SYNTHESIS AND CHARACTERISATION OF A SERIES OF NOVEL MONONUCLEAR AND SURFACE ACTIVE DINUCLEAR RUTHENIUM(II) AND OSMIUM(II) POLYPYRIDYL COMPLEXES.

By

Adrian Liam Guckian, B.Sc.

A Thesis presented to Dublin City University for the degree of Doctor of Philosophy.

Supervisor Prof. J. G. Vos
School of Chemical Sciences
Dublin City University

August 2002

To my parents…

Isaac Newton (1642 –1727)

On how he made discoveries,

"By always thinking unto them. I keep the subject constantly before me and wait till the first dawnings open little by little into the full light."

I hereby certify that this material, which I now submit for assessment on the programme of study leading to award of Doctor of Philosophy by research and thesis, is entirely my own work and has not been taken from work of others, save and to extent that such work has been cited and acknowledged with the text of my work.

Signed: Adrian Guckian

Adrian Guckian

I. D. number: 98970682

Date: 16-09-2002

Acknowledgements:

I would like to thank Prof. Han Vos firstly. I appreciate the chance you gave me to work in your research group. Without your enthusiasm and help, this thesis would not have come about. I really appreciate the amount of reading you have done over the past couple of months. Your comments and direction has made the time a little more bearable.

The first half of this thesis introduces a series of ruthenium and osmium complexes containing a series of novel ligands. These ligands were provided by Prof. Manfred Doering. I owe Prof. Doering a huge debt of gratitude for providing me with these ligands to work with. Thank you for sending the ligands in the first place and for sending more when the first lot ran out. The X-Ray Crystallography has also been provided by Prof. Doering. Thank you for achieving such excellent results so quickly. Prof. Villani from the University of Rome has also been involved in this project. The expertise provided by his group have provided many answers for us.

The first year of my Ph. D. was spent in the University of Bologna, in the research group of Prof. Balzani. I would like to take this opportunity to thank Prof. Balzani for providing the opportunity to work in his group. Special thanks must go to my surrogate Italian mother Prof. Teresa Gandolfi (Mother Teresa). Thanks for having the patience to teach me about photophysics, I cannot imagine a better place to have learnt about this area of chemistry. Not only was she an excellent supervisor while I worked in the group, she also greatly eased the move to Italy and the language barrier. I am delighted to have met her, and am looking forward to meeting her again. Thanks also to Roberto Ballardini, Albertos Juris and Credi, Margherita, Luca Prodi, Mauro, Nelsi, Anna, Pierre, Nunzio and Andreas. The year was made more enjoyable because of your company. I hope to see you all shortly.

A huge thank you should go to the technicians in DCU. Damien, Maurice, Veronica, Ann, Ambrose, Vinny, John and Mary. Thanks for everything. Special thanks goes to Mick. I learned a lot about NMR from you and appreciate how much more there is to

learn. Thanks for always having the time to talk even though you would always have 15 more things to do.

To my fellow postgrads (and postdocs). The HVRG group past Anthea (Wales forever), Christine (21 forever), Egbert, Frances, Luke (nothing like a drop of Red Breast), Marco (what can I say – remember the blue hair and the pillow), Moss, Scott (Mr. Ice, not), Stefano. I learnt a lot in the first couple of months of my Ph.D and not a lot of it was chemistry. The present group Dec (Yo!), Fiona1 and 2, Helen, Noel, Stefania and Wesley. Thanks a lot. Special thanks has to go to the lads for helping sanity to be maintained. Frank (coldest house in Ireland), Cathal (I like to ----), and Ger (Gerrr-rrard) and Johan (of the Dubillin accent). Thanks to everyone else who was there – you all know who you are. For all the coffees and breaks in the corridor before we had a room. Thanks to my friends from the outside – Brian and Mark (and their girlfriends Nathalie and Jane). Roger, Eddie, Galtee, John. Those nights out when talking about chemistry or work was banned were a lifesaver. I'll be doing a lot more of that soon too.

Thanks Michelle. For always being there to listen, and to encourage me. Thanks for having patience and always knowing what to say. I promise I'll have more free time soon. We'll always remember that it was through this that we met

Finally, thanks to my family. My sister Julie and brother Philip. Maybe you can stop making fun of me for still being at school now. Most of all thanks Mam and Dad. I really couldn't have done it without you. You have never stopped believing in me and have made this possible.

Abstract:

The synthesis, spectroscopic and electrochemical characterisation of a series of mononuclear and dinuclear ruthenium (II) and osmium (II) complexes is described. Chapter 1 provides an introduction to the area of supramolecular chemistry. The complex $[Ru(bpy)_3]^{2+}$, the parent complex of modern supramolecular chemistry is also introduced. Chapter 2 is a general introduction to the physical measurements of the complexes which have been synthesised. The techniques of High Performance Liquid Chromatography (HPLC), Nuclear Magnetic Resonance (NMR), UV/Visible spectroscopy, fluorimetry, spectroelectrochemistry and electrochemistry are all briefly described to provide an insight into the application of these techniques later in the thesis.

Chapter 3 provides an introduction to the ligands used to synthesise the complexes described in Chapters 3, 4 and 5. The ligands all contain a fused 5 and 6 membered ring, with the 5 membered ring having an imidazo-type functionality in the case of all the ligands with the exception of one, where the 5 membered ring contains a third nitrogen and becomes a triazo-type system. The ^{1}H NMR spectra of the ligands have been assigned where possible, and the photophysics and electrochemistry of the free ligands are discussed. The synthesis of a series of novel ruthenium(II) mononuclear complexes, $[Ru(bpy)_2(LL)]^{2+}$ is described as is the synthesis of several deuterated analogues, $[Ru(d_8\text{-bpy})_2(LL)]^{2+}$. The characterisation of these complexes by X-Ray Crystallography and ^{1}H NMR is discussed with an isomerisation effect being discussed in detail using analysis from ^{1}H NMR and HPLC experiments. The characterisation of the complexes is completed with an examination of the photophysical, photochemical and electrochemical properties. Chapter 4 is structured similarly. The synthesis of the osmium(II) bipyridyl complexes using the ligands discussed in Chapter 3 is described. The same isomerisation effect appears for several of the ligands and is again discussed in detail. Again, the characterisation of the complexes is completed with an examination of the photophysical, photochemical and electrochemical properties. The LL7 ligand is used to synthesise a ruthenium(II) monomer as well as a series of homonuclear and heteronuclear ruthenium(II) and osmium(II) dimers. The deuterated analogues of the Ru-Ru homonuclear dimer has also been synthesised. These complexes provide the material for discussion in Chapter 5. The photophysical and electrochemical examination of this series of complexes indicates that little or no communication exists between the metal centres, even in the case of the mixed-metal complex. The spectroelectrochemistry of the complexes agree with this supposition.

Chapter 6 introduces a different type of complex and a detailed survey of previous work in this area using the bridging ligands 4,4'bipyridyl, P2P, P3P and PEP precedes the discussion of the synthesis and characterisation of the series of mononuclear ruthenium(II) and osmium(II) complexes. It proved important to understand the properties of these compounds as these monomeric species provide the starting material for the synthesis of the series of dimers discussed in Chapter 7. The synthesis and spectroscopic behaviour of this series of dinuclear complexes is presented. The dinuclear complexes have been synthesised with the intention of attaching them to surfaces. This is described for one of the complexes and a brief examination of the behaviour of the complex confined to a surface is performed.

The final chapter, Chapter 8 provides a conclusion to the work carried out on the two projects that make up this thesis. The chapter also suggests further work, which may be carried out in future studies.

Table of Contents:

Chapter 1 Introduction

Chapter 2 Experimental Procedures

Chapter 7 Synthesis and Characterisation of a Series of Surface Active Dinuclear Ruthenium(II) and Osmium(II) Complexes

Chapter 8 Conclusions and Future Work

Chapter 1: Introduction

Abstract:

Chapter 1 serves as an introduction to many of the subjects that are discussed in this thesis. Firstly, supramolecular chemistry is introduced. The development of this area of chemistry is outlined and its relevance to this thesis is highlighted. In order to understand the processes involved in a supramolecular species, it is important to first understand the fundamental properties of the simpler subunits of the supramolecular species. Coordination and the effect of coordination on ligands is mentioned as is molecular photochemistry. The "parent" complex of many of the compounds discussed in this thesis, $[Ru(bpy)_3]^{2+}$, and its importance to the area of inorganic chemistry is highlighted.

Several other concepts are introduced including excited state molecular processes, intervalence transfer bands and the techniques used to examine these processes, such as spectroelectrochemistry, are also discussed. The topics discussed in Chapter 1 have been limited to those that are relevant to this thesis as the area of inorganic and supramolecular chemistry is now so large. Chapter 3 and Chapter 6 of this thesis contain more detailed examination of the specific areas which are relevant to those particular sections of this thesis.

1.1 Introduction to Supramolecular Chemistry:

In nature photons are used by living organisms as energy in photosynthetic processes. The aim of supramolecular chemistry is the design and construction of artificial energy-conversion and information processing devices, devices that in the future will allow us to power and control the machines that form the basis of our civilisation. [1] Since the 1970s, using the "bottom up" approach proposed by Richard Feynman, [2] the design and construction of these machines and devices began for the first time with atoms and molecules. This area has branched and diversified since and now self-assembly, self organisation and self replication, actions central to nature's forms and functions are feasibly being used to construct large and intricate functional molecular and supramolecular entities. [3]

The interaction of light with matter is dependent on the nature of the receiving matter [4], with the simplest form being represented by a molecule. This interaction of light with a molecule can have a number of outcomes, such as a change in molecular structure, and some of these may be exploited for our purposes. Solar energy, for example, can be converted into chemical energy by transforming a molecule into its higher energy isomer. [5]

In order to utilise this potential fully a high level of organisation within the molecule is required. The assembly of a number of discrete molecular components allows the synthesis of supramolecular species. [4,6,7,8,9] Organisation of components can be achieved by various types of intermolecular forces (Coulombic interactions, hydrogen bonding, etc.) or by linking the components using covalent or coordination bonding. This means that it is possible therefore to design structurally organised systems which incorporate a certain function, (Photochemical Molecular Devices (PMDs) [10,11,12]) i.e. the molecular components have the desired light related properties: absorption spectrum, excited state lifetime, luminescence spectrum or redox properties, capable of converting the energy and input of the photons to perform complex functions (such as light harvesting, conversion of light into electrical energy, data processing and storage).

The simplest definition of supramolecular chemistry is the chemistry of systems (supermolecules) made up of molecular components in the same way as molecules are made up of atoms. [13] More recently this has been expanded to become "the chemistry beyond the molecule, bearing on the organized entities of higher complexity that result from the association of two or more chemical species held together by intermolecular forces." [6] This definition can be simplified. The distinction between a large molecule and a supramolecular species can be based on the degree of interaction between the subunits of the components, regardless of the nature of the intercomponent bonding. [1] (Figure 1.1) When the interaction energy between subunits is small compared to other relevant parameters, the system can be considered to be a supramolecular species.

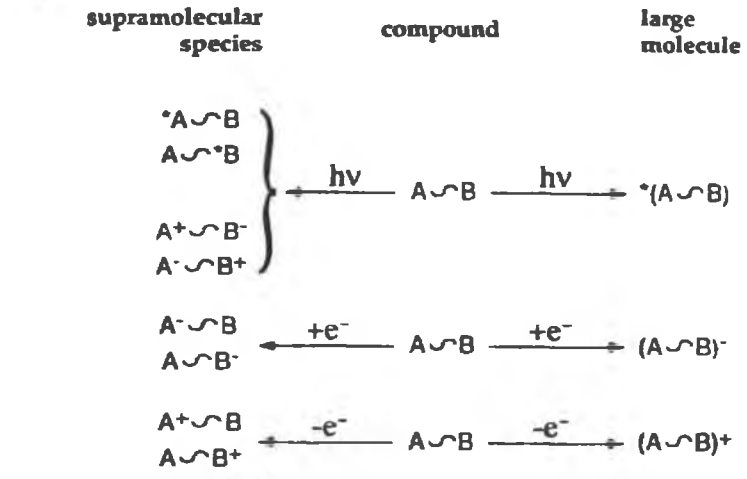

[a] The symbol "∽" indicates any type of "bond" that keeps together the A and B moieties.

Figure 1.1 Illustration of the photochemical and electrochemical criteria used to classify a complex as a supramolecular species or as a large molecule.

In order to discuss supramolecular chemistry further, the basics of photophysics and photochemistry must be examined. The next section provides an introduction to coordination chemistry and to the processes that are used to investigate the photophysical properties of coordination complexes.

1.2 Examination of Ligand Orbitals

Consider the case of the free pyridine molecule which possesses a nonbonding electron pair (*n*) on the N atom which can be promoted to antibonding orbitals π* on the aromatic ring. The first $n \rightarrow \pi^*$ transition lies at low energy, and excitation of a nonbonding electron into the ring is the lowest energy transition possible. This is followed closely by a $\pi \rightarrow \pi^*$ transition which is characteristic of an aromatic ring. [14]

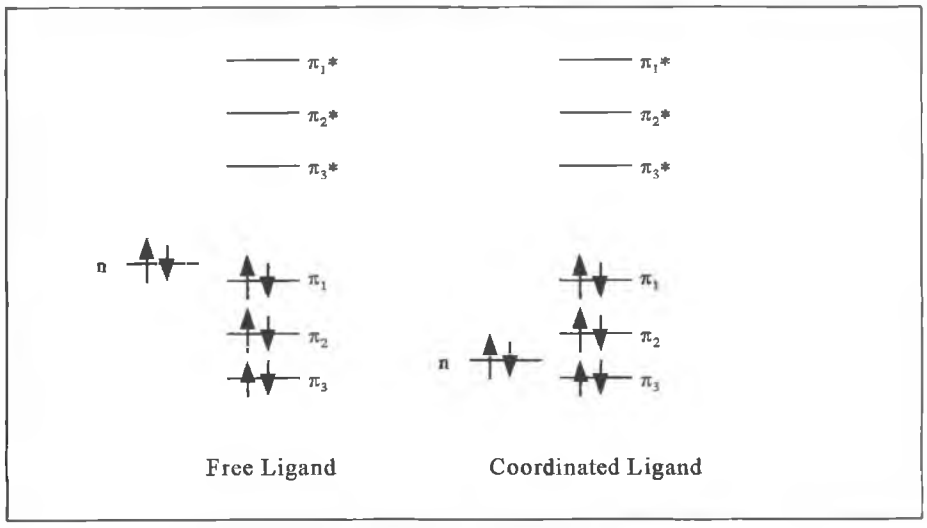

Figure 1.2 Representation of the orbitals of a N-heterocycle ligand. Nonbonding (n) electrons in the free ligand are lowered in energy with respect to the π-system when coordination occurs.

On coordination however the *n* electrons on the nitrogen atom form a σ- bond with the metal ion, which lowers their energy so they can no longer be excited by low energy light. (Figure 1.2) The $\pi \rightarrow \pi^*$ transitions on the ring are not greatly affected by complexation and it can be said that generally the $\pi \rightarrow \pi^*$ transitions of coordinated moieties are not shifted greatly by complexation whereas the $n \rightarrow \pi^*$ transitions are usually shifted to higher energies. The case for a ligand coordinated in a d^6 complex is discussed below. [14]

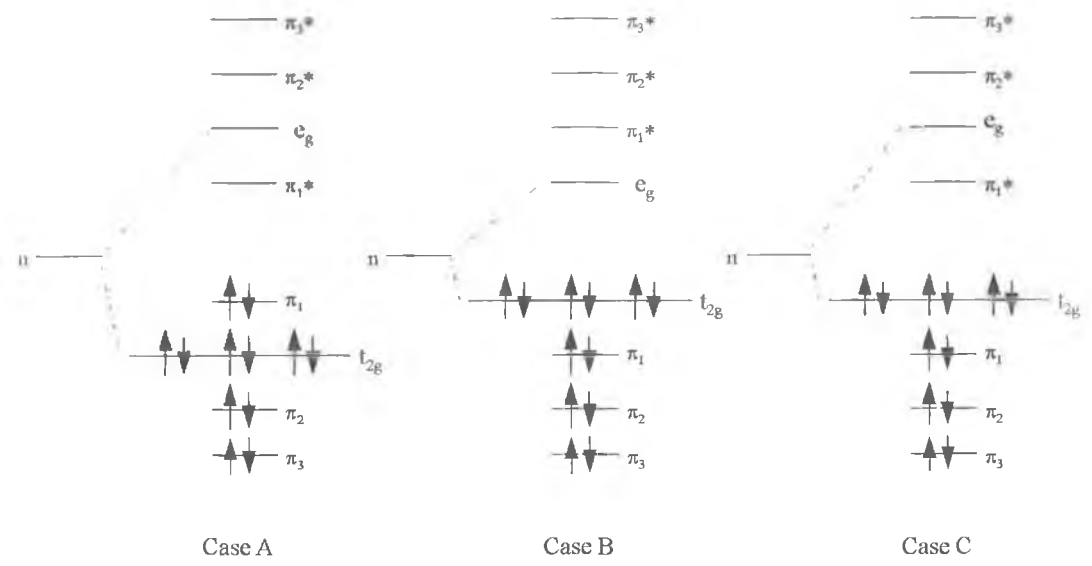

Figure 1.3 Schematic representation of orbital dispositions for strong field d^6 complexes.

In Case A (Figure 1.3), the $\pi \rightarrow \pi^*$ Excited Configuration is Lowest. Here the energy levels of the filled t_{2g} orbitals are placed below the filled orbitals of the ligands and the energy levels of the e_g set are placed above the π^* set. The lowest excited state is therefore derived from a $\pi\pi^*$ configuration. This is the case for the compounds $[Rh(bpy)_3]^{3+}$, and $[Rh(phen)_3]^{3+}$. The metal orbital plays a negligible role in the excitation process. As the lowest energy transitions are ligand localised, chemical processes occurring subsequent to excitation would be suspected to be ligand photochemistry. In Case B above the dd excited state configuration is lowest. An example of this is $[Co(CN)_6]^{3-}$, a diamagnetic ion, the absorption and emission spectra of which indicates a $(t_{2g})^6$ closed shell with all spins paired in the ground state. When light is absorbed the action occurs on the metal ion with $(t_{2g})^6 \rightarrow (t_{2g})^5(e_g)^1$ orbital promotion. Excitation of $[Co(CN)_6]^{3-}$ leads to characteristic ligand field photochemistry. Substitution photochemistry is the usual photochemical process expected to occur upon $t_{2g} \rightarrow e_g$ orbital promotion. This takes place when $[Co(CN)_6]^{3-}$ is irradiated in aqueous solution to produce the $[Co(CN)_5(H_2O)]^{2-}$ ion in high quantum efficiency. Case C above is the most relevant to this thesis. The $d \rightarrow \pi^*$ excited state configuration is lowest. The

absorption spectrum of 2,2'-bipyridine shows the expected lowest energy $\pi \rightarrow \pi^*$ transitions. Spectral measurements of $[Ru(bpy)_3]^{2+}$ however reveal an entirely new set of electronic transitions which are neither metal centred nor ligand localised. These intense visible transitions are charge transfer in nature. [15] Absorption of a photon promotes an electron from the t_{2g} orbital on the Ru(II) ion to an antibonding π^* orbital on the bipyridine system. This is represented in Case C of the inferred orbital diagram above (Figure 1.3). The first antibonding orbital is a ligand π^* and the highest filled orbital is a metal t_{2g}.

In a charge transfer excited configuration the complex has a hole in the t_{2g} orbital set with the excited electron resting on the ligand, which is a different species to the ground state complex. The excitation energy can be transferred to another molecule, can undergo reduction by filling the hole or act as a reductant by transferring the promoted electron on the ligand to another species.

1.3 Principles of molecular photochemistry:

The photochemical process begins when a molecule absorbs a photon. The gain in energy promotes an electron from the highest occupied molecular orbital (HOMO) to the lowest unoccupied molecular orbital (LUMO). The excited molecule, now unstable decays quickly to its original state, the ground state, by losing the energy it acquired from the photon. This energy loss may take different forms - radiative decay and non radiative decay. These will both be examined more closely later.

The behaviour of an electronically excited molecule differs from ordinary chemical species. These molecules have an excess of free energy above equilibrium which can cause bond rupture and other reactions. [16,17] Absorption of infra-red and microwave radiation is normally excluded from the subject as the energy per photon is too small to cause photoreaction.[18]

Transitions that are nearly fully allowed are charge transfer and intraligand. Charge transfer can either be metal to ligand charge transfer (MLCT) or ligand to metal charge transfer (LMCT), where an electron can be represented as being transferred from one orbital to another localised in different regions of the molecule without net spin change. This is less so the greater the atomic number of the metal ion.

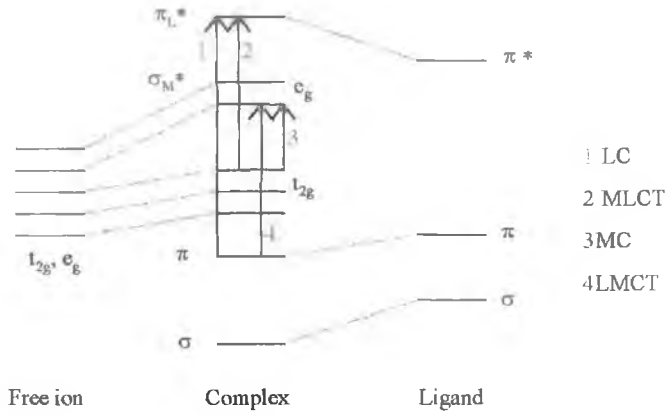

Figure 1.4 Relative disposition of metal and ligand orbitals and possible electronic transitions in an octahedral ligand field of a transition metal complex.

At the instant of absorption of light, the Franck-Condon effect dictates that molecules are formed in non-equilibrated vibrational states. Photochemical reactions of inorganic molecules normally take place in solution and therefore internal conversion leading to equilibration of the vibrational energy with the substrate is fast, so unless a competing process is very fast, a thermally excited state is produced following the absorption of light. [19]

There are two emission processes to consider - phosphorescence and fluorescence. Whether an emission process is fluorescence or phosphorescence depends on whether or not there is a spin quantum number change associated with the transition.

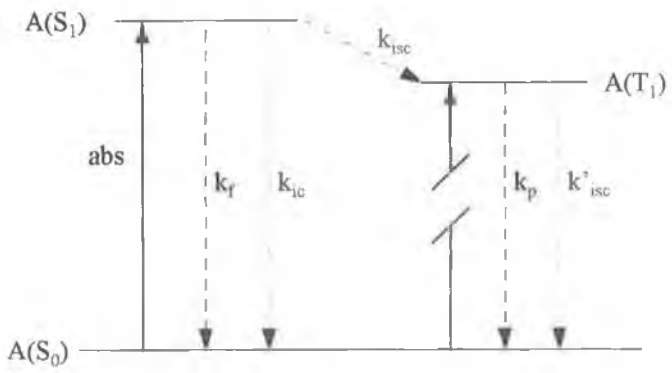

Figure 1.5 Schematic energy level diagram of a molecule showing the possible paths of energy degradation.

k_f = fluorescence

k_{ic} = internal conversion

k_{isc} = intersystem crossing

k_p = phosphorescence

The Jablonski diagram above shows three of the states involved in a photochemical process (ground state singlet and excited singlet and triplet). As mentioned already, emission of light (luminescence) is called fluorescence or phosphorescence depending on whether the excited state has the same or different spin compared to the ground state. In the same way, radiationless deactivation is called internal conversion when it occurs between states of the same spin and intersystem crossing when it occurs between states of different spin.[20] Fluorescence and internal conversion are spin-allowed steps, whereas phosphorescence and intersystem crossing are spin-forbidden steps.

Where the transitions do not involve a change in multiplicity, inorganic and organic systems tend to be similar. However where changes in multiplicity are involved the differences can be substantial. These differences arise in part due to the larger coupling constants associated with the high atomic number metal ions relative to C, H and N. The increased spin orbit coupling causes mixing of the singlet and triplet states which results in a breakdown of the selection rules which prohibit changes in multiplicity. For organic molecules containing low atomic number atoms, intersystem crossing processes are

formally forbidden and therefore are very slow or hindered, with rate constants, k_{isc} typically 1-1000 x 10^{-6} s^{-1}. In inorganic systems where spin orbit coupling is greater, k_{isc} of 10^{9} - 10^{12} s^{-1} are the rule rather than the exception. These can be so fast as to make it impossible to distinguish them from internal conversions that are not spin forbidden.[21]

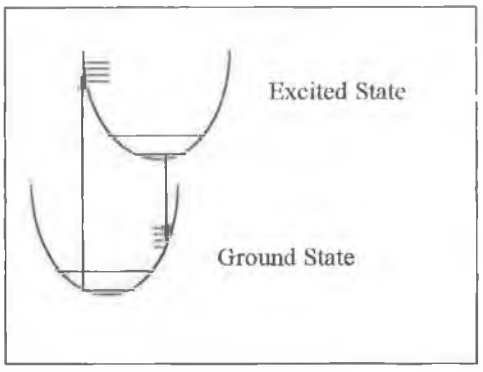

Figure 1.6 Illustration of the origin of the Stokes' Shift.

Application of the Franck-Condon effect indicates that on absorption of light, excited vibrational levels of the excited state will be formed. This implies that the energy of maximum emission will be smaller than the energy of maximum absorption. This Stokes' Shift means that emission occurs on the lower energy side or red side of absorption (assuming that they correspond to the same transition).

1.4 Emission Spectroscopy:

Photochemical processes predominantly involve the lowest excited states of molecules. These lowest excited states are the ones that are responsible for emission. Emission is usually observed from the lowest singlet state or from the lowest triplet state (fluorescence or phosphorescence). Emission is guided by the fact that in the absence of photochemistry from upper excited states, emission from a transition metal complex with an unfilled d-shell will occur from the lowest electronic excited state of the molecule, or from those states that can achieve a significant Boltzmann population relative to the lowest excited state.

This rule tells us that an emissive complex is one that possesses a large energy gap between its lowest excited state and the ground state, because otherwise, the energy would degrade rapidly to lower levels and not produce light, this is known as the Energy Gap Law. Consequently, in order to design photoluminescent compounds we search for complexes that will give a large energy gap between the ground state and the lowest excited configuration. [22]

Experiments at 77K have permitted the classification of the lowest, or emitting states of complexes.

⇨ ^{3}dd Excited states.

The emission is broad and structureless and is rarely observed in solution. The quantum yield is generally quite low, but the yield can be improved by removing high frequency vibrations from the coordination sphere. This can be accomplished by perdeuteration of the ligands and complexes.

⇨ ^{3}dπ^* Excited States.

The emission is intense and highly structured. Often a single vibrational progression dominates the band. Luminescence is often observed at room temperature. When the complex is unsymmetrical and has a static dipole moment, the energy of the emission band can be shifted markedly by changing the polarity of the medium.

⇨ $^3\pi\pi^*$ Excited States.

Normally highly structured, and sometimes resembles the $\pi\pi^*$ emission from the uncoordinated ligand, but is usually red shifted upon complexation. The energy of the emission is not highly solvent dependent.

1.5 The photophysical properties of $[Ru(bpy)_3]^{2+}$

$[Ru(bpy)_3]^{2+}$ has been one of the most extensively studied compounds of the second half of the past century.[23] The photophysical properties of $[Ru(bpy)_3]^{2+}$ are well understood at this stage and it has become the standard and reference compound for comparison with other ruthenium(II) diimine complexes. [24,25,26,27,28] Interest in the chemical conversion of solar light into energy has provided additional driving force to the field. Unfortunately however, $[Ru(bpy)_3]^{2+}$ is not the ideal catalyst for this process. The most serious problem is the fact that population of the ^3MC state results in photodecomposition. The compounds absorption spectrum in the solar spectrum is another obstacle to its application in catalysis. It makes inefficient use of the suns energy as only a relatively narrow band of the suns light is absorbed by the complex. The ground state structure of one enantiomer of the hexaflourophosphate salt of $[Ru(bpy)_3]^{2+}$ is represented in Figure 1.7. [29]

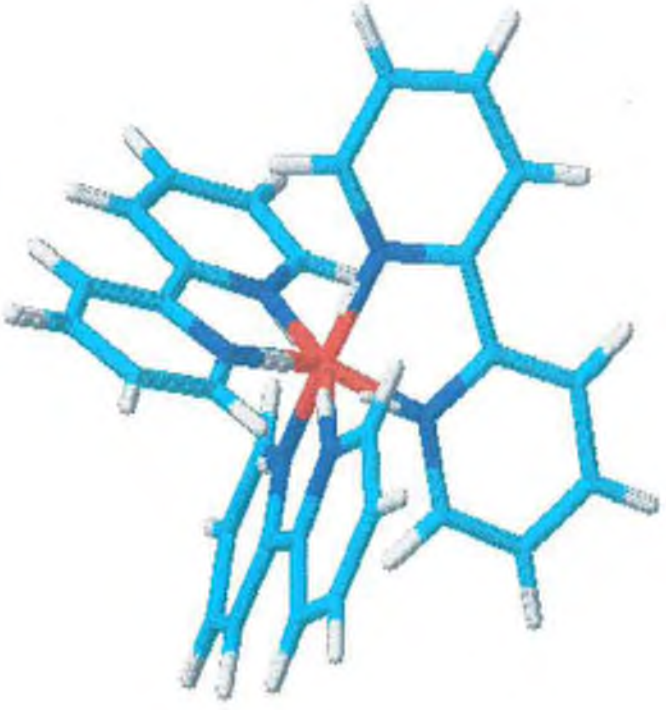

Figure 1.7 3D structure of $[Ru(bpy)_3]^{2+}$

The complex possesses D_3 symmetry and the Ru-N bond length of 205.6pm is shorter than the normal Ru-N bond length of 210.4pm. This indicates the presence of significant π-backbonding interaction between the ruthenium and the π* orbitals of the bipyridyl ligand. The solution ^1H NMR data confirm the retention of the D_3 symmetry for the solvated species, and can be interpreted in terms of four coupled spins in each of the six equivalent pyridine rings.

The assignment of spin states to electronically excited states has already been discussed. The differences arise in part due to the larger coupling constants associated with the high atomic number metal ions relative to C, H and N. This increased spin orbit coupling causes mixing of the singlet and triplet states which results in a breakdown of the selection rules which prohibit changes in multiplicity. This means that for ruthenium and osmium, transitions that are normally formally forbidden can become partially allowed. Overall this means that the rate of radiative and non radiative transitions which are formally spin forbidden become enhanced. For $[Ru(bpy)_3]^{2+}$ excitation to all higher excited states undergo rapid internal conversion (IC) and inter-system crossing (ISC) to the lowest lying manifold of the ^{3}MLCT states.[30]

Figure 1.8 depicts the most important photophysical properties of $[Ru(bpy)_3]^{2+}$. The absorption spectrum exhibits an intense absorption band at 452 nm with an extinction coefficient of 14,600 $M^{-1}cm^{-1}$ (Figure 1.9). This band has been assigned as a metal to ligand charge transfer (MLCT) transition. Fast intersystem crossing (ISC) from singlet to triplet states occurs with an efficiency of unity. Emission from the triplet state to the ground state (k_r) (Figure 1.9) or radiationless deactivation (k_{nr}) to the ground state can occur. Another deactivation pathway is provided by population of the metal centred excited state (^{3}MC) which leads to radiationless deactivation or to photodecomposition of the complex.[18,31,32,33,34]

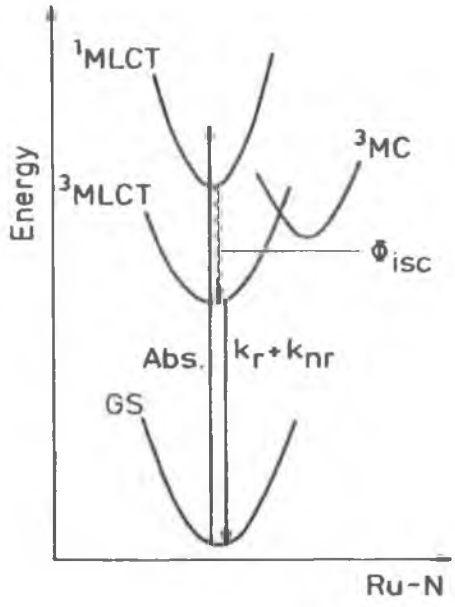

Figure 1.8 Potential Energy diagram showing the relative positions of the excited states of $[Ru(bpy)_3]^{2+}$

The lowest ^{3}MLCT excited state consists of three electronic components with the upper two members situated approximately 10 and 60 cm^{-1} above the lowest. These are distinguishable only at very low temperatures (< 5K). A fourth ^{3}MLCT, which lies approximately 600cm^{-1} above these and is only thermally populated at higher temperatures (> 77K), has considerably more singlet character than the lower lying ^{3}MLCT states and therefore greatly enhances the radiative and nonradiative ISC rates to the ground states.[35]

The photochemistry of $[Ru(bpy)_3]^{2+}$ therefore arises mostly from the ^{3}MC excited state which can be populated thermally by internal conversion from the ^{3}MLCT state. This can at best lead to non radiative decay, but can also lead to ligand loss photochemistry. The reason for this is the lengthening and therefore weakening of the Ru-N bond, which is the result of population of the ^{3}MC state. The ^{3}MC state has considerable e_g orbital character and electron density is placed between the ruthenium centre and the nitrogen donor atoms. The resulting electronic repulsion of placing electron density in the e_g

orbitals and the loss of backbonding from the t_{2g}-π^* orbital weakens the Ru-N bond. [36, 37, 38]

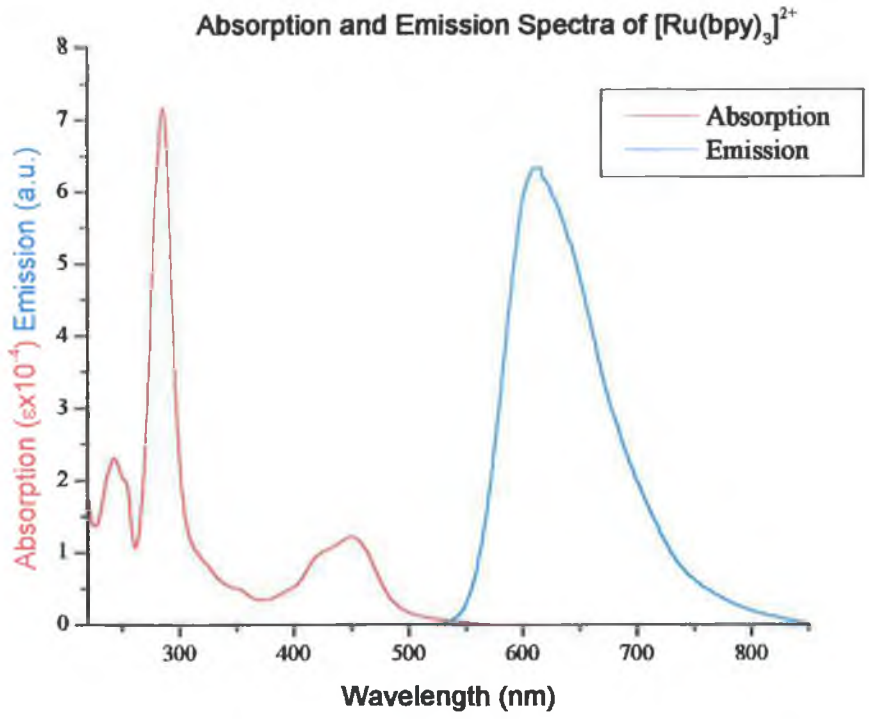

Figure 1.9 Absorption and Emission spectra of $[Ru(bpy)_3]^{2+}$ in MeCN.

A good deal of the photochemical interest in $[Ru(bpy)_3]^{2+}$ stems from its photoredox properties. The values of the ground state standard potentials for the oxidation and reduction of $[Ru(bpy)_3]^{2+}$ are useful in establishing the excited state redox potentials.

$$[Ru(bpy)_3]^{2+} + e^- \rightarrow [Ru(bpy)]_3^{+} \qquad E^0 = -1.35 \text{ V } vs \text{ SCE}$$

$$[Ru(bpy)_3]^{3+} + e^- \rightarrow [Ru(bpy)_3]^{2+} \qquad E^0 = +1.26 \text{ V } vs \text{ SCE}$$

The monovalent, divalent and trivalent cations are known for their thermal inertness towards the labilisation of 2,2'-bipyridyl which leads to their participation in a variety of reversible electron transfer processes.

Oxidation of the $[Ru(bpy)_3]^{2+}$ complex normally involves a metal centred orbital, with formation of Ru(III) centres, which are inert to ligand substitution. The oxidation potential of $[Ru(bpy)_3]^{2+}$ is centred at +1.26V *vs* SCE, but substitution of one or more of the bipyridine ligands can drastically change this potential. Reduction of $[Ru(bpy)_3]^{2+}$ takes place on the ligand π^* orbital at -1.35V *vs* SCE and is usually the same as that involved in the ^{3}MLCT transition.

Due to the higher energy content, the excited state is both a stronger reductant and a stronger oxidant than the corresponding ground state. The properties of ruthenium(II) complexes are governed by the σ-donor and π-acceptor properties of the ligands. A σ-donor donates electron density to the metal centre lowering the oxidation potential and causing more negative reduction potentials. On the other hand π-acceptor ligands remove electron density from the metal centre of the complex, stabilising the filled metal orbitals which results in higher oxidation potentials and lower reduction potentials.

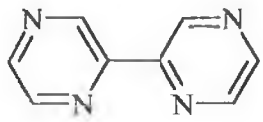

2,2'-bipyrazine

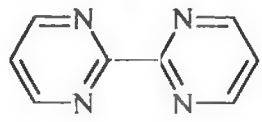

2,2'-bipyrimidine

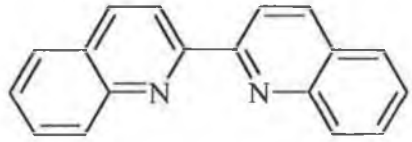

2,2'-biquinoline

Figure 1.10 Examples of π–acceptor ligands.

Much attention has been focused on systems containing strong π-accepting ligands. Apart from bpy these include 2,2' bipyrazine, 2,2'-bipyrimidine, 2,2'-biquinoline and derivatives. [39,40,41,42] (Figure 1.10) The mixed ligand complexes which result, i.e. $[Ru(bpy)_2(LL)]^{2+}$ display a red shift in the absorption and emission energy relative to the

parent $[Ru(bpy)_3]^{2+}$ compound. As a result these complexes harvest a larger portion of the available solar energy. Unfortunately, due to the fact that often strong π-acceptor ligands are weak σ-donor ligands, the ligand field splitting of Ru(II) becomes much smaller and therefore after excitation the ^{3}MC state is more easily accessible, the emission yield is diminished and the compound becomes less photostable than $[Ru(bpy)_3]^{2+}$.

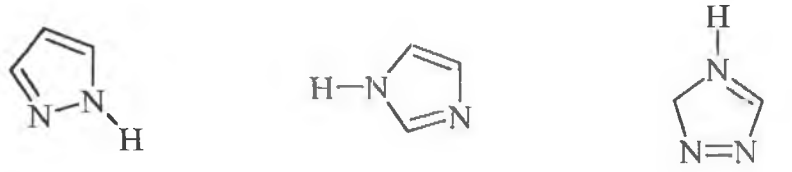

Pyrazole Imidazole 1,2,4-triazole

Figure 1.11 Examples of σ-donor ligands.

Ligands with strong σ-donor properties include imidazole, pyrazole and 1,2,4-triazole. (Figure 1.11) The strong σ-donor capacities of these ligands result in larger ligand field splitting which helps stop photodecomposition.[43,44,45,46,47,48,49,50] These ligands are weaker π-acceptors and their empty π* orbitals are higher in energy than that of bpy. This results in a blue shift in the absorption and emission spectra leading to a smaller proportion of the solar energy available being absorbed.

By combining the two systems, a π-acceptor and a σ-donor, e.g. a compound containing two bpy ligands and one azole ligand, the lowest π* level is still bpy based, but the filled d orbitals are destabilised by strong σ-donor ligands which lower the oxidation potential. Photophysical measurements on such compounds have indicated that such systems are more stable than the parent $[Ru(bpy)_3]^{2+}$ compound and still they have retained the useful photophysical and electrochemical properties.

1.6 Excited State Bimolecular Processes

There are two bimolecular reactions of vital importance, energy transfer and electron transfer. Energy transfer is a physical process where through contact, an excited state molecule transfers its excitation energy to another, different molecule. Electron transfer involves the transfer of an electron from or to the excited state molecule and simultaneous oxidation or reduction of another separate species in the solution. [51,52,53,54]

From the point of view of the quenching species, its reactions are sensitised by the energy transfer process, and for this reason a molecule can be caused to undergo photoreaction by light in a region of wavelengths in which the molecule does not absorb. The limitation to energy transfer is that the acceptor (of energy) must have an excited state that lies lower than that of the donor. Also the lifetime of the donor must be long enough for the two species to come together. The donor and acceptor interact rapidly once they come in contact, and hence energy transfer is usually diffusion-controlled.

1.7 Energy-Transfer Processes

An electronically excited state *D, obtained when a molecule D absorbs a photon of suitable energy (Equation 1.1) is a new chemical species which has the potential to transfer energy to another species (Equation 1.2).

$$D + h\nu \rightarrow {}^*D \qquad \textbf{Equation 1.1}$$

$${}^*D + A \rightarrow D + {}^*A \qquad \textbf{Equation 1.2}$$

The simultaneous deactivation of the original excited molecule and the promotion of the acceptor molecule to an electronically excited state is known as energy transfer. What is observed is the quenching of the emission or photochemistry associated with *D and its replacement by the emission or photochemistry characteristic of *A.

Energy transfer may occur by radiative or nonradiative mechanisms. [4] Radiative energy transfer is the simpler of the two and involves emission of a quantum of light by the donor excited state which is followed by absorption of the emitted photon by the acceptor, and can occur over any distance.

$$^{*}D \rightarrow D + h\nu \qquad \textbf{Equation 1.3}$$

$$h\nu + A \rightarrow {}^{*}A \qquad \textbf{Equation 1.4}$$

In this process the absorbing molecule cannot influence the emission of the donor molecule but merely intercepts the emitted photon.

Electronic energy transfer can occur by two mechanisms: the Förster-type mechanism, based on Coulombic interactions (1), and the Dexter-type mechanism which is based on exchange interactions (2). [17] Figure 1.12 illustrates the differences between the two mechanisms.

1. The first may occur by dipole-dipole interaction between an electronically excited donor and an acceptor in its ground state. This type of energy transfer is distance dependant and can operate at distances of up to 100 Å. This is known as the Förster mechanism and is the better understood mechanism of the two.
2. The second method is the Dexter mechanism and involves a simultaneous electron exchange mechanism where a spatial overlap of the donor and acceptor is required, and therefore they must be in van der Waals or hard sphere contact with each other.

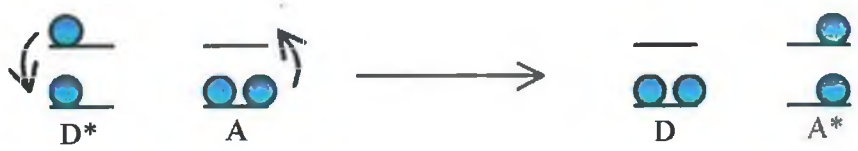

Energy Transfer by dipole-dipole mechanism (Förster mechanism).

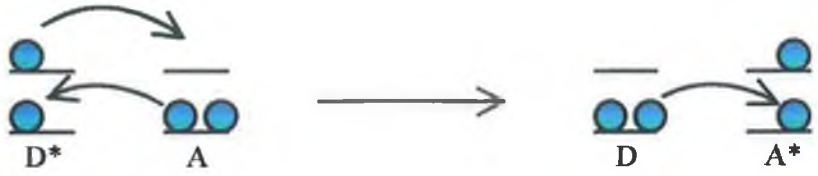

Energy Transfer by electron exchange (Dexter mechanism).

Figure 1.12 Pictorial representation of the energy transfer processes of electronically excited states.

1.8 Electron Transfer Reactions of Excited States

There are two types of electron transfer involving excited states, photoinduced electron transfer which follows light excitation of a component, and optical electron transfer which takes place directly upon light excitation. These will be dealt with separately.

1.8.1 Photoinduced Electron Transfer:

Light excitation increases both the oxidizing and the reducing power of a molecule. In a multicomponent supramolecular system light excitation is often followed by an electron transfer process.

$$A \sim B + h\nu \rightarrow {}^{*}A \sim B \qquad \textbf{Photoexcitation} \qquad \textbf{Equation 1.5}$$

$$* A \sim B \rightarrow A^{+} \sim B$$ **Photoinduced oxidative electron transfer** **Equation 1.6**

$$* A \sim B \rightarrow A^{-} \sim B^{+}$$ **Photoinduced reductive electron transfer** **Equation 1.7**

The reduction potentials for the excited state couples may be calculated from the reduction potentials of the ground state couples and the one-electron potential corresponding to the zero-zero excitation energy:

$$E(A^{+}/{}^{*}A) \approx E(A^{+}/A) - E^{0-0}$$ **Equation 1.8**

$$E({}^{*}A/A^{-}) \approx E(A/A^{-}) - E^{0-0}$$ **Equation 1.9**

Therefore the feasibility of an excited state electron transfer process occurring is given by the Weller equation: [17]

$$\Delta G^{0} \approx -E^{0-0} - E(B/B^{-})' + E(A^{+}/A)' - E_{IP}$$ **Equation 1.10**

where ΔG^0 is the free energy change of the process, E^{0-0} is the spectroscopic change of the excited state, $E(B/B^-)'$ and $(E(A^+/A)'$ are the one electron energies corresponding to the reduction of the two species, and E_{IP} is the Coulombic stabilisation energy of the products.

1.8.2 Optical Electron Transfer.

Optical electron transfer may be described by the model developed by Marcus, Hush and Sutin and is known as the Marcus model. [55,57] This model makes it clear that reactants and products of an electron-transfer process are related by a ground/excited state relationship.

$$A\sim B \longrightarrow A^{+}\sim B^{-}$$ **Equation 1.11**

If a ground state reaction is considered where $\Delta G^0 < 0$ then according to the Marcus model, for a unimolecular electron transfer process the rate of electron transfer, k_{et}, can be expressed as

$$k_{et} = \nu_N K \exp(-\Delta G^{\neq}/RT)$$ **Equation 1.12**

Where ν_N = the average nuclear frequency factor of the reaction, K = the transmission coefficient of the reaction, and ΔG^{ζ} = the experimental Gibbs energy of activation for the electron transfer process.

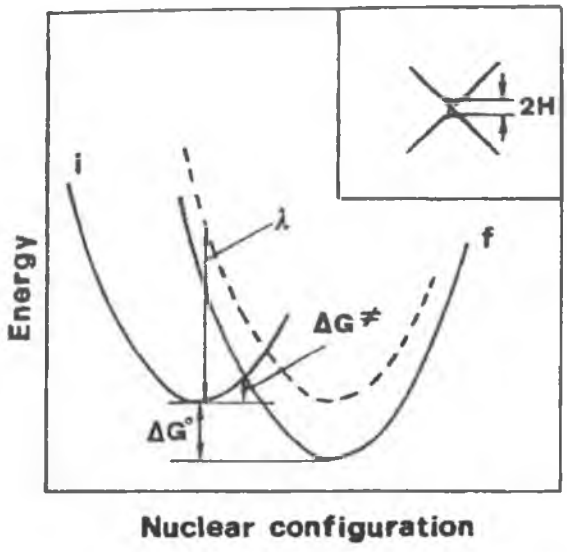

Figure 1.13 Profile of the potential energy curves of an electron transfer reaction. i and f indicate initial (A-B) and final (A^{+}-B^{-}) states.

In Figure 1.13, the two curves represent the potential energies of the reactants and products as a function of the reaction coordinate. The activation free energy, ΔG^{ζ} in Equation 1.12 and 1.13 corresponds to the energy difference between the crossing point and the reactant minimum in Figure 1.13. The term K is the probability that the reactants, on reaching the geometry of the crossing point, convert into products.

From Figure 1.13, the activation free energy is determined by the combined effects of the degree of distortion between products and reactants (horizontal displacement) and the driving force of the reaction (vertical displacement). Marcus Theory expresses this in the equation below.

$$\Delta G^{\neq} = (\lambda/4)(1+\Delta G^0/\lambda)^2 \qquad \textbf{Equation 1.13}$$

The parameter λ is the reorganisational energy. This can be split into the sum of two independent contributions (Equation 1.14), corresponding to reorganisation of "inner" (bond lengths and angles within A and B) and "outer" (solvent reorganisation around the reacting pair) nuclear modes.

$$\lambda = \lambda_i + \lambda_o \qquad \textbf{Equation 1.14}$$

The behaviour predicted by the Marcus model in the highly exoergonic ΔG^0 region has attracted much attention. According to Equation 1.13, $\Delta G^{\ddagger}$ equals $\lambda/4$ at $\Delta G^0 = 0$, goes to 0 at $\Delta G^0 = -\lambda$, and increases again for more negative ΔG^0 values. This is represented in Figure 1.14 below.

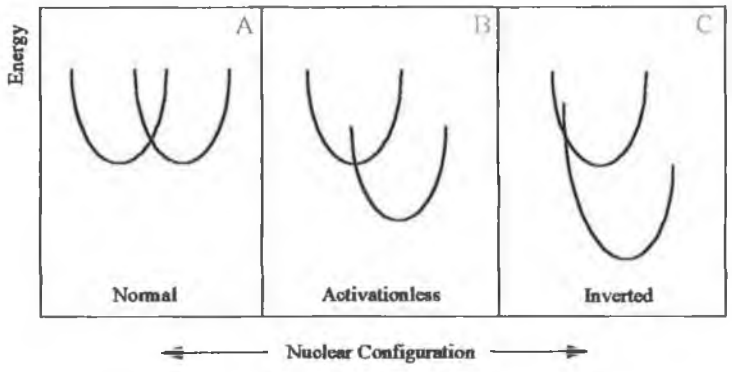

Figure 1.14 The potential energy curves for the reactant and product of an electron transfer process in the 3 types of system identified by the Marcus model.

This predicts that for moderately exoergonic reactions the driving force is expected to help the reaction kinetics, but for strongly exoergonic reactions the driving force is predicted to act against it. The ΔG^0 region in which this happens is known as the "Marcus inverted region."

Both optical and photoinduced electron transfer may be followed by a thermal back-electron transfer process.

$$A^+ \sim B^- \rightarrow A \sim B \qquad \textbf{Equation 1.15}$$

The relationships between optical, photoinduced and thermal back electron-transfer processes are illustrated in Figure 1.15. [17]

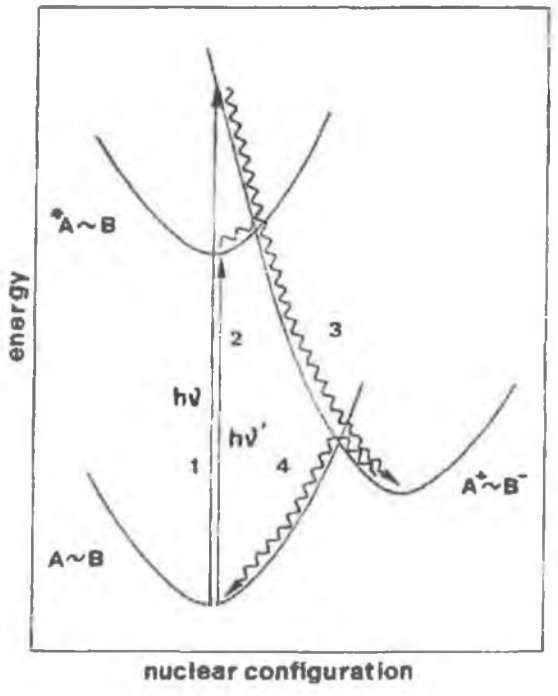

Figure 1.15 Relationship between optical (1), photoinduced (2 and 3) and thermal back (4) electron transfer processes in supramolecular species.

Optical electron transfer is often observed for mixed-valence compounds where partially oxidised forms show structureless bands in the Near Infra-Red (NIR) region (7000-10000 cm^{-1}) and are called Intervalence Transfer (I.T.) bands or metal to metal charge transfer (MMCT) bands.

The energy of an IT band consists of an inner and an outer sphere part. The inner sphere part is due to the fact that the metal-ligand bond lengths and the force constants are different for M(II) and M(III) ions (λ_i in Equation 1.14). The changing nuclear configurations give rise to an activation barrier to electron transfer as nuclear motion occurs on a timescale of 10^{-11}-10^{-13} s whereas electronic motion occurs in $<10^{-15}$ s. The outer sphere part is due to the changes solvent dipoles which have to reorientate themselves when the oxidation state is changed (λ_o in Equation 1.14).

It is obvious therefore that λ_i is an intrinsic property of the supermolecule, whereas λ_o depends on the reorganisation of the solvent environment. By measuring the IT band in different solvents the influence of the inner-sphere and the outer-sphere energies on the IT band may be calculated.

The extent of electron delocalisation in a mixed valence compound, α^2, can be calculated from the properties of the IT band.

$$\alpha^2 = (4.2\text{x}10^{-4})\varepsilon_{max}\Delta\nu_{1/2} / d^2.E_{op} \qquad \textbf{Equation 1.16}$$

where α^2 = extent of electron delocalisation,

ε_{max} = extinction coefficient of the IT band ($M^{-1}cm^{-1}$)

$\Delta\nu_{1/2}$ = peak width at half the peak height

d = distance between the metal centres (Å)

E_{op} = energy of the IT band (cm^{-1})

The bandwidth at half the peak height can be derived from

$$\Delta\nu_{1/2} = [2310(E_{op}.\ \Delta E)]^{1/2} \qquad \textbf{Equation 1.17}$$

where ΔE = the energy difference induced by the asymmetrical environment.

The nature of valence delocalisation in mixed valence systems has been classified by Robin and Day. [56] The classifications can better be explained while considering an example of a binuclear complex such as that in Figure 1.16.

$$[Ru(NH_3)_5\text{-BL-}Ru(NH_3)_5]^{5+} \qquad \textit{Figure 1.16}$$

Class I The electronic coupling between the centres is very small or totally absent, and the properties of the supermolecule are essentially a superposition of those of the individual components. An example of this type of system would be $[Ru(NH_3)_5(P2P)Ru(NH_3)_5]^{5+}$ (where P2P = 1,2-di-(pyrid-4'-yl-ethane)).[57] The system exhibits properties which are simply a superposition of the properties of the isolated mononuclear components $[Ru(NH_3)_5]^{2+}$ and $[Ru(NH_3)_5]^{3+}$. The electronic interaction between the metal centres is absolutely negligible. The curves in Figure 1.17A represent the system. Even if the system does acquire sufficient activation energy to reach the intersection region, the probability of electron exchange is still negligible.

Class II The electronic coupling between the metal centres is appreciable, either as a consequence of direct orbital overlap or via a through bridge mechanism, and a number of new properties of the supermolecule appear in the spectra (e.g. IT bands). Systems of this type can still be considered as valence localised, and will still exhibit the properties of the isolated $[Ru(NH_3)_5]^{2+}$ and $[Ru(NH_3)_5]^{3+}$ components. However new properties associated with the Ru(II)-Ru(III) interaction can also be observed. An example of this type of behaviour can be observed for the complex $[Ru(NH_3)_5(POP)Ru(NH_3)_5]^{5+}$ where POP = 4,4'-bipyridine. [57] Figure 1.17B represents the potential energy curves of such a system.

Class III The properties of the isolated components of the supermolecule are absent and the electronic coupling of the metal centres is strong. In this case the binuclear compound is best considered a fully delocalised $Ru(II^{1/2})$-$Ru(II^{1/2})$ system with properties that are mostly unrelated to those of the $[Ru(NH_3)_5]^{2+}$ and $[Ru(NH_3)_5]^{3+}$ components. An example of this type of behaviour is found when the bridging ligand in Figure 1.17C is NC-CN. [57] In this case the true first order curves show a single minimum at an intermediate geometry (Figure 1.17C).

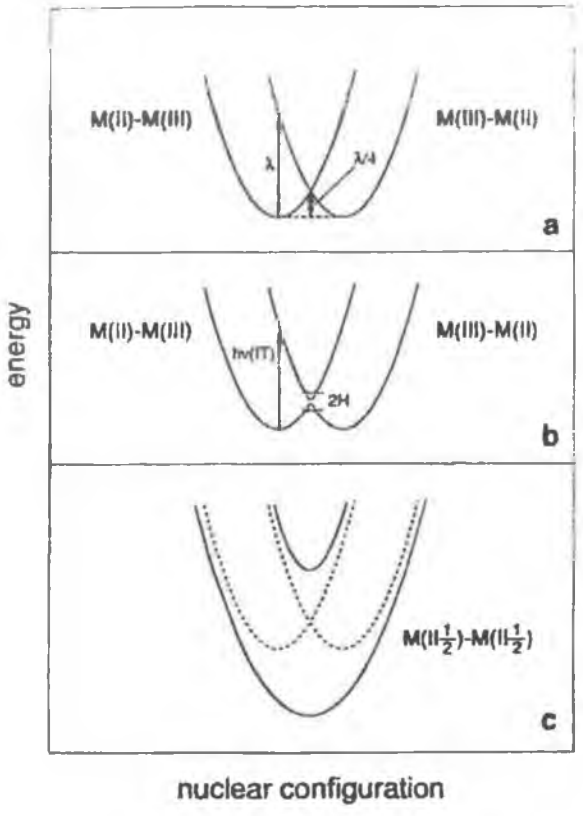

Figure 1.17 Potential Energy curves for mixed valence compounds with (a) negligible (b) weak and (c) strong electronic coupling. The dotted lines represent zero order states.

1.9 Spectroelectrochemistry:

Spectroelectrochemistry involves the combination of an electrochemical technique with a spectroscopic one, so that the measurements may be performed simultaneously. This allows the electrochemical technique to serve as the excitation signal while the response of the system to this is measured spectroscopically. Optical spectroelectrochemistry ensures the integrity of the one electron transfer as a chemically and electrochemically reversible step. In addition, this impressive procedure provides valuable information about the constitution of the product from the resultant spectra. [58] Other advantages of this method incude (i) the species are studied near their ground state, avoiding large perturbations as in photochemically triggered reactions, (ii) the measurement, being static, is relatively simple and easy to perform, and (iii) interfaces from intermolecular effects are absent/negligible. [59]

Spectroelectrochemistry is most commonly used in the analysis of mixed valence dinuclear species to examine the nature and extent of metal-metal interaction and electronic coupling between the metal centres.

Much work has concentrated on the examination of the intervalence transitions in mixed valence compounds, but spectroelectrochemistry can also be used to probe ligand to metal charge transfer (LMCT) states. This is due to the relatively weak intensities ($\varepsilon < 500 cm^{-1}$) and non-emissive nature of the transitions. For example the visible spectrum of $[Ru(bpy)_3]^{3+}$ has two bands with maxima at 670 nm and 415 nm.

In general, low energy LMCT transitions are favourable when the metal is oxidising and the ligand reducing. These properties can be introduced into complexes by changing the nature of the 2,2'-bipyridyl ligand. Reasonably intense LMCT bands can be generated with Ru(III) and Os(III) complexes with substituted bpy ligands. The properties of these LMCT bands were examined by Kalyanassundarum and co-workers. The donor strength of the bpy ligand was systematically tuned using different substituents (Me, OMe, NH_2, NMe_2) on the 4,4'- position. [60] It was found that the intensity of the LMCT transition

increased with decreasing values of the redox potential. Also noted was the fact that replacement of a donor ligand, by a poorer donor or acceptor ligand caused a red shift in the observed LMCT transition.

Nazeeruddin et al. have examined the effects of increasing electron donating capacity of the donor ligand on the intensity of the LMCT state. [61] Their findings indicate that the larger the σ-donor capacity of the ligand the more intense the band observed.

1.10 Scope of thesis

Chapter 1 has provided an introduction to supramolecular chemistry and some of the most important features of supramolecular species. The next sections of this thesis describes the synthesis and characterisation of mononuclear and dinuclear ruthenium(II) and osmium(II) bisbipyridyl complexes. In Chapter 2 the experimental methodology used to synthesise and characterise the complexes is described.

Chapter 3 introduces previous work in areas relevant to the complexes discussed in Chapters 3, 4 and 5. The ligands used (LL_x) to synthesise the ruthenium complexes (Chapter 3), the osmium complexes (Chapter 4) and the dinuclear complexes (Chapter 5) are introduced and characterised in Chapter 3, which also contains the synthesis of the ruthenium complexes containing the LL_x ligands. Chapter 4 describes the synthesis and characterisation of the osmium LLx complexes while Chapter 5 deals with a series of dinuclear complexes bridged by the LL7 ligand.

Chapter 6 acts as an introduction to Chapter 7. In Chapter 6 previous work in the area relevant to both chapters is reported, as is the synthesis of the monomeric precursors used in Chapter 7 to synthesise a series of surface active dinuclear complexes. The complexes described in Chapter 6 have been previously reported and their surface chemistry is well understood. Chapter 8 concludes this thesis with a brief outline of the work successfully undertaken and the future work necessary to conclude the characterisation of the novel complexes introduced in the previous chapters is outlined.

Finally, two appendices are supplemented to this thesis. The first consists of X-Ray Crystal data for the complexes described in Chapter 3.4 and Chapter 5.4. The second relates to presentations made, poster presentations and contributions to a publication during the course of my research.

1.11 Bibliography:

[1] Balzani V., Scandola F., ***"Comprehensive Supramolecular Chemistry"***, Vol. 10; "***Supramolecular Technology"***. Eds Atwood J., Davies E. E. D., MacNicol D. D., Vögtle F., Pergannon, **1996**

[2] Feynman R. P., ***Sat. Rev.***, **1960**, 43, 45

[3] Dietrich-Buchecker C. O., Sauvage J. P., ***Chem. Rev.***, **1987**, 87, 795

[4] Balzani V., Scandola F., ***"Supramolecular Photochemistry,"*** Ellis Horwood, Chichester, **1991.**

[5] Hautala R. R., King R. B., and Kutal C., ***"Solar Energy Chemical Conversion and Storage,"*** Humana Press, Clifton, NJ, **1979**.

[6] Lehn J.-M., ***Angew. Chem., Int. Ed. Engl.***, **1988**, 27, 89

[7] Vögtle F., ***"Supramolecular Chemistry,"*** Wiley, Chichester, **1991.**

[8] Balzani V. and De Cola L., ***"Supramolecular Chemistry,"*** Kluwer, Dordrecht, **1992**.

[9] Lehn J.-M., **Angew. Chem., *Int. Ed. Engl.***, **1990**, 29, 1304

[10] Balzani V., Moggi L. and Scandola F., ***"Supramolecular Photochemistry,"*** ed. V. Balzani, Reidei, Dordrecht, **1987**.

[11] Balzani V., ***Tetrahedron***, **1992,** 48, 10443.

[12] Bissel R. A., de Silva A. P., Gunaratne H. Q. N., Lynch P. L. M., Maguire G. E. M., and Sandanayake K. R. A. S., ***Top. Curr. Chem.,*** **1993**, 168, 223.

[13] Stoddart, J. F., ***Chem. Brit***, **1988,** 24, 1203.

[14] Crosby G. A., ***J. Chem. Ed.,*** **1983**, 60, 791

[15] Klassen, D. M., Crosby G. A., ***J. Chem. Phys.,*** **1968,** 48, 1853

[16] Porter, G. B., ***J. Chem. Ed.,*** **1983**, 60, 785

[17] Balzani V., Juris A., Venturi M., Campagna S., Serroni S., ***Coord. Chem. Rev***., **1996**, 2, 759

[18] A. Juris, V. Balzani, F. Barigelleti, S. Campagna, P. Belser, A. Von Zelewsky, ***Coord. Chem. Rev.,*** **1988**, 84, 85

[19] Demas J. N., ***J. Chem. Ed.*** **1983**, 60, 803.

[20] Endicott J. F., ***J. Chem. Ed***. **1983**, 60, 785

[21] Demas J. N., ***J. Chem. Ed.***, **1983,** 60, 803.

[22] Demas J. N., Crosby G. A., ***J. Am. Chem. Soc***., **1970**, 92, 7262

[23] Paris J. P., Brandt W. W., ***J. Am. Chem. Soc***., **1959**, 81, 5001

[24] Durham B., Casper J. V., Nagle J. K., Meyer T. J., ***J. Am. Chem. Soc***., **1982**, 104, 4803.

[25] Watts R. J., ***J. Chem. Ed***., **1983**, 60, 834.

[26] Casper J. V., Meyer T. J., ***J. Am. Chem. Soc***., **1983**, 105, 5583

[27] Damrauer N. H., Cerullo G., Yeh A., Boussie T. R., Shank C. V., McCusker J. K., ***Science***, **1997**, 275, 54.

[28] Li C., Hoffman M. Z., ***Inorg. Chem***., **1998**, 37, 830.

[29] Rillema P., Jones D. S., Levy H., ***J. C. S. Chem. Comm***., **1979**, 849

[30] Hage R., ***Ph. D Thesis***, Leiden University, **1991**.

[31] Van Houten J., Watts R. J., ***J. Am. Chem. Soc***., **1975**, 97, 3843

[32] Demas J. N., Crosby G. A., ***J. Am. Chem. Soc***., **1971**, 93, 2841

[33] Demas J.N., Taylor G. A., ***Inorg. Chem.,*** **1979,** 18, 3177

[34] Kober E. M., Meyer T. J., ***Inorg. Chem.,*** **1984,** 23, 3877

[35] Van Houten J., Watts R. J., ***J. Am. Chem. Soc***., **1960**, 33, 1261.

[36] Kober E. M., Meyer T.J., ***Inorg. Chem.,*** **1982**, 21 3967.

[37] Kober E. M., Meyer T.J., ***Inorg. Chem.,* 1983,** 22, 1614.

[38] Kober E. M., Meyer T.J., ***Inorg. Chem.,* 1984,** 23, 3877.

[39] Juris A., Campagna S., Balzani V., Gremaud G., von Zelewsky A., ***Inorg. Chem.*, 1988**, 27, 3652

[40] Barigelleti F., Juris A., Balzani V., Belser P., von Zelewsky A., ***Inorg. Chem.,* 1988,** 27, 3652

[41] Barigelleti F., Belser P., von Zelewsky A., Juris A., Balzani V., ***J. Phys. Chem.,* 1985,** 89, 3680

[42] Juris A., Belser P., Barigelleti F., Balzani V., von Zelewsky A., ***Inorg. Chem.,* 1986,** 25, 256

[43] Bond A. M., Haga M., ***Inorg. Chem.,* 1986**, 25, 4507

[44] Steel P. J., Constable E. C., ***J. Chem. Soc., Dalton Trans*, 1990,** 1389

[45] Vos J. G., Haasnoot J. G., Vos G., ***Inorg. Chim. Acta,* 1983,** 71, 155

[46] Hage R., Dijkhuis A. H. J., Haasnoot J. G., Prins R., Reedijk J., Buchanan B. E., Vos J. G., ***Inorg. Chem.,* 1988**, 27, 2185

[47] Hage R., Prins R., Haasnoot J. G., Reedijk J., Vos J. G., ***J. Chem. Soc., Dalton Trans*, 1987,** 1389

[48] Hage R., Haasnoot J. G., Reedijk J., Vos J. G., ***Inorg. Chim. Acta.,* 1986,**

118, 73,

[49] Hage R., Haasnoot J. G., Stufkens D. J., Snoeck T. L., Reedijk J., Vos J. G., ***Inorg. Chem.,* 1989,** 28, 1413

[50] Barigelleti F., De Cola L., Balzani V., Hage R., Haasnoot J. G., Reedijk J., Vos J. G., ***Inorg. Chem.,* 1989**, 28, 4344

[51] Balzani V., Scandola F., Comp. ***Supramol. Tech,.* 1996**, 10, 687

[52] Balzani V., Scandola F., ***J. Chem. Ed.,* 1983**, 60, 814

[53] Balzani V., Juris A. ***Coor. Chem. Rev.,* 2001,** 211, 97

[54] Adamson A. W*., J. Chem. Ed.,* **1983**, 60, 797

[56] Robin, M. B. and Day, P., ***Adv. Inorg. Chem. Radiochem***, **1967**, 10, 247

[57] Creutz, C., ***Prog. Inorg. Chem.***, **1963**, 30, 1.

[58] Hage R., Haasnoot J. G., Niewenhuis H. A., Reedijk J., De Ridder D. H., Vos J. G., Wang R., ***J. Am. Chem. Soc.***, **1990**, 112, 9245

[59] Weldon, F*., Ph.D Thesis,* Dublin City University, **1998.**

[60] Thummel R. P., Lefoulon F., Chirayil S., ***Inorg. Chem***., **1987**, 26, 3072.

[61] Nazeeruddin M. K., Zakeeruiddin S. M., Kalyanasundaram K., ***J. Phys. Chem.***, **1993**, 97, 9607.

Chapter 2: Experimental Procedures

Abstract:

In this chapter details of experimental and basic synthetic procedures used in subsequent chapters are described. In addition a limited discussion of practical aspects of both synthetic procedures and physical measurements is included, in particular where major difficulties were encountered and where improvements to standard procedures were made.

2.1 Materials and reagents

All synthetic reagents were of commercial grade and no further purification was employed, unless otherwise stated. All solvents used for spectroscopic measurements were of HPLC or UVASOL (Merck) grade. For luminescence measurements UVASOL grade solvents have been found to be the purest with respect to emissive contaminants. The ligands used in Chapters 3, 4 and 5 were provided by Prof. Doering and were used without further purification.

Deuteriation of 2,2'-bipyridyl was carried out in accordance with the literature procedure.[1] After 3 days in the bomb (a general-purpose dissolution Bomb P/N 4744 from Scientific Medical Products, which included a Teflon cup and cover), it was found that approximately 90% atom deuteriation had been achieved. This percentage improved only slightly with increased reaction times. However, following a repeat of the procedure, i.e. another 3 days in the bomb with fresh reagents it was found that atom deuteriation of >99% was achieved. The percentage deuteriation was calculated by ^{1}H NMR experiments. A known amount of the undeuteriated ligand was dissolved in a known volume of solvent (d_6-DMSO). The ratio of the peak integration of the ligand to the peak integration of the solvent was found. After obtaining a spectrum of the same amount of the perdeuterio ligand in the same volume of solvent, a second ratio was obtained. Comparison of the ratios led to a measurement of the percentage of the atoms which have been successfully exchanged. The ^{1}H NMR spectra of the deuteriated 2,2'-bipyridyl ligand is shown in Figure 2.1. The size of the solvent peak relative to the size of the 2,2'-bipyridyl ligand peaks should be noted. It is the ratio of the peak integration of these peaks that allow the second ratio to be calculated.

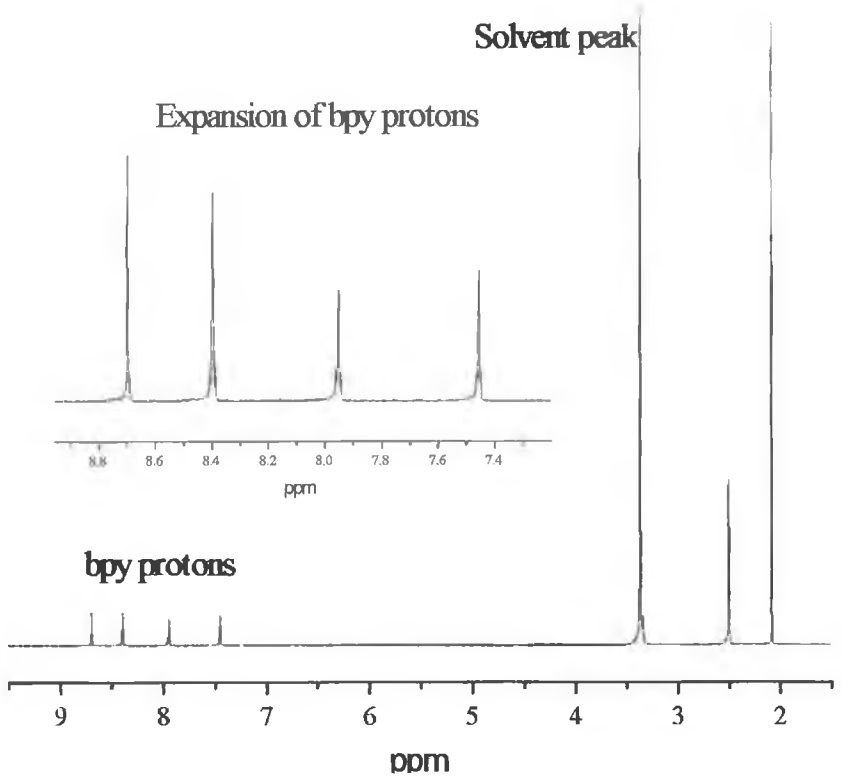

Figure 2.1 ^1H NMR of d_8-bpy in d_6-DMSO. Note size of solvent peak relative to the bipyridyl protons.

2.2 Chromatographic techniques

Analytical HPLC

Analytical High Performance Liquid Chromatography (HPLC) experiments were carried out using a JVA analytical HPLC system consisting of a Varian Prostar HPLC pump fitted with a 20 μL injection loop, a Varian Prostar PDA detector connected to a dedicated PC, and a HiChrom Partisil P10SCX-3095 cation exchange column. The mobile phase used was 80:20 (v:v) CH_3CN:H_2O containing typically 0.08-0.01 M $LiClO_4$, the flow rate was between 1.8 and 2.5 cm^3/min. The monitoring wavelength used was 280 nm.

Column Chromatography

Column chromatography was carried out on activated neutral alumina (Al_2O_3, 150 mesh) or on silica gel (80/20 (v:v) CH_3CN/H_2O saturated with KNO_3).

2.3 Nuclear Magnetic Resonance spectroscopy

NMR spectroscopy is an invaluable tool not only in the identification of compounds but also in the monitoring of reactions and the determination of purity. It is used extensively throughout this thesis and where practical full assignment of ^1H spectra have been made using a combination of 2-dimensional techniques.[2]

^1H and ^1H Cosy Spectroscopy

All ^1H (400 MHz) and ^2D (75 MHz) NMR experiments were recorded on a Bruker Avance 400 NMR Spectrometer and the free induction decay (FID) profiles processed using XWIN-NMR software package. All measurements were carried out in $(CD_3)_2SO$, CD_3Cl or $(CD_3)_2CO$ for ligands and CD_3CN or $(CD_3)_2CO$ for complexes. Peak positions are relative to residual solvent peaks. For ^1H Cosy NMR experiments 256 FID's, each of 8 scans, consisting of 1K data points were accumulated. After digital filtering using a sine bell squared function, the FID's were zero filled in the F1 dimension. Acquisition parameters were F1 = +/- 500 Hz, F2 = 1000 Hz, $t_{1/2}$ = 0.001 s and the recycle delay was 1.5 s.

2.4 Absorption and Emission Spectroscopy

UV/Vis spectra were recorded on a Shimadzu UV.Vis/NIR 3100 spectrophotometer interfaced with an Elonex-466 PC using UV.Vis data manager. Samples were held in 0.1 or 1 cm pathlength quartz cuvettes.

Emission spectra were recorded at all temperatures using a Perkin-Elmer LS50 or LS50-B Luminescence spectrophotometer interfaced with an Elonex-466 PC using windows 3.1 based fluorescence data manager software. Emission and excitation slit widths were typically 3, 5 or 10 nm depending on conditions. Measurements at 77 K were carried out

in liquid nitrogen filled glass cryostat, with sample held in a NMR tube. Measurements between 90 K and 280 K were carried out using an Oxford Instruments liquid nitrogen cooled cryostat model 39426 with samples being held in a home made quartz or glass cuvette. Spectra are uncorrected for photomultiplier response.

Emission Quantum yield measurements

Quantum yield measurements were carried out by the optically dilute method [3] by comparison with $[Ru(bpy)_3](PF_6)_2$ [4] in aerated/deaerated acetonitrile. Emission spectra were obtained at a wavelength where the absorption by $[Ru(bpy)_3](PF_6)_2$ and the sample under examination are equal. The area under the emission spectrum (A) of each sample was calculated using the spectrometer supplied software and the quantum yield was calculated from Equation 2.1:

Equation 2.1
$$\Phi_{unkown} / \Phi_{[Ru(bpy)_3](PF_6)_2} = A_{unkown} / A_{[Ru(bpy)_3](PF_6)_2}$$

Where Φ is the quantum yield and A is the area under the emission spectrum. As all quantum yield measurements were carried out in acetonitrile, compensation for refractive indices is unnecessary.

2.5 Luminescent Lifetime Measurements

All lifetime measurements reported have been determined using TCSPC (Time Correlated Single Photon Counter) either at DCU using an Edinburgh Instruments nf900 ns flashlamp and CD900 TAC (time to amplitude converter) or at the Department of Photochemistry, "G. Ciamician", University of Bologna, Italy using an Edinburgh Instruments instrument of similar design but with manual TAC control. Lifetimes were measured using Uvasol Solvents (Lennox chemicals) (MeCN at room temperature, butyronitrile at 77K) and either degassed using Ar purge for 15 min or by undergoing four freeze-pump-thaw cycles. Deconvolution of the lamp profile was carried out for samples, which showed either very weak emission and/or had emission lifetimes < 50

ns. The lamp profile was obtained using a colloidal suspension of silica in water as scattering agent. Data correlation and manipulation was carried out using the program F900, Version 5.13.

2.6 Photochemical studies

Photolysis studies were carried out by placing samples in Quartz matched cuvettes for both UV/Vis and ^{1}H NMR studies, and placing them before a 100 W Tungsten filament light source slide projector (Kodak Carousel S-AV2020). This produces light with a broad spectrum similar to that of solar energy. Sample heating was prevented using a water filter.

2.7 Electrochemical Measurements:

Cyclic voltammetry (100 mV/s) and DPV (step height: 50 mV, increment: 4 mV, pulse duration: 60 ms, sampling interval: 20 ms, frequency: 5 Hz that is: 5 pulses per second, or a "pulse period" of 0.2 seconds) carried out in acetonitrile with 0.1 M $TBABF_4$. A conventional three-electrode cell was used. A 2 mm Pt disk electrode sealed in Kel-F (purchased from CH Instruments) was used as the working electrode, the counter (auxiliary) electrode was a coiled Pt-wire, and a Ag/Ag^+ (acetonitrile + 10mM $AgNO_3$ + 0.1 M $TBABF_4$) half-cell was used as reference electrode. The solutions were degassed with argon and a blanket of argon was maintained over the solutions during the experiments. Glassware used was dried in a vacuum oven at 80°C overnight or flamed using a Bunsen burner previous to preparing solutions and running experiments. The salt was dried in the vacuum oven overnight at 80°C. The electrodes were polished on a soft polishing pad (Struers, OP-NAP) with an aqueous slurry of 0.3 micron alumina (Buehler) and sonicated for at least 5 min in MQ-water to remove any remaining polishing material from the surface of the electrode. The working electrodes were rinsed thoroughly with acetone and dried in air before insertion into the cell. The reference electrode was calibrated externally by carrying out cyclic voltammetry (also at 100

mV/s) in solutions of ferrocene of roughly the same concentration as that of the complexes (0.4 – 2 mM) in the same electrolyte at the end of each day of experiments.

Spectroelectrochemistry was carried out using an optically transparent thin layer electrode (OTTLE) set-up comprising of a homemade Pyrex glass, thin layer cell (1mm). The optically transparent working electrode was made from platinum gauze, the counter electrode used was a platinum wire, and the reference electrode was a pseudo Ag/AgCl reference electrode. Spectroelectrochemistry[5] was carried out in anhydrous acetonitrile (Aldrich), and the electrolyte employed was 0.1 M TEAP perchlorate. The working electrode was held at the required potential throughout the measurement using an EG&G PAR Model 362 scanning potentiostat. In order to perform the experiment properly, the Ag/Ag^+ wire was calibrated against the Fc/Fc^+ standard before each experiment was carried out. This allows the oxidation potentials observed during the electrochemical measurements to correlate with the spectroelectrochemical measurements. All references are quoted as being Fc/Fc^+ using the relevant conversion factor. [6,7] Absorption spectra of the species generated in the OTTLE cell were recorded on a Shimadzu 3100 UV-Vis/NIR spectrophotometer interfaced with an Elonex PC-433.

2.8 Elemental Analysis

Elemental analysis on C, H, and N was carried out at the Microanalytical Laboratory of University College Dublin (UCD). The CHN analyser used is an Exador analytical **CE440**.

2.9 Bibliography

[1] Keyes T., Weldon F., Muller E., Pechy P., Gratzel M., Vos J. G., ***J. Chem. Soc. Dalton Trans.***, **1995**, 2705.

[2] (a) Binsch G. and Kessler H., ***Angew. Chem., Int. Ed. Engl.,*** **1980**, *19* ,411 (b) King R. W. and Williams K. R., ***J. Chem. Ed.,*** **1990**, *67*, A101 (useful glossary of NMR terms) (c) Dybowski C., Glatfelter A. and Cheng N. H., ***Encyclopaedia of***

Analytical Chemistry, Academic press, 149 (d) Williams K. R., and King R.W., ***J. Chem. Ed.,*** **1990**, *67*, A125 (e) Crews P., Rodriguez J., ***Organic Structural Analysis***, Oxford University press, Oxford, **1998**

[3] Demas J. N. and Crosby G. A., ***J. Phys. Chem.***, **1971**, *75*, 991

[4]. Nakamaru N., ***Bull. Chem. Soc. Jpn.***, **1982**, *55*, 2697

[5] Heineman W. R., ***J. Chem. Ed.,*** **1983**, *60*, 4

[6] Chang J. P., Fung E. Y., Curtis J. C., ***Inorg. Chem.,*** **1986**, 25, 4233.

[7] Connelly N. G., Geiger W. E., ***Chem. Rev.***, **1996**, 96, 877.

Chapter 3: Synthesis and Characterisation of a series of $[Ru(bpy)_2(LL_x)]^{2+}$ complexes:

Abstract:

Chapter 3 introduces a series of novel bidentate ligands (LL_x) and the corresponding ruthenium(II) bisbipyridyl complexes of these ligands. This chapter begins with an investigation of the photophysical, electrochemical and photochemical properties of previously reported complexes which are expected to have similar properties to the ruthenium(II) complexes presented here. The introduction and the discussion of the properties of the ligands in Chapter 3 are relevant also for the complexes discussed in Chapter 4 (osmium(II) complexes) and the dinuclear complexes discussed in Chapter 5.

An involved chemistry has been observed for the ruthenium(II) complexes of the LL_x ligands. In order to understand this better, the properties of the free ligands have also been examined and this serves as an introduction to the interesting properties of the complexes.

3.1 Introduction

Chapter 3 introduces a series of ligands which has been used to prepare a series of novel ruthenium(II) and osmium(II) complexes. The synthesis and characterisation of the ruthenium complexes are discussed in this chapter, while the osmium(II) complexes are discussed in Chapter 4 of this thesis. These complexes take the form $[M(bpy)_2(LL_x)](PF_6)_2$ (where M = Ru or Os and LL_x is one of ligands detailed below). The structures of the ligands are detailed in Figure 3.1.

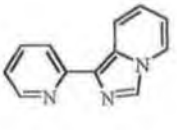

LL1 = 2-pyridyl imidazo[1,5-a] pyridine

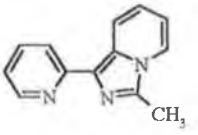

LL2 = methyl (2-pyridyl imidazo[1,5-a] pyridine)

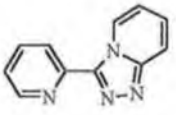

LL3 = 2-pyridyl triazo[1,5-a] pyridine

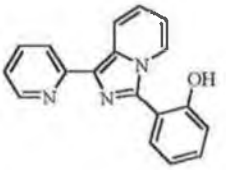

LL4 = 2-phenol-(2-pyridyl imidazo[1,5-a] pyridine)

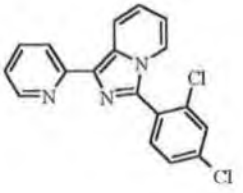

LL5 = 2,4 dichlorophenyl-(2-pyridyl imidazo[1,5-a] pyridine)

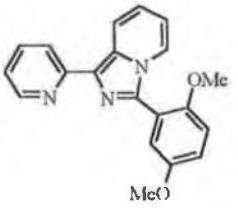

LL6 = 2,5-dimethoxyphenyl-(2-pyridyl imidazo[1,5-a] pyridine)

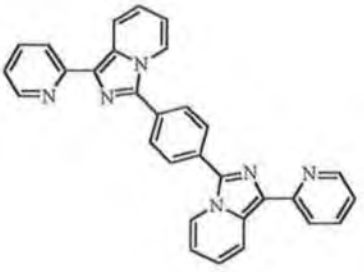

LL7 = 1,4-phenylene-bis-(2-pyridyl imidazo[1,5-a] pyridine)

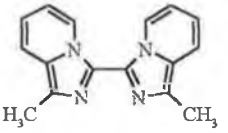

LL8 = bis-2-pyridyl imidazo[1,5-a]

Figure 3.1 Ligands used to synthesise the complexes discussed in Chapters 3,4 and 5.

With the exception of the LL1 ligand which was reported in 1992 by Grigg *et al.* [1] none of the other ligands, and no attempt to synthesise either the ruthenium(II) or osmium(II) complexes containing these ligands has been reported previously. The ligands consist of a pyridine ring fused to a 5 membered imidazo (or triazo, LL3) type ring system. This conjugated, fused 5 and 6 membered ring system is bound to a second pyridine ring, and the free nitrogens on this pyridine ring, and the free nitrogen on the imidazo/triazo ring provide the opportunity for bidentate binding of metallic species. The uniqueness of these ligands is provided by the extended conjugated π-system afforded by the fused 5 and 6 membered rings.

Before the properties of the $[Ru(bpy)_2(LL_x)](PF_6)_2$ complexes are introduced, it is important to examine the properties of ruthenium and osmium complexes whose results are expected to be comparable to those reported here. Examination of these results will greatly ease the characterisation of the new complexes being introduced in this chapter and Chapters 4 and 5. What follows in this section details some of the relevant work carried out in this area.

The ligands with which comparisons will be drawn are represented in Figure 3.2.

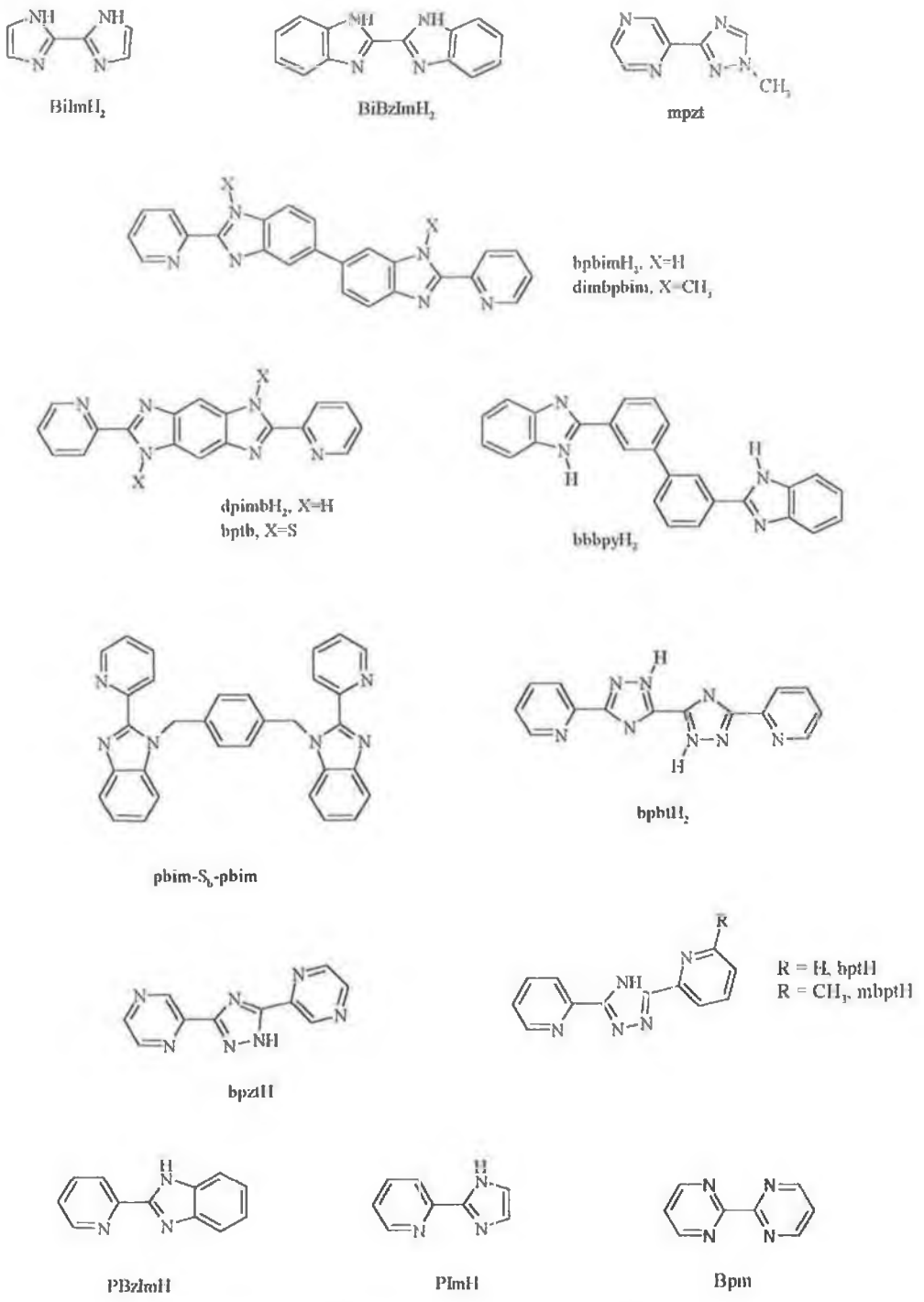

Figure 3.2 Ligands with which comparisons can be made.

The abbreviations used in Figure 3.2 are expanded upon in Table 3.1.

Abbreviation	Full Name	Abbreviation	Full Name
$biImH_2$	Protonated 2,2'-biimidazole	btpb	2,6-bis(2'-pyridyl)-2,2':6,2''-thiazolo[4,5-d]benzothiazole
$bibzImH_2$	Protonated 2,2'-bibenzimidazole	$bbbpyH_2$	2,2'-bis(2-benzimidazolyl)-4,4'-bipyridine
Mpzt	1-methyl-3-(pyrazine-2-yl)-1,2,4-triazole	PBim-SB-pBim	
$bpbimH_2$	2,2'-bis(2-pyridyl)bibenzimidazole	$bpbtH_2$	5,5'-bis(2-pyridyl)-3,3'-bi(1,2,4-triazole)
dimbpbim	1,1'-dimethyl-2,2'-bis(2-pyridyl)-6,6'-bibenzimidazole	BpztH	Protonated 3,5-bis(pyrazine-2-yl)-1,2,4-triazole
$dpimbH_2$	2,6-bis(2'-pyridyl)benzimidazole	bptH	Protonated 3,5-bis(pyridine-2-yl)-1,2,4-triazole
Bpm	2,2'-Bipyrimidine	mbptH	3-(6-methyl-2-pyridyl)-5-(2-pyridyl)-1,2,4-triazole)
PBzImH	2-(2-pyridyl)benzimidazole	PimH	2-(2-pyridyl)imidazole

Table 3.1 Explanation of the abbreviations used to label the ligands in Figure 3.2.

Complexes of the ligands $BiImH_2$ and $BiBzImH_2$ have been studied by Haga *et al* since the early 1980s. [2,3,6,7] These ligands were used for their coordinating ability toward

transition metal ions as three possible species: neutral molecule (A), monoanion (B), or dianion (C) (Figure 3.3).

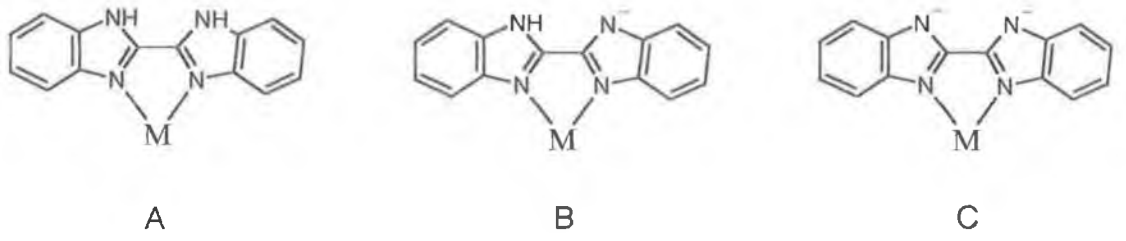

Figure 3.3 Representation of the three different protonation states possible with the $BiBzIm^{2-}$ ligand.

The dianion ($BiBzIm^{2-}$ or $BiIm^{2-}$) ligands can also function as a bridging ligand between two metal ions to form binuclear compounds, which had been done before as in the case of $[(\eta^5\text{-}C_5H_5)_2Ti]_2(BiBzIm)$ [4] and $[Cu_2(Me_5dien)_2(BiBzIm)](BPh_4)_2$. [5] Of more interest however is the complex $[Ru(bpy)_2(biBzImH_2)](ClO_4)_2$ [6]. The electronic absorption spectrum of this complex contains an absorption band at around 460nm which has been assigned to a ruthenium to ligand π* charge transfer. As the pH is increased however the transition is shifted to lower energy with isosbestic points at 487nm and 513nm. This confirms the presence of the two protonation states in Figure 3.3 and the complex (A) undergoes two successive deprotonations. Electrochemistry of the monomer shows a reversible Ru(II)/Ru(III) couple with $E_{1/2}$= +1.11 V (vs SCE and ΔE_p = 70 mV). The dimeric species $[(bpy)_2Ru(BiBzIm)Ru(bpy)_2](ClO_4)_2$ exhibits two pairs of anodic and cathodic waves at $E_{1/2}$ = +0.74 and +1.04V (vs SCE), both of which are quasi-reversible. (ΔE_p=95mV)

Following on from the ruthenium benzimidazole complexes, further similar ligands were synthesised and the ruthenium complexes made.[7] These complexes are of the form $[Ru(bpy)_2(LL)]^{n+}$ where LL = PbzImH and PimH. From the spectral and electrochemical measurements made on these complexes, the metal to ligand charge transfer bands and

the oxidation potentials were rationalised based on the σ-donor properties of the LL ligand which was found to increase in the order bpy < PbzImH < PimH < $BiBzImH_2$ < $BiImH_2$. The deprotonated forms of the ligands have a stronger π-donor property than the protonated forms. It was also found that the emission lifetime decreases with increasing number of imidazole groups, which was suggested to provide a rapid deactivation pathway to the excited state.

The electronic spectra of the ruthenium complexes all contain low energy bands at 460~470 nm which may be assigned to ^{1}MLCT transitions and the two bands with maxima at 290 and 240 nm to bipyridine intraligand $\pi \rightarrow \pi^*$ transitions. The ^{1}MLCT transition energies of $[Ru(bpy)_2(LL)](ClO_4)_n$ (n = 1 or 2) decrease in the order of LL = bpy > PbzImH > PimH > $BiBzImH_2$ > $BiImH_2$.

Comparison of the pK_a values of the PImH and PbzImH complexes (7.9 and 6.8) with those of the free ligands (13.4 and 12 respectively [8]) indicates that the acidity of the ligands increase upon complexation to the metal ion. The pKa values of the complexes of the benzimidazole derivatives are smaller than those of the imidazole derivatives which is due to the electron withdrawing effect of the benzene ring of the benzimidazole.

It is clear that one of the most important features of the chemistry of complexes of these ligands is their acid-base chemistry. This is not relevant for comparison with the ligands used in Chapters 3, 4 and 5 and therefore much of the acid-base chemistry of these systems will be ignored in this introduction and concentration will be focussed on the protonated monomeric species and on the dimers of these ligands as these most closely represent the compounds which will be discussed in the following chapters.

The electrochemical data for these complexes are given in Table 3.2.

Ligand (LL)	$E_{1/2}$, V *vs* SCE	
	Oxidation	Reductions
PBzImH	+1.17	-1.49, -1.76
PImH	+1.14	-1.52, -1.78
$BiBzImH_2$	+1.12	-1.60, -1.90
$BiImH_2$	+1.04	-1.66, -1.96

Table 3.2 Electrochemical Data for the protonated $[Ru(bpy)_2(LL)](ClO_4)_2$ complexes.

Again the increasing donor property of the ligands is represented by the $Ru^{(II)} \rightarrow Ru^{(III)}$ oxidation potentials which move cathodically in the order $BiImH_2$ > $BiBzImH_2$ > PimH > PbzImH > bpy. The two reduction waves, both of which are reversible, are due to stepwise one electron reductions at the bpy ligands.

The preparation, spectroscopic and electrochemical properties of 2,2-bibenzimidazolate-($BiBzIm^-$) bridged binuclear complexes of the formula $[(bpy)_2M(BiBzIm)M'(bpy)_2]^{n+}$ (M = Ru, Os; M' = Ru, Os, Co, Ni) were reported in 1987.[9] The $Os^{(II)}$-$Os^{(III)}$ mixed valence complex shows multiple intervalence transfer (IT) absorption bands in the near infra-red region. The $Ru^{(II)}$-$Ru^{(III)}$ and $Ru^{(II)}$-$Os^{(III)}$ mixed valence complexes also exhibit IT bands. The UV-visible absorption spectral data contain the expected π-π^*(bpy) transitions at circa 245 and 290 nm. The BiBzIm ligand contributes its own π-π^* transitions to the absorption spectra of the complexes, at 318 and 355 nm, and 362 nm for the homonuclear Ru-Ru and Os-Os complexes respectively. The heteronuclear Ru-Os dimer has π-π^*(BiBzIm) transitions at 357 nm. The λ_{max} of the MLCT bands for the Ru-Ru complex is 505 nm, for Ru-Os it is 501 nm, 683 nm and 740 nm, while the Os-Os complex contains absorption bands associated with the dπ-π^*(bpy) transitions at 518 nm. The additional absorption bands in the osmium dinuclear complexes, observed between 670-740 nm, have been assigned to a triplet dπ-π^*(bpy) MLCT transition.

For the homobinuclear Ru-Ru and Os-Os complexes, two successive reversible electrode oxidation couples are observed, each corresponding to a one electron process. The heterobinuclear Ru-Os complex also shows two reversible couples. The first being assigned to a $Os^{(II)}$-$Os^{(III)}$ couple and the second a $Ru^{(II)}$-$Ru^{(III)}$ couple.

If the oxidation potentials are compared to those of the analogous mononuclear compounds, it is found that the first oxidation potential of the binuclear complexes is 0.3V lower than those of the mononuclear analogues. This indicates that the bridging ligand, i.e. BiBzIm, has a greater electron donating ability in the binuclear complexes. This compares to the results found for the binuclear compound $[(bpy)_2Ru(bpm)Ru(bpy)_2]^{4+}$ which has an oxidation potential of 0.2V higher than for its analogous monomer. Bpm (see Figure 3.2) has been shown to act a good π-acceptor. The electrochemical data for the complexes are given in Table 3.3.

M-M'	**$E_{1/2}$, V *vs* SCE (ΔE_p, mV)**	
	$Ru^{(II)}$-$Ru^{(III)}$	**$Os^{(II)}$-$Os^{(III)}$**
Ru-Ru	+0.77 (61), +1.06 (63)	-
Ru-Os	+1.01 (64)	+0.39 (66)
Os-Os	-	+0.40 (68), +0.58 (65)
Ru	+1.12 (70)	-
Os	-	+0.66 (63)

Table 3.3 Oxidative electrochemical data for the binuclear and mononuclear complexes $[(bpy)_2M(BiBzIm)M'(bpy)_2](ClO_4)_2$ and for $[M(bpy)_2(BiBzImH_2)](ClO_4)_2$ in MeCN (0.1M TBAP) at a platinum electrode. [9]

Further work was carried out on the monomeric $BiImH_2$ and $BiBzImH_2$ ruthenium complexes by Rillema and co-workers.[10] $[(Ru(bpy)_2)_2BiIm]^{2+}$ and the series $[Ru(bpy)_n(BiImH_2)_{3-n}]^{2+}$, $[Ru(bpy)_n(BiBzImH_2)_{3-n}]^{2+}$ and $[Ru(bpy)_n(BiBzIm)Ru(bpy)_2)_{3-n}]^{2+}$, where n = 0-2 were synthesised and examined. It was found that the redox potential for the first $Ru^{(II)}$-$Ru^{(III)}$ couple shifted negatively from +1.26 V *vs* SSCE to –0.26 V as

bpy ligands were replaced by $BiImH_2$, $BiBzImH_2$ and "$BiBzImRu(bpy)_2$" ligands. Reduction waves were found in the –1.5 to -1.6 V region for complexes containing a bpy ligand, but none were observed out to –2 V for $[Ru(BiImH_2)_3]^{2+}$ or $[Ru(BiBzImH_2)_3]^{2+}$.

Complex	**$d\pi\rightarrow\pi_1^*$ (nm)**	**$d\pi\rightarrow\pi_2^*$ (nm)**	**$\pi\rightarrow\pi^*$BiBzIm (nm)**	**$\pi\rightarrow\pi^*$ (nm)**
$[Ru(bpy)_2(BiBzImH_2)]^{2+}$	463	-	350	291
	483	-	332	243
$[Ru(bpy)(BiBzImH_2)_2]^{2+}$	465	-	350	292
	-	-	332	245
$[Ru(BiBzImH_2)_3]^{2+}$	483	-	351	242
	-	-	333	-
$[Ru(bpy)_2(BiImH_2)]^{2+}$	473	340	-	289
	432	-	-	242
$[Ru(bpy)(BiImH_2)_2]^{2+}$	487	366	-	294
	-	-	-	287
	-	-	-	248
$[Ru(BiImH_2)_3]^{2+}$	401	-	-	297
	-	-	-	285
	-	-	-	276
$BiBzImH_2$	-	-	-	309
$BiImH_2$	-	-	-	276

Table 3.4 Visible-UV Spectral Data for the Ruthenium(II) Bibenzimidazole and Biimidazole complexes and free ligands in MeCN. [10]

The spectral changes associated with the $[Ru(bpy)_n(BiBzImH_2)_{3-n}]^{2+}$ series should be examined more closely. The low energy bands are related to $d\pi\rightarrow\pi^*$ transitions and are found to red shift as bpy is replaced by $BiBzImH_2$. For $[Ru(BiImH_2)_3]^{2+}$ the absorption at 483 nm can be assigned as a $d\pi\rightarrow\pi^*(BiBzImH_2)$ transition. However for the compounds $[Ru(bpy)_2(BiBzImH_2)]^{2+}$ and $[Ru(bpy)(BiBzImH_2)_2]^{2+}$ the low energy

maxima are more likely to be $d\pi \rightarrow \pi^*$(bpy) due to the fact that coordinated bpy is reduced electrochemically preferentially with respect to coordinated $BiBzImH_2$. The substantial red shift (circa 20 nm) of the low energy MLCT absorption maxima of $[Ru(BiBzImH_2)_3]^{2+}$ in comparison to $[Ru(bpy)_2(BiBzImH_2)]^{2+}$ and $[Ru(bpy)(BiBzImH_2)_2]^{2+}$ could be explained by loss of the $d\pi \rightarrow \pi^*$(bpy) component or by increased steric crowding around the ruthenium centre.

The complexes are weak emitters with the tris chelates $[Ru(BiImH_2)_3]^{2+}$ and $[Ru(BiBzImH_2)_3]^{2+}$ having no emission at both room temperature and 77K. This rules out direct involvement of the $BiImH_2$ or $BiBzImH_2$ ligands in the emission decay of the mixed-ligand complexes. Therefore, absorption of light most likely populates the ^{3}MLCT state associated with one of the bipyridine ligands and emission is observed from this level.

Complex	**Oxidation (V)**	**Reduction (V)**	
	$E_{1/2}(1)$	$E_{1/2}(1)$	$E_{1/2}(2)$
$[Ru(bpy)_2(BiBzImH_2)]^{2+}$	1.04	-1.66	-1.96
$[Ru(bpy)(BiBzImH_2)_2]^{2+}$	0.80	-1.61	
$[Ru(BiBzImH_2)_3]^{2+}$	0.54		
$[Ru(bpy)_2(BiImH_2)]^{2+}$	1.12	-1.60	-1.90
$[Ru(bpy)(BiImH_2)_2]^{2+}$	0.91	-1.48	
$[Ru(BiImH_2)_3]^{2+}$	0.80		

Table 3.5 Cyclic Voltammetry data for the ruthenium Biimidazole and Bibenzimidazole Complexes in MeCN (0.1M TEAP or TBAH). Potentials are in V vs SSCE. [10]

The $E_{1/2}(1)$ values for these monometallic species follow the sequence $[Ru(BLH_2)(bpy)_2]^{2+} > [Ru(BLH_2)_2(bpy)]^{2+} > [Ru(BLH_2)_3]^{2+}$, where BLH_2 is either $BiImH_2$ or $BiBzImH_2$. Also the $E_{1/2}(1)$ values for analogous $BiBzImH_2$ based complexes are more positive than $BiImH_2$ based complexes which indicates that $BiImH_2$ is a

stronger σ donor than $BiBzImH_2$. The systematic negative shift as bpy is replaced by BLH_2 results from an increase in the electron density on the ruthenium metal centre.[11]

Since the early 1990's focus has shifted from the biimidazole and bibenzimidazole ligands. Haga *et al.* were again at the forefront of this work. The ligand $bpbzimH_2$ is an example of this.[12,13] Comparison of the structure of the $bpbzimH_2$ ligand (Figure 3.2) with the LL7 ligand shows the similarities of the two bridging ligands. One of the more interesting features is the fused five membered imidazo moiety with a six membered ring. The structures of the $bpbzimH_2$ and LL7 ligands can be seen in Figure 3.4.

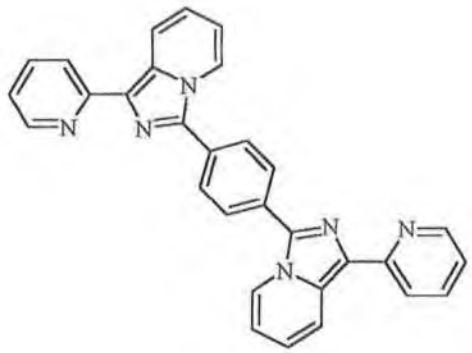

LL7 = 1,4-phenylene-bis-(2-pyridyl imidazo[1,5-a] pyridine)

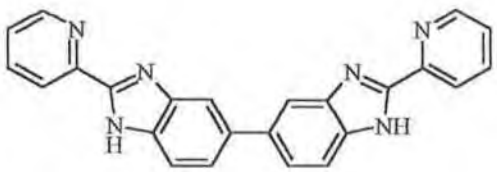

$BPBzImH_2$

Figure 3.4 $BPBzImH_2$ ligand studied by Haga et al. compared to LL7.

The oxidation potentials of the dimeric forms of the homonuclear Ru-Ru and Os-Os bipyridine complexes have been reported.[12] For $[Ru(bpy)_2(BPBzImH_2)Ru(bpy)_2]^{4+}$ this was found to be 0.94V *vs* Ag/AgCl, whereas for the $[Os(bpy)_2(BPBzImH_2)Os(bpy)_2]^{4+}$ this oxidation potential is lowered at 0.53V *vs* Ag/AgCl. What is interesting to note is

that for the diprotonated complexes, there is only one oxidation potential reported, which would indicate that the coupling between the metal centres could be described as weak. This is confirmed by the spectroelectrochemisty results which indicate the presence of a very weak, broad Intervalence Transfer band for the mixed valence $Ru^{(II)}$-$Ru^{(III)}$ complex. This IT band appears at 7300 cm^{-1}, on the edge of an LMCT transition which is centered at 14,400 cm^{-1}. The assignment of the IT band was confirmed by its disappearance on fully oxidising the complex. The mixed valence osmium complex $Os^{(II)}$-$Os^{(III)}$ also has a very weak IT band at 9100 cm^{-1} as well as the $d\pi$-$d\pi$ and LMCT transitions.

Until this point, dinuclear complexes with σ/π donor bridging ligands were relatively sparse.[14,15,16] The ligand above with its benzimidazole groups, has a σ/π donor property. Once the benzimidazole unit is coordinated to the metal ion, the imino N-H proton becomes more acidic and is easier to remove. The metal-metal interaction can be controlled by proton transfer on the bridging ligand. The degree of metal-metal interaction of the deprotonated dinuclear complexes becomes 4-6 times larger than that of the protonated species. This can be explained in several ways – the total charge is decreased from +4 to +2 and thus electrostatic repulsions between metal ions decreases. In addition electrostatic attraction between cationic metal and anionic bridging ligand may arise.

Another compound investigated was the bridging tetradentate ligand 2,6-bis(2-pyridyl)benzoimidazole, ($dpimbH_2$) (see Figure 3.5), which was found to have strong σ-donor properties in comparision to bpy.[17,18] The extent of electronic exchange interaction had seldom been determined for metal to ligand CT excited states in binuclear compounds before this. Emission energy shifts of binuclear compounds compared with the corresponding mononuclear compounds do not necessarily indicate the extent of electronic interaction between ruthenium ions bridged by 2,3-bis(2-pyridyl)pyrazine [19] or 2,2'-bipyrimidine [20], as a positive charge on the remote ruthenium ion shifts the reduction potential of the bridging ligand to less negative values which in turn lowers the energy of the metal to ligand CT emission. In the case of the compound

$[(Ru(bpy)_2)_2(dbimbH_2)]^{4+}$ it was found that chromophore-chromophore interaction in the CT state allowed delocalisation of the excited state through the whole binuclear compound. The rate of the CT exchange depends on the extent of electronic exchange interaction between the excited $Ru^{(III)}$ site and the unexcited $Ru^{(II)}$ site, as the $Ru^{(III)}$-$Ru^{(II)}$ interaction is small compared to intraligand interaction.

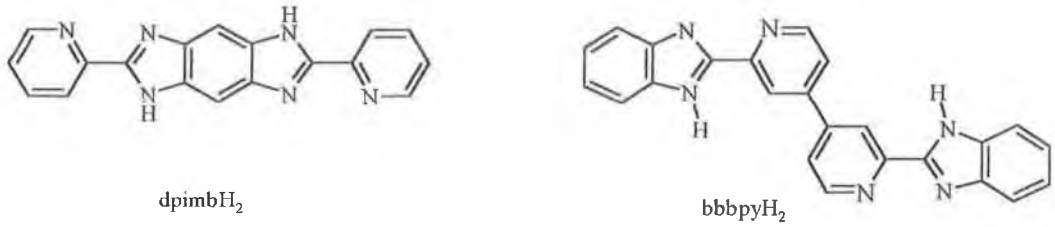

dpimbH$_2$ bbbpyH$_2$

Figure 3.5 Schematic of the ligands being discussed in this section.

The ligand $bbbpyH_2$ (2,2'-bis(2-pyridyl)-6,6'-bibenzimidazole) was prepared. [21] (Figure 3.5) As with many similar systems, it was found that its complexes exhibited proton induced switching of metal-metal interaction by proton transfer in the bridging $bbbpyH_2$ ligand.

The absorption spectra of the mononuclear complex $[Ru(bpy)_2(bbbpyH_2)](ClO_4)_2$ consists of three well resolved bands. The band at 459 nm is assigned to the $Ru^{(II)}$-bpy and $bbbpyH_2$ metal to ligand charge transfer transitions from comparison with the spectra of $[Ru(bpy)_3](ClO_4)_2$ and $[Ru(bpy)_2(BiBzImH_2)](ClO_4)_2$. The MLCT band occurs at almost the same wavelength as that of $[Ru(bpy)_3](ClO_4)_2$. Since free $bbbpyH_2$ has a $\pi\rightarrow\pi^*$ intraligand transition at 337 nm (in MeCN) the band at 346 nm can be assigned as a $\pi\rightarrow\pi^*(bbbpyH_2)$ intraligand transition. The lowering of this transition in comparison to $bibzImH_2$ reflects the destabilisation of the π orbital and the stabilisation of the π^* orbital based in the interaction of the two $BiBzImH_2$ chromophores. The higher band at 289 nm is assigned as a $\pi\rightarrow\pi^*$(bpy) intraligand transition. The corresponding osmium complex has an additional absorption band at 606 nm which can be assigned to a $d\pi\rightarrow\pi^*$ triplet transition.

On coordination of a second Ru or Os metal centre to the monomeric complex, the MLCT at 406 nm remains almost unaltered except that it becomes twice as intense compared to the mononuclear compounds. For π-accepting bridging ligands a shift to longer wavelength is expected on coordination of a second metal.[22] In this case the energy of the π* orbital of the bridging ligand is slightly lower than that of bpy and the energy of the MLCT band is almost unaltered on going from the mono to the dinuclear compound.

Work has continued with these types of ligands with benzimidazolate bridging ligands. Recently Khalil et al. has coordinated the 2-(2'-pyridyl)benzimidazole ligand with $Ru_3(CO)_{12}$ and $Os_3(CO)_{12}$. [23] The intervalence transfer properties of the binuclear ruthenium complexes containing benzotriazolate or benzimidazolate bridging ligands are being examined and reported by Rocha *et al.* [24,25] More recently again, benzimidazoles are being used to model important bioinorganic systems. Benzimidazole complexes have been evaluated for antifungal activity and as antitumour agents.[26,27,28]

The majority of the ligands used in Chapters 3 and 4 are based on 2-pyridyl and imidazo type structures. The ligand LL3 however is based on a 2-pyridyl and a triazo type system. In order to allow the photophysical and electrochemical results found for the ruthenium and osmium complexes of LL3 examination of some ruthenium and osmium triazole compounds are examined next.

Another type of ligand whose properties are of relevance are the triazole and pyridyl triazole series. The first report of 1,2,4-triazole ligands and their ruthenium complexes was by Vos and co-workers in 1983. [29] It was noted in these reports that the triazoles possess weak π-acceptor properties in comparison to bpy. The triazole contains two different coordination sites, which gives rise to the possibility of coordination isomers. It has been found that these isomers are easily separated by chromatographic techniques or by fractional crystallisation.[30,31,32] The coordination isomers possess different photophysical and electrochemical properties. Examination of the diagram below indicates why those differences may arise.

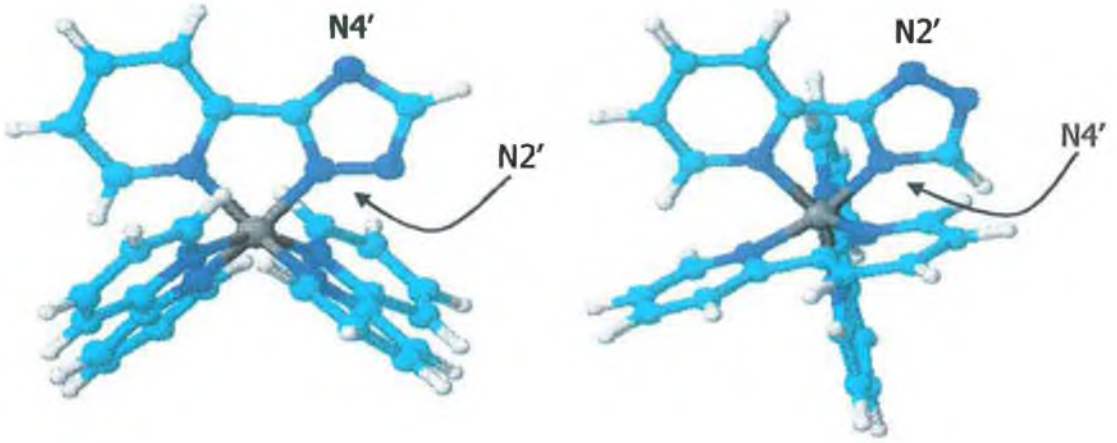

Figure 3.6 N2' and N4' bound coordination isomers of $[Ru(bpy)_2(ptr)]^+$

The ruthenium may bind via the N2' or the N4' of the triazole. The N4' site is known to be a stronger σ-donor than the N2' site. This is noticeable in the pK_a for the protonation of the free nitrogen in the complex, where the pK_a for the N4' bound complex is higher than that of the N2' bound complex. [33] The complexes of pyridyl triazoles show interesting acid-base chemistry also. The properties of the complexes are pH sensitive. [34] Normally the triazole is deprotonated when coordinated to the metal centre, which means a negatively charged ligand. This is easily protonated in acidic media, and protonation results in significant changes in the photophysical and electrochemical properties of the complexes. The changes are caused by the loss of some of its σ-donor ability due to the fact that protonation removes the negative charge from the ligand. This results in a considerable loss of emission intensity and the MLCT of the complex is shifted to lower energy on protonation.

One of the most studied triazolate type bridging ligands is 3,5-bis(pyridin-2-yl)-1,2,4-triazole (Hbpt) (Figure 3.2). The photophysical and electrochemical properties of the ruthenium and osmium compounds containing this ligand have been reported since the late 1980s [35,36,37,38,39] and are summarised in the Tables 3.6-8.

Compound	Absorption 298K (a)	Emission (b)				
		77K		298K		
	λ_{max}(nm)	λ_{max}(nm)	τ, μs	λ_{max}(nm)	τ, μs (c)	τ, μs (d)
$[Ru(bpy)_3]^{2+}$	452	582	4.8	615	0.80	0.17
$[Ru(bpy)_2(bpt)]^{+}$	480	628	2.8	678	0.16	0.07
$[(Ru(bpy)_2)_2(bpt)^{3+}$	453	608	3.6	648	0.10	0.056

(a) MeCN solution. (b) Butyronitrile solution. (c) deaerated solution (d) aerated solution.

Table 3.6 Absorption and Luminescence Properties of the ruthenium bpt⁻ compounds.

Replacement of a bpy ligand of $[Ru(bpy)_3]^{2+}$ by bpt^- to give $[Ru(bpy)_2(bpt)]^+$ causes an increase in the electronic charge of the metal, with a consequent red shift of the metal to ligand charge transfer absorption. Coordination of a second $Ru(bpy)_2^{2+}$ unit to the bpt-bridging ligand implies the sharing of its negative charge between the two $[Ru(bpy)_2]^{2+}$ units with a decrease of the electronic charge on the $Ru^{(II)}$ ions and a consequent blue shift of the Ru→bpy CT levels. This behaviour has already been discussed in the section on imidazole type ligands.

It was also mentioned earlier that the σ-donor ability on the N2' position is stronger than that on the N4' position. On these grounds, for the binuclear species, the lowest energy luminescent ^{3}MLCT state (which is Ru→bpy in origin) is expected to be centred on the Ru-containing unit attached to the N2' position.

Compound	Absorption 298K (a)	Emission (b)			
		90K		298K	
	λ_{max}(nm)	λ_{max}(nm)	τ, ns	λ_{max}(nm)	τ, ns (c)
$[Os(bpy)_3]^{2+}$	479	712	940	725	62
$[Os(bpy)_2(bpt)]^{+}$	486	750	250	762	55
$[(Os(bpy)_2)_2(bpt)^{3+}$	475	765	340	762	33
$[(bpy)_2Ru(bpt)Os(bpy)_2]^{3+}$	459	741	670	756	30
$[(bpy)_2Os(bpt)Ru(bpy)_2]^{3+}$	453	744	590	762	25

(a) MeCN solution. (b) Butyronitrile solution. (c) Deaerated solution.

Table 3.7 Absorption and luminesence properties of the osmium bpt and mixed metal bpt compounds.

Replacement of a bpy ligand of $[Os(bpy)_3]^{2+}$ by bpt^- to give $[Os(bpy)_2(bpt)]^{+}$ causes small red shifts in the metal to ligand (Os→bpy) charge transfer absorption and emission bands.[40,41] Coordination of a second $Os(bpy)_2$ unit to the bpt- bridging ligand implies the sharing of the negative charge between the two $Os(bpy)_2^{2+}$ units with an expected decrease in the electronic density on the metal ions and a consequent blue shift of the Os→bpy CT levels. This however is negligible which contrasts with the analogous ruthenium complexes. This could be due to a compensation effect for osmium due to the more covalent character of the M-bpy bond. The case for the binuclear complex is the same as that of the ruthenium complex with the σ-donor ability on the N2' position being stronger than that on the N4' position which leads to the lowest energy luminescent ^{3}MLCT state (which is Os→bpy in origin) being centred on the Os-containing unit attached to the N2' position.

$[(bpy)_2Ru(bpt)Os(bpy)_2]^{3+}$ and $[(bpy)_2Os(bpt)Ru(bpy)_2]^{3+}$ have intense absorption bands between 350-500nm which have been assigned as ^{1}MLCT bands. At lower energies the additional bands visible have been attributed to forbidden transitions to the triplet state and are due to the increased spin orbit coupling caused by the osmium.

Compound	Oxidation Potential			Reduction Potential		
$[Os(bpy)_2bpt]^-$	0.49	-	-	-1.41	-1.69	-2.22
$[Ru(bpy)_2bpt]^-$	0.85	-	-	-1.47	-1.72	-2.28
$[(Os(bpy)_2)_2bpt]^-$	0.64	0.85	0.21	-1.34	-1.57	-2.23
$[(Os(bpy)_2)_2bpt]^-$	1.04	1.34	0.30	-1.40	-1.62	-1.67
$[(bpy)_2Ru(bpt)Os(bpy)_2]^{3+}$	0.73	1.20	0.47	-1.33	-1.41	-1.59
$[(bpy)_2Os(bpt)Ru(bpy)_2]^{3+}$	0.65	1.30	0.65	-1.36	-1.63	-2.17

Table 3.8 Electrochemical data for the various complexes containing bispyridyltriazole. All compounds measured in MeCN with 0.1M NBu_4PF_6. Potentials in V vs SCE.

As expected the oxidation potentials of the osmium complexes were approx. 0.4 V lower than for the analogous ruthenium complexes.[42,43,44,45] The difference in oxidation potential of the mixed metal complexes Ru-Os and Os-Ru gives information on the influence of the different modes of coordination possible for the bpt- ligand. If both coordination sites were the same the potentials for both Ru-Os and Ru-Os should be the same – they are not however which indicates that the differences in chemical environment is an important consideratory factor when discussing these complexes. The reduction potentials for the dinuclear compounds have similar values. These along with resonance Raman data indicate that the lowest π^* level of these complexes is bpy based rather than based on the bpt^- ligand.

The next section describes the synthesis of the ruthenium(II) bisbipyridyl complexes of the LL_x ligands. These complexes have been structurally characterised by both ^1H NMR and in some cases X-Ray Crystallography. The chapter concludes with an examination of the photophysical, photochemical and electrochemical properties of this series of novel ruthenium(II) complexes.

3.2 Synthesis of the $[Ru(bpy)_2(LL_x)]^{2+}$ complexes

The previous section has dealt with the properties, both photophysical and electrochemical of ruthenium and osmium complexes which are expected to have some similar properties to those exhibited by the $[M(bpy)_2(LL_x)]^{2+}$ complexes. It has been found that while the LL_x ligands behave in many ways as expected, they do have several unique characteristics that can not simply be dismissed. It is therefore essential to investigate the properties of the free ligands.

The next sections of this chapter details the synthesis of the ruthenium(II) complexes and a full characterisation of these complexes. In order to characterise the ruthenium complexes properly, the properties of the free ligands are introduced and discussed also, which simplifies the characterisation of the complexes formed using the LL_x ligands.

Synthesis of *cis*-$[Ru(bpy)_2Cl_2].2H_2O$

This procedure has been modified slightly to that described by Meyer *et al.* [46] A suspension containing $RuCl_3.3H_2O$ (3.90 g, $1.5x10^{-2}$ mol), 2,2' bipyridine (4.68 g, $3x10^{-2}$ mol) and LiCl (4.30 g, 0.10 mol) was refluxed in dimethylformamide (25 cm^3). After 8 hours the mixture was allowed to cool to room temperature and 125 cm^3 of acetone was added. This was left at 0^0C for 24 hours. The resulting violet precipitate was filtered and the isolated solid washed with water until the filtrate was no longer coloured. The solid was washed with diethylether and dried to yield 4.40 g of a microcrystalline solid. (57% yield).

Synthesis of $[Ru(bpy)_2(LL1)](PF_6)_2$

The LL1 ligand (100 mg, $5.1x10^{-4}$ mol) and $[Ru(bpy)_2Cl_2].2H_2O$ (250 mg, $4.8x10^{-4}$ mol) were placed in 10 cm^3 of a 1:1 $EtOH/H_2O$ mixture. This suspension was heated at reflux for 3 hours and after this time the EtOH removed in vacuo. The solution was filtered to remove any excess unreacted ligand. 10 cm^3 of a saturated aqueous solution of

ammonium hexafluorophosphate was added to the filtrate to precipitate an orange/brown product. This product was isolated by filtration, washed with water and dried with diethylether. The compound was purified by column chromatography (stationary phase silica gel, mobile phase 80% acetonitrile, 20% water, 0.05M KNO_3 buffer). The second band to elute yielded the desired product. The acetonitrile was removed in vacuo and an aqueous solution of NH_4PF_6 added to reprecipitate the pure product product which was filtered, washed with cold water and diethyl ether and allowed to dry to yield 315mg. (73%)

^{1}H NMR (400 MHz, d_6-acetone) δ = 7.09 (dd, 1H), 7.26 (dd, 1H), 7.45 (dd, 1H), 7.58 (m,4H), 7.81 (d, 1H), 8.05 (dd, 1H), 8.2 (m, 8H), 8.41 (m, 2H), 8.45 (m, 2H), 8.79 (m, 4H). Total = 25 aromatic protons.

Elemental Analysis for $C_{32}H_{25}N_7RuP_2F_{12}$: Calculated C 42.71, H 2.80, N 10.90. Found C 42.59, H 2.83, N 11.20 %.

Synthesis of $[Ru(d_8\text{-bpy})_2(LL1)](PF_6)_2.5H_20$

LL1 (51 mg, $2.6x10^{-4}$ mol) and $[Ru(bpy)_2Cl_2].2H_2O$ (137 mg, $2.6x10^{-4}$ mol) were placed in 10 cm^3 of a 1:1 EtOH/H_2O mixture. This suspension was heated at reflux for 4 hours and after this time the EtOH removed *in vacuo*. The solution was filtered to remove any excess unreacted ligand. 10 cm^3 of a saturated aqueous solution of ammonium hexafluorophosphate was added to the filtrate to precipitate an orange/brown product. This product was isolated by filtration, washed with water and dried with diethylether. The compound was purified by column chromatography (stationary phase silica gel, mobile phase 80% acetonitrile, 20% water, 0.05M KNO_3 buffer). The second band to elute yielded the desired product. The acetonitrile was removed in vacuo and an aqueous solution of NH_4PF_6 added to reprecipitate the pure product which was filtered and washed with water and diethyl ether and allowed to dry yielding 195 mg. (82%)

^{1}H NMR (400 MHz, d_6-acetone) δ = 6.99 (dd, 1H), 7.12 (dd, 1H), 7.38 (dd, 1H), 7.56 (d, 1H), 7.90 (s, 1H), 7.94 (dd, 1H), 8.14 (m, 2H), 8.20 (d, 1H). Total = 9 aromatic protons.

Elemental Analysis for $C_{32}H_{19}N_7D_{16}RuO_5P_2F_{12}$: Calculated C 38.25, H 2.99, N 9.76. Found C 37.96, H 2.49, N 9.99 %.

Synthesis of $[Ru(bpy)_2(LL2)](PF_6)_2.2H_2O$

The LL2 ligand (100 mg, $4.8x10^{-4}$ mol) and $[Ru(bpy)_2Cl_2].2H_2O$ (225 mg, $4.3x10^{-4}$ mol) were placed in 10 cm^3 of a 1:1 $EtOH/H_2O$ mixture. This suspension was heated at reflux for 3 hours and after this time the EtOH removed in vacuo. The solution was filtered to remove any excess unreacted ligand. 10 cm^3 of a saturated aqueous solution of ammonium hexafluorophosphate was added to the filtrate to precipitate an orange/brown product. This product was isolated by filtration, washed with water and dried with diethylether. The compound was purified by column chromatography (stationary phase silica gel, mobile phase 80% acetonitrile, 20% water, 0.05M KNO_3 buffer). The second band to elute yielded the desired product. The acetonitrile was removed in vacuo and an aqueous solution of NH_4PF_6 added to reprecipitate the pure product which was filtered and washed with cold water and diethyl ether and allowed to dry. Yield 325mg (74% yield).

^1H NMR (400 MHz, d_6-acetone) δ = 1.88 (s, 3H), 7.25 (m, 2H), 7.35 (dd, 1H), 7.56 (m, 4H), 7.83 (d, 1H), 7.86 (d, 1H), 8.0 (d, 1H), 8.08 (d, 1H), 8.19 (m, 7H), 8.69 (d, 1H), 8.82 (m, 4H), 9.19 (d, 1H). Total = 24 aromatic protons + 3 aliphatic protons.

Elemental Analysis for $C_{33}H_{35}N_7RuO_2P_2F_{12}$: Calc: C 41.78, H 3.29, N 10.34. Found: C 41.24, H 2.90, N 10.49 %.

Synthesis of $[Ru(bpy)_2(LL3)](PF_6)_2$

The LL3 ligand (100 mg, $5.0x10^{-4}$ mol) and $Ru(bpy)_2Cl_2.2H_2O$ (236 mg, $4.5x10^{-4}$ mol) were placed in 10 cm^3 of a 1:1 $EtOH/H_2O$ mixture. This suspension was heated at reflux for 3 hours and after this time the EtOH removed in vacuo. The solution was filtered at

this stage to remove any excess unreacted ligand. An aqueous solution of ammonium hexafluorophosphate was added to the filtrate to precipitate an orange/brown product. This product was isolated by filtration, washed with water and dried with diethylether. No further purification of the product was necessary. The yield from the reaction was 391 mg. (87%)

^{1}H NMR (400 MHz, d_6-acetone) δ = 7.48 (dd, 2H), 7.58 (m, 4H), 7.79 (dd, 1H), 7.90 (d, 1H), 8.05 (d, 1H), 8.17 (m, 9H), 8.77 (m, 2H), 8.87 (m, 3H), 9.32 (d, 1H). Total = 24 aromatic protons.

Elemental Analysis for $C_{31}H_{25}N_8RuP_2F_{12}$: Calc: C 41.32, H 2.69, N 12.45. Found: C 41.34, H 2.83, N 11.82 %.

Synthesis of $[Ru(bpy)_2(LL4)](PF_6)_2.2H_2O$

The LL4 ligand (100 mg, $3.5x10^{-4}$ mol) and $[Ru(bpy)_2Cl_2].2H_2O$ (165 mg, $3.1x10^{-4}$ mol) were placed in 10 cm^3 of a 1:1 EtOH/H_2O mixture. This suspension was heated at reflux for 3 hours and after this time the EtOH removed in vacuo. The solution was filtered to remove any excess unreacted ligand. Ammonium hexafluorophosphate was added to the filtrate to precipitate an orange/brown product. This product was isolated by filtration, washed with water and dried with diethylether. The compound was purified by column chromatography (stationary phase silica gel, mobile phase 80% acetonitrile, 20% water, 0.05M KNO_3 buffer). The second band to elute yielded the desired product. The acetonitrile was removed in vacuo and an aqueous solution of NH_4PF_6 added to reprecipitate the product which was filtered, washed with water and diethyl ether and allowed to dry yielding 202 mg (66% yield).

^{1}H NMR (400 MHz, d_6-acetone) δ = 6.36 (d, 1H), 6.58 (dd, 1H), 6.66 (dd, 1H), 6.80 (m, 2H), 7.06 (m, 6H), 7.23 (m, 2H), 7.60 (m, 17H), 7.91 (m, 2H), 8.12 (m, 10H), 8.35 (m, 2H), 8.50 (m, 6H), 8.75 (m, 6H), 9.64 (s, 1H), 10.90 (s, 1H). Total = 56 aromatic protons + 2 OH protons.

Elemental Analysis for $C_{38}H_{33}N_7RuO_3P_2F_{12}$: Calc: C 45.16, H 3.29, N 9.70. Found: C 44.74, H 2.83, N 9.55 %.

Synthesis of $[Ru(d_8\text{-bpy})_2(LL4)](PF_6)_2.2H_2O$

The LL4 ligand (100 mg, $3.5x10^{-4}$ mol) and $[Ru(bpy)_2Cl_2].2H_2O$ (165 mg, $3.1x10^{-4}$ mol) were placed in 10 cm^3 of a 1:1 $EtOH/H_2O$ mixture. This suspension was heated at reflux for 3 hours and after this time the EtOH removed in vacuo. The solution was filtered to remove any excess unreacted ligand. Ammonium hexafluorophosphate was added to the filtrate to precipitate an orange/brown product. This product was isolated by filtration, washed with water and dried with diethylether. The compound was purified by column chromatography (stationary phase silica gel, mobile phase 80% acetonitrile, 20% water, 0.05M KNO_3 buffer). The second band to elute yielded the desired product. The acetonitrile was removed in vacuo and an aqueous solution of NH_4PF_6 added to reprecipitate the product which was filtered, washed with water and diethyl ether and allowed to dry. yield 185 mg (53% yield).

^1H NMR (400 MHz, d_6-acetone) δ = 6.40 (d, 1H), 6.55 (dd, 1H), 6.70 (m, 2H), 6.79 (d, 1H), 7.15 (m, 6H), 7.48 (m, 3H), 7.65 (d, 1H), 7.72 (m, 3H), 8.06 (m, 2H), 8.52 (m, 4H), 8.86 (s, 1H), 9.87 (s, 1H). Total = 24 aromatic protons + 2 OH protons.

Elemental Analysis for $C_{38}H_{17}N_7D_{16}O_2P_2F_{12}$. Calculated: C 44.62, H 3.03, N 9.59. Found: C 44.01, H 2.97, N 9.17 %.

Synthesis of $[Ru(bpy)_2(LL5)](PF_6)_2.4H_2O$

The LL5 ligand (100 mg, $2.95x10^{-4}$ mol) and $[Ru(bpy)_2Cl_2].2H_2O$ (140 mg, $2.65x10^{-4}$ mol) were placed in 10 cm^3 of a 1:1 $EtOH/H_2O$ mixture. This suspension was heated at reflux for 3 hours and after this time the EtOH removed in vacuo. The solution was filtered to remove any excess unreacted ligand. Ammonium hexafluorophosphate was added to the filtrate to precipitate an orange/brown product. This product was isolated by

filtration, washed with water and dried with diethylether. The compound was purified by column chromatography (stationary phase silica gel, mobile phase 80% acetonitrile, 20% water, 0.05M KNO_3 buffer). The second band to elute yielded the desired product. The acetonitrile was removed in vacuo and an aqueous solution of NH_4PF_6 added to reprecipitate the pure product which was filtered, washed with water and diethyl ether and allowed to dry. yield 190mg (65% yield).

^{1}H NMR (400 MHz, d_6-acetone) δ = 6.62 (m, 2H), 7.16 (m, 4H), 7.25 (m, 4H), 7.33 (m, 2H), 7.56 (m, 6H), 7.69 (m, 2H), 7.68 (m, 2H), 7.77 (m, 4H), 7.88 (m, 6H), 8.13 (m, 10H), 8.44 (m, 2H), 8.59 (m, 4H), 8.76 (m, 8H). Total = 54 aromatic protons.

Elemental Analysis for $C_{38}H_{35}N_7RuO_4P_2F_{12}Cl_2$: Calc: C 41.19, H 2.80, N 8.85. **Found**: C 40.84, H 2.45, N 9.12 %.

Synthesis of $[Ru(bpy)_2(LL6)](PF_6)_2.2H_2O$

The LL6 ligand (100 mg, $3x10^{-4}$ mol) and $Ru(bpy)_2Cl_2.2H_2O$ (157 mg, $3.1x10^{-4}$ mol) were placed in 50 cm^3 of a 1:1 $EtOH/H_2O$ mixture (high volume used to aid dissolution of the ligand). This suspension was heated at reflux for 6 hours and after this time the EtOH removed in vacuo. The solution was filtered to remove any excess unreacted ligand. Ammonium hexafluorophosphate was added to the filtrate to precipitate an orange/brown product. This product was isolated by filtration, washed with water and dried with diethylether. The compound was purified by column chromatography (stationary phase silica gel, mobile phase 80% acetonitrile, 20% water, 0.05M KNO_3 buffer). The second band to elute yielded the desired product. The acetonitrile was removed in vacuo and an aqueous solution of NH_4PF_6 added to reprecipitate the which was filtered, washed with water and diethyl ether and allowed to dry to yield 238 mg (72% yield).

^{1}H NMR (400 MHz, d_6-acetone) δ = 3.28 (s, 3H), 3.64 (s, 3H), 3.68 (s, 3H), 3.78 (s, 3H), 6.05 (m, 1H), 6.731 (m, 1H), 6.86 (m, 3H), 7.05 (m, 3H), 7.12 (dd, 1H), 7.23 (m,

2H), 7.72 (m, 18H), 8.20 (m, 12H), 8.68 (m, 13H). Total = 54 aromatic protons, 12 aliphatic protons.

Elemental Analysis for $C_{40}H_{37}N_7RuO_4P_2F_{12}$: Calc: C 44.86, H 3.27, N 9.16. Found: C 45.10, H 2.87, N 9.44 %.

Synthesis of $[Ru(bpy)_2(LL8)](PF_6)_2.4H_2O$

The LL8 ligand (100 mg, $3.8x10^{-4}$ mol) and $Ru(bpy)_2Cl_2.2H_2O$ (198 mg, $3.8x10^{-4}$ mol) were placed in 20 cm^3 of a 1:1 $EtOH/H_2O$ mixture. This suspension was heated at reflux for 6 hours and after this time the EtOH removed in vacuo. The solution was filtered to remove any excess unreacted ligand. 10 cm^3 of a saturated aqueous solution of ammonium hexafluorophosphate was added to the filtrate to precipitate an orange/brown product. This product was isolated by filtration, washed with water and dried with diethylether. The compound was purified by column chromatography (stationary phase silica gel, mobile phase 80% acetonitrile, 20% water, 0.05M KNO_3 buffer). The second band to elute yielded the desired product. The acetonitrile was removed in vacuo and an aqueous solution of NH_4PF_6 added to reprecipitate the pure product which was filtered, washed with cold water and diethyl ether and allowed to dry to yield 268 mg.(73 %)

^{1}H NMR (400 MHz, d_6-acetone) δ = 7.09 (m, 4H), 7.51 (m, 4H), 7.70 (d, 2H), 8.15 (m, 8H), 8.69 (d, 2H), 8.80 (d, 4H).

Elemental Analysis for: Calculated. Found $C_{36}H_{38}N_8O_4RuP_2F_{12}$: Calculated: C 41.98, H 3.30, N 10.88. Found C 41.44, H 2.86, N 10.77 %.

3.2.1 Discussion of the synthesis of the ruthenium(II) complexes:

The preparation of the starting materials for the synthesis of the ruthenium bipyridyl complexes was carried out with slight differences to literature methods. [46] This reaction can be problematic, sometimes leading to the formation of carbonyl containing compounds, which must be removed before the compound is used. Reaction of the $[Ru(bpy)_2Cl_2].2H_2O$ with the ligands in refluxing ethanol/water (1:1 v/v) led to the replacement of the two chlorides by the bidentate ligands. As the reaction proceeds, the deep violet colour of the $[Ru(bpy)_2Cl_2]$ solution is gradually replaced by an orange/red colour, which indicates the presence of the N6 $[Ru(bpy)_2(LL)]^{2+}$ complexes. The ethanol was removed at this stage and the chloride counter ion replaced by a PF_6^- counter ion which led to the precipitation of the complex from an aqueous solution. The PF_6^- salts of this type of complex tend to be only sparingly water soluble, and soluble in many organic solvents, which greatly eases the isolation, purification and analysis of these compounds.

The purity of the compounds was checked at this stage using TLC and HPLC. Further purification was necessary in most cases and this was generally performed by column chromatography on silica gel, using an 4:1 (v/v) $MeCN:H_2O$ mobile phase which contained 0.05M KNO_3 as a buffer. The desired band was generally the second band to elute. After the purity was determined again by HPLC, the compounds were analysed by ^1H NMR spectroscopy, CHN elemental analysis and in some cases by X-Ray Crystal structure analysis. These results follow in the next sections.

3.3 HPLC Analysis of the purified complexes:

The purification of the complexes has been detailed in the experimental section (Section 3.2). High Performance Liquid Chromatography (HPLC) has been an important tool in the determination of the purity of the desired complexes. The instrument provides the opportunity to analyse the product at various stages of the synthetic process, for example during the reaction, after isolation but before purification and finally after purification. Not only does the HPLC analysis provide details of the percentage purity of the desired complex, but often provides information about the nature of the impurities. Analysis of a reaction mixture before completion of the reaction generally results in three main peaks. The first corresponds to the free ligand, the second band due to $[Ru(bpy)_2(solvent)_n]$ with the desired complex often the last to elute. The nature of the impurities can be determined by examination of their UV/Vis spectra. Generally speaking, the ligand absorbs predominantly in the UV region, with the $[Ru(bpy)_2(solvent)_2]^{2+}$ species having a λ_{max} at *circa* 470 nm (compared to 450 nm for the desired complex).

As discussed in the previous section, it proved necessary in most cases to purify the reaction mixture by column chromatography. The desired band was generally the second orange band to elute, and as expected the first band proved to be the solvated $Ru(bpy)_2$ complex. This has been proven by HPLC. In conjunction with ^1H NMR, HPLC has proven very important and efficient at verifying the desired complexes are free of impurities. The results of the analysis of the complexes is presented in Figure 3.7.

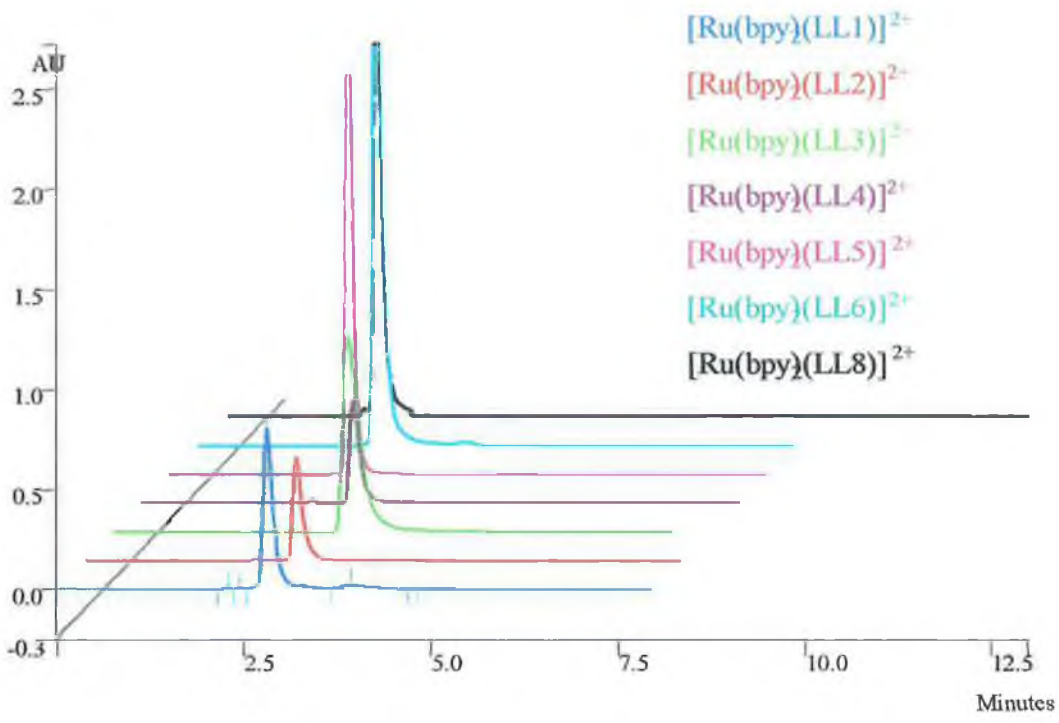

Figure 3.7 Examples of the HPLC traces of the purified ruthenium(II) complexes.

Compound	Retention Time (min)
$[Ru(bpy)_2(LL1)]^{2+}$	2.82
$[Ru(bpy)_2(LL2)]^{2+}$	2.75
$[Ru(bpy)_2(LL3)]^{2+}$	3.13
$[Ru(bpy)_2(LL4)]^{2+}$	2.40
$[Ru(bpy)_2(LL5)]^{2+}$	2.39
$[Ru(bpy)_2(LL6)]^{2+}$	2.45
$[Ru(bpy)_2(LL8)]^{2+}$	2.25

Table3.9 HPLC data obtained for the ruthenium(II) complexes.

As can be seen from Figure 3.7 the complexes were successfully purified by column chromatography and appear pure by HPLC. The analysis of the complexes by HPLC indicates a purity of >97% in all cases. The retention times (Table 3.9) are typical of ruthenium(II) complexes and are comparable to that of $[Ru(bpy)_3]^{2+}$ when examined under similar conditions.

The lack of variation in the retention times indicate that the LL_x ligand interacts little with the column, and is less important than the charge of the complex in determining the behaviour of the complex on the chromatography column. This is an expected result as the column is a cation exchange column, and is less sensitive to changes in the "organic" structures of compounds than to differences in charge.

HPLC has provided an excellent starting point in the structural characterisation of these complexes. This characterisation is completed by X-Ray Crystal Structure analysis (Chapter 3.4) and ^1H NMR (Chapter 3.6).

3.4 X-Ray Crystal Structure Analysis:

X-Ray Crystallography can be used to investigate and elucidate the structure of metal complexes. This technique has been used since the 1970s on ruthenium complexes, with the X-Ray Crystallographic determination of $[Ru(bpy)_3](PF_6)_2$ being reported in 1979. [47] The investigation revealed the $[Ru(bpy)_3]^{2+}$ cation has crystallographic symmetry, D_3-32, and has an octahedral coordination with a propeller-like arrangement of the ligands around the central metal ion. The Ru-N bond lengths of 2.056 Å is shorter than those found for the complexes $[Ru(NH_3)_6]^{3+}$ [48] and $[(bpy)_2(NO_2)Ru^{(III)}\text{-}O\text{-}Ru^{(III)}(NO_2)(bpy)_2]^{2+}$ [49] which were found to have average Ru-N bond lengths of 2.104 Å and 2.080 Å respectively. The shorter bond length found for the $[Ru(bpy)_3]^{2+}$ complex is contrary to the expected increase due to the larger ionic radius of $Ru^{(II)}$ *vs* $Ru^{(III)}$. The bond length decrease can be explained by the considerable π-bonding between the delocalised π* orbitals on the bpy ligands and the t_{2g} orbitals of the $Ru^{(II)}$ ion. In the $Ru^{(III)}$ complexes

the π-bonding is reduced or absent because the energy of the d-orbitals of $Ru^{(III)}$ is lowered.

X-Ray Crystallography has been used to unequivocally determine the structure of three of the ruthenium complexes of the LL_x ligands. The results are presented in this section. Crystals suitable for X-Ray Crystal structure analysis were grown for the $[Ru(bpy)_2(LL1)](PF_6)_2$, $[Ru(bpy)_2(LL2)](PF_6)_2$ and $[Ru(bpy)_2(LL3)](PF_6)_2$ complexes. The complexes were recrystallised slowly from acetone:water (3:1 v/v). Suitable crystals of the $[Ru(bpy)_2(LL8)](PF_6)_2$ complex have also been grown. The results of the analysis have not been completed to date and are not included here.

The results of the X-Ray Crystal Structure determination can be seen in Figures 3.8. 3.9 and 3.10. Selected data from this analysis is presented in Tables 3.10, 3.11 and 3.12. The complete set of results from the analysis of the three complexes are collated in Appendix A. The labelling used in Figures 3.8, 3.9 and 3.10 is used to identify the atoms during the discussion on the results of the analysis.

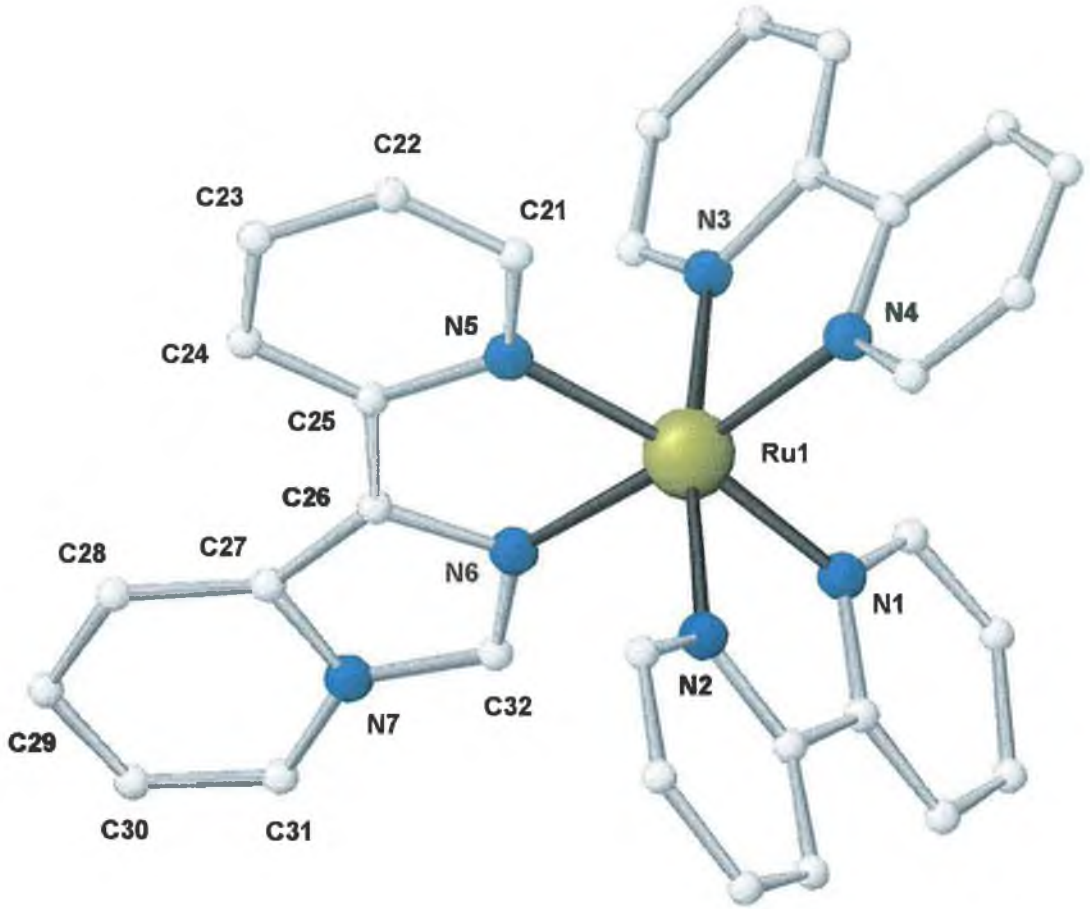

Figure 3.8 Results of the crystal structure analysis of the complex $[Ru(bpy)_2(LL1)](PF_6)_2$ showing the relevant atomic numbering used. The PF_6^- ions and hydrogen atoms have been omitted for clarity.

The $[Ru(bpy)_2(LL1)](PF_6)_2$ complex exhibits octahedral symmetry around the central metal ion. The LL1 ligand is bound to the metal centre via the N5 and N6 nitrogens. The length of the Ru-N5 and Ru-N6 bonds are 2.09 and 2.064 Å respectively.

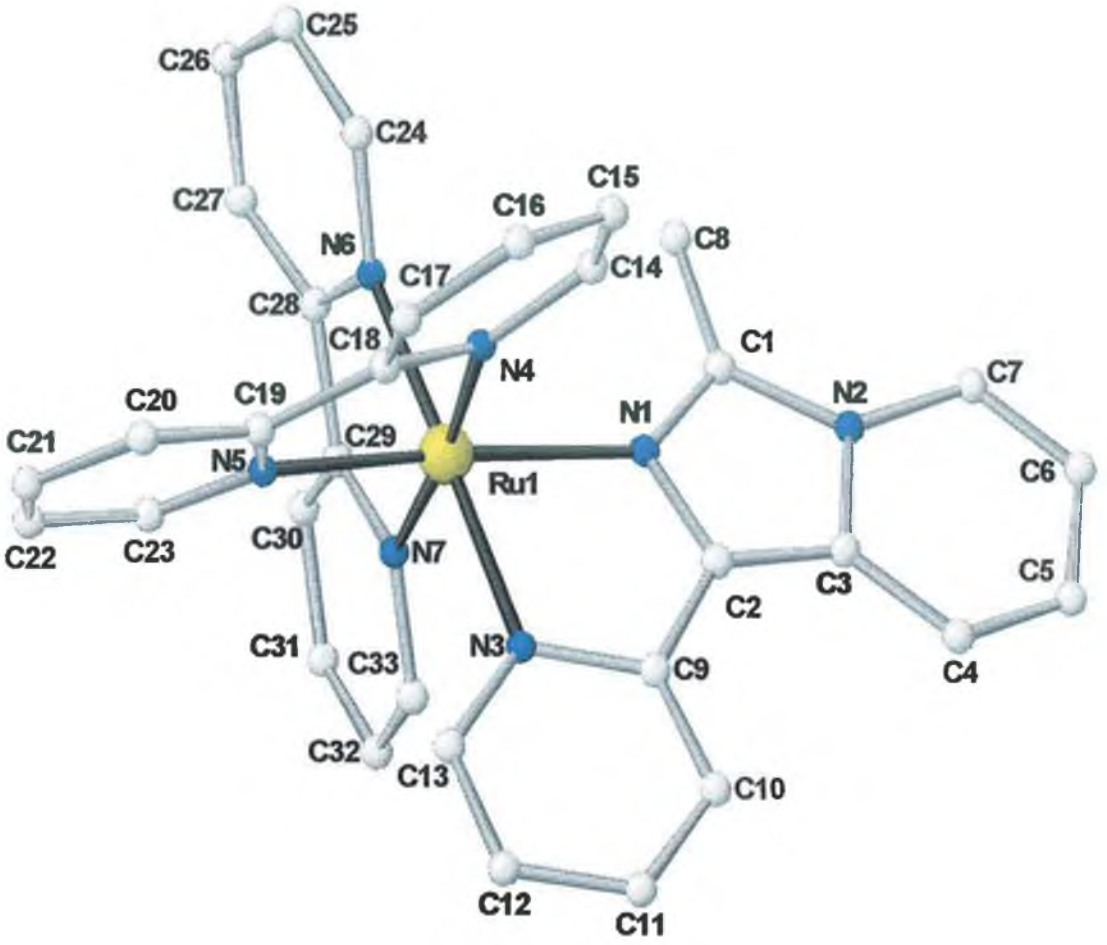

Figure 3.9 Results of the crystal structure analysis of the complex $[Ru(bpy)_2(LL2)](PF_6)_2$ showing the relevant atomic numbering used. The PF_6^- ions and hydrogen atoms have been omitted for clarity.

The $[Ru(bpy)_2(LL2)](PF_6)_2$ complex also exhibits octahedral symmetry around the central metal ion. The LL2 ligand is bound to the metal centre via the N1 and N3 nitrogens. The length of the Ru-N1 and Ru-N3 bonds are 2.074 and 2.086 Å respectively. The difference between the $[Ru(bpy)_2(LL1)](PF_6)_2$ and $[Ru(bpy)_2(LL2)](PF_6)_2$ complexes can clearly be seen with the methyl group on C1 evident in the structure of the $[Ru(bpy)_2(LL2)](PF_6)_2$ complex.

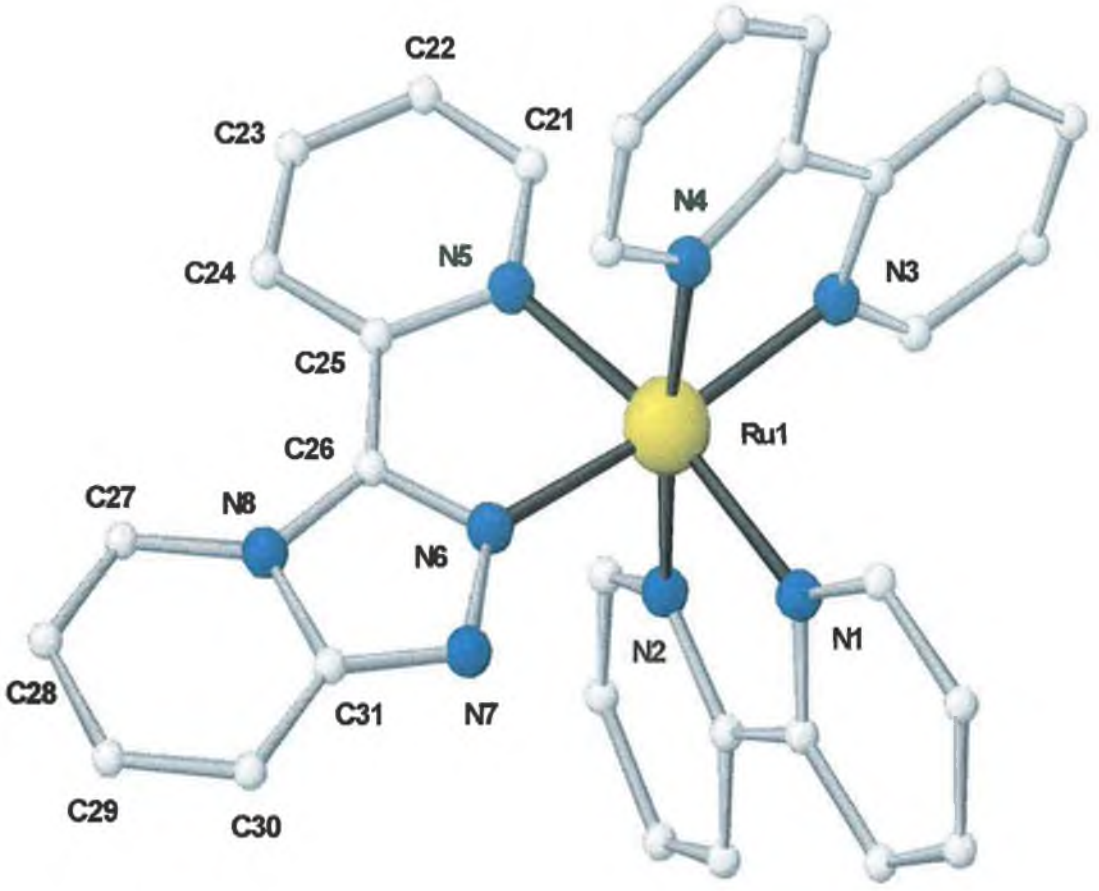

Figure 3.10 Results of the crystal structure analysis of the complex $[Ru(bpy)_2(LL3)](PF_6)_2.H_20$ showing the relevant atomic numbering used. The PF_6^- ions, water molecule and hydrogen atoms have been omitted for clarity.

The $[Ru(bpy)_2(LL3)](PF_6)_2$ complex also exhibits octahedral symmetry around the central metal ion. The LL3 ligand is bound to the metal centre via the N5 and N6 nitrogens. The length of the Ru-N5 and Ru-N6 bonds are 2.082 and 2.030 Å respectively. The extra nitrogen in the five membered ring of the $[Ru(bpy)_2(LL3)](PF_6)_2$ complex differentiates between this complex and the $[Ru(bpy)_2(LL1)](PF_6)_2$ complex. Unlike the previous two structures, the $[Ru(bpy)_2(LL3)](PF_6)_2$ complex contains a water of crystallisation. Selected data from the structures presented in Figures 3.8, 3.9 and 3.10 is detailed in Tables 3.10, 3.11 and 3.12.

Compound	$[Ru(bpy)_2(LL1)](PF_6)_2$	$[Ru(bpy)_2(LL2)](PF_6)_2$	$[Ru(bpy)_2(LL3)](PF_6)_2$
Formula	$C_{32}H_{25}F_{12}N_7P_2Ru$	$C_{33}H_{27}F_{12}N_7P_2Ru$	$C_{34}H_{30}F_{12}N_8OP_2Ru$
M_r	898.6	912.63	957.67
Space Group	$P2_{(1)}/n$	$P2_{(1)}/n$	$P2_{(1)}/c$
Crystal Class	Monoclinic	Monoclinic	Monoclinic
	Unit Cell Dimensions		
a/ Å	10.8719 (11)	13.0742 (9)	17.716 (12)
b/ Å	19.670 (2)	12.6822 (9)	13.8631 (9)
c/ Å	15.7347 (16)	21.5808 (15)	16.397 (11)
β^0	94.846 (2)	101.59 (10)	112.345 (10)
Volume/ $Å^3$	3353	3505.3	3724
Calculated Density, D_{calc}	1.780	1.729	1.708
	Data Collection Range		
H	-14 to 14	-16 to 17	-23 to 23
K	-25 to 26	-16 to 16	-18 to 18
L	-20 to 20	-27 to 28	-21 to 21
Reflections Collected	35986	36830	39757

Table 3.10 Summary of Crystal Data and Collection of Intensities of the compounds $[Ru(bpy)_2(LL1)](PF_6)_2$, $[Ru(bpy)_2(LL2)](PF_6)_2$ and $[Ru(bpy)_2(LL3)](PF_6)_2$.

$[Ru(bpy)_2(LL1)]^{2+}$ Bond - (Å)	$[Ru(bpy)_2(LL2)]^{2+}$ Bond - (Å)	$[Ru(bpy)_2(LL3)]^{2+}$ Bond - (Å)
Ru-N(1) (2,2'-bpy) - 2.054	Ru-N(1) (imidazo-LL2) - 2.074	Ru-N(1) (2,2'-bpy) - 2.058
Ru-N(2) (2,2'-bpy) - 2.061	Ru-N(3) (py-LL2) - 2.086	Ru-N(2) (2,2'-bpy) - 2.067
Ru-N(3) (2,2'-bpy) - 2.061	Ru-N(4) (2,2'-bpy) - 2.064	Ru-N(3) (2,2'-bpy) - 2.058
Ru-N(4) (2,2'-bpy) - 2.057	Ru-N(5) (2,2'-bpy) - 2.059	Ru-N(4) (2,2'-bpy) - 2.065
Ru-N(5) (py-LL1) - 2.090	Ru-N(6) (2,2'-bpy) - 2.057	Ru-N(5) (py-LL3) - 2.082
Ru-N(6) (imidazo-LL1) - 2.064	Ru-N(7) (2,2'-bpy) - 2.050	Ru-N(6) (triazo-LL3) - 2.030

Table 3.11 Selected Bond distances of $[Ru(bpy)_2(LL1)]^{2+}$, $[Ru(bpy)_2(LL2)]^{2+}$ and $[Ru(bpy)_2(LL3)]^{2+}$

The length of the ruthenium-nitrogen bonds provide a good basis for comparison with previously reported structures. In the case of all three structures, the length of the Ru-N 2,2'-bipyridyl bonds are between 2.050 → 2.067 Å. The bond lengths of the Ru-N (LL_x) bonds vary between 2.03 → 2.09 Å. These distances are similar to those found for other ruthenium(II) complexes. [50,51,52,53] Generally speaking, the σ-donor and π-acceptor character of the ligands is reflected in the Ru-N bond length. A shortening of this bond length may indicate enhanced σ-donating ability of the ligand relative to 2,2'-bipyridyl. [53] Due to the similarity of the Ru-N bond lengths to both the 2,2'-bipyridyl ligands and the LL_x ligands, this information cannot be gleaned from these structures.

Bond Angles (degrees)					
$[Ru(bpy)_2(LL1)]^{2+}$		$[Ru(bpy)_2(LL2)]^{2+}$		$[Ru(bpy)_2(LL3)]^{2+}$	
N(1)-Ru-N(4)	92.62	N(1)-Ru-N(3)	78.43	N(6)-Ru-N(3)	173.87
N(1)-Ru-N(3)	95.27	N(4)-Ru-N(3)	87.35	N(6)-Ru-N(1)	95.70
N(4)-Ru-N(3)	78.63	N(5)-Ru-N(3)	94.15	N(3)-Ru-N(1)	88.53
N(1)-Ru-N(2)	78.64	N(6)-Ru-N(3)	175.62	N(6)-Ru-N(4)	96.36
N(4)-Ru-N(2)	95.38	N(7)-Ru-N(3)	96.44	N(3)-Ru-N(4)	78.62
N(3)-Ru-N(2)	171.35	N(4)-Ru-N(1)	95.28	N(1)-Ru-N(4)	97.81
N(1)-Ru-N(6)	93.09	N(5)-Ru-N(1)	170.85	N(6)-Ru-N(2)	87.68
N(4)-Ru-N(6)	173.48	N(6)-Ru-N(1)	100.92	N(3)-Ru-N(2)	97.52
N(3)-Ru-N(6)	97.70	N(7)-Ru-N(1)	89.37	N(1)-Ru-N(2)	78.67
N(2)-Ru-N(6)	88.83	N(5)-Ru-N(4)	78.90	N(4)-Ru-N(2)	174.92
N(1)-Ru-N(5)	170.76	N(6)-Ru-N(4)	97.03	N(6)-Ru-N(5)	77.48
N(4)-Ru-N(5)	96.09	N(7)-Ru-N(4)	174.52	N(3)-Ru-N(5)	98.89
N(3)-Ru-N(5)	89.48	N(6)-Ru-N(5)	86.89	N(1)-Ru-N(5)	169.86
N(2)-Ru-N(5)	97.42	N(7)-Ru-N(5)	96.83	N(4)-Ru-N(5)	90.46
N(6)-Ru-N(5)	78.39	N(7)-Ru-N(6)	79.20	N(2)-Ru-N(5)	93.43

Table 3.12 Selected Bond Angles of $[Ru(bpy)_2(LL1)]^{2+}$, $[Ru(bpy)_2(LL1)]^{2+}$ and $[Ru(bpy)_2(LL3)]^{2+}$

The bite angles of the LL1, LL2 and LL3 ligands in the complexes are 78.39°, 78.43° and 77.48°. The bite angles of the coordinated 2,2'-bipyridyl ligands lie between 78.62° and 79.2°. These values are in agreement with those found for the 2,2'-bipyridyl ligands in other ruthenium(II) complexes. [47,50,52,53]

Closer examination of the angles in the complexes exhibit deviations from the trans angular value (180°). The N1-Ru-N5, N2-Ru-N3 and N4-Ru-N6 angles of the $[Ru(bpy)_2(LL1)]^{2+}$ complexes are 170.76°, 171.35° and 173.48° respectively. This deviation originates from the acute bite angles of both the 2,2'-bipyridyl ligands (78.62°

to 79.2°) and to a greater extent from the bite angle of the LL1 ligand (78.39°). The pattern is the same for both the $[Ru(bpy)_2(LL2)]^{2+}$ and $[Ru(bpy)_2(LL3)]^{2+}$ complexes. The N1-Ru-N5, N3-Ru-N6 and N4-Ru-N7 angles are 170.85°, 175.62° and 174.52° respectively for the $[Ru(bpy)_2(LL2)]^{2+}$ complex while the N1-Ru-N5, N2-Ru-N4 and N3-Ru-N6 angles are 169.86°, 174.92°, and 173.87° respectively for the $[Ru(bpy)_2(LL3)]^{2+}$ complex. These values are typical for ruthenium complexes containing 2,2'-bipyridyl and imidazo type ligands. [54]

A full list of all the crystallography data can be found in Appendix A.

3.5 ^{1}H NMR spectroscopy of the ligands:

^{1}H NMR spectroscopy has proven to be an invaluable tool in the analysis of the purity and in the elucidation and characterisation of the structure of the ruthenium(II) bisbipyridyl complexes. The ^{1}H NMR spectra of the complexes become complicated owing to the large number of aromatic protons present on the ligands. In order to assign the ^{1}H NMR of the complexes it was necessary to investigate the ^{1}H NMR of the free ligands. In Figure 3.11 the labelling of the LL1, LL2, LL3 and LL8 ligands is given. The ^{1}H NMR spectra of these ligands have been assigned first as the spectra are simpler than those of the other LL_x ligands which are complicated by the additional substituted phenyl ring. The ^{1}H NMR spectra of the LL4 and LL5 ligands are introduced later in this section. The ^{1}H NMR of the LL7 ligand is discussed in Chapter 5.4 while analysis of the LL6 ligand by ^{1}H NMR has not proved possible as it is insoluble in a suitable solvent. Figures 3.12 and 3.13 illustrate the ^{1}H NMR spectra of the LL1, LL2, LL3 and LL8 ligands.

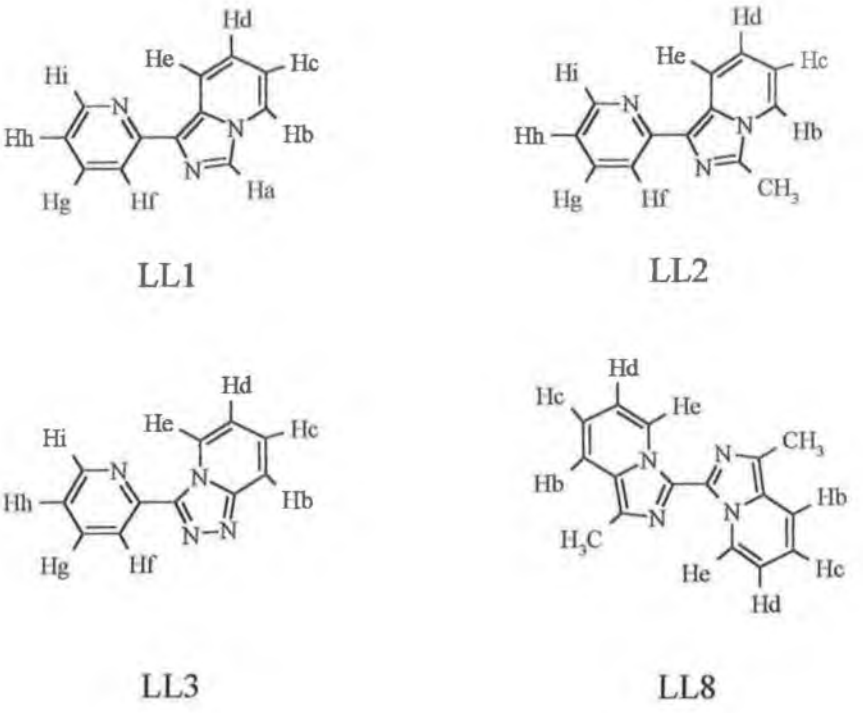

Figure 3.11 Labelling of the ligand protons for assignment.

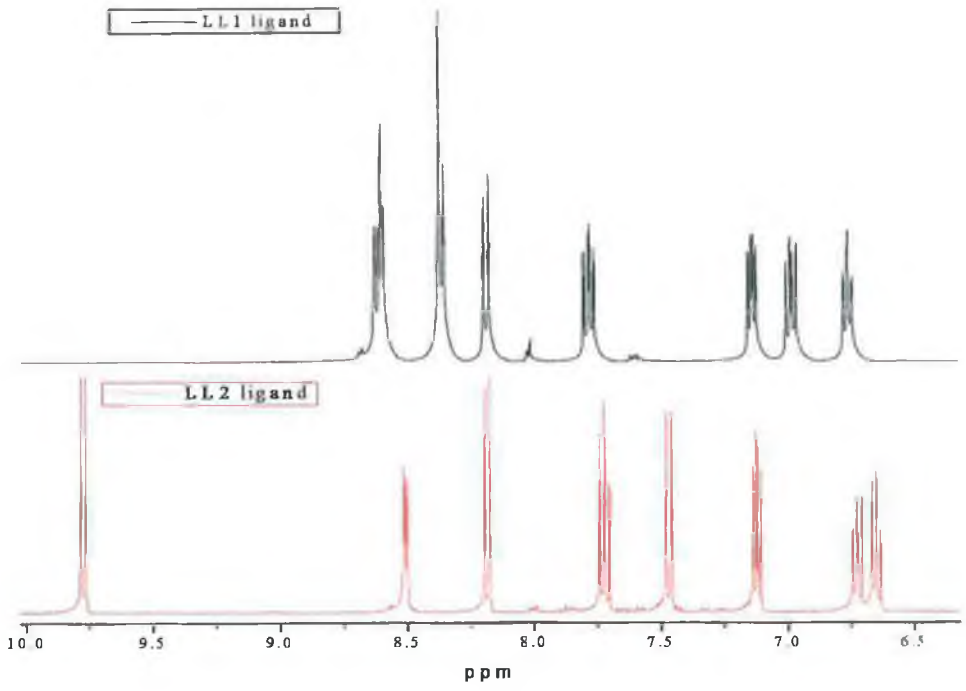

Figure 3.12 ^1H NMR spectra of LL1 and LL2 ligands in d_6-acetone.

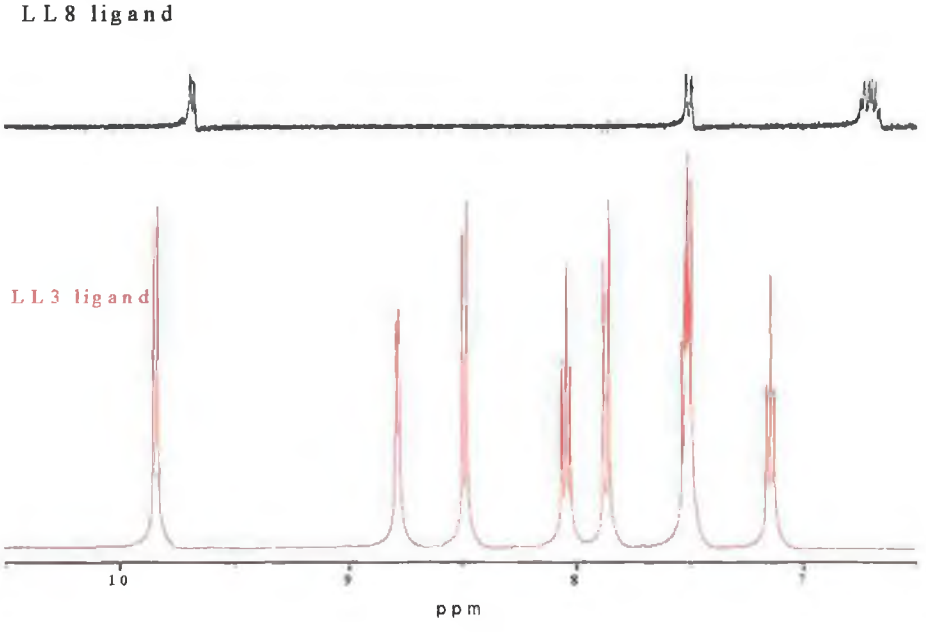

Figure 3.13 ^1H NMR spectra of LL3 and LL8 in d_6-acetone.

2D COSY NMR has proven very important in aiding the elucidation of the ^1H NMR spectra of these ligands. An illustrative 2D COSY NMR spectrum of the LL1 ligand is given in Figure 3.14 below. The assignments of the individual protons of the LL1, LL2, LL3 and LL4 ligands are given in Table 3.13.

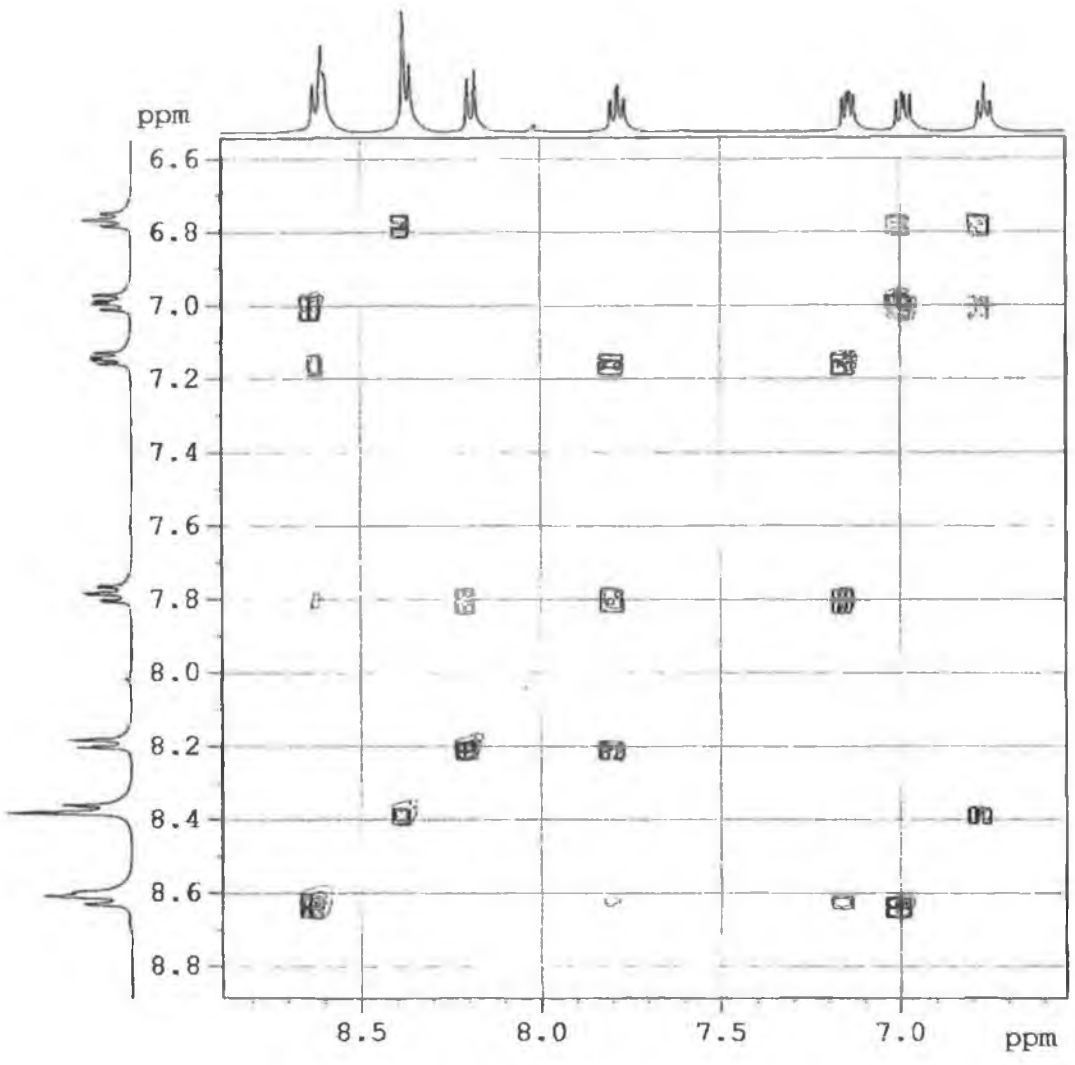

Figure 3.14 2D COSY NMR spectrum of LL1 ligand in d_6-acetone.

Ligand	LL1 (ppm)	LL2 (ppm)	LL3 (ppm)	LL8 (ppm)
H_a	8.37 (s)	-	-	-
H_b	8.38 (m)	7.47 (d)	8.50 (d)	7.51 (m)
H_c	6.77 (dd)	6.72 (dd)	8.04 (dd)	6.70 (m)
H_d	6.99 (dd)	6.63 (dd)	7.50 (m)	6.70 (m)
H_e	8.59 (m)	9.78 (d)	9.84 (d)	9.68 (d)
H_f	8.18 (d)	8.17 (d)	7.85 (d)	-
H_g	7.78 (dd)	7.72 (dd)	7.50 (m)	-
H_h	7.14 (dd)	7.14 (dd)	7.14 (dd)	-
H_i	8.62 (m)	8.49 (d)	8.78 (d)	-
Other protons	-	2.38 (s)	-	2.46 (s)

Table 3.13 ^1H NMR data for the ligands LL1, LL2 and LL3 in d_6-acetone.

Several important points should be noted from the results in Table 3.13. As expected, substitution of the H_a proton in LL1 for the methyl group in LL2 has very little effect on the chemical shifts of the protons in the free pyridine ring ($H_f \rightarrow H_i$). Closer examination of this reveals that the chemical shifts of the H_f protons are found between 7.85 and 8.18 ppm. The H_g protons lie between 7.50 and 7.78 ppm. The H_h protons are all found at 7.14 ppm which indicates the similarity of the chemical environment of this proton even between the different ligands, while the H_i protons can be found from 8.49 to 8.78 ppm.

The closeness of the chemical shifts of these protons indicate that substitution, or alteration of the fused 5 and 6 membered ring has little effect on the "free" pyridine ring in these ligands. This has proven useful in the assignment of the LL4 and LL5 ligands.

The H_e proton is found furthest downfield. This can be attributed to the orientation adopted by the ligands in solution. . As can be seen from Figure 3.11, the H_e proton is

positioned in such a way as to facilitate interaction with the nitrogen on the pyridine ring. This leads to a hydrogen bonding interaction between the H_e protons and the free nitrogen, causing the proton to be shifted downfield relative to the other protons. The replacement of the H_a proton in LL1 by a methyl group in LL2 leads to an upfield shift of the H_b, H_c and H_d protons of the LL2 ligand relative to the LL1 ligand. This is due to the shielding nature of the methyl group in comparison to H. The introduction of a third hydrogen into the 5-membered ring increases the electron density over both the five membered and fused pyridine ring, and a subsequent shift to higher ppm is observed for the H_b, H_c and H_d protons.

This sensitivity to electron density is evident in the comparison of the LL1 and LL3 ligands. In moving from an imidazo type ligand to a triazo type 5 membered ring system, the extra nitrogen in the triazo ligand will have an electron withdrawing effect resulting in a downfield shift in the chemical shifts of the protons on the affected rings.

The ^1H NMR of the LL8 ligand differs from that of the LL1, LL2 and LL3 ligands on account of its symmetrical nature. This symmetry is reflected in the ^1H NMR where three signals which integrate to 4 protons are observed. Allowing each of these signals to represent two equivalent protons accounts for the 8 protons which should be present in the spectrum. The chemical shifts of the H_b, H_c and H_d protons are similar to those of the analogous protons in the LL2 ligand. The substituted phenyl group adds complexity to the ^1H NMR spectra of LL4 and LL5.

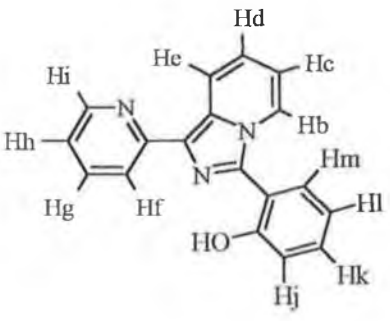

LL4

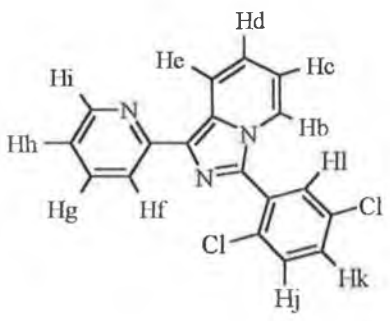

LL5

Figure 3.15 Labelling of the protons of the ligands LL4 and LL5.

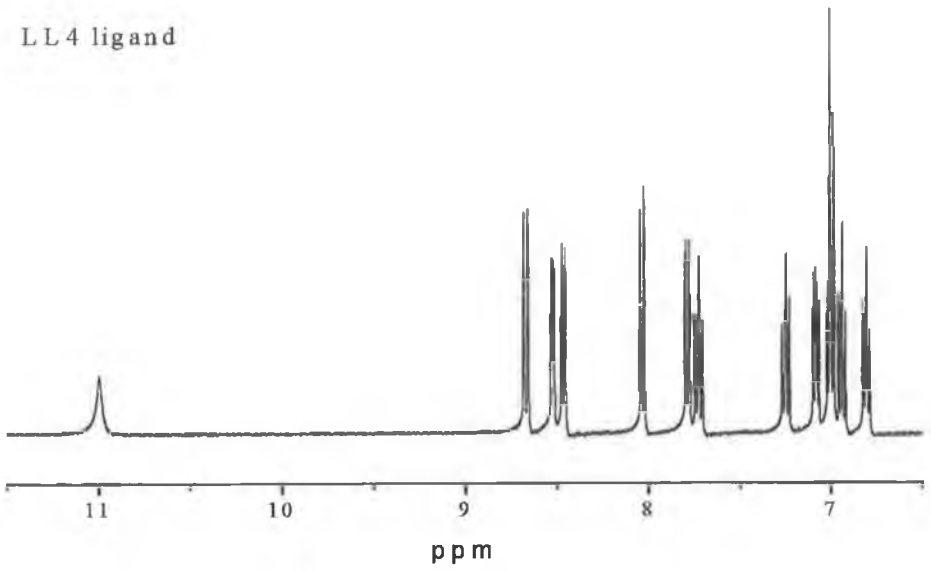

Figure 3.16 ^1H NMR of the LL4 ligand in d_6-acetone.

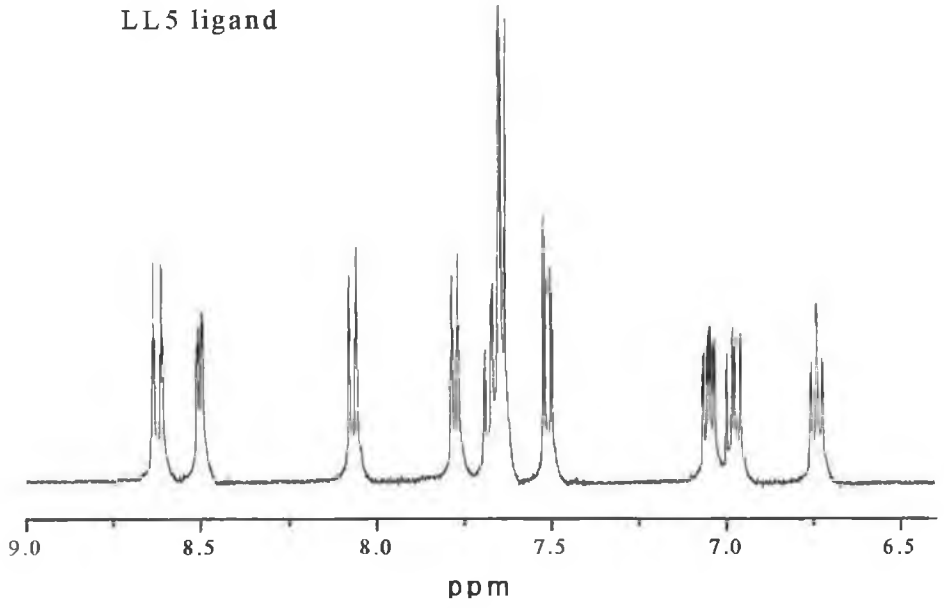

Figure 3.17 ^1H NMR of the LL5 ligand in d_6-acetone.

As in the case of the simpler LL1, LL2, LL3 and LL8 ligands, 2D COSY NMR proved decisive in the assignment of the LL4 and LL5 protons. The protons of the phenyl rings proved readily identifiable by their splitting patterns, with the H_l proton in the LL5 ligand appearing as a singlet. As expected, substituting a phenyl group for the H_a proton of the LL1 ligand had little effect on the chemical shifts of the free pyridine ring ($H_f \rightarrow$

H_j). The chemical shifts of the $H_f \rightarrow H_i$ protons are comparable to those observed for the LL1, LL2 and LL3 ligands. The OH proton in the LL4 ligand is observed at 11 ppm and is broader than the other signals.

Proton	LL4 (ppm)	LL5 (ppm)	Proton	LL4 (ppm)	LL5 (ppm)
H_a	-	-	H_h	7.00 (m)	7.05 (dd)
H_b	7.00 (m)	7.77 (d)	H_i	8.51 (d)	8.50 (d)
H_c	6.95 (dd)	6.75 (dd)	H_j	8.68 (d)	7.65 (m)
H_d	6.80 (dd)	6.98 (dd)	H_k	7.08 (dd)	7.75 (m)
H_e	8.45 (d)	8.61 (d)	H_l	7.72 (dd)	7.52 (d)
H_f	7.78 (d)	8.08 (d)	H_m	8.03 (d)	-
H_g	7.25 (dd)	7.65 (m)	Other ^{1}Hs	11.00 (s)	-

Table 3.14 ^{1}H NMR data for the ligands LL4 and LL5 in d_6-acetone.

The effect of coordination on the chemical shifts of the LL_x ligand protons is examined in Chapter 3.6.

3.6 ^{1}H NMR spectroscopy of the $[Ru(bpy)_2(LL_x)](PF_6)_2$ complexes

The analysis of the ^{1}H NMR spectra of the complexes can be divided into two categories. The complexes containing LL_x ligands with no substituted phenyl ring (i.e. LL1, LL2, LL3 and LL8), and those LL_x ligands containing a substituted phenyl ring (i.e. LL4, LL5 and LL6). The differences between the spectra of these two categories of LL_x ligand are substantial and are discussed in detail in this section.

The ^{1}H NMR spectra of the mixed ligand complexes are more complicated and more difficult to assign than the free ligands. Several techniques have been used to aid the assignment of the spectra, including deuteriation of the 2,2'-bipyridyl ligands (introduced in Chapter 2.1) and 2D COSY NMR. In this way it has been possible to assign the protons of the LL1, LL2, LL3 and LL8 ligands while coordinated to the ruthenium(II) bisbipyridyl unit. This has not proved possible in the case of the ligands which contain the substituted phenyl ring (LL4, LL5 and LL6) due to an unforeseen isomerisation effect which complicates the ^{1}H NMR spectra. This will be discussed in more detail later in this section. The ^{1}H NMR spectra of the complexes $[Ru(bpy)_2(LL1)](PF_6)_2$ and its deuteriated analogue can be seen in Figure 3.18. The 2D COSY NMR of the deuteriated complex is presented in Figure 3.19, while the ^{1}H NMR spectra of $[Ru(bpy)_2(LL2)](PF_6)_2$, $[Ru(bpy)_2(LL3)](PF_6)_2$, and $[Ru(bpy)_2(LL8)](PF_6)_2$ can be seen in Figures 3.20 to 3.23.

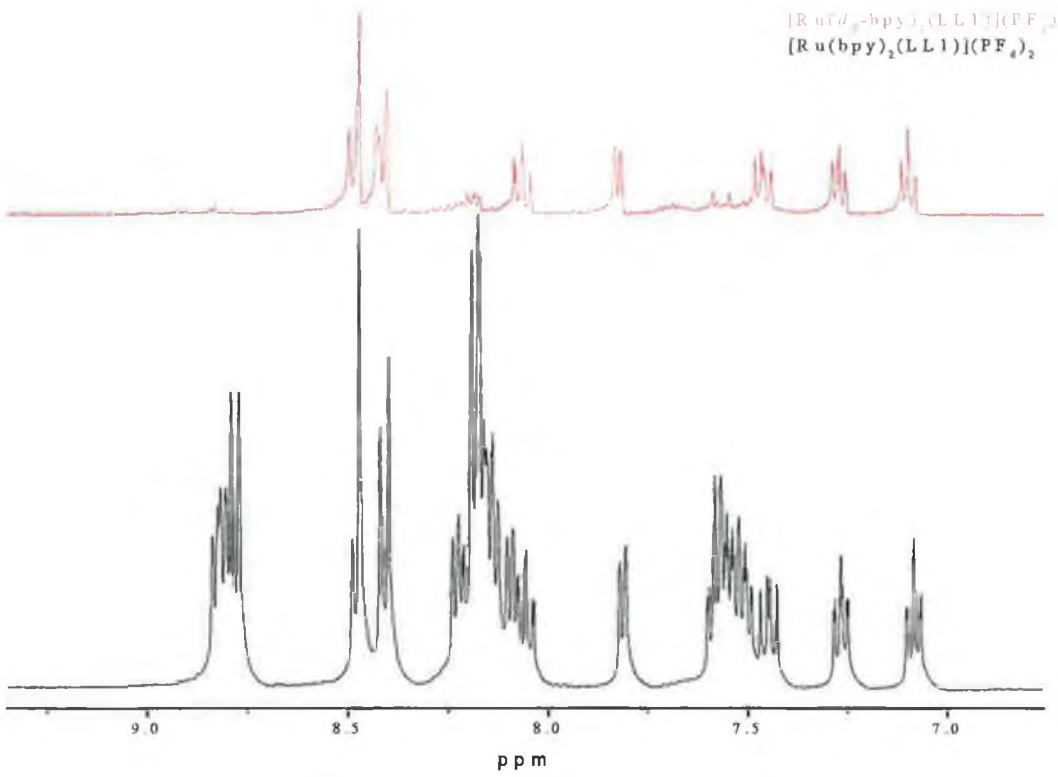

Figure 3.18 ^{1}H NMR of $[Ru(d_8\text{-bpy})_2(LL1)](PF_6)_2$ (red) and $[Ru(bpy)_2(LL1)](PF_6)_2$ (black) in d_6-acetone.

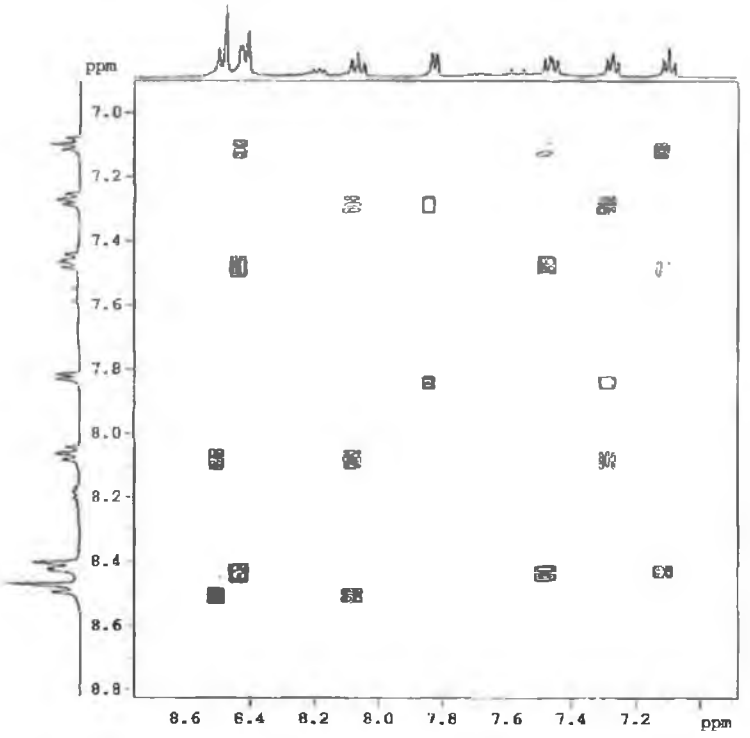

Figure 3.19 2D COSY NMR of the deuterated complex, $[Ru(d_8\text{-bpy})_2(LL1)](PF_6)_2$ in d_6-acetone. Used to assign the peaks of the LL1 ligand in the ruthenium(II) complex.

Figures 3.18 and 3.19 illustrate the ^{1}H NMR spectra and 2D COSY NMR spectra of the simplest of the complexes, $[Ru(bpy)_2(LL1)]^{2+}$ and its deuteriated analogue $[Ru(d_8\text{-bpy})_2(LL1)]^{2+}$. Deuteriation has been applied to the elucidation of ^{1}H NMR spectra of large polynuclear complexes where the number of inequivalent protons result in spectra otherwise difficult to assign. [55,56] Deuteriation has the effect of removing protons from the ^{1}H NMR spectrum while not affecting the signals of the undeuterated ligands. This can simplify a spectrum greatly, and allow complicated spectra to be assigned more easily. Figure 3.18 compares the ^{1}H NMR of $[Ru(bpy)_2(LL1)]^{2+}$ and its deuteriated analogue $[Ru(d_8\text{-bpy})_2(LL1)]^{2+}$. It should be noted that the apparent impurities in the spectrum of the $[Ru(d_8\text{-bpy})_2(LL1)]^{2+}$ complex are in fact residual signals from the 2,2'-bipyridyl protons which have not been fully deuterated. Deuteriation of the 2,2'-bipyridyl protons has also been used to aid the assignment of the spectra of the

$[Ru(bpy)_2(LL2)]^{2+}$, $[Ru(bpy)_2(LL3)]^{2+}$ and $[Ru(bpy)_2(LL8)]^{2+}$ complexes. The ^1H NMR of the undeuteriated complexes are presented in Figures 3.20, 3.21 and 3.22.

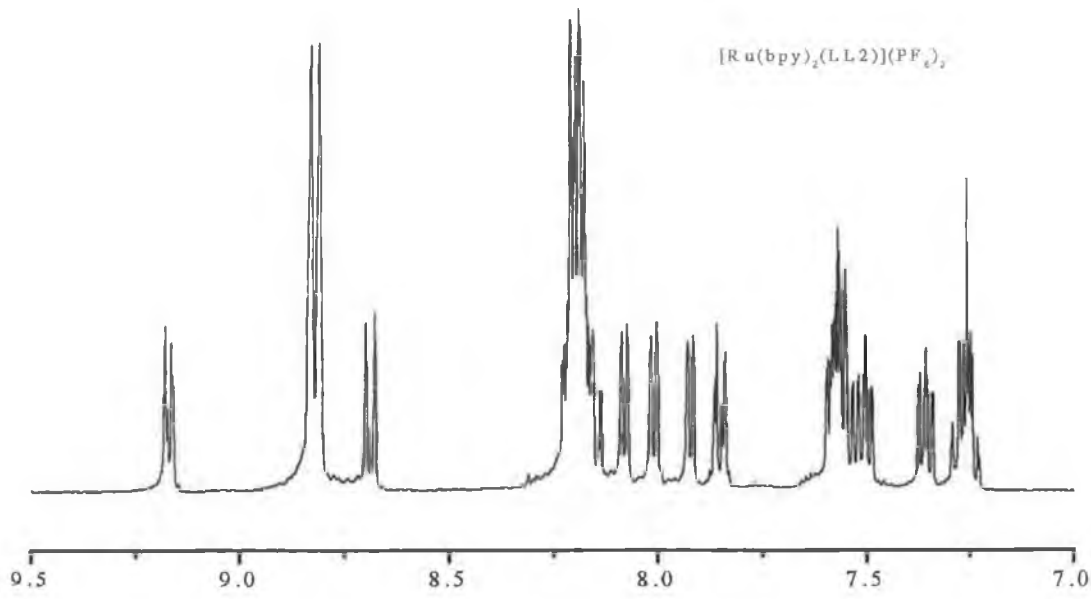

Figure 3.20 ^1H NMR of $[Ru(bpy)_2(LL2)](PF_6)_2$ in d_6-acetone.

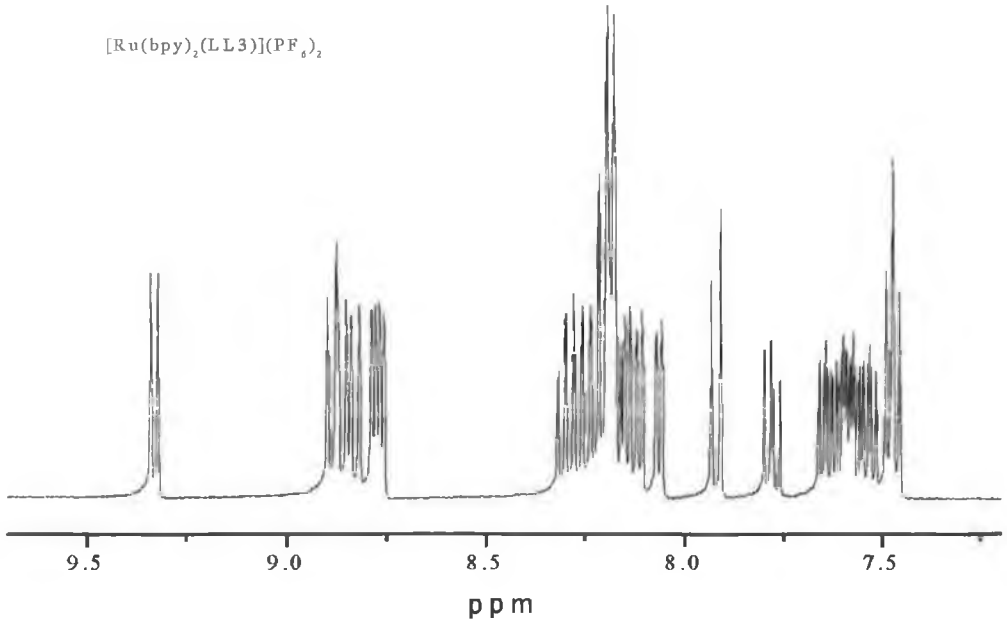

Figure 3.21 ^1H NMR of $[Ru(bpy)_2(LL3)](PF_6)_2$ in d_6-acetone.

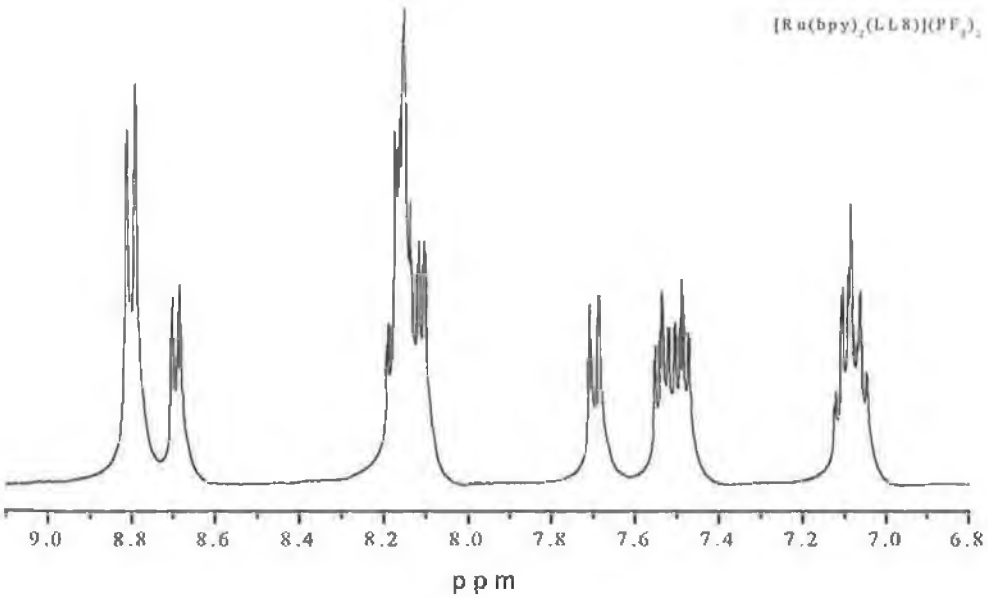

Figure 3.22 ^1H NMR of $[Ru(bpy)_2(LL8)](PF_6)_2$

Table 3.15 contains the assignment of the LL1, LL2, LL3 and LL8 ligands while complexed to the ruthenium(II) bisbipyridyl unit. The labelling of the protons has been illustrated in Figure 3.11.

Proton	Chemical Shift in d_6-acetone			
	$[Ru(bpy)_2(\mathbf{LL1})]^{2+}$ (ppm)	$[Ru(bpy)_2(\mathbf{LL2})]^{2+}$ (ppm)	$[Ru(bpy)_2(\mathbf{LL3})]^{2+}$ (ppm)	$[Ru(bpy)_2(\mathbf{LL8})]^{2+}$ (ppm)
H_a	8.49 (8.37)	No H_a	No H_a	No H_a
H_b	8.40 (8.38)	7.91 (7.47)	8.05 (8.50)	7.70 (7.51)
H_c	7.09 (6.77)	7.36 (6.72)	7.53 (8.04)	7.10 (6.70)
H_d	7.48 (6.99)	8.18 (6.63)	8.14 (7.50)	7.10 (6.70)
H_e	8.40 (8.59)	8.18 (9.78)	8.13 (9.85)	8.70 (9.68)
H_f	8.49 (8.18)	8.82 (8.17)	8.81 (7.85)	No H_f
H_g	8.06 (7.78)	8.18 (7.72)	8.19 (7.50)	No H_g
H_h	7.27 (7.14)	7.50 (7.14)	7.64 (7.14)	No H_h
H_i	7.83 (8.62)	8.08 (8.49)	8.17 (8.78)	No H_i

Table 3.15 ^1H NMR data for the complexes $[Ru(bpy)_2(LL1)](PF_6)_2$, $[Ru(bpy)_2(LL2)](PF_6)_2$, $[Ru(bpy)_2(LL3)](PF_6)_2$ and $[Ru(bpy)_2(LL8)](PF_6)_2$ in d_6-acetone. The values in parentheses are the chemical shifts of the free ligands.

Figure 3.24 provides a graphic illustration of the effect coordination has on the chemical shifts of the LL1 protons. It can be seen from Table 3.15 that most of the protons are shifted slightly in comparison to the free ligand. This is due to the altered electron density the ligand experiences on coordinating to a metal centre. Coordination has an electron withdrawing or deshielding effect, and lowers the electron density of the ligand. This leads to most of the ligand protons being shifted slightly downfield. There are two exceptions to this however and they are in the cases of the H_e and H_i protons. There are two different reasons for the upfield shift experienced by both these protons. In the case of the H_i proton, the upfield shift is due to the orientation of the proton, which in the complex is directed towards one of the pyridine rings of the adjacent aromatic 2,2'-bipyridine rings. The ring current of the 2,2'-bypyridine induces a diamagnetic anisotropic interaction effect which results in a large upfield shift (approx. 1 ppm in the case of the H_i proton). [30] Figure 3.23 illustrates this with respect to the

$[Ru(bpy)_2(LL1)]^{2+}$ complex.

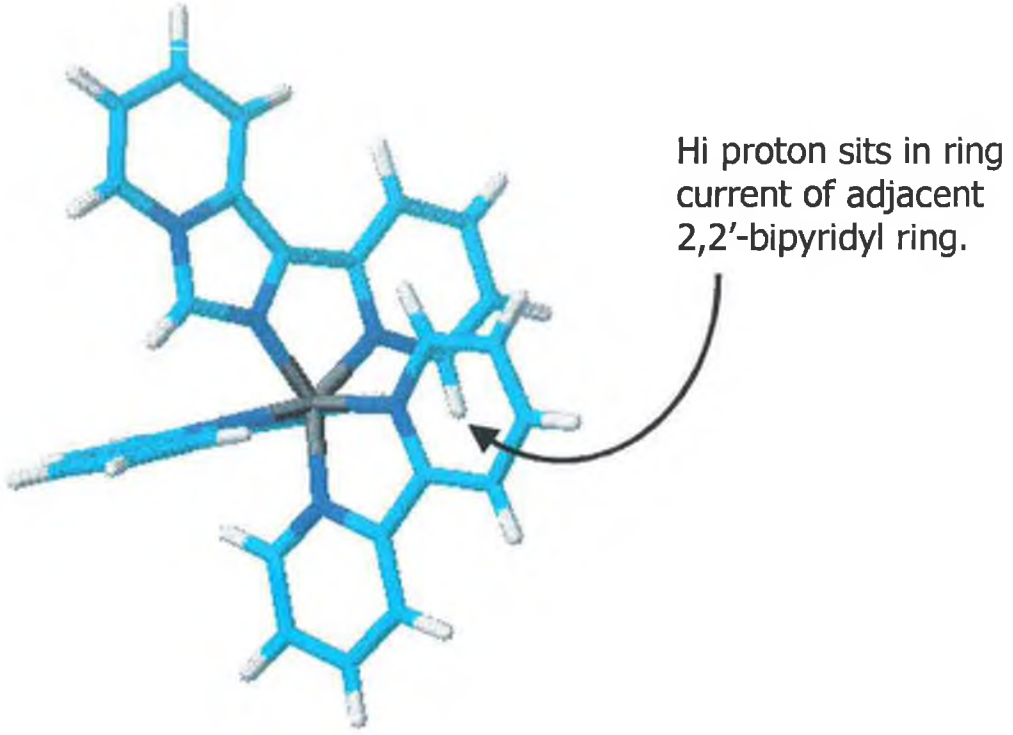

Figure 3.23 Diagram illustrating the orientation of the Hi protons in relation to the adjacent 2,2'-bipyridyl rings in the complex $[Ru(bpy)_2(LL1)]^{2+}$

The H_e proton is also upfield shifted. This is because in order to achieve bidentate coordination with the ruthenium centre, the ligand must adopt a less favoured configuration. The "free" pyridine ring in the ligand rotates so that its nitrogen is in a favourable position for coordination. The hydrogen bonding interaction between the H_e and the nitrogen is lost on coordination, leading to the upfield shift observed for the H_e proton. This is more pronounced in the complexes of the LL2, LL3 and LL8 ligands, where before complexation the chemical shift of the H_e protons were 9.78, 9.84 and 9.68 ppm respectively. On complexation, the chemical shifts of the protons are 8.18, 8.13 and 8.70 ppm respectively.

Figure 3.24 graphically illustrates the effect of coordination on each proton of the LL1 ligand. As explained already, coordination induces a downfield shift for most of the protons, with the exception of the H_e and H_i protons which are shifted upfield. This upfield shift is strongest for the H_i proton in this instance, resulting in the chemical shift of the H_i proton being shifted from 8.60 ppm in the free ligand to 7.83 ppm in the complex. The effect is less for the H_e proton which is shifted from 8.60 ppm in the free ligand to 8.49 ppm in the complex. The comparison of the two spectra also highlights the effect deuteriation of the 2,2'-bipyridyl ligands has on the ^1H NMR spectra of the mixed ligand complexes, and the simplification it provides to the elucidation of those spectra.

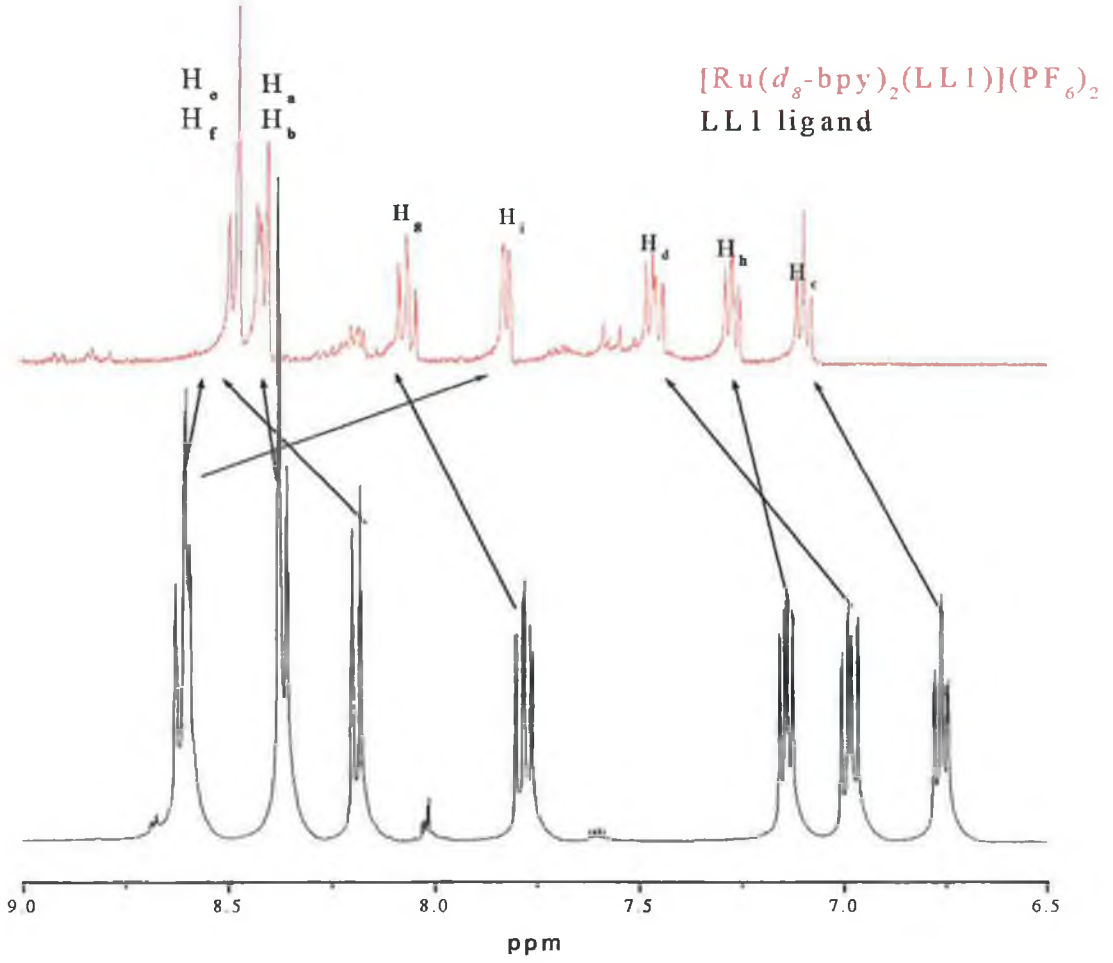

Figure 3.24 ^1H NMR of $[Ru(d_8\text{-bpy})_2(LL1)](PF_6)_2$ and the free ligand LL1 in d_6-acetone.

Before the ^1H NMR spectra of the ruthenium(II) complexes of the LL4, LL5 and LL6 ligands are discussed, the presence of enantiomers in coordination chemistry is briefly examined. It has been known for many years of the existence of the Δ and Λ enantiomers that occur on coordination of a third bidentate ligand to octahedral $M(LL)_2$ species. [57] Previous studies have shown that these enantiomers exhibit no observable differences in their electrochemical or electronic properties. The synthetic process used to synthesise the $[Ru(bpy)_2(LL_x)]^{2+}$ complexes produces both the Δ and Λ isomers of the each complex. The ^1H NMR spectra of the complexes containing the LL1, LL2 and LL3 complexes have been assigned. The presence of the Δ and Λ isomers of each complex is not evident from the ^1H NMR spectra of these complexes. For example, 25 individual protons are expected in the ^1H NMR spectrum of the $[Ru(bpy)_2(LL1)]^{2+}$ complex and 25 individual signals can be elucidated.

This compares to the ^1H NMR spectra of the ruthenium(II) complexes of the LL4, LL5 and LL6 ligands. Examination of the integration of the ^1H NMR spectra reveals a doubling of the expected number of signals. The $[Ru(bpy)_2(LL4)]^{2+}$ complex contains 56 aromatic protons, the $[Ru(bpy)_2(LL5)]^{2+}$ complex contains 54 protons while the $[Ru(bpy)_2(LL6)]^{2+}$ complex contains 54 aromatic protons.

The origin of the doubling of the number of protons in the ^1H NMR of the complexes $[Ru(bpy)_2(LL4)](PF_6)_2$, $[Ru(bpy)_2(LL5)](PF_6)_2$ and $[Ru(bpy)_2(LL6)](PF_6)_2$ can be explained using molecular modelling of the compounds using Hyperchem®.

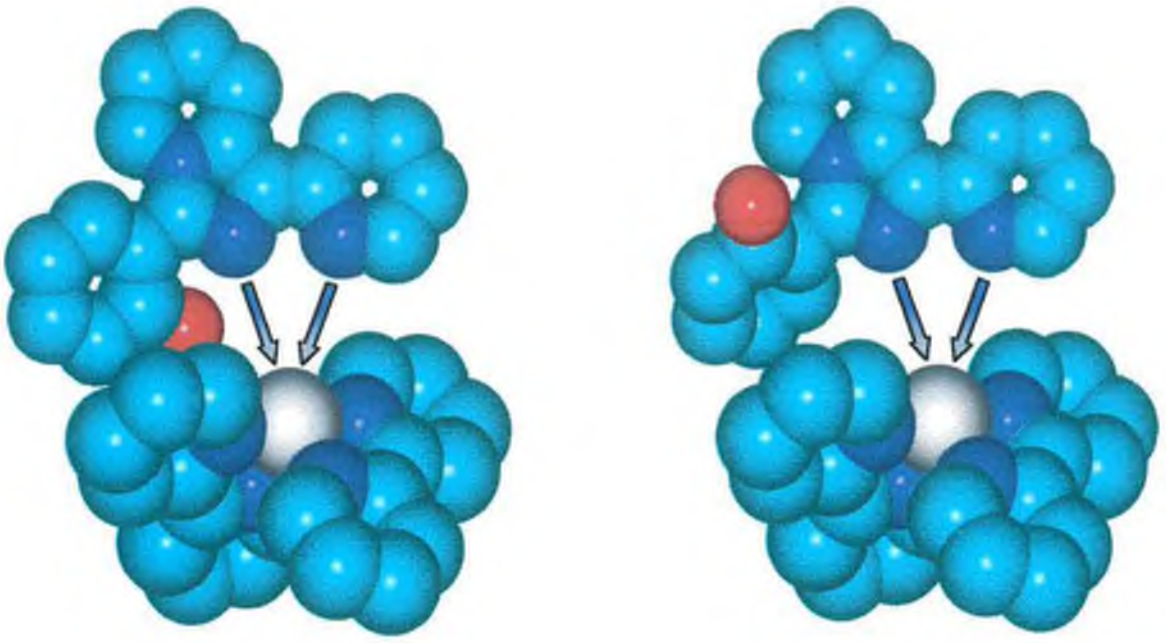

Figure 3.25 Representation of the origin of the conformational isomers for $[Ru(bpy)_2(LL4)]^{2+}$.

Figure 3.25 is a pictorial representation of two possible modes of coordination that will lead to the formation of isomers of the complex. In reality coordination takes place by substitution of solvent molecules which have already replaced the chlorides of the starting material. From this diagram it can clearly be seen that the OH group of the LL4 ligand (red group) will be in two different chemical environments after coordination. In Case A, the red OH group will be stacked above a 2,2'-bipyridyl ring, and will be influenced by the ring current produced by the aromatic ring. In Case B, the phenyl ring sits above one of the 2,2'-bipyridyl moieties allowing the OH group to point into space.

In the free ligand, the phenyl ring on which the OH group is located is free to rotate. Figure 3.25 shows clearly that this is not the case after coordination and leads to the phenyl ring adopting one of two orientations. (Case A or Case B in Figure 3.25). The differences in environment are not detectable by HPLC, but these differences become apparent in the ^{1}H NMR spectrum of the complex where a doubling of the expected number of protons occurs (each set of protons represent the complex containing the LLx ligand in one of two different conformations). The HyperChem diagram above is the representation of the case for the LL4 ligand. The hypothesis can be extended to include the LL5 and LL6 ligands which also contain substituted phenyl rings. For the LL5 ligand, the two chloro substituents cause the ligand to adopt two different orientations on coordination, while the methoxy groups of the LL6 ligand cause the same problem. In each case a doubling of the number of protons expected in the ^{1}H NMR spectrum occurs.

The ^{1}H NMR spectrum of the complex $[Ru(bpy)_2(LL4)]^{2+}$ is given in Figure 3.26. The spectrum of the LL4 ligand is also given for comparison. In order to prove that the peaks at 9.65 and 10.89 ppm in the ^{1}H NMR spectrum of the complex were indeed those of the OH group of the substituted phenyl ring a simple ^{1}H NMR experiment was performed. A few of drops of D_2O were added to the NMR sample after the original spectrum had been run and a second proton spectrum was run. The disappearance of the OH peaks can clearly be seen (Figure 3.26). The most important observations to make about the spectrum of the complex are to do with the relative positions of the proton of the OH group. It is clear that there are two OH groups present in the spectrum of the complex, whereas the free ligand contains only one. The relative chemical shifts of the OH peaks are given in Table 3.16.

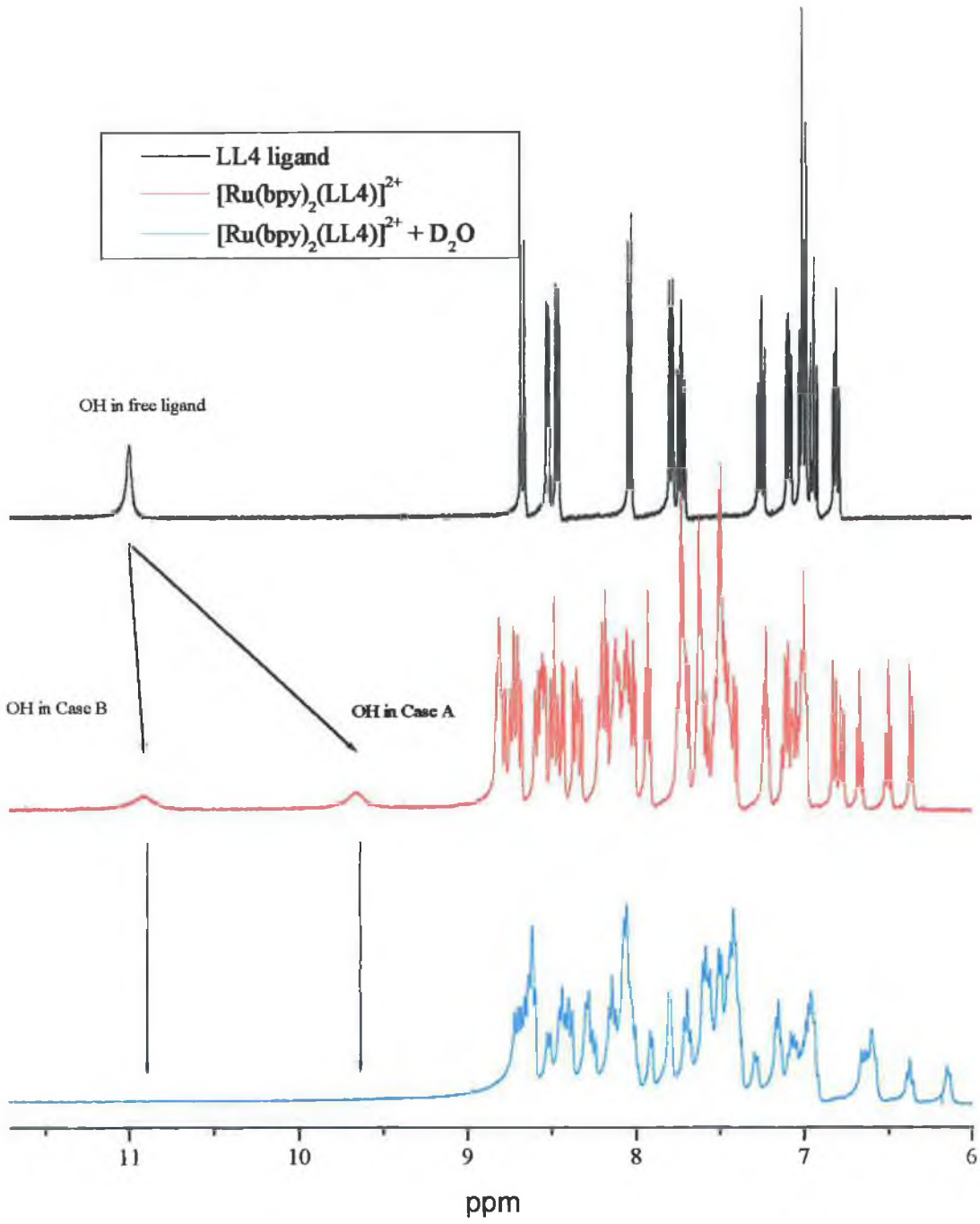

Figure 3.26 ^{1}H NMR of the free ligand LL4 (black) and the corresponding $[Ru(bpy)_2(LL4)](PF_6)_2$ complex (red) in d_6-acetone. Note the relevant positions of the OH groups. Case A and B refer to the environment of the OH groups in Figure 3.25. The blue spectrum is the $[Ru(bpy)_2(LL4)](PF_6)_2$ complex + D_2O.

Proton	Chemical Shift in d_6-acetone (ppm)	
OH in free ligand	10.99	N/A
OH in complex	10.89	9.65

Table 3.16 Relative chemical shifts of the OH protons in the free ligand and in the ruthenium(II) complex.

The reason two OH groups are observed is due to the two different orientations adopted by the phenyl ring on coordination. The same criteria can be used to explain the difference in the chemical shifts of the two OH groups as has been used to explain the upfield shift experienced by the H_i proton on coordination. Again it is due to the diamagnetic anisotropic effect it feels while sitting in the ring current of an adjacent 2,2' bipyridyl unit (Figure 3.23). The modelling of the LL4 ligand indicates that one of the conformational isomers places the OH proton directly over a bipyridyl ring (Case A in Figure 3.25) and this causes a shift of 1.3 ppm in the position of the proton in the spectrum. The second OH proton evident in the spectrum of the complex is also shifted in comparison to the free ligand but to a lesser extent (Case B in Figure 3.25). Even though it is not sitting directly in the ring current it still feels the effect and is therefore shifted upfield also.

Again efforts were made to simplify the spectrum, and a complex containing deuteriated 2,2'-bipyridyl moieties was synthesised, $[Ru(d_8\text{-bpy})_2(LL4)](PF_6)_2$. The ^1H NMR spectrum of the deuterated complex should be similar to that of the free ligand, with the exception of one or two of the signals which would be shifted upon coordination. The ^1H NMR of the deuteriated complex can be seen in Figure 3.27. Integration of the spectrum of the complex $[Ru(d_8\text{-bpy})_2(LL4)](PF_6)_2$ results in 26 individual protons including both of the OH protons already discussed. This is double the expected number of protons and is further proof of the existence of the conformational isomers. The residual non deuteriated 2,2'-bipyridyl protons are also evident in the Figure 3.27 and should be ignored.

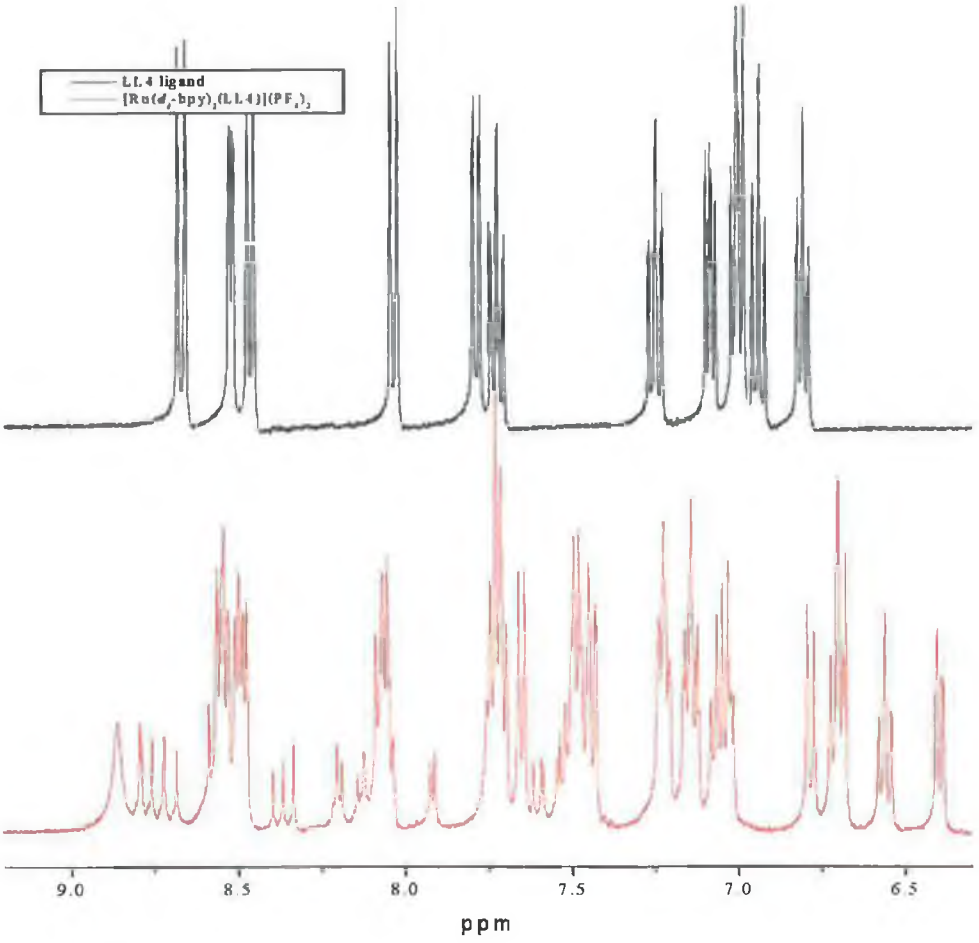

Figure 3.27 ^{1}H NMR spectra of the aromatic protons of the free ligand LL4 and the complex $[Ru(d_8\text{-bpy})_2(LL4)](PF_6)_2$ in d_6-acetone.

The ^{1}H NMR spectra of the complexes $[Ru(bpy)_2(LL5)](PF_6)_2$ and $[Ru(bpy)_2(LL6)](PF_6)_2$ show the same evidence of the presence of rotamers and are given in Figures 3.28 and 3.29 respectively.

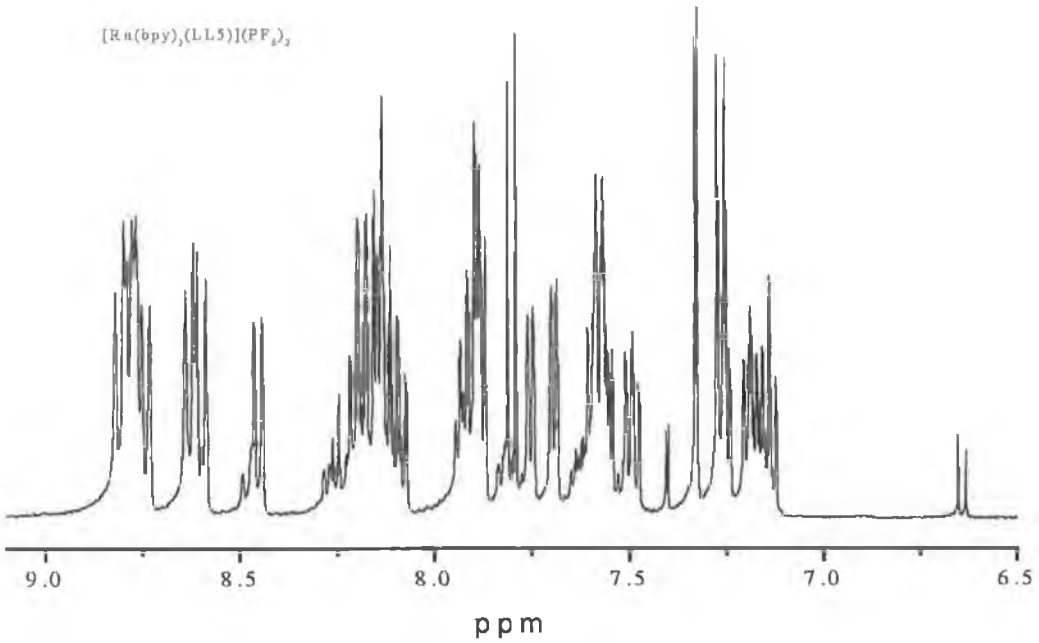

Figure 3.28 ^1H NMR spectrum of $[Ru(bpy)_2(LL5)](PF_6)_2$ in d_6-acetone.

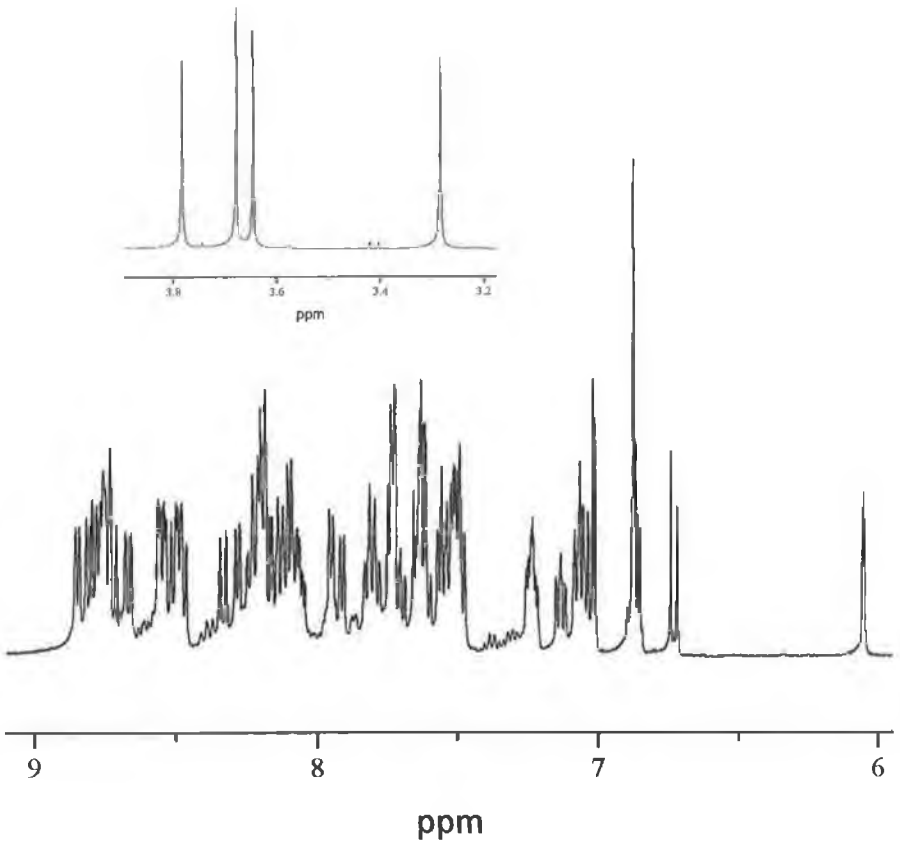

Figure 3.29 ^1H NMR spectrum of $[Ru(bpy)_2(LL6)](PF_6)_2$ in d_6-acetone.

The presence of the conformational isomers is evident from both Figure 3.28 and Figure 3.29. The doubling of the expected number leads to cluttering of the aromatic region and discrete signals are difficult to isolate. The exception is in the spectra of $[Ru(bpy)_2(LL5)](PF_6)_2$. The doublet centred at 6.64 ppm represents the H_1 proton (Figure 3.15) as does the doublet centred at 6.05 ppm. Again, the reason that these peaks are so far upfield is due to the orientation of the phenyl ring in relation to the 2,2'-bipyridyl rings. The proton is again sitting in the ring current of the aromatic 2,2'-bipyridyl unit and this is causing the shielding which leads to the upfield shift. This upfield shift has been typically *circa* 1 ppm for the other protons in the spectra.

There is further evidence of the presence of conformational isomers in the ^1H NMR spectra of $[Ru(bpy)_2(LL6)](PF_6)_2$. Examination of the ligand LL6 (Figure 3.15), indicates that two singlets in the aliphatic region of the ^1H NMR should be evident, each integrating to three protons representing the two sets of three equivalent methoxy protons. As can be seen from Figure 3.29 above, the actual ^1H NMR contains not 2 sets of methoxy protons as expected but 4 sets of methoxy protons, each integrating to 3 protons. These protons further prove the existence of the conformational isomers.

To conclude the ^1H NMR discussion. The complexes of the LL1, LL2, LL3 and LL8 ligands all behave as expected and the protons of the LL_x ligands in the complexes have been assigned. The complications which arise on examination of the ^1H NMR spectra of the complexes of the LL4, LL5 and LL6 ligands can be explained in terms of two different conformations adopted by the phenyl ring on coordination, leading to the formation of two isomers, which can be described as **rotamers**. As can be appreciated, the problems associated with these rotamers needed to be examined further. This is described in Chapter 3.12.

3.7 Absorption and Emission Spectra of the Ligands:

The photophysical, photochemical and electrochemical properties of the complexes have been studied, and provide a picture of the interaction between the LL_x ligands and the metal centre. To understand this interaction better, the UV/Vis and emission spectra of the free ligands in MeCN were recorded. It is hoped that this investigation of the spectroscopic properties of the free ligands will enhance the ability to understand the behaviour of the complexes. The absorption spectra of the LLx ligands are given in Figures 3.30 and 3.31 while the emission spectra are provided in Figures 3.32 and 3.33.

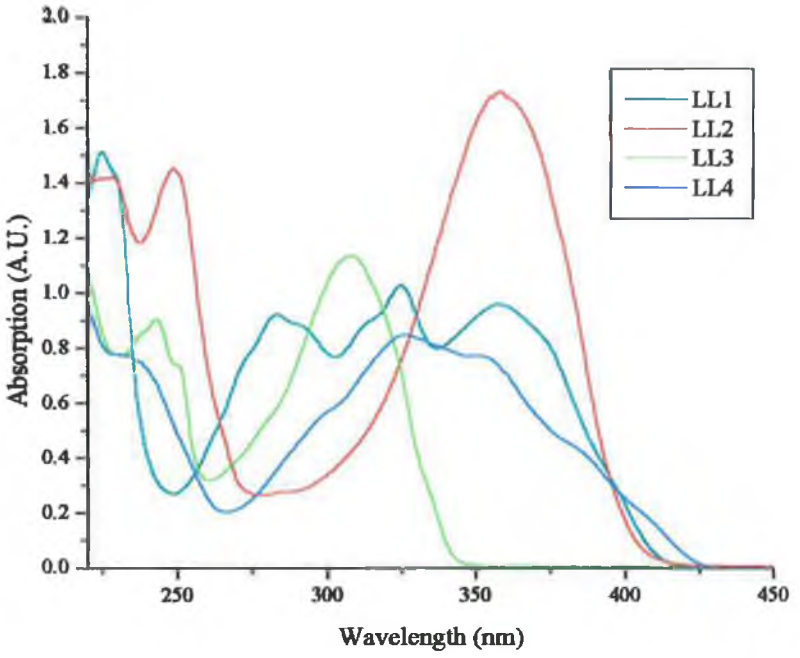

Figure 3.30 UV-visible spectra of the free ligands LL1, LL2, LL3 and LL4 in MeCN.

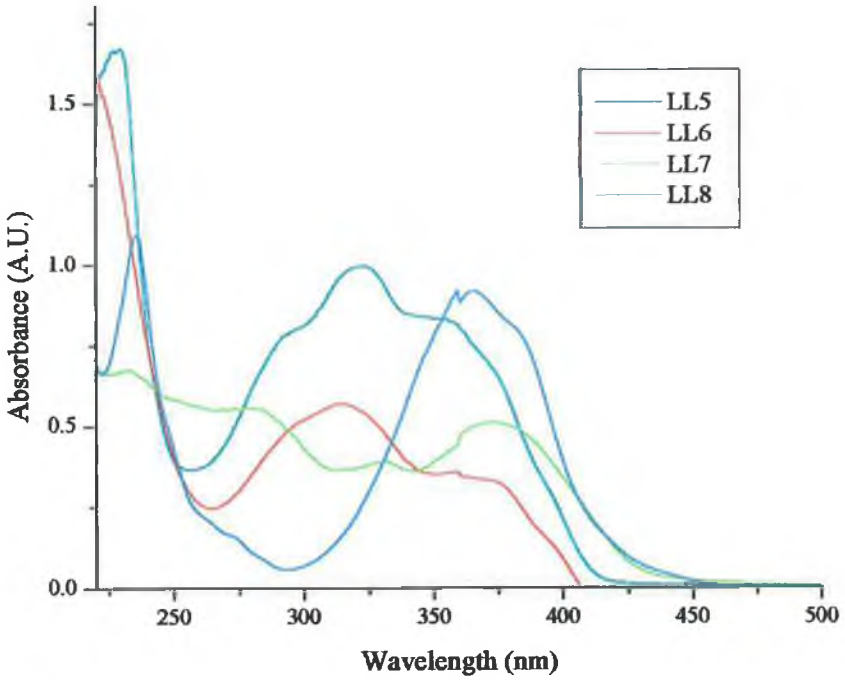

Figure 3.31 UV-visible spectra of the free ligands LL5, LL6, LL7 and LL8 in MeCN.

Ligand	Absorption (λ_{max}) (nm)	Emission (λ_{max}) (nm)
LL1	225, 282, 325, 357	446
LL2	248, 358	448
LL3	243, 308	371
LL4	326, 349	462
LL5	228, 322, 351	449
LL6	315, 361 (sh)	450
LL7	277, 331, 373	456
LL8	236, 365	475

Table 3.17 Table of the absorption and emission data of the free ligands in MeCN.

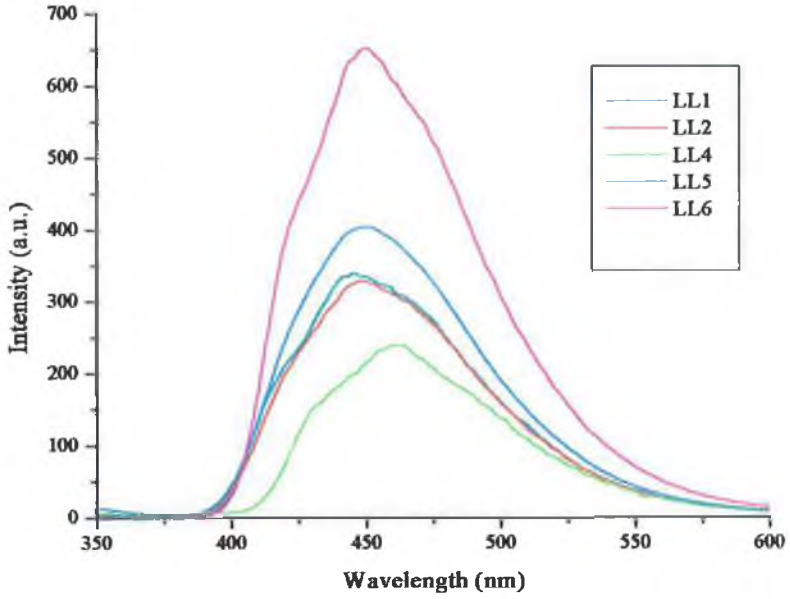

Figure 3.32 Emission Spectra of the free ligands LL1, LL2, LL4, LL5 and LL6 in MeCN. Excitation was in the maximum of absorption.

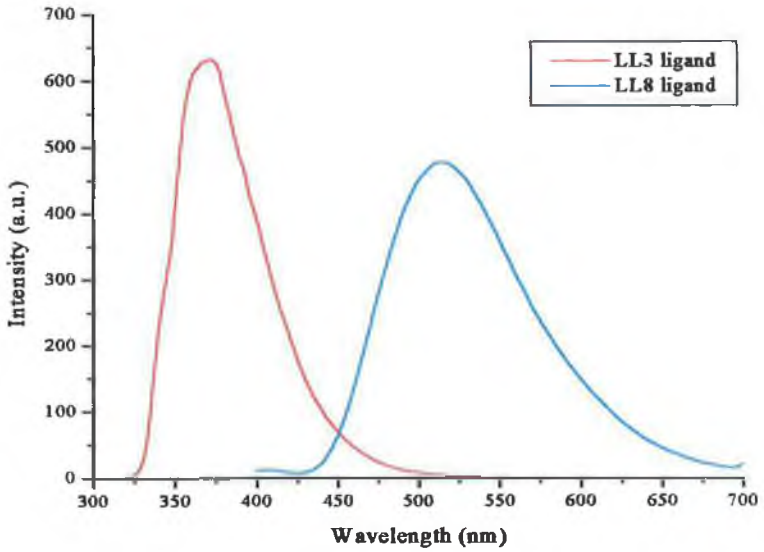

Figure 3.33 Emission Spectra of the free ligands LL3 and LL8 in MeCN. Excitation was performed in the maximum of absorption.

The absorption spectra of the LL_x ligands are dominated by $\pi \rightarrow \pi^*$ transitions. In the case of the LL1 ligand, three peaks are observed. These may correspond to absorption from the three different rings in the molecule (i.e. the two pyridine rings and the five membered imidazo type ring). The absorption spectra of the ligands are unusual in that they absorb in the high energy side of visible region. This becomes important on examination of the absorption spectra of the mixed ligand ruthenium and osmium complexes.

The emission spectra of the ligands are also unusual, and variations in the λ_{max} of the different ligands exist. The λ_{max} of most of the ligands is centred at circa 450 nm, with the exception of the LL3 and LL8 ligands. The LL3 ligand differs from the other LL_x ligand by virtue of the additional nitrogen in the 5 membered ring. The λ_{max} of the LL3 ligand is shifted to higher energy and is centred at 371 nm. The LL8 ligand consists of two fused 5 and 6 membered rings. The emission of this symmetrical ligand is red shifted in comparison to the other LL_x ligands, and its λ_{max} is centred at 475 nm.

The low energies of the absorption and emission spectra of the LL_x ligands may be interpreted in such a way as to presume that the emissive state in the ruthenium bisbipyridyl complex should be based on the LL_x ligands as the energy of the emission from this ligand is low and as has been discussed in Chapter 1.4 (emission occurs from the lowest emitting state). [58] It is important to remember however that the energy of the emission observed for these ligands corresponds only to the difference in energy between the ground and excited states of the ligands and comparison of the energy of this process with for example the emission of 2,2'-bipyridyl is pointless without knowing the relative ground state energies of both compounds. This is investigated further as the photophysics and electrochemistry of the complexes are examined.

3.8 UV/Vis Absorption, Emission Spectroscopy and Luminescence Lifetimes of the Ruthenium (II) Complexes.

The electronic absorption spectra of the parent compound $[Ru(bpy)_3]^{2+}$ and the ligands have already been discussed. (Chapter 1.5 and Chapter 3.7). The absorption spectra of the ruthenium(II) compounds to be discussed are presented in Figures 3.34 and 3.35. The electronic properties of the complexes are listed in Table 3.19.

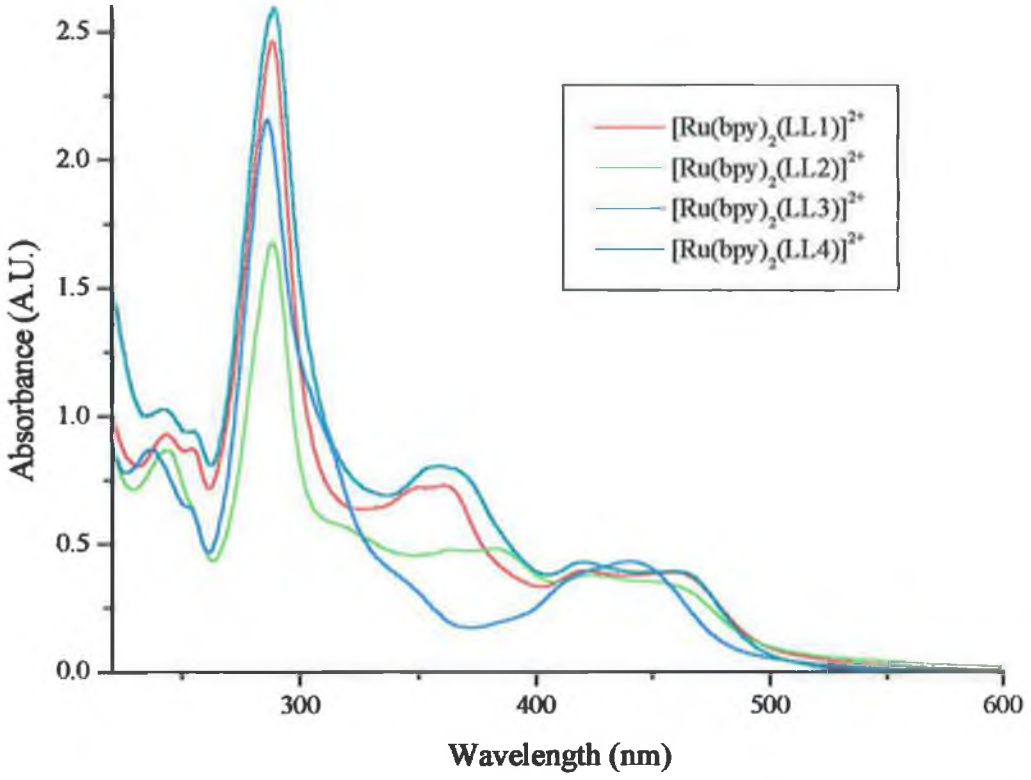

Figure 3.34 Absorption spectra of the listed complexes in MeCN.

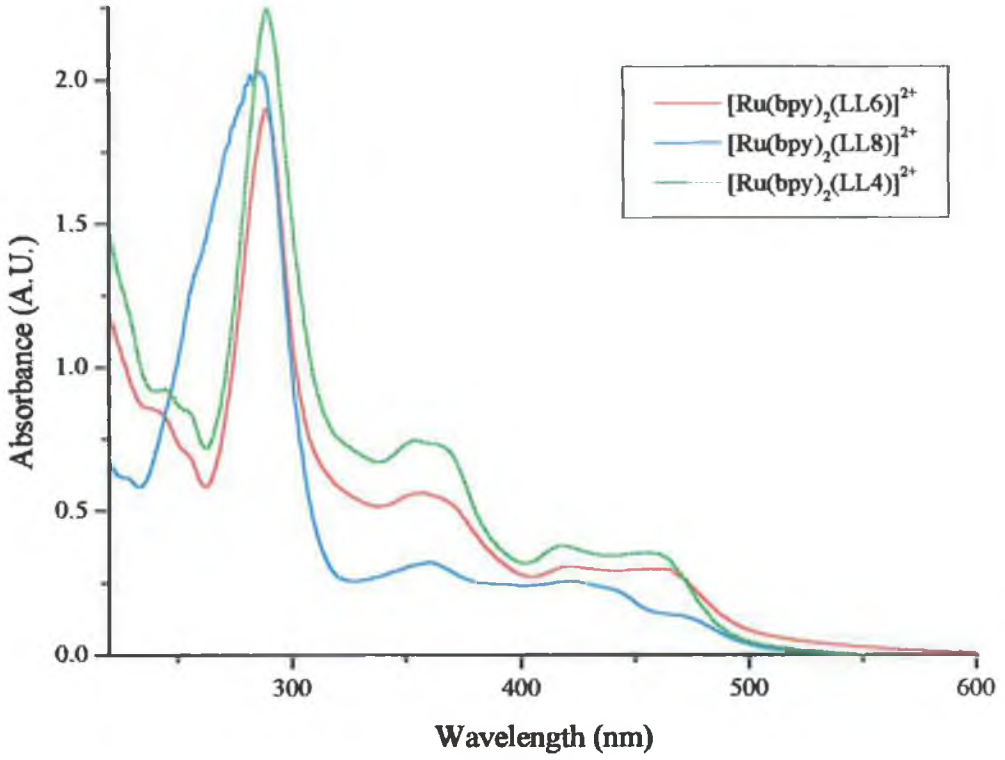

Figure 3.35 Absorption spectra of listed complexes in MeCN.

Figure 3.36 compares the absorption spectra of the complexes $[Ru(bpy)_2(LL1)]^{2+}$, $[Ru(bpy)_3]^{2+}$ and the free LL1 ligand. As well as the normal 2,2'-bipyridyl centred (LC) $\pi \rightarrow \pi^*$ bands (λ_{max} at *circa* 290 nm) a new absorption band in the region 320 nm to 400 nm has appeared. Comparison of this band to the free ligand shows that this band may be attributed to the introduction of the LL1 ligand into the complex and that this band may be attributed to ligand centered (LC) $\pi \rightarrow \pi^*$ transitions on the LL1 ligand. Similar bands are observed in the absorption spectra of the other complexes. (Figure 3.34 and 3.35).

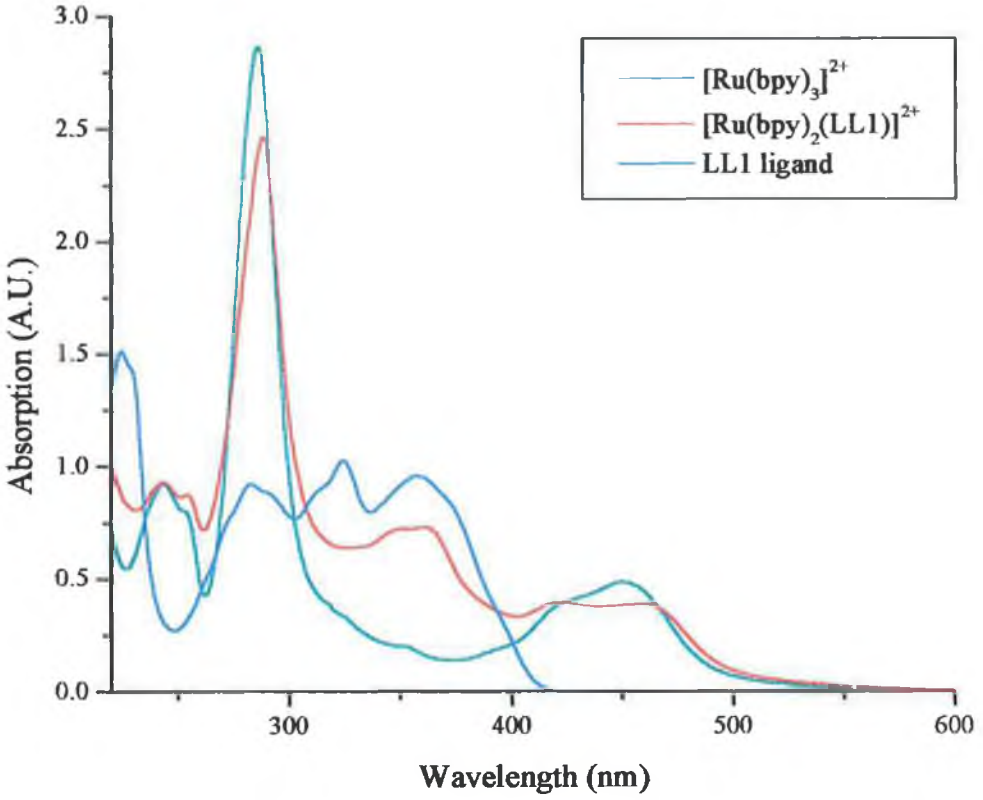

Figure 3.36 Comparison of the absorption spectra of $[Ru(bpy)_3]^{2+}$, $[Ru(bpy)_2(LL1)]^{2-}$ and the free ligand LL1.

The bands which are of most interest in these complexes are the $d\pi \rightarrow \pi^*$ metal to ligand charge transfer bands. These intense bands have extinction coefficients typically in the range of 10^4 $M^{-1}cm^{-1}$. The position of these bands provide information about the electronic structure of the complex.[59] The presence of strong σ-donating results in the ruthenium centre being more electron rich and this causes the MLCT band to be shifted to the red (i.e. to lower energy).[60] As discussed in the introduction to this chapter, similar ruthenium complexes of imidazole, benzimidazole and triazole ligands have absorption spectra whose ^{1}MLCT bands have been shifted to lower energy due to the σ-donating properties of the ligands. Figure 3.37 is a comparison of the absorption spectra of $[Ru(bpy)_3]^{2+}$ with some of the complexes being discussed. Attention is focussed on the ^{1}MLCT bands, which are red shifted slightly for the complexes containing LL_x ligands.

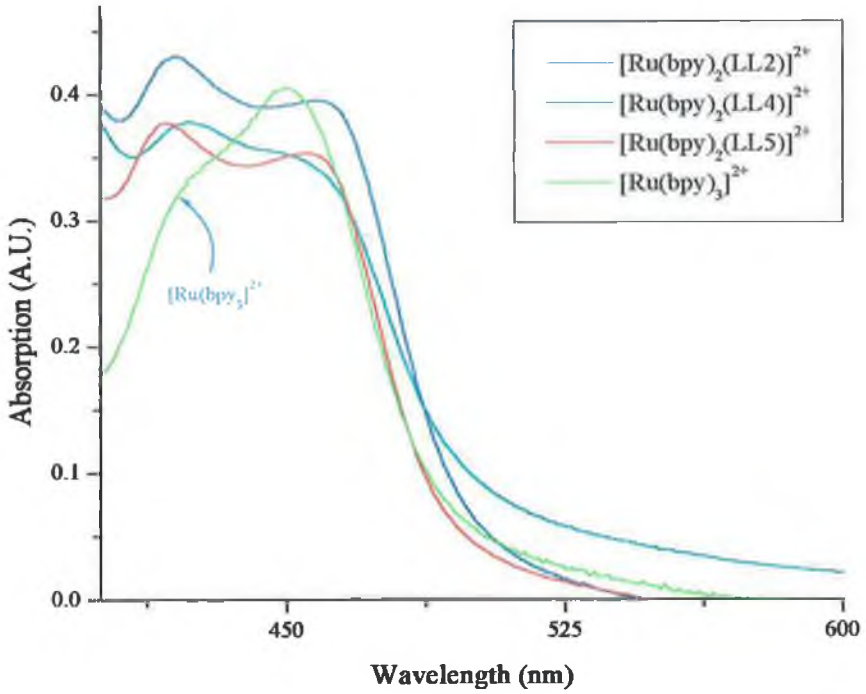

Figure 3.37 Comparison of the position of the MLCT band of selected complexes with $[Ru(bpy)_3]^{2+}$ in MeCN.

Deuteration of the ligands is not expected to have any effect on either the position or the intensity of the MLCT of ruthenium(II) complexes. [63] The extinction coefficients of the $[Ru(d_8\text{-bpy})_2(LL_x)]^{2+}$ complexes have not been measured as they should be the same as for the undeuterated complexes.

Compound	Absorption λ_{max} (nm)	ε ($M^{-1}cm^{-1}$)	Emission, 298K λ_{max} (nm)	Emission, 77K λ_{max} (nm)
$[Ru(bpy)_2(LL1)]^{2+}$	460	10500	630	591
	420	10200		
$[Ru(bpy)_2(LL2)]^{2+}$	453	10100	630	593
	423	10200		
$[Ru(bpy)_2(LL3)]^{2+}$	455	10450	630	572
	420	10100		
$[Ru(bpy)_2(LL4)]^{2+}$	460	10100	640	598
	420	10600		
$[Ru(bpy)_2(LL5)]^{2+}$	456	10200	630	592
	440	9950		
$[Ru(bpy)_2(LL6)]^{2+}$	457	10300	632	596
	422	9800		
$[Ru(bpy)_2(LL8)]^{2+}$	465 (sh)	9900	645	615
	421	9450		

Table 3.18 Electronic Properties of the Ruthenium(II) complexes in MeCN.

The compounds studied exhibit luminescence at room temperature and at 77K. This emission originates from a triplet MLCT state.[60] The emission spectra of the complexes studied can be seen in Figures 3.38-3.41.

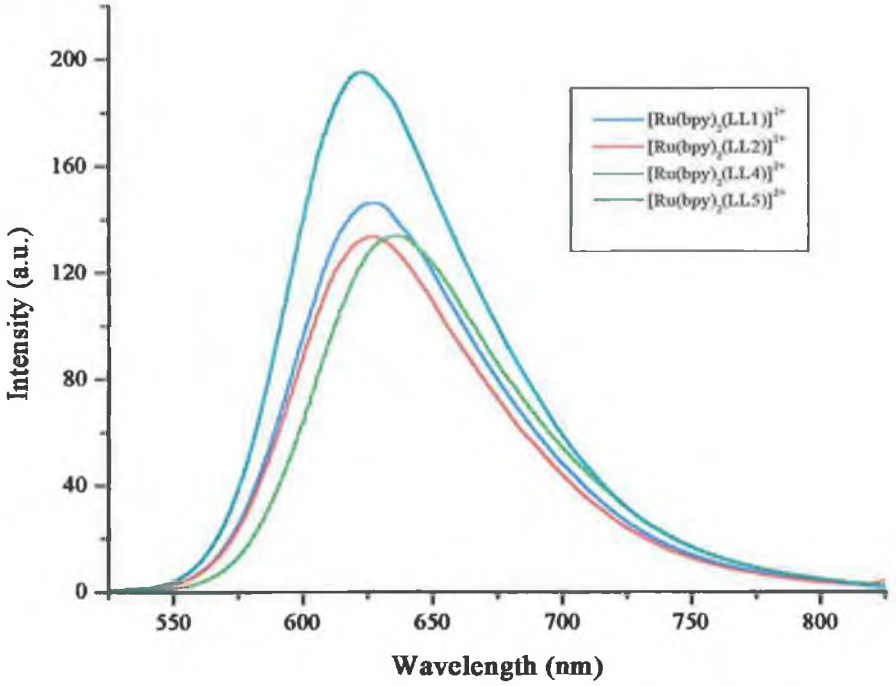

Figure 3.38Emission spectra of the listed complexes in MeCN.

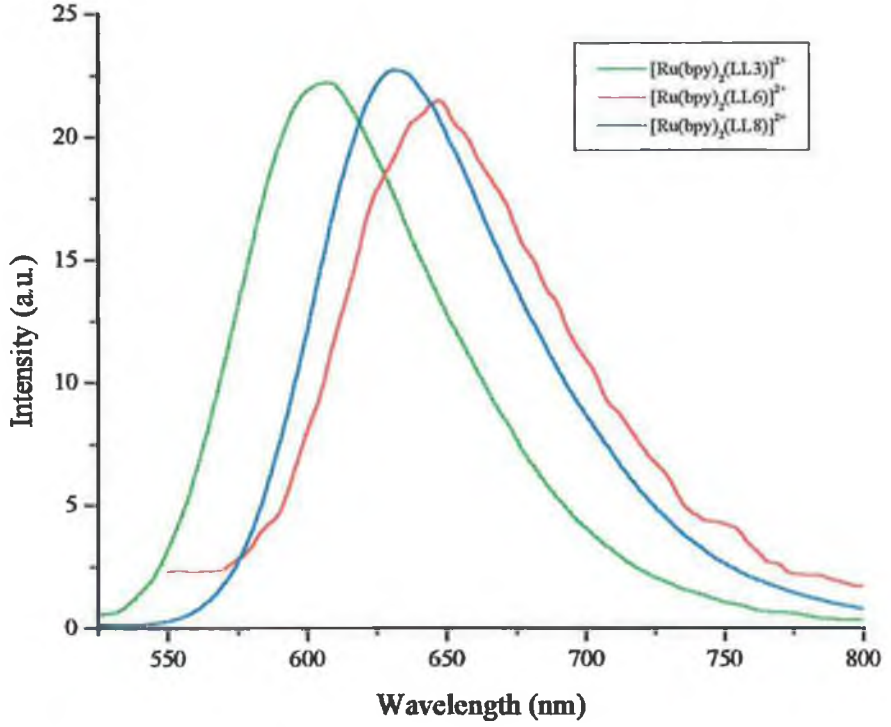

Figure 3.39 Emission spectra of the listed complexes in MeCN.

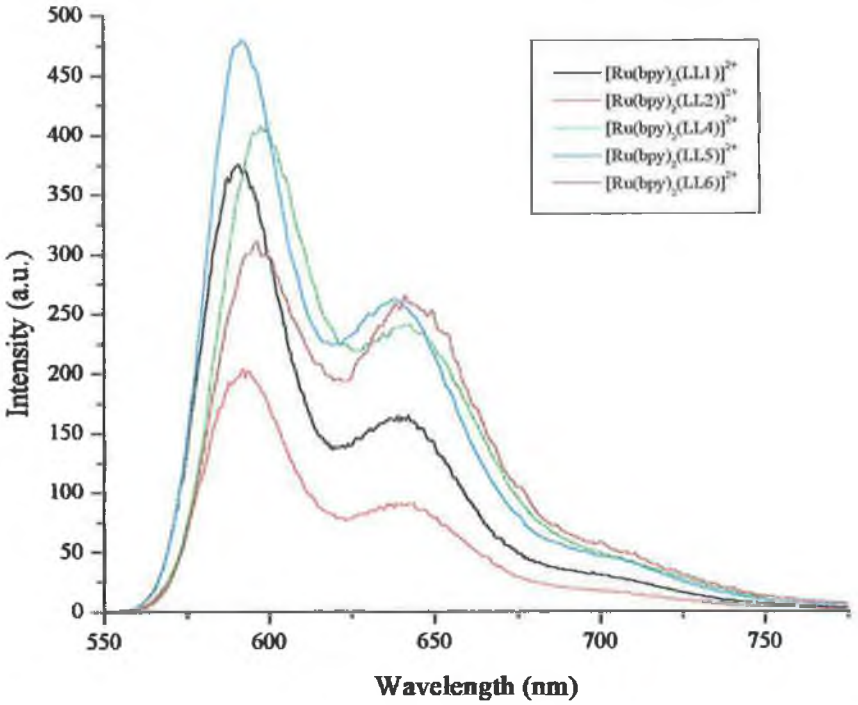

Figure 3.40 Emission of ruthenium complexes at 77K in butyronitrile.

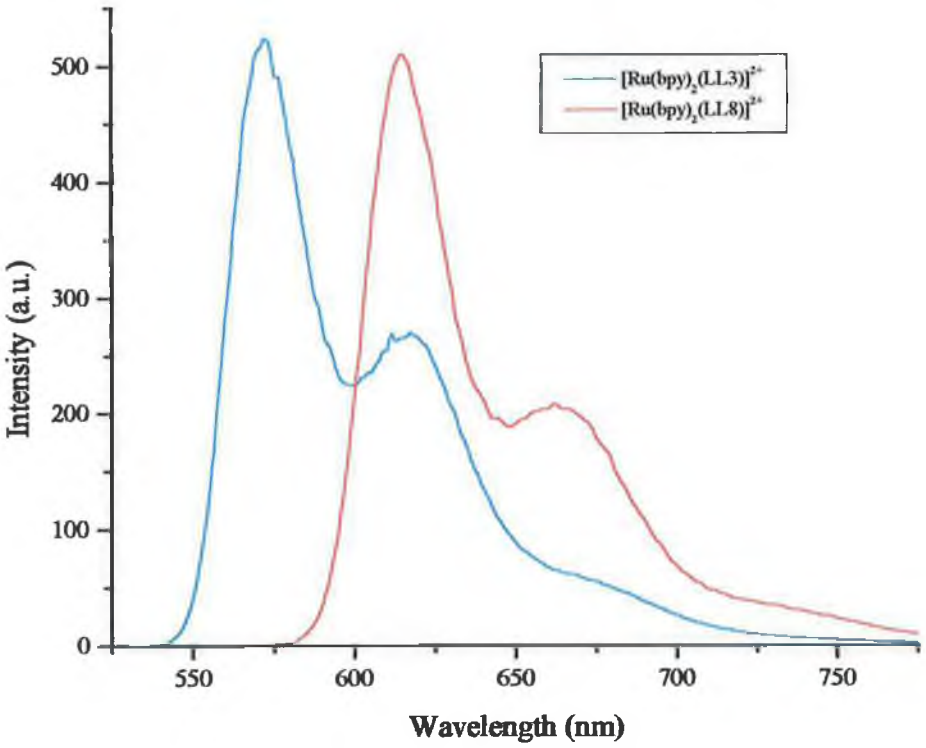

Figure 3.41 Low temperature emission of ruthenium complexes in butyronitrile.

As in the case of the absorption spectra there is a shift of *circa* 15 nm to the red in comparison to $[Ru(bpy)_3]^{2+}$. This shift to lower energy can be explained by the fact that the mixed ligand species now contains a ligand which has a better σ-donating capacity than the bipyridyl ligands in the parent complex $[Ru(bpy)_3]^{2+}$. The new ligands increase the charge on the metal relative to the bipyridyl ligands and the metal to ligand charge transfer process, which is a $d\pi \rightarrow \pi^*$(bpy) process becomes easier and therefore occurs at lower energy.

At 77K, all the complexes exhibit a strong emission with vibrational structure. This vibrational fine structure has been attributed to relaxation via bipyridine-based vibrations [61] and is common for both ruthenium and osmium complexes. Cooling to 77K leads to a blue shift in the emission maxima of the complexes. This shift to higher energy is caused by a phenomenon known as "rigidchromism". [62] In the glass matrix formed at 77K, the solvent dipoles are immobile on the timescale of the excited state, and therefore cannot respond to the change in electronic configuration between the ground and excited state of the molecule. The increase in intensity is attributable to several factors, the first of which is solvent dependent. At 77K the environment in which both the solvent and complex are held is rigid, preventing deactivation of the excited state by vibronic coupling to low frequency, high amplitude Ru-N vibrations which contribute to radiationless decay. Another factor to note is the population of the ^{3}MC level which can act as a deactivation pathway for the excited state. The ^{3}MC state cannot be populated at 77K (it is a thermally populated energy level), which also leads to an increase in the intensity of the emission at 77K. Finally, quenching by O_2 is considerably reduced at 77K as diffusion of oxygen to the excited state is restricted.

Having shown that the complexes emit at both room temperature and at 77K, the nature of this emitting state was investigated. Deuteration of the 2,2'-bipyridyl ligand and the subsequent use of this deuterated ligand to synthesise the mixed ligand complexes containing the LL_x ligands have allowed the nature of the emissive state to be determined. The synthesis of the deuterated complexes are detailed in Section 3.2.

Deuteriation has been used as a tool for the study of the photophysical properties of organic and inorganic systems since the 1960s. [63] The effect of solvent deuteriation has been of most interest, but the effect of ligand deuteriation has also been studied in order to increase lifetimes and improve the quantum yield of complexes. In the area of supramolecular chemistry this has proved to be very useful as often complex molecular assemblies are involved.

For aromatic compounds, both the S_0 and T_1 states are $\pi \rightarrow \pi^*$ in nature and therefore out of plane C-H bending modes would be potential channels for radiationless decay. Deuteration reduces both the amplitude and the frequency of C-H vibrational modes and therefore C-D vibrations are of a lower frequency and amplitude than the equivalent C-H vibrations which results in an increase in the observed lifetime of the electronically excited state. This is more pronounced for free aromatic compounds than for transition metal complexes since the excited state of the complexes are generally more distorted with respect to the ground state and hence lower frequency vibrational modes, such as ring breathing, are more important.

It was hoped therefore that a comparison of the lifetimes of both the undeuterated complexes and the deuterated complexes may yield information on the nature of the excited state. The results of this analysis is listed in Table 3.19.

The emission quantum yields of the complexes are also given in Table 3.19. The values range from 0.6×10^{-3} to 1.0×10^{-3}. The reference used to calculate these is $[Ru(bpy)_3]^{2+}$ (whose emission quantum yield is 1.2×10^{-3}.)

Complex	298K (aerated solution)		298K (deaerated) [a]		77K
	τ (ns)	Φ x 10^{-3} [c]	τ (ns)	Φ x 10^{-3} [c]	τ (μs)
$[Ru(bpy)_2(LL1)]^{2+}$	122	1	801	3.1	6
$[Ru(d_8\text{-bpy})_2(LL1)]^{2+}$	128	1	1050	4.4	N/A
$[Ru(bpy)_2(LL2)]^{2+}$	116	0.95	758	4.1	5.54
$[Ru(bpy)_2(LL3)]^{2+}$	128	0.8	970	4.6	6.4
$[Ru(bpy)_2(LL4)]^{2+}$	134	0.8	872	3.3	5.67
$[Ru(d_8\text{-bpy})_2(LL4)]^{2+}$	140	0.8	980	4.1	N/A
$[Ru(bpy)_2(LL5)]^{2+}$	165	1.1	902	3.8	5.6
$[Ru(bpy)_2(LL6)]^{2+}$	151	0.8	789	3.7	5.25
$[Ru(bpy)_2(LL8)]^{2+}$	95	0.6	502	3.1	4.75

[a] *Compounds degassed with argon.*

[b] *Lowest energy absorption bands.*

[c] *Reference is $[Ru(bpy)_3]^{2+}$ in acetonitrile.*

Table 3.19 Results of Emission Lifetime Experiments

The lifetimes of the complexes in degassed acetonitrile lie between 500 ns for the $[Ru(bpy)_2(LL8)](PF_6)_2$ complex and 970 ns for the $[Ru(bpy)_2(LL3)](PF_6)_2$. This compares to the value of 1000 ns for $[Ru(bpy)_3]^{2+}$. The undeuterated complex $[Ru(bpy)_2(LL1)](PF_6)_2$ has a lifetime of 122 ns in aerated acetonitrile. The lifetime of the compound in deaerated acetonitrile was measured as 800 ns. The lifetime for this deuterated complex in aerated acetonitrile was 128 ns while the lifetime for the complex in deaerated acetonitrile was found to be 1050 ns. The same increase is observed for the deuterated analogue of the $[Ru(bpy)_2(LL4)]^{2+}$ complex. In deaerated MeCN the lifetime

is 870 ns, while the lifetime of the deuterated complex is 980 ns. These increases of *circa* 20% in the lifetimes of complexes containing deuterated 2,2'-bipyridyl ligands indicates that the emitting state is most likely 2,2'-bipyridyl based on the mixed ligand complexes, and the emission does not originate from the LL_x ligands. The increase in lifetime has occurred for the compound with the deuterated 2,2'-bipyridyl ligands.

In answering whether the emitting state is localised on the bipyridyl ligand or located on one of the ligands it should be realised also that deuteration is not the only tool used to assign the excited state. It is important at this stage to mention the relationship that has been established between the electrochemical potentials and both the absorption and emission maxima. [60,64]

In a MLCT process, an electron is removed from the filled metal orbital to an empty ligand orbital ($d\pi \rightarrow \pi^*$). Oxidation is also the removal of an electron from the d-orbitals while upon reduction, an electron is added to the lowest unoccupied molecular orbital (LUMO) of the complex. This also helps to explain what happens in an MLCT process. By probing the energy of the LUMO using electrochemical means, this provides information about the nature of the emissive state. From the electrochemical measurements obtained for the mixed ligand complexes, the first two reduction potentials appear to be directed to the two 2,2'-bipyridyl ligands. (This is discussed further in Chapter 3.10). This indicates that the π^* levels of the 2,2'-bipyridyl ligands are lower in energy than those of the new ligand. It is expected, therefore, that for the mixed ligand complexes that the observed emission is 2,2'-bipyridyl-based.

3.9 Photochemistry of the complexes:

It was noticed during the characterisation of the complexes, that the samples very often changed colour on exposure to light. This is not an uncommon occurrence, the photochemistry and photodecomposition of $[Ru(bpy)_3]^{2+}$ has been well documented, [65, 66] The photochemistry of the complexes were examined by UV/Vis spectroscopy and ^1H NMR. The results of this analysis are presented in Figures 3.42 and 3.43.

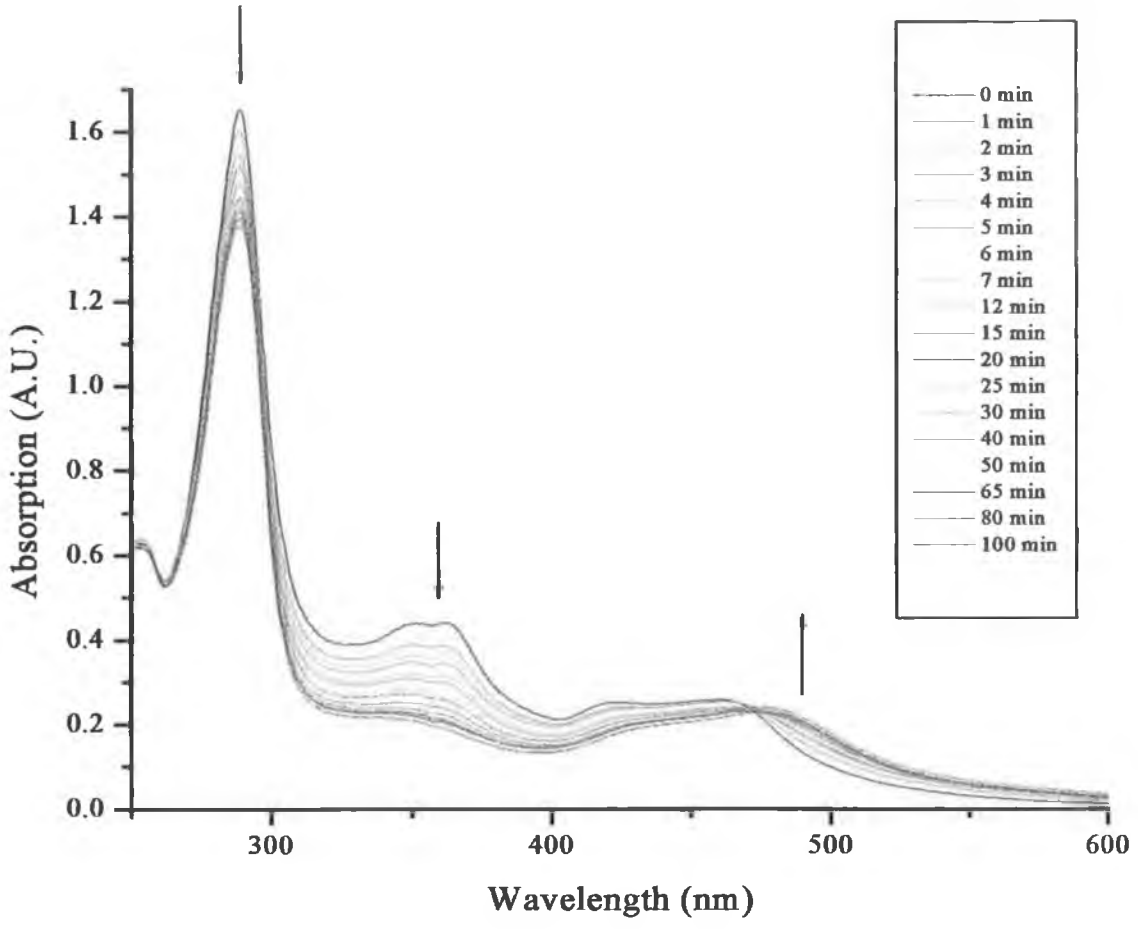

Figure 3.42 Photochemistry of the $[Ru(bpy)_2(LL1)]^{2+}$ complex in MeCN.

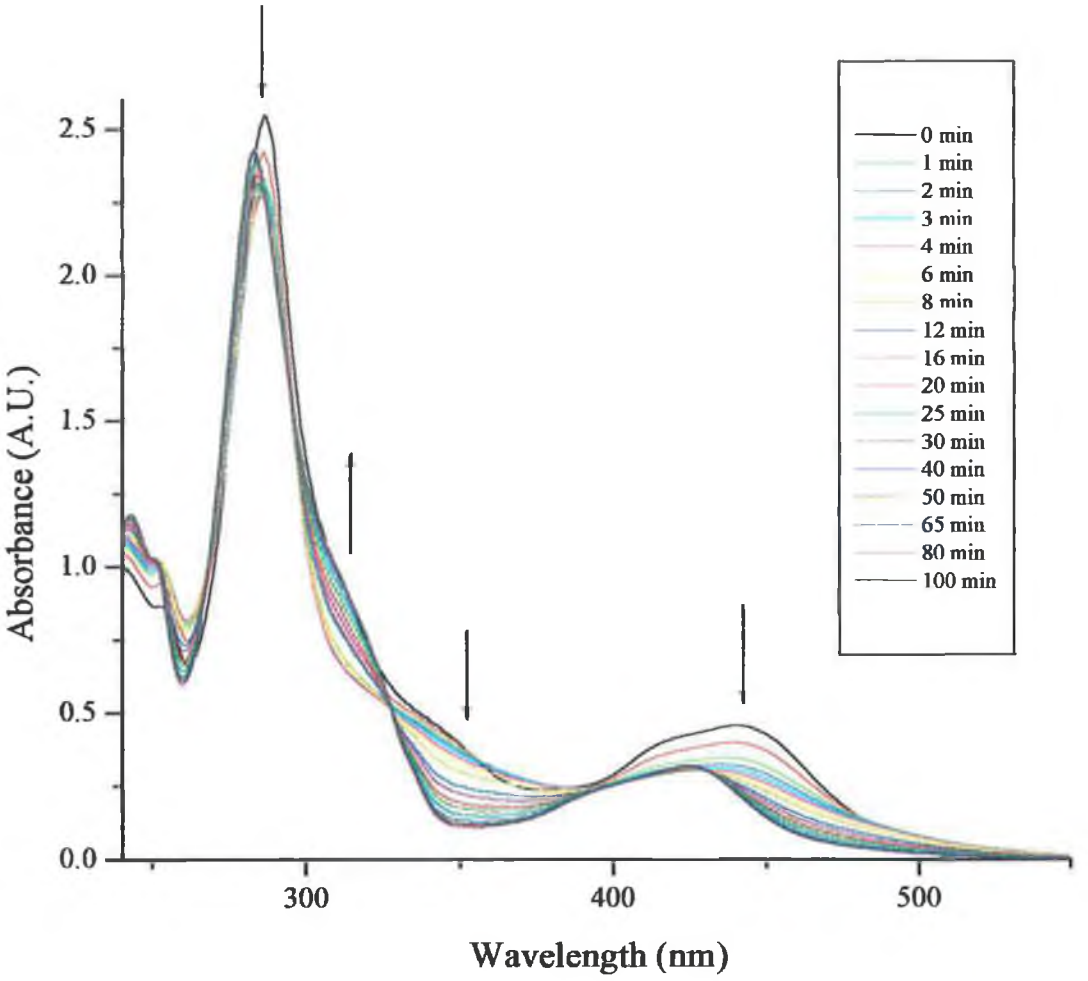

Figure 3.43 Photochemistry of the $[Ru(bpy)_2(LL3)]^{2+}$ complex in MeCN.

The two complexes studied were $[Ru(bpy)_2(LL1)]^{2+}$ and $[Ru(bpy)_2(LL3)]^{2+}$. It was felt that it was important to examine both an imidazo and a triazo containing ligand. It is obvious that changes have occurred, and these changes have occurred on a relatively short timescale (less than 100 min). There are slight changes in the intensity of the $\pi \rightarrow \pi^*$(bpy) bands, but the real differences occur in the ligand centred $\pi \rightarrow \pi^*$ of the LL1 and LL3 ligands which seems to collapse and in the MLCT bands of both complexes which change in both intensity and position. The changes in the region from 250 nm to 400 nm is discussed later, but first the changes to the ^{1}MLCT band should be examined.

The ^{1}MLCT band of the $[Ru(bpy)_2(LL1)]^{2+}$ and the $[Ru(bpy)_2(LL3)]^{2+}$ complex is affected differently on irradiation of the sample. The band is shifted to lower energy in the $[Ru(bpy)_2(LL1)]^{2+}$ complex (from a λ_{max} of 460 nm to λ_{max} of 476 nm). The opposite is the case for the $[Ru(bpy)_2(LL3)]^{2+}$ complex where the λ_{max} is shifted to higher energy (from 455 nm to 427 nm). This shift to lower energy produces a spectrum similar to that of the complex $[Ru(bpy)_2(MeCN)_2]^{2+}$, which has a λ_{max} at 425 nm. [67] This is consistent with the photolysis leading to the loss of the LL3 ligand with subsequent replacement by MeCN. This mechanism does not explain the behaviour of the $[Ru(bpy)_2(LL1)]^{2+}$ complex however.

The bands from 250 nm to 400 nm have been assigned to transitions on the LL_x ligands. It was decided therefore that the photochemistry of the LL1 and LL3 ligands needed to be examined. The results of this examination are presented in Figure 3.44.

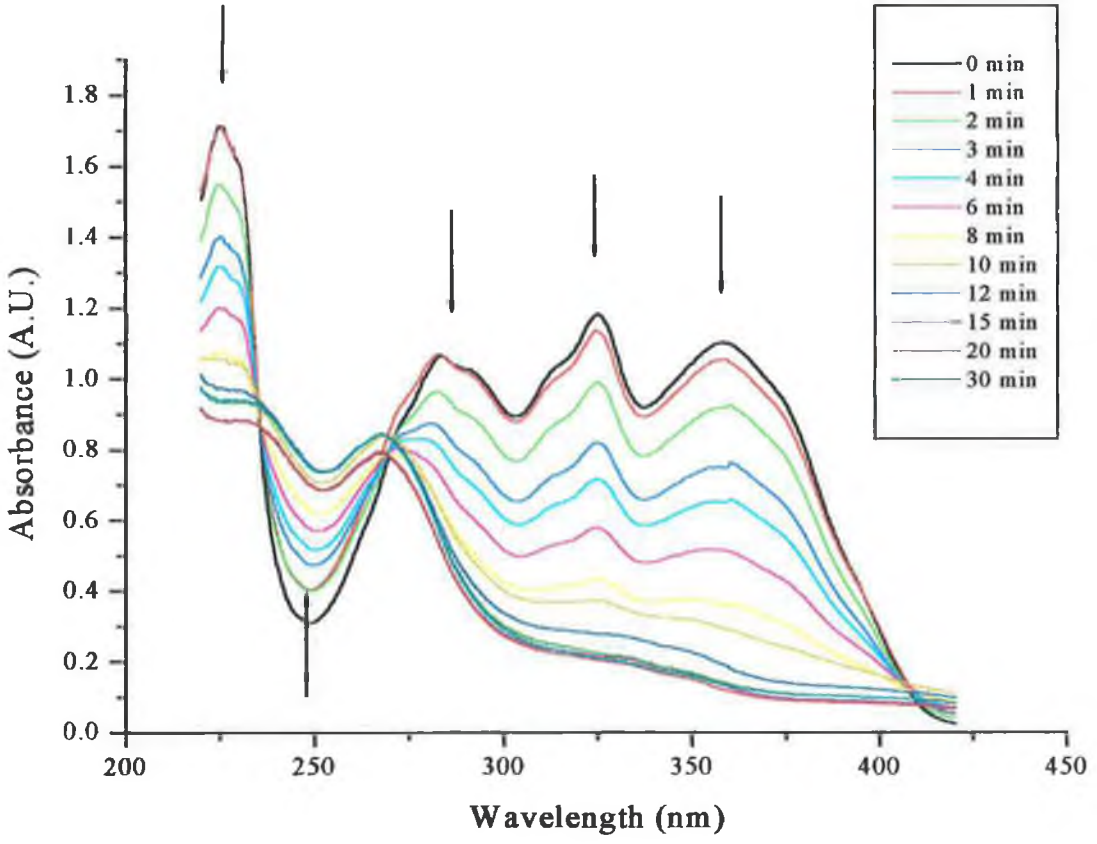

Figure 3.44 Photochemistry of the LL1 ligand in MeCN.

No photochemistry was observed for the LL3 ligand over a similar timescale. The photochemistry exhibited by the LL1 ligand was surprising. The presence of the isosbestic point at 270 nm indicates that the photochemistry may result in the growth of a single photoproduct, however as the isosbestic point is not very well defined, it is not possible to rule out the presence of more than two species in the solution. It was decided to follow this process by ^{1}H NMR. As before, the sample was dissolved in d_3-MeCN and placed in a quartz cuvette which was irradiated by a 100W slide projector. Samples were taken from this solution in order to perform the NMR experiments. The photochemistry of the $[Ru(bpy)_2(LL1)]^{2+}$ complex was also followed by ^{1}H NMR.

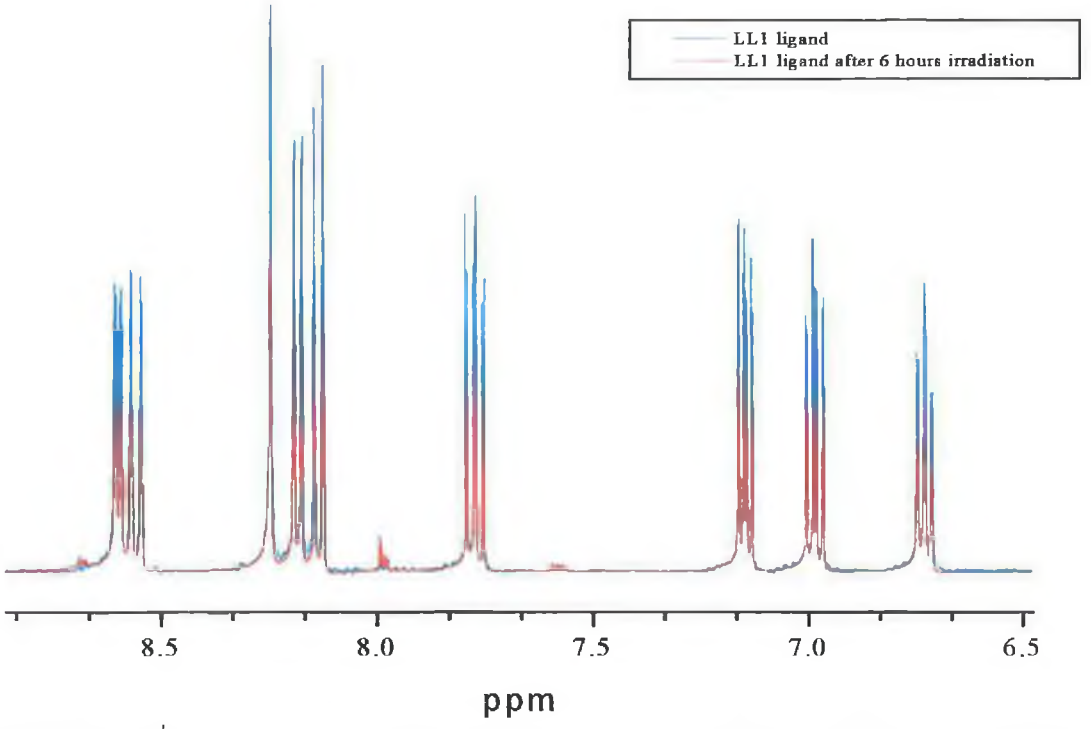

Figure 3.45 ^{1}H NMR spectra of the LL1 ligand in d_3-MeCN before (blue) and after 6 hours irradiation (red).

As can be seen from Figure 3.45, the examination of the photodecomposition of the LL1 ligand by ^{1}H NMR merely shows a decrease in the intensity of the signals, but does not indicate the change in structure which is expected on examination of the UV/Vis data. This result was surprising, but may be due to the differences in concentration between the two experiments. In order to perform the ^{1}H NMR experiment, the concentration of

the sample must be high, whereas this is not the case in the UV/Vis experiment. Changes in the aliphatic region were noted also in the ^1H NMR of the irradiated sample. These changes however appear to be solvent related.

Examination of the photolysis of the $[Ru(bpy)_2(LL1)]^{2+}$ complex by ^1H NMR yielded the expected changes in the spectra. The results of this analysis is presented in Figure 3.46.

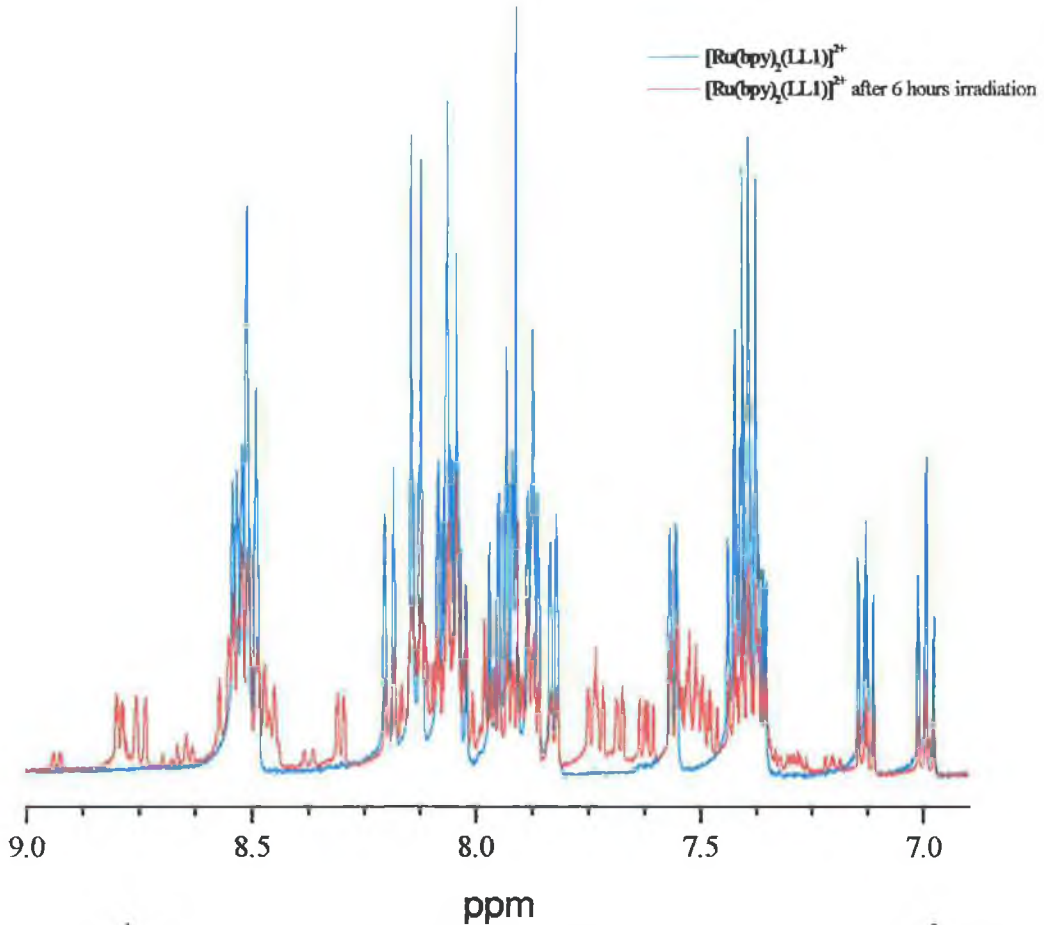

Figure 3.46 ^1H NMR of the aliphatic region of the complex $[Ru(bpy)(LL1)]^{2+}$ in d_3-MeCN before (blue) and after 6 hours irradiation (red).

The differences between the before (blue) and after (red) spectra in Figure 3.46 are quite pronounced. Coupled to the decrease in intensity of the signal, a number of additional peaks have formed. This growth has been followed over time (only the initial and final spectra have been included). Assignment of the spectrum is complicated, and the nature of the photoproducts has not been revealed by this experiment.

The photochemistry of these complexes is discussed and explained further in the next chapter (Chapter 4.7) with emphasis on the comparison of the photochemistry of the osmium complexes to those presented here.

3.10 Electrochemistry of the ligands:

It was realised during the electrochemical analysis of the ruthenium complexes that the LL_x ligands are electrochemically active in the oxidative region being examined. For this reason the electrochemical properties of the free LL_x ligands has been investigated.

Complete electrochemical analysis of each of the LLx ligands has not been performed. This is due to the insolubility of the LL4, LL6 and LL7 ligands in a suitable solvent in concentrations that would provide reproducible results. The analysis of the LL1, LL2, LL3, LL4 and LL8 ligands is discussed in this section. Illustrative cyclic voltammograms are presented in Figures 3.47 and 3.48.

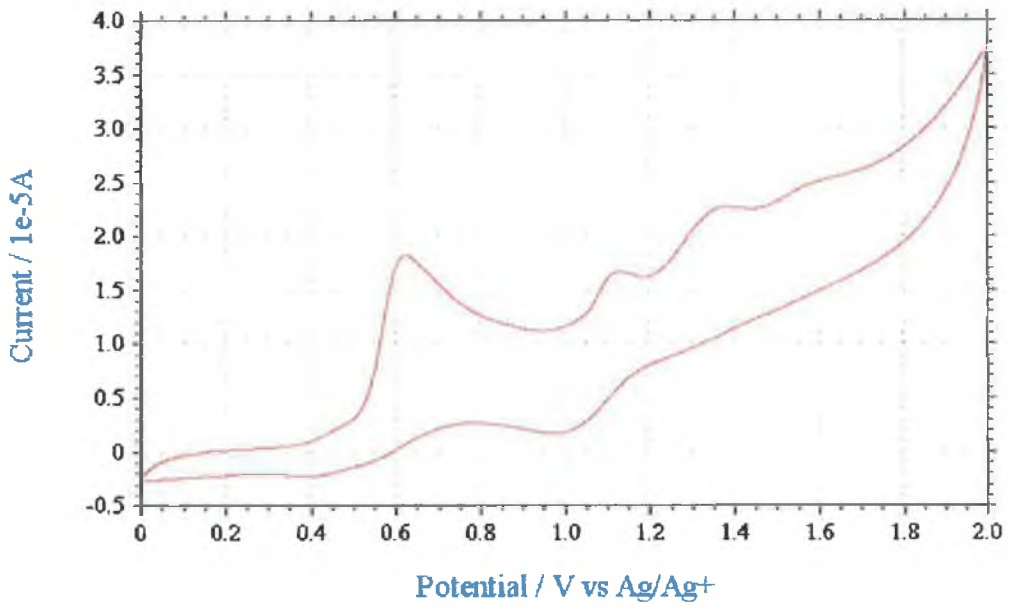

Figure 3.47 Illustrative CV of the oxidation potentials of the LL1 ligand in MeCN with 0.1M $TBABF_4$.

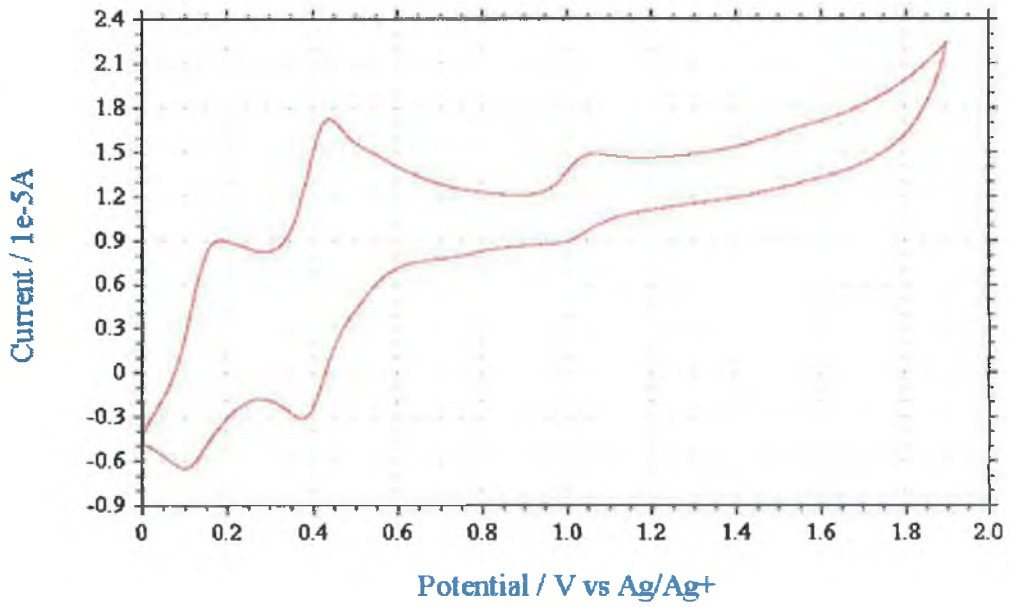

Figure 3.48 CV of the oxidation potentials of the LL8 ligand in MeCN with 0.1M $TBABF_4$.

Figures 3.47 and 3.48 present the oxidative behaviour of the free LL1 and LL8 ligands in MeCN. As in all the electrochemistry discussed in this thesis, the reference electrode used during the experiment was Ag/Ag^+. This reference electrode has been calibrated versus ferrocene at the end of each days experiments. The CVs presented in Figures 3.49, 3.50 and 3.51 present the oxidation potentials *vs* Ag/Ag^+ whereas the tabulated data throughout this thesis present the data *vs* Fc/Fc^+.

Compound	Oxidation Potentials ($E_{1/2}$) V *vs* Fc/Fc^+
LL1	0.52, 1.02, 1.26
LL2	0.49, 0.98
LL3	1.20
LL4	0.55, 1.15
LL8	0.15, 0.34

Table 3.20 Oxidation potentials of the LL1, LL2, LL3, LL4 and LL8 ligands in MeCN with 0.1M TBABF4 as supporting electrolyte.

Table 3.20 lists the oxidation potential of the free ligands that were soluble in the electrolyte. No reduction potentials were observable in the potential window available. The multiple oxidation potentials present for the free ligands indicate the ligands are electron rich species. This study will help to explain the electrochemistry of the ruthenium(II) bisbipyridyl complexes, although it should be remembered that coordination will alter the electron density of the LL_x ligands.

3.11 Electrochemistry of the ruthenium(II) complexes:

Many electrochemical investigations on mononuclear and polynuclear ruthenium(II) complexes containing polypyridyl ligands have been previously reported and some relevant data has already been discussed in Chapter 3.1. From these studies it is generally accepted that oxidation processes are metal-centred while reduction processes are ligand centred. Surprisingly, however for the complexes reported in this section

several oxidation potentials are present for each of the ruthenium(II) complexes studied. This is an unusual characteristic, and is likely a property related to the LL_x ligands. (Section 3.10) This observation will be examined in the following section.

The complex $[Ru(bpy)_3]^{2+}$ is again used as a comparison for the results achieved during the electrochemical analysis of the compounds. It was therefore important to perform the electrochemistry of $[Ru(bpy)_3]^{2+}$ under the same experimental conditions as those used for the other complexes, to allow for direct comparison. The results of the experiments on $[Ru(bpy)_3]^{2+}$ can be found in the diagram Figure 3.49, while Figure 3.50 illustrates the redox potentials observed for the complex $[Ru(bpy)_2(LL3)]^{2+}$. The anodic region of the cyclic voltammogram features a reversible metal-centered oxidation, while the cathodic region exhibits three very clearly defined waves. The first two waves (i.e. the least negative waves) result from the reduction of both of the coordinated 2,2'-bipyridyl ligands while the third results from the reduction of the LL3 ligand.

The width of the potential window is illustrated clearly by these experiments. The potential window can be substantially widened once precautions are taken to ensure the purity and especially the dryness of the apparatus, solvent and compounds being used to perform the experiment.

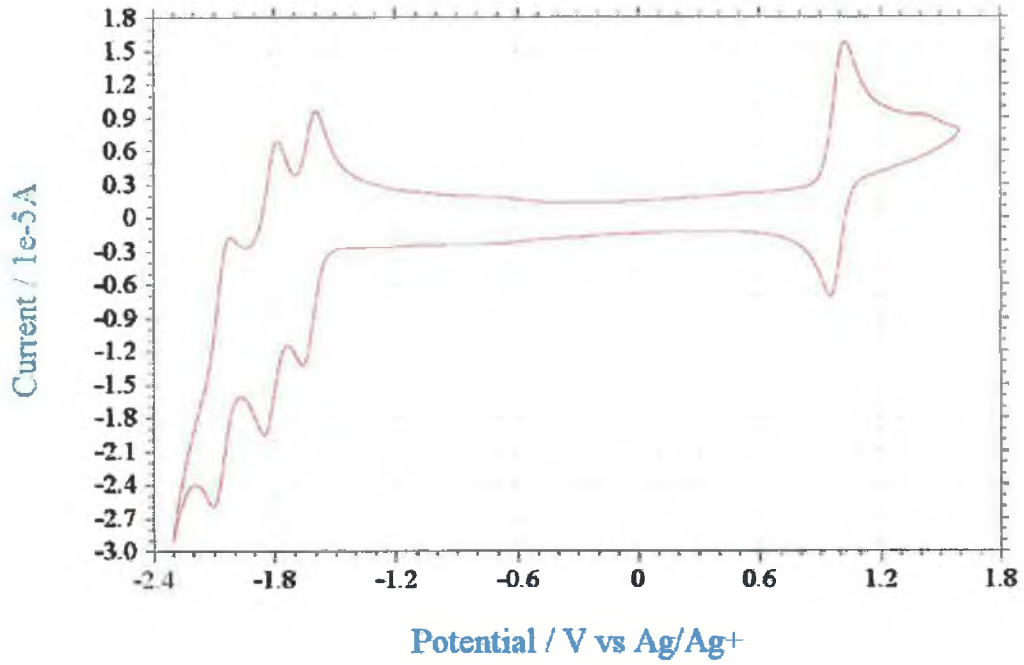

Figure 3.49 CV of $[Ru(bpy)_3]^{2+}$ in MeCN with 0.1M $TBABF_4$.

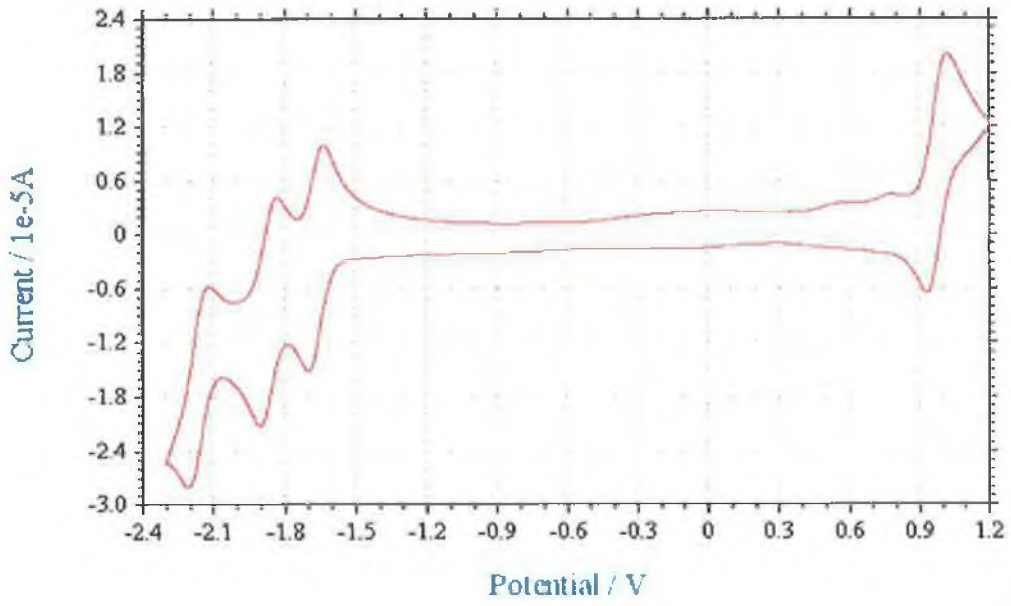

Figure 3.50 Oxidation and reduction potentials of the complex $[Ru(bpy)_2(LL3)]^{2+}$ in MeCN with 0.1M $TBABF_4$.

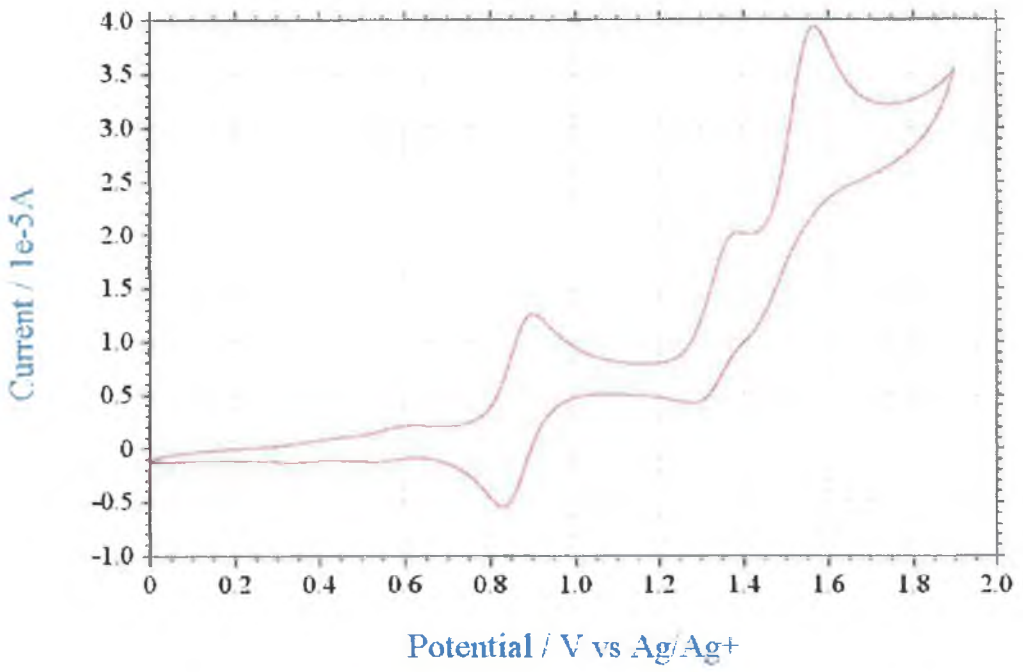

Figure 3.51 Oxidation potentials of the complex $[Ru(bpy)_2(LL6)]^{2+}$ in MeCN with 0.1M $TBABF_4$.

Figure 3.51 provides a good example of the additional oxidation potentials being observed for these complexes. A table of the results of the electrochemical analysis of all the ruthenium(II) bipyridyl complexes in the series is presented in Table 3.21.

The potentials of the metal based $Ru^{(II)}/Ru^{(III)}$ oxidation are taken as being the lowest oxidation potential observed for the complexes listed in Table 3.21 except in the case of $[Ru(bpy)_2(LL8)]^{2+}$ which appears to have a ligand based oxidation wave as the lowest potential. This follows from the electrochemical study of the free ligands. The oxidation waves observed for the LL8 ligand were circa 300 mV lower than for the corresponding LLx ligands. Defining the reversibility of electrochemical processes is complicated, but in this case, based on the assumptions derived from the Nernst equation the reversibility of the process is based on whether the system is thermodynamically or electrochemically reversible. [68] This information can be extracted for each wave in the voltammogram by examining the difference between the anodic and cathodic peak currents. Assuming

Nernstian behaviour, a system with peak to peak separation of between 60 and 100mV is considered reversible. [69]

Compound	Oxidation Potentials, $E_{1/2}$	Reduction potentials, $E_{1/2}$. Ligand based.
$[Ru(bpy)_3]^{2+}$		-1.82 (69)
	0.88 (69)	-2.01 (64)
		-2.26 (89)
$[Ru(bpy)_2(LL1)]^{2+}$	0.78 (83)	-1.79 (64)
	1.36 (irr)	-2.01 (97)
$[Ru(bpy)_2(LL2)]^{2+}$	0.77 (73)	-1.77 (72)
	1.21 (irr)	-1.99 (85)
$[Ru(bpy)_2(LL3)]^{2+}$		-1.76 (67)
	0.87 (76)	-1.96 (78)
	1.97 (irr)	-2.27 (110)
$[Ru(bpy)_2(LL4)]^{2+}$	0.82 (150)	-1.82 (67)
	1.79 (irr)	
$[Ru(bpy)_2(LL5)]^{2+}$	0.81 (77)	-1.77 (78)
	1.22(irr)	-2.02 (161)
	1.43 (irr)	
$[Ru(bpy)_2(LL6)]^{2+}$	0.77 (69)	-1.80 (74)
	1.29 (irr)	-2.07 (82)
	1.46 (irr)	
$[Ru(bpy)_2(LL8)]^{2+}$	0.41 (67)	
	0.73 (75)	-1.70 (69)
	1.38 (irr)	-1.93 (88)
	1.71 (irr)	

Table 3.21 Oxidation and reduction potentials for the ruthenium(II) complexes in MeCN with 0.1M $TBABF_4$ (V vs Fc/Fc^+).

The $Ru^{(II)}/Ru^{(III)}$ potentials are all lower than the oxidation potential found for $[Ru(bpy)_3]^{2+}$ performed under similar experimental conditions. (Table 3.22). This agrees with the analysis of the photophysical results and indicates that the metal ion has more electron density, which is caused by the ligand being either a strong σ-donating or weak π-accepting ligand. Comparison of this with the complexes discussed in Chapter 3.1 are in agreement with this supposition. The similarities in structure between the LL_x ligands and ligands such as imidazole, bisimidazole and bisbenzimidazole indicated that the ligands should be σ-donating and this is indeed the case. The results for some of these similar ruthenium(II) complexes and those achieved for the $[Ru(bpy)_2(LL_x)]^{2+}$ complex are compared in Table 3.22.

Compound	$E_{1/2}$, V *vs* Fc/Fc$^+$	
	Oxidation	Reductions
$[Ru(bpy)_2$**(LL1)**$]^{2+}$	+0.78	-1.82
		-2.01
$[Ru(bpy)_2$**(PbzImH)**$]^{2+}$	+0.79	-1.87
		-2.14
$[Ru(bpy)_2$**(PimH)**$]^{2+}$	+0.76	-1.90
		-2.16
$[Ru(bpy)_2$**(BiBzImH$_2$)**$]^{2+}$	+0.74	-1.98
		-2.28
$[Ru(bpy)_2$**(BiImH$_2$)**$]^{2+}$	+0.68	-2.04
		-2.34

Table 3.22 Comparison of the redox potential of $[Ru(bpy)_2(LL1)]^{2+}$ with the protonated complexes of some of the ligands studied by Haga et al. [2,3,6]

Table 3.22 indicates clearly that the σ-donating ability of the LL1 ligand is comparable to that of the PbzImH and PimH ligands, but not as strongly donating as the $BiImH_2$ ligands. The oxidation potentials of these ligands move cathodically in the order $BiImH_2$ > $BiBzImH_2$ > PimH > PbzImH > bpy, and the LL1 ligand sits in the centre of this group. [2,3,6]

The effect on the metal based oxidation potentials of the different substituents at the 2' position of the 5 membered ring, and the effect of changing from an imidazo to a triazo type 5 membered ring is examined in this section. Taking the simplest, unsubstituted $[Ru(bpy)_2(LL1)]^{2+}$ as the parent complex, we will compare its $Ru^{(II)}/Ru^{(III)}$ oxidation potential of 0.78 V *vs* Fc/Fc^+ with that of the other complexes in the series.

The LL2 ligand contains a methyl group in the 2' position of the 5 membered imidazo ring. The electron donating group should increase the electron density on the ligand. The metal based oxidation potential of this complex is 0.77 V *vs* Fc/Fc^+. The difference between this and the oxidation potential of the complex containing LL1 is almost negligible, indicating that the methyl group affects the electron donating ability of the LL2 ligand very little. The LL4 and LL5 ligands both contain a substituted phenyl ring in the 2' position of the imidazo moiety. In the case of the LL4 ligand, the phenyl ring contains an OH group which is ortho to the phenyl-imidazo bond. Generally speaking, ortho substituents exert a steric crowding influence, being much closer to the sensitive binding site than meta or para substituents, and are therefore less able to exert their withdrawing effect. However in the case of the LL4 ligand, with the OH group being strongly electron withdrawing, and the phenyl ring also pulling electron density from the "parent" ligand, it was expected that the metal should be harder to oxidise, and the $Ru^{(II)}/Ru^{(III)}$ was found to be 0.82 V *vs* Fc/Fc^+, over 50mV higher than for the ruthenium(II) complex of LL1. The LL5 ligand contains electron withdrawing chlorine atoms in both the ortho and the para position (relative to the phenyl-imidazo bond). Again the ortho chlorine is not expected to affect the electron affinity felt by the phenyl ring as much as the chlorine in the para position. The complex has a metal based oxidation potential of 0.81 V *vs* Fc/Fc^+ which is 40mV higher than for the "parent" complex, meaning the LL5 ligand has less electron donating ability than the LL1 ligand towards the complexed ruthenium cation, due to the electron donating effects of the substituent in the 2' position of the imidazo ring, i.e. the metal is more difficult to oxidise.

The methoxy group much like the methyl group (LL2) is expected to have an electron donating effect. This effect appears to be quite small however and an $E_{1/2}$ of 0.77 V *vs* Fc/Fc^+ was found experimentally for the complex $[Ru(bpy)_2(LL6)]^{2+}$.

The oxidation potential observed of 0.87 V vs Fc/Fc^+ was the highest found, and indicates that the triazo moiety appears to be less electron rich than the imidazo moiety or even the substituted imidazo moieties. As discussed already in Chapter 3.1, the pyridyl-triazole complexes studied by Vos *et al*, [29,30,31,32] contain many similarities to the LL3 ligand. These similarities are obvious from Figure 3.52.

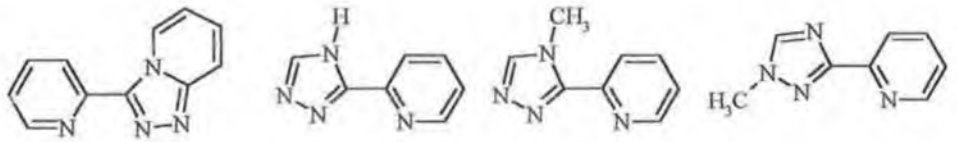

LL3 Hptr 4Mptr 1M3ptr

Figure 3.52 Comparison of the LL3 ligand with the pyridyl triazole ligands studied by Vos et al. [29,30,31,32]

Table 3.23 is a comparison with the results found for similar pyridyl-triazole/2,2'-bipyridyl type systems. In order for the comparisons to be valid the protonated forms of the complexes and the N2' bound isomers of the pyridyl-triazole systems are quoted.

Compound	$E_{1/2}$, V *vs* SCE	
	Oxidation	Reductions
$[Ru(bpy)_2(\mathbf{LL3})]^{2+}$	+1.25	-1.38
		-1.58
		-1.89
$[Ru(bpy)_2(\mathbf{Hptr})]2^{+}$	+1.14	-1.49
		-1.73
		-2.25
$[Ru(bpy)_2(\mathbf{4Mptr})]^{2+}$	+1.19	-1.39
		-1.61
		-1.94
$[Ru(bpy)_2(\mathbf{1M3ptr})]^{2+}$	+1.20	-1.39
		-1.61
		-2.05

Table 3.23 Comparison with of the $[Ru(bpy)_2(LL3)]^{2+}$ complex with the pyridyl-triazole complexes studied by Vos et al.

The oxidation potential of the $[Ru(bpy)_2(LL3)]^{2+}$ complex is higher than that observed for the pyridyl-triazole complexes, indicating that the LL3 ligand is not as strongly σ-donating as the pyridyl-triazoles.

For all the complexes, with the exception of the $[Ru(bpy)_2(LL3)]^{2+}$, the first two reduction potentials were the only observable reduction waves. These reduction waves are comparable to the first two reduction potentials found for $[Ru(bpy)_3]^{2+}$ [70]and is in agreement with the results from the luminescence lifetime studies of the complexes, and of the deuterated analogues, that the first two reduction potentials are 2,2'-bipyridyl based. As mentioned the complex $[Ru(bpy)_2(LL3)]^{2+}$ has an observable third reduction potential and from Table 3.23 it can be seen that this is to be expected from previous studies. The third reduction potential is at a more negative potential than that observed for $[Ru(bpy)_3]^{2+}$, indicating that the third reduction is based on the LL3 ligand proving

that the LL3 ligand, and by analogy, the other ligands in the series, are weaker π-acceptors than 2,2'-bipyridyl.

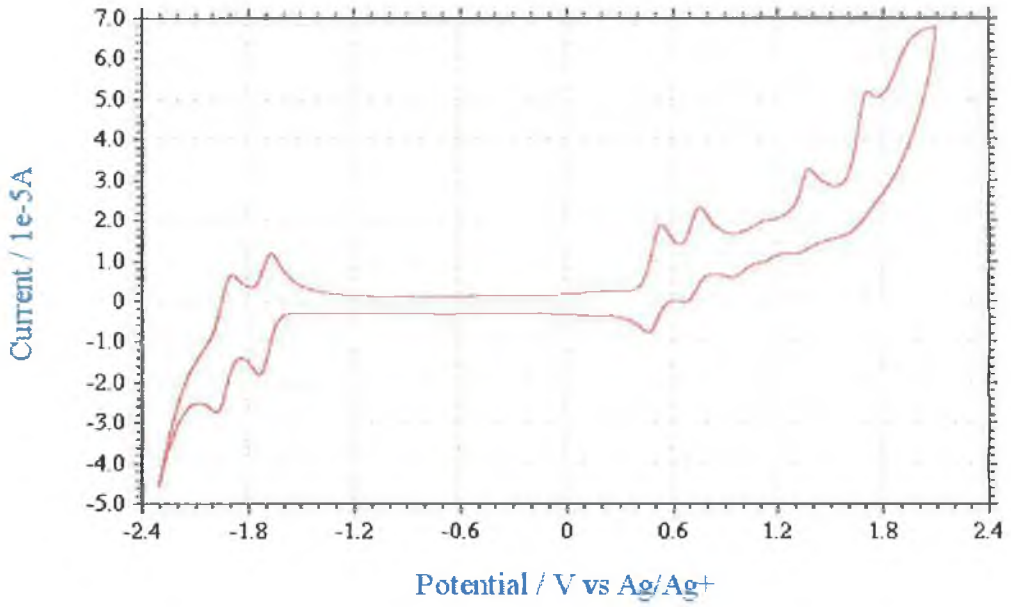

Figure 3.53 Oxidation and reduction potentials of the complex $[Ru(bpy)_2(LL8)]^{2+}$ in MeCN with 0.1M $TBABF_4$.

The final ruthenium(II) bipyridyl complex in the series is that containing the LL8 ligand. The LL8 ligand contains two 5 membered imidazo rings fused to a 6 membered pyridyl type moiety. The other ligands contain only one of these fused conjugated systems. The oxidation potentials of the $Ru(bpy)_2$ complex of the LL8 ligand can be seen in Figure 3.57. Assignment of the metal based oxidation is not as straightforward as for the other complexes, as the complex contains several oxidation potentials in the region being examined. The free LL8 ligand contains oxidation potentials at 0.15 V, and 0.34 V *vs* Fc/Fc^+. This compares to oxidation potentials of 0.41 V, 0.73 V, 1.38 V and 1.71 V vs Fc/Fc^+ observed for the ruthenium complex. Comparison with the oxidation potential of the previously detailed complexes indicate that the oxidation potential at 0.73 V should correspond to the $Ru^{(II)}/Ru^{(III)}$ couple. This is lower than the other complexes and indicates that it is the fused 5 and 6 membered ring system that is responsible for the σ-donating ability of the ligand. Assignment of the wave at 0.73 V as metal based allows

the wave at 0.41 V to be assigned as a ligand centred oxidation wave. Again, this is lower than observed for the other complexes studied, but by comparison to the oxidation potentials of the free ligand, this is a reasonable assumption to make.

3.12 Further Discussion of the Rotamers Issue:

The presence of isomers has already been discussed in the ^{1}H NMR section of this chapter. Here we look into the phenomenon further and examine more fully the properties of these rotamers.

In order to prove that the doubling of the number of signals observed in the ^{1}H NMR spectra of the complexes $[Ru(bpy)_2(LL4)]^{2+}$, $[Ru(bpy)_2(LL5)]^{2+}$ and $[Ru(bpy)_2(LL6)]^{2+}$ is due to an isomerisation effect and not merely a consequence of sterically hindered rotation of the substituted phenyl ring, temperature dependent ^{1}H NMR was performed on the complex $[Ru(bpy)_2(LL6)]^{2+}$. This experiment may prove whether the phenomenon is due to the orientation adopted by the ligand at the point of coordination, which resulted in the formation of the two rotamers or whether another process is responsible for the effect observable only by NMR. The results of this experiment may be seen in Figure 3.55. The experiment indicates whether an increase in temperature provides the energy to the substituted phenyl to overcome the barrier to rotation it may experience at room temperature. Should this be the case, performing the ^{1}H NMR experiment at temperatures higher than this temperature should lead to a change in the spectrum.

It was decided to perform this experiment on the $[Ru(bpy)_2(LL6)]^{2+}$ complex in d_6-DMSO to allow higher temperatures to be reached during the experiment. The $[Ru(bpy)_2(LL6)]^{2+}$ complex was used because the four methoxy signals allow the experiment to be followed easily. At temperatures beyond the barrier to rotation, the four methoxy signals should appear as two singlets.

This experiment has been used to study the fluxional behaviours in solution of a number of lopsided heterocycles previously. [71] The dynamic solution behaviour of the three different monodentate ligands, 1-methylimidazole, 1,2-dimethylimidazole and 1-methyldenzimidazole as complexes of the type $[Ru(bpy)_2(L)_2]$ have been investigated. The smallest ligand rotate around the Ru-N axis fastest, while the larger ligands experience steric hindrance, rotate fast at 55°C, but slowly at low temperature leading to the appearance of atropisomers.

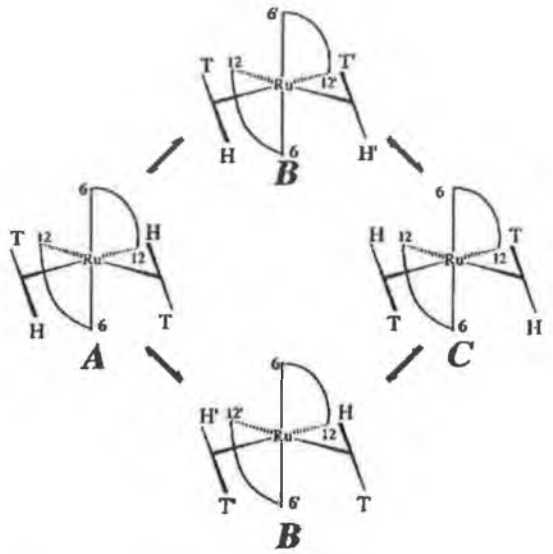

[a] The arrows represent the interconversion pathway of the atropisomers, each via a single rotation of one of the imidazole ligands by about 180°.

Figure 3.54 Schematic representations of the four atropisomers with the arcs representing the bpy ligands and the rods representing the unsymmetric imidazole derivatives. [72]

The results of the temperature dependent ^1H NMR study on the $[Ru(bpy)_2(LL6)]^{2+}$ complex in d_6-DMSO can be seen in Figure 3.55.

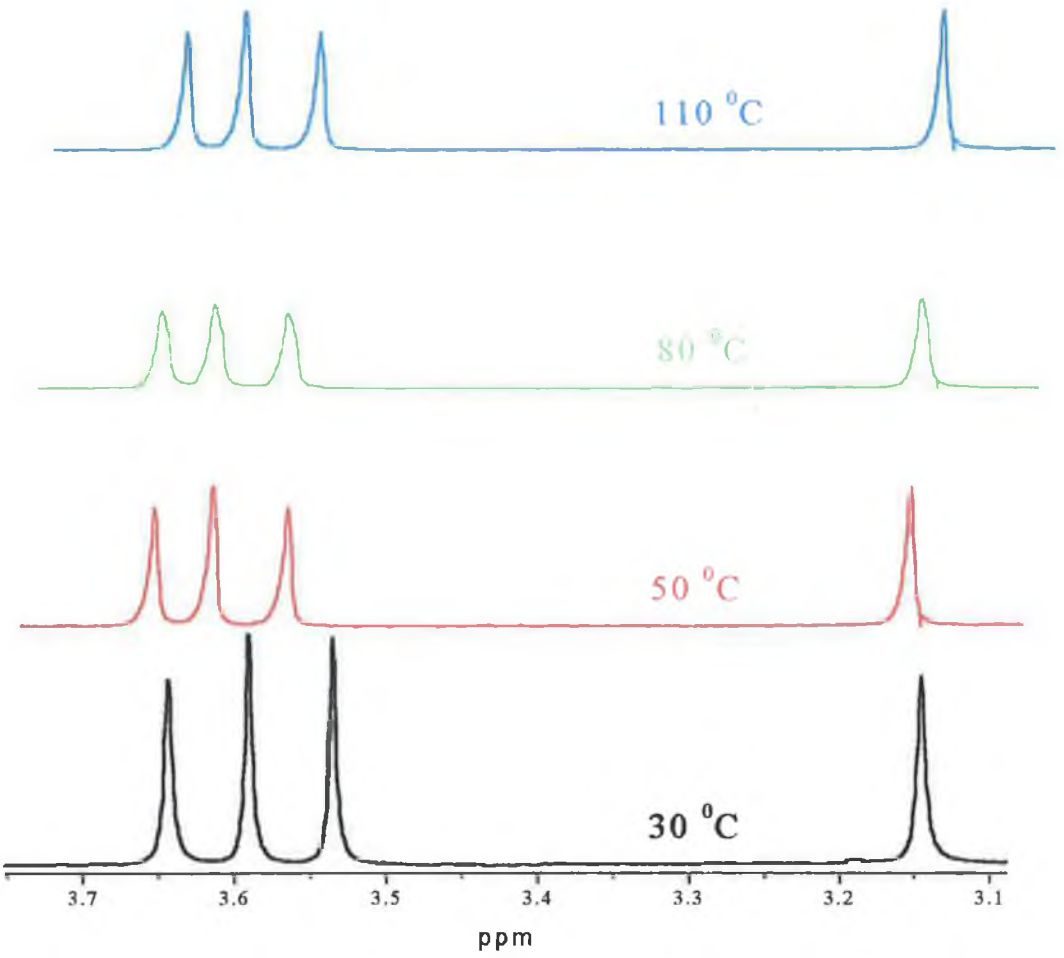

Figure 3.55 Results from the Temperature Dependent ^1H NMR study of $[Ru(bpy)_2(LL6)]^{2+}$ in d_6-DMSO.

In order to simplify the results, only the aliphatic region, which contain the signals of the methoxy groups has been shown. As discussed in Section 3.5, four methoxy signals are observed as opposed to the two expected signals. Should the doubling of the peaks be due to steric hindrance of the substituted phenyl ring, increasing the temperature, and thereby increasing the kinetic energy of the compound in solution, could result in the disappearance of the effect caused by the steric interaction. i.e. the four signals could become the expected two at higher temperatures. This does not happen however, and the only change observed on increasing the temperature is a very slight broadening and shift of the signals which can be explained by changes in the viscosity of the solvent on

changing the temperature. This was the first experiment to investigate the rotamers, and the results added credence to the supposition that the effect seen in the ^1H NMR spectra is due to the presence of two separate isomeric species which were formed on coordination of the ligand with the $[Ru(bpy)_2]$ unit.

In order to investigate the effect further, another set of experiments, on the compound $[Ru(bpy)_2(LL6)]^{2+}$, were undertaken by Prof. Villani in the University of Rome. Prof. Villani has managed to separate the two isomers on a HPLC column. This trace is pictured below.

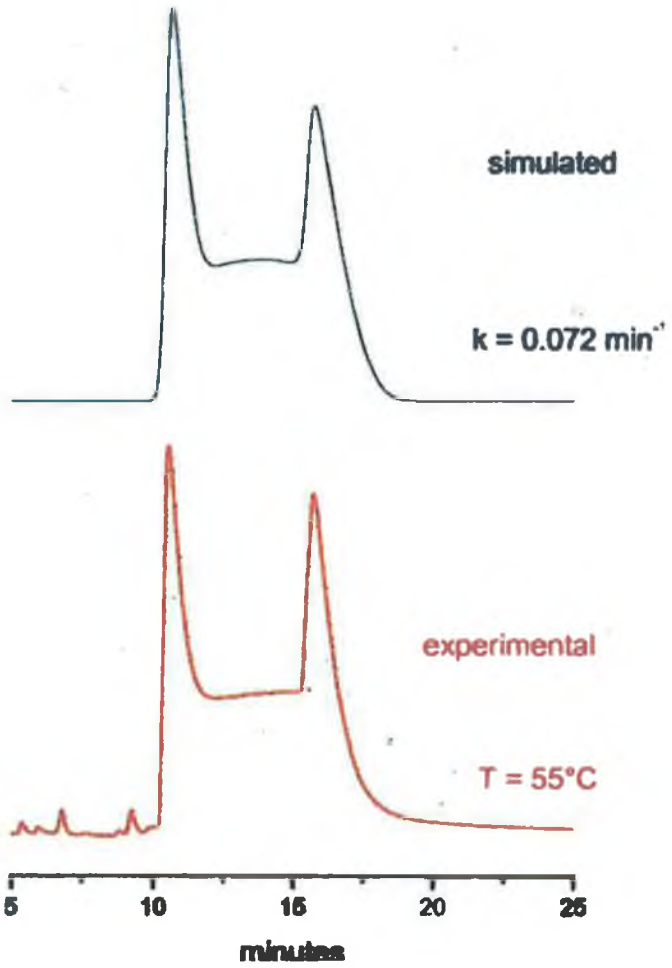

Figure 3.56 HPLC trace of the two rotamers of the complex $[Ru(bpy)_2(LL6)]^{2+}$.

The upper trace in Figure 3.56 is a computer simulated prediction of the expected behaviour of the rotamers on the column. The red trace is the actual experiment. Prof. Villani's experiments have shown that the isomers interconvert on a C18 column at temperatures greater than 45°C. At 55°C the on-column isomerisation produces a plateau between the two peaks. Computer simulation of the exchange modified chromatogram gives the (apparent) rate constant for this interconversion. The rate constant is an averaged value of the rate constants, k_m and k_s, (where k_m is the interconversion rate in the mobile phase and k_s is the interconversion rate on the stationary phase). The value for this interconversion rate calculated by Prof. Villani roughly translates to the rotamers having a half-life of about 6 hours at 25°C.

This result differs from the view on the presence of the rotamers. Before these results, it was believed that the two different isomers were formed in roughly equal ratios at the moment of coordination, and that interconversion from one isomer to another was not possible. The results achieved in Rome leads to a different approach to this issue being necessary. The results indicate that interconversion from one isomer to another is possible in solution, and at higher temperatures this interconversion is faster. The results so far have been on equilibrated solutions of the two isomers. It had previously been believed that if one of the isomers was isolated, that it would be stable as that isomer. This is not now the case, as an isolated isomer will eventually return to a mixture of the two isomers in solution, and that this process will be faster the higher the temperature. It was decided however that the isomers should be separated in amounts suitable for a ^1H NMR experiment. This has only recently been achieved, and the HPLC traces of the isolated isomers can be seen in Figure 3.57. One thing both the simulated and actual HPLC traces of the interconversion of the isomers is that this process has an interconversion rate that is not observable by NMR. (The interconversion rate is > seconds and needs to be much shorter for coalescence to be observed by NMR).

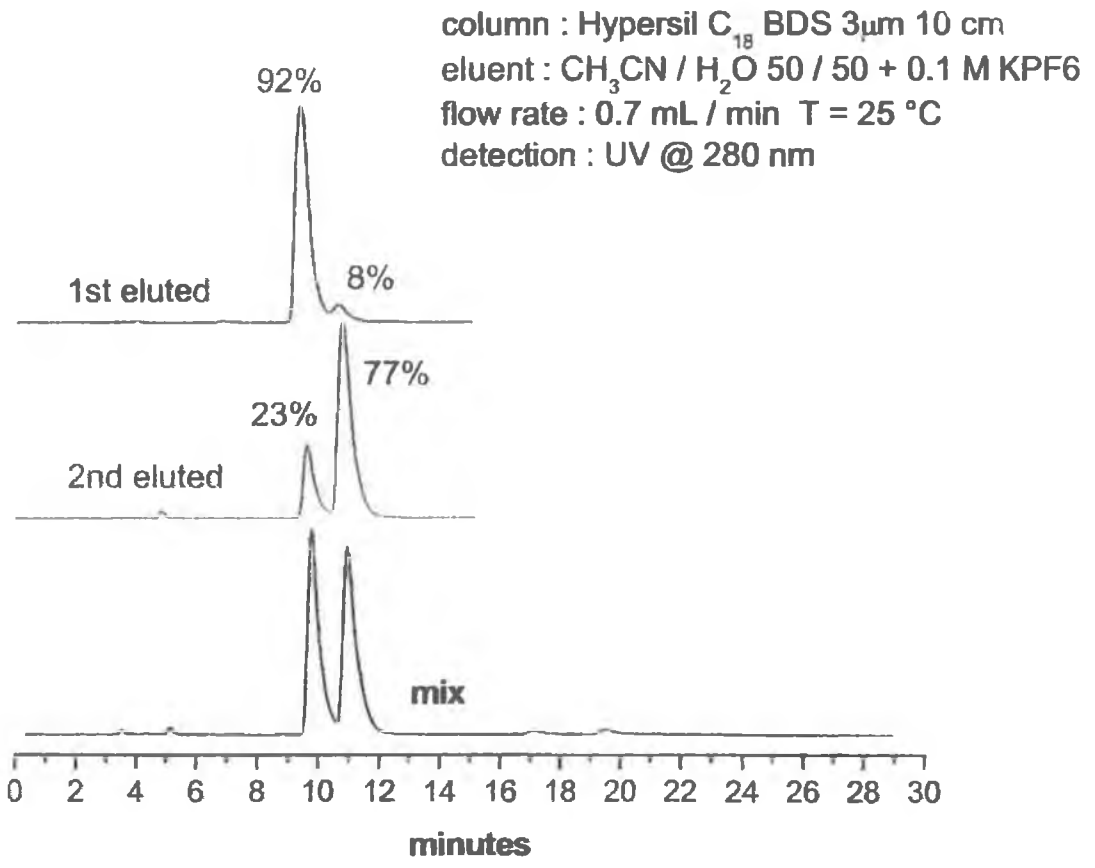

Figure 3.57 HPLC traces of the mixture of isomers (bottom trace) and of the isolated isomers (middle and top traces).

As can be seen from Figure 3.57, the isomers have successfully been separated. The trace at the bottom represents an injection of the re-equilibrated mixture of isomers of the first eluted isomers, proving the complexes reorientate in solution. Much work needs to be completed in order to fully understand this issue. This is discussed further in Chapter 8.

3.13 Bibliography:

[1] Grigg R., Kennewell P., Savic V., Sridharan V., ***Tetrahedron***, **1992,** 10432

[2] Haga M., ***Inorg. Chim. Acta.,*** **1983**, 77, 39.

[3] Haga M., Matsumura-Inoue T., Shimizu K., Sato G. P., ***J. Chem. Soc. Dalton Trans.***, **1989**, 371.

[4] Fieselmann B. F., Hendrickson D. N., Stucky G. D., ***Inorg. Chem.***, **1978,** 17, 2078

[5] Haddad M. S., Hendrickson D. N., ***Inorg. Chem.***, **1978,** 17, 2660

[6] Haga, M., ***Inorg. Chim. Acta.***, **1980**, 45, 183

[7] Haga, M., ***Inorg. Chim. Acta.***, **1983,** 75, 29

[8] Bogess R. K., Martin R. B., ***Inorg. Chem.***, **1974**, 13, 1525

[9] Haga, M. A., Matsumura-Inoue, T., Yamabe S., ***Inorg. Chem.***, **1987**, 26, 4148

[10] Rillemma D. P., Sahai R., Matthews P., Edwards A. K., Shaver R. J., and Morgan L., ***Inorg. Chem.***, **1990**, 29, 167

[11] Rillemma, D. P., Endicott, J. F., Papaconstantinou, E., ***Inorg. Chem.***, **1971**, 10, 1739

[12] Haga, M., Ano, T., Kano K., Yamabe S., ***Inorg. Chem.***, **1991**, 30, 3843

[13]Ohno T., Nozaki K., Haga M., ***Inorg. Chem.***, **1992**, 31, 548

[14] Haga, M., Matsumura-Inoue, T., Yamabe, S., ***Inorg. Chem.***, **1987**, 26, 4148

[15] Kaim W., Kasack, V., ***Inorg. Chem.***, **1990**, 29, 4696

[16] Krentzien, H., Taube, H., ***J. Am. Chem. Soc.***, **1976**, 98, 6379. Krentzien, H., Taube, H., ***Inorg. Chem.***, **1982**, 21, 4001. Neyhart, G., Meyer T. J., ***Inorg. Chem.***, **1986**, 25, 4807. Hage, R., Dijkhuis, A. H. J., Haasnoot, J. G., Prins, R., Reedijk, J., Buchanan, B. E., Vos, J. G., ***Inorg. Chem.***, **1988**, 27, 2185

[17] Ohno T., Nozaki K., Haga M., ***Inorg. Chem.***, **1992**, 31, 4256

[18] Nozaki K., Ohno T., Haga M., ***J. Phys. Chem.***, **1992**, 96, 10880.

[19] Braunstein, C. H., Baker A. D., Strekas T. C., Gafney, H. D., ***Inorg. Chem.***, **1984**, 23, 857. Fuchs, Y., Lofters S., Diester T., Shi W., Morgan R., Strekas T. C., Gafney H. D., Baker A. D., ***J. Am. Chem. Soc.***, **1987**, 109, 2691. Wallace A. W., Murphy W. W., Petersen J. D., ***Inorg. Chim. Acta.***, **1989**, 166, 47. Murphy W. R., Brewer K. J., Gettliffe G., Petersen J. D., ***Inorg. Chem.***, **1989**, 28, 81. Kalyanasundaram, K., Nazeeruddin, M. K., ***Inorg. Chem.***, **1990**, 29, 1888. Berger R. M., ***Inorg. Chem.***, **1990**, 29, 1920. Denti, G., Campagna, S., Sabbatino, L., Serroni S., Ciano M., Balzani V., ***Inorg. Chem.***, **1990**, 29, 4750. Campagna, S., Denti, G., Serroni S., Ciano M., Balzani V., ***Inorg. Chem.***, **1991**, 30, 3728

[20] Hunziker, M., Ludi, A., ***J. Am. Chem. Soc.***, **1977**, 99, 7370. Dose E., Wilson L. J., ***Inorg. Chem.***, **1978**, 17, 2660. Sahai R., Rillemma D. P., Shaver R., Van Wallendael S., Jackman D. C., Boldaji M., ***Inorg. Chem.***, **1989**, 28, 1022

[21] Haga M., Ano T., Ishizaki T., Kano K., Nozaki K., Ohno T., ***J. Chem. Soc., Dalton Trans.***, **1994**, 263

[22] Rillemma D. P., Callahan R. W., Mack K. B., ***Inorg. Chem.***, **1982**, 21, 2589. Murphy W. R., Brewer K. J., Gettliffe G., Petersen J. D., ***Inorg. Chem.***, **1989**, 28, 81. Fuchs Y., Lofters S., Dieter T., Shi W., Morgan R., Strekas T. C., Gafney H. D., Baker A. D., ***J. Am. Chem. Soc.***, **1987**, 109, 2691. Hunziger M., Ludi A., ***J. Am. Chem. Soc.***, **1977**, 99, 7370

[23] Khalil M. M. H., Ali S. A., Ramadan R. M., ***Spectrochimica Acta, Part A***, **2001**, 57, 1017

[24] Rocha R. C., Araki K., Toma H., ***Inorg. Chim. Acta***, **1999**, 285, 197

[25] Rocha R. C., Toma H., ***Inorg. Chim. Acta***, **2000**, 310, 65

[26] Kucukbay H., Durmaz B., ***Arzneimittel-Forschung/Drug Res.***, **1997**, 47, 667

[27] Mylonas S., Valavanids Y. A., Dimitropoulos K., Polissiou M., Tsiftsoglou A. S., Vizirianakis I. S., ***J. Inorg. Biochem.***, **1988**, 34, 265

[28] Kabanos T. A., Kersmidas A. D., Mentafos D., Russo U., Terzis A., Tsangaris J. M., ***J. Chem. Soc., Dalton Trans.***, **1992**, 2729

[29] Vos J. G., Haasnoot J. G., Vos G., ***Inorg. Chim. Acta***, **1983**, 162, 155

[30] Hage R., ***Ph. D Thesis***, Leiden University, **1991**.

[31] Browne W. R., O'Connor C. M., Villani C., Vos J. G., ***Inorg. Chem.***, **2001**, 40, 5461

[32] Buchanan B. E., Mc Govern E., Harkin P., Vos J. G., ***Inorg. Chim. Acta***, **1988**, 154, 1

[33] Hage R., Haasnoot J. G., Nieuwenhuis H. A., Reedijk J., Wang R., Vos J. G., ***J. Chem. Soc., Dalton Trans.***, **1991**, 3271

[34] Wang R., Vos J. G., Schmehl R. H., Hage R., ***J. Am. Chem. Soc.***, **1992**, 114, 1964

[35] Hage R., Dijkhuis A. H. J., Haasnoot J. G., Prins R., Reedijk J., Buchanan B. E., Vos J. G., ***Inorg. Chem.***, **1988**, 27, 2185

[36] Hage R., Haasnoot J.G., Stufkens D. J., Snoeck T. L., Vos J. G., Reedijk J., ***Inorg. Chem.***, **1989**, 28, 1413

[37] Barigelletti F., De Cola L., Balzani V., Hage R., Haasnoot J. G., Reedijk J., Vos J. G., ***Inorg. Chem.***, **1989**, 28, 4344

[38] Hage R., Haasnoot J.G., Nieuwenhuis H. A., Reedijk J., De Ridder D. J. A., Vos J. G., ***J. Am. Chem. Soc.***, **1990**, 112, 9245

[39] Barigelletti F., De Cola L., Balzani V., Hage R., Haasnoot J. G., Reedijk J., Vos J. G., ***Inorg. Chem.***, **1991**, 30, 641

[40] Pankuch B. J., Lacky D. E., Crosby G. A., ***J. Phys. Chem.***, **1980**, 84, 2061

[41] Lacky D. E., Pankuch B. J., Crosby G. A., ***J. Phys. Chem.***, **1984**, 88, 2068

[42] Creutz, C., Chou M. H., ***Inorg. Chem.***, **1987**, 26, 2995

[43] Pipes D. W., Meyer T. J., ***Inorg. Chem.***, **1984**, 23, 2466

[44] Kober E. M., Sullivan B. P., Dressick W. J., Casper J. V., Meyer T. J., ***J. Am. Chem. Soc.***, **1980**, 102, 7385

[45] Bond A., Haga M., ***Inorg. Chem.***, **1986**, 25, 4507

[46] Sullivan B. P., Salmon D. J., Meyer T. J., ***Inorg. Chem.***, **1978**, 17, 3334

[47] Rillema D. P., Jones D. S., Levy H. A., ***J. Chem. Soc., Chem. Comm.***, **1979**, 849

[48] Stynes H. C., Ibers J. A., ***Inorg. Chem.***, **1971**, 10, 2304

[49] Phelps D. W., Kahn E. M., Hodgson D. J., ***Inorg. Chem.***, **1975**, 14, 2486

[50] Hage R., Turkenburg J. P., De Graaf R. A. G., Haasnoot J. G., Reedijk J., Vos J. G., ***Acta Cryst.***, **1989**, C45, 381

[51] Rilemma D. P., Jones D. S., Woods C., Levey H. A., ***Inorg. Chem.***, **1992**, 31, 2935

[52] Hage R., Haasnoot J. G., Nieuwenhuis H. A., Reedijk J., De Ridder D. J. A., Vos J. G., ***J. Am. Chem. Soc***., **1990**, 112, 9245.

[53] Haga M., Meser Ali M., Koseki S., Fujimoto K., Yoshimura A., Nozaki K., Ohno T., Nakajima K., Stufkens D. J., ***Inorg. Chem***., **1996**, 35, 3335.

[54] Pal S., Misra T. K., Sinha C., Slawin A. M. Z., Woolins J. D., ***Polyhedron***, **2000**, 19, 1925.

[55] Thummel R. P., Williamson D., Hery C., ***Inorg. Chem.***, **1993**, 32, 1587.

[56] Chirayil S., Thummel R. P., ***Inorg. Chem.***, **1989,** 28, 812.

[57] Hesek D., Hembury G. A., Drew M. G. B., Taniguchi S., Inoue Y***., Inorg. Chem***., **2001**, 40, 2478.

[58] Demas J. N., Crosby G. A., ***J. Am. Chem. Soc.,* 1970,** 92, 7262

[59] Barlgelleti F., DeCola L., Balzani V., Hage R., Haasnoot J. G., Reedijk J., Vos J. G., ***Inorg. Chem.***, **1991**, 30, 641.

[60] Juris A, Balzani V., Barigelleti F, Campagna S., Belser P., von Zelewsky A., ***Coord. Chem. Rev.,* 1988**, 84, 85.

[61] Lumpkin R. S., Kober E. M., Worl L., Murtaza Z., Meyer T J., ***J. Phys. Chem.***, **1990**, 94, 239.

[62] Wrighton, M., Morse D. L., ***J. Am. Chem. Soc.***, **1974,** 96, 996.

[63] Browne W. R., Vos J. G., ***Coord. Chem. Rev.***, **2001,** 219, 761.

[64] Dodsworth E. S., Lever A. B. P., ***Chem. Phys. Lett***., **1986**, 124, 152.

[65] Rillema P., Jones D. S., Levy H., ***J. C. S. Chem. Comm***., **1979,** 849

[66] Paris J. P., Brandt W. W., ***J. Am. Chem. Soc***., **1959**, 81, 5001

[67] Buchanan B. E., McGovern E., Harkin P., Vos J. G., ***Inorg. Chim. Acta.*, 1988,** 154, 1.

[68] Bard A. J., Faulkner L. R., ***Electrochemical Methods,*** 2nd Edition, **2001.**

[69] Kaifer A. E., Gomez-Kaifer M., ***Supramolecular Electrochemistry***, Wiley, **1999.**

[70] Wallace A. W., Murphy W. R., Petersen J. D., ***Inorg. Chim. Acta.***, **1989,** 166, 47

[71] Velders A. H., Hotze A. C. G., van Albada G. A., Haasnoot J. G., Reedijk J., ***Inorg. Chem.***, **2000**, 39, 4073.

[72] Velders A. H., Hotze A. C. G., van Albada G. A., Haasnoot J. G., Reedijk J., ***Inorg. Chem.***, **2000**, 39, 4073.

Chapter 4: Synthesis and characterisation of the $[Os(bpy)_2(LL_x)](PF_6)_2$ complexes.

Abstract:

Chapter 4 details the synthesis and characterisation of a series of osmium(II) bisbipyridyl complexes based on the LL_x ligands which were introduced in Chapter 3. The reasons for synthesising the complexes are outlined in the introduction. The complexes were characterised using the same techniques as outlined in Chapter 3. Again, ^1H NMR has proven a valuable tool in the determination of the structure of the osmium(II) complexes. As with the ruthenium(II) complexes the rotamers complications are observed for the LL4, LL5 and LL6 complexes. This is not discussed in as much detail here, as it has been well documented for the ruthenium(II) complexes. The complexes exhibit typical osmium(II) absorption and emission behaviour. However, interestingly, the $[Os(bpy)_2(LL1)]^{2+}$ complex exhibits photochemistry in MeCN which appears to defeat one of the main reasons for the synthesis of the osmium(II) complexes. As in the case of the ruthenium(II) complexes, the electrochemistry is complicated by the electron rich LL_x ligands. As expected the metal centred oxidation potentials appear at potentials roughly 0.4 V less positive than the analogous ruthenium(II) complexes.

4.1 Introduction to Chapter 4

It was decided to synthesise these osmium complexes for several reasons. A very important feature of osmium(II) complexes is that the metal-nitrogen bond distances are very similar to those found for the analogous ruthenium(II) complexes.[1,2] This means that the differences between steric and solvation effects should be very small for the ruthenium and osmium complexes, allowing easy comparison of the two systems. The lanthanide contraction results in surprisingly short osmium-nitrogen bond distances. This is because the 4f orbital is filled before the 5d orbital, but as the 4f electrons are very diffuse, the 5d electrons are not effectively screened from the nuclear charge, causing their average distance from the nucleus to lessen. This leads to average metal-ligand bonds to be very similar for both second and third row metal ions.[3]

The chemistry of osmium polypyridyl complexes differs from that of ruthenium polypyridyl complexes in four main ways. Firstly, the oxidation potentials of osmium(II) compounds are generally lower than those of the analogous ruthenium compounds. This means that higher oxidation states of osmium complexes are more stable. Secondly, the lower oxidation potentials mean that the luminescent ^{3}MLCT states are lower than those of the corresponding ruthenium compounds. Thirdly, the metal-ligand interaction is stronger for osmium than for ruthenium due to the larger ligand field splitting. Reactions of osmium with ligands are slower than for ruthenium.[4] Finally, complexes of osmium tend to be more photochemically stable as a consequence of the higher 10Dq for Os, which raises the energy of the low lying dd states preventing significant population at room temperature.

The increased spin-orbit coupling associated with third row transition elements opposed to second row elements leads to greater mixing of the singlet and triplet states. Formally forbidden transitions may be observed for osmium compounds that are not present for ruthenium compounds. The best example of this is probably the ($d\pi \rightarrow \pi^*$) ^{3}MLCT

absorption band which is very weak for $[Ru(bpy)_3]^{2+}$ but is quite intense for $[Os(bpy)_3]^{2+}$. This will be discussed in more detail at a later stage in this chapter.

The ligands being used to synthesise the osmium(II) complexes are the same as those used in Chapter 3. It is expected that, as in the case of the ruthenium(II) complexes, the properties of the free ligands will need to be examined in conjunction with the properties of the complexes to best explain the observations. The approach used is therefore going to be the same as in Chapter 3, and the ligands with which reference is made have already been detailed in Chapter 3.1.

4.2 Synthesis of the $[Os(bpy)_2(LL_x)](PF_6)_2$ complexes

Synthesis of *cis*-$[Os(bpy)_2Cl_2].2H_2O$ [5]

K_2OsCl_6 (300mg, $6.2x10^{-4}$ mol) and 2,2' bipyridine (203mg, $1.3x10^{-3}$ mol) were refluxed in $3cm^3$ ethylene glycol with constant stirring. The resulting solution was allowed to cool to room temperature and $5cm^3$ of a saturated aqueous solution of sodium dithionite ($Na_2S_2O_4$) was added. The solid which formed was isolated by filtration and washed with water until the filtrate was colourless. The solid was further washed with diethylether and placed in a dessicator overnight to yield 298mg of product. (79% yield)

Synthesis of $[Os(bpy)_2(LL1)](PF_6)_2.H_2O$

LL1 (55mg, $2.8x10^{-4}$ mol) and $[Os(bpy)_2Cl_2].2H_2O$ (171mg, $2.8x10^{-4}$ mol) were placed in $15cm^{-3}$ of a 1:1 ethylene glycol/water mixture. This suspension was heated at reflux for 24 hours and allowed to cool to room temperature. The solution was filtered at this stage to remove any excess unreacted ligand. A solution of aqueous ammonium hexafluorophosphate was added to the filtrate to precipitate a brown/green product. This product was isolated by filtration, washed with water and dried with diethylether. The compound was purified by column chromatography (stationary phase silica gel, mobile phase 80% acetonitrile, 20% water, 0.05M KNO_3 buffer) to yield 136 mg of pure compound. (49%)

^{1}H NMR (400 MHz, d_6-acetone) δ = 7.11 (dd, 1H), 7.21 (dd, 1H), 7.45 (m, 5H), 7.75, (d,1H), 7.94 (m, 5H0, 8.03 (dd, 2H), 8.10 (d, 1H), 8.17 (d, 1H), 8.36 (m, 2H), 8.44 (d, 1H), 8.50 (d, 1H), 8.78 (m, 4H).

Elemental Analysis for $C_{32}H_{27}N_7OsOP_2F_{12}$: Calculated C 38.20, H 2.59, N 9.75. Found C 38.30, H 2.38, N 10.07 %.

Synthesis of $[Os(d_8\text{-bpy})_2(LL1)](PF_6)_2.4H_2O$

LL1 (25.2mg, $1.28x10^{-4}$ mol) and $[Os(d_8\text{-bpy})_2Cl_2].2H_2O$ (78mg, $1.28x10^{-4}$ mol) were placed in $15cm^{-3}$ of a 1:1 ethylene glycol/water mixture. This suspension was heated at reflux for 24 hours and allowed to cool to room temperature. The solution was filtered at this stage to remove any excess unreacted ligand. A solution of aqueous ammonium hexafluorophosphate was added to the filtrate to precipitate a brown/green product. This product was isolated by filtration, washed with water and dried with diethylether. The compound was purified by column chromatography (stationary phase silica gel, mobile phase 80% acetonitrile, 20% water, 0.05M KNO_3 buffer) to yield 62 mg of pure compound. (48% yield)

^{1}H NMR (400 MHz, d_6-acetone) δ = 6.97 (dd, 1H), 7.06 (dd, 1H), 7.29 (dd, 1H), 7.60 (d, 1H), 7.79 (dd, 1H), 8.22 (m, 2H), 8.30 (d, 1H), 8.36 (d, 1H).

Elemental Analysis for $C_{32}H_{31}N_7OsO_4P_2F_{12}$: Calculated C 35.71, H 2.70, N 9.11. Found C 35.84, H 1.93, N 8.70 %.

Synthesis of $[Os(bpy)_2(LL2)](PF_6)_2$

The LL2 ligand (20mg, $9.5x10^{-5}$ mol) and $[Os(bpy)_2Cl_2].2H_2O$ (58mg, $9.5x10^{-5}$ mol) were placed in $15cm^{-3}$ of a 1:1 ethylene glycol/water mixture. This suspension was heated at reflux for 24 hours and allowed to cool to room temperature. The solution was filtered at this stage to remove any excess unreacted ligand. A solution of aqueous

ammonium hexafluorophosphate was added to the filtrate to precipitate a brown/green product. This product was isolated by filtration, washed with water and dried with diethylether. The compound was purified by column chromatography (stationary phase silica gel, mobile phase 80% acetonitrile, 20% water, 0.05M KNO_3 buffer) to yield 59 mg of pure product. (62% yield)

^{1}H NMR (400 MHz, d_6-acetone) δ = 7.11 (m, 3H), 7.30 (m, 4H), 7.68 (m, 2H), 7.73 (d, 1H), 7.82 (m, 6H), 7.97 (m, 2H), 8.55 (d, 1H), 8.64 (m, 4H), 9.07 (d, 1H), 1.79 (s, 3H).

Elemental Analysis for $C_{33}H_{27}N_7OsP_2F_{12}$. Calculated C 39.57, H 2.72, N 9.79. Found C 39.53, H 2.64, N 9.77 %.

Synthesis of $[Os(bpy)_2(LL3)](PF_6)_2$

LL3 (32mg, $1.64x10^{-4}$ mol) and $[Os(bpy)_2Cl_2].2H_2O$ (100mg, $1.64x10^{-4}$ mol) were placed in $10cm^{-3}$ of a 1:1 ethylene glycol/water mixture. This suspension was heated at reflux for 24 hours and allowed to cool to room temperature. The solution was filtered at this stage to remove any excess unreacted ligand. A solution of aqueous ammonium hexafluorophosphate was added to the filtrate to precipitate a brown/green product. This product was isolated by filtration, washed with water and dried with diethylether. The compound was purified by column chromatography (stationary phase silica gel, mobile phase 80% acetonitrile, 20% water, 0.05M KNO_3 buffer) to yield 123 mg of pure compound. (76%)

^{1}H NMR (400 MHz, d_6-acetone) δ = 7.39 (dd, 1H), 7.48 (m, 4H), 7.55 (dd, 1H), 7.80 (dd, 1H), 7.88 (d, 1H), 8.06 (m, 10H), 8.80 (m, 5H), 9.36 (d, 1H).

Elemental Analysis for $C_{31}H_{24}N_8OsP_2F_{12}$. Calculated C 37.66, H 2.45, N 11.33. Found C 37.52, H 2.01, N 10.34 %.

Synthesis of $[Os(bpy)_2(LL4)](PF_6)_2.H_2O$

LL4 (71mg, $2.46x10^{-4}$ mol) and $[Os(bpy)_2Cl_2].2H_2O$ (150mg, $2.46x10^{-4}$mol) were placed in $15cm^{-3}$ of a 1:1 ethylene glycol/water mixture. This suspension was heated at reflux for 24 hours and allowed to cool to room temperature. The solution was filtered at this stage to remove any excess unreacted ligand. A solution of aqueous ammonium hexafluorophosphate was added to the filtrate to precipitate a brown/green product. This product was isolated by filtration, washed with water and dried with diethylether. The compound was purified by column chromatography (stationary phase silica gel, mobile phase 80% acetonitrile, 20% water, 0.05M KNO_3 buffer) to yield 175mg of pure compound. (66% yield)

^{1}H NMR (400 MHz, d_6-acetone) δ = 6.36 (d, 1H), 6.53 (dd, 1H), 6.71 (m, 2H), 6.79 (d, 1H), 6.92 (m, 2H), 7.14 (m, 7H), 7.47 (m, 12H), 7.62 (m, 3H), 7.69 (d, 1H), 7.90 (m, 11H), 8.07 (d, 1H), 8.32 (m, 3H), 8.67 (m, 11H), 9.22 (s, 1H), 10.40 (s, 1H).

Elemental Analysis for $C_{38}H_{29}N_7OsOP_2F_{12}$. Calculated C 42.27, H 2.71, N 9.08. Found C 42.67, H 2.70, N 9.50 %.

Synthesis of $[Os(bpy)_2(LL5)](PF_6)_2.((CH_3)_2CO)$

LL5 (70mg, $2.05x10^{-4}$ mol) and $[Os(bpy)_2Cl_2].2H_2O$ (127mg, $2.05x10^{-4}$mol) were placed in $15cm^{-3}$ of a 1:1 ethylene glycol/water mixture. This suspension was heated at reflux for 24 hours and allowed to cool to room temperature. The solution was filtered at this stage to remove any excess unreacted ligand. A solution of aqueous ammonium hexafluorophosphate was added to the filtrate to precipitate a brown/green product. This product was isolated by filtration, washed with water and dried with diethylether. The compound was purified by column chromatography (stationary phase silica gel, mobile phase 80% acetonitrile, 20% water, 0.05M KNO_3 buffer). Further purification was carried out and this complex was recrystallised from acetone/water to yield 160mg of pure compound. (69% yield)

^{1}H NMR (400 MHz, d_6-acetone) δ = 6.62 (m, 1H), 7.09 (m, 2H), 7.17 (m, 5H), 7.26 (m, 1H), 7.37 (m, 4H), 7.49 (m, 7H), 7.61 (m, 2H), 7.75 (m, 8H), 7.86 (m, 1H), 7.96 (m, 10H), 8.15 (m, 2H), 8.43 (m, 2H), 8.72 (m, 11H).

Elemental Analysis for $C_{41}H_{33}N_7OsOCl_2P_2F_{12}$. Calculated C 41.34, H 2.77, N 8.23. Found C 41.65, H 2.44, N 8.90 %.

Synthesis of $[Os(bpy)_2(LL6)](PF_6)_2.((CH_3)_2CO)$

LL6 (54.3mg, $1.64x10^{-4}$ mol) and $[Os(bpy)_2Cl_2].2H_2O$ (100mg, $1.64x10^{-4}$ mol) were placed in $15cm^{-3}$ of a 1:1 ethylene glycol/water mixture. This suspension was heated at reflux for 24 hours and allowed to cool to room temperature. The solution was filtered at this stage to remove any excess unreacted ligand. A solution of aqueous ammonium hexafluorophosphate was added to the filtrate to precipitate a brown/green product. This product was isolated by filtration, washed with water and dried with diethylether. The compound was purified by column chromatography (stationary phase: alumina, mobile phase: acetonitrile) and recrystallised from acetone/water to yield 55mg of pure compound. (30 % yield).

^{1}H NMR (400 MHz, d_6-acetone) δ = 8.69 (m, 11H), 8.45 (d, 1H), 8.30 (d, 1H), 8.22 (d, 1H), 8.07 (d, 1H), 7.96 (m, 9H), 7.80 (m 2H), 7.55 (m, 16H), 7.08 (m, 7H), 6.88 (m, 3H), 6.75 (d, 1H), 6.05 (s, 1H), 3.79 (s, 3H), 3.67 (s, 3H), 3.65 (s, 3H), 3.29(s, 3H).
Total = 54 aromatic protons, 12 aliphatic.

Elemental Analysis for $C_{43}H_{39}N_7O_3OsP_2F_{12}$. Calculated C 44.54, H 3.63, N 7.91. Found C 44.48, H 3.07, N 9.06.

Synthesis of $[Os(bpy)_2(LL8)](PF_6)_2.H_2O.CH_3CN$

LL8 (52 mg, $1.97x10^{-4}$ mol) and $[Os(bpy)_2Cl_2].2H_2O$ (120 mg, $1.97x10^{-4}$ mol) were placed in $15cm^{-3}$ of a 1:1 ethylene glycol/water mixture. This suspension was heated at

reflux for 24 hours and allowed to cool to room temperature. The solution was filtered at this stage to remove any excess unreacted ligand. A solution of aqueous ammonium hexafluorophosphate was added to the filtrate to precipitate a brown/green product. This product was isolated by filtration, washed with water and dried with diethylether. The compound was purified by column chromatography (stationary phase silica gel, mobile phase 80% acetonitrile, 20% water, 0.05M KNO_3 buffer) to yield 152 mg of pure compound. (73%)

^{1}H NMR (400 MHz, d_6-acetone) δ = 8.84 (d, 1H), 8.77 (m, 2H), 7.96 (m, 4H), 7.68 (d, 1H), 7.44 (dd, 1H), 7.36 (dd, 1H), 7.09 (m, 2H).

Elemental Analysis for $C_{38}H_{35}N_9O_1OsP_2F_{12}$. Calculated C 42.61, H 3.18, N 11.77. Found C 42.89, H 2.91, N 11.09 %.

4.3 Discussion of the Synthesis of the $[Os(bpy)_2(LL_x)](PF_6)_2$ complexes:

The osmium complexes proved more difficult to synthesise than the analogous ruthenium complexes. Synthesis of the starting materials *cis*-$[Os(bpy)_2Cl_2].2H_2O$ and *cis*-$[Os(d_8\text{-bpy})_2Cl_2].2H_2O$ was carried out according to literature procedures. [5] The reaction proved to be problematic however with great care needed to fully reduce the Os(III) compound to its Os(II) species. This was achieved by stirring the reaction mixture with a saturated solution of sodium dithionite for 12 hours. The presence of the paramagnetic Os(III) species was readily identifiable by ^{1}H NMR. It also proved extremely important that the product was washed properly with water to remove impurities after isolation. The major impurity present generally seemed to be $[Os(bpy)_3]^{2+}$. As the chloride salt of $[Os(bpy)_3]^{2+}$ is water soluble, complete removal of this impurity was achieved by continuous washing of the product until the filtrate was colourless. The purity of the starting materials were confirmed by HPLC and ^{1}H NMR.

Reaction of the osmium bisbipyridyl dichloride with the ligands in a 1:1 (v/v) mixture of ethylene glycol/water led to replacement of the chlorides, firstly by solvent molecules and subsequently by the ligands. The larger field splitting for osmium in comparison to ruthenium meant that the higher reaction temperature offered by ethylene glycol (b.p. 197 °C) rather than ethanol (b.p. 78 °C) or methanol (b.p. 65 °C) meant ethylene glycol would lead to the reaction to taking place with efficiency. For the same kinetic reasons the reaction time was increased from typically 4 hours for the ruthenium complexes to 24 hours for the osmium complexes. As the reaction proceeded, the deep violet colour of the refluxing $[Os(bpy)_2Cl_2]$ solution was replaced by a black/green colour typical of a solvated osmium N6 complex. The solid was precipitated by exchanging the chloride counter ion for a PF_6^- counter ion. The PF_6^- complexes are soluble in many organic solvents but are only slightly soluble in water. This greatly eases their purification and characterisation. The yield of these reactions were affected by the fact that ethylene glycol was used in the reaction mixture. The ethylene glycol was not removed before the addition of the saturated aqueous solution of NH_4PF_6 (due to its very high boiling point), and therefore while most of the desired complex precipitated as its PF_6 salt, some of the product remained in solution and was lost in the filtrate, resulting in reduced yields.

The reactions were all monitored by HPLC. This allowed for accurate determination of the end point of the reaction and gave an indication as to the type of purification necessary. The complexes were purified by column chromatography on silica gel and a mobile phase of 4:1(v/v) acetonitrile/water containing 0.05M KNO_3 proved to be the most effective. The desired complex generally eluted as the main band, was dark green in colour and was often preceded by a minor band which consisted of unreacted starting materials, i.e. free ligand and solvated osmium bisbipyridyl.

4.4 HPLC Analysis of the $[Os(bpy)_2(LL_x)](PF_6)_2$ complexes:

The purification of the osmium bisbipyridyl LLx complexes has been detailed in the experimental section (Chapter 4.2). As for the ruthenium(II) complexes, High Performance Liquid Chromatography (HPLC) has been an important tool in determining

the purity of the desired complexes. As before, HPLC provides the opportunity to analyse the progress of the reaction, the purity of the crude product, the nature of impurities, and the purity of the desired complex quickly and simply. Again, analysis of the crude product resulted in three main peaks. The first corresponded to the uncharged free ligand, the second to solvated $[Os(bpy)_2]$ while the third, the main band, corresponded to the desired product.

The HPLC traces of the purified complexes are presented in Figure 4.1, and is followed by the tabulated results of the HPLC analysis in Table 4.1.

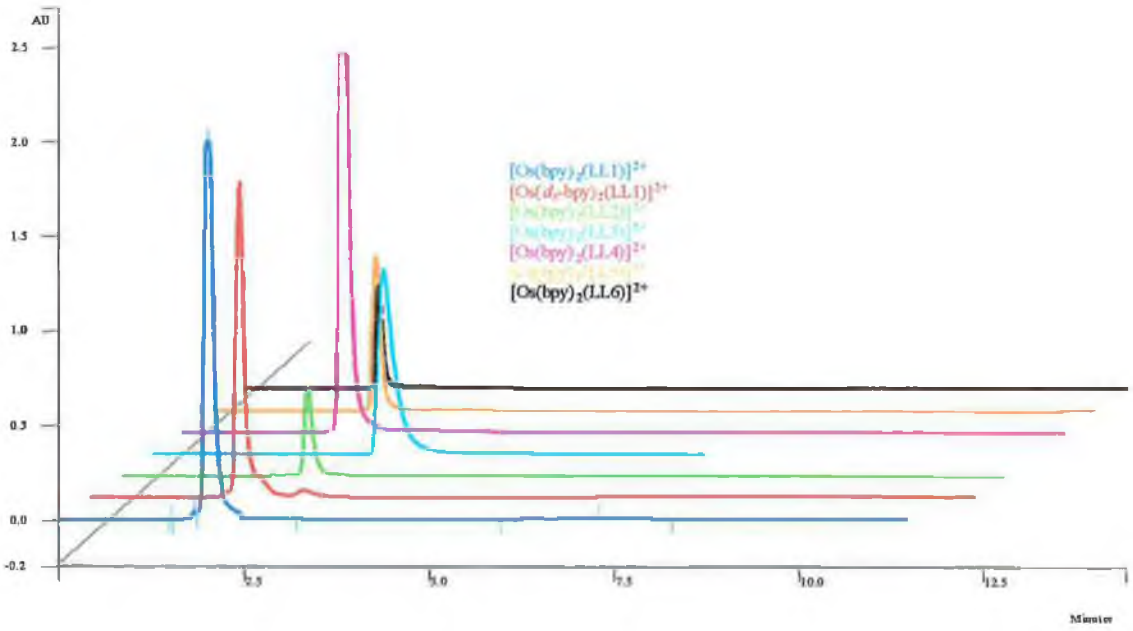

Figure 4.1HPLC traces of the purified osmium complexes.

Compound	Retention Time (min)	Compound	Retention Time (min)
$Os(bpy)_2Cl_2.2H_2O$	1.49	$Os(bpy)_2(LL3)^{2+}$	2.67
$Os(bpy)_2(LL1)^{2+}$	2.01	$Os(bpy)_2(LL4)^{2+}$	2.18
$Os(d_8\text{-}bpy)_2(LL1)^{2+}$	2.01	$Os(bpy)_2(LL5)^{2+}$	2.20
$Os(bpy)_2(LL2)^{2+}$	2.53	$Os(bpy)_2(LL6)^{2+}$	1.81

Table 4.1 HPLC data from osmium complexes.

As can be seen from Figure 4.1 the complexes were successfully purified by column chromatography and appear pure by HPLC. The analysis of the complexes by HPLC indicated a purity of >97% in all cases. The retention times are typical of osmium(II) polypyridyl complexes and are comparable to the retention time of $[Os(bpy)_3]^{2+}$ when examined under similar conditions.

The lack of variation in the retention times between the complexes containing LL_x ligands indicate that the LL_x ligand interacts little with the column, and is less important than the charge of the complex in determining the amount of time the compound spends on the column. This is further illustrated on examination of the retention time of the neutral complex $[Os(bpy)_2Cl_2].2H_2O$, which was found to have a retention time of 1.49 min which compares to times ranging from 1.80 to 2.67 minutes for the other compounds. This is expected as the column is a cation exchange column and therefore is more responsive to changes in charge than changes in the "organic" make up of the complexes.

As before HPLC has proven a useful starting point in the structural and purity determination of the complexes. This charaterisation is completed by ^1H NMR which is the topic of the next section.

4.5 ^{1}H NMR Spectroscopy of the Osmium(II) complexes:

As in the case of the ruthenium(II) complexes discussed in Chapter 3, ^{1}H NMR has proved to be an invaluable tool in determining both the structure and the purity of the osmium(II) complexes which are being discussed. As in the case for the ruthenium analogues, complete assignment of each proton in each complex was not possible due to the complexity of the aromatic region of the ^{1}H spectrum. It has proved possible to assign all the protons of the LL_x ligands for the osmium(II) complexes of LL1, LL2 and LL3.

The resonances of the protons of the osmium(II) bound complexes are found at higher field than those of the analogous ruthenium(II) bound complexes. This is due to the greater shielding effect experienced by the ligands in osmium complexes because of the relatively stronger metal $d\pi \rightarrow \pi^*$(bpy) back donation compared to ruthenium. [4] (The Os(II) orbitals are higher in energy). This phenomenon is illustrated in Figure 4.3, whereby the protons of the osmium complexes appear at slightly higher field than the analogous ruthenium complexes. Despite this however, comparison with the spectra of the ruthenium analogues is possible, and therefore reference will be made to the ^{1}H NMR discussion in Chapter 3.5 as appropriate. The labelling of the ligand protons used in the assignment is the same as that used in Chapter 3 (Figure 4.2). The ^{1}H NMR of the complexes containing the LL1, LL2 and LL3 ligands can be seen in Figure 4.5.

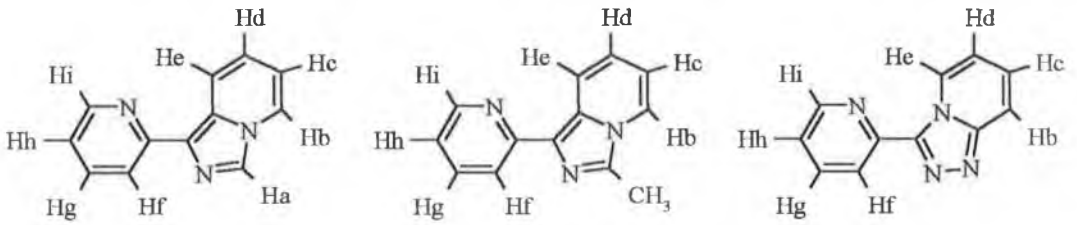

LL1 LL2 LL3

Figure 4.2 Labelling of the protons of LL1, LL2 and LL3 for ^{1}H NMR discussion.

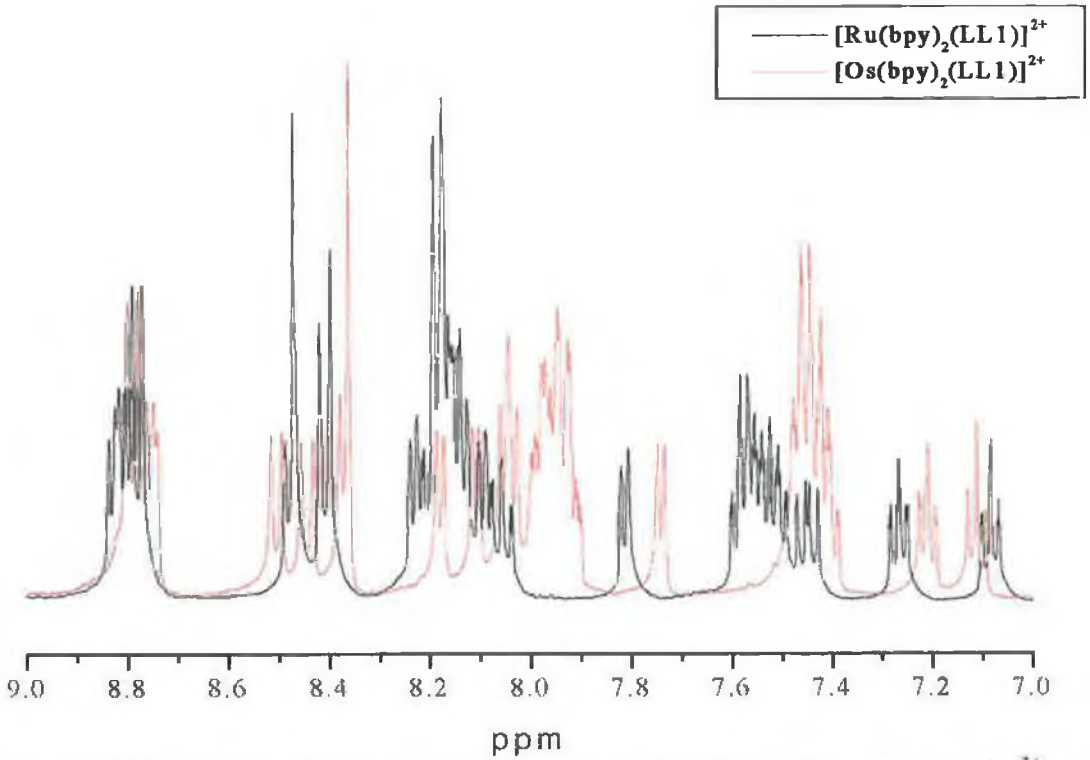

Figure 4.3 Illustration of the phenomenon where the protons of $[Os(bpy)_2(LL1)]^{2+}$ appear at slightly higher field than those of the analogous $[Ru(bpy)_2(LL1)]^{2+}$ complex. Both complexes in d_6-acetone.

The next section involves a detailed examination and assignment of the peaks in the ^1H NMR spectrum of $[Os(bpy)_2(LL1)](PF_6)_2$, $[Os(bpy)_2(LL2)](PF_6)_2$ and $[Os(bpy)_2(LL3)](PF_6)_2$. The spectra can be seen in Figure 4.4.

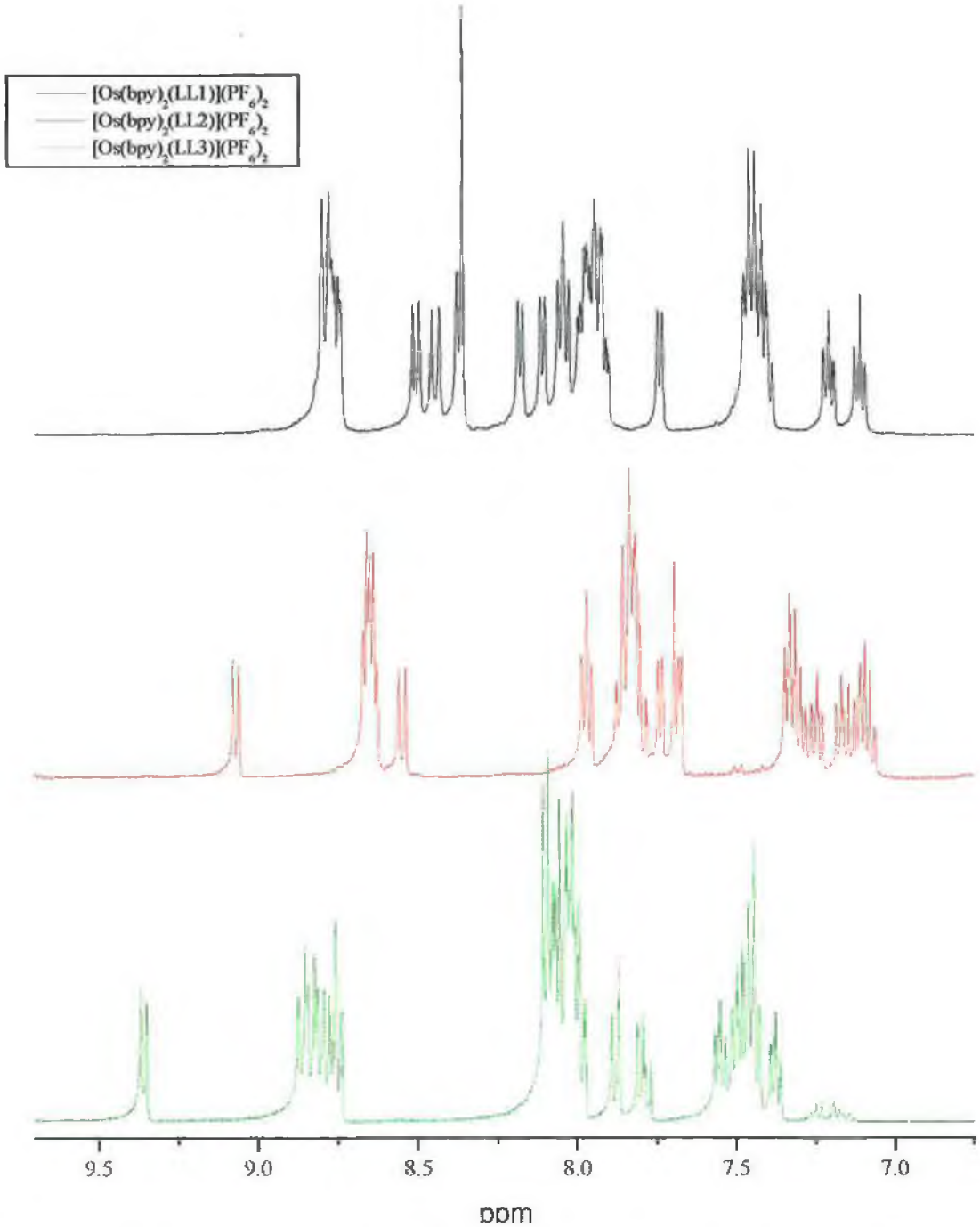

Figure 4.4 ^1H NMR of the complexes $[Os(bpy)_2(LL1)](PF_6)_2$, $[Os(bpy)_2(LL2)](PF_6)_2$ and $[Os(bpy)_2(LL3)](PF_6)_2$ in d_6-acetone.

In order for the protons of the LL1, LL2 and LL3 ligands in the osmium(II) complexes to be assigned accurately it was important to synthesise the complexes with deuteriated

2,2'-bipyridyl ligands in order to remove these resonances from the proton spectra. [6,7] As in the case of the ruthenium(II) complexes, this approach in conjunction with 2D COSY NMR of the deuteriated complexes, and using the ^{1}H NMR spectra and assignment of the free ligands eased the assignment substantially. The 2D COSY NMR of $[Os(d_8\text{-bpy})_2(LL1)]^{2+}$ is presented in Figure 4.5.

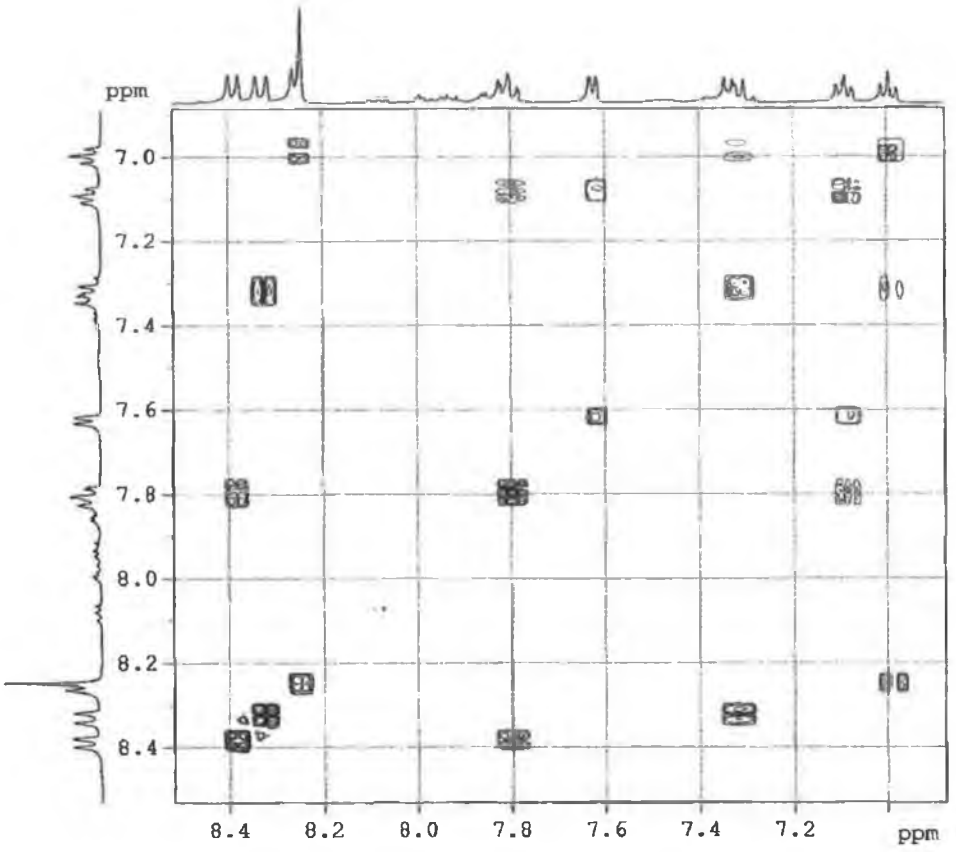

Figure 4.5 2D COSY NMR of the deuterated complex $[Os(d_8\text{-bpy})_2(LL1)]^{2+}$ in d_6-acetone. This spectrum was used to assign the peaks of the LL1 ligand in the osmium(II) complex.

Table 4.2 provides a significant insight into what happens to the LL_x ligands upon coordination. It can be seen that most of the protons are shifted slightly in comparison to the free ligand. This is due to the altered electron density the ligand will experience when bonded to the metal. There is an exception however and that is in the case of the H_i proton. This is most likely due to the orientation of the proton, which is directed

towards one of the pyridine rings of the adjacent 2,2'-bipyridiyl rings. The ring current induces a diamagnetic anisotropic interaction effect which results in a large upfield shift (approx. 1ppm).[4] This phenomenon has been discussed in Chapter 3.5 in more detail.

Proton	Chemical Shift in d_6-acetone (ppm)		
	$[Os(bpy)_2$**(LL1)**$](PF_6)_2$	$[Os(bpy)_2$**(LL2)**$](PF_6)_2$	$[Os(bpy)_2$**(LL3)**$](PF_6)_2$
H_a	8.21 (8.37)	No Ha	No Ha
H_b	8.23 (8.38)	8.64 (7.47)	7.72 (8.50)
H_c	6.97 (6.77)	7.11 (6.72)	7.67 (8.04)
H_d	7.29 (6.99)	7.30 (6.63)	7.31 (7.50)
H_e	8.30 (8.59)	8.55 (9.78)	7.95 (9.84)
H_f	8.18 (8.18)	8.64 (8.17)	9.23 (7.85)
H_g	7.78 (7.78)	7.97 (7.72)	7.31 (7.50)
H_h	7.14 (7.14)	7.11 (7.14)	7.95 (7.14)
H_i	7.60 (8.62)	7.73 (8.49)	8.76 (8.78)

Table 4.2 Comparison of the chemical shifts of the LL1, LL2 and LL3 aromatic protons in their complexed and free (in parenthesis) forms, measured in d_6-acetone.

It did not prove possible to deuteriate the LL1 ligand however. Several attempts to deuteriate the ligand were made but the conditions seem to have been too harsh and led to decomposition of the ligand. This has complicated the assignment of the 2,2'-bipyridyl rings of the ^{1}H NMR spectra as many of the peaks overlap.

As in Chapter 3.5 the situation for the complexes of the ligands LL4, LL5 and LL6 is much different. The ^{1}H NMR spectra contain exactly double the expected number of protons for each of osmium complexes.

The ^{1}H NMR spectra of the LL4 ligand is as expected with 11 well defined, well resolved peaks visible (Figure 3.16). Without the isomerisation effect, the ^{1}H NMR spectrum of $[Os(d_8\text{-bpy})_2(LL4)](PF_6)_2$ should resemble that of the free ligand for many of the protons. This is not the case, and the integration of the spectrum indicates the presence of 26 individual protons, even though only 13 protons should be present. This

doubling of the number of signals means that even this ^{1}H NMR spectrum, which should be easily assigned becomes impossible to. The most important observations to make about the spectra of the complex involve the relative position of the proton of the OH group.

Proton	Chemical Shift in d_6-acetone (ppm)	
OH in free ligand	10.99	
OH in complex	10.40	9.23

Table 4.3 Comparative positions of the OH protons in the free and osmium(II) complex containing the LL4 ligand.

As in the case for the ruthenium(II) complex containing the LL4 ligand, it was verified that the signals were in fact due to OH groups by simply adding D_2O to the ^{1}H NMR sample. The disappearance of both signals proved they were OH groups. This experiment is illustrated in Figure 4.6.

The position of these protons are slightly upfield in comparison to the ruthenium complex, however the principle remains the same. This effect has been discussed in detail in Chapter 3.5 and need not be discussed again here. The ^{1}H NMR spectra of the ligand, the complex and the spectrum of the complex after the addition of D_2O to the sample are illustrated in Figure 4.6.

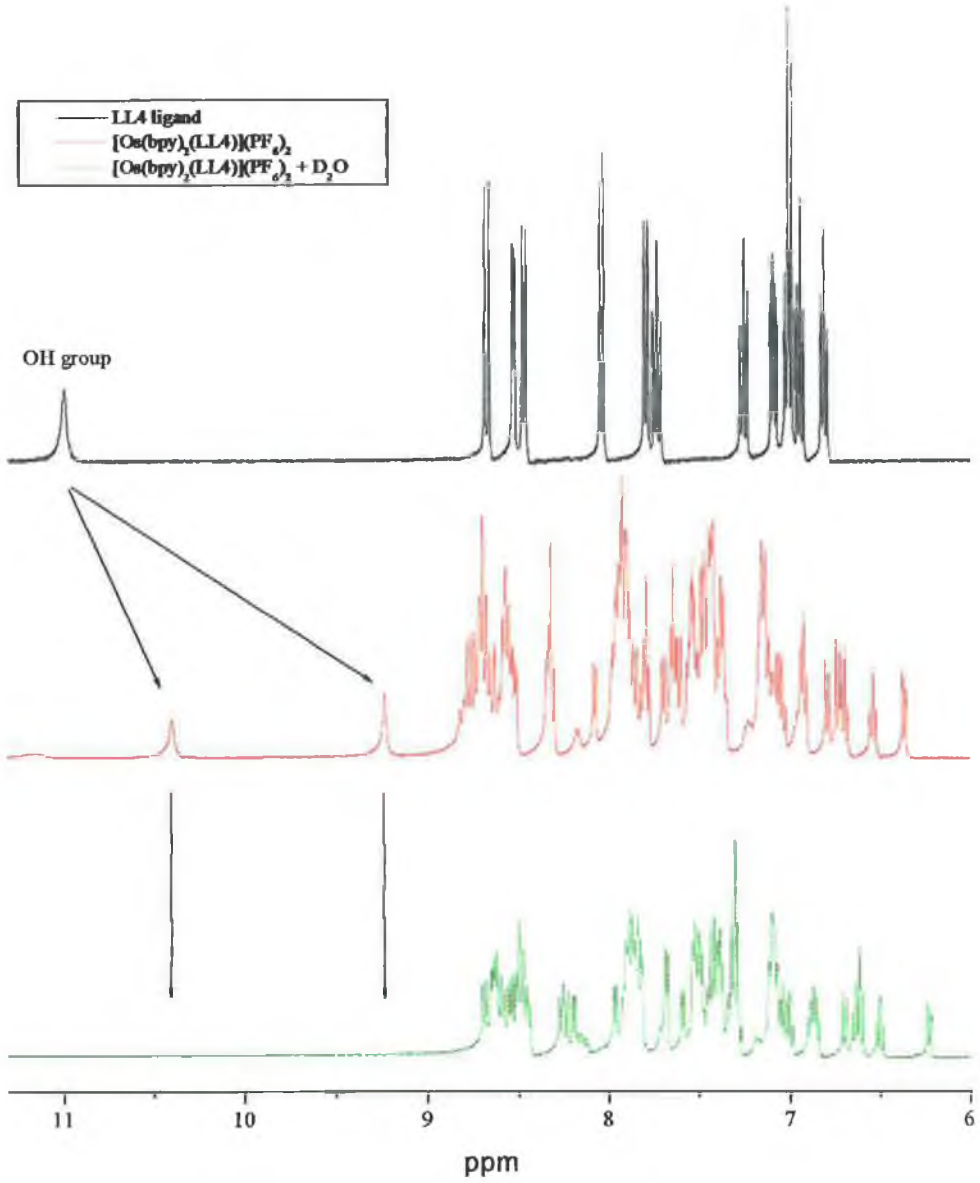

Figure 4.6 ^1H NMR spectra of LL4 ligand, $[Os(bpy)_2(LL4)](PF_6)_2$ and $[Os(bpy)_2(LL4)](PF_6)_2$ with D_2O in d_6-acetone.

The ^1H NMR spectra of the other complexes which exhibit this type of isomerism are given in Figures 4.7 and 4.8.

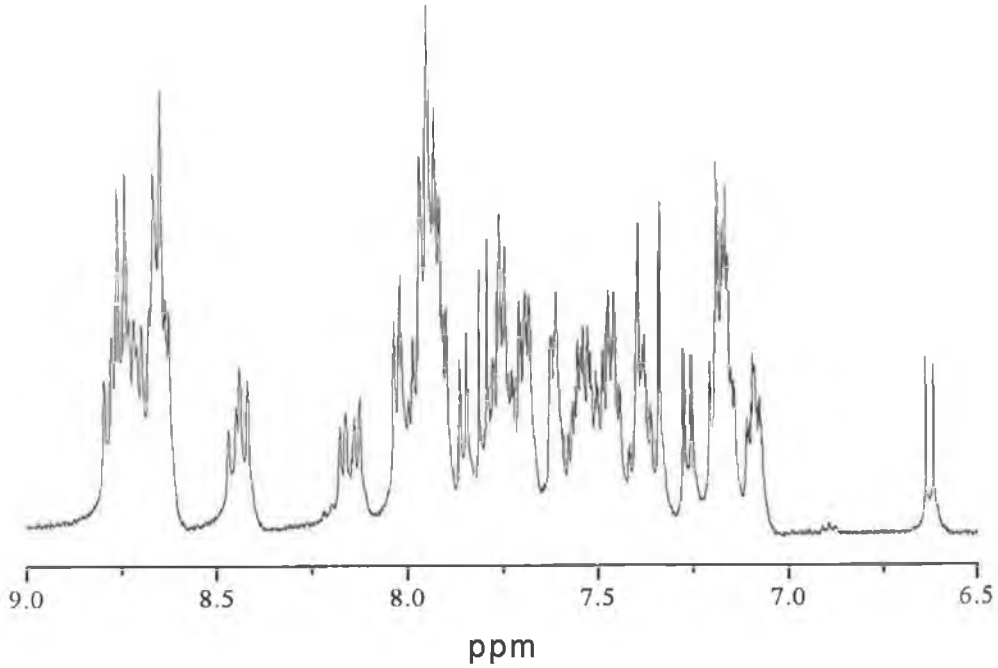

Figure 4.7 ^1H NMR of $[Os(bpy)_2(LL5)](PF_6)_2$ in d_6-acetone

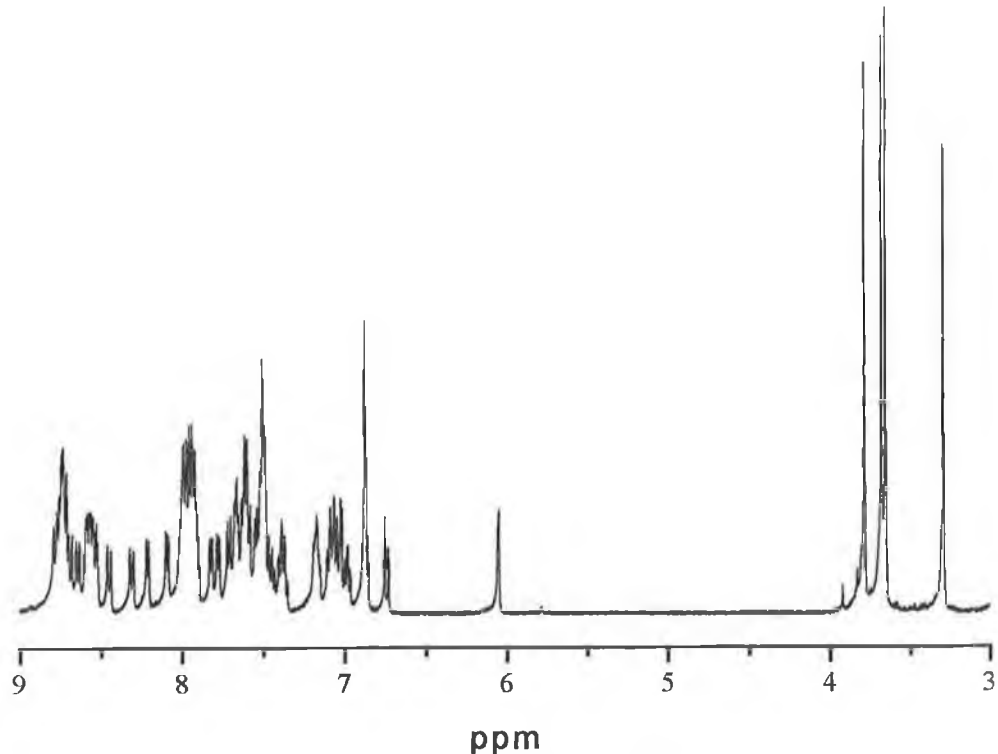

Figure 4.8 ^1H NMR of $[Os(bpy)_2(LL6)](PF_6)_2$ in d_6-acetone

As in the case of the ruthenium complexes of the LL5 and LL6 ligands the presence of the conformational isomers is evident in both of the above spectra. In the case of $[Os(bpy)_2(LL5)](PF_6)_2$, the peak at 6.61 ppm appears to be a doublet. This peak however should be a singlet. (See Chapter 3, Figure 3.29).

The evidence is even more pronounced in the ^1H NMR spectra of $[Os(bpy)_2(LL6)](PF_6)_2$. Examination of the LL6 ligand, indicates that two singlets should be observed in the aliphatic region of the ^1H NMR, integrating to three protons and representing the methoxy protons. As can be seen from the ^1H NMR in Figure 4.8, the reality is different and 4 methoxy signals, each integrating to 3 protons are clearly visible providing further proof of the presence of these conformational isomers.

The final complex in the series is that synthesised with the symmetrical LL8 ligand. The ^1H NMR of the $[Os(bpy)_2(LL8)](PF_6)_2$ complex can be seen in Figure 4.9. Unlike in the previous three examples, no isomerisation is evident in the ^1H spectra of the complex, and due to its symmetrical nature, the spectrum has been simplified, with each signal representing two equivalent protons.

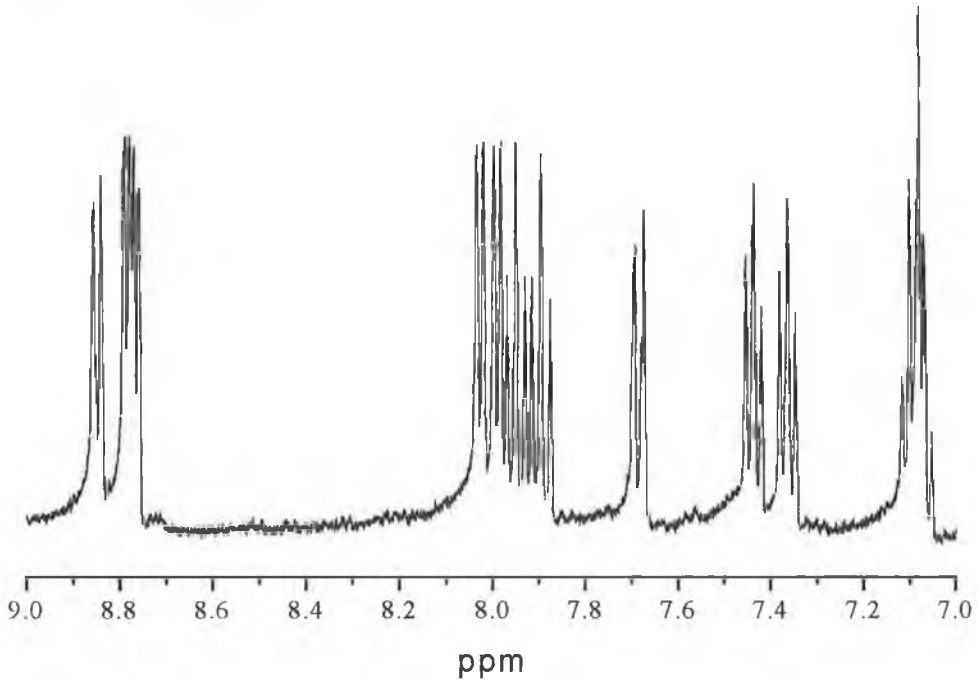

Figure 4.9 ^1H NMR of the $[Os(bpy)_2(LL8)](PF_6)_2$ complex in d_6-acetone.

The protons of the LL8 ligand have been assigned and are listed in Table 4.4.

Proton	Chemical Shift (ppm)
H_b	7.69 (7.51)
H_c	7.08 (6.70)
H_d	7.08 (6.70)
H_e	8.77 (9.68)

Table 4.4 Chemical shifts of the LL8 ligand in the complex $[Ru(bpy)2(LL8)]^{2+}$ and as a free ligand (in parenthesis).

Coordination has altered the electron density of the ligand. Coordination has an electron withdrawing or deshielding effect, and lowers the electron density of the ligand. This leads to most of the ligands protons being shifted downfield, with the exception of the He proton which experiences an upfield shift of *circa* 1 ppm. This is due to the change in orientation experienced by the ligand on coordination. In the free ligand, the H_e proton is hydrogen bonded to the free nitrogen of the pyridyl ring, however on coordination, this nitrogen coordinates to the metal centre, and the hydrogen bonding interaction is lost resulting in the large upfield shift of the H_e proton on coordination.

4.6 UV/Vis Absorption and Emission Spectroscopy and Emission Luminescence Lifetimes of the Osmium(II) complexes:

As discussed in the introduction to this chapter, the photophysics of analogous ruthenium and osmium complexes have many similarities, but they also exhibit several differences. (Figure 4.10). These differences arise from the larger spin-orbit coupling of third-row transition elements in comparison to second row metals. This increased coupling results in increased mixing of the singlet and triplet states and results in formally forbidden transitions such as the ($d\pi \rightarrow \pi^*$) ^{3}MLCT absorption band, which is weak for $[Ru(bpy)_3]^{2+}$ but quite intense for $[Os(bpy)_3]^{2+}$. [8]

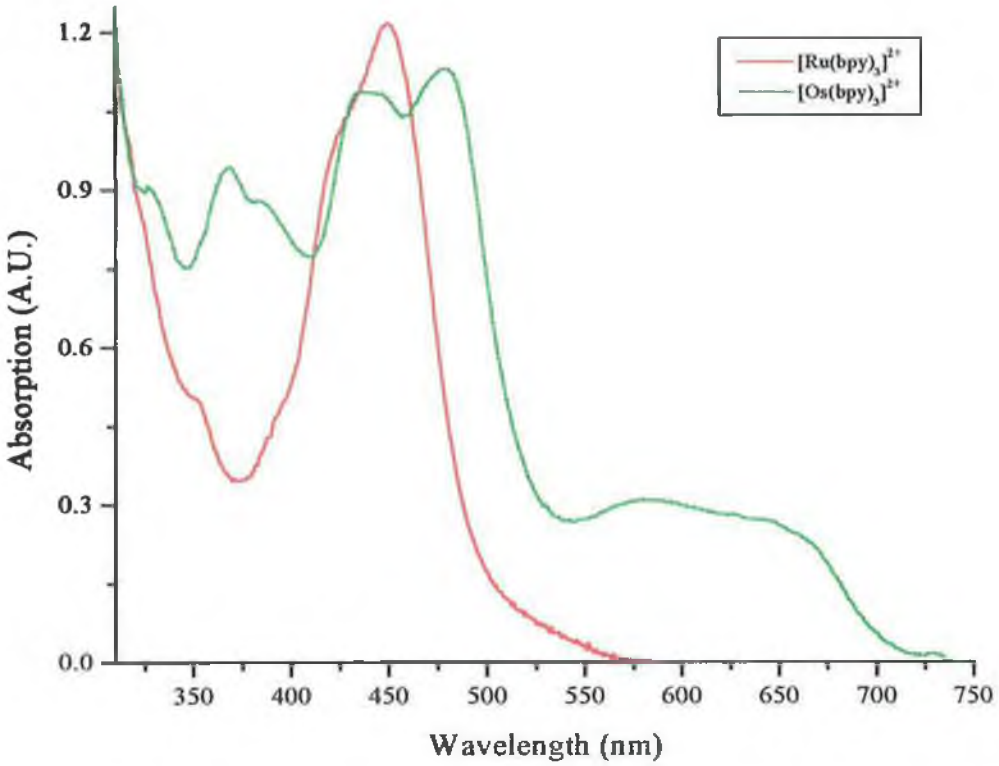

Figure 4.10 Comparison of the absorption spectra of $[Os(bpy)_3]^{2+}$ and $[Ru(bpy)_3]^{2+}$ in MeCN.

The absorption spectra of the range of compounds synthesised are presented here (Figures 4.11 and 4.12). The absorption spectra of the complexes show only slight differences between the different complexes of the series.

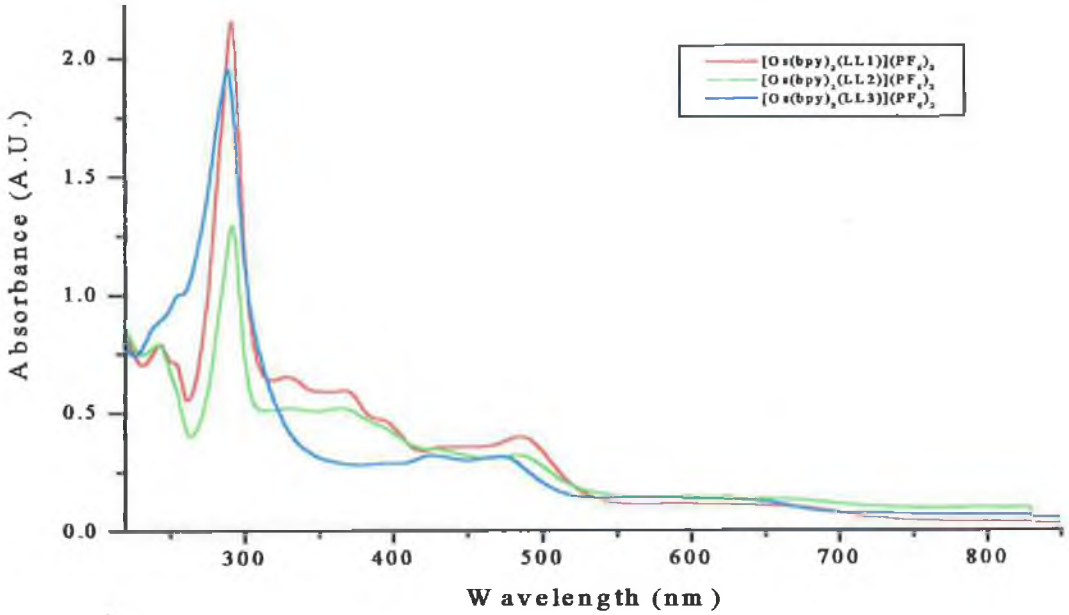

Figure 4.11 Absorption spectra of the complexes $[Os(bpy)_2(LL1)](PF_6)_2$ (black), $[Os(bpy)_2(LL2)](PF_6)_2$ (red) and $[Os(bpy)_2(LL3)](PF_6)_2$ (blue) in MeCN.

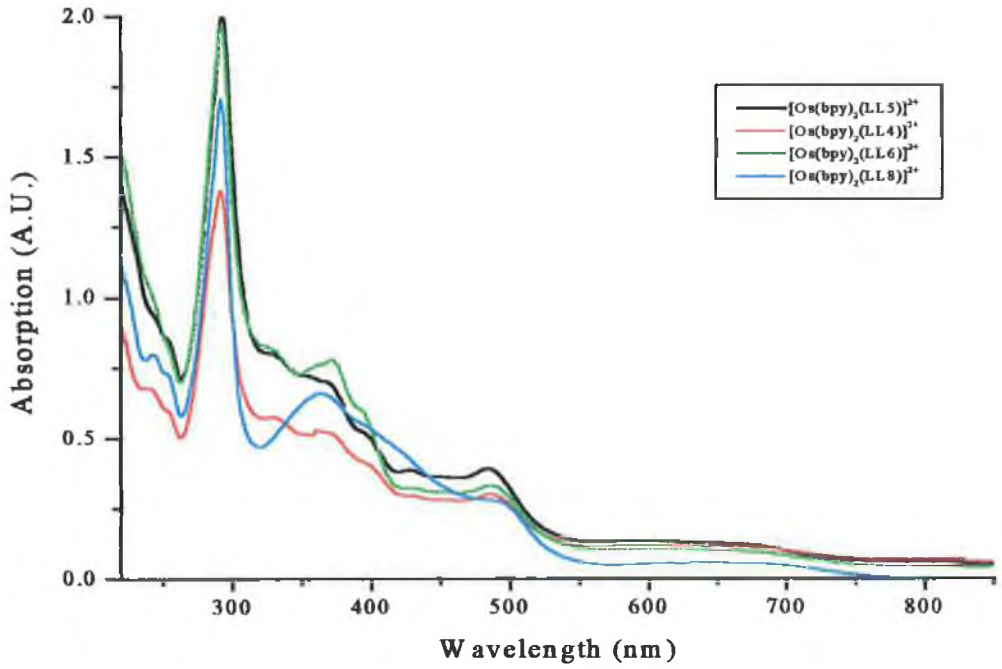

Figure 4.12 Absorption spectra of the complexes $[Os(bpy)_2(LL5)](PF_6)_2$ (black), $[Os(bpy)_2(LL4)](PF_6)_2$ (red), $[Os(bpy)_2(LL6)](PF_6)_2$ (green) and $[Os(bpy)_2(LL8)](PF_6)_2$ (blue) in MeCN.

Figure 4.13 shows a comparison of the absorption spectra of the complexes $[Os(bpy)_2(LL1)]^{2+}$ and the free LL1 ligand. As well as the normal bipyridyl centred (LC) $\pi \rightarrow \pi^*$ bands (λ_{max} at *circa* 290 nm) a new absorption band in the region 320 nm to 400 nm has appeared. Comparison of this band to the free ligand shows that this band may be attributed to the introduction of the ligand into the complex and that this band may be attributed to ligand centred (LC) $\pi \rightarrow \pi^*$ transitions on the LL1 ligand. This pattern is the same for each of the osmium complexes.

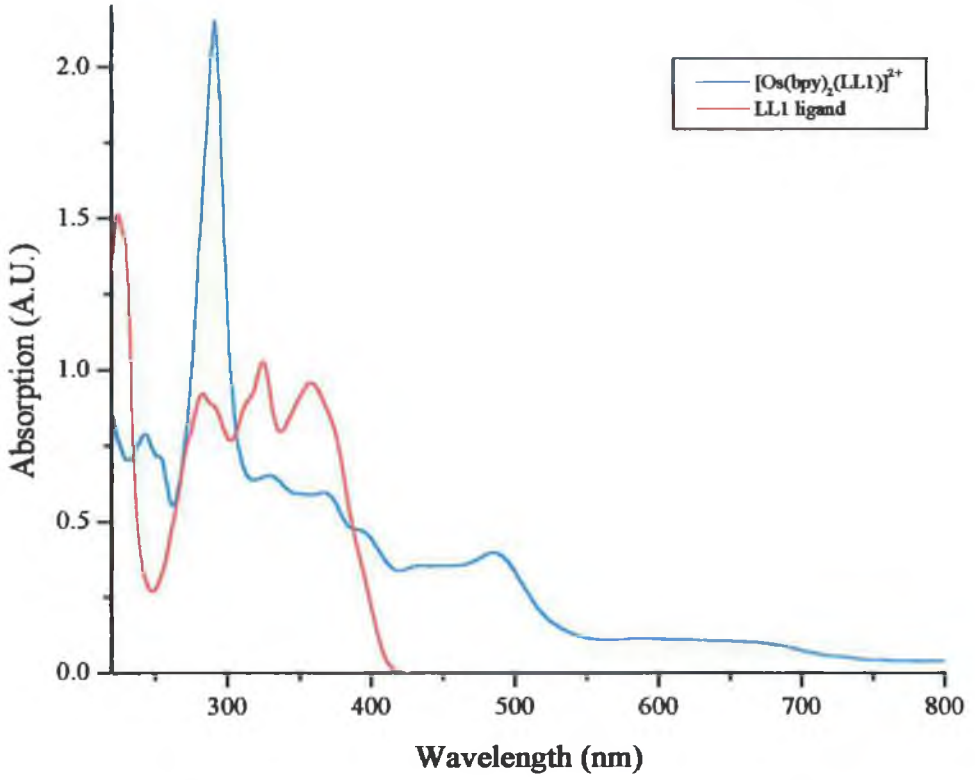

Figure 4.13 Comparison of the absorption spectra of the complex $[Os(bpy)_2(LL1)]^{2+}$ and the free LL1 ligand in MeCN.

Replacement of the ruthenium(II) metal centre with osmium(II) causes a shift to lower energy of the MLCT absorption bands. This has been observed for other systems, and is due to the higher energy of the osmium 5d orbitals, compared to the ruthenium 4d orbitals. [9] Osmium complexes contain absorption bands which are not present in the

absorption spectra of the ruthenium analogues in the range 600-660 nm.[10] Table 4.5 lists the data from the spectroscopic investigations of the osmium(II) complexes containing LL_x ligands.

For osmium(II) polypyridyl complexes, the room temperature excited state properties are determined by a series of three low energy Boltzmann populated MLCT states. These states have considerable triplet character and behave kinetically as a single state.[11]

All the complexes exhibit room temperature emissions in acetonitrile. The emission maxima of the osmium complexes occur at lower energy than that of $[Os(bpy)_3]^{2+}$ with the exception of the complex containing the LL3 ligand. It appears that the exchange of the imidazo ring for a triazo ring has the effect of reducing the σ-donating ability of the LLx ligand. In general however, as in the case of the ruthenium(II) complexes the emission at lower energy is indicative of the LL_x ligands having stronger σ-donating ability in the osmium complex than 2,2'-bipyridyl. As before, this leads to an increase of electron density on the metal (relative to $[Os(bpy)_3]^{2+}$), which causes a decrease in the t_{2g}-^{3}MLCT energy gap, and therefore a lowering of the emission energy, i.e. a red shift in the emission maxima.

The emission maxima of the osmium complexes occur at lower energy than those of the analogous ruthenium(II) complexes. This is as expected and this observation is in agreement with the lower oxidation potentials observed for the osmium complexes in comparison with their ruthenium counterparts. As already observed, this is due to the energy difference between the metal t_{2g} and bpy π* orbitals, which is smaller for osmium than ruthenium which in turn means the energy of the MLCT transitions will be lower.

Compound	Absorption		Emission	
	λ_{max} (nm)	$\varepsilon \times 10^{-4}$ ($M^{-1}cm^{-1}$)	λ_{max} (nm) 298K	λ_{max} (nm) 77K
$[Os(bpy)_3]^{2+}$	640	—	725	712
$[Os(bpy)_2(LL1)]^{2+}$	488	1.46	753	730
	609	0.41		
$[Os(bpy)_2(LL2)]^{2+}$	485	1.34	753	728
	622	0.60		
$[Os(bpy)_2(LL3)]^{2+}$	475	1.54	718	693
	567	0.69		
$[Os(bpy)_2(LL4)]^{2+}$	489	1.53	769	731
	599	0.60		
$[Os(bpy)_2(LL5)]^{2+}$	486	1.69	751	726
	589	0.59		
$[Os(bpy)_2(LL6)]^{2+}$	488	1.20	764	731
	595	0.41		
$[Os(bpy)_2(LL8)]^{2+}$	486	1.39	782	760
	655	0.65		

Table 4.5 Absorption and emission data of the $[Os(bpy)_2(LL_x)]^{2+}$ complexes. Measurements performed in acetonitrile except for those at 77K which were performed in butyronitrile.

The room temperature emission spectra of the osmium(II) bisbipyridyl complexes are given in Figures 4.14 and 4.15.

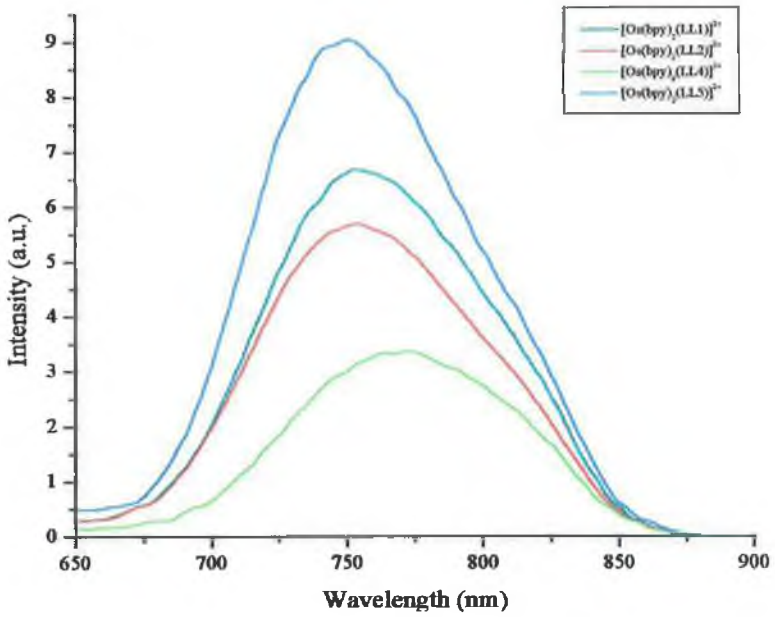

Figure 4.14 Room temperature emission spectra of the $[Os(bpy)_2(LL1)]^{2+}$, $[Os(bpy)_2(LL2)]^{2+}$, $[Os(bpy)_2(LL4)]^{2+}$, and $[Os(bpy)_2(LL5)]^{2+}$ complexes in MeCN. Emission spectra measured at the maxima of absorbance.

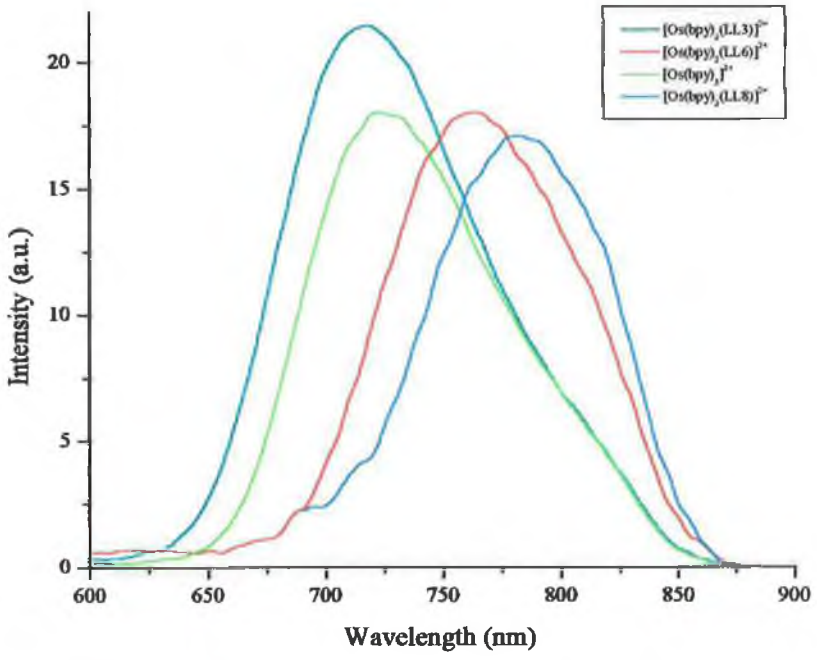

Figure 4.15 Room temperature emission spectra of the $[Os(bpy)_2(LL3)]^{2+}$, $[Os(bpy)_2(LL6)]^{2+}$, $[Os(bpy)_2(LL8)]^{2+}$, and $[Os(bpy)_3]^{2+}$ complexes in MeCN. Emission spectra measured at the maxima of absorbance.

At 77K, all the complexes exhibit strong emission showing a vibrational structure. This vibrational fine structure has been attributed to relaxation via 2,2'-bipyridine-based vibrations [12] and is common for both ruthenium and osmium complexes. As discussed in Chapter 3, cooling to 77K leads to a blue shift in the emission maxima of the complexes. [13] This shift is due to a phenomenon known as "rigidchromism" and has been discussed in Chapter 3.8. Illustrative low temperature emission spectra are presented in Figure 4.16.

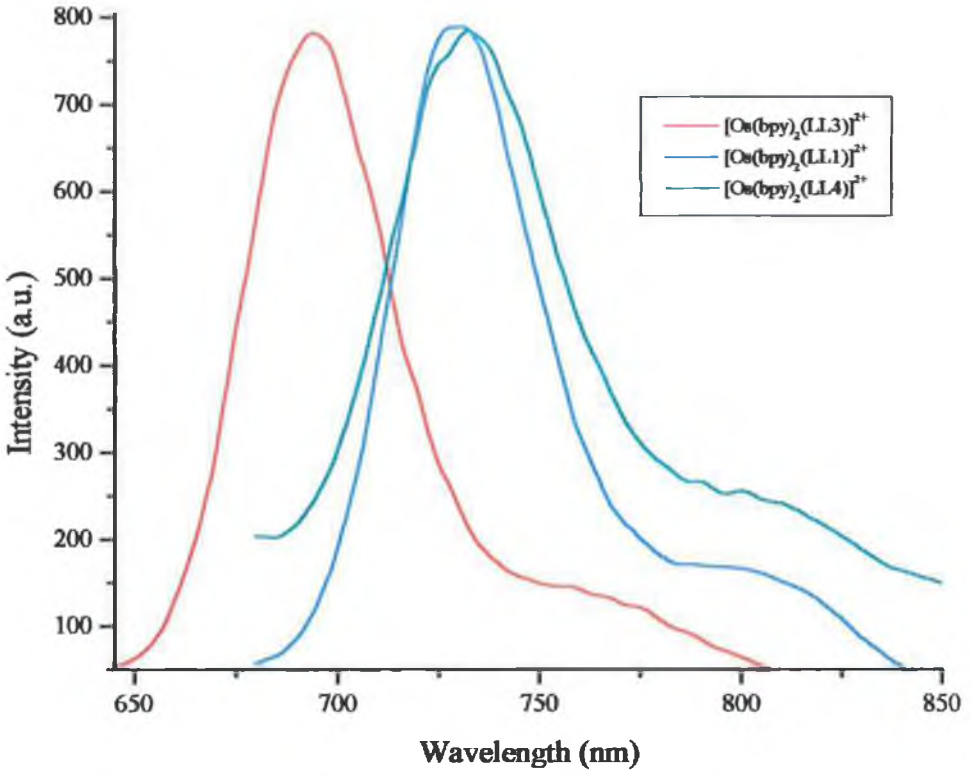

Figure 4.16 Typical emission spectra of the $[Os(bpy)_2(LL_x)]^{2+}$ complexes at 77K in butyronitrile. Spectra have been normalised for comparison.

The luminescent lifetimes of the osmium complexes have also been determined. The results are collated in Table 4.6.

Compound	298K, aerated	298K, deaerated	77K
	τ (ns)	τ (ns)	τ (ns)
$[Os(bpy)_3]^{2+}$	--	62	940
$[Os(bpy)_2(LL1)]^{2+}$	29	34	856
$[Os(d_8\text{-bpy})_2(LL1)]^{2+}$	39	56	2254
$[Os(bpy)_2(LL2)]^{2+}$	28	37	864
$[Os(bpy)_2(LL3)]^{2+}$	46	71	1350
$[Os(bpy)_2(LL4)]^{2+}$	21	24	842
$[Os(bpy)_2(LL5)]^{2+}$	31	37	853
$[Os(bpy)_2(LL6)]^{2+}$	23	26	783
$[Os(bpy)_2(LL8)]^{2+}$	16	18	470

Table 4.6 Emission data for the $[Os(bpy)_2(LLx)]^{2+}$ complexes. Measurements at 298K in MeCN, at 77K in butyronitrile.

The results of both the room temperature and low temperature lifetime data of the osmium complexes are comparable to those of the "parent" $[Os(bpy)_3]^{2+}$. The lifetime of MLCT excited states of both ruthenium and osmium polypyridyl complexes in fluid solution are expected to be dominated by non-radiative processes. [14] The energy gap law [15] predicts that the rate of non-radiative decay should increase as the gap between the ground and excited state decreases. This means that complexes with low energy bands are generally weakly emitting and have short-lived excited state.[16]

As in the case of the ruthenium complexes, the luminescent lifetime study has been used to aid in the characterisation and location of the excited state. The use of the selective deuteration of moieties within the molecule and the examination of the effect this selective deuteration has on the lifetime of the complex has been discussed in relation to the ruthenium complexes (Chapter 3.8) whereby deuteration reduces both the amplitude and the frequency of C-H vibrational modes and therefore C-D vibrations are of a lower

frequency and amplitude than the equivalent C-H vibrations which results in an increase in the observed lifetime of the electronically excited state. [6] As in the analogous ruthenium complexes, the bipyridyl ligands have been deuterated and the effect this has on the lifetime of the $[Os(bpy)_2(LL1)]^{2+}$ complex was examined. It was observed that the lifetime in deaerated MeCN increased from 34 ns for the undeuterated complex to 62 ns for the deuterated analogue. This is an increase of over 80%. The effect deuteration had on the lifetime of the complex at 77K was even more pronounced with the lifetime increasing from 850 ns to 2250 ns in butyronitrile, an increase of over 250%. An increase was observed also in the case of the lifetimes in aerated MeCN, however this results may prove unreliable as quenching by oxygen may have a greater effect on the lifetime than deactivation of the excited state by C-H vibrations.

A relationship can be established between the photophysical data and the electrochemical potentials [17]. In a MLCT process, an electron is removed from the filled metal orbital to an empty ligand orbital ($d\pi \rightarrow \pi^*$). Oxidation is also the removal of an electron from the d-orbitals and in the case of reduction, an electron is transferred to the lowest unoccupied molecular orbital (LUMO) of the complex. This also helps to explain what happens in an MLCT process. By determining the LUMO using electrochemical means, this information may be used to elucidate the nature of the emissive state. From the electrochemical measurements achieved for the mixed ligand complexes, the first two reduction potentials appear to be directed to the two 2,2'-bipyridyl ligands, indicating that the π^* levels of the 2,2'-bipyridyl ligands are lower in energy than those of the new ligand. It is expected therefore that for the mixed ligand complexes that the observed emission is bipyridyl-based. This is discussed further in Chapter 4.8.

These observations allow us to locate the 2,2'-bipyridyl ligand as the location of the excited state. This is as expected and agrees with the observations made for other polypyridyl osmium complexes containing σ- donating ligands where the excited state has been located on the bipyridyl ligands rather than on the σ- donating ligands.

4.7 Photochemistry of the osmium(II) complexes:

The previous section has detailed the photophysical properties of a series of polypyridyl complexes of osmium(II) which, as expected, are closely related to those of the analogous ruthenium complexes discussed in Chapter 3. In general, a major difference does exist between osmium and ruthenium complexes, and that is in terms of photochemical instability towards ligand loss. [18,19,20] As already explained, for $[Ru(bpy)_3]^{2+}$ and related complexes, thermal population of low-lying dd states reduces the excited state lifetimes, and leads to decomposition of the complex by loss of ligands. [21,22,23,24] This ligand loss photochemistry compares to a remarkable lack of photochemistry observed for osmium polypyridine complexes. This photochemical stability is a consequence of the higher 10Dq for Os, which raises the energy of the low lying dd states preventing significant population at room temperature. This is not to say that photosubstitution has not been observed for osmium complexes. For the complex $[Os(bpy)_2(Me_2SO)_2]^{2+}$, [18] where the high energy emitting MLCT state(s) may approach the dd state in energy this has been observed, as for certain terpy complexes of Os where the terpy ligand causes mixing of the $d\pi$ and $d\sigma^*$ orbitals. Most interestingly it is believed that photosubstitution could occur from the MLCT states containing weak σ donor ligands. [18] The results of the experiments to examine photochemistry of the $[Os(bpy)_2(LL1)]^{2+}$ complex in MeCN are presented in Figure 4.17.

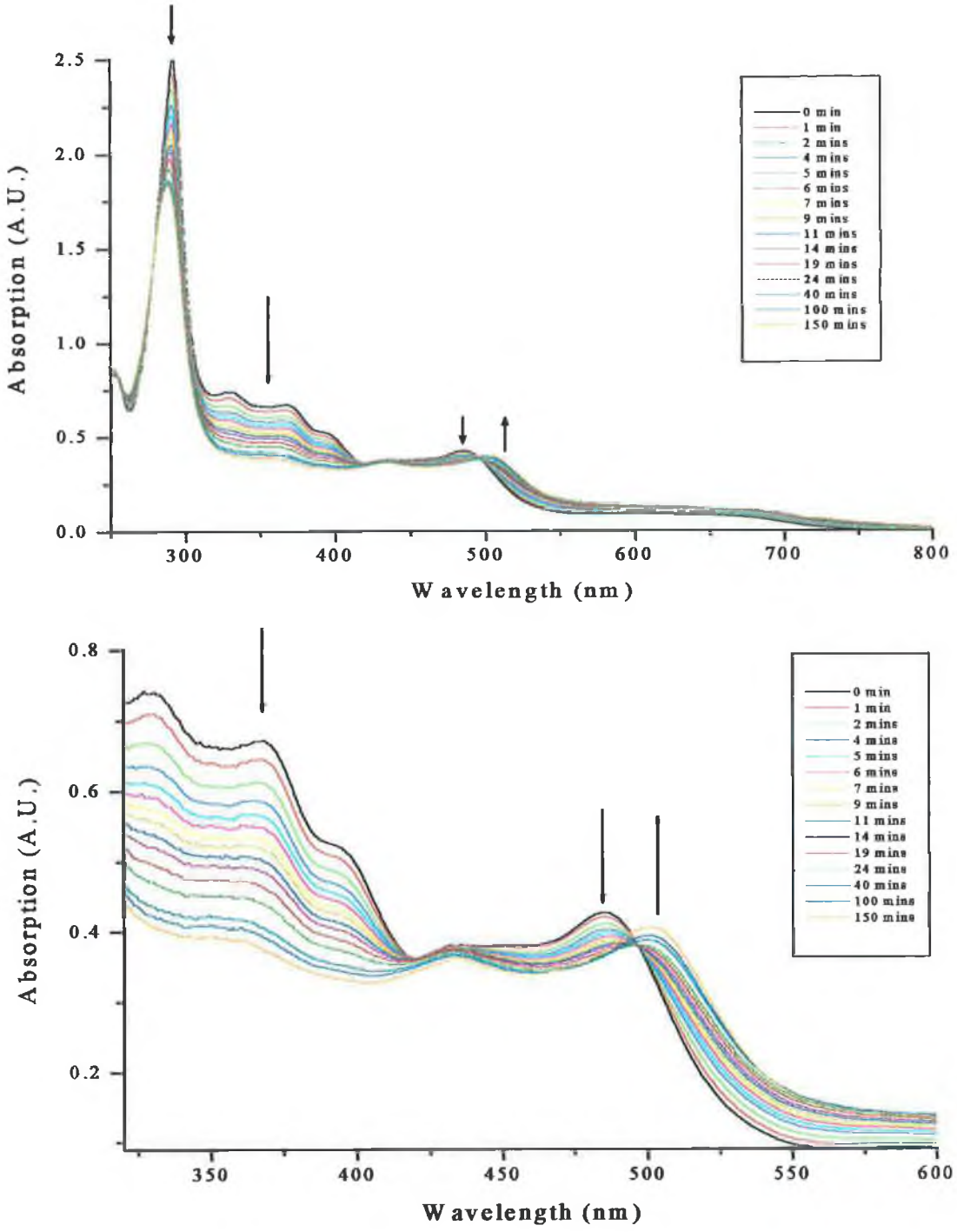

Figure 4.17 Results of the study to examine the photochemistry of the $[Os(bpy)_2(LL1)]^{2-}$ complex in MeCN.

As can be seen from Figure 4.17, the complex $[Os(bpy)_2(LL1)]^{2+}$ in MeCN surprisingly exhibits photochemistry. As in the case of the ruthenium(II) complexes, the photochemical properties of the ligand must be considered. This proved of vital significance while examining the photochemistry of the ruthenium complexes, and it is of even more significance now. The photochemistry of the LL1 ligand has previously been described in Chapter 3.9, Figure 3.46, and similar changes were observed in the ligand centred transitions for the ruthenium complex. This is also the case for the analogous osmium complex. The UV spectrum changes in several ways. The π-π*(bpy) bands at 280 – 290 nm lose some intensity but are not significantly shifted on irradiation. The bands in the region from 310 – 400 nm, which have been assigned as π-π*(LL1) transitions for the ruthenium complex by comparison with the free ligand and also using molecular mechanics to predict the electronic structure and therefore by extension as π-π* transitions in the osmium complexes collapse to half their original intensity. The MLCT band at 485 nm is red shifted to 502 nm and the dπ→π* bpy MLCT between 600 – 660 nm disappear.

The photochemistry of the $[Os(bpy)_2(LL3)]^{2+}$ complex has also been examined. No noticeable photochemistry from the complex was observed in the time scale of the experiment.

Compound	Photochemistry
LL1 ligand	Yes
$[Ru(bpy)_2(LL1)]^{2+}$	Yes
$[Os(bpy)_2(LL1)]^{2+}$	Yes
LL3 ligand	No
$[Ru(bpy)_2(LL3)]^{2+}$	Yes
$[Os(bpy)_2(LL3)]^{2+}$	No

Table 4.7 Compounds examined for exhibition of photochemistry.

From Table 4.7 it can be seen that each of the LL1 compounds exhibits photochemistry, as does the ruthenium(II) LL3 complex. Neither the LL3 ligand nor the osmium complex containing the LL3 ligand exhibit photochemistry. This seems to indicate that the ruthenium complexes exhibit photochemistry whether the ligand is responsible for this process or not. Basically, two photochemical process are possible, the first due to population of the ^{3}MC state leading to lengthening of the Ru-N bonds causing the bonds to break [25] and the second due to the photochemistry of the LL_x ligand itself. The photochemistry of the osmium complexes is dependent solely on the LL_x ligand as population of the ^{3}MC level is not possible. If the LL_x ligand exhibits photochemistry, the corresponding osmium complex also exhibits photochemistry, as in the case of the LL1 ligand. If, as for the LL3 ligand, the ligand is photochemically stable, the osmium complex is also photostable.

4.8 Electrochemistry of osmium (II) complexes:

The electrochemistry of the ligands has been reported in Chapter 3.10, and as in the case of the ruthenium(II) complexes it has proved necessary to first understand the properties and characteristics of the ligands before the voltammograms of the complexes can be assigned. The electrochemistry of the ruthenium(II) complexes has been examined and described in detail in Chapter 3.10 and much of the discussion contained within that is valid by extension to the discussion of the osmium(II) complexes. As in the case of the ruthenium complexes several oxidation waves are observed in the potential window of the experiments. As expected the oxidation potentials of the $Os^{(II)}/Os^{(III)}$ couple is approximately 400mV lower than for the $Ru^{(II)}/Ru^{(III)}$ couple in the analogous complexes. This has been reported in previous studies and is caused by the higher energy of the 5d orbitals compared to the 4d orbitals of ruthenium. [26]

The oxidation and reduction potentials of the complexes are given in Table 4.8. All values are given *vs* ferrocene whereas the diagrams used to illustrate the redox waves of the examples given have not been corrected *vs* Fc/Fc^+ and therefore appear against the reference used in the experiment, Ag/Ag^+.

The complex $[Os(bpy)_3]^{2+}$ is used as a comparison for the results achieved during the electrochemical analysis of the compounds. It was therefore important to perform the electrochemistry of $[Os(bpy)_3]^{2+}$ under the same experimental conditions as those used for the other complexes, to allow for direct comparison. The results of the experiments on $[Os(bpy)_3]^{2+}$ can be found in Figure 4.18.

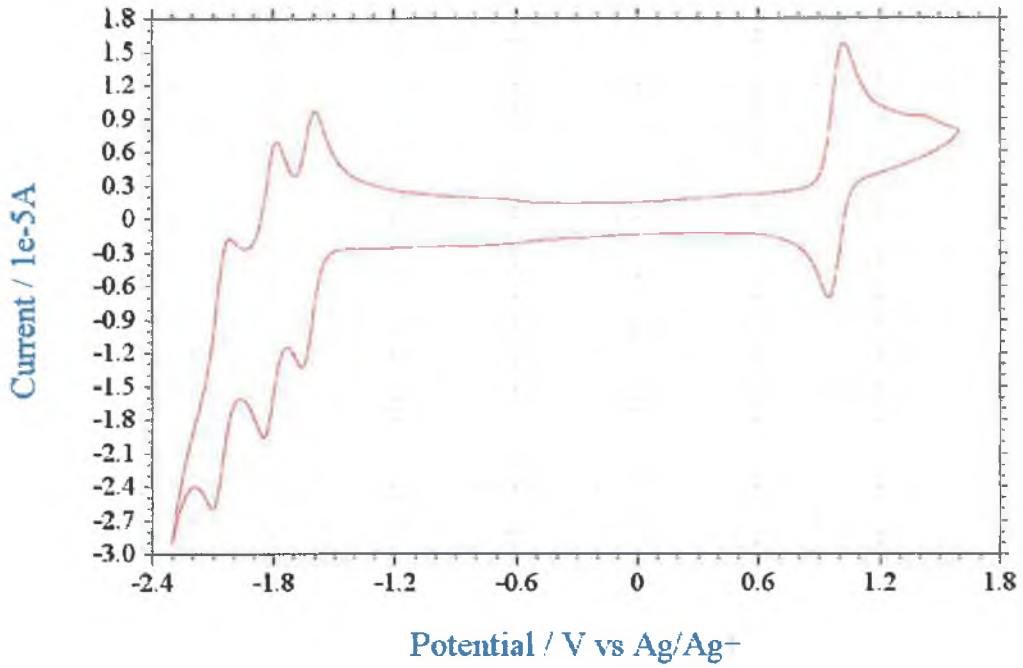

Figure 4.18 Cyclic Voltammogram of $[Os(bpy)_3]^{2+}$ in MeCN with 0.1M $TBABF_4$.

The literature value for the $Os^{(II)}/Os^{(III)}$ couple in $[Os(bpy)_3]^{2+}$ is 0.45 V *vs* Fc/Fc^+. [27] Under the experimental conditions employed, this was found to be 0.45 V vs Fc/Fc^+ which allows direct comparison of the results achieved for the osmium complexes being measured here with those of similar complexes from previously reported work was possible.

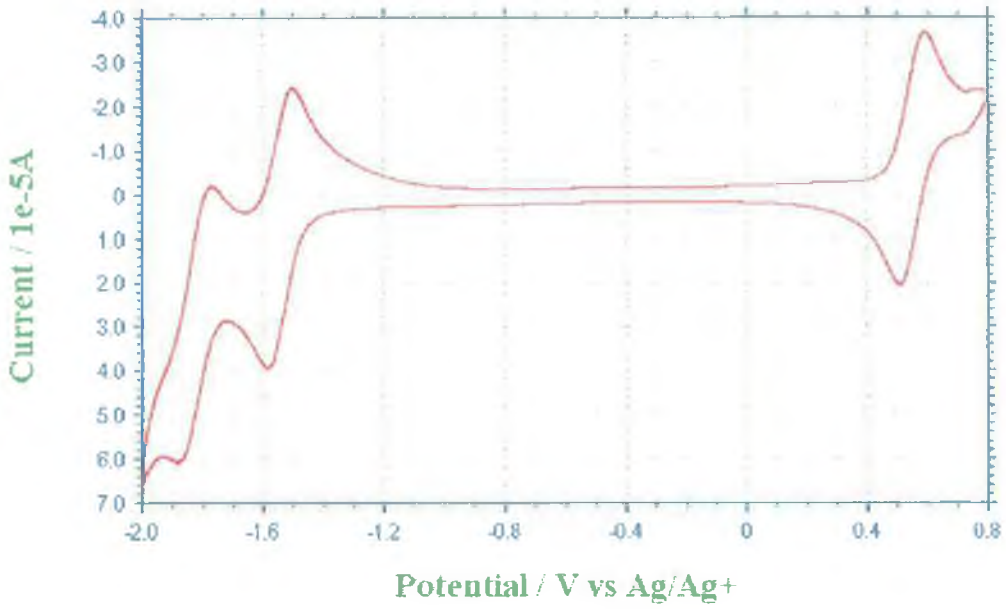

Figure 4.19 Cyclic voltammogram of the oxidation and reduction potentials of the $[Os(bpy)(LL5)]^{2+}$ complex in MeCN with 0.1M $TBABF_4$.

Figure 4.19 illustrates a typical cyclic voltammogram achieved for the osmium(II) complexes. The anodic region of the cyclic voltammogram above features a reversible metal-centred oxidation, while the cathodic region exhibits two clearly defined waves. These first two reduction waves result from the reduction of both of the coordinated bipyridyl ligands.

As mentioned already, as in the case of the ruthenium(II) complexes, several oxidation waves are observed upon scanning to +2 V *vs* Fc/Fc^+. The diagrams on the next page are typical examples of these oxidation waves which can be assigned as ligand centred oxidations on the LL_x ligands by comparison with the CVs of the free ligands (Chapter 3.10).

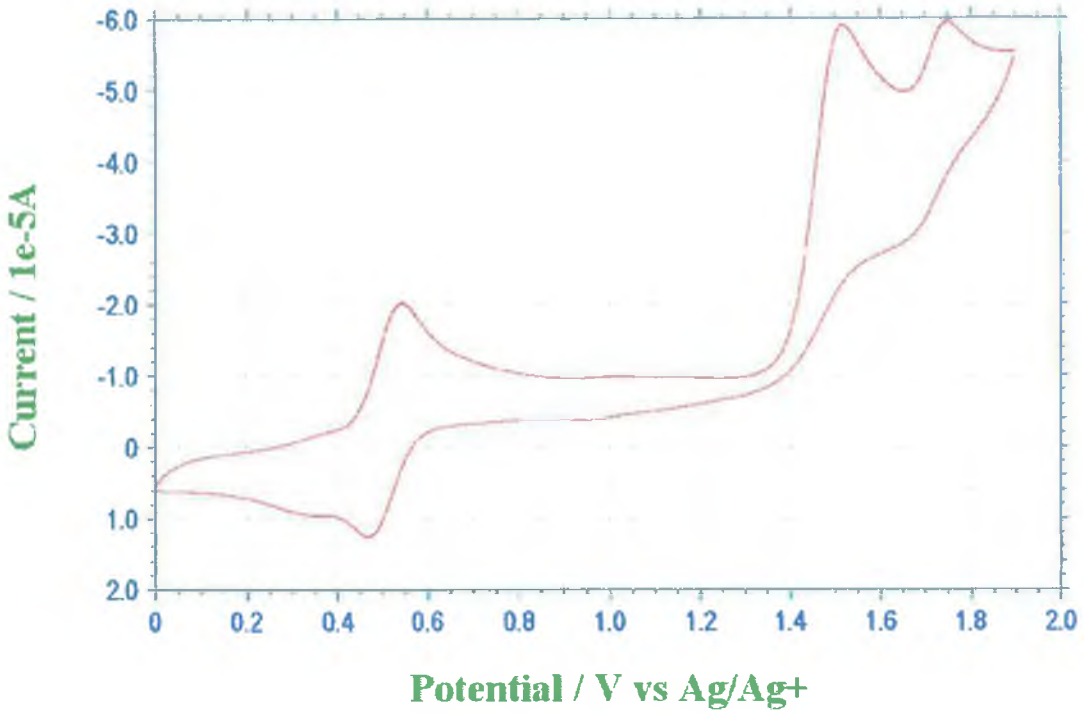

Figure 4.20 Oxidation potentials of the complex $[Os(bpy)_2(LL1)]^{2+}$ in MeCN with 0.1M $TBABF_4$.

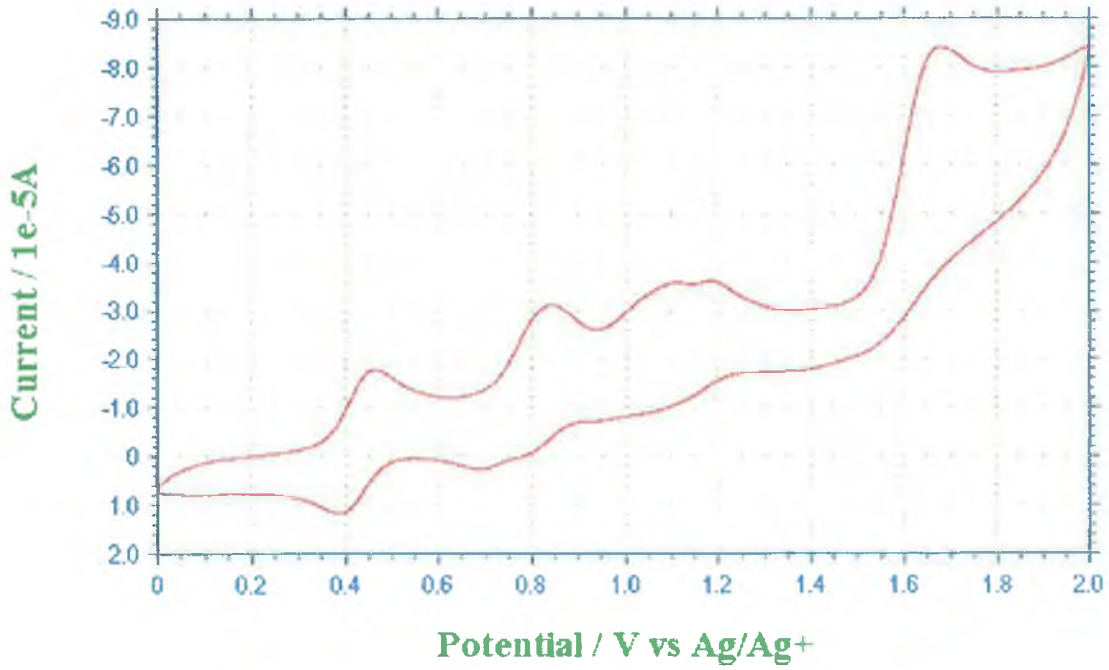

Figure 4.21 Oxidation potentials of the complex $[Os(bpy)_2(LL8)]^{2+}$ in MeCN with 0.1M $TBABF_4$.

Compound	Oxidation Potentials, $E_{1/2}$	Reduction potentials, $E_{1/2}$. Ligand based.
$[Os(bpy)_3]^{2+}$		-1.66 (72)
	0.44 (65)	-1.85 (82)
		-2.17 (80)
$[Os(bpy)_2(LL1)]^{2+}$	0.38 (78)	-1.67 (65)
	1.35 (irr)	-1.89 (90)
	1.58 (irr)	
$[Os(bpy)_2(LL2)]^{2+}$	0.35 (70)	-1.70 (80)
	1.28 (irr)	-1.94 (95)
$[Os(bpy)_2(LL3)]^{2+}$	0.43 (76)	-1.68 (70)
	1.93 (irr)	-1.90 (90)
$[Os(bpy)_2(LL4)]^{2+}$	0.29 (125)	-1.75 (irr)
	1.34 (irr)	-2.09 (irr)
$[Os(bpy)_2(LL5)]^{2+}$	0.39 (78)	-1.71 (80)
	1.28 (irr)	-1.99 (90)
	1.45 (irr)	
$[Os(bpy)_2(LL6)]^{2+}$	0.32 (78)	-1.73 (84)
	1.32 (irr)	-2.02 (90)
	1.85 (irr)	
$[Os(bpy)_2(LL8)]^{2+}$	0.25 (71)	
	0.67 (irr)	-1.74 (70)
	0.95 (irr)	-2.00 (86)
	1.49 (irr)	

Table 4.8 Oxidation and reduction potentials of the $[Os(bpy)_2(LLx)]^{2+}$ complexes in MeCN with 0.1M $TBABF_4$ in V vs Fc/Fc^+.

Comparison of the electrochemical data presented in Table 4.8 with previously studied osmium complexes synthesised by Haga *et al.* [28] shows many similarities. The complex

$[Os(bpy)_2(BiBzIm)](ClO_4)_2$ [28] was found to have an oxidation potential of 0.28 V *vs* Fc/Fc^+ in MeCN (0.1M TBAP) and this has been assigned as the $Os^{(II)}/Os^{(III)}$ couple. This compares to values of between 0.25 V and 0.44 V *vs* Fc/Fc^+ which have been listed in Table 4.8. What is important to note is that the metal based oxidation potential is lower in the case of each of the complexes relative to the $[Os(bpy)_3]^{2+}$ complex. This result is as expected owing to the already established σ-donating ability of the LLx ligands.

Comparison of the complex $[Os(bpy)_2(LL3)]^{2+}$ with the osmium complexes studied by Hage [4] shows similarities. In order for the comparisons to be valid, comparison must be made with the protonated complexes. The oxidation potential for the protonated complex $[Os(bpy)_2(Hbpt)]^{2+}$ was found to be 0.42 V *vs* Fc/Fc^+ which compares to the value of 0.43 V *vs* Fc/Fc^+ found for the LL3 complex. [4]

As in the case of the ruthenium(II) complexes the electrochemistry has been studied for the series of compounds. The effect on the metal based oxidation potentials of the different substituents at the 2' position of the 5 membered ring is expected to be the same of was found for the ruthenium complexes. Taking the simplest, unsubstituted $[Os(bpy)_2(LL1)]^{2+}$ as the parent complex, its $Os^{(II)}/Os^{(III)}$ oxidation potential of 0.38 V *vs* Fc/Fc^+ is compared with that of the other complexes in the series.

The LL2 ligand contains a methyl group in the 2' position of the 5 membered imidazo ring. This slightly electron donating group should increase the electron density on the ligand and this in turn should lower the oxidation potential of the metal in the complex due to the increased ability of the LL2 ligand to push electron density onto the metal. The metal based oxidation potential of this complex is 0.35 V *vs* Fc/Fc^+ which is 30mV lower than that of the LL1 complex which agrees with our supposition.

The metal centred oxidation potential of the $[Os(bpy)_2(LL4)]^{2+}$ complex appears to be different from those observed for the other complexes in the series. The $Os^{(II)}/Os^{(III)}$ couple appears at a lower potential than that expected, with the OH group being electron

withdrawing, and the phenyl ring also pulling electron density from the "parent" ligand, and therefore it was expected that the metal should be harder to oxidise. This is not the case however, and the metal oxidation wave is observed at 0.29 V *vs* Fc/Fc^+. The peak to peak separation was found to be 125 mV which makes the wave quasi-reversible at best.

The LL5 ligand contains electron withdrawing chlorine atoms in both the ortho and the para position. Again the ortho chlorine is not expected to affect the electron affinity felt by the phenyl ring as much as the chlorine in the para position. The complex has a metal based oxidation potential of 0.39 V *vs* Fc/Fc^+ which indicates that the substituted phenyl ring has a slightly the electron withdrawing effect in comparison to H. The LL6 ligand again contains a phenyl ring with two methoxy groups (ortho and meta to the binding site). Methoxy groups have an electron donating effect relative to H, and therefore as in the case of the LL2 ligand, the potential of the metal oxidation wave is expected to be lower than for that of the LL1 ligand. This is indeed the case with an $E_{1/2}$ of 0.32 V *vs* Fc/Fc^+ found experimentally for the complex $[Os(bpy)_2(LL6)]^{2+}$.

The oxidation potential observed of 0.43 V *vs* Fc/Fc^+ for the $[Os(bpy)_2(LL3)]^{2+}$ complex was the highest found, and indicates that the triazo moiety appears to be less electron rich than the imidazo moiety or even the substituted imidazo moieties. The result indicates that the LL3 ligand is only slightly more σ-donating than the 2,2'-bipyridyl ligand. However as already discussed the results for this complex are comparable to those of previously studied osmium polypyridine triazole containing complexes. [4]

For all the complexes the first two reduction potentials were the only observable reduction waves. These reduction waves are comparable to the first two reduction potentials found for $[Os(bpy)_3]^{2+}$ and is in agreement with the results from the lifetime studies of the complexes, and of the deuterated analogues, that the first two reduction potentials are bipyridyl based.

The final osmium(II) bis-bipyridyl complex in the series is that containing the LL8 ligand. The LL8 ligand contains two 5 membered imidazo rings fused to a 6 membered

pyridyl type moiety. The other LL_x ligands contain only one fused conjugated system. The oxidation potentials of the osmium complex of the LL8 ligand can be seen in Figure 4.21. As in the case of the ruthenium(II) complexes the oxidation potential for the $Os^{(II)}/Os^{(III)}$ couple was found to be lower for this complex than for the other complex in the series (0.25 V *vs* Fc/Fc^{+}).

4.9 Bibliography

[1] Constable E. C., Raithby P. R., Smit D. N., ***Polyhedron***, **1989,** 8, 367

[2] Rillema D. P., Jones D. S., Levy H. A., **J. Chem. Soc., Chem. Comm**., **1979,** 849

[3] Conner J. A., Meyer T. J., Sullivan B. P**.,** ***Inorg. Chem***., **1979**, 18, 1388

[4] Hage, R., *Ph. D Thesis*, Leiden University, **1991**.

[5]. P. Lay, A. M. Sargeson, H. Taube, M. H. Chou and C. Creutz, ***Inorg. Synth.,*** **1986**, 24, ***John Wiley and Sons (Publishers)***

[6] Browne W. R., Vos J. G., ***Coord. Chem. Rev***., **2001**, 219, 761.

[7] Chirayil S., Thummel R. P**.,** ***Inorg. Chem***., **1989**, 28, 813.

[8] Kober E. M., Meyer T. J., ***Inorg. Chem***., **1983**, 22, 1614

[9] Ernst S., Kasack V., Kaim W**.,** ***Inorg. Chem***., **1989**, 28, 1520.

[10] Haga M., Matsumura-Inoue T., Yamabe S., ***Inorg. Chem***., **1987**, 26, 4148.

[11] Vining W. J., Caspar J. V., Meyer T. J., ***J. Phys. Chem***., **1985**, 89, 1095.

[12] Lumpkin R. S., Kober E. M., Worl L., Murtaza Z., Meyer T J., ***J. Phys. Chem.***, **1990**, 94, 239.

[13] Wrighton, M., Morse D. L., ***J. Am. Chem. Soc***., **1974**, 96, 996.

[14] Juris A., Balzani V., Barigelleti F., Campagna S., Belser P., von Zelewsky A., ***Coord. Chem. Rev.***, **1988,** 84, 85

[15] Kober E. M., Caspar J. V., Lumpkin R. S., Meyer T. J., ***J. Phys. Chem.***, **1990**, 94, 239

[16] Strouse G. E., Schnoover J. R., Duesing R., Boyde S., Jones W. E., Meyer T. J., ***Inorg. Chem.***, **1995,** 34, 473.

[17] Dodsworth E. S., Lever A. B. P., ***Chem. Phys. Lett.***, **1986**, 124, 152.

[18] Kober E. M., Marshall J. L., Dressick W. J., Sullivan P., Caspar J. V., Meyer T. J., ***Inorg. Chem.***, **1985**, 24, 2755.

[19] Caspar J. V., Meyer T. J., ***J. Am. Chem. Soc.,*** **1983**, 105, 5583.

[20] Hoggard P. E., Porter G. B., ***J. Am. Chem. Soc***., **1978,** 100, 1457.

[21] Van Houten J., Watts R. J., ***J. Am. Chem. Soc.,*** **1976**, 98, 4853.

[22] Van Houten J., Watts R. J., ***Inorg. Chem.,*** **1978**, 17, 3381.

[23] Durham B., Caspar J. V., Nagle J. K., Meyer T. J., ***J. Am. Chem. Soc***., **1982**, 104, 4803.

[24] Caspar J. V., Meyer T. J., ***Inorg. Chem.***, **1983,** 22, 2444.

[25] Barigelleti F., Juris A., Balzani V., Belser P., von Zelewsky A., ***Inorg. Chem.***, **1983**, 22, 3335.

[26] Goldsby K. A., Meyer T. J., ***Inorg. Chem.***, **1984,** 23, 3002.

[27] Kober E. M., Casper J. V., Sullivan B. P., Meyer T. J., ***Inorg. Chem.***, **1989**, 27, 4587.

[28] Haga, M. A., Matsumura-Inoue, T., Yamabe S., ***Inorg. Chem.***, **1987**, 26, 4148

Chapter 5:

The synthesis and characterisation of homo and hetero dinuclear complexes based on the bridging ligand LL7.

Abstract:

The LL7 ligand is introduced in this chapter. Unlike the other LL_x ligands, the LL7 ligand provides the opportunity to coordinate two metal centres. This chapter details the synthesis and characterisation of dinuclear complexes using the bridging ligand, LL7. The complexes take the form $[M(bpy)_2(LL7)(bpy)_2]^{2+}$ (where M = Ru or Os). The synthesis of the ruthenium(II) monomer, the homo-nuclear Ru-Ru and Os-Os dimers and the hetero-nuclear Ru-Os bis-bipyridyl dinuclear complexes bridged by the LL7 ligand is described. The complexes have been structurally determined by elemental analysis, ^1H NMR and in the case of the Ru-Ru dimer, X-Ray Analysis. The photophysical and electrochemical properties are also examined. The chapter concludes with an examination of the metal-metal interactions by spectroelectrochemistry.

5.1 Introduction:

The compounds in Chapter 5 are based on the LL7 ligand (see Figure 5.1 below).

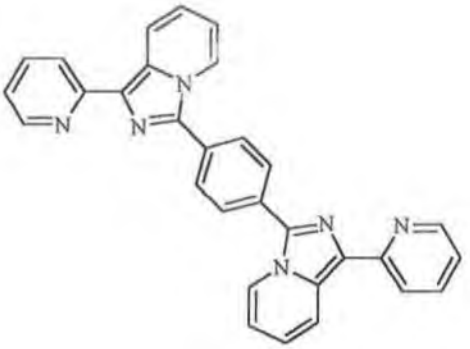

LL7 = 1,4-phenylene-bis-(2-pyridyl imidazo[1,5-a] pyridine)

Figure 5.1 Pictorial representation of the LL7 ligand.

Unlike the LLx ligands introduced in Chapter 3 and 4, the LL7 ligand provides the opportunity to synthesise dinuclear complexes. The synthesis of the dinuclear complexes proved a relatively simple task, however the synthesis of a monomeric complex containing the LL7 ligand proved to be a more difficult proposition. Chapter 5.2 details the synthesis of the complexes and is followed by a discussion of the problems encountered during the synthesis and explanations of how these problems were overcome. Chapter 5.3 discusses the X-Ray Crystal structure obtained for the $[Ru(bpy)_2(LL7)(bpy)_2Ru](PF_6)_4$ dimer. As in the previous chapters the structural characterisation of this and the other complexes is completed by ^1H NMR. The photophysical, electrochemical and spectroelectrochemical properties have also been examined.

5.2 Synthesis of the complexes:

The synthesis of the starting materials, *cis*-$[Ru(bpy)_2Cl_2].2H_2O$ and *cis*-$[Os(bpy)_2Cl_2].xH_2O$ have already been discussed in Chapter 3.2 and Chapter 4.2 respectively and will not be discussed here.

Synthesis of $[Ru(bpy)_2(LL7)](PF_6)_2.2H_2O$

The LL7 ligand (102 mg, $2.19x10^{-4}$ mol) was heated to reflux in 300 cm^{-3} of a 1:1 EtOH/H_2O mixture. To this $[Ru(bpy)_2Cl_2].2H_2O$ (114 mg, $2.19x10^{-4}$ mol) in 20cm^3 EtOH was added over 90 minutes. After 3 hours the reaction was allowed to cool and the EtOH was removed *in vacuo*. Unreacted ligand was removed by filtration. 10 cm^3 of a saturated aqueous solution of ammonium hexafluorophosphate was added to the filtrate to precipitate an orange/brown product. This product was isolated by filtration, washed with water and dried with diethylether. The compound was purified by column chromatography (stationary phase silica gel, mobile phase 80% acetonitrile, 20% water, 0.05M KNO_3 buffer). The first orange band to elute yielded the desired product, with the second band containing the homonuclear dinuclear complex. The acetonitrile was removed *in vacuo* and an excess of NH_4PF_6 added to reprecipitate the pure product which was filtered, washed with cold water and diethyl ether and allowed to dry to yield 95mg. (37%)

^1H NMR (400 MHz, d_6-DMSO) δ = 6.95 (dd, 1H), 7.24 (m, 4H), 7.44 (m, 2H), 7.60 (m, 7H), 7.78 (d, 1H), 7.82 (d, 1H), 7.88 (m, 2H), 7.97 (d, 1H), 8.14 (m, 7H), 8.29 (d, 1H), 8.53 (m, 5H), 8.66 (d, 1H), 8.74 (m, 3H). Total = 36 aromatic protons.

Elemental Analysis for $C_{50}H_{40}N_{10}Ru_1O_2P_2F_{12}$: Calculated C 50.04, H 3.17, N 11.68. Found C 49.45, H 3.01, N 11.19 %.

$[Ru(bpy)_2(LL7)(bpy)_2Ru](PF_6)_4.4H_2O$

The LL7 ligand (200 mg, $4.3x10^{-4}$ mol) and $[Ru(bpy)_2Cl_2].2H_2O$ (492 mg, $9.46x10^{-4}$ mol) were placed in 30 cm^3 of a 1:1 EtOH/H_2O mixture. This suspension was refluxed overnight and after this time the EtOH removed *in vacuo*. The solution was filtered to remove any excess unreacted ligand. 10 cm^3 of a saturated aqueous solution of ammonium hexafluorophosphate was added to the filtrate to precipitate an orange/brown product. This product was isolated by filtration, washed with water and dried with diethylether. The compound was purified by column chromatography (stationary phase silica gel, mobile phase 80% acetonitrile, 20% water, 0.05M KNO_3 buffer). The second orange band to elute yielded the desired product. The acetonitrile was removed *in vacuo* and aqueous ammonium hexafluorophosphate added to reprecipitate the pure product which was filtered and washed with cold water and diethyl ether and allowed to dry. Yield 650 mg (81% yield).

^{1}H NMR (400 MHz, d_6-DMSO) δ = 6.75 (dd, 1H), 6.94 (dd, 1H), 7.24 (m, 8H), 7.43 (m, 7H), 7.60 (m, 10H), 7.80 (d, 1H), 7.90 (d, 1H), 8.16 (m, 12H), 8.40 (d, 1H), 8.63 (m, 6H), 8.75 (m, 4H). Total = 52 aromatic protons.

Elemental Analysis for $C_{70}H_{60}N_{14}Ru_2O_4P_4F_{24}$: Calculated C 43.43, H 2.90, N 10.13. Found C 43.11, H 3.08, N 10.01 %.

$[Ru(d_8\text{-bpy})_2(LL7)(d_8\text{-bpy})_2Ru](PF_6)_4.4H_2O$

The LL7 ligand (50 mg, $1.07x10^{-4}$ mol) and $[Ru(d_8\text{-bpy})_2Cl_2].2H_2O$ (127 mg, $2.37x10^{-4}$ mol) were placed in 30 cm^3 of a 1:1 EtOH/H_2O mixture. This suspension was refluxed overnight and after this time the EtOH removed *in vacuo*. The solution was filtered to remove any excess unreacted ligand. 10 cm^3 of a saturated aqueous solution of ammonium hexafluorophosphate was added to the filtrate to precipitate an orange/brown product. This product was isolated by filtration, washed with water and dried with diethylether. The compound was purified by column chromatography (stationary phase silica gel, mobile phase 80% acetonitrile, 20% water, 0.05M KNO_3 buffer). The second orange band to elute yielded the desired product. The acetonitrile was removed *in vacuo*

and an aqueous solution of ammonium hexafluorophosphate added to reprecipitate the pure product which was filtered and washed with cold water and diethyl ether and allowed to dry. Yield 112 mg (55% yield).

^{1}H NMR (400 MHz, d_6-DMSO) δ = 7.27 (m, 3H), 7.41 (d, 2H), 7.60 (m, 2H), 8.05 (dd, 1H), 8.63 (m, 2H). Total = 10 aromatic signals, each corresponding to 2 protons.

Elemental Analysis for $C_{70}H_{28}N_{14}D_{32}Ru_2O_4P_4F_{24}$: Calculated C 42.73, H 2.85, N 9.97. Found C 43.21, H 2.98, N 9.51 %.

$[Os(bpy)_2(LL7)(bpy)_2Os](PF_6)_4.4H_2O$

The LL7 ligand (200 mg, $4.3x10^{-4}$ mol) and $[Os(bpy)_2Cl_2].2H_2O$ (523 mg, $9.46x10^{-4}$ mol) were placed in 30 cm^3 of a 1:1 ethylene glycol/H_2O mixture. This suspension was refluxed for 72 hours. The solution was filtered to remove any excess unreacted ligand. 10 cm^3 of a saturated aqueous solution of ammonium hexafluorophosphate was added to the filtrate to precipitate a green/brown product. This product was isolated by filtration, washed with water and dried with diethylether. The compound was purified by column chromatography (stationary phase silica gel, mobile phase 80% acetonitrile, 20% water, 0.05M KNO_3 buffer). The second band to elute yielded the desired product. The acetonitrile was removed in vacuo and an excess of an aqueous solution of ammonium hexafluorophosphate added to reprecipitate the pure product which was filtered and washed with cold water and diethyl ether and allowed to dry. Yield 549 mg (62 % yield).

^{1}H NMR (400 MHz, d_6-acetone) δ = 6.81 (dd, 2H), 7.06 (dd, 1H), 7.25 (m, 7H), 7.53 (m, 13H), 7.74 (d, 1H), 7.94 (m, 14H), 8.26 (d, 1H), 8.40 (d, 1H), 8.46 (m, 2H), 8.65 (m, 10H). Total = 52 aromatic protons.

Elemental Analysis for $C_{70}H_{60}N_{14}Os_2O_4P_4F_{24}$: Calculated C 39.77, H 2.65, N 9.28. Found C 39.44, H 2.39, N 9.41 %.

$[Os(bpy)_2(LL7)(bpy)_2Ru](PF_6)_4.3H_2O$

The complexes $[Ru(bpy)_2(LL7)](PF_6)_2$ (97 mg, $8.3x10^{-5}$ mol) and $[Os(bpy)_2Cl_2].2H_2O$ (51 mg, $8.3x10^{-5}$ mol) were placed in 20 cm^{-3} of a 1:1 ethylene glycol/H_2O mixture. This suspension was refluxed for 72 hours. 10cm^3 of a saturated aqueous solution of ammonium hexafluorophosphate was added to the filtrate to precipitate a green/brown product. This product was isolated by filtration, washed with water and dried with diethylether. The compound was purified by column chromatography (stationary phase silica gel, mobile phase 80% acetonitrile, 20% water, 0.05M KNO_3 buffer). The second green band to elute yielded the desired product. The acetonitrile was removed in vacuo and an excess of an aqueous solution of ammonium hexafluorophosphate added to reprecipitate the pure product which was filtered and washed with cold water and diethyl ether and allowed to dry. Yield 90 mg after purification. (54 % yield).

^{1}H NMR (400 MHz, d_6-DMSO) δ = 6.81 (m, 2H), 7.08 (dd, 1H), 7.38 (m, 17H), 7.62 (dd, 2H), 7.67 (d, 2H), 7.73 (d, 1H), 7.83 (d, 1H), 7.94 (m, 12H), 8.26 (d, 1H), 8.40 (d, 1H), 8.46 (m, 2H), 8.62 (m, 10H). Total = 52 aromatic protons.

Elemental Analysis for $C_{70}H_{58}N_{14}RuOsO_3P_4F_{24}$: Calculated C 41.85, H 2.74, N 9.76. Found C 42.31, H 3.16, N 9.43 %.

5.3 Discussion of the synthesis of the complexes:

The synthesis of the ruthenium(II) and osmium(II) homonuclear dinuclear complexes proved a straightforward reaction of two equivalents of metal with one equivalent of the bridging LL7 ligand in ethanol/water and ethylene glycol/water respectively. The yield for the Os-Os dimer is lower due to the presence of ethylene glycol, which unlike the ethanol used in the reaction to make the Ru-Ru dimer is not removed before the precipitation of the product from the reaction mixture. Some of the desired product

inevitably dissolves in the ethylene glycol and is not recovered. The purification of the dimers proved reasonably straightforward, with the product eluting as the main band.

The ease with which the homo-nuclear complexes were made contrasts with the difficulties experienced during the synthesis of the hetero-nuclear complex. In order to synthesise the mixed metal heteronuclear ruthenium-osmium dinuclear complex, either the $[Ru(bpy)_2(LL7)]^{2+}$ or the $[Os(bpy)_2(LL7)]^{2+}$ monomer is needed in order to use the "complexes as ligands" approach which was developed at the beginning of the 1990s.[1,2,3] This approach was used as it was believed the one-pot synthetic approach would have little success due to the different reaction rates of ruthenium and osmium relative to each other.

Considering the differences in reaction rates, it was believed that the osmium mononuclear complex would prove easier to synthesise than the analogous ruthenium complex as osmium is less reactive than ruthenium and therefore would be less likely to form the dinuclear species. This however did not prove possible, and any attempt to synthesise the osmium mononuclear complex resulted in the synthesis of relatively small amounts of the mononuclear complex in comparison to the amount of dinuclear complex made in the same reaction.

The reasons for the problems incurred during the synthesis of the mononuclear complexes were due to the insolubility of the ligand. The only solvent the ligand seemed to be partially soluble in was refluxing DMSO, and then dissolution needed to be aided by sonication. Therefore, under the reaction conditions employed, i.e. refluxing ethanol/water or ethylene glycol/water, the free ligand will remain undissolved until after it reacts with a $[M(bpy)_2Cl_2]$ molecule, forming the chloride salt of the monomeric complex which is soluble in the reaction mixture. This complex then, because it is dissolved in the reaction medium has greater opportunity to react with a second equivalent of $[M(bpy)_2Cl_2]$ leading to the formation of the homodinuclear complex, leaving very small amounts of the mononuclear complex in the reaction mixture. Proof of this theory is provided by the large amounts of undissolved free ligand present after

any reaction to make the monomer. In order to prevent the formation of dimer, and therefore increase the yield of the desired monomer, several approaches were attempted.

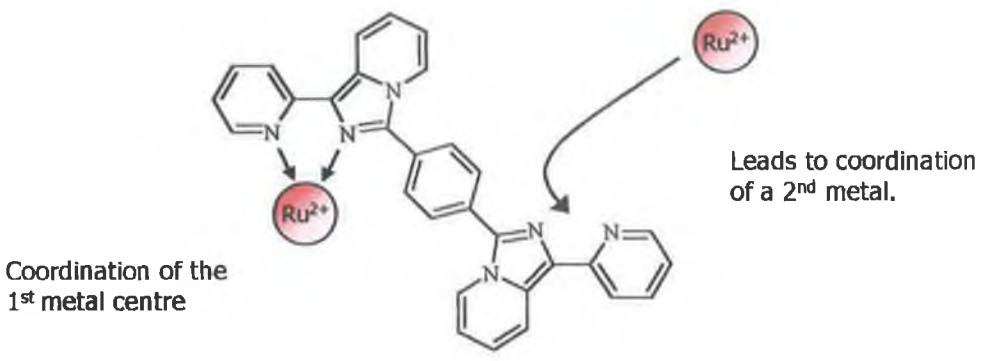

Figure 5.2 Illustration of the reaction that proceeds under normal conditions.

The successful approach used a very large amount of solvent, and the ligand was refluxed in this before the metal was slowly added to the reaction mixture. The reaction was stopped shortly after the metal was added to try to prevent any further reaction of the mononuclear complex. This attempt proved successful, and the desired complex was successfully isolated by chromatography from this reaction as described.

Once the monomer had been formed the heteronuclear ruthenium-osmium dimer was synthesised in a 1:1 reaction between the $[Ru(bpy)_2(LL7)]^{2+}$ complex and $[Os(bpy)_2Cl_2].xH_2O$.

5.4 X-Ray Crystallography:

X-Ray Crystallography, and its uses in synthetic inorganic chemistry has been introduced and discussed in Section 3.4. In this chapter, X-Ray Crystallography has been used to unequivocally determine the structure of the $[Ru(bpy)_2(LL7)(bpy)_2Ru](PF_6)_4$ complex. The results are presented in Figure 5.3, while selected data from this analysis has been collated in Tables 5.1, 5.2 and 5.3.

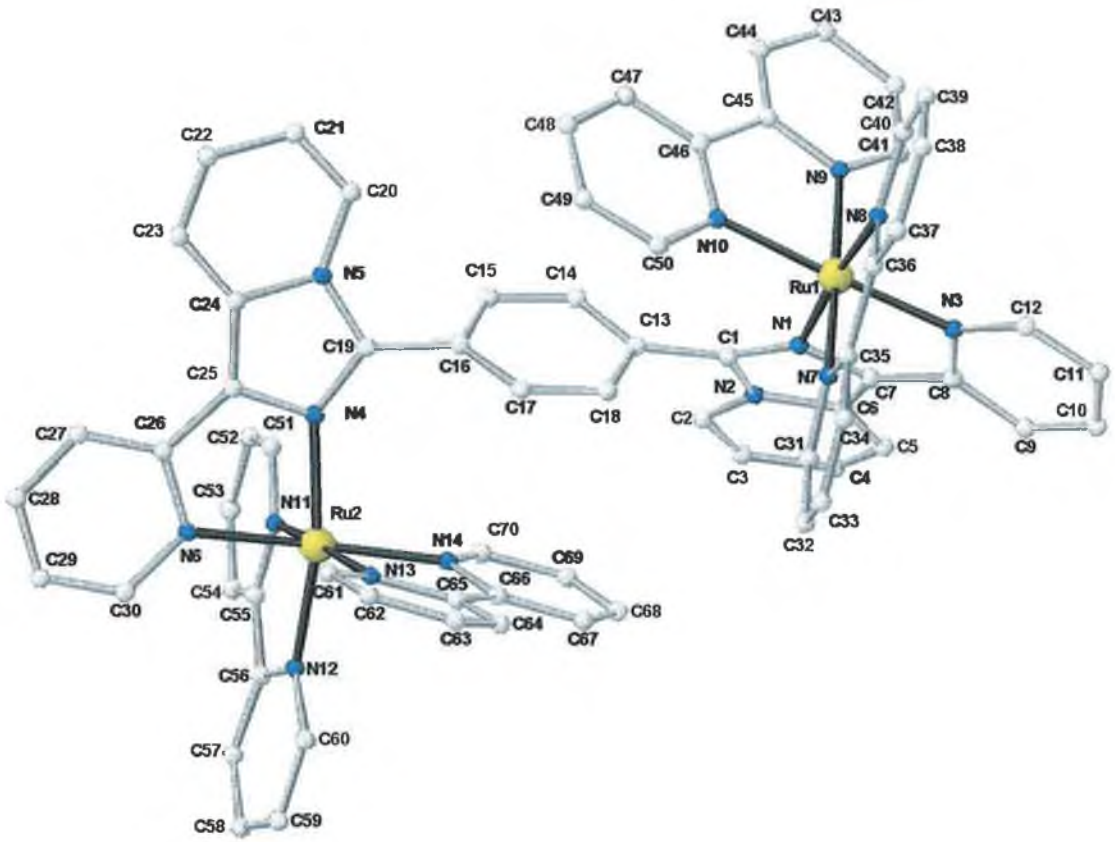

Figure 5.3 Pictorial representation of the results of the crystal structure analysis of the complex $[Ru(bpy)_2(LL7)(bpy)_2Ru]^{4+}$ showing the relevant atomic numbering used. The PF_6^- ions, acetone molecules and hydrogen atoms have been omitted for clarity.

Compound	$[Ru(bpy)_2(LL7)(bpy)_2Ru](PF_6)_4$
Formula	$C_{75.1}H_{52}F_{24}N_{14}P_4O_{1.7}Ru_2$
M_r	1959.73
Space Group	$P2_{(1)}/c$
Crystal Class	Monoclinic
Unit Cell Dimensions	
a/ Å	15.0193 (15)
b/ Å	24.332 (3)
c/ Å	21.810 (2)
Volume/ $Å^3$	7911.9
Calculated Density, D_{calc}, Mg/m^3	1.645
Data Collection Range	
H	-20 to 19
K	-30 to 32
L	-26 to 28
Reflections Collected	85840

Table 5.1 Summary of Crystal Data and Collection of Intensities of the compound $[Ru(bpy)_2(LL7)(bpy)_2Ru](PF_6)_4$

Bond Lengths (Å) $[Ru(bpy)_2(LL7)(bpy)_2Ru]^{4+}$			
Ru(1)-N(7) (2,2'-bpy)	2.046	Ru(2)-N(12) (2,2'-bpy)	2.046
Ru(1)-N(10) (2,2'-bpy)	2.053	Ru(2)-N(11) (2,2'-bpy)	2.048
Ru(1)-N(8) (2,2'-bpy)	2.060	Ru(2)-N(13) (2,2'-bpy)	2.052
Ru(1)-N(9) (2,2'-bpy)	2.069	Ru(2)-N(14) (2,2'-bpy)	2.065
Ru(1)-N(3) (imidazo)	2.073	Ru(2)-N(6) (pyridine)	2.079
Ru(1)-N(1) (pyridine)	2.081	Ru(2)-N(4) (imidazo)	2.084

Table 5.2 Selected Bond distances of $[Ru(bpy)_2(LL7)(bpy)_2Ru]^{4+}$

Bond Angles (degrees) $[Ru(bpy)_2(LL7)(bpy)_2Ru]^{4+}$			
N(7)-Ru(1)-N(10)	98.01	N(12)-Ru(2)-N(11)	78.88
N(7)-Ru(1)-N(8)	78.87	N(12)-Ru(2)-N(13)	97.10
N(10)-Ru(1)-N(8)	85.10	N(11)-Ru(2)-N(13)	172.85
N(7)-Ru(1)-N(9)	176.45	N(12)-Ru(2)-N(14)	87.64
N(10)-Ru(1)-N(9)	79.30	N(11)-Ru(2)-N(14)	95.02
N(8)-Ru(1)-N(9)	98.52	N(13)-Ru(2)-N(14)	78.82
N(7)-Ru(1)-N(3)	85.89	N(12)-Ru(2)-N(6)	92.15
N(10)-Ru(1)-N(3)	175.77	N(11)-Ru(2)-N(6)	89.10
N(8)-Ru(1)-N(3)	97.30	N(13)-Ru(2)-N(6)	97.01
N(9)-Ru(1)-N(3)	96.87	N(14)-Ru(2)-N(6)	175.76
N(7)-Ru(1)-N(1)	97.55	N(12)-Ru(2)-N(4)	169.19
N(10)-Ru(1)-N(1)	99.16	N(11)-Ru(2)-N(4)	94.95
N(8)-Ru(1)-N(1)	174.82	N(13)-Ru(2)-N(4)	89.91
N(9)-Ru(1)-N(1)	85.22	N(14)-Ru(2)-N(4)	101.83
N(3)-Ru(1)-N(1)	78.62	N(6)-Ru(2)-N(4)	78.79

Table 5.3 Selected Bond angles of $[Ru(bpy)_2(LL7)(bpy)_2Ru]^{4+}$.

The structure examined crystallised with 1.7 molecules of acetone per unit. The H-atoms of the solvent molecules are omitted so the final formula has to be corrected as the H-atoms for the 1.7 molecules of acetone have not been included. The results of the X-Ray analysis of the $[Ru(bpy)_2(LL7)(bpy)_2Ru]^{4+}$ complex is presented in Figure 5.3. Selected data from this analysis has been detailed in Tables 5.1, 5.2 and 5.3. As before, length of

the ruthenium-nitrogen bonds provide a good basis for comparison with previously reported structures. The length of the Ru-N (2,2' bpy) bonds are between 2.046 → 2.069 Å. The bond lengths of the Ru-N (LL_x) bonds vary between 2.073 → 2.084 Å. These distances are similar to those found for the ruthenium complexes bisbipyridyl complexes of the LL1, LL2 and LL3 ligands as well as those of previously studied ruthenium(II) complexes. [4,5,6]

The complex exhibits octahedral symmetry around both of the ruthenium atoms, with the LL7 ligand coordinated to Ru1 via the N1 and N3 atoms, while the LL7 ligand is coordinated to the Ru2 atom via the N4 and N6 atoms. Closer examination of the angles in the complexes exhibit deviations from the expected trans angular value of 180°. The N1-Ru1-N8, N3-Ru1-N10 and N7-Ru1-N9 angles are 174.82°, 175.22° and 176.45° respectively, while the trans angular bond angles around the Ru2 atom are 169.19°, 175.76° and 172.85° for N4-Ru2-N12, N6-Ru2-N14 and N11-Ru2-N13 respectively. This deviation originates from the acute bite angles of both the 2,2'-bipyridyl ligands, and of the bite angles of the LL7 ligand. The bite angles of the LL7 ligands in the complexes are 78.79° for the Ru(1)-LL7 bond and 78.62° for the Ru(2)-LL7 bond. The bite angles of the coordinated 2,2'-bipyidyl ligands lie between 78.82° and 79.30°. These values are in agreement with those found for the 2,2'-bipyridine ligands of the complexes discussed in Chapter 3 as well as in other ruthenium(II) complexes. [4,7,8,9]

A full list of all the crystallographic data can be found in Appendix A.

5.5 ^{1}H NMR spectroscopy:

As in the case of the ruthenium and osmium complexes discussed in Chapters 3 and 4, ^{1}H NMR has proved to be one of the most valuable tools in the structural determination of these compounds. The use of ^{1}H NMR with 2D COSY NMR has allowed the peaks of the free LL7 ligand to be assigned. In order to assign the peaks of the coordinated LL7 ligand successfully, the above techniques coupled with selective deuteriation of the 2,2'-

bipyridyl ligands has been used. [10,11] The labels used for the protons in the ligand are illustrated below. In order to compare the resonances of the LL7 ligand to those of the complexes, the ^{1}H NMR of the complexes was performed in d_6-DMSO as the free ligand is insoluble in d_6-acetone (it is only sparingly soluble in d_6-DMSO). The insolubility of the ligand is evident from the baseline of the ^{1}H NMR spectrum of the ligand even though the experiment consisted of 128 scans rather than the normal 16 scans.

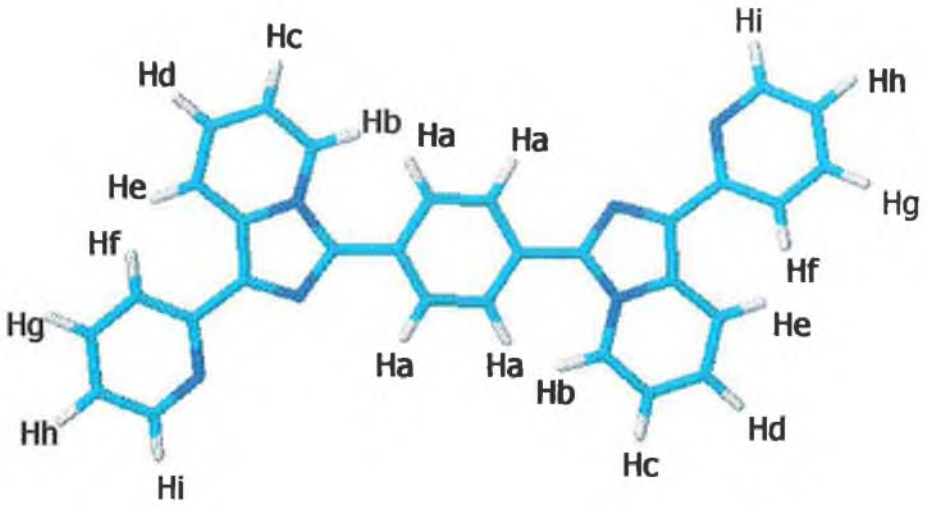

Figure 5.4 Labelling of the protons for the LL7 ligand.

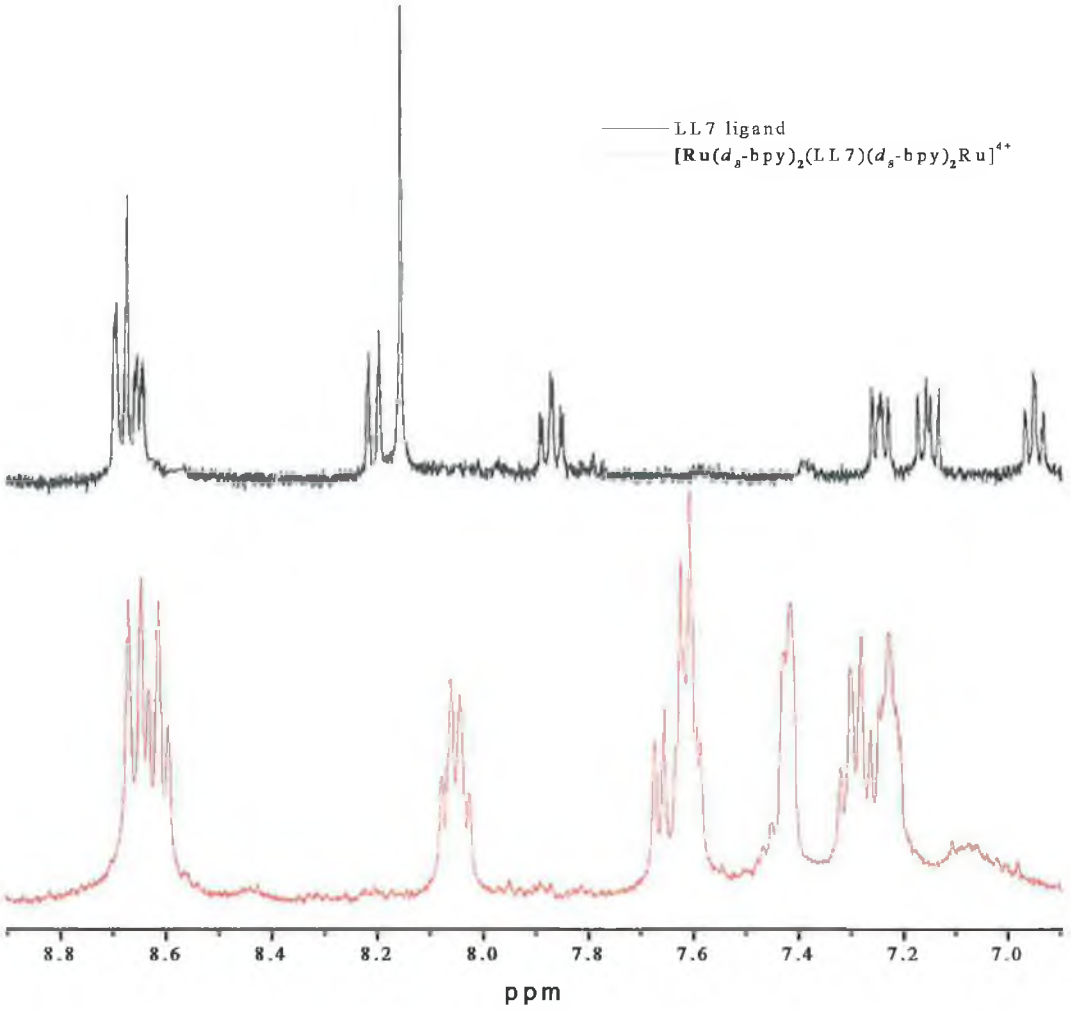

Figure 5.5 ^1H NMR of the LL7 ligand and the complex $[Ru(d_8\text{-bpy})_2(LL7)(d_8\text{-bpy})_2Ru](PF_6)_4$. Both in d_6-DMSO.

The protons of the LL7 ligand have been assigned both as the free ligand, and coordinated in the $[Ru(d_8\text{-bpy})_2(LL7)(d_8\text{-bpy})_2Ru]^{4+}$ complex. This was done with the aid of 2D COSY NMR. The ^1H NMR of the ligand while coordinated to the metal centres has proven more difficult to assign than the free ligand. The 2D COSY NMR of both the free ligand and the deuteriated complex can be seen in Figures 5.6 and 5.7. The assignment of the LL7 protons are given in Table 5.4. The LL7 ligands of the mononuclear complex $[Ru(bpy)_2(LL7)]^{2+}$ have not been assigned as the deuteriated complex has not been synthesised.

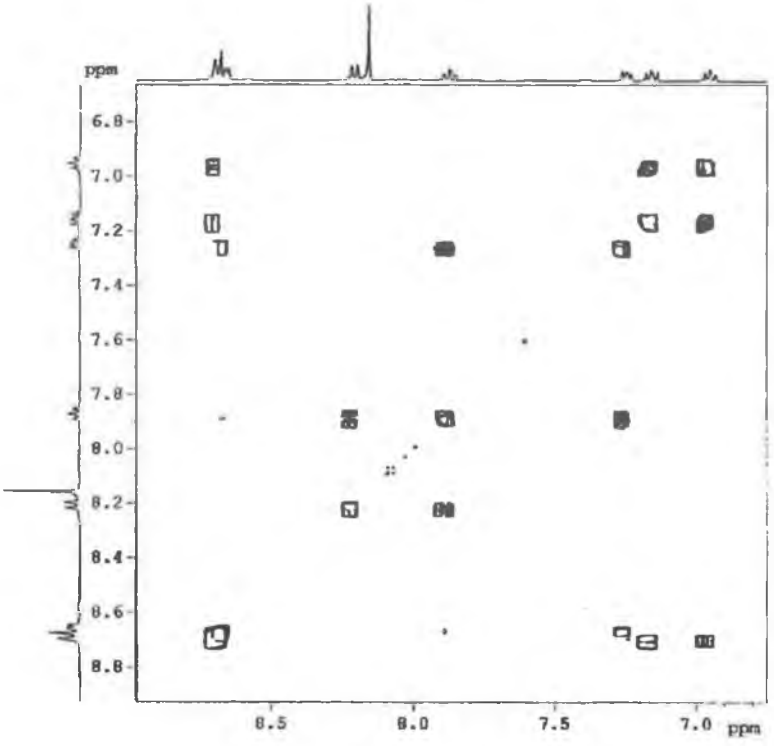

Figure 5.6 2D COSY NMR of the free LL7 ligand in d_6-DMSO.

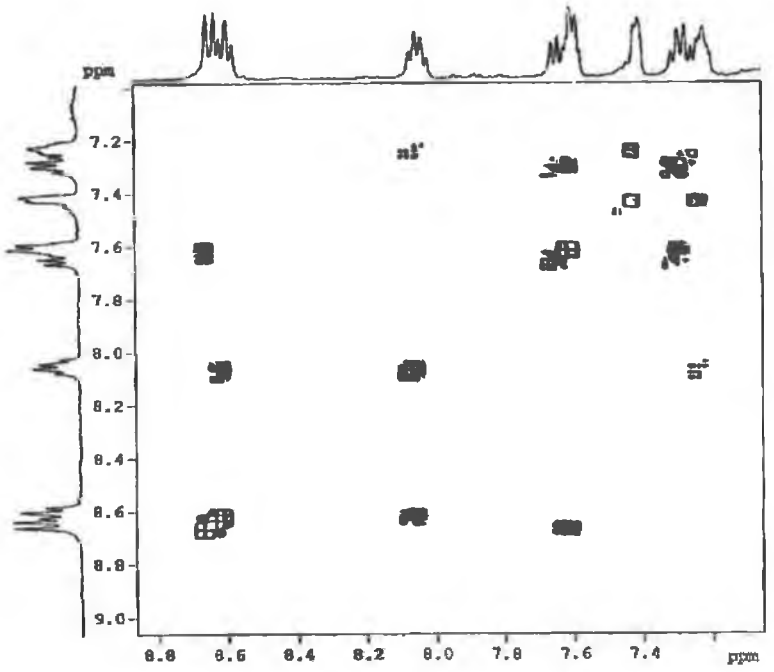

Figure 5.7 2D COSY NMR of the deuterated complex $[Ru(d_8\text{-bpy})_2(LL7)(d_8\text{-bpy})_2Ru]^{4+}$ in d_6-DMSO.

Proton	**Free LL7** Ligand	[Ru(d_8-bpy)$_2$(**LL7**) (d_8-bpy)Ru]$^{4+}$
H_a	8.15 (s)	7.60 (m)
H_b	8.67 (m)	7.60 (m)
H_c	6.95 (dd)	7.27 (m)
H_d	7.15 (dd)	7.27 (m)
H_e	8.67 (m)	8.63 (m)
H_f	8.67 (m)	8.63 (m)
H_g	7.87 (m)	8.05 (dd)
H_h	7.25	7.22 (m)
H_i	8.21	7.42 (d)

Table 5.4 Assignment of the ^1H spectrum of the LL7 ligand protons in the free ligand and in [Ru(d_8-bpy)$_2$(LL7)(d_8-bpy)$_2$Ru](PF$_6$)$_4$, in d_6-DMSO.

It is important to note that no doubling of the number of signals for [Ru(d_8-bpy)$_2$(LL7)(d_8-bpy)$_2$Ru]$^{4+}$ is found. The 10 signals correspond to 20 protons with each signal therefore representing two protons indicating clearly that coordination of metal centres to both sides of the bridging ligand maintains the symmetrical nature of the compound.

This is further proof of the rotamers theory discussed in Chapter 3.5. The reason the osmium or ruthenium complexes containing the LL4, LL5 and LL6 ligands exhibit the rotamer phenomenon is due to the bulky nature of the substituents on the phenyl ring i.e. an OH group, two chloro moieties and two methoxy groups are large enough to prevent rotation of the phenyl ring leading it to be "locked" into one of two orientations. However, even though the LL7 ligand contains a phenyl ring in the 2' position of the imidazo ring, rotation of the phenyl ring must be possible. Examination of the crystal structure indicates that the unsubstituted phenyl ring should be free to rotate.

The majority of the LL7 ligands protons resonances are shifted slightly downfield on coordination to the metal centres. This is due to the electron withdrawing or deshielding effect coordination has on the electron density of the ligand. There is an exception to this however and that is in the case of the H_i protons. This is most likely due to the orientation of the protons, which are directed towards one of the pyridine rings of the adjacent 2,2' bipyridine rings. The ring current induces a diamagnetic anisotropic interaction effect which results in a large upfield shift (approx. 1ppm in the case of the H_i proton).[6] This phenomenon has been explained in Chapter 3.5 in more detail.

The ^{1}H NMR spectra of the undeuterated compounds become very complicated in the aromatic region. Illustrative spectra of the $[Ru(bpy)_2(LL7)]^{2+}$ monomer and $[Ru(bpy)_2(LL7)(bpy)_2Ru]^{4+}$ dimer are presented below.

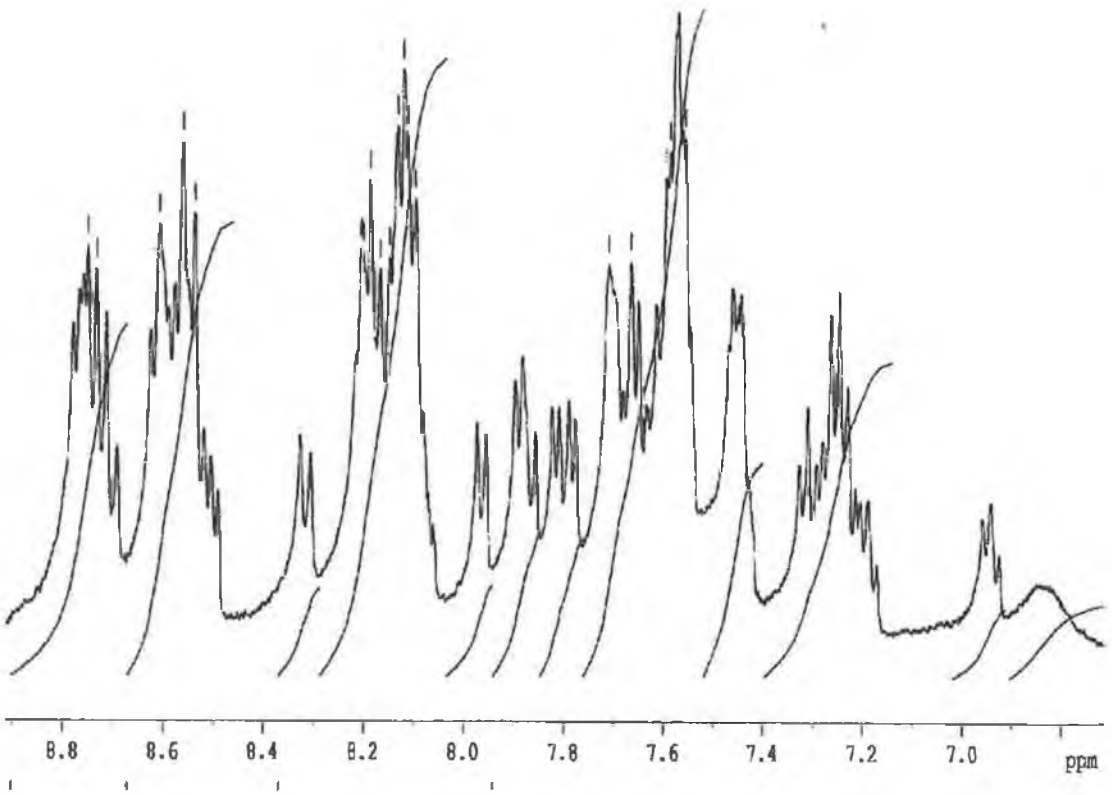

Figure 5.8 Illustrative ^{1}H NMR spectrum of the $[Ru(bpy)_2(LL7)]^{2+}$ monomer in d_6-acetone

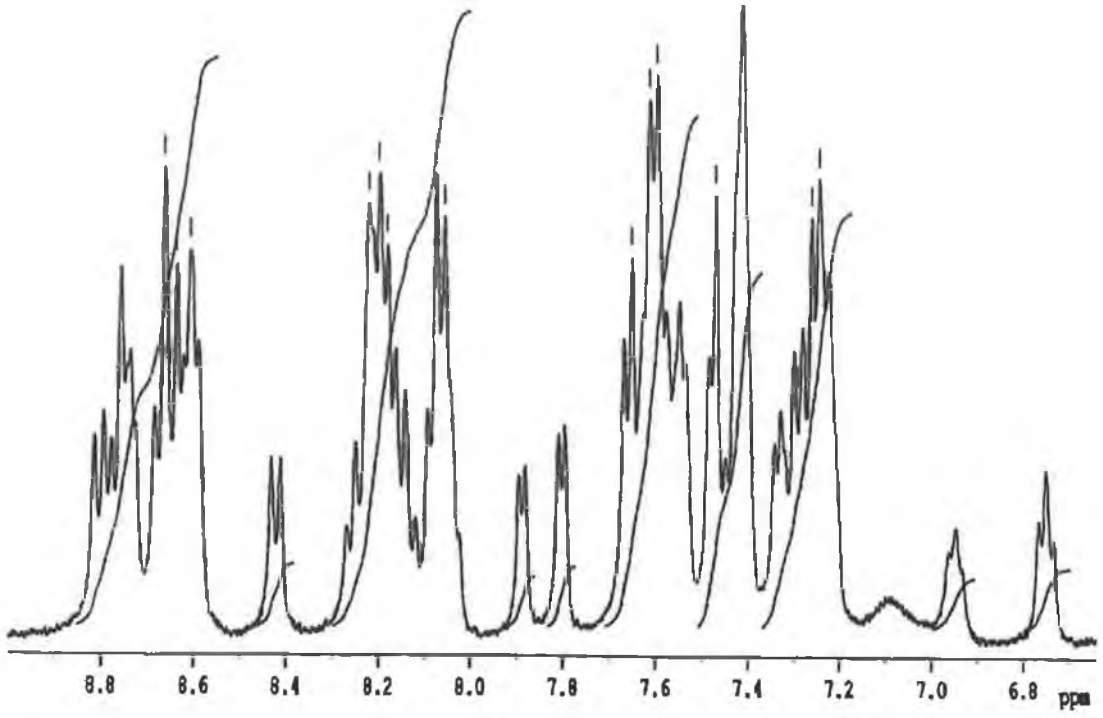

Figure 5.9 Illustrative ^1H NMR spectrum of the $[Ru(bpy)_2(LL7)(bpy)_2Ru]^{4+}$ dimer in d_6-acetone

Owing to the complexity of the spectra, individual assignment of the protons in the spectra illustrated in Figures 5.8 and 5.9 has not been possible. The monomer integrates to 36 protons while the dimer integrates to 52 protons. This difference is explained by the extra two 2,2'-bipyridyl units introduced by coordination of the second ruthenium centre.

The coordination of the second metal centre, as well as adding 16 more proton signals in the aromatic region also introduces symmetry to the complex as is evident from the spectrum of the deuterated complex $[Ru(d_8\text{-bpy})_2(LL7)(d_8\text{-bpy})_2Ru]^{4+}$ which has already been shown to exhibit symmetry (Figure 5.7 – each signal corresponds to two protons). For example, examination of the region between circa 7.7 – 7.95 ppm in the spectrum of the Ru-Ru dimer reveals two doublets (Figure 5.9). This region in the monomer contains four signals (Figure 5.8). The complexity evident in the spectrum of the monomer,

relative to the dinuclear complex provides strong evidence that the mononuclear complex has indeed been made.

The ^{1}H NMR spectra for the Os-Os and Os-Ru dinuclear complexes exhibit the same characteristics as those observed in that of the Ru-Ru dimer and so will not be dwelt on here.

5.6 Photophysical Characterisation of the complexes:

The photophysical properties are presented and discussed in this section. In order to simplify the discussion, the ruthenium complexes are discussed first, the osmium dinuclear complexes second and finally the mixed metal Ru-Os complex is discussed. Unlike in the previous chapters, where the properties of the free ligands have been reported first, no results are reported for the ligand (LL7) owing to its lack of solubility in a suitable solvent. Reference is made to the properties of $[Ru(bpy)_3]^{2+}$ and $[Os(bpy)_3]^{2+}$. These complexes have already been discussed in relation to the monomeric complexes discussed in Chapters 3.8 and 4.6 and their photophysical characteristics are detailed there.

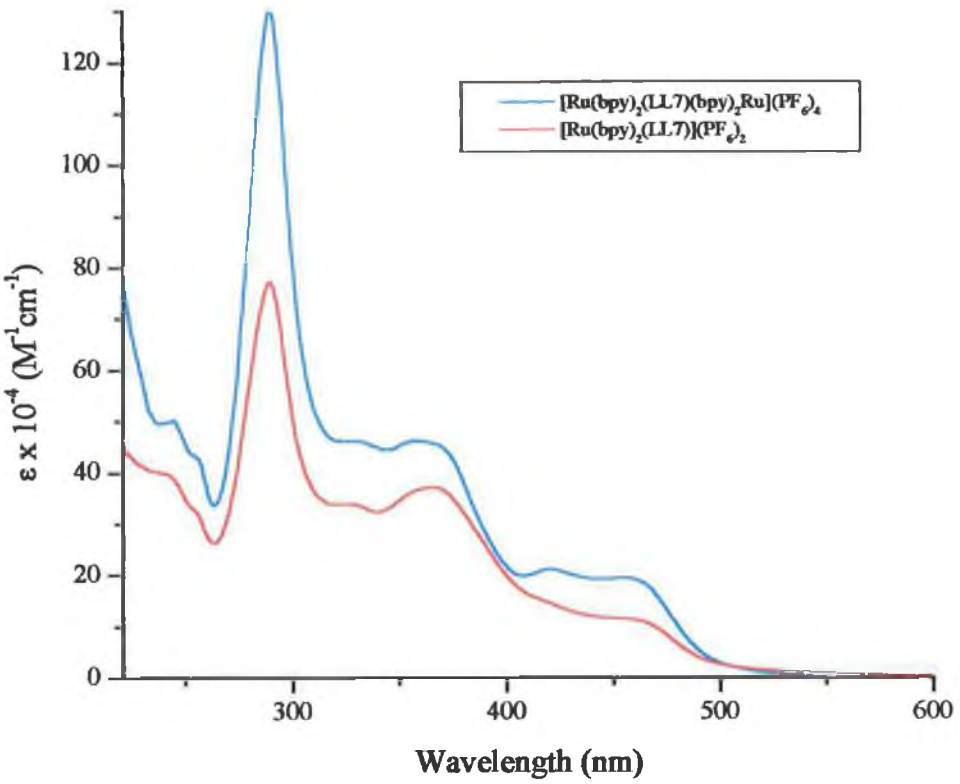

Figure 5.10 Absorption spectra of the monomer $[Ru(bpy)_2(LL7)]^{2+}$ and the dimer $[Ru(bpy)_2(LL7)(bpy)_2Ru]^{4+}$ in MeCN.

The absorption spectra of the two ruthenium complexes, $[Ru(bpy)_2(LL7)]^{2+}$ and $[Ru(bpy)_2(LL7)(bpy)_2Ru]^{4+}$, detailed above are quite similar (Figure 5.10). The visible regions of the spectra are dominated by $d\pi \rightarrow \pi^*$ MLCT transitions which are typical of complexes of this type. As in the case of the other ruthenium complexes studied and detailed in Chapter 3.8, the UV region contains the expected $\pi \rightarrow \pi^*$ (bpy) transitions associated with transitions on the bipyridyl ligands, and also of $\pi \rightarrow \pi^*$ (LL7) transitions located on the LL7 ligand. These transitions being located at *circa* 290 nm and 350 nm respectively. As expected the absorbance spectra of the complexes are red shifted with respect to $[Ru(bpy)_3]^{2+}$, indicating that as in the case of the other LL_x ligands, the LL7 ligand is a stronger σ-donor than 2,2' bipyridyl.

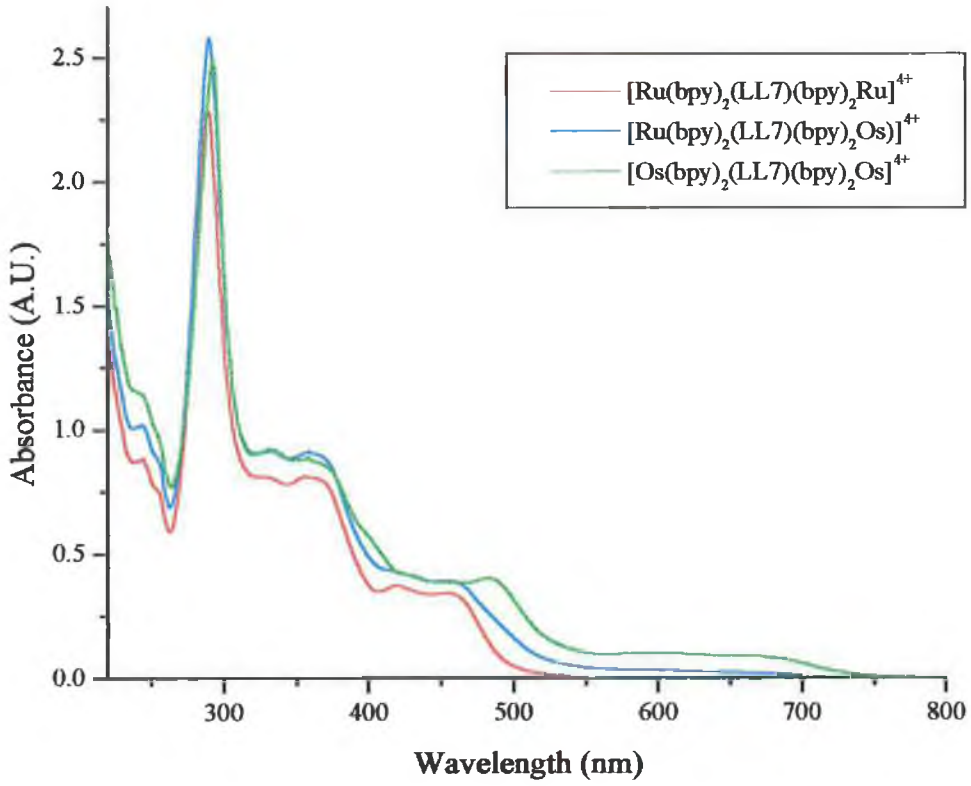

*Figure 5.11 Absorption spectra of the complexes [**Ru**(bpy)$_2$(LL7)(bpy)$_2$**Ru**]$^{4+}$ (red trace), [**Ru**(bpy)$_2$(LL7)(bpy)$_2$**Os**]$^{4+}$ (blue trace) and [**Os**(bpy)$_2$(LL7)(bpy)$_2$**Os**]$^{4+}$ (green trace) in MeCN.*

In the mixed metal complex, replacement of a ruthenium metal centre with an osmium metal centre leads to a shift to lower energy of the MLCT absorption bands (Figure 5.11). This phenomenon has been well documented [12] and has been described Chapter 4.6. As in the case of the osmium monomeric LL_x complexes, an additional band between 580 and 700 nm is visible. These bands can be assigned to formally forbidden $d\pi \rightarrow \pi^*$ (bpy) MLCT transitions.

This is true also of the homonuclear osmium complex [Os(bpy)$_2$(LL7)(bpy)$_2$Os]$^{4+}$, which has bands which absorb even more strongly in this region due to the coordination of the second osmium bis bipyridyl unit.

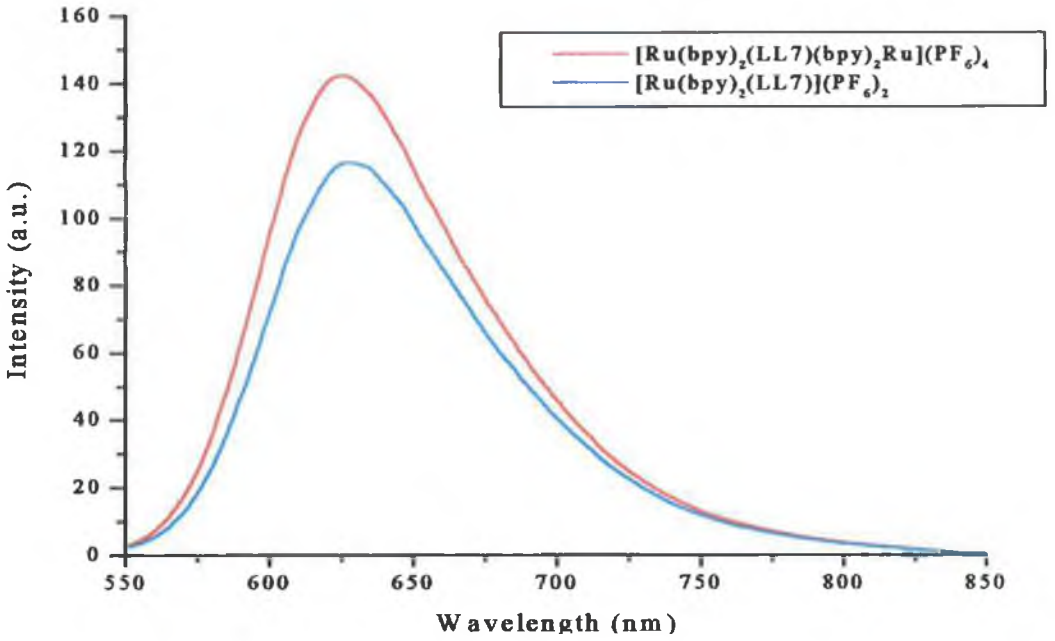

Figure 5.12 Room temperature emission spectra of $[Ru(bpy)_2(LL7)(bpy)_2Ru]^{4+}$ (red trace) and $[Ru(bpy)_2(LL7)]^{2+}$ (blue trace) in MeCN.

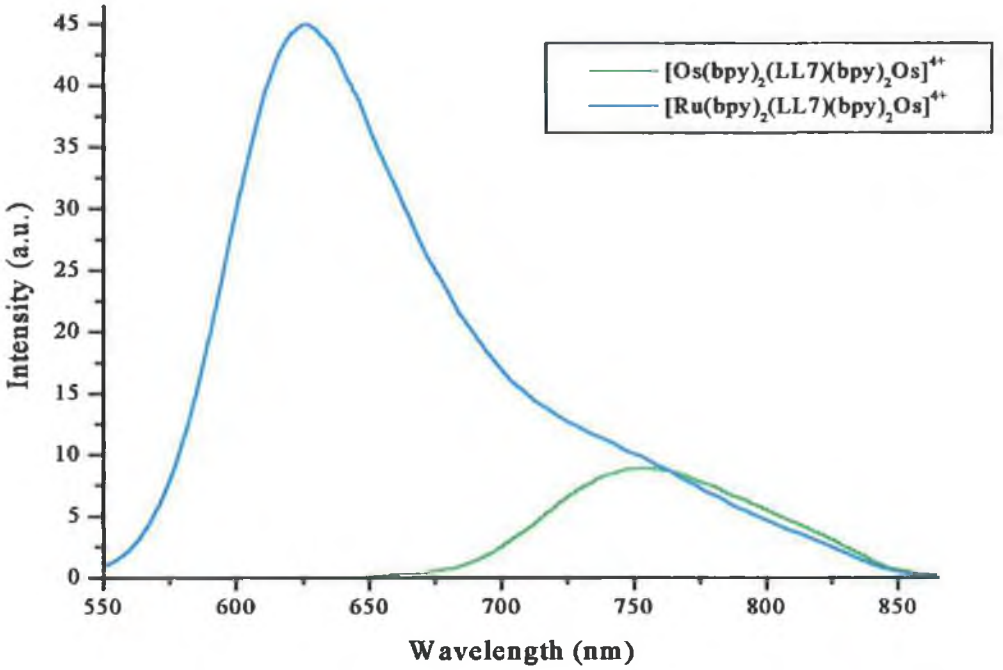

Figure 5.13 Room temperature emission spectra of $[Ru(bpy)_2(LL7)(bpy)_2Os]^{4+}$ (blue trace) and $[Os(bpy)_2(LL7)(bpy)_2Os]^{4+}$ (green trace) in MeCN.

All the complexes exhibited room temperature emissions in acetonitrile. (Figures 5.12 and 5.13) As with the absorption spectra the λ_{max} of the emission spectra are red shifted with respect to $[Ru(bpy)_3]^{2+}$ or $[Os(bpy)_3]^{2+}$. As expected, the emission maxima of the osmium complexes were lower in energy than the emission maxima of the analogous ruthenium complexes. [13] The emission spectral features of the heteronuclear Os-Ru dimer are more complicated and therefore need more careful analysis. The results are tabulated in Table 5.5. Comparison shows that the emission of the homodinuclear complexes correspond closely to the emissions observed for the mononuclear complexes discussed in Chapters 3 and 4.

Compound	**Absoprtion, λ_{max}** (nm)	Extinction coefficent, ε	**Emission, λ_{max}** 298K (nm)	**Emission, λ_{max}** 77K (nm)
$[Ru(bpy)_2(LL7)]^{2+}$	290	77,250		
	365	36,700	628	598
	454	11,350		
$[Ru(bpy)_2(LL7)$	290	129,700		
$(bpy)Ru]^{4+}$	357	46,200	625	602
	457	19,500		
$[Ru(bpy)_2(LL7)$	290	128,900		
$(bpy)Os]^{4+}$	357	47,000	755	713
	457	19,300	626	602
	506 (sh)	7,700		
$[Os(bpy)_2(LL7)$	293	135,000		
$(bpy)Os]^{4+}$	359	47,300	753	738
	484	17,890		
	624	7,200		

Table 5.5 Absorption and emission data for the complexes. All room temperature measurements carried out in MeCN. 77K emission studies carried out in butyronitrile.

As in Chapters 3 and 4 all the complexes exhibit a strong emission with vibrational structure at 77K. [14] Cooling to 77K leads to a blue shift in the emission maxima of both the osmium and ruthenium centred emissions as expected. [15] The emission spectra of the complexes at 77K can be seen in Figures 5.14 and 5.15.

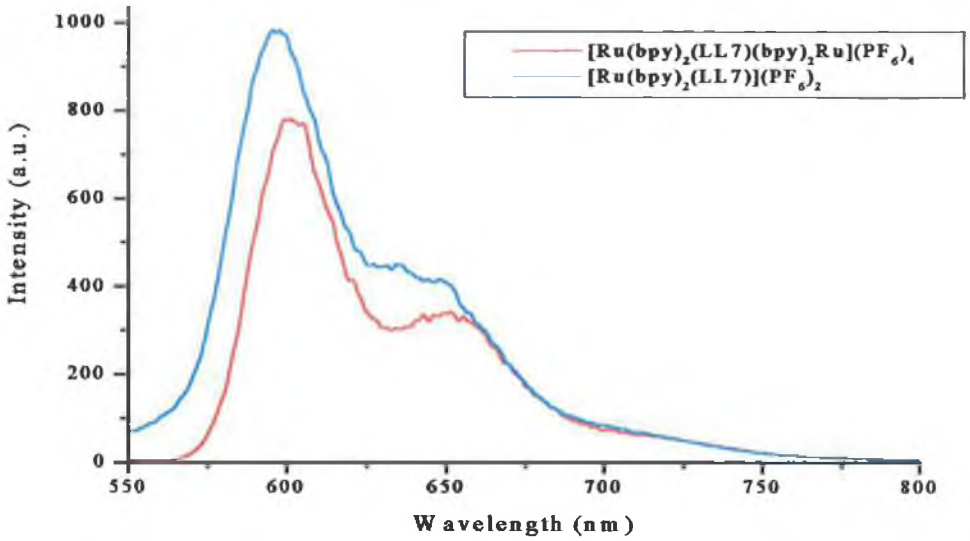

Figure 5.14 Low temperature emission spectra of $[Ru(bpy)_2(LL7)(bpy)_2Ru]^{4+}$ (blue trace) and $[Ru(bpy)_2(LL7)]^{2+}$ (red trace) in butyronitrile.

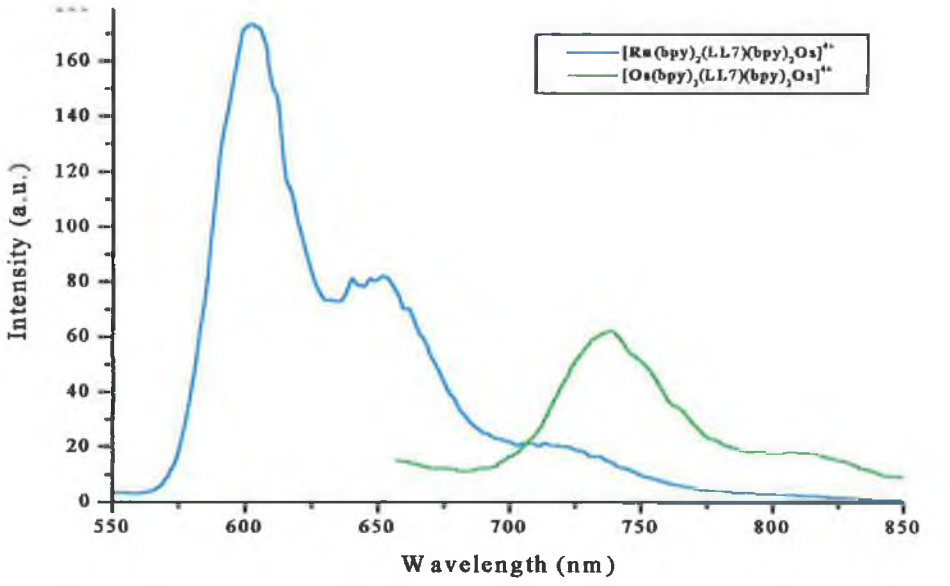

Figure 5.15 Low temperature emission spectra of $[Ru(bpy)_2(LL7)(bpy)_2Os]^{4+}$ (blue trace) and $[Os(bpy)_2(LL7)(bpy)_2Os]^{4+}$ (green trace) in butyronitrile.

Compound	Room Temperature		77K (ns)
	Aerated (ns)	Degassed (ns)	
$[Ru(bpy)_2(LL7)]^{2+}$	142	690	N/A
$[Ru(bpy)_2(LL7)(bpy)_2Ru]^{4+}$	143	506	N/A
$[Ru(d_8\text{-bpy})_2(LL7)(d_8\text{-bpy})_2Ru]^{4+}$	155	940	N/A
$[Os(bpy)_2(LL7)(bpy)_2Os]^{4+}$	30	39	890
$[Os(d_8\text{-bpy})_2(LL7)(d_8\text{-bpy})_2Os]^{4+}$	33	65	1750

Table 5.6 Single Photon Counting Lifetime Data of complexes $[Ru(bpy)_2(LL7)]^{2+}$, $[Ru(bpy)_2(LL7)(bpy)_2Ru]^{4+}$ and $[Os(bpy)_2(LL7)(bpy)_2Os]^{4+}$ and their deuterated analogues in Uvasol acetonitrile. 77K measurements in butyronitrile.

The lifetimes of the ruthenium monomer, $[Ru(bpy)_2(LL7)]^{2+}$ (142 ns and 690 ns) and the dimer $[Ru(bpy)_2(LL7)(bpy)_2Ru]^{4+}$ (143 ns and 506 ns) in both aerated and deaerated MeCN correspond closely with the lifetimes of the $[Ru(bpy)_2(LL_x)]^{2+}$ complexes which were between 116 and 165 ns for the deaerated lifetimes and 750 and 970 ns for the deaerated lifetimes. The use of the selective deuteriation of moieties within the molecule and the examination of the effect this selective deuteriation has on the lifetime of the complex has been discussed in relation to the ruthenium and osmium complexes already (Chapter 3.8 and 4.6). The 2,2'-bipyridyl ligands have been deuteriated and the effect this has on the lifetime of the complexes was examined. This is illustrated in Figure 5.16 below and recorded in Table 5.6.

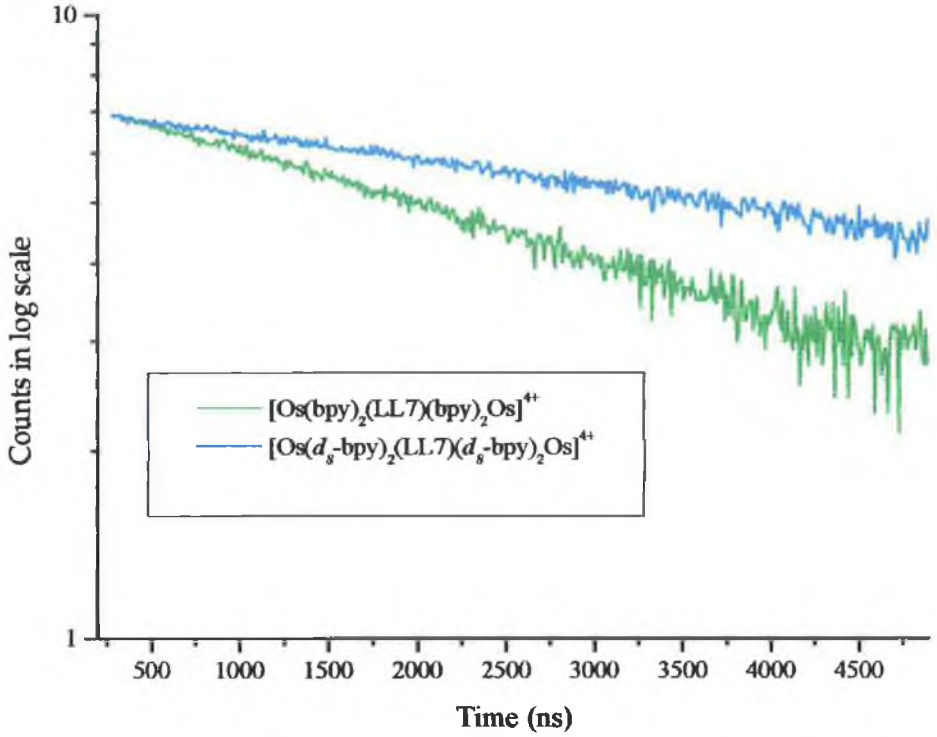

Figure 5.16 Decay profile of the complexes $[Os(bpy)_2(LL7)(bpy)_2Os]^{4+}$ (green trace) and $[Os(d_8\text{-}bpy)_2(LL7)(d_8\text{-}bpy)_2Os]^{4+}$ (blue trace) at 77K (in butyronitrile).

Deuteration of the bipyridyl ligands leads to a lengthening of the lifetime of the Ru-Ru dimer from 506 to 940 ns (185%) in deaerated MeCN and from 39 to 65 ns (166%) for the Os-Os complex in MeCN. The lifetimes of the Os-Os dimer at 77 K in butyronitrile show greater differences with the non deuterated complex having a luminescent lifetime of 890 ns. This is increased to 1750 ns on deuteration of the bipyridyl moieties. (Figure 5.16) As in the case of the monomers (Chapters 3 and 4) this indicates strongly that the excited state lies on the bipyridyl units and not on the LL7 ligand. This supposition is backed-up by the observed reduction potentials of the complexes. (Section 5.6)

The emissive properties of the mixed metal complex $[Ru(bpy)_2(LL7)(bpy)_2Os]^{4+}$ (Ru-Os) are more complicated than those of the homonuclear osmium(II) or ruthenium(II) dinuclear complexes. The luminescence spectra of the Ru-Os complex at room temperature and at 77K can be seen in Fig. 5.13 and Fig. 5.15 respectively. In both cases

there appears to be a dual emission. At room temperature, a strong emission at 626 nm is observed, while the emission at lower energy, i.e. circa 755 nm appears as a shoulder on the low energy side of the stronger emission. These may, by comparison with the data for both the ruthenium mono- and dinuclear complexes and the osmium dinuclear complex, be assigned as a ruthenium(II) emission and an osmium(II) emission. The Ru based component is the stronger of the two. The situation is the same at 77K. The strong ruthenium emission is centred at 602 nm. The osmium centred emission once again appears as a shoulder on the low energy side of the ruthenium emission. Exact location of the λ_{max} is more difficult, but this emission appears to be centred at 713 nm. Both osmium and ruthenium emission have been blue shifted with respect to the room temperature values.

Dual luminescence is not uncommon. Barigelleti and coworkers have reported dual emission for rodlike Ru(II)/Os(II) dinuclear complexes where the bridging ligand contains dipyridylbenzene fragments separated by phenylene spacers. [16,17] De Cola *et al.* have shown that Ru/Os dimers separated by rigid bicyclooctane spacer show dual luminescence behaviour. [18]

Compound	Excitation at 620nm (ns)		Excitation at 750nm (ns)	
	Aerated	Degassed	Aerated	Degassed
$[Ru(bpy)_2(LL7)(bpy)_2Os]^{4+}$	144	520	143 31	530 41

Table 5.7 Single Photon Counting Lifetime Data of the complex $[Ru(bpy)_2(LL7)(bpy)_2Os]^{4+}$ in Uvasol acetonitrile.

The luminescent lifetime data of the mixed metal Ru-Os complex has been tabulated in Table 5.7. Both aerated and deaerated experiments were measured in the maxima of the Ru centred emission and the Os centred emission. As can be seen from Table 5.6,

measuring in the Ru centre results in a single lifetime corresponding to emission from the Ru centre. The lifetimes are comparable to those of the ruthenium LL7 monomer and dimer. Measuring at 750 nm leads to a dual emissive behaviour. The lifetime of the Ru component is almost the same when recording at 620 nm, while a shorter lifetime of 31 ns and 41 ns (in aerated and deaerated respectively) corresponding to emission from the osmium centre are also observed.

Comparison of the results of the luminescence lifetime data achieved for the mixed metal Ru-Os dinuclear complex with the lifetimes found for the homodinuclear Ru-Ru and Os-Os complexes provide information on the metal-metal interaction. In the Ru-Os dimer the lifetime of the emission corresponding to the ruthenium centre is measured as being *circa* 143 ns in aerated MeCN or 520 ns in deaerated MeCN. This compares to lifetimes of 142 ns and 690 ns found for the $[Ru(bpy)_2(LL7)]^{2+}$ complex and 143 and 506 ns found for the $[Ru(bpy)_2(LL7)(bpy)_2Ru]^{4+}$. The lifetime of the emission corresponding to emission from the osmium centre of the mixed metal complex is 31 ns and 41 ns aerated and deaerated respectively. This compares to the lifetimes of the $[Os(bpy)_2(LL7)(bpy)_2Os]^{4+}$ dinuclear complex of 30 ns and 39 ns aerated and deaerated respectively. The similarities between the lifetimes of the emissions from both metal centres in the heteronuclear Ru-Os complex to those of the homonuclear Ru-Ru and Os-Os complexes indicate that there is little interaction between the metal centres, even in the mixed metal species.

5.7 Electrochemistry of the complexes:

As with the electrochemistry of the monomeric complexes discussed in both Chapter 3.10 and 4.8, the electrochemistry of the ruthenium(II) and osmium(II) complexes of the LL7 ligand is not as straightforward as could be expected, and careful study and several experiments have been necessary to understand and be able to describe more fully the electrochemical processes at work.

The complexes $[Ru(bpy)_3]^{2+}$ and $[Os(bpy)_3]^{2+}$ have again been used for comparisons' sake. The cyclic voltammograms of these "parent" complexes have already been described in Section 3.11 and Section 4.8 and will not be discussed again here. Unfortunately, the electrochemistry of the free ligand could not performed due to the insolubility of the ligand in a suitable solvent. The results of the electrochemical analysis are listed in Table 5.8.

Compound	Oxidation	Reduction
$[Ru(bpy)_2(LL7)]^{2+}$	0.79 (93)	-1.67
	1.42 (irr)	-1.92
$[Ru(bpy)_2(LL7)(bpy)_2Ru]^{4+}$	0.79 (85)	-1.63
	1.10 (67)	-1.84
$[Os(bpy)_2(LL7)(bpy)_2Os]^{4+}$	0.43 (74)	-1.58
	0.78 (63)	-1.82
	1.39 (irr)	
$[Ru(bpy)_2(LL7)(bpy)_2Os]^{4+}$	0.36 (92)	-1.56
	0.79 (79)	-1.81
	1.10 (111)	

Table 5.8 Results of electrochemistry of complexes containing LL7.

All results are in V vs Fc/Fc^+ standard.

The cyclic voltammogram of the oxidation waves of the $[Ru(bpy)_2(LL7)]^{2+}$ complex is presented in Figure 5.17. Comparison with the voltammograms of the monomeric ruthenium(II) complexes of the LL_x ligands discussed in Chapter 3 indicate that the first oxidation wave is most likely due to a $Ru^{(II)}/Ru^{(III)}$ couple, while the second wave is due to oxidation of the LL7 ligand. The presence of ligand oxidation waves has been discussed for ruthenium(II) complexes containing similar ligands in Section 3.10. The cyclic voltammogram of the reduction potentials is interesting also and can be seen in the Figure 5.18.

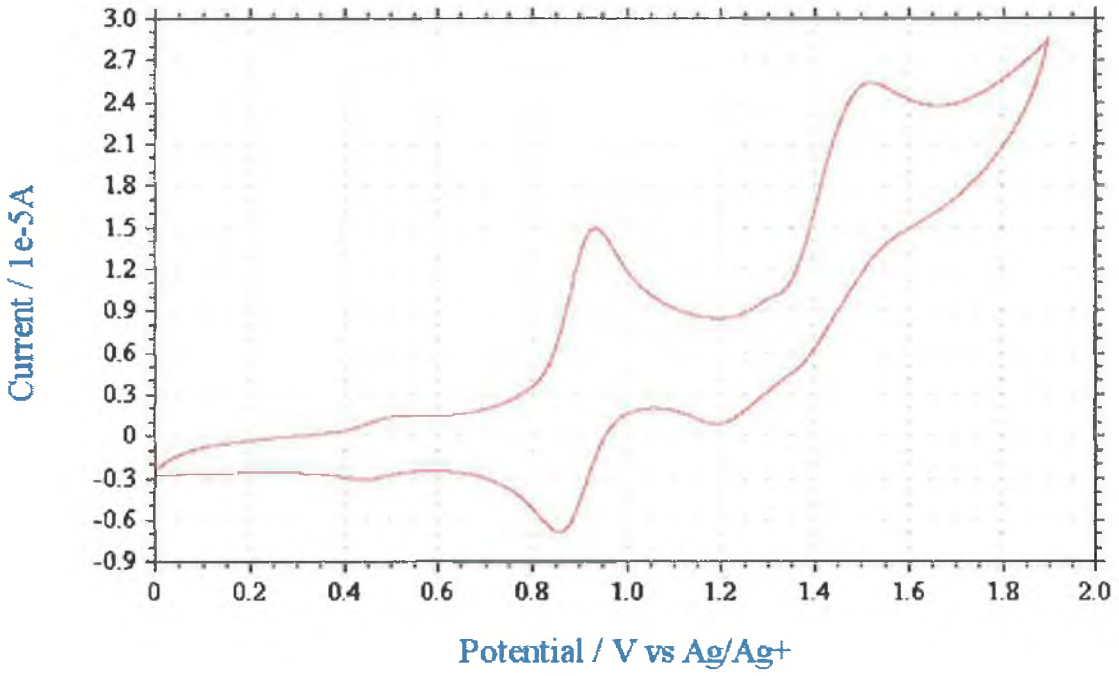

Figure 5.17 Cyclic Voltammogram of the oxidation potentials of the monomer $[Ru(bpy)_2(LL7)]^{2+}$ in MeCN with 0.1M $TBABF_4$.

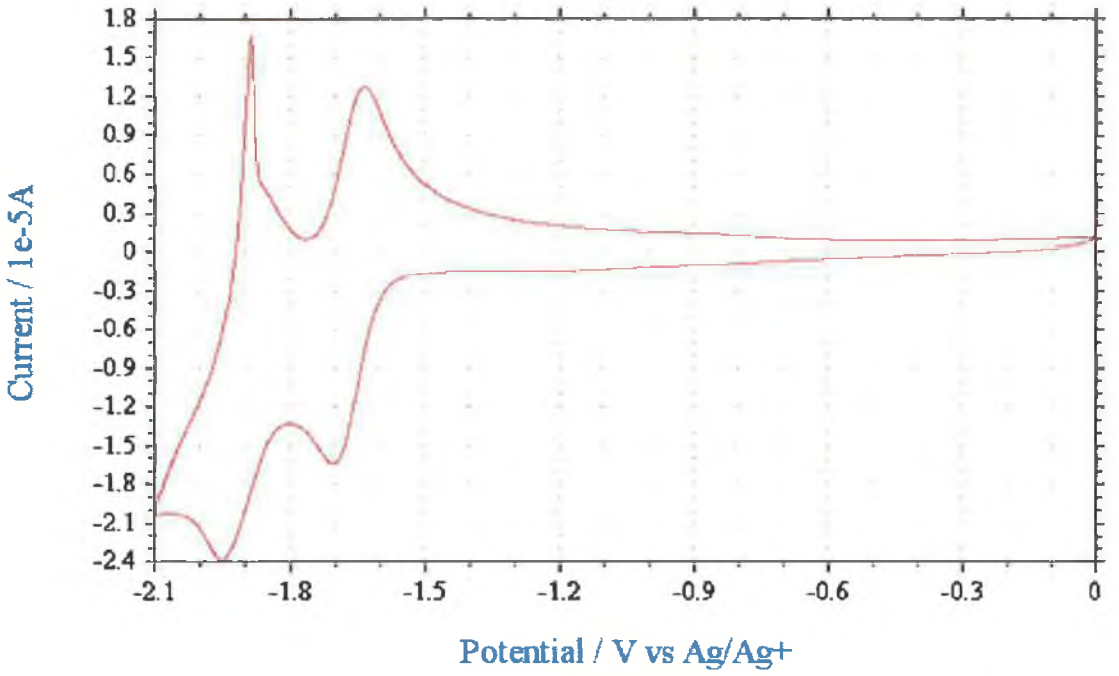

Figure 5.18 Reduction potentials of the complex $[Ru(bpy)_2(LL7)]^{2+}$ in MeCN with 0.1M $TBABF_4$.

In the experiment to examine the reduction potentials of the complex $[Ru(bpy)_2(LL7)]^{2+}$, the applied potential is initially scanned in a negative direction from 0 V *vs* Ag/Ag^+. The spike seen on the return wave in this instance can tentatively be described as a "desorption spike" and is likely to be due to the desorption of complex from the electrode surface at the applied potential. [19,20]

This desorption spike may be caused by more than one factor. After the applied potential reaches -2.1 V *vs* Ag/Ag^+, the complex in solution has experienced two reductions, i.e. the complex has gained two electrons, and therefore should be a neutral species at this potential. This sudden neutrality may cause the complex to become insoluble at this applied potential and this in turn leads to the deposition of the complex onto the working Pt electrode. The desorption spike can therefore be due to the complex being oxidised from the neutral species, and therefore re-dissolving in the electrolyte at a particular potential which results in a larger than expected current flowing at that voltage.

Alternatively, it should be remembered also that the LL7 ligand in the monomeric complex will contain free nitrogens which have the ability to "adsorb" on the electrode. On the return scan the electrode becomes less negatively charged, and at a specific voltage, the interaction between electrode and free nitrogens becomes too weak to bind the complex to the surface resulting in the desorption spike found in Figure 5.18. This is an interesting result, and if this was the case, provides proof that the complex being examined is the monomer, as the adsorption to the electrode would not be possible without the free nitrogens available on the monomer. In favour of this supposition, this phenomenon does not occur for any of the dimeric complexes.

The voltammogram of the dinuclear Ru-Ru complex is given in Figure 5.19. In order to aid the assignment of the oxidation potentials, the voltammogram of the mononuclear ruthenium complex is presented for comparison.

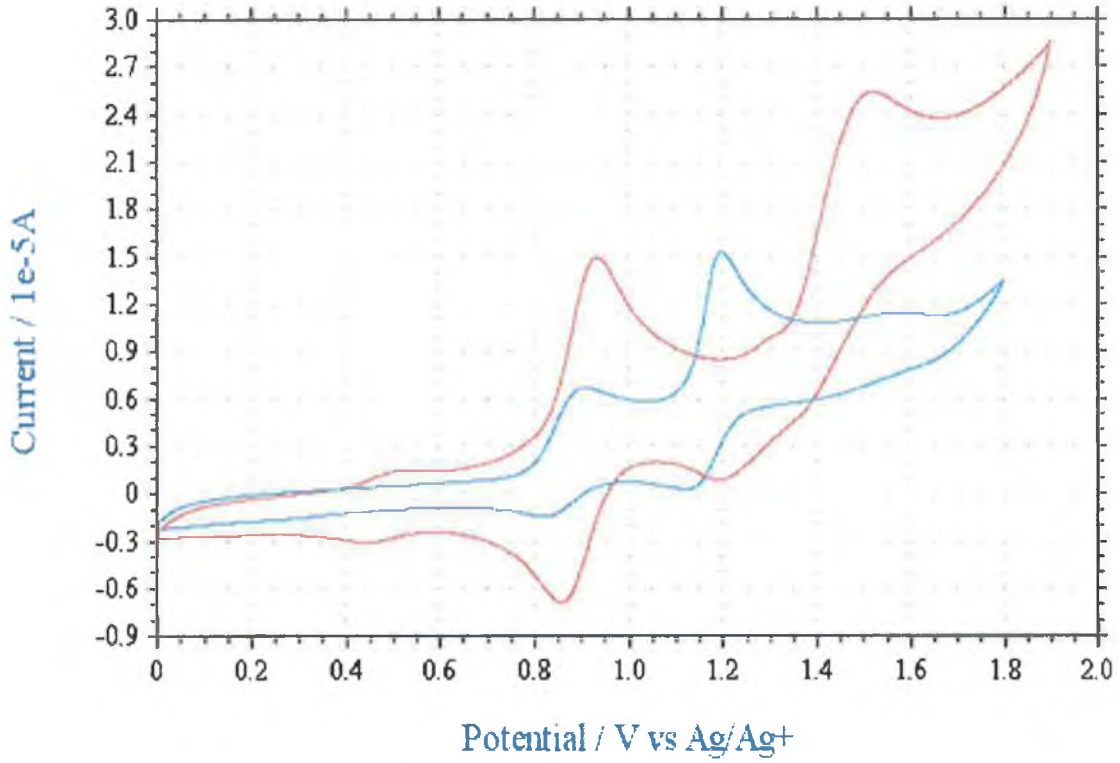

Figure 5.19 Oxidation potentials of $[Ru(bpy)_2(LL7)]^{2+}$ (red) and $[(Ru(bpy)_2)_2(LL7)]^{4+}$ (blue) in MeCN with 0.1M $TBABF_4$.

The first oxidation wave of the $[(Ru(bpy)_2)_2(LL7)]^{4+}$ dimer corresponds very closely with that of the monomer, and has also been assigned as due to a $Ru^{(II)}/Ru^{(III)}$ couple. What is interesting is the two electron process appears as a single redox wave with no sign of splitting. This can be attributed to the simultaneous oxidation of the two metal units of the dimer and is a known phenomenon. [21] Molecules containing a number of identical, noninteracting centres exhibit electrochemical responses of the same shape as that obtained for the corresponding molecule containing a single centre. The presence of the extra units simply enhances the magnitude of the current.

This is the case for the $[(Ru(bpy)_2)_2(LL7)]^{4+}$ complex and the $[(Os(bpy)_2)_2(LL7)]^{4+}$ complex which will be discussed next. The oxidation potential of the ruthenium metal centre in both the monomer and dimer are almost identical. This is characteristic of dinuclear complexes where electrostatic and resonance stabilisation effects are small and

therefore serves as evidence of small electronic coupling between the two metal centres. [22] A metal-metal interaction through space, or through the bridging ligand would lead to stabilisation of the mixed-valence complex, and lead in turn to the presence of discrete oxidation waves for each metal centre. [23,24] Attempts to resolve the peaks using the more sensitive technique of differential pulse voltammetry has also failed. [25]

The stability of the intermediate species towards redox dissociation is measured by the comproportionation equilibrium constant, K_c. The intermediate exists in a comproportionation equilibrium which can be represented as,

$$2M^{(II)}\text{-LL-}M^{(III)} \rightleftharpoons M^{(II)}\text{-LL-}M^{(II)} + M^{(III)}\text{-LL-}M^{(III)} \qquad \textbf{Equation 5.1}$$

$$K_c = e^{\Delta E(mV)/25.69} \text{ at } T = 298K \qquad \textbf{Equation 5.2}$$

A single oxidation wave for the homodinuclear complexes $[(Ru(bpy)_2)_2(LL7)]^{4+}$ and $[(Os(bpy)_2)_2(LL7)]^{4+}$ means that K_c is near its statistical limit of 4. [26]

The second oxidation potential for the mononuclear complex is 1.42 V *vs* Fc/Fc^+, whereas the second oxidation potential of the dimer appears at 1.10 V *vs* Fc/Fc^+. The electronic properties of the ligand are changed upon coordination of a second $[Ru(bpy)_2]$ unit.

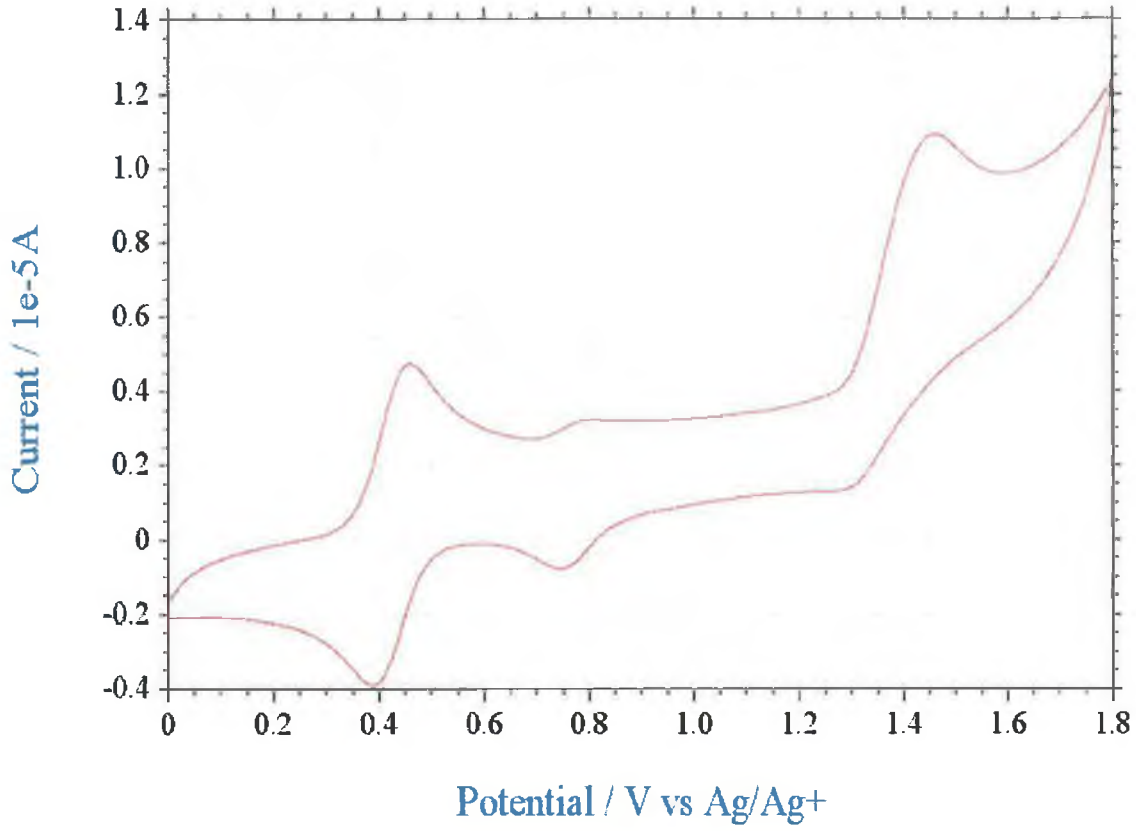

Figure 5.20 Cyclic Voltammogram of the oxidation of the complex $[Os(bpy)_2(LL7)(bpy)_2Os]^{4+}$.

Section 4.8, has already discussed the electrochemistry of osmium(II) complexes. The first oxidation wave (0.43 V *vs* Fc/Fc^+) can be assigned as a two electron $Os^{(II)}/Os^{(III)}$ couple (this has been proven by bulk electrolysis and is described in the next section). As expected this is approximately 350mV lower than for the analogous $Ru^{(II)}/Ru^{(III)}$ couple. [27] (Figure 5.20) The reasons for this difference have already been discussed and will not be repeated here. As for the ruthenium dimer, the two electron process appears as a single redox wave with no sign of splitting. The irreversible ligand oxidation is centred at 1.38 V *vs* Fc/Fc^+, which is much closer to the ligand centred oxidation potential found for the ruthenium monomer, than for that of the ruthenium dimer.

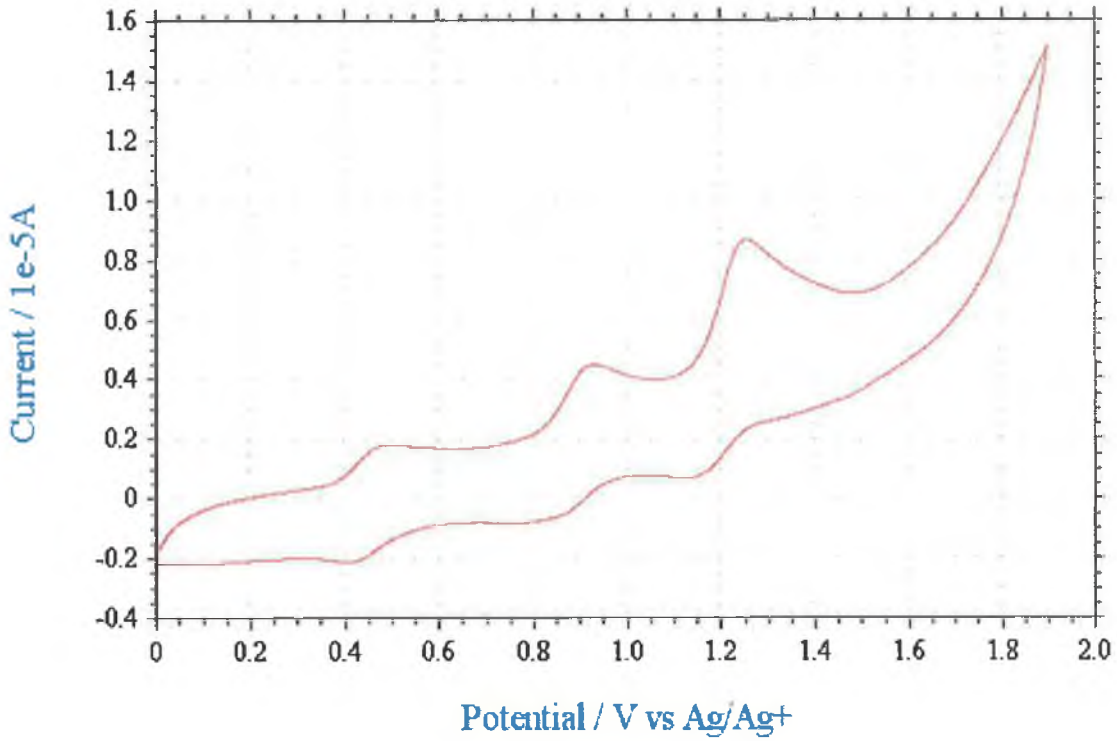

Figure 5.21 Cyclic Voltammogram of the oxidation potentials of the mixed metal complex $[Ru(bpy)_2(LL7)(bpy)_2Os]^{4+}$.

The oxidation potentials of the mixed metal heteronuclear dimer can be seen in Figure 5.21. As expected, for a system where the communication between the metal centres is weak, the oxidation potential of the $Ru^{(II)}/Ru^{(III)}$ and $Os^{(II)}/Os^{(III)}$ are the same as for the corresponding monomer and homonuclear dimers. Again, a ligand based oxidation is found at higher potentials. (1.10 V *vs* Fc/Fc^+)

The results of the electrochemistry to examine the reduction potentials of the complexes can be seen in Table 5.8. Each of the complexes exhibits two one electron reduction potentials before we reach the solvent limit, with the first between –1.56 and –1.62 V and the second lying between –1.81 and –1.84 V *vs* Fc/Fc^+. These compare favourably to the first two reduction potentials found for other ruthenium(II) and osmium(II) complexes and correspond to the first two reductions of the 2,2'-bipyridyl moieties. [28]

The similarity of the reduction potentials to those of previously studied complexes allow us to locate the excited state of these compounds on the 2,2'-bipyridyl unit and not on the bridging ligand. This agrees with the excited state lifetimes discussed in Section 5.5. The fact that the 2,2'-bipyridyl units are easier to reduce than the bridging ligand also suggests that 2,2'-bipyridyl is a stronger π-acceptor than the bridging LL7 ligand.[29]

5.8 Bulk electrolysis of the $[Os(bpy)_2(LL7)(bpy)_2Os](PF_6)_4$ complex:

In this experiment bulk electrolysis was used to confirm that the first oxidation potential is a two electron process, i.e. that the oxidation potential at 0.43 V *vs* Ag/Ag^+ is due to simultaneous oxidation of the both osmium(II) centres to osmium(III). In the electrochemical experiments that have been performed thus far, the ratio of the electrode surface to the volume of solution has been low. This permits the experiments to be performed without changing the overall composition of the solution, i.e. the experiments are not destructive. In this instance however, we attempt to convert 100% of the electroactive species in the solution to a different oxidation state by applying an appropriate constant potential to the surface of the working electrode. To speed up the electrochemical conversion, working electrodes with a large surface area are used, while mass transport is enhanced by magnetically stirring the experiment. Figure 5.24 illustrates the bulk electrolysis set-up.

The set-up used was a 3 compartment, 3 electrode cell. The reference electrode was Ag/Ag^+, the working electrode was a cylinder of Pt guaze, 1 cm x 1 cm (52 mesh) and the counter electrode used was a coiled Pt wire. (Figure 5.22)

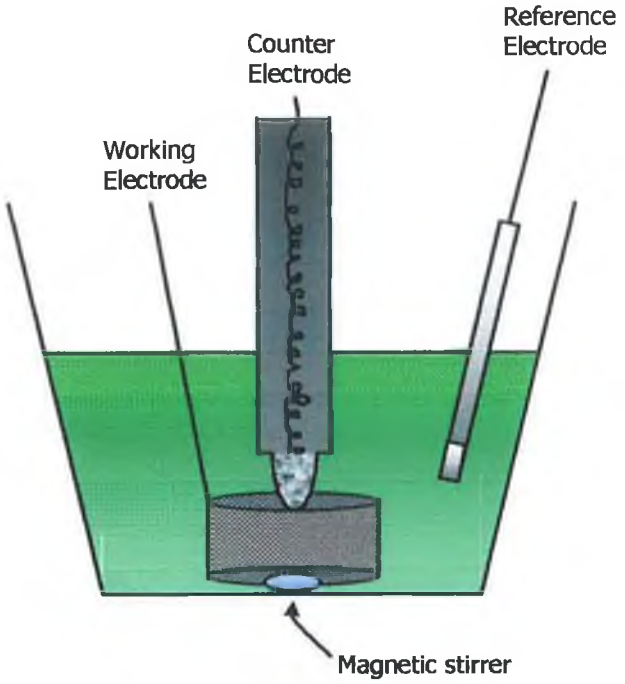

Figure 5.22 Illustration of the apparatus used to perform the bulk electrolysis experiment.

During the bulk electrolysis experiment, the current decays exponentially with time as the remaining concentration of the original electroactive species is lowered by the electrochemical reaction. Integration of the current *vs* time leads to the total electrical charge passed, which can be converted to the number of moles converted using Faraday's Law. In our case we use the measured charge (Q) to determine the number of electrons (n) involved in the electrochemical reaction, where F is Faradays Constant, V is the volume of the solution and C is the concentration of the electroactive species in solution. The result of the experiment is presented in Figure 5.23.

$$n = \frac{Q}{FVC}$$

Equation 5.3

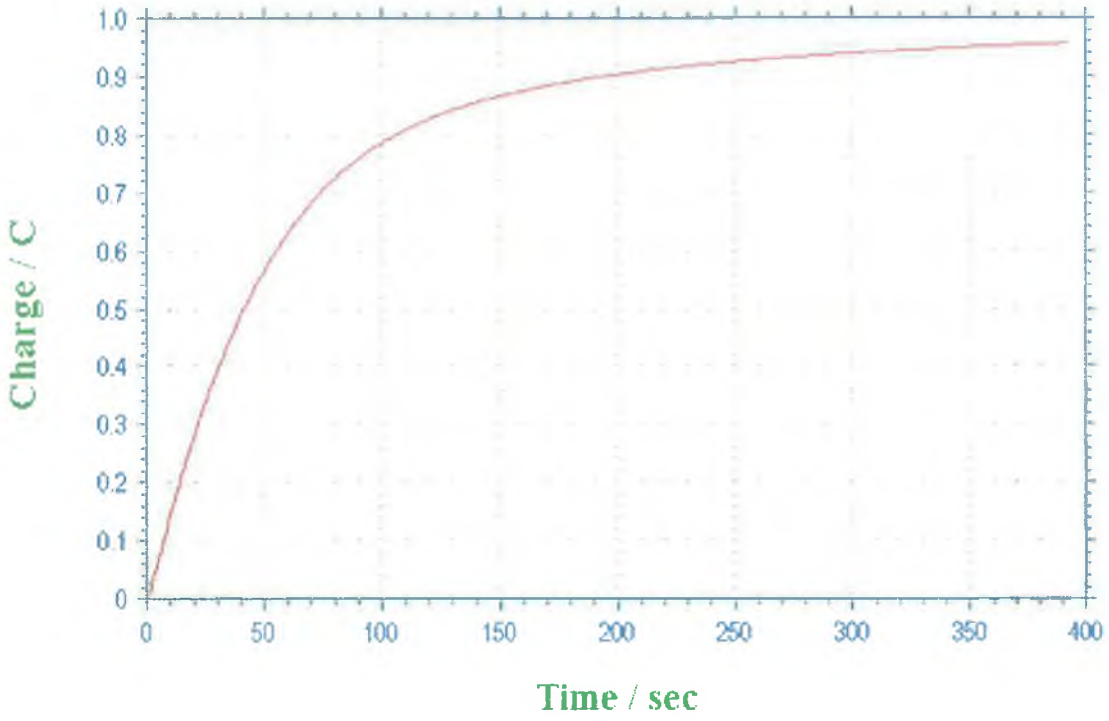

Figure 5.23 Bulk oxidation trace of $[Os(bpy)_2(LL7)(bpy)_2Os]^{4+}$.

In our experiment, the value of **n = 1.92**. This compares to an expected value of 2. The value of n = 1.92 is well within experimental error and proves that both osmium(II) centres are oxidised simultaneously. The results of this experiment can be used by extension to assert that the oxidation potential observed at 0.79 V *vs* Fc/Fc^+ in the voltammogram of the $[Os(bpy)_2(LL7)(bpy)_2Os]^{4+}$ dimer is also a 2 electron process.

5.9 Spectroelectrochemistry of the complexes:

The spectroelectrochemical properties of the dinuclear complexes have also been examined. Spectroscopic and electrochemical data indicates that communication between the metal centres in the ground state is weak. The most effective way to measure directly the coupling between two metal centres in a dinuclear complex is to examine mixed valence species. Section 1.10 provides an introduction to this section.

As discussed in the previous section, the ruthenium and osmium homonuclear dimers exhibit a single metal centred oxidation couple, which corresponds to oxidation of both metal centres simultaneously. The bulk electrolysis experiment described in the previous section has confirmed this. This does not provide an obstacle to the formation of the mixed-valence species of these complexes. Intervalence Transitions have been observed for other dinuclear systems which exhibit a single metal centred redox couple. [30,31,32]

The results of the spectroelectrochemical examination of the complexes, $[Ru(bpy)_2(LL7)(bpy)_2Ru]^{4+}$, $[Os(bpy)_2(LL7)(bpy)_2Os]^{4+}$ and $[Ru(bpy)_2(LL7)(bpy)_2Os]^{4+}$ are described in this section. The procedure has been outlined in Chapter 2.7.

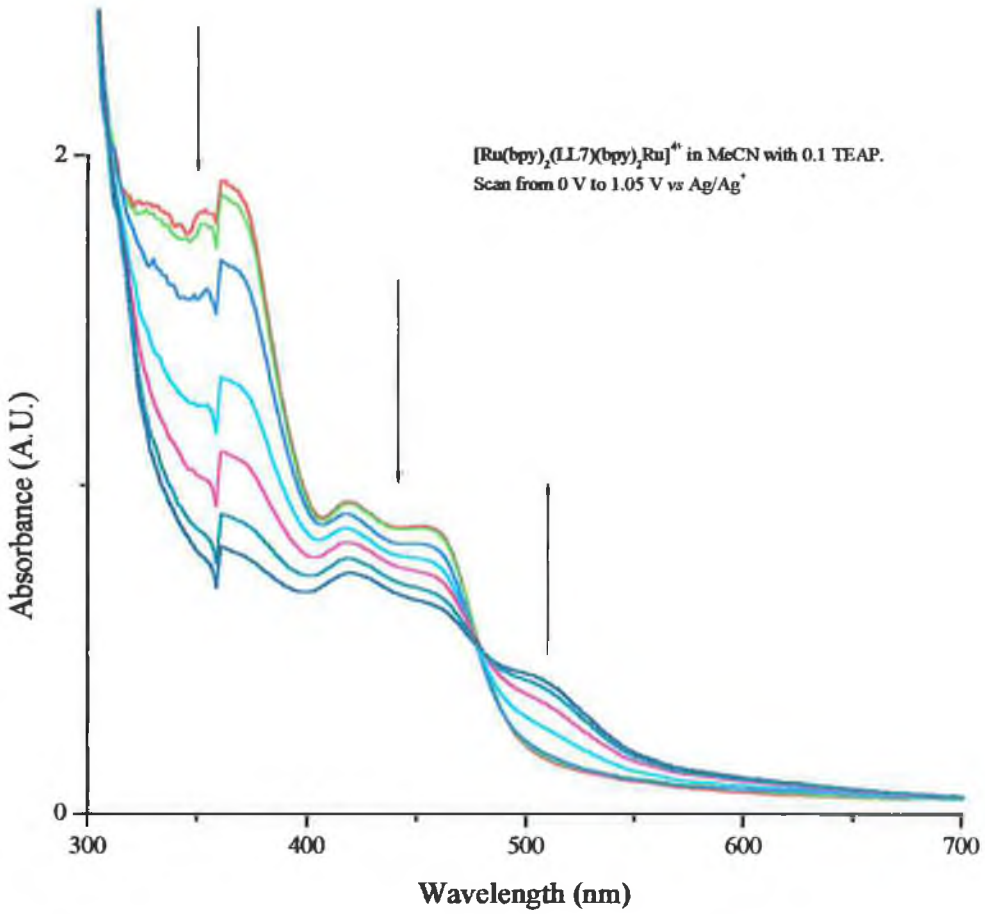

Figure 5.24 Spectroelectrochemistry of the complex $[Ru(bpy)_2(LL7)(bpy)_2Ru]^{4+}$ in MeCN with 0.1M TEAP at intervals from 0V to 1.05V vs Ag/Ag^+ wire.

The results in Figure 5.24 correspond to oxidative spectroelectrochemistry of the $[Ru(bpy)_2(LL7)(bpy)_2Ru]^{4+}$ complex. Scanning to 1.05 V *vs* Fc/Fc^+ has fully oxidised the metal, whose oxidation potential has been determined as being 0.79 V *vs* Fc/Fc^+, but has not led to oxidation of the ligand, which occurs at 1.10 V *vs* Fc/Fc^+. Scanning at these potentials has seen the gradual disappearance of the MLCT band and a decrease in the intensity and red-shift in the $\pi \rightarrow \pi^*$ transition around 280 nm. This characteristic splitting and shift to lower energy of the band is indicative of oxidation of metal centres which are bound to 2,2'-bipyridyl ligands. [33]

With the bleaching of the MLCT band, a concurrent increase in the intensity of band in the region 470 nm to 700 nm is observed. These bands can be assigned as ligand to metal charge transfer (LMCT) bands based on their energy and intensity in comparison to similar spectroelectrochemical measurements. [6,33]

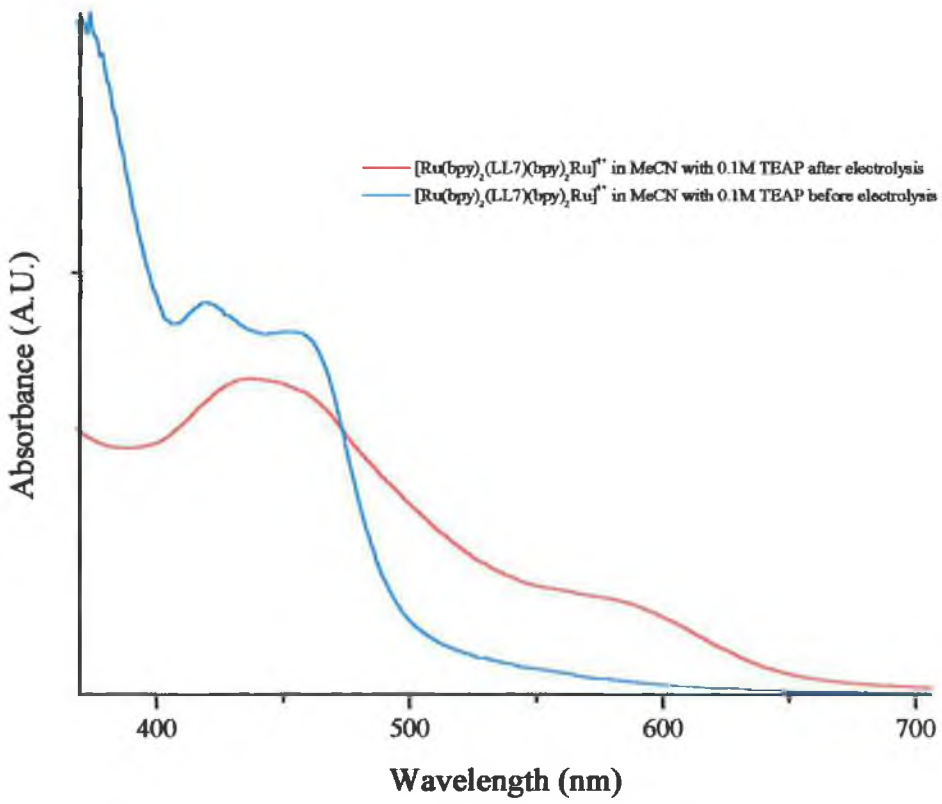

Figure 5.25 Result of scanning beyond 1.05 V vs Fc/Fc^+.

The reversibility of the process observed on scanning from 0 V to 1.05 V *vs* Fc/Fc^- was ascertained at this stage by electrolysis of the complex to its original oxidation state and analysis of the absorption spectrum. At this stage the original complex was regenerated on scanning the complex at 0 V. Figure 5.25 indicates that regeneration of the original starting material is not possible, when the complex is scanned beyond 1.05 V *vs* Fc/Fc^+. Figure 5.25 shows the complex in its original oxidation state and the complex at 0 V after scanning as far as 1.6 V *vs* Fc/Fc^+. In the spectroelectrochemical experiment, scanning from 0V to 1.05 V and back to 0V allows us to oxidise and reduce the metal reversibly. Scanning beyond this potential begins to oxidise the ligand, which is an irreversible process, and therefore on cycling back to 0V from these higher potentials a different species can be observed corresponding to the metal centres in their original oxidation states bridged by an oxidised ligand.

The spectroelectrochemical behaviour of the $[Os(bpy)_2(LL7)(bpy)_2Os]^{4+}$ dimer is very similar to that of its ruthenium analogue. The results of the spectroelectrochemical experiments on the Os-Os dimer can be seen in Figure 5.26. From the electrochemistry of the dimer, the first oxidation has been assigned as simultaneous oxidation of the osmium centres. Again oxidation of the LL7 ligand is responsible for the second wave observed in the voltammogram.

Scanning to 0.75 V *vs* Fc/Fc^+ has seen the gradual disappearance of the MLCT band and a decrease in the intensity and red-shift in the $\pi \rightarrow \pi^*$ transition around 280 nm. Unlike the Ru-Ru complex, no concurrent increase in the intensity of band in the region 470 nm to 700 nm with the bleaching of the MLCT band was observed. This may be due to the fact that the complex contains absorption bands which are not present in the absorption spectra of the ruthenium analogues in the range 600-660 nm which have been assigned as formally forbidden $d\pi \rightarrow \pi^*$ bpy MLCT transitions. These absorption bands may mask the appearance of LMCT bands. The reversibility of this process has been examined. It proved possible to return to the original oxidation states of the complex on returning to 0V after oxidation of the metal centres. As in the case of the Ru-Ru dimer, higher

potentials leads to oxidation of the ligand bridge, a process that has been found to be irreversible.

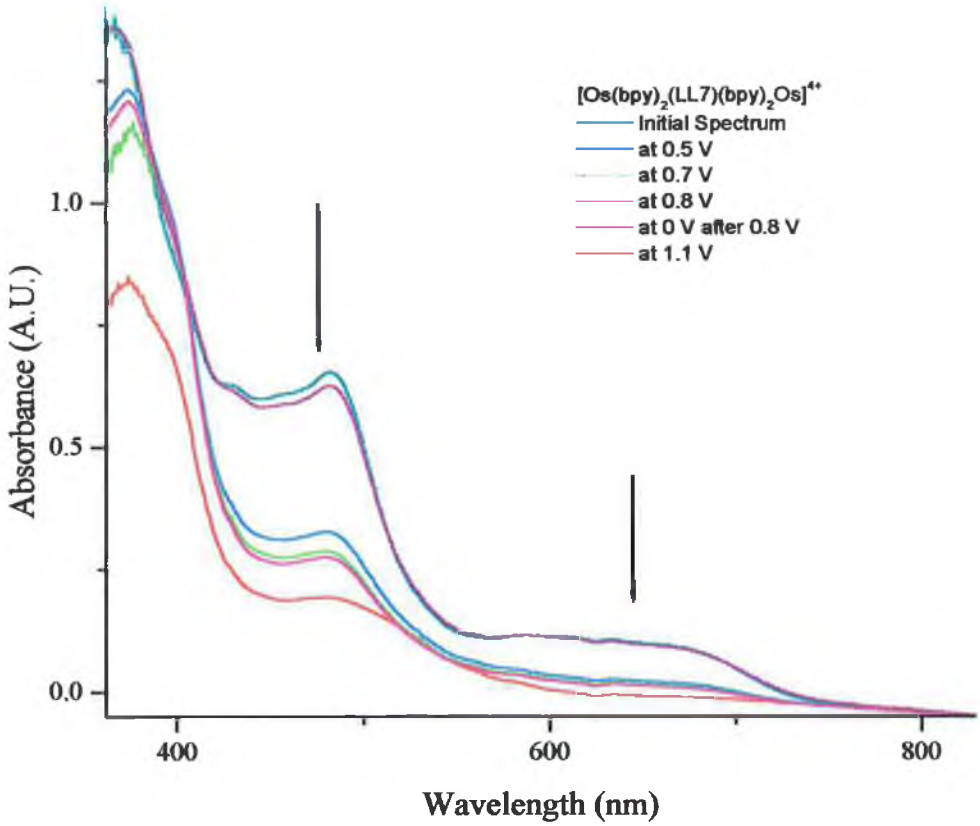

Figure 5.26 Spectroelectrochemistry of the complex $[Os(bpy)_2(LL7)(bpy)_2Os]^{4+}$ in MeCN with 0.1M TEAP at intervals from 0V to 1.05V vs Fc/Fc^+.

The spectroelectrochemistry of the mixed metal complex $[Ru(bpy)_2(LL7)(bpy)_2Os]^{4+}$ was also performed. The results can be analysed more accurately by complementing the results of the spectroelectrochemistry with the electrochemical data. As discussed in the previous section, the first oxidation wave is centred at 0.36 V *vs* Fc/Fc^+ and has been assigned as oxidation of the osmium centre. The second oxidation at 0.79 V *vs* Fc/Fc^+ has been assigned as based on the ruthenium centre while the third irreversible wave corresponds to oxidation of the ligand bridge and is centred at 1.39 V *vs* Fc/Fc^+.

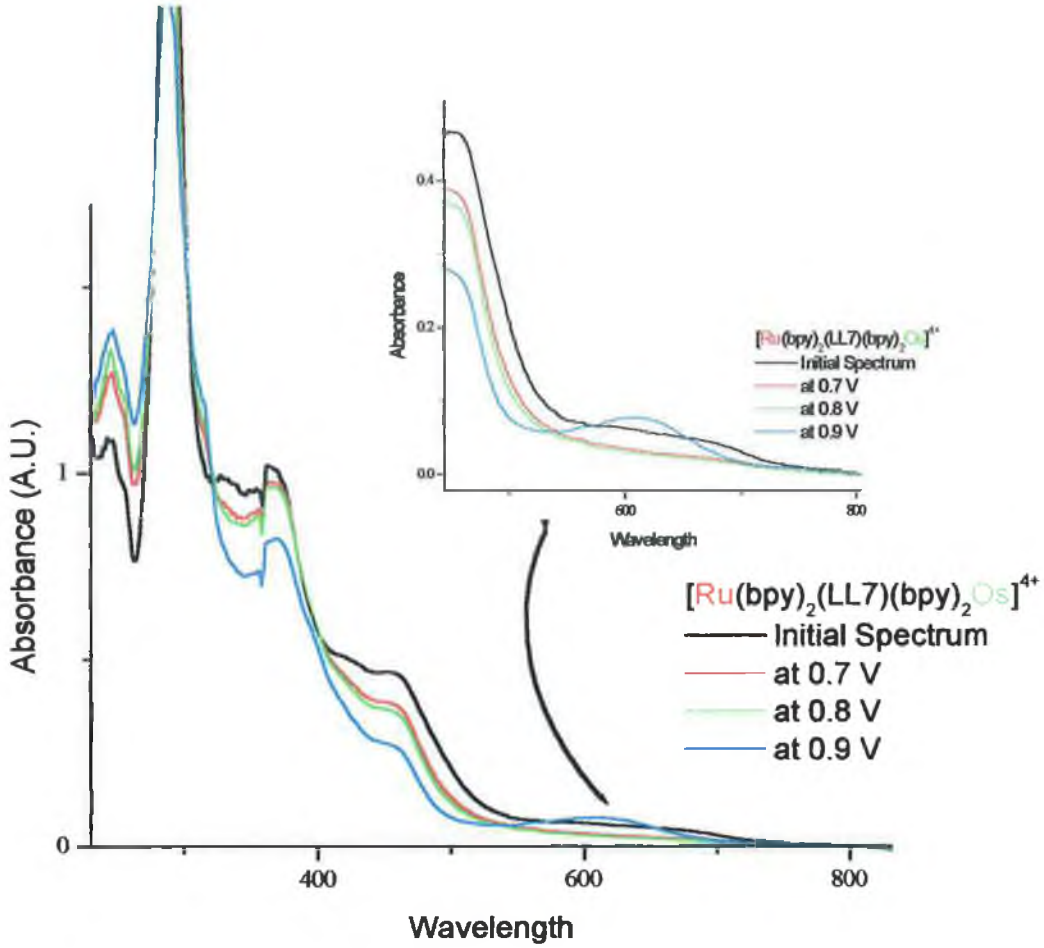

Figure 5.27 Spectroelectrochemistry of the mixed metal complex $[Ru(bpy)_2(LL7)(bpy)_2Os]^{4+}$ in MeCN with 0.1M TEAP at intervals from 0V to 0.9V vs Fc/Fc^+.

As can be seen from Figure 5.28 the results are very similar to those observed for the Ru-Ru and Os-Os dimers. Scanning to 0.7 V *vs* Fc/Fc^+ has seen the gradual disappearance of the MLCT band and a decrease in the intensity and red-shift in the $\pi \rightarrow \pi^*$ transition around 280 nm. With the bleaching of the MLCT band, which continues at potentials higher than 0.7 V *vs* Fc/Fc^+, a concurrent increase in the intensity of band in the region 500 nm to 800 nm. These bands can be assigned as ligand to metal charge transfer (LMCT) bands based on their energy and intensity in comparison to similar spectroelectrochemical measurements.

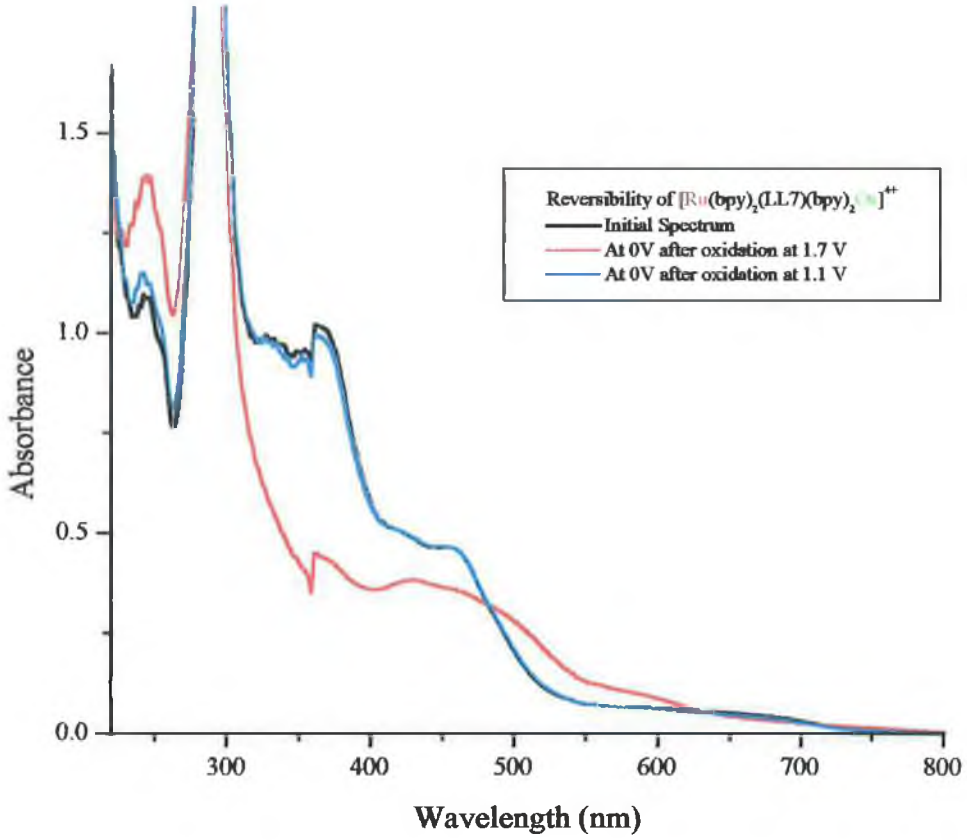

Figure 5.28 Illustration of the irreversibility associated with potentials above the oxidation potential of the bridging ligand.

As in the case of the Ru-Ru and Os-Os dimers, scanning to potentials higher than that of the bridging ligand oxidation prevents re-reduction back to the original oxidation state due to the irreversibility of the ligand oxidation process.

The results of the spectroelectrochemical analysis presented here do not include the data points of the near IR region where IT bands are expected as no interesting bands have been observed in this region. This does not necessarily mean that there are no IT bands, but the intensity may be so low that they are not differentiable from the baseline (which tends to be very noisy in this region). These results agree with those of the electrochemistry, the and photophysics of these dimers and allow us to say confidently that interaction between the metal centres may be described as weak at best.

5.10 Bibliography:

[1] Marco G. D., Bartollota A., Ricevuto V., Campagna S., Denti G., Sabatino L., Rosa G. D., ***Inorg. Chem.,* 1991**, 30, 270.

[2] Denti G., Campagna S., Serroni S., Ciano M., Balzani V., ***J. Am. Chem. Soc.,* 1992**, 114, 2944.

[3] Denti G., Serroni S., Campagna S., Juris A., Ciano M., Balzani V., ***Perspectives in Coordination Chemistry*; 1992**.

[4] Hage R., Turkenburg J. P., De Graaf R. A. G., Haasnoot J. G., Reedijk J., Vos J. G., ***Acta Cryst.*,1980**, C45, 381

[5] Rilemma D. P., Jones D. S., Woods C., Levey H. A., ***Inorg. Chem.*, 1992**, 31, 2935

[6] Hage R., ***Ph. D Thesis***, Leiden University, **1991.**

[7] Rillema D. P., Jones D. S., Levy H. A., ***J. Chem. Soc., Chem. Comm.*, 1979**, 849

[8] Hage R., Haasnoot J. G., Nieuwenhuis H. A., Reedijk J., De Ridder D. J. A., Vos J. G., ***J. Am. Chem. Soc*., 1990**, 112, 9245.

[9] Haga M., Meser Ali M., Koseki S., Fujimoto K., Yoshimura A., Nozaki K., Ohno T., Nakajima K., Stufkens D. J., ***Inorg. Chem.***, **1996**, 35, 3335.

[10] Browne W. R., Vos J. G., ***Coord. Chem. Rev.***, **2001**, 219, 761.

[11] Chirayil S., Thummel R. P., ***Inorg. Chem.***, **1989**, 28, 813.

[12] Haga M., Matsumura-Inoue T., Yamabe S., ***Inorg. Chem.***, **1987**, 26, 4148.

[13] Vining W. J., Caspar J. V., Meyer T. J., ***J. Phys. Chem.,*** **1985**, 89, 1095.

[14] Lumpkin R. S., Kober E. M., Worl L., Murtaza Z., Meyer T J., ***J. Phys. Chem.***, **1990**, 94, 239.

[15] Wrighton, M., Morse D. L., ***J. Am. Chem. Soc.***, **1974,** 96, 996.

[16] Barigelleti F., Flamigni L., Gaurdigli M., Juris A., Deley M., Chodorowski-Kimmes S., Collin J. P., Sauvage J.-P., ***Inorg. Chem.***, **1996**, 35, 136.

[17] Barigelleti F., Flamigni L., Collin J. P., Sauvage J.-P., ***J. Chem. Soc., Chem. Commun.***, **1997**, 333

[18] de Cola L., Balzani V., Barigelleti F., Flamigni L., Belser P., von Zelewsky A., Frank M., Voegtle F., ***Inorg. Chem.***, **1993**, 32, 5228.

[19] Cleary R. L., Byrom K. J., Bardwell D. A., Jeffrey J. C., Ward M. D., Calogero G., Armoli L., Flamigni L., Barigelleti F., ***Inorg. Chem.,*** **1997**, 36, 2601.

[20] Tokel-Takvoryan N. E., Hemingway R. E., Bard A. J., ***J. Am. Chem. Soc.***, **1973,** 95, 6582.

[21] Flanagan J. B., Margel S., Bard A. J., Anson F. C., ***J. Am. Chem. Soc***, **1978**, 100, 4248.

[22] Curtis J. C., Bernstein J. S., Meyer T. J., ***Inorg. Chem.***, **1985**, 24, 385.

[23] Giuffrida G., Calogero G., Guglielmo G., Ricevuto V, Ciano M., Campagna S., ***Inorg. Chem.***, **1993**, 32, 1179.

[24] Hage R., Haasnoot J.G., Reedijk J., Vos J.G., ***Inorg. Chim. Acta.,*** **1986,** 118, 73.

[25] Woitellier S., Launay J.P., Spangler C. W., ***Inorg. Chem.***, **1989**, 28, 758.

[26] Richardson D. E., Taube H., ***Inorg. Chem.,*** **1981**, 20, 1278.

[27] Goldsby K. A., Meyer T. J., ***Inorg. Chem.***, **1984**, 23, 3002.

[28] Wallace A. W., Murphy W. R., Petersen J. D.**.,** ***Inorg. Chim. Acta***., **1989**, 166, 47.

[29] Ernst S. D., Kaim W., ***Inorg. Chem.***, **1989**, 28, 1520

[30] Ribou A. C., Launay J.-P., Takahashi K., Nihira T., Tarutani S., Spangler C. W., ***Inorg. Chem.,*** **1994**, 33, 1325.

[31] Laine P., Marvaud V., Gourdon A., Launay J.-P., Argazzi R., Bignozzi C. A., ***Inorg. Chem.***, **1996**, 35, 711.

[32] Ribou A. C., Launay J.-P., Sachtleben M. L., Li H., Spangler C. W., ***Inorg. Chem.***, **1996**., 35, 3735.

[33] Weldon F., ***Ph. D. Thesis***, Dublin City University, **1998**.

Chapter 6:

Ruthenium(II) and Osmium(II) Mononuclear Complexes as Precursors to the Synthesis of Surface Active Dinuclear Complexes:

Abstract:

Chapter 6 introduces a number of monomeric ruthenium(II) and osmium(II) complexes based on variations of the 4,4'-bipyridyl ligand. These monodentate ligands have been used to synthesise a series of ruthenium and osmium N6 complexes containing two 2,2'-bipyridyl rings and two monodentate coordinating PnP ligands. A series of N5-chloride ruthenium complexes have also been synthesised. These complexes have been synthesised previously by other groups and this chapter begins with an introduction to the work that has been done before using these ligands. The complexes have been structurally characterised by ^{1}H NMR and the spectroscopic and electrochemical properties have also been investigated.

Chapter 6 is used in this thesis as an introduction to Chapter 7, as the monomeric complexes studied here form the structure of a series of dinuclear complexes that are introduced in Chapter 7. It is important therefore to understand properly the properties of the monomeric "starting materials" in order to best explain the processes taking place in the more complicated dinuclear complexes.

6.1 Introduction:

In recent years much work has focussed on the synthesis of polynuclear transition metal complexes and the study of their photochemical, photophysical and electrochemical properties. This interest is stimulated by attempts to design and construct multicomponent systems (often called supramolecular species) which are capable of performing useful light – and/or redox induced functions. [1] For assemblies of this type to perform a particular function, it must be possible to probe, and preferably control the properties of the individual components.[2] The formation and characterisation of ordered structures produced by self assembly or spontaneous adsorption of transition metal complexes is one way of gaining this control. Chapter 6 introduces a series of mononuclear ruthenium(II) and osmium(II) bis bipyridyl complexes which contain either one or two monodentate ligands. Chapter 7 uses these mononuclear complexes as building blocks to synthesise a series of dinuclear ruthenium-ruthenium and osmium-ruthenium complexes. Both the monomers (Chapter 6) and the dinuclear complexes (Chapter 7) are capable of attachment to specific surfaces. The monodentate ligands that are used as bridging ligands both from metal to metal, and also from metal to surface are introduced below.

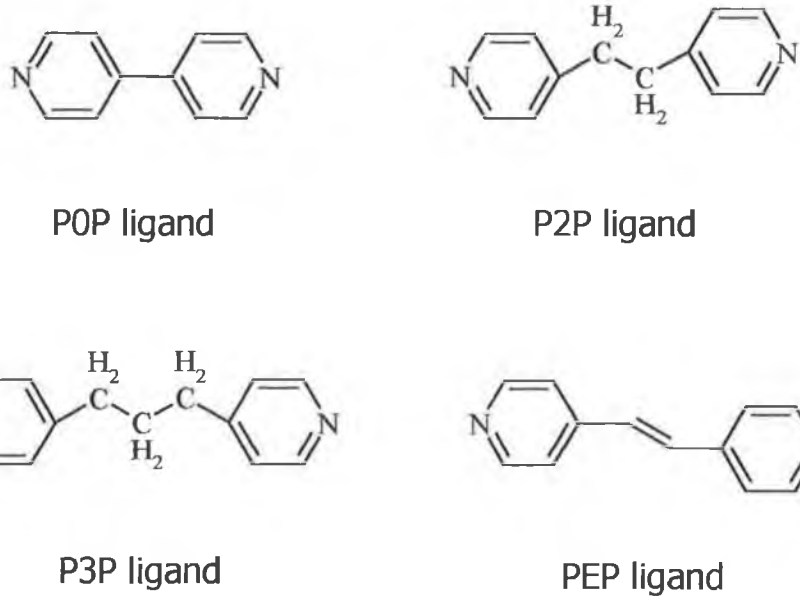

Figure 6.1 Schematic of the ligands used in this Chapter.

The ligands used in this chapter to synthesise complexes of the type $[M(bpy)_2(L)_2](PF_6)_2$ and $[Ru(bpy)_2(L)Cl](PF_6)$ where M = Ru or Os and L = 4,4' bipyridine (P0P), 1,2-bis(4-pyridyl)ethylene (PEP), 1,2-bis(4-pyridyl)ethane (P2P) or 4,4'-trimethylenepyridine (P3P) are illustrated on the previous page. (Figure 6.1) It must be reiterated that the complexes being discussed in the chapter ***have been synthesised previously*** by other groups (many of them in order to examine the behaviour of the complexes on a surface). What follows in this section includes information and data relevant to the compounds discussed both in this chapter and more importantly in Chapter 7. It is important to note that the photophysical properties of these complexes do not appear to have been studied previously. This chapter therefore contains a detailed analysis of the absorption, emission and excited state lifetime properties of these series of complexes.

One of the simplest complexes formed using 4,4' bipyridine (POP) or 1,2-bis(4-pyridyl)ethylene (PEP) is the monomeric pentaammineruthenium(II) complex $[(NH_3)_5RuL]^{2+}$ with L= POP or PEP.[3] Dimeric compounds of the type $[(NH_3)_5Ru]_2L^{4+}$ where L = POP or PEP have also been synthesised and characterised. The pK_a of the POP ligand are pK_1=3.2 and pK_2 = 4.9. For the P2P ligand the pK_a are pK_1 = 4.4 and pK_2 = 5.9. The ruthenium complex $[(NH_3)_5RuL]^{2+}$ has a pK_a of 4.4 for L = POP and 5.0 for L = PEP. The absorption of these complexes in the ultraviolet region is generally very close in energy to the transitions of the free ligand and arises from transitions between molecular orbitals which are localised on the ligand (i.e. $\pi \rightarrow \pi^*$). In the visible region an intense absorption band corresponding to a MLCT process appears. The more easily the ligand is reduced the lower the energy of the absorbance associated with the charge transfer is.

Both the POP and PEP have a second nitrogen atom available for bonding and pentaammineruthenium(II) complexes of both undergo significant bathochromic shifts in acidic solution.

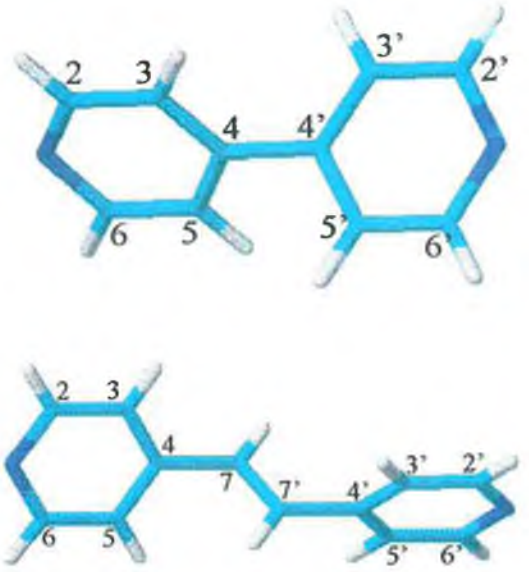

Figure 6.2 Labelling of the positions in the ligands POP and PEP. For ^{1}H-NMR analysis.

The ^{1}H NMR spectrum of 4,4'-bipyridine consists of two doublets which are further split into superimposed doublets. The downfield set (δ 8.55) set of "doubled doublets" are assigned as the chemical shifts of the $H_{2,6}$ and $H_{2',6'}$ atoms while the upfield set (δ 7.60) are assigned to the $H_{3,5}$ and $H_{3',5'}$ atoms. [3,4]

In order to assign the chemical shifts of the ring protons in the complex 4,4'-bipyridine-pentaammineruthenium(II) more easily, the chemical shifts of the pyridine-pentaammineruthenium(II) complex were assigned first and were found to be δ 8.45 for $H_{2,6}$ and shifts of δ 7.75 and δ 7.30 for H_4 and $H_{3,5}$ respectively.[4]

The peaks at δ 7.88 are assigned to $H_{3,5}$ on the basis of the similarity in the shift change upon complexation (δ -0.28) of $H_{3,5}$ in pyridine (δ -0.30) and to a change of (δ -0.28) for 1,2-bis(4-pyridyl)ethylene on complexation. The downfield or diamagnetic shift indicates a π electron deficiency on the ring.

The ^{1}H-NMR spectrum of the 1,2-bis(4-pyridyl)ethylene ligand consists of the "doubled doublet" at δ 8.35 ($H_{2,6}$, $H_{2',6'}$) and one at δ 7.30 ($H_{3,5}$, $H_{3',5'}$) and a single spike at δ 7.06

(H_7, and $H_{7'}$). The NMR of the 1,2-bis(4-pyridyl)ethylene complex consists of a doublet assigned to the $H_{2,6}$ protons which is shifted by δ 0.10 upfield in comparison to the free ligand. Another doublet occurs downfield at δ 8.56 corresponding to the $H_{2',6'}$ protons. Doublets at δ 7.66 and 7.57 are assigned to $H_{3',5'}$ respectively while the peaks at δ 7.51 and 7.48 are assigned to H_7 and $H_{7'}$. [3,4]

Mononuclear ruthenium and osmium complexes containing the POP, P2P, P3P and PEP ligands have also been synthesised by Forster, Faulkner, Tirado and Abruna.[5,6,7,8,9,10] The complexes take the form $[M(bpy)_2(L)Cl]^+$ or $[M(bpy)_2(L)_2]^{2+}$ where M = Ru or Os, bpy = 2,2' bipyridyl and L = POP, P2P, PEP or P3P. These compounds have been synthesised for their ability to form self-assembling, dense, spontaneously absorbing monolayers onto microelectrodes. The compounds bind to the surface through one of the free pyridine groups. The exchange dynamics, desorption and displacement reactions, the electrochemistry and the effects of solvent, electrolyte and temperature on these results have all been studied. Chronoamperometry has allowed the heterogenous electron transfer rate constants to be calculated for both $Ru^{2+/3+}$ and $Os^{2+/3+}$ redox reactions.

A table containing the relevant electrochemical data corresponding to the metal based oxidation from $M^{(II)}$ to $M^{(III)}$ has been compiled below.[11] (Table 6.1)

Compound	Formal potential (V)
$[Os(bpy)_2(POP)Cl]^+$	0.47
$[Os(bpy)_2(P2P)Cl]^+$	0.43
$[Os(bpy)_2(P3P)Cl]^+$	0.40
$[Os(bpy)_2(POP)_2]^{2+}$	0.88
$[Os(bpy)_2(P2P)_2]^{2+}$	0.86
$[Os(bpy)_2(P3P)_2]^{2+}$	0.85
$[Ru(bpy)_2(P2P)Cl]^+$	0.65
$[Ru(bpy)_2(P3P)Cl]^+$	0.75

Table 6.1 Electrochemical results corresponding to the metal based oxidation $M^{(II)} \rightarrow M^{(III)}$. All measurements on osmium compounds were carried out in acetonitrile with 0.1 M $TBABF_4$ as electrolyte.

The electronic spectra of these compounds have also been reported. The UV spectra of the $[Os(bpy)_2(L)Cl]^+$ compounds show sharp bands at 280nm which correspond to $\pi \rightarrow \pi^*$ transitions. The bands in the visible region correspond to metal to ligand charge transfer bands. The spectra of the $[Os(bpy)_2(L)_2]^{2+}$ compounds also contain a high energy $\pi \rightarrow \pi^*$ band at 180nm and a broad MLCT band in the visible region between 320 and 520nm. The electronic spectra of the ruthenium complexes will be discussed in more detail later.

More recent studies have examined in greater detail the photostability, electrochemistry and monolayers of $[M(bpy)_2(PEP)L]^+$ (M = Ru, Os; L = Cl, H_2O).[2] In principle the two monodentate Cl^- ligands and PEP can be photochemically displaced where M = Ru. Previous investigations on related systems indicate that the loss of chloride rather than the monodentate PEP ligand is favoured in water. [12] The rapid loss of chloride in aqueous solution, triggered by low intensity visible light means that monolayers of $[Ru(bpy)_2(PEP)Cl]^+$ can only be prepared by avoiding exposure to ambient light. On the other hand irradiation represents a convenient way of preparing $[Ru(bpy)_2(PEP)(H_2O)]^{2+}$ *in situ*.

In contrast to the high lability of the monodentate ligands within the ruthenium complex, no photosubstitution reactions were found for the osmium complexes. This is consistent with the higher energy of the triplet MC excited state of Os polypyridyl complexes compared to their Ru analogues.

In the case of the $[M(bpy)_2Cl(L)]^+$ or $[M(bpy)_2(L)_2]^{2+}$ compounds examined by Forster *et al*, [13] the ligands act as a bridge between the metallic centre and the surface. In the next section the ability of these ligands to act as a bridge between two metal centres will be reviewed. The metal centres may be both the same metal, mixed valence compounds and mixed metal complexes.

One of the simplest and earliest dimeric compounds synthesised was of the type $[(NH_3)_5Ru(L)RuCl(bpy)_2].(PF_6)_3$ where L = POP, PEP and P2P.[14] These 3+ dimeric ions undergo a reversible one-electron oxidation in acetonitrile to give the mixed-valence ($Ru^{(III)}$-$Ru^{(II)}$) ions, $[(NH_3)_5Ru(L)RuCl(bpy)_2]^{4+}$, with the site of oxidation being largely localised on the $(NH_3)_5Ru$- group. The results of the electrochemical measurements are given below. The voltammograms for the dimeric complexes give two anodic waves which arise from the oxidation of the 3+ ions to $[(NH_3)_5Ru(L)RuCl(bpy)_2]^{4+}$ and then followed at higher potentials by a second one electron oxidation to give $[(NH_3)_5Ru(L)RuCl(bpy)_2]^{5+}$.

Compound	$E_{1/2}(1)$, V	$E_{1/2}(2)$, V
$[(NH_3)_5Ru(P2P)RuCl(bpy)_2]^{4+,3+}$	0.37	
$[(NH_3)_5Ru(P2P)RuCl(bpy)_2]^{5+,4+}$		0.79
$[(NH_3)_5Ru(P0P)RuCl(bpy)_2]^{4+,3+}$	0.43	
$[(NH_3)_5Ru(P0P)RuCl(bpy)_2]^{5+,4+}$		0.83
$[(NH_3)_5Ru(PEP)RuCl(bpy)_2]^{4+,3+}$	0.41	
$[(NH_3)_5Ru(PEP)RuCl(bpy)_2]^{5+,4+}$		0.81

Table 6.2 First and Second Oxidation potentials for $[(NH_3)_5Ru(PnP)RuCl(bpy)_2]^{3+}$. (Pt electrode and are referred to the SCE in 0.1M TBAH-CH_3CN at 25 ± 2°C) [14]

As can be seen from the data in Table 6.2 the oxidations occur at well separated potentials. Oxidation potentials for the first redox process fall in the same range as potentials for the related $[Ru(NH_3)_5L]^{3+,2+}$ couples while potentials for the second process are in the same range for the related $[Ru(bpy)_2(L)Cl]^{2+,+}$ couples. This is consistent with a model for dimeric complexes where the oxidation states are localised, and, in which the interactions between the metal centres are relatively weak. The most clear cut conclusions can be drawn for the P2P bridged dimer. From the electronic spectra of the ions $[(NH_3)_5Ru^{II}(P2P)Ru^{II}Cl(bpy)_2]$ and $[(NH_3)_5Ru^{III}(P2P)Ru^{II}Cl(bpy)_2]$ the two ruthenium ions in both the 3+ and 4+ ions do not interact electronically because of the saturated $-CH_2-CH_2-$ linkage. Due to the absence of an extended π system the two separated ruthenium groups behave as non-interacting chromophores. This is reinforced by the fact that the UV spectrum for $[(NH_3)_5Ru^{II}(P2P)Ru^{II}Cl(bpy)_2]$ is essentially the sum of the spectra of the monomeric ions $[Ru(NH_3)_5(P2P)]^{2+}$ and $[Ru(bpy)_2(P2P)Cl]^{+}$.

For the other dimeric complexes bridged by the POP or PEP ligands, the π systems linking the metal ions are uninterrupted in comparison to P2P, however, the changes in $E_{1/2}(1)$ and $E_{1/2}(2)$ values for these compounds when compared to the monomers is insufficient, preventing meaningful conclusions.

The presence of Intervalence Transfer (IT) bands has also been investigated. Mixed valence compounds often have relatively intense bands in the visible and near infra-red regions of their spectra. These occur due to light induced electron transfer between the metal centres. [15] I.T. bands have been introduced in Section 1.8 and again does not need to be expanded upon here.

The shoulders at 14.4 and 14.7 kK in the infra-red absorption spectrum of $[(NH_3)_5Ru^{III}(POP)Ru^{II}Cl(bpy)_2]^{4+}$ and $[(NH_3)_5Ru^{III}(PEP)Ru^{II}Cl(bpy)_2]^{4+}$ respectively are due to intervalence transfer. The shift to higher energies relative to $[(NH_3)_5Ru^{III}(pyz)Ru^{II}Cl(bpy)_2]^{4+}$ may result from the greater distance separating the metal centres. No IT band is observed for the $[(NH_3)_5Ru^{III}(P2P)Ru^{II}Cl(bpy)_2]^{4+}$ compound. Fischer, Tom and Taube measured the first order specific rates for the

reduction of Co(III) with Ru(II) in complexes of the type $[(NH_3)_5Co^{(III)}(L)Ru^{(II)}(NH_3)_4(H_2O)]^{5+}$ with L = POP, PEP and P2P.[16] The first order rate constants were found to be 44 x 10^{-3}, 18.7 x 10^{-3} and 1.2 x $10^{-3}s^{-1}$ for L as POP, PEP and P2P respectively. The results suggest that the Franck-Condon barrier for electron transfer is constant for the series, and that the differences arise from the slower reactions being not quite adiabatic. The bridging ligand appears to mediate in electron transfer, but in the reaction with L as P2P, electron transfer appears to take place directly between the metal centres. A series of dimers, $[(bpy)_2ClRu(L)RuCl(bpy)_2]^{2+}$ where bpy is 2,2'-bipyridine and L = POP, PEP and P2P were synthesised by Powers and Meyer.[17] One electron oxidation of these compounds gave solutions containing the mixed-valence $Ru^{(III)}$-$Ru^{(II)}$ dimers. For the mixed-valence dimers where the bridging ligand is unsaturated, intervalence transfer bands were observed. The formal reduction potentials of these mixed valence dimers are detailed in the Table 6.3.

Compound	$E_{1/2}$, V
$[(bpy)_2ClRu(POP)RuCl(bpy)]^{4+,3+}$	0.82
$[(bpy)_2ClRu(POP)RuCl(bpy)]^{3+,2+}$	
$[(bpy)_2ClRu(PEP)RuCl(bpy)]^{4+,3+}$	0.78
$[(bpy)_2ClRu(PEP)RuCl(bpy)]^{3+,2+}$	
$[(bpy)_2ClRu(P2P)RuCl(bpy)]^{4+,3+}$	0.77
$[(bpy)_2ClRu(P2P)RuCl(bpy)]^{3+,2+}$	

Table 6.3 Formal reduction potentials of the mixed valence dimers. The CV experiments were carried out in CH_3CN with 0.1 M TBAH vs SSCE at 25 ^0C. [17]

The UV spectra of the series of dimers are all similar and the spectra of the mixed valence ions in the UV/Vis spectral region are nearly the sum of the spectra of $[(bpy)_2ClRu^{II}(L)]^+$ and $[(bpy)_2ClRu^{III}(L)]^{2+}$. In the near infrared region, new absorption bands appear for the mixed-valence ions which are not present for either the 2^+ or 4^+ dimeric ions.

Meyer, Schanze and Neyhart have used these ligands to form mixed valence dimers of osmium.[18,19] The photophysical properties of these unsymmetrical ligand bridged dimers, $[(bpy)_2(CO)Os^{II}(L)Os^{II}(phen)(dppe)(Cl)]^{3+}$ and $[(bpy)_2(CO)Os^{II}(L)Os^{III}(phen)(dppe)(Cl)]^{3+}$ where L = POP, P2P, phen = 1,10-phenanthroline and dppe = 1,2-bis(diphenylphosphino)-cis-ethene have been investigated and reported. Due to the difference of coordination environments at the two metal centres, there is a moderate difference in energy between the localised MLCT excited states, e.g. $[(bpy^{-})_2(CO)Os^{III}(L)Os^{II}(phen)(dppe)(Cl)]^{3+}$ (E ~ 2.1 eV) and $[(bpy)_2(CO)Os^{II}(L)Os^{III}(phen^{-})(dppe)(Cl)]^{3+}$ (E ~ 1.9 eV). Excited and ground state redox potentials are also different at the two sites.

$E_{1/2}$ values are close to those of the associated monomers, which indicates that at best slight resonance and/or electrostatic interactions exist between the two metal centres. The P2P bridged dimer has three ligand based reductions, whereas the POP bridged dimer has a fourth due to the ability of the POP ligand to act as an electron acceptor in the dimer. The absorption spectra for the (II,II) dimers are essentially the sum of the absorption spectra of the monomers. In the mixed valence (II,III) dimers there is a decrease in the absorption in the region λ = 400 - 500 nm which is due to the loss of the $d\pi(Os)\rightarrow\pi^*(phen)$ MLCT absorption band. The POP bridged dimer has a weak absorption band in the region 700 - 1000 nm in its near-IR spectra which is not observed for the P2P compound. Emission from the dimer $[(bpy)_2(CO)Os(P2P)Os(phen)(dppe)(Cl)]^{3+}$ is superimposable on emission from the monomer $[(phen)Os(dppe(Cl)(P2P)]^{2+}$ except for a weak band appearing on the high energy side of the major band which corresponds in energy to the emission from $[(bpy)_2Os(CO)(P2P)]^{2+}$. Emission lifetime data at room temperature and 77K gives further evidence in support of a dual emission.

The monomers $[(phen)Os(dppe)(Cl)(POP)]^{2+}$ and $[(bpy)_2Os(CO)(POP)]^{2+}$ display typical MLCT luminescence with λ_{max} values slightly blue shifted in comparison to the P2P bridged dimers. The dimer $[(bpy)_2(CO)Os(POP)Os(phen)(dppe)(Cl)]^{3+}$ however does not luminesce at room temperature. Emission spectra and lifetimes have been obtained at

77K and these suggest that the luminescence from $[(bpy)_2(CO)Os(P2P)Os(phen)(dppe)(Cl)]^{3+}$ occurs nearly exclusively from an Os(phen) localised state. The fact that the weak emission attributable to the high energy MLCT state $[(bpy)(bpy^{-})(CO)Os^{III}POPOs^{II}(phen)(dppe)(Cl)]^{3+*}$ is 1/10 as intense than for the P2P dimer suggests that intramolecular quenching is even more rapid for the POP bridged dimer (electronic coupling between the two metal centres is greater). [18,19]

It is expected that as for other biphenyl-like molecules, the pyridyl rings will be twisted away from co-planarity due to steric effects, but after addition of an electron the rings will become almost planar to maximise delocalisation. Therefore in the ground state the preferred conformation of the POP bridging ligand is expected to be twisted while following optical excitation, the bridging ligand in the Os(phen)→POP MLCT excited state is expected to adopt the flattened configuration. At 77K the ligand is unable to adopt the planar configuration and its ability to act as an electron acceptor is greatly reduced and the photophysics are much the same as that for the P2P bridged dimer. However in fluid solution, the bipyridine rings are free to become planar and act as an extremely efficient electron trap.

Meyer et al.[20] also did work with these ligands on ruthenium mixed valence dimers of the type $[(dpte)_2ClRu^{II}(L)Ru^{III/II}Cl(bpy)_2]^{3+/2+}$ and $[(NH_3)_5Ru^{II/III}(L)Ru^{II}Cl(bpy)_2]^{4+/3+}$ where dpte = $PhSCH_2CH_2SPh$ and L = POP, PEP and P2P in both cases. The electrochemistry for $[(dpte)_2ClRu(POP)RuCl(bpy)_2]^{2+}$ does not differ significantly to the electrochemistry of its component monomers. This is characteristic for mixed valence ions where electrostatic and resonance stabilisation effects are small and provides evidence that the electronic coupling between the two sites in the ground state is small. The UV visible spectrum of the $Ru^{(II)}$-$Ru^{(II)}$ dimers is dominated by the $\pi^*(bpy)\leftarrow d\pi(Ru^{(II)})$ transitions at the $[(bpy)_2ClRu^{(II)}(L)]^{+}$ site. The $Ru^{(II)}$-$Ru^{(III)}$ spectra are somewhat simplified in comparison due to the disappearance of the $\pi^*(bpy)\leftarrow d\pi(Ru^{(II)})$ band. A weak band is observed at about 420 nm and is a $d\pi Ru \leftarrow p\pi(Cl^{-})$ (LMCT) transition arising at the $-Ru^{III}Cl(bpy)_2$ end of the dimer.

The Near-Infrared bands for the dimers $[(dpte)_2ClRu^{II}(L)Ru^{III}Cl(bpy)_2]^{3+}$ where L is POP and PEP occur at 823 nm and 781 nm respectively. The shift to lower energy for the PEP bridged dimer is to be expected due to the longer separation between the metal centres. For the unsymmetrical dimer $[(NH_3)_5Ru^{III}(L)Ru^{II}Cl(bpy)_2]^{4+}$ the intervalence transfer band overlaps strongly with the tail of the $\pi^*(bpy)\leftarrow d\pi(Ru^{II}Cl(bpy)_2)$ MLCT band, and so the maximum is difficult to resolve. Optical excitation of the $[(dpte)_2ClRu^{II}(L)Ru^{II}Cl(bpy)_2]^{2+}$ dimers leads to a sequence of photochemical events which has been largely established for the related monomers. Therefore, for the POP and P2P dimers, following excitation, the usual ^{3}MLCT state is formed, decays and is unaffected by the presence of the second metal site which suggests that the electronic coupling between the two metals is weak. The situation is different for the PEP dimer $[(dpte)_2ClRu^{II}(PEP)Ru^{II}Cl(bpy)_2]^{2+}$, where the lifetime of the dimer is 2.5 times shorter than that of the monomer and may be attributable to population and decay from a lower lying, bridging ligand based MLCT state $[(dpte)_2ClRu^{II}(PEP^-)Ru^{III}Cl(bpy)_2]^{2+*}$, or from a $\pi\pi^*$ state localised on PEP, $[(dpte)_2ClRu^{II}(PEP^*)Ru^{III}Cl(bpy)_2]^{2+}$.

For the $[(NH_3)_5Ru^{II}(L)Ru^{II}Cl(bpy)_2]^{3+}$ dimers with L = POP and PEP, the absorption spectra and excited state manifold are complicated by the presence of the low-lying $\pi^*(L)\leftarrow d\pi(Ru^{II}(NH_3)_5)$ states. With L = P2P, the transient absorbance and emission properties of the dimer are practically the same as for that of the monomer.

Excitation of the mixed valence dimers of $[(dpte)_2ClRu^{II}(L)Ru^{III}Cl(bpy)_2]^{3+}$ resulted in the emission and decay characteristics of the Ru(II)-bpy site, even though the other site is in the III oxidation state. The excited state reached must have nearly the same redox potential as a reducing agent as the Ru(bpy) MLCT states of the monomer $(bpy)_2ClRu(POP)^+$ and the Ru(II) dimer $[(dpte)_2ClRu(POP)RuCl(bpy)_2]^{2+}$. The evidence points towards the appearance of the bpy based ^{3}MLCT state -(L)Ru(III)Cl(bpy$^{-\xi}$)(bpy) following excitation even though the corresponding chromophore does not exist for the $Ru^{(II)}$-$Ru^{(III)}$ dimers. The appearance of this can most reasonably be explained via initial $Ru^{(II)}\rightarrow\pi^*(L)$ excitation followed by intramolecular, ligand to ligand electron transfer.

The mixed valence dimers of $[(NH_3)_5Ru^{III}(L)Ru^{II}Cl(bpy)_2]^{4+}$ are different. The site of oxidation, at the pentaamine and the $\pi^*(bpy) \leftarrow d\pi(Ru^{II})$ site is maintained in the $Ru^{(II)}$-$Ru^{(II)}$ compound and is maintained in the mixed valence state.

A series of luminescent bimetallic complexes of rhenium(I) were synthesised by Guarr, Lin *et al.*[21] who also prepared bimetallic complexes containing an (α-diimine)$(CO)_3Re^I$ chromophore and a covalently attached ruthenium pentaammine moiety. $[(LL)(CO)_3Re(BL)Ru(NH_3)_5]^{3+}$ where LL = 4,4' Di(isopropylcarboxylate)-2,2'-bipyridine (DCObpy), 4,4'-dimethyl-2,2'-bipyridine (Me_2bpy), 4,4', 5,5'-tetramethyl-2,2'-bipyridine (Me_4bpy), 2,2'-bipyridine (bpy), and BL = P2P and P3P. [22] The direction of electron transfer can be controlled simply by changing the oxidation state of the quencher portion of the molecule. Assuming a through bond pathway, observation of a rapid rate for the oxidative quenching direction, (Re chromophore as electron donor) suggests that the unoccupied orbitals of the bridging ligand serve to mediate the electron transfer process. Rapid reductive quenching with the Re chromophore as electron acceptor, would imply metal-metal coupling through the occupied orbitals of the bridging ligand. The spectrophotometric data from $[(LL)(CO)_3Re(BL)Ru(NH_3)_5]^{3+}$ spectra are essentially the sum of the spectra of $[Ru(NH_3)^+(BL)]^{2+}$ and $[(LL)(CO)_3Re(BL)]^+$ suggesting that interaction between the metal centres is weak. Oxidation of $[(LL)(CO)_3Re(BL)Ru(NH_3)_5]^{3+}$ causes the disappearance of the Ru$\rightarrow$BL MLCT band at 410 nm. Initial oxidation of the $[(LL)(CO)_3Re(BL)Ru(NH_3)_5]^{3+}$ complexes appears to be localised on the ruthenium centre and is observed at $E_{1/2}$ = +0.30 V vs SCE. The rhenium centre undergoes a one electron chemically irreversible oxidation at more positive potentials. The $E_{ox}[Re^{II}/Re^I]$ values for $[(LL)(CO)_3Re(BL)Ru(NH_3)_5]^{3+}$ decreases with the increasing electron donating ability of the substituents DCObpy > bpy > Me_4bpy.

The lifetime data and emission intensities of the Re/Ru^{II} complexes indicate that the α-diimine ligand based MLCT states are efficiently quenched by the attached $-Ru(NH_3)_5^{2+}$ moiety. This could be caused by intermolecular transfer, or energy transfer to the

Ru→BL MLCT state, but most likely occurs by intramolecular electron transfer. i.e. electron transfer from the ruthenium to the rhenium centre. [21,22]

Since the early 1990's the ligands POP and PEP have been used to synthesise a new type of supramolecular compound. The earlier systems were derived from Pt(II) or Pd(II) triflate species and were tetranuclear in regard to the metal content. These therefore arranged in a square or box-like geometry, with the metal centres occupying the corners. These rigid macrocycles represent a new and unusual class of compounds which have tremendous possibilities in host-guest, inclusion and molecular recognition chemistry.[23] Expansion of this field has led to the synthesis of visible, light addressable, luminescent metal-ligand components within a square or rectangular assembly. The growth in this field coincides with the growth in the area of self assembly, and these supramolecular species have this common factor, that they self-assemble.

Molecular self assembly is a new strategy for the preparation of organised nanostructures. It is based on the phenomenon whereby the individual subunits are quickly driven together and held in place by multiple, accurately positioned non-covalent interactions. Transition metals and coordination based design allows the formation of a variety of self-organised nanosystems in a few highly convergent synthetic steps. In order to synthesise materials with specific properties and functions the form, shape and distribution of the individual units must be controlled. This necessary control places limits on the nature, type and directionality of the bonding that can operate throughout the system. The bonding of the subunits must be relatively weak, thermodynamically stable, yet kinetically labile allowing the self-rearrangement of the subunits within the entire structure. Another important requirement is the conformational rigidity of the building blocks which reduces entropic factors upon self-organisation.

Self assembly offers some important advantages over stepwise bond formation. Since it proceeds via the simultaneous assembly of pre determined building blocks, the resulting synthesis is highly convergent and requires fewer steps. Also, since non covalent interactions are usually established very rapidly, final product formation is fast and

facile. These non-covalent interactions between the subunits generally results in defect free assemblies with self maintained integrity since the usual equilibria between the constituents and products contribute towards the self rearrangement of the components. Nature has been exploiting the advantages of self assembly for a long time.

Transitions metals have coordination sites with specific geometries that depend on their electronic structure and therefore can serve perfectly as acceptor subunits. These acceptor subunits can be linked together via donor building blocks, which form the rigid frame of the assembled entity. Both of these subunits must possess specific geometries and remain multidentate, or at least bidentate. These subunits should also be readily available. The ligands which have been discussed so far in this chapter are perfectly suited to molecular self assembly, and in fact most of the early systems were based on the POP ligand. .[24,25,26,27,28,29]

Fujita *et al* have been at the forefront of the synthesis of macrocyclic metal complexes, where the metals are bridged by bidentate ligands and the synthesis leads to the formation of cyclised products quantitatively without using special conditions. One of the early examples is the complex $[(en)Pd(POP)]_4(NO_3)_8$ (where en = ethylenediamine). A significant feature of this complex is its ability for molecular recognition in aqueous media.[30] This work was expanded and the synthesis of the same Pd complex was attempted using the P2P ligand. It was anticipated that displacement of the rigid POP ligand by a flexible one may lead to unfavourable oligomerisation rather than cyclisation. Against that anticipation, synthesis gave the dimeric $[(en)Pd(P2P)]_2(NO_3)_4$ complex.[31] This complex is notable for its high ability for molecular recognition of electron rich aromatic compounds with high shape specificity.

A series of square and box type compounds were reported by Hupp *et al* in 1995.[32] These compounds are capable of incorporating light addressable, luminescent metal-ligand components within a square assembly. Induction of photoluminescent characteristics are attractive in the context of molecular sensing applications as it provides an alternative to ^1H NMR spectroscopy for the detection of guest inclusion.

This also opens the possibility of electronic excited state reactivity and possible manipulation of the encapsulated guests. The light emitting square complex was prepared by combining the chrompophore fac-$Re(CO)_3Cl(POP)_2$ [33] with $[Pd(dppp)(triflate)]_2$ (where dppp = 1,3-(diphenylphosphino)propane). Square formation induces a red-shift in both absorption and emission from the nominally triplet MLCT excited state. The emission is also decreased circa 25-fold. The excited state lifetime is similarly affected from 645 ns to 17 ns on formation of the square. These changes are attributed to quenching by the Pd(II) fragments. Attempts to extend the synthetic chemistry by replacing the POP ligand with P2P yielded a dimeric metal complex, a phenomenon already noted by Fujita.[34,35,36] Further work in the area by Hupp led to the synthesis of luminescent molecular squares featuring octahedral rhenium corners. [37,38] The squares based on the bridging ligands pyrazine or POP luminesce at room temperature, while the complex based on the P2P ligand decays exclusively via nonradiatve pathways. This absence of luminescence may possibly be associated with nonradiative decay via torsional motion about the ethylene bond.[39] It should also be noted that the emissive excited state lifetimes for the squares are significantly shorter than for the corresponding monomeric "corner" complexes. This could be caused by quenching by further charge transfer to proximal chromophores in the squares.[40,41]

Further expansion of the field has led to the development of this type of "square" complex as a molecular sieving and ion exchange device. [27,42,43,44,45,46] Having successfully built molecular squares, Hupp *et al* concentrated on varying the size of the cavity contained within the four bridging ligands, and realised that this could be altered more easily if molecular "rectangles" rather than squares were synthesised. Previous attempts by the group to make rectangles from mixtures of singly functional bridging ligands such as pyrazine and POP with $Re(CO)_5Cl$ yielded squares, rather than the mixed bridge dimers.[47] A different approach however, the reaction of the dimeric complex $[(CO)_4Re(\mu\text{-}SR)]_2$ with the POP ligand gave a molecular rectangle. [48] This reaction provided the stepping stone to the synthesis of other molecular rectangles containing POP on two sides while the other sides consist of η^2-alkoxy or hydroxy bridges.[49,50]

Since 1990, the groups of Fujita and Stang reported many different molecular square complexes based on the square planar Pd(II), Pt(II) and Cd(II) centres.[37,47,51,52] There have been however much fewer cases reported based on an octahedral geometry at the metal centre.[53,54] The metal Re(I) was used because of its well known photophysical and redox properties. [55] The P2P ligand was also used as it was reasoned that increasing the overall length of the bridging ligand may induce the formation of a new triangular structure.[56] The triangular structures exhibit increased thermal and photodecomposition in THF than square molecules of the same components. This is probably due to the larger strain that exists on the triangular structure.

The area is continuing to grow, and the complexity of the structures are increasing. The geometry of the metal centres is no longer limited to square planar, and octahedral metal centres are being used more. The reaction conditions are evolving also with a photochemical synthesis of organometallic squares being reported in 1999. [57,58]

Finally, an interesting application for osmium complexes of the type $[AsPh_4]_2[Cl_5Os(L)OsCl_5]$ where L = pyrazine or POP has been reported. [59] These complexes can be used for the preparation of humidity sensors by thick film technology. The resistance of these complexes exhibit a strong dependence on the humidity of the environment they are in.

6.2 Synthesis of the complexes $[M(bpy)_2(PnP)_2](PF_6)_2$ and $[Ru(bpy)_2(PnP)Cl](PF_6)$

This section details the synthetic procedure followed which resulted in the synthesis of the monomeric complexes outlined below. The synthesis has been modified from those previously reported in the literature, [9,10,60] while the purification of the complexes is completely different. As these complexes have been synthesised and studied previously, elemental analysis has not been deemed necessary in the characterisation process. The synthesis of the starting materials, *cis*-$[Ru(bpy)_2Cl_2].2H_2O$ and *cis*-$[Os(bpy)_2Cl_2].xH_2O$ have been described in Chapter 3.2 and 4.2.

Synthesis of $[Ru(bpy)_2(P0P)Cl](PF_6)$

$[Ru(bpy)_2Cl_2].2H_2O$ (250 mg, $4.8x10^{-4}$ mol) and P0P ligand (75 mg, $4.8x10^{-4}$ mol) were refluxed in 10ml methanol for 4 hours. The methanol was removed *in vacuo* and the residue dissolved in water. A saturated solution of ammonium hexafluorophosphate was added to the solution to precipitate the product. This was isolated by filtration, washed with water and dried with diethylether. The product was purified by column chromatography on alumina (using MeCN as eluent). The yield of pure product was 302 mg. (70 %).

^1H NMR (400 MHz, d_6-acetone) δ = 7.38 (dd, 1H), 7.41 (dd, 1H), 7.73 (m, 2H), 7.82 (m, 5H), 7.94 (m, 4H), 8.19 (m, 4H), 8.62 (m, 2H), 8.67 (m, 2H), 8.76 (m, 3H), 10.10 (d, 1H).

Synthesis of $[Ru(bpy)_2(P2P)Cl](PF_6)$

$[Ru(bpy)_2Cl_2].2H_2O$ (250 mg, $4.8x10^{-4}$ mol) and P2P ligand (89 mg, $4.8x10^{-4}$ mol) were refluxed in 10ml methanol for 4 hours. The methanol was removed *in vacuo* and the

residue dissolved in water. A saturated solution of ammonium hexafluorophosphate was added to the solution to precipitate the product. This was isolated by filtration, washed with water and dried with diethylether. The product was purified by column chromatography on alumina (using MeCN as eluent). The yield of pure product was 283 mg. (64%).

^{1}H NMR (400 MHz, d_6-acetone) δ = 3.08 (m, 4H), 7.18 (dd, 1H), 7.31 (m, 3H), 7.497 (dd, 1H), 7.70 (dd, 1H), 7.87 (m, 4H), 8.12 (m, 4H), 8.62 (m, 9H), 10.06 (d, 1H).

Synthesis of $[Ru(bpy)_2(P3P)Cl](PF_6)$

$[Ru(bpy)_2Cl_2].2H_2O$ (250 mg, 4.8 x 10^{-4} mol) and P3P ligand (95 mg, 4.8 x 10^{-4} mol) were refluxed in 10ml methanol for 4 hours. The methanol was removed *in vacuo* and the residue dissolved in water. A saturated solution of ammonium hexafluorophosphate was added to the solution to precipitate the product. This was isolated by filtration, washed with water and dried with diethylether. The product was purified by column chromatography on alumina (using MeCN as eluent). The yield of pure product was 265 mg. (59 %).

^{1}H NMR (400 MHz, d_6-acetone) δ = 2.07 (m, 6H), 7.26 (m, 4H), 7.79 (m, 6H), 8.14 (m, 4H), 8.64 (m, 9H), 10.08 (d, 1H).

Synthesis of $[Ru(bpy)_2(PEP)Cl](PF_6)$

$[Ru(bpy)_2Cl_2].2H_2O$ (250 mg, 4.8 x 10^{-4} mol) and PEP ligand (87 mg, 4.8 x 10^{-4} mol) were refluxed in 10ml methanol for 4 hours. The methanol was removed *in vacuo* and the residue dissolved in water. A saturated solution of ammonium hexafluorophosphate was added to the solution to precipitate the product. This was isolated by filtration, washed with water and dried with diethylether. The product was purified by column chromatography on alumina (using MeCN as eluent). The yield of pure product was 295 mg. (67 %).

^{1}H NMR (400 MHz, d_6-acetone) δ = 7.35 (m, 2H), 7.52 (m, 3H), 7.78 (m, 2H), 7.93 (m, 4H), 8.15 (m, 4H), 8.70 (m, 8H), 10.06 (d, 1H).

Synthesis of $[Ru(bpy)_2(picolene)_2](PF_6)_2$

$[Ru(bpy)_2Cl_2].2H_2O$ (50 mg, 9.6 x 10^{-5} mol) was heated to reflux in a 1:1 EtOH/H_2O mixture. Picolene (0.074 ml, 7.6x10^{-4} mol) was added by syringe to the hot mixture and this solution was heated at reflux for a further 4 hours. At this point the ethanol was removed *in vacuo* and the solution allowed to cool to room temperature. An excess of a saturated solution of ammonium hexafluorophosphate was added and the resulting precipitate was isolated by filtration. The precipitate was washed with water and dried with diethyl ether to yield 61mg of pure product. 71% yield.

^{1}H NMR (400 MHz, d_6-acetone) δ = 2.92 (s, 6H), 7.28 (m, 4H), 7.53 (dd, 2H), 7.94 (dd, 2H), 8.07 (dd, 2H), 8.28 (m, 4H), 8.48 (d, 4H), 8.60 (d, 2H), 8.67 (d, 2H), 9.30 (d, 2H).

Synthesis of $[Ru(bpy)_2(POP)_2].(PF_6)_2$

$[Ru(bpy)_2Cl_2].2H_2O$ (250 mg, 4.8 x 10^{-4} mol) and $AgNO_3$ (163 mg, 9.6 x 10^{-3} mol) were refluxed in a 1:1 EtOH/H_2O solution (10 ml) until the formation of a grey precipitate was observed. This precipitate was removed by filtration and the filtrate returned to the reaction flask. POP ligand (750 mg, 4.8 x 10^{-3} mol) was dissolved in EtOH/H_2O and added to the filtrate and this was refluxed until the solution was bright orange in colour. The ethanol was removed *in vacuo* and the aqueous solution was left at 4^0C overnight. The excess unreacted ligand was removed by filtration and a saturated solution of ammonium hexafluorophosphate was added to the filtrate to precipitate an orange product which was isolated by filtration. This product was washed with water and dried with diethylether. The product was purified by column chromatography (silica gel, 80% acetonitrile, 20% water, 0.05M KNO_3). The desired product was collected as the second band to elute. The yield of pure product was 277mg (57%).

^{1}H NMR (400 MHz, d_6-acetone) δ = 7.59 (dd, 2H), 7.72 (d, 4H), 7.85 (d, 4H), 7.98 (dd, 2H), 8.14 (dd, 2H), 8.32 (m, 4H), 8.64 (d, 2H), 8.71 (m, 6H), 8.87 (d, 4H), 9.43 (d, 2H).

Synthesis of $[Ru(bpy)_2(P2P)_2](PF_6)_2$

$[Ru(bpy)_2Cl_2].2H_2O$ (250 mg, 4.8×10^{-4} mol) and $AgNO_3$ (163 mg, 9.6×10^{-3} mol) were refluxed in a 1:1 $EtOH/H_2O$ solution (10 ml) until the formation of a grey precipitate was observed. This precipitate was removed by filtration and the filtrate returned to the reaction flask. P2P ligand (1.76 g, 9.6×10^{-3} mol) was dissolved in $EtOH/H_2O$ and added to the filtrate and this was refluxed until the solution was bright orange in colour. The ethanol was removed *in vacuo* and the aqueous solution was left at 4^0C overnight. The excess unreacted ligand was removed by filtration and a saturated solution of ammonium hexafluorophosphate was added to the filtrate to precipitate an orange product which was isolated by filtration. This product was washed with water and dried with diethylether. The product was purified by column chromatography (silica gel, 80% acetonitrile, 20% water, 0.05M KNO_3). The desired product was collected as the second band to elute. The yield of pure product was 230 mg (46%).

^{1}H NMR (400 MHz, d_6-acetone) δ = 3.06 (s, 8H), 7.34 (d, 4H), 7.42 (m, 4H), 7.53 (dd, 2H), 7.93 (dd, 2H), 8.08 (dd, 2H), 8.28 (m, 4H), 8.55 (m, 5H), 8.68 (d, 2H), 9.25 (d, 2H).

Synthesis of $[Ru(bpy)_2(P3P)_2](PF_6)_2$

$[Ru(bpy)_2Cl_2].2H_2O$ (250 mg, 4.8×10^{-4} mol) and $AgNO_3$ (163 mg, 9.6×10^{-3} mol) were refluxed in a 1:1 $EtOH/H_2O$ solution (10 ml) until the formation of a grey precipitate was observed. This precipitate was removed by filtration and the filtrate returned to the reaction flask. P3P (1.90 g, 9.6×10^{-3} mol) was dissolved in $EtOH/H_2O$ and added to the filtrate and this was refluxed until the solution was bright orange in colour. The ethanol was removed *in vacuo* and the aqueous solution was left at 4^0C overnight. The excess unreacted ligand was removed by filtration and a saturated solution of ammonium

hexafluorophosphate was added to the filtrate to precipitate an orange product which was isolated by filtration. This product was washed with water and dried with diethylether. The product was purified by column chromatography (silica gel, 80% acetonitrile, 20% water, 0.05M KNO_3). The desired product was collected as the second band to elute. The yield of pure product was 230 mg (44%).

^{1}H NMR (400 MHz, d_6-acetone) δ = 2.07 (m, 8H), 3.06 (s, 4H), 7.26 (m, 8H), 7.53 (dd, 2H), 7.94 (dd, 2H), 8.07 (dd, 2H), 8.28 (m, 3H), 8.47 (m, 3H), 8.59 (d, 2H), 8.66 (d, 2H), 9.25 (d, 2H).

Synthesis of $[Ru(bpy)_2(PEP)_2](PF_6)_2$

$[Ru(bpy)_2Cl_2].2H_2O$ (250 mg, 4.8 x 10^{-4} mol) and $AgNO_3$ (163mg, 9.6 x 10^{-3} mol) were refluxed in a 1:1 $EtOH/H_2O$ solution (10 ml) until the formation of a grey precipitate was observed. This precipitate was removed by filtration and the filtrate returned to the reaction flask. PEP ligand (1.76 g, 9.6 x 10^{-3} mol) was dissolved in $EtOH/H_2O$ and added to the filtrate and this was refluxed until the solution was bright orange in colour. The ethanol was removed *in vacuo* and the aqueous solution was left at 4^0C overnight. The excess unreacted ligand was removed by filtration and a saturated solution of ammonium hexafluorophosphate was added to the filtrate to precipitate an orange product which was isolated by filtration. This product was washed with water and dried with diethylether. The product was purified by column chromatography (silica gel, 80% acetonitrile, 20% water, 0.05M KNO_3). The desired product was collected as the second band to elute. The yield of pure product was 260 mg (51%).

^{1}H NMR (400 MHz, d_6-acetone) δ = 7.43 (dd, 2H), 7.56 (m, 8H), 7.74 (d, 4H), 7.84 (dd, 2H), 7.97 (dd, 2H), 8.17 (m, 4H), 8.49 (d, 2H), 8.56 (d, 2H), 8.61 (m, 8H), 9.27 (d, 2H).

Synthesis of $[Os(bpy)_2(POP)_2](PF_6)_2$

$[Os(bpy)_2Cl_2].2H_2O$ (250 mg, $4.11x10^{-4}$ mol) and $AgNO_3$ (140 mg, $8.22x10^{-4}$ mol) were refluxed in a 1:1 ethylene glycol/H_2O solution (10 ml) until the formation of a grey precipitate was observed. This precipitate was removed by filtration and the filtrate returned to the reaction flask. POP ligand (640 mg, $4.11x10^{-3}$ mol) was dissolved in ethylene glycol/H_2O and added to the filtrate and this was refluxed for 96 hours. At this stage the solution was green/brown in colour. The solution was left at 4^0C overnight. The excess unreacted ligand was removed by filtration and a saturated aqueous solution of ammonium hexafluorophosphate was added to the filtrate to precipitate a brown/green product which was isolated by filtration. This product was washed with water and dried with diethylether. The product was purified by column chromatography (silica gel, 80% acetonitrile, 20% water, 0.05M KNO_3). The desired product was collected as the second green band to elute. The yield of pure product was 150 mg (33 %).

^{1}H NMR (400 MHz, d_6-acetone) δ = 7.50 (dd, 2H), 7.79 (m, 8H), 7.92 (m, 4H), 8.08 (dd, 2H), 8.20 (d, 2H), 8.62 (d, 2H), 8.71 (m, 6H), 8.83 (m, 6H), 9.26 (d, 2H).

Synthesis of $[Os(bpy)_2(P2P)_2](PF_6)_2$

$[Os(bpy)_2Cl_2].2H_2O$ (250 mg, $4.11x10^{-4}$ mol) and $AgNO_3$ (140 mg, $8.22x10^{-4}$ mol) were refuxed in a 1:1 ethylene glycol/H_2O solution (10 ml) until the formation of a grey precipitate was observed. This precipitate was removed by filtration and the filtrate returned to the reaction flask. P2P ligand (756 mg, $4.11x10^{-3}$ mol) was dissolved in ethylene glycol/H_2O and added to the filtrate and this was refluxed for 96 hours. At this stage the solution was green/brown in colour. The solution was allowed to stand at 4^0C overnight. The excess unreacted ligand was removed by filtration and a saturated aqueous solution of ammonium hexafluorophosphate was added to the filtrate to precipitate a brown/green product which was isolated by filtration. This product was washed with water and dried with diethylether. The product was purified by column chromatography (silica gel, 80% acetonitrile, 20% water, 0.05M KNO_3). The desired

product was collected as the second green band to elute. The yield of pure product was 134 mg (28 %).

^{1}H NMR (400 MHz, d_6-acetone) δ = 3.02 (m, 8H), 7.36 (m, 10H), 7.86 (m, 4H), 8.04 (dd, 2H), 8.13 (d, 2H), 8.44 (d, 4H), 8.57 (d, 4H), 8.65 (d, 4H), 9.07 (d, 2H).

Synthesis of $[Os(bpy)_2(P3P)_2](PF_6)_2$

$[Os(bpy)_2Cl_2].2H_2O$ (250 mg, $4.11x10^{-4}$ mol) and $AgNO_3$ (140 mg, $8.22x10^{-4}$ mol) were refluxed in a 1:1 ethylene glycol/H_2O solution (10 ml) until the formation of a grey precipitate was observed. This precipitate was removed by filtration and the filtrate returned to the reaction flask. P3P ligand (813 mg, $4.11x10^{-3}$ mol) was dissolved in ethylene glycol/H_2O and added to the filtrate and this was refluxed for 96 hours. At this stage the solution was green/brown in colour. The solution was left at 4^0C overnight. The excess unreacted ligand was removed by filtration and a saturated aqueous solution of ammonium hexafluorophosphate was added to the filtrate to precipitate a brown/green product which was isolated by filtration. This product was washed with water and dried with diethylether. The product was purified by column chromatography (silica gel, 80% acetonitrile, 20% water, 0.05M KNO_3). The desired product was collected as the second green band to elute. The yield of pure product was 190 mg (39 %).

^{1}H NMR (400 MHz, d_6-acetone) δ = 2.77 (s, 4H), 3.07 (s, 8H), 7.28 (dd, 2H), 7.39 (m, 4H), 7.84 (m, 4H), 8.06 (m, 8H), 8.54 (m, 8H), 8.91 (m, 4H), 9.06 (d, 2H).

Synthesis of $[Os(bpy)_2(PEP)_2](PF_6)_2$

$[Os(bpy)_2Cl_2].2H_2O$ (250 mg, $4.11x10^{-4}$ mol) and $AgNO_3$ (140 mg, $8.22x10^{-4}$ mol) were refluxed in a 1:1 ethylene glycol/H_2O solution (10 ml) until the formation of a grey precipitate was observed. This precipitate was removed by filtration and the filtrate returned to the reaction flask. PEP ligand (748 mg, $4.11x10^{-3}$ mol) was dissolved in ethylene glycol/H_2O and added to the filtrate and this was refluxed for 96 hours. At this

stage the solution was green/brown in colour. The solution was left at 4^0C overnight. The excess unreacted ligand was removed by filtration and a saturated aqueous solution of ammonium hexafluorophosphate was added to the filtrate to precipitate a brown/green product which was isolated by filtration. This product was washed with water and dried with diethylether. The product was purified by column chromatography (silica gel, 80% acetonitrile, 20% water, 0.05M KNO_3). The desired product was collected as the second green band to elute. The yield of pure product was 141 mg (29 %).

^{1}H NMR (400 MHz, d_6-acetone) δ = 7.21 (dd, 2H), 7.34 (m, 10H), 7.63 (m, 6H), 7.80 (dd, 2H), 7.93 (d, 2H), 8.38 (m, 12H), 8.94 (d, 2H).

6.3 Discussion of the synthesis of the monomers:

In general the synthesis of both types of ruthenium(II) complexes proved slightly easier than for the osmium(II) complexes which was expected considering the unreactive nature of osmium. Problems arose for several reasons. The first is that the ligands being used are monodentate. For bidentate ligands, coordination of the first nitrogen places the second nitrogen in an orientation that favours the binding of the second nitrogen to the metal centre. This does not occur for monodentate ligands, and coordination of the first ligand actually hinders replacement of the second chloride by a second monodentate ligand. For the bidentate ligands introduced in Chapter 3, reaction of the $[Ru(bpy)_2Cl_2].2H_2O$ with the LL_x ligands in refluxing ethanol/water led to the replacement of both chlorides by the bidentate ligands. The mechanism was that the solvent molecules first replace the chlorides, and the solvent molecules are replaced in turn by the ligand. This reaction mechanism works for the monodentate PnP ligands, but the yield of the reaction becomes very low, with the major products being the monosubstitued chloro or aquo complexes.

Synthesis of the complexes of the type $[M(bpy)_2(PnP)_2](PF_6)_2$ did not prove simple. Several different methods were employed to improve the yield of the reactions. The

most important was the pre-removal of the two chloride ions from the starting material. This was done using silver nitrate. Addition of two molar equivalents of $AgNO_3$ to a suspension of $[Ru(bpy)_2Cl_2].2H_2O$ in refluxing ethanol/water leads to the complexation of the chloride ions by the silver which precipitates a grey/white solid, AgCl, and leads to the subsequent binding of water molecules to the vacant coordination sites on the metal. Filtration of the solution at this stage removes the AgCl and the filtrate is returned to the reaction vessel. A large excess of the ligand is added to force the replacement of the water molecules from the metal centre by the desired monodentate ligands. After the reaction is complete, the ethanol is removed *in vacuo*, and the solution cooled at 4^0C overnight. This precipitates much of the excess ligand which is then removed by filtration. The addition of a saturated aqueous solution of NH_4PF_6 leads to the precipitation of the complex from the aqueous solution.

The purity of the compounds was checked at this stage using TLC and HPLC. Further purification was necessary in most cases and this was generally performed by column chromatography on silica gel, using a 4:1 MeCN:H_2O mobile phase which contained 0.05M KNO_3 as a buffer. The desired band was generally the second band to elute. After the purity was determined again by HPLC and the compounds were analysed by ^1H NMR spectroscopy. The results of this analysis follow in the next sections.

The synthesis of the osmium(II) complexes was carried out in similar fashion. Ethylene glycol was used instead of ethanol to provide a higher refluxing temperature. Due to the high boiling point of ethylene glycol, it was not removed after the reaction, the reaction solution was cooled overnight, filtered and the product precipitated using a saturated aqueous solution of NH_4PF_6. The osmium(II) complexes were purified in a similar way to the ruthenium(II) complexes.

The complexes of the type $[Ru(bpy)_2(L)Cl]^+$ were simpler to synthesise than either the $[Ru(bpy)_2(L)_2]^{2+}$ or $[Os(bpy)_2(L)_2]^{2+}$ where L = P0P, P2P, P3P or PEP. As only one of the chlorides was being removed, the reactions were carried in MeOH. A 1:1 ratio of ligand to metal was used. Problems were found to arise if water was used at any stage of

the reaction, as this led to exchange of the second chloride, resulting in a mixture of both the aquo complex and the chloro complex in solution. Purification was therefore carried out on alumina using MeCN as eluent. It is important at this stage however to discuss the aquo/chloro issue more. The displacement of chloride ions for water molecules is well known and has been reported for the complex $[Ru(bpy)_2(py)Cl]^+$ (where py = pyridine). [61,62] The studies indicated that loss of the chloride ion rather than the monodentate pyridine ligand was favoured in water. In contrast, loss of the PEP ligand is expected on irradiation of the $[Ru(bpy)_2(PEP)Cl]^+$ complex in organic solvents such as acetonitrile or acetone. [2,63] These studies have been assigned by comparison of the UV/Vis spectra of the photoproducts with those of known complexes. For example, irradiation of the the $[Ru(bpy)_2(PEP)Cl]^+$ complex in acetonitrile results in a product with a λ_{max} of 481 nm. This compares to the value reported in literature of 480 nm for the complex $[Ru(bpy)_2(MeCN)Cl]^+$. [63] The photostability of the complex $[Ru(bpy)_2(PEP)Cl]^+$ has also been performed in aqueous solution. Following irradiation with visible light, dilute suspensions of the complex form solutions which exhibit an absorption maximum at 468 nm. This agrees closely with the value reported by Meyer *et al.* [64,65] for $[Ru(bpy)_2(py)(H_2O)]^{2+}$ of 470 nm.

From these studies it is apparent that great care must be taken in order to ensure the $[Ru(bpy)_2(PnP)Cl]^+$ products retains both the PnP ligand and also the Cl^- ion in solution. As has been detailed in the previous section, care has been taken to avoid using water in the reaction to synthesise these complexes, or the purification process of these complexes. Care has also been taken to avoid the exposure of solutions of these complexes to light. The results presented in the following section in relation to the $[Ru(bpy)_2(PnP)Cl]^+$ can safely be assigned to results corresponding to that complex and not the aquo or solvated analogue. This problem is a pertinent problem in the synthesis and use of these complexes, and is discussed further in Chapter 7.

6.4 ^{1}H NMR spectroscopy:

As in the case of the previous chapters ^{1}H NMR spectroscopy has proven to be the most valuable tool is assigning the structure and determining the purity of these complexes. ^{1}H NMR spectroscopy not only allows the percentage purity of the crude products to be determined, but will also give a good indication as to the nature of the impurities present in the sample which is a useful aid in the purification process of a complex. Because of the symmetrical nature of the complex of the type $[M(bpy)_2(PnP)_2]^{2+}$ (where M = Ru or Os) both the bipyridyl protons and the PnP protons have been completely assigned. This symmetry means that each signal in the ^{1}H NMR spectrum actually represents two equivalent protons, and therefore the number of signals observed is halved in comparison to asymmetrical $[Ru(bpy)_2(PnP)Cl]^+$ complexes. This asymmetry leads to each proton being represented by an individual signal making the assignment more complicated. Figure 6.4 illustrates the symmetry found for the $[M(bpy)_2(PnP)_2]^{2+}$ complexes.

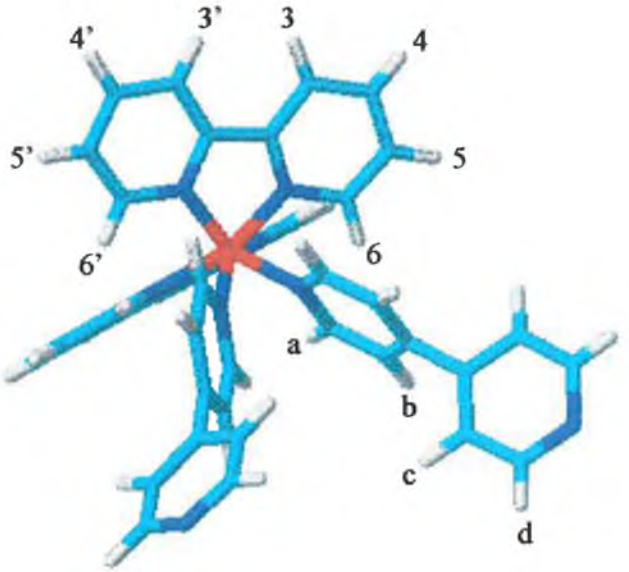

Figure 6.3 Illustration and labelling of the protons in the complexes of the type $[M(bpy)_2(PnP)_2]^{2+}$

Unlike the ^{1}H spectra of the complexes discussed in Chapters 3, 4 and 5 it proved possible to assign the 2,2'-bipyridyl protons in the case of these complexes. Once again 2D COSY NMR proved useful in the assignment of the spectra. Representative 2D COSY spectra are presented in Figures 6.4 and 6.5. The assignment of the spectra follow in Table 6.4, 6.5, 6.6 and 6.7.

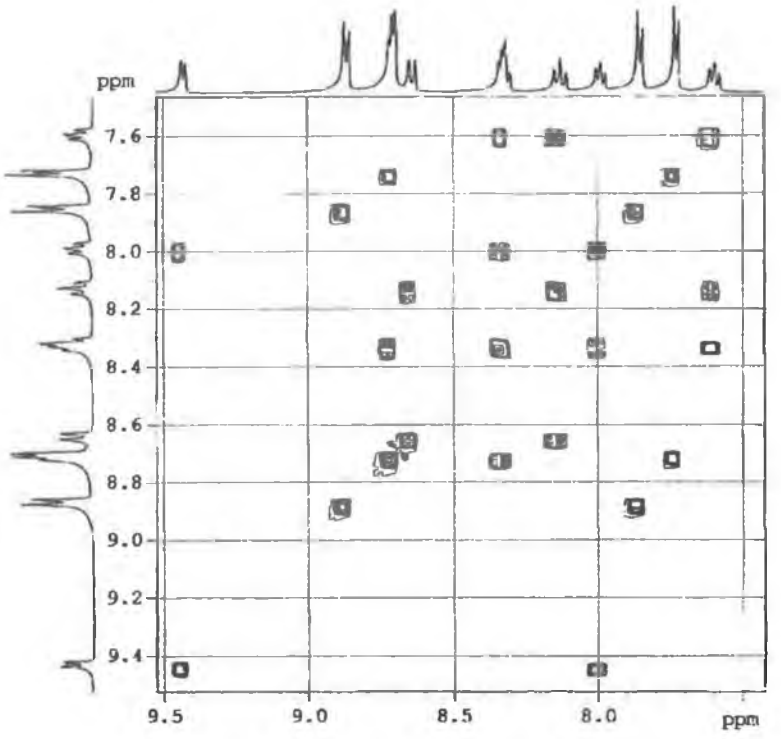

Figure 6.4 2D COSY NMR of the complex $[Ru(bpy)_2(POP)_2](PF_6)_2$ in d_6-acetone.

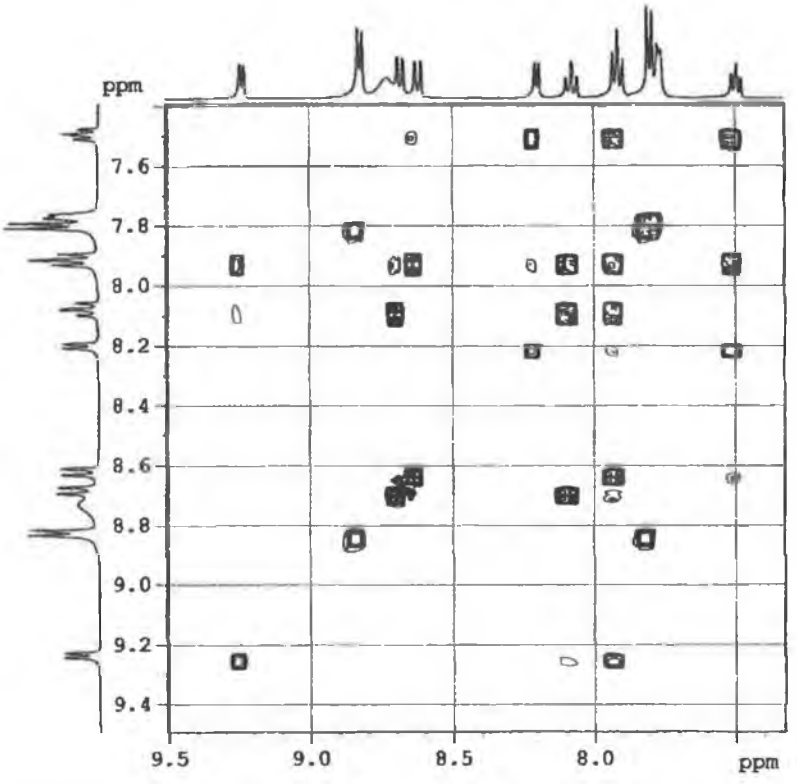

Figure 6.5 2D COSY NMR of the complex $[Os(bpy)_2(POP)_2](PF_6)_2$ in d_6-acetone.

Compound	H_3	H_4	H_5	H_6	H_3'	H_4'	H_5'	H_6'
2,2' bpy	8.48	7.93	7.42	8.67				
$[Ru(bpy)_2(picolene)_2]^{2+}$	8.55	8.15	7.80	9.18	8.47	7.93	7.39	8.14
$[Ru(bpy)_2(P0P)_2]^{2+}$	8.71	8.32	7.97	9.43	8.65	8.13	7.58	8.33
$[Ru(bpy)_2(PEP)_2]^{2+}$	8.66	8.24	7.89	9.10	8.61	8.05	7.50	7.96
$[Ru(bpy)_2(P2P)_2]^{2+}$	8.68	8.28	7.92	9.24	8.59	7.92	7.53	8.25
$[Ru(bpy)_2(P3P)_2]^{2+}$	8.54	8.15	7.80	9.12	8.46	7.93	7.38	8.10

Table 6.4 Assignment of the bpy protons for the complexes $[Ru(bpy)_2(PnP)_2](PF_6)_2$. All measurements have been performed in d_6-acetone and are measured in ppm vs Me_4Si.

Compound	H_3	H_4	H_5	H_6	H_3'	H_4'	H_5'	H_6'
$[Os(bpy)_2(P0P)_2]^{2+}$	8.63	8.07	7.79	9.24	8.60	7.89	7.51	8.19
$[Os(bpy)_2(PEP)_2]^{2+}$	8.40	7.84	7.68	9.01	8.40	7.60	7.32	7.93
$[Os(bpy)_2(P2P)_2]^{2+}$	8.66	8.04	7.85	9.08	8.58	7.85	7.41	8.13
$[Os(bpy)_2(P3P)_2]^{2+}$	8.52	8.06	7.78	9.01	8.33	7.75	7.36	7.97

Table 6.5 Assignment of the bpy protons for the complexes $[Os(bpy)_2(PnP)_2](PF_6)_2$. All measurements have been performed in d_6-acetone and are measured in ppm vs Me_4Si.

Compound	H_a	H_b	H_c	H_d
$[Ru(bpy)_2(picolene)_2]^{2+}$	8.34	7.14		
$[Ru(bpy)_2(P0P)_2]^{2+}$	8.71	7.73	7.85	8.71
$[Ru(bpy)_2(PEP)_2]^{2+}$	8.41	7.57	7.57	8.61
$[Ru(bpy)_2(P2P)_2]^{2+}$	8.49	7.35	7.52	8.49
$[Ru(bpy)_2(P3P)_2]^{2+}$	8.41	7.18	7.02	8.34

Table 6.6 Assignment of the aromatic PnP protons for the complexes $[Ru(bpy)_2(PnP)_2].(PF_6)_2$ in d_6-acetone.

Compound	H_a	H_b	H_c	H_d
$[Os(bpy)_2(POP)]^{2+}$	8.83	7.80	7.80	8.83
$[Os(bpy)_2(PEP)_2]^{2+}$	8.40	7.35	7.35	8.40
$[Os(bpy)_2(P2P)]^{2+}$	8.45	7.32	7.32	8.45
$[Os(bpy)_2(P3P)_2]^{2+}$	8.62	7.27	7.27	8.62

Table 6.7 Assignment of the aromatic PnP protons for the complexes $[Os(bpy)_2(PnP)_2].(PF_6)_2$. All measurements have been performed in d_6-acetone and are measured in ppm vs Me_4Si.

Comparison of the spectra of the ruthenium and osmium analogues shows that the protons of the osmium(II) bound ligands are found at higher field than those of the analogous ruthenium(II) bound ligands (Figure 6.6). This has been observed in earlier chapters (comparison of spectra in Chapters 3 and 4), and is due to the greater shielding effect experienced by the ligands in osmium complexes because of the relatively stronger metal $d\pi \rightarrow \pi^*$(bpy) back donation compared to ruthenium. (The Os(II) orbitals are higher in energy). This phenomenon is illustrated in Figure 6.6.

Figure 6.7 represents a typical spectrum of a $[Ru(bpy)_2(PnP)_2]^{2+}$ complex, while Figure 6.8 represents a typical spectrum of an $[Os(bpy)_2(PnP)_2]^{2+}$ complex. The broadening of some of the peaks should be noted, for example the peaks at 7.42 and 8.56 ppm in Figure 6.7 and at 7.33 and 8.51 ppm in Figure 6.8. This broadening effect on these signals are most likely due to hindered rotation of the coordinated pyridyl rings of the PnP ligands.

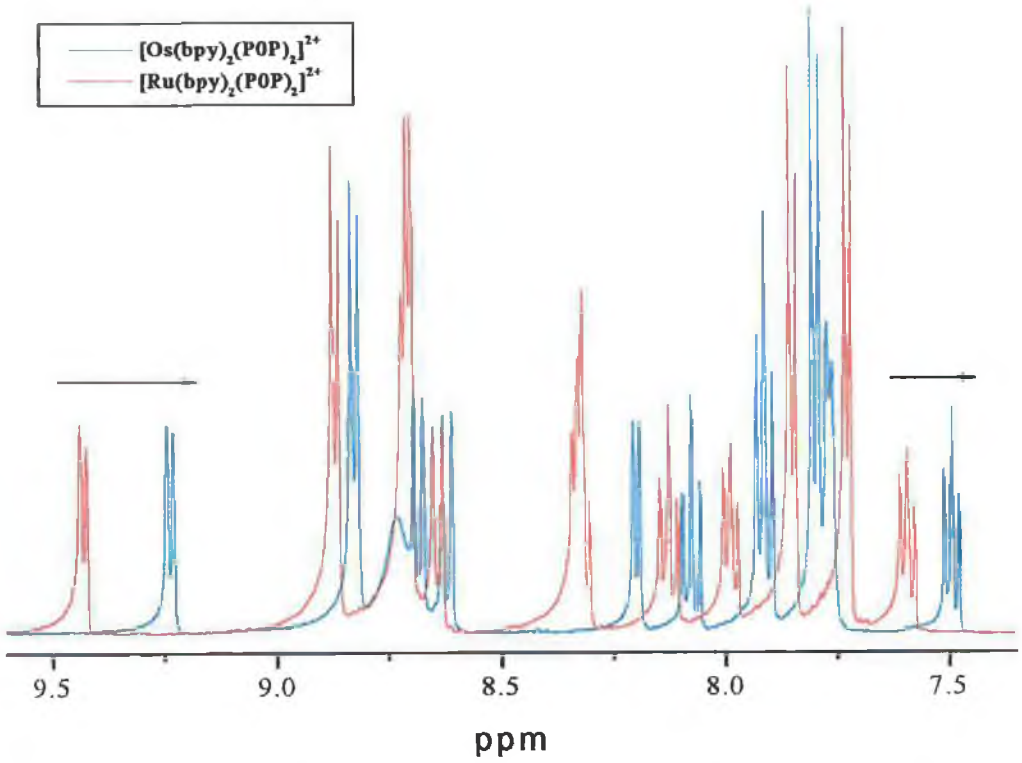

Figure 6.6 Comparison of the ^{1}H NMR spectra of $[Os(bpy)_2(POP)_2]^{2+}$ and $[Ru(bpy)_2(POP)_2]^{2+}$. Both in d_6-acetone.

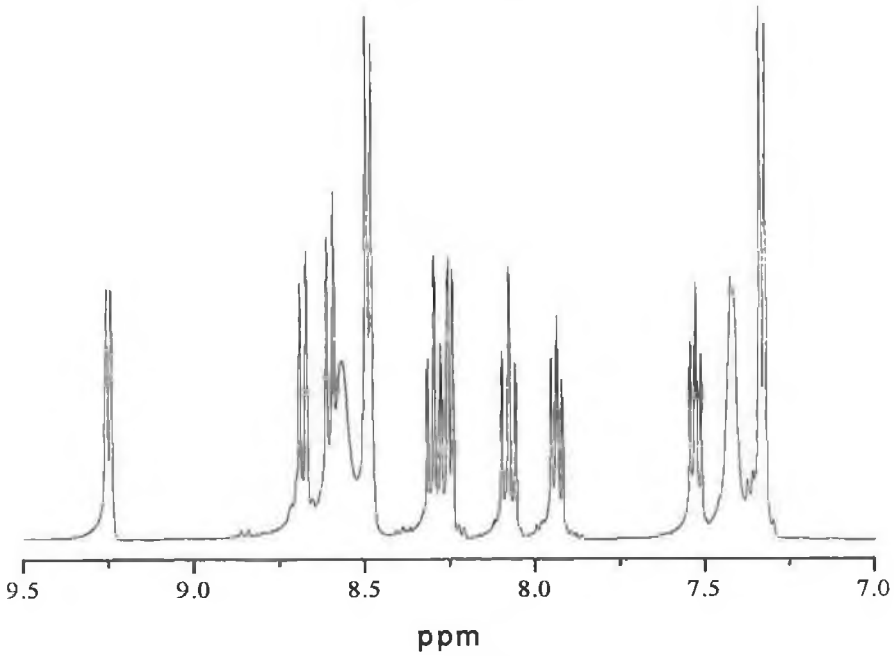

Figure 6.7 Illustrative ^{1}H NMR of $[Ru(bpy)_2(P2P)_2]^{2+}$ in d_6-acetone.

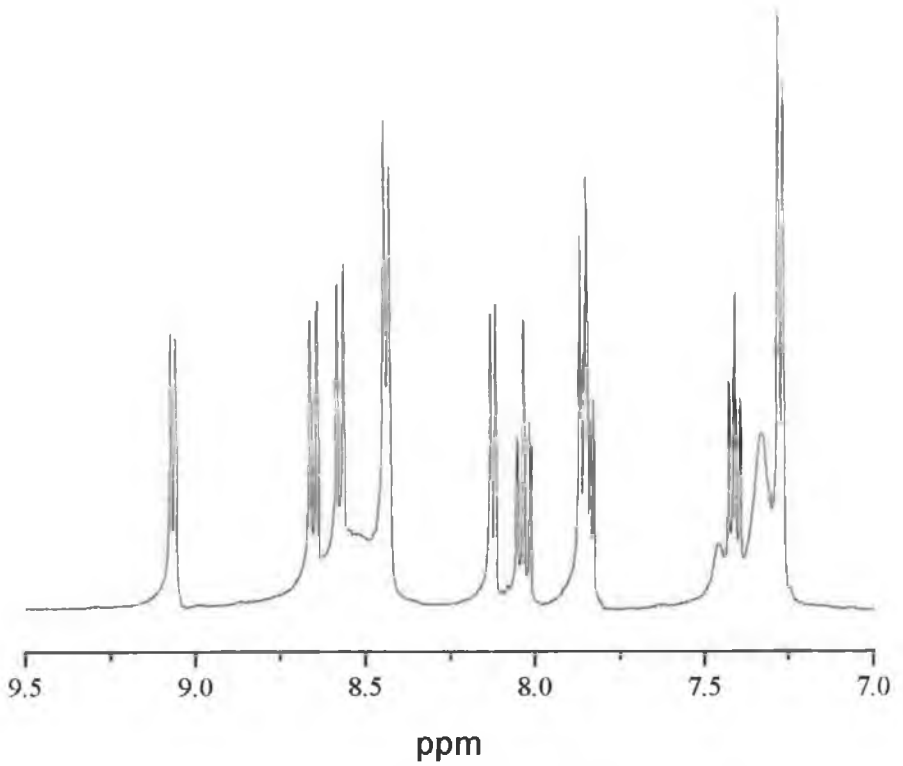

Figure 6.8 Illustrative ^1H NMR of $[Os(bpy)_2(P2P)_2]^{2+}$ in d_6-acetone.

A fingerprint proton can be identified in the spectra of each of these complexes. It is shifted downfield relative to the other protons. The reason for this becomes clear when the three dimensional structure of the complex is considered. An illustration of this can be seen in Figure 6.3. An analogy can be drawn between the H6 proton being discussed here and the H_i protons discussed in the ^1H NMR sections of Chapters 3 and 4. The H_i protons were shifted upfield dramatically on coordination of the ligand to the metal centre. The H_i protons experience a diamagnetic anisotropic effect is caused by the interaction of the proton with the ring current of a neighbouring 2,2'-bipyridyl unit.

The H6 proton on the other hand, interacts with the aromatic pyridyl ring of the PnP ligand which is bound to the ruthenium(II) (or osmium(II)) centre. This pyridyl ring is free to rotate due to the monodentate bond of the PnP ligand to the metal, unlike in the H_i protons discussed above. Therefore the H6 proton does not sit in the ring current of a static aromatic ring, instead it experiences an increase in electron density caused by the electron cloud surrounding the spinning aromatic ring – causing it to shift to higher ppm.

This is seen for the spectra of both the ruthenium and osmium complexes of the type $[M(bpy)_2(PnP)_2]^{2+}$.

The second type of complex is that containing one PnP ligand and a chloride ion, $[Ru(bpy)_2(PnP)Cl]^+$. As discussed already, the chloride ion removes the symmetry found in the complexes, causing each proton to give an individual signal, resulting in 24 discrete signals in the aromatic region. Many of these signals overlay each other and elucidation of the spectrum becomes very difficult. Once again however a fingerprint proton is found for these complexes. The H6 proton is shifted to even higher ppm for these complexes than for the complexes of the type $[M(bpy)_2(PnP)_2]^{2+}$. This is illustrated in Figure 6.9.

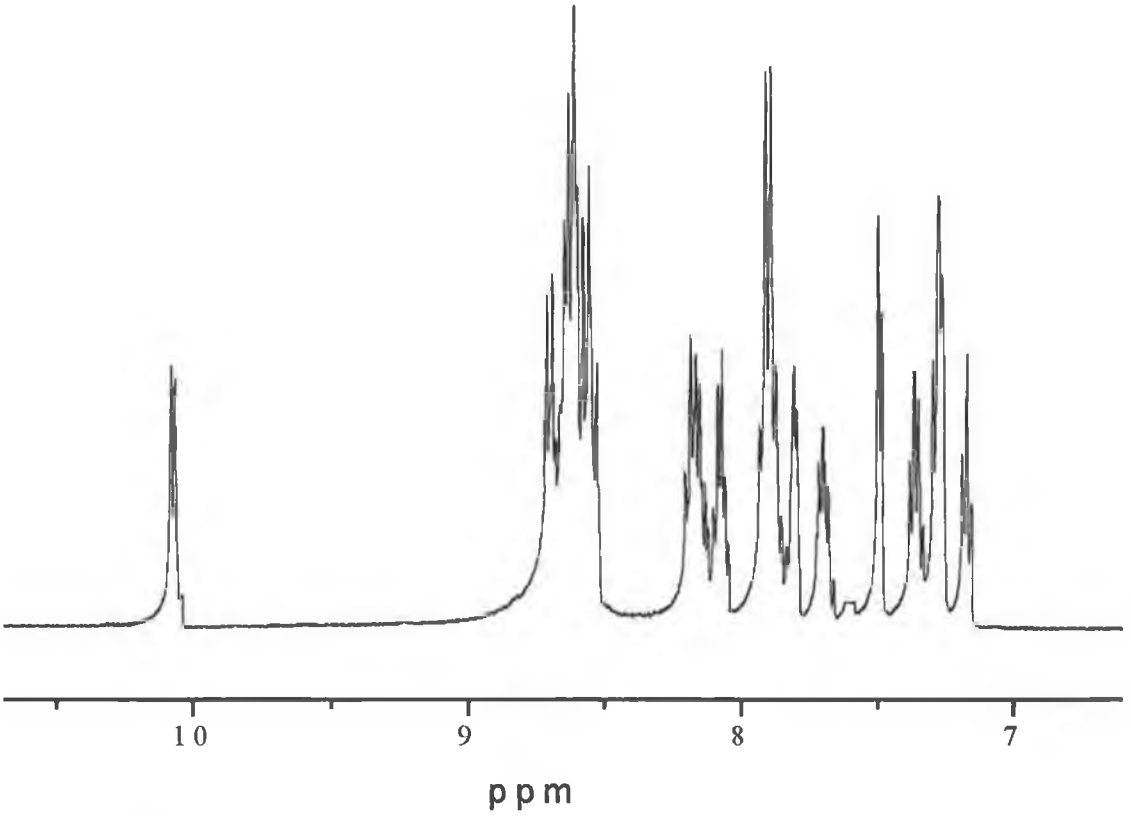

Figure 6.9 ^1H NMR of the complex $[Ru(bpy)_2(P2P)Cl]^+$ in d_6-acetone. Typical of the ^1H NMR of the $[Ru(bpy)_2(PnP)Cl]^+$ complexes.

The orientation of the H6 proton is such that its nearest "neighbour" is the chloride ion, and not the rotating aromatic ring experienced by the H6 protons in the $[M(bpy)_2(PnP)_2]^{2+}$ complexes, or the ring current of a neighbouring 2,2'-bipyridyl ring as in the case of $[Ru(bpy)_3]^{2+}$. This is illustrated graphically in Figure 6.10. The lack of interaction with an aromatic ring leaves the H6 proton further downfield than could be expected. Table 6.5 below details the positions of the H6 protons in the complexes of interest.

Comparison of the position of the H6 protons of the $[Ru(bpy)_2(PnP)_2]^{2+}$ complexes with the H6 protons of the $[Ru(bpy)_2(PnP)Cl]^{+}$ complexes show clearly a difference to higher ppm of *circa* 1 ppm in the chemical shift of the protons. As discussed the complexity of the spectra of the $[Ru(bpy)_2(PnP)Cl]^{+}$ ligands prevents assignment of the protons. The chemical shifts of the fingerprint H6 protons are given in Table 6.8.

Compound	Position of H6 proton (ppm) in $[Ru(bpy)_2(PnP)Cl]^{+}$
$[Ru(bpy)_2(POP)Cl]^{+}$	10.09
$[Ru(bpy)_2(PEP)Cl]^{+}$	10.05
$[Ru(bpy)_2(P2P)Cl]^{+}$	10.07
$[Ru(bpy)_2(P3P)Cl]^{+}$	10.07

Table 6.8 Positions of the H6 protons of the $[Ru(bpy)_2(PnP)Cl]^{+}$ complexes in d_6-acetone.

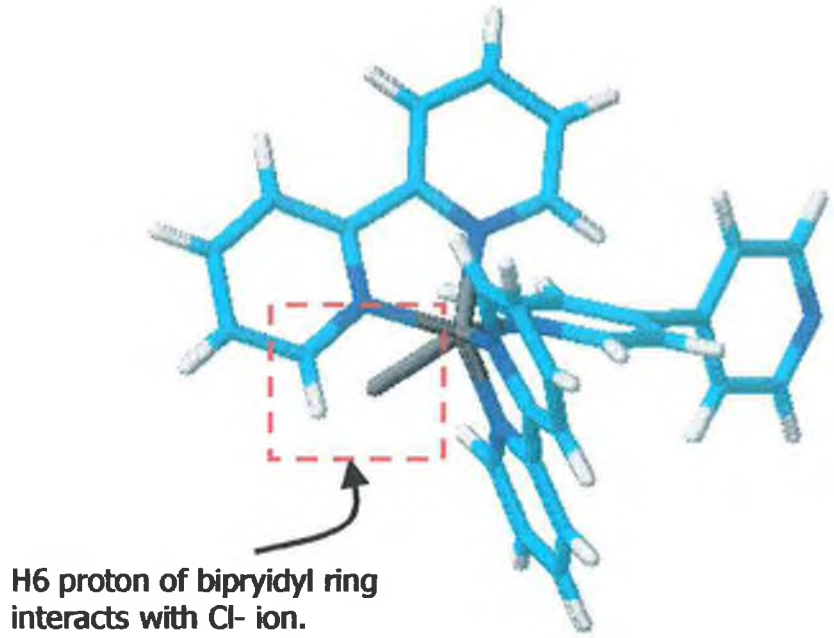

Figure 6.10 Illustration of the interaction between the H6 proton of the bipyridyl ring with the Cl⁻ ion which results in the large downfield shift observed in the ^1H NMR of these complexes.

6.5 Photophysics of the complexes

The photophysical behaviour of the complexes of the ruthenium(II) and osmium bipyridyl complexes of the P0P, P2P, P3P and PEP ligands have been investigated in a number of ways. Extensive analysis of the absorption and emission spectra has been performed and the lifetime measurements of the samples in aerated and degassed solutions, and in a glassy matrix at 77K have also been performed. The results of these experiments are detailed in the diagrams and the tables below.

6.5.1 Absorption Spectra of the complexes

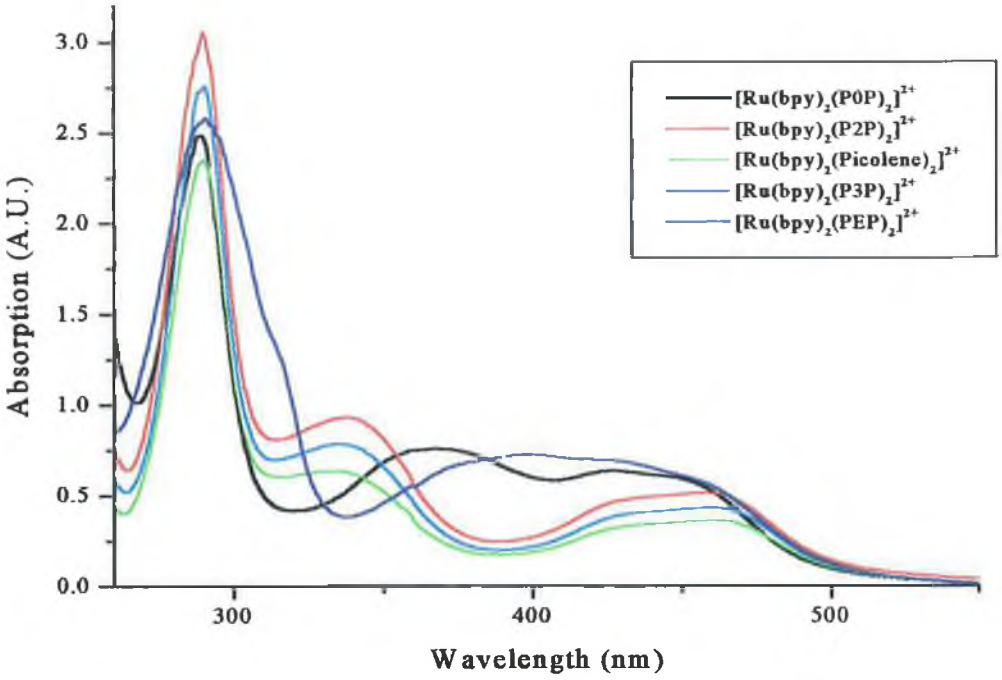

Figure 6.11 Absorption spectra of the $[Ru(bpy)_2(PnP)_2]^{2+}$ complexes in MeCN.

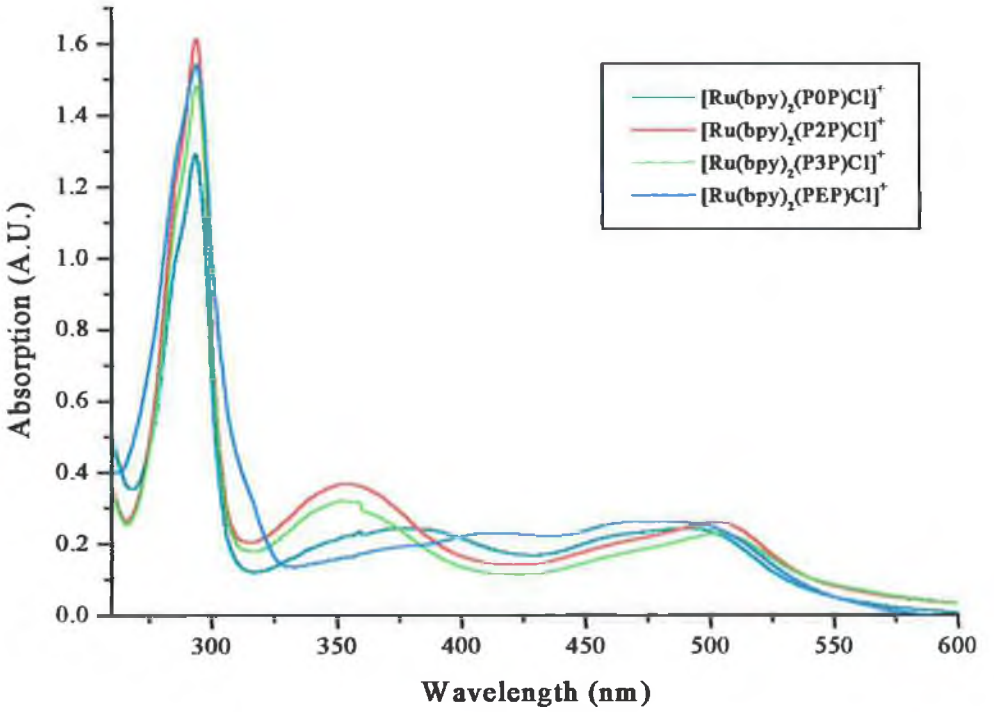

Figure 6.12 Absorption spectra of the $[Ru(bpy)_2(PnP)Cl]^+$ complexes in MeCN.

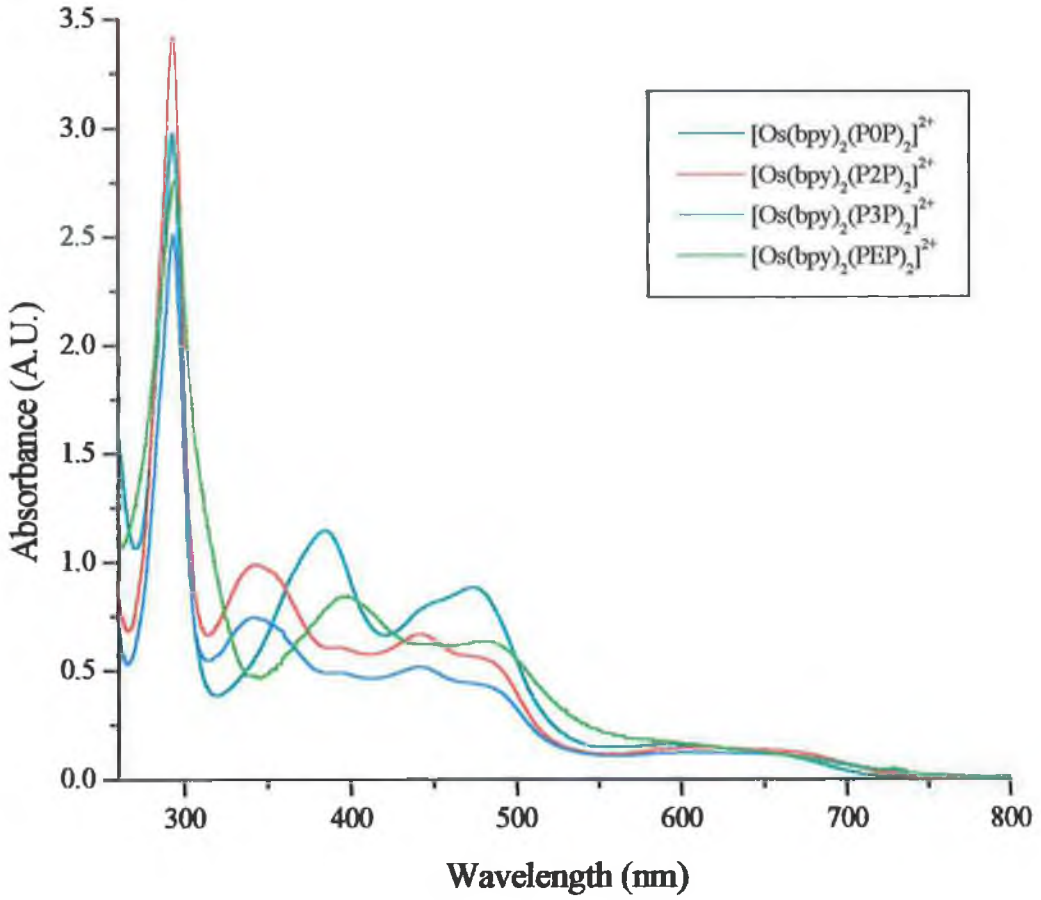

Figure 6.13 Absorption spectra of the $[Os(bpy)_2(PnP)_2]^{2+}$ complexes in MeCN.

The discussion of the absorption (Figures 6.11, 6.12 and 6.13) and the emission (Figures 6.15 and 6.16) spectra of the complexes has been divided into a separate examination of the three types of complex, i.e. $[Ru(bpy)_2(PnP)_2]^{2+}$, $[Ru(bpy)_2(PnP)Cl]^{+}$ and $[Os(bpy)_2(PnP)_2]^{2+}$. Both $[Ru(bpy)_3]^{2+}$ is used for comparison with the ruthenium complexes and $[Os(bpy)_3]^{2+}$ for comparison with the osmium complexes.

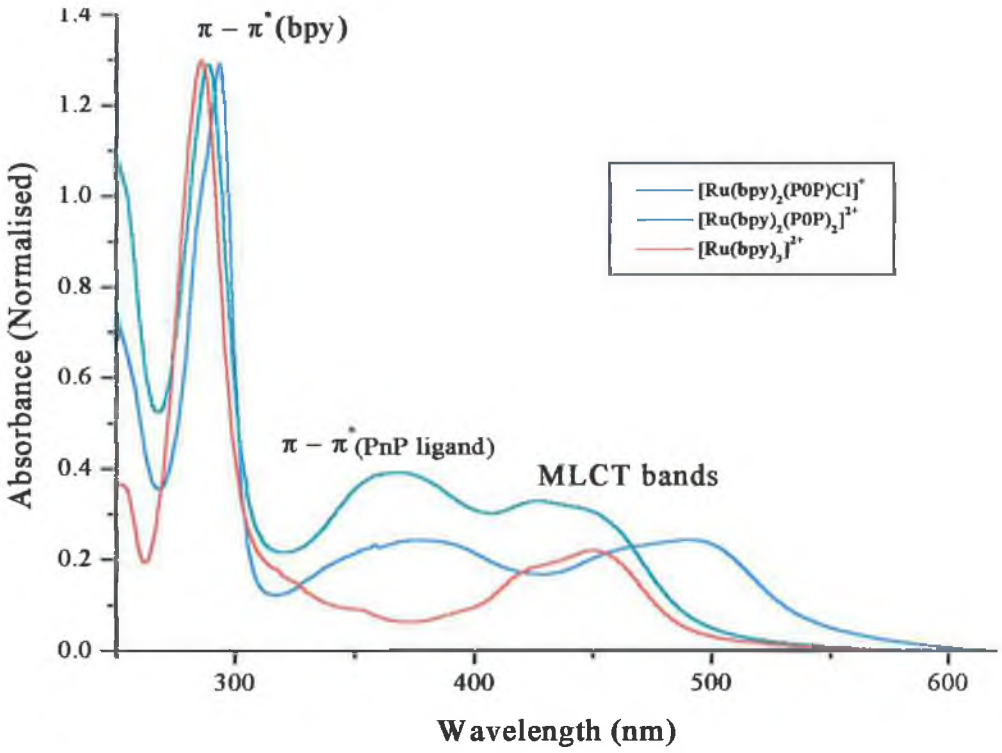

Figure 6.14 Comparison of the absorption spectra of $[Ru(bpy)_3]^{2+}$ with $[Ru(bpy)_2(P0P)_2]^{2+}$ and $[Ru(bpy)_2(P0P)Cl]^{+}$ in MeCN.

The absorption spectra of the $[Ru(bpy)_2(PnP)_2]^{2+}$ complexes contain ligand centred (LC) $\pi \rightarrow \pi^*$ (bpy) based transitions at *circa* 290 nm. A new absorption band in comparison to the spectrum of $[Ru(bpy)_3]^{2+}$ (Figure 6.14) in the region 320 nm to 400 nm has appeared. Comparison of this band to the free PnP ligands shows that this band may be attributed to a ligand centred (LC) $\pi \rightarrow \pi^*$ transitions on the PnP ligands. The bands which are of most interest in these complexes are the $d\pi \rightarrow \pi^*$ metal to ligand charge transfer (MLCT) bands. These are very intense bands with extinction coefficients typically in the range of 10^4 $M^{-1}cm^{-1}$. The position of these bands say much about the electronic structure of the complex.[66] Strong σ-donating ligands are electron rich, and coordination of these ligands result in the ruthenium being more electron rich and this causes the MLCT band to be shifted to the red (i.e. to lower energy).[67] As discussed in Chapter 1.6 and 3.1, ruthenium complexes of imidazole, benzimidazole and triazole ligands have absorption spectra whose MLCT bands have been shifted to lower energy due to the σ-donating properties

of the ligands. However in this case, the ligands that have been introduced are bipyridyl ligands also, and therefore it is not expected that the position of this band should change much as the σ-donating and π-accepting properties of 4,4'-bipyridyl and the related ligands are expected to be almost the same as that found for 2,2' bipyridyl. This is found to be the case, and from Figure 6.14 it can be seen that the λ_{max} of the absorption changes little when comparing $[Ru(bpy)_3]^{2+}$ and $[Ru(bpy)_2(PnP)_2]^{2+}$. As expected, the ^{1}MLCT band of the $[Ru(bpy)_2(PnP)_2]^{2+}$ complex has a higher extinction coefficient.

The ^{1}MLCT band of the $[Ru(bpy)_2(PnP)Cl]^+$ complex differs in the position of the ^{1}MLCT band which is shifted to lower energy. This is due to the presence of the chloride ion, which affects the ^{1}MLCT level of the complex, moving it to lower energy because the chloride ion destabilises the ground state. As discussed in Section 6.3 the UV/Vis spectra of the complexes is the most effective proof that the complex continues to contain the chloride ion in solution. Previous studies indicate that the λ_{max} of the complexes should shift to circa 480 nm should the PnP ligand be replaced by MeCN, and be further blue shifted, to circa 470 nm on replacement of the chloride by water. [2] The λ_{max} of the ^{1}MLCT bands of the $[Ru(bpy)_2(PnP)Cl]^+$ complexes fall between 492 nm and 503 nm which is an excellent indication that the chloride ion remains bound to the ruthenium centre.

Replacement of the ruthenium(II) metal centre with osmium(II) causes a shift to lower energy of the MLCT absorption bands. This has been observed for other systems, and is due to the higher energy of the osmium 5d orbitals, compared to the ruthenium 4d orbitals. [68] Absorption bands that are not present in the absorption spectra of the ruthenium analogues in the range 600-660 nm can be assigned to formally forbidden $d\pi \rightarrow \pi^*$ bpy MLCT transitions, which becomes partially allowed due to the increased spin orbit coupling associated with the larger osmium ion. [69] These bands are centred between 620 and 630 nm for the $[Os(bpy)_2(PnP)_2]^{2+}$ complexes.

6.5.2 Emission Spectra of the complexes:

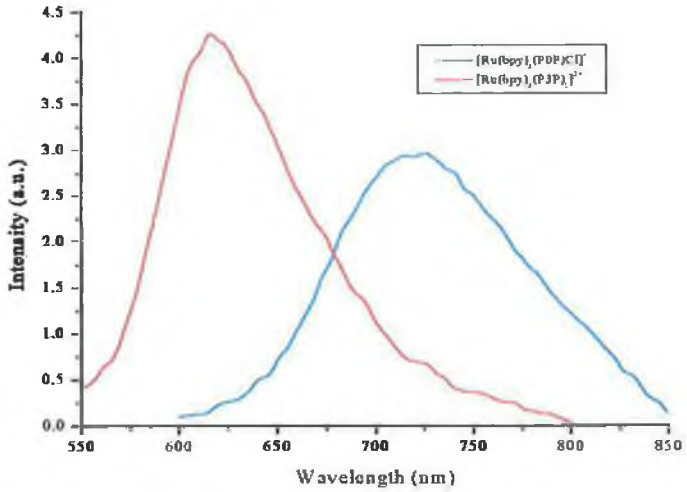

Figure 6.15 Emission spectra of the $[Ru(bpy)_2(P3P)_2]^{2+}$ (red) and $[Ru(bpy)_2(P0P)Cl]^{+}$ (blue) complexes in MeCN.

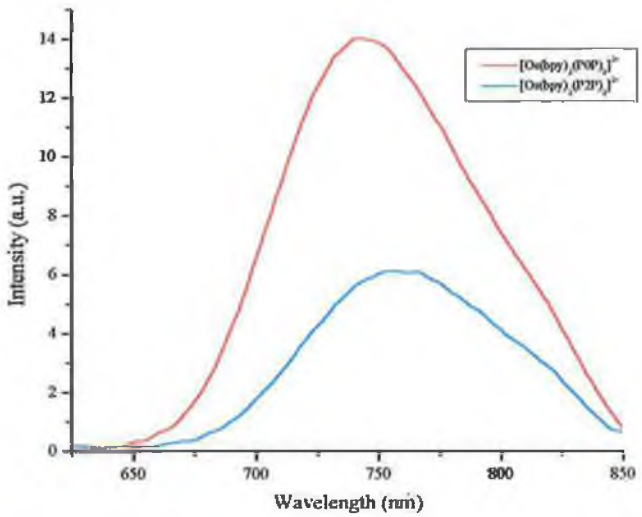

Figure 6.16 Emission spectra of the $[Os(bpy)_2(P0P)_2]^{2+}$ (red) and $[Os(bpy)_2(P2P)_2]^{2+}$ (blue) complexes in MeCN.

Compound	Absorption		Emission	
	λ_{max} (nm)	ε ($M^{-1}cm^{-1}$)	λ_{max} (nm), 298K	λ_{max} (nm), 77K
$[Ru(bpy)_2(Picolene)_2]^{2+}$	290	38,000	620	596
	335	9,200		
	463	5700		
$[Ru(bpy)_2(POP)_2]^{2+}$	288	45,300	615	595
	368	13,800		
	430	11,800		
$[Ru(bpy)_2(P2P)_2]^{2+}$	290	41,300	620	606
	338	11,700		
	458	6,500		
$[Ru(bpy)_2(P3P)_2]^{2+}$	290	48,700	620	605
	335	13,000		
	450	7,400		
$[Ru(bpy)_2(PEP)_2]^{2+}$	291	44,300	618	601
	438	11,500		
$[Ru(bpy)_2(POP)Cl]^{+}$	291	53,000	722	685
	380	12,600		
	492	13,000		
$[Ru(bpy)_2(P2P)Cl]^{+}$	293	47,500	730	696
	354	10,600		
	503	8,000		
$[Ru(bpy)_2(P3P)Cl]^{+}$	290	48,700	720	695
	335	13,070		
	503	7,400		
$[Ru(bpy)_2(PEP)Cl]^{+}$	293	42,000		
	414	13,300	718	690
	495	8,100		

Table 6.9 Results of absorption and emission measurements of Ru(II) complexes in MeCN.

Compound	Absorption		Emission	
	λ_{max} (nm)	ε ($M^{-1}cm^{-1}$) x10^{-4}	λ_{max} (nm), 298K	λ_{max} (nm), 77K
$[Os(bpy)_2(P0P)_2]^{2+}$	293	7.94		
	386	1.97	744	721
	475	1.34		
	623	0.29		
$[Os(bpy)_2(P2P)_2]^{2+}$	293	8.83		
	344	2.87	759	752
	444	1.91		
	632	0.39		
$[Os(bpy)_2(P3P)_2]^{2+}$	293	10.8		
	342	3.24	757	749
	442	2.31		
	617	0.55		
$[Os(bpy)_2(PEP)_2]^{2+}$	294	10.6		
	398	3.28	749	725
	480	2.46		
	630	5.4		

Table 6.10 Absorption and Emission data from the osmium(II) complexes in MeCN.

The compounds studied, exhibit luminescence at room temperature and at 77K. This emission originates from a triplet MLCT state. [67] The ruthenium(II) N6 compounds emit around 620 nm which is comparable to the room temperature emission of $[Ru(bpy)_3]^{2+}$. However, this emission is weak at room temperature. There are a number of reasons for this. The strength of the emission is determined by the contribution of and the ratio between the radiative (k_r) and the non-radiative (k_{nr}) deactivation pathways present for a complex. Although the energy of the emission is the same for the $[Ru(bpy)_2(PnP)_2]^{2+}$ complexes and $[Ru(bpy)_3]^{2+}$ the intensity is greatly reduced, i.e. for the $[Ru(bpy)_2(PnP)_2]^{2+}$ complexes the non radiative deactivation pathways contribution is greater than for the parent complex. This can be readily explained. $[Ru(bpy)_3]^{2+}$ contains

three bidentate ligands, with the nature of the bidentate bond restricting the movement of the ligands. Compare this to the case of the $[Ru(bpy)_2(P0P)_2]^{2+}$ for example which contains two "rigid" 2,2'-bipyridyl units, but also has two 4,4'-bipyridyl moieties which are monodentate coordinationed. The monodentate nature of their coordination to the metal provides both the pyridine rings bound to the metal free rotation, while the pendant arms can also dissipate energy efficiently. [39]

At 77K, all the complexes exhibit strong emission with vibrational structure. This vibrational fine structure has been attributed to relaxation via ligand-based vibrations. [70] As expected cooling to 77K leads to a blue shift in the emission maxima of the complexes. [71] This has been introduced and discussed in earlier chapters and will not be explained again here. In order to discuss the emissive properties of the complexes in more detail, the luminescent lifetimes of the complexes should be examined. Experiments have also been performed to calculate the emission quantum yields. The lifetimes were measured using the single photon counting technique and were measured in the maxima of the emission. These results can be seen in Table 6.11 and 6.12.

	Aerated RT		Deaerated RT		77K
Compound	τ(ns)	Φ(x 10^{-4})	τ(ns)	Φ(x 10^{-4})	τ(μs)
$[Ru(bpy)_2(P0P)_2]^{2+}$	0.9	1	1.1	1	4.2
$[Ru(bpy)_2(P2P)_2]^{2+}$	1.7	2	1.6	2	3
$[Ru(bpy)_2(P3P)_2]^{2+}$	2.3	1.7	2.9	2	4
$[Ru(bpy)_2(PEP)_2]^{2+}$	1.2	1.1	1.4	1	3.7
$[Ru(bpy)_2(P0P)Cl]^{+}$	32	8	46	11	0.7
$[Ru(bpy)_2(P2P)Cl]^{+}$	37	7	54	11	0.6
$[Ru(bpy)_2(P3P)Cl]^{+}$	35	7	56	10	0.7
$[Ru(bpy)_2(PEP)Cl]^{+}$	29	6.3	37	9	0.58

Table 6.11 Results of Emission Quantum Yield and Excited State Lifetime experiments. All measurements at 298K in MeCN, at 77K in butyronitrile

Compound	τ, aerated (ns)	τ, deaerated (ns)	τ, 77K (ns)
$[Os(bpy)_2(POP)_2]^{2+}$	31	46	670
$[Os(bpy)_2(P2P)_2]^{2+}$	25	37	478
$[Os(bpy)_2(P3P)_2]^{2+}$	25	35	506
$[Os(bpy)_2(PEP)_2]^{2+}$	28	38	617

Table 6.12 Results of the excited state lifetime measurements on the $[Os(bpy)_2(PnP)_2]^{2+}$ complexes.

The emission of the $[Ru(bpy)_2(PnP)Cl]^+$ differs from that of the RuN6 complexes. At room temperature the $[Ru(bpy)_2(PnP)Cl]^+$ complexes have a weak emission at around 720 – 730 nm. There are several reasons for this lack of emission. The chloride lowers the ^{3}MC state of the complex while also raising the ground state. The ^{3}MC state is a thermally populated state and therefore at room temperature, lowering the energy of the state allows it to be populated more easily. The chloride also affects the ^{3}MLCT level of the complex, moving it to lower energy. This then leads to a shortening of the lifetime, which is due to the energy gap law. Also, as discussed for the N6 complex, these compounds contain monodentate ligands and the freedom of motion provided by this mode of coordination leads to loss of the intensity of the emission.

The emission maxima of the osmium complexes also occurs at lower energy than those of the analogous ruthenium(II) complexes. This is as expected and this observation is in agreement with the lower oxidation potentials observed for the osmium complexes in comparison with their ruthenium counterparts.

The lifetime data of the complexes can be explained by comparison to the luminescence properties of the complexes. The weakly emitting RuN6 complexes have a short lifetime, and this can be associated with the efficient non-radiative decay processes afforded by the two pendant PnP ligands. The lifetime of the RuN5-Cl complexes are

surprisingly long (between 9 and 11 ns in deaerated MeCN). Unlike the RuN6 complexes the RuN5-Cl complexes have only one pendant PnP ligand to dissipate the excited state energy. This leads to the RuN5-Cl having longer lifetimes at room temperature.

At 77K the lifetime for the RuN6 complexes increase to between 3 and 4.2 μs. The RuN5-Cl complexes lifetimes increase to between 580 and 700 ns. The torsional rotation of the PnP ligands, which shorten the lifetime and lessens the intensity of the emission of both the RuN6 and RuN5-Cl complexes is "frozen" out in the glassy butyronitrile matrix at 77K. The lifetimes correlate more closely with the energy of the emission, with the higher energy emitting species (RuN6) having a longer lived excited state.

The lifetimes of the OsN6 complexes lie between 35 – 46 ns in deaerated MeCN and increase to between 500 – 700 ns at 77K. These values are typical for osmium N6 complexes.

6.6 Electrochemistry of the complexes:

One of the most important techniques used in the characterisation of the dinuclear complexes synthesised using these monomeric precursors will be electrochemistry. Two techniques have been used extensively for the electrochemical characterisation of these complexes, cyclic voltammetry (CV) and differential pulse voltammetry (DPV). Of these cyclic voltammetry has proved the more important. Once again, the complexes $[Ru(bpy)_3]^{2+}$ (Section 3.11) and $[Os(bpy)_3]^{2+}$ (Section 4.8) will be used as reference complexes for comparison with the results obtained. Illustrative CVs of the three type of complex are presented in Figures 6.17, 6.18 and 6.19, while the results of the electrochemical analysis of the complexes are listed in Table 6.13.

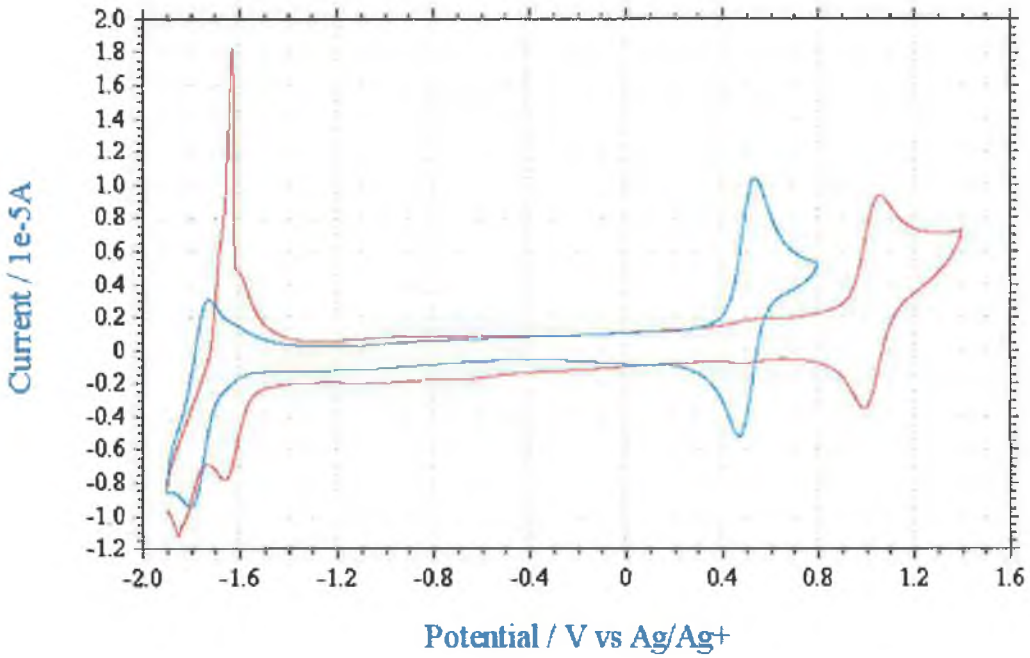

Figure 6.17 Overlay of the CVs of $[Ru(bpy)_2(POP)Cl]^+$ (blue) and $[Ru(bpy)_2(POP)_2]^{2+}$ in MeCN with 0.1M $TBABF_4$.

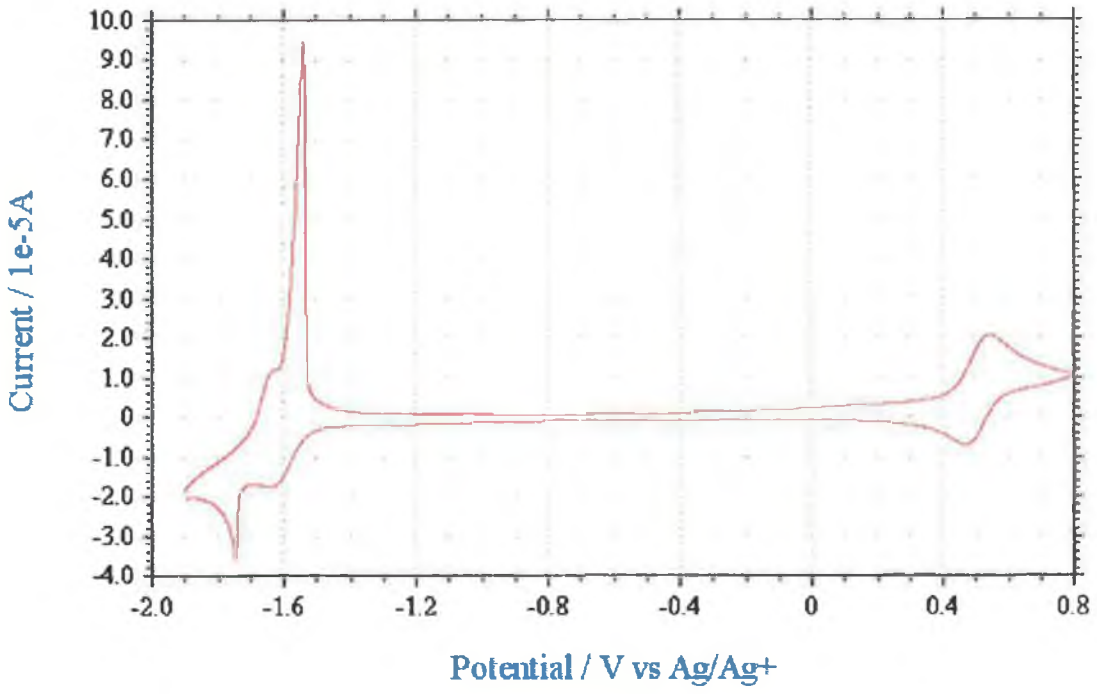

Figure 6.18 CV of $[Os(bpy)_2(P0P)_2]^{2+}$ in MeCN with 0.1M $TBABF_4$.

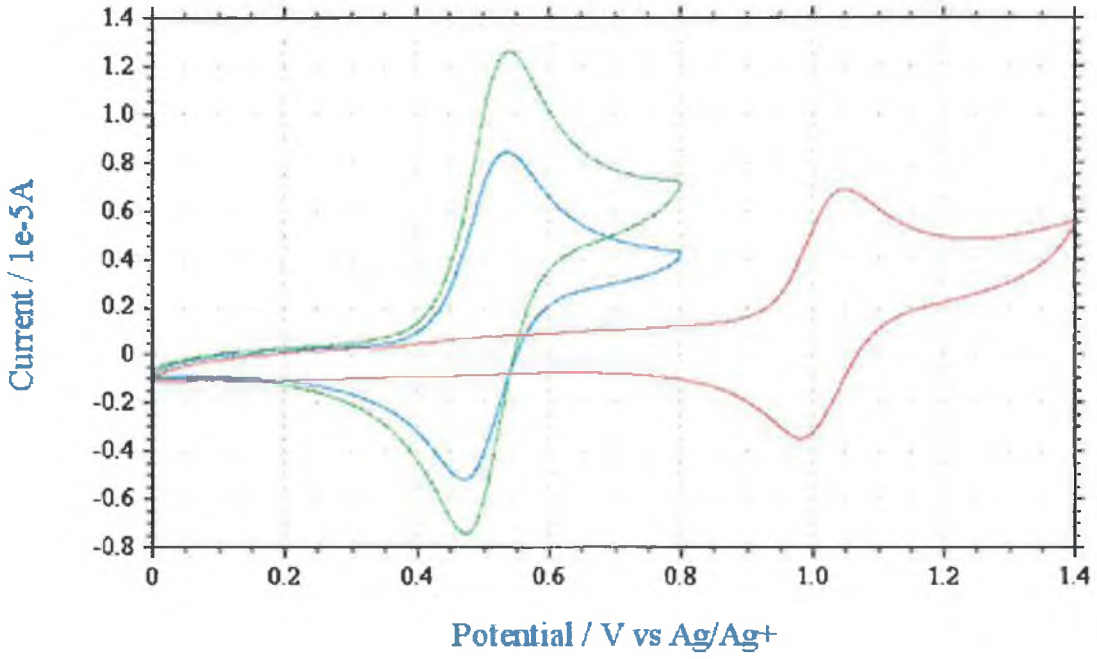

Figure 6.19 Overlay of the oxidation waves of the complexes $[Ru(bpy)_2(P0P)Cl]^+$ (blue), $[Os(bpy)_2(POP)_2]^{2+}$ (green) and $[Ru(bpy)_2(POP)_2]^{2+}$ in MeCN with 0.1M $TBABF_4$.

Compound	Oxidation potential, M(II)/M(III)	Reduction potential, Ligand based.
$[Ru(bpy)_2(picolene)_2]^{2+}$	0.84	-1.75
		-1.97
$[Ru(bpy)_2(POP)_2]^{2+}$	0.91	-1.73
		-1.86
$[Ru(bpy)_2(P2P)_2]^{2+}$	0.86	-1.75
		-1.95
$[Ru(bpy)_2(P3P)_2]^{2+}$	0.84	-1.75
		-1.96
$[Ru(bpy)_2(PEP)_2]^{2+}$	0.89	-1.73
$[Ru(bpy)_2(POP)Cl]^{+}$	0.41	-1.86
$[Ru(bpy)_2(P2P)Cl]^{+}$	0.38	-1.87
$[Ru(bpy)_2(P3P)Cl]^{+}$	0.37	-1.88
$[Ru(bpy)_2(PEP)Cl]^{+}$	0.40	-1.65
		-1.89
$[Os(bpy)_2(POP)_2]^{2+}$	0.45	-1.65
	1.67 (irr)	
$[Os(bpy)_2(P2P)_2]^{2+}$	0.39	-1.69
	1.64 (irr)	-1.91
$[Os(bpy)_2(P3P)_2]^{2+}$	0.38	-1.70
	2.01 (irr)	-1.92
$[Os(bpy)_2(PEP)_2]^{2+}$	0.40	-1.71
	1.94 (irr)	

Table 6.13 Oxidation and reduction potentials of the mononuclear ruthenium(II) and osmium(II) complexes (V vs Fc/Fc^+). All measurements carried out in MeCN with 0.1M $TBABF_4$.

The electrochemical properties of these mononuclear complexes have already been investigated and reported [5,6,7,8,9,10,11] and so detailed analysis of the results is not necessary. It is important that the electrochemistry of these complexes was carried out under the same experimental conditions as those of the dimeric complexes which will be discussed in the next chapter as this will allow for comparison of the monomers with the results obtained for the dimers.

The anodic region of the cyclic voltammograms exhibit well defined reversible metal-centred oxidation waves, while the cathodic region features waves which results from the reduction of the coordinated polypyridyl ligands. [67] As expected the oxidation potentials of the osmium compounds are approximately 400mV lower than for those of the analogous ruthenium complexes. This is consistent with the fact that the 5d orbitals of osmium are higher in energy than the 4d orbitals of ruthenium. [72,73,74]

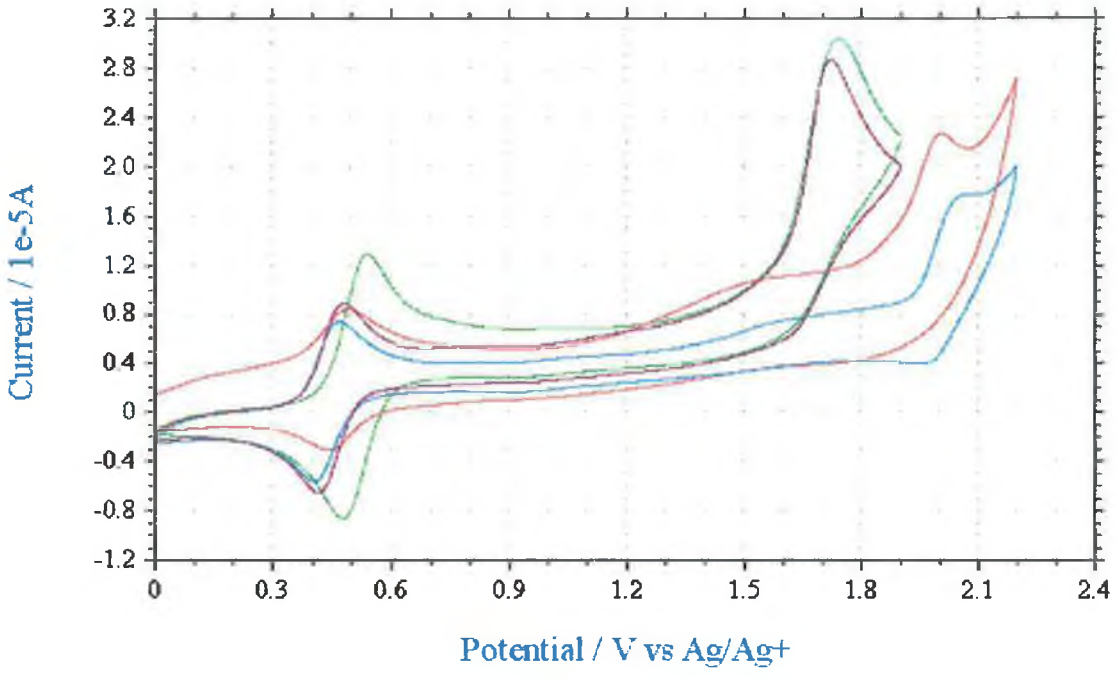

Figure 6.19 Examination of the oxidation waves of the complexes $[Os(bpy)_2(P0P)_2]^{2+}$ (green), $[Os(bpy)_2(P2P)_2]^{2+}$ (purple), $[Os(bpy)_2(P3P)_2]^{2+}$ (blue) and $[Os(bpy)_2(PEP)_2]^{2+}$ (red).

Figure 6.19 illustrates an unusual process observed for each of the $[Os(bpy)_2(PnP)_2]^{2+}$ complexes. A second irreversible oxidation process is observed at higher potentials. This oxidation process has not been reported for these complexes before, and this may be due to the width of the potential window achieved during the electrochemical examination of these complexes, it is possible the other groups were unable to scan this far. Extreme care to exclude water from the organic media was taken and this is reflected in the electrochemical results achieved not only in this chapter but throughout the thesis. Two explanations for these oxidation wave are possible, and are examined in detail in Chapter 7.9.

6.7 Bibliography

[1] Balzani V., Juris A., Venturi M., Camapgna S., Serroni S., ***Chem. Rev.***, **1996**, 96, 759.

[2] Forster R. J., Figgemeier E., Lees A., Hjelm J., Vos J. G., ***Langmuir***, **2000**, 16, 7867.

[3] Lavallee, D. K., Fleischer E. B., ***J. Am. Chem. Soc.,*** **1972**, 94, 2583.

[4] Lavallee, D. K., Fleischer E. B., ***J. Am. Chem. Soc.,*** **1972**, 94, 2599.

[5] Forster R. J., Faulkner L. R., ***J. Am. Chem. Soc.,*** **1994**, 116, 5444

[6] Forster R. J., Faulkner L. R., ***Langmuir***, **1995**, 11, 1014

[7] Forster R. J., Faulkner L. R., ***J. Am. Chem. Soc.,*** **1994**, 116, 5453

[8] Forster R. J., Faulkner L. R., ***Anal. Chem.,*** **1995**, 67, 1232

[9] Forster R. J., O' Kelly J. P., ***J. Phys. Chem.,* 1996**, 100, 3695

[10] Tirado J. D., Abruna H. D., ***J. Phys. Chem.***, **1996**, 100, 4556

[11] O' Halloran D., ***Ph. D. Thesis***, Dublin City University, **1999.**

[12] Haas O., Kriens M., Vos J. G., ***J. Am. Chem. Soc.***, **1981**, 103, 1318.

[13] Forster R. J., Figgemeier E., Loughman P., Lees A., Hjelm J., Vos J. G., ***Langmuir*, 2000**, 16, 7871.

[14] Meyer T. J., Callahan R. W., Brown G. M., ***Inorg. Chem.,* 1975**, 14, 1443

[15] Hage R., ***Ph. D Thesis***, Leiden University, **1991**

[16] Taube H., Fischer H., Tom G. M., ***J. Am. Chem. Soc.,* 1976**, 98, 5512

[17] Powers M. J., Meyer T. J., ***J. Am. Chem. Soc.,* 1980**, 102, 1289

[18] Schanze K. S., Meyer T. J., ***Inorg. Chem.,* 1985**, 24, 2122

[19] Schanze K. S., Neyhart G. A., Meyer T. J., ***J. Phys. Chem.,* 1986,** 90, 2182

[20] Curtis J. C., Bernstein J. S., Meyer T. J., ***Inorg. Chem.,* 1985**, 24, 385

[21] Lin R., Fu Y., Brock C. P., Guarr T. F., ***Inorg. Chem.,* 1992**, 31, 4346

[22] Lin R., Guarr T. F., ***Inorg. Chim. Acta.,* 1994**, 226, 79.

[23] Olenyuk B., Fechtenkotter, A., Stang, P. J., ***J. Chem. Soc., Dalton Trans.,*** **1998**, 1707.

[24] MacGillivray L. M., Subramanian S., Zaworotko M. J., ***J. Chem. Soc., Chem. Commun.,*** **1994**, 1325.

[25] Carlucci, L., Ciani, G., Proserpio, D. M., Sironi, A., ***J. Chem. Soc., Chem. Commun.,*** **1994**, 2755.

[26] Fujita M, Kwon Y. J., Washizu S., Ogura K., ***J. Am. Chem. Soc.,*** **1994**, 116, 1151.

[27] Gable R. W., Hoskins B. F., Robson R., ***J. Chem. Soc. Chem. Commun.,*** **1990**, 1677.

[28] Robson R., Abrahams, B. F., Batten S. R., Gable R. W., Hoskins B. F., Liu J., ***Supramolecular Architecture***; ACS Symposium 499, Chapter 19.

[29] Stang, P. J., Cao D. H., Saito, S., Aif, A. M., ***J. Am. Chem. Soc***., **1995**, 117, 6273.

[30] Fujita, M., Yazaki, J., Ogura, K., ***J. Am. Chem. Soc***., **1990**, 112, 5645.

[31] Fujita, M.,Nagoa, S., Ilida, M., Ogata, K., Ogura K., ***J. Am. Chem. Soc***., **1993**, 115,1574.

[32] Slone R. V., Yoon D. I., Calhoun R. M., Hupp J. T., ***J. Am. Chem. Soc.,*** **1995**, 117, 11813.

[33] Wrighton M.S., Giordano P. J., ***J. Am. Chem. Soc***., **1995**, 117, 6273.

[34] Fujita M., Ibukuro F., Hagihara H., Ogura K., ***Nature,* 1994**, 367, 720.

[35] Fujita M., Yakazi J., Ogura K., ***Tetrahedron Lett,* 1991,** 32, 5589.

[36] Fujita M., Kwon Y., J., Washizu s., Ogura K., ***J. Am. Chem. Soc***., **1994**, 116, 4981.

[37] Slone R. V., Hupp J. T., Stern C L., Albrecjt-Schmitt T E***., Inorg. Chem***., **1996**, 35, 4096.

[38] Hunter C. A., ***Angew. Chem***., **1995**, 107, 1181.

[39] Ashton P. R., Ballardini R., Balzani V., Credi A., Gandolfi M. T., Menzer S., Perez L., Prodi L., Stoddart, J. F., Venturi M., White, A. J. P., Williams D. J., ***J. Am. Chem. Soc.***, **1995**, 117, 11171.

[40] Tapolsky G., Duessing R., Meyer T. J., ***J. Phys. Chem***., **1989**, 93, 3885.

[41] Tapolsky G., Duessing R., Meyer T. J., ***Inorg. Chem.,* 1990**, 29, 2285.

[42] Yaghi O. M., Li H., Groy, T. J., ***Inorg. Chem***., **1997**, 36, 4292.

[43] Yaghi O.M., Davis C. E., Li G. Li H., ***J. Am. Chem. Soc.***, **1997**, 119, 2861.

[44] Gardner G., Kiang, Y. H., Lee S., Asgaonkar A., Venkataraman D., ***J. Am. Chem. Soc.***, **1996**, 118, 9096.

[45] Parmrasad D., Pez G. P., Toby B. H., Markley T. J., Pearlstein R. M., ***J Am. Chem. Soc., 1995***, 117, 10694.

[46] Subramanian S., Zaworotko M. J., ***Angew, Chem., Int. Ed. Engl.,*** **1995**, 34, 2127.

[47] Slone R. V., Benkstein K. D., Belanger S., Hupp J T., Guzei I A., Rheingold A. L., ***Coord. Chem. Rev.,*** **1998**, 171, 221.

[48] Benkstein K. D., Hupp J. T., Stern C. L., ***Inorg. Chem.***, **1998**, 37, 5404.

[49] Woessner S. M., Helms J. B., Shen Y., Sullivan B. P., ***Inorg. Chem.***, **1998**, 37, 5406.

[50] Benkstein K. D., Hupp J. T., Stern C. L., ***J. Am. Chem. Soc.,*** **1998**, 120, 12982.

[51] Slone R. V., Hupp J. T., ***Inorg. Chem.***, **1997**, 36, 5422.

[52] Belanger S., Hupp T. J., Stern C. L., Slone R. V., Watson D. F., Carrell T. G., ***J. Am. Chem. Soc.,*** **1999**, 121, 557.

[53] Stricklen P. M., Volcko E. J., Verkade J. G., ***J. Am. Chem. Soc.,*** **1983**, 105, 2494.

[54] Kajiwara, T., Ito T. J., ***J. Chem. Soc., Chem. Commun.,*** **1994**, 1773.

[55] Sun S, Lees, A. J., ***Inorg. Chem.,*** **1999,** 38, 4181.

[56] Lee S. B., Hwang S. C., Chung D. S., Yun H., Hong J. I., ***Tetrahedron Lett.,*** **1998**, 39, 873.

[57] Leadbeater N. E., Cruse H. A., ***Inorg. Chem. Commun. 2***, **1999**, 93.

[58] Rajendran, T., Manimaran B., Lee F. Y., Lee G. H., Peng S. M., Wang C. M., Lu K. L., ***Inorg. Chem.***, **2000,** 39, 2016.

[59] Maiboroda A., Fechner A., Zahn D., Hietscold M., Lang H., ***Sensors and Actuators,*** **2001**, B 75, 188.

[60] Forster R. J., ***Inorg. Chem.***, **1996**, 35, 3394.

[61] Haas O., Kriens M., Vos J. G., ***J. Am. Chem. Soc.,*** **1981**, 103, 1318.

[62] Forster R. J., Vos J. G., ***Macromolecules,*** **1990**, 23, 4372.

[63] Buchanan B. E., McGovern E., Harkin P., Vos J. G., ***Inorg. Chim. Acta.,*** **1988**, 154, 1.

[64] Moyer B. A., Meyer T. J., ***J. Am. Chem. Soc.,*** **1978**, 100, 3601.

[65] Moyer B. A., Meyer T. J., ***Inorg. Chem.,*** **1981,** 20, 436.

[66] Barigelleti F. DeCola L., Balzani V., Hage R., Haasnoot J. G., Reedijk J., Vos J. G., ***Inorg. Chem.,*** **1991**, 30, 641.

[67] Juris A, Balzani V., Barigelleti F, Campagna S., Belser P., von Zelewsky A., ***Coord. Chem. Rev.,*** **1988**, 84, 85.

[68] Ernst S., Kasack V., Kaim W., ***Inorg. Chem.,*** **1989**, 28, 1520.

[69] Haga M., Matsumura-Inoue T., Yamabe S., ***Inorg. Chem***., **1987**, 26, 4148.

[70] Lumpkin R. S., Kober E. M., Worl L., Murtaza Z., Meyer T. J., ***J. Phys. Chem.,*** **1990**, 94, 239.

[72] Goldsby K. A., Meyer T. J., ***Inorg. Chem.***, **1984**, 23, 3002.

[73] Kalyanasundaram K., Nazeeruddin K., ***Inorg. Chim. Acta***, **1990,** 171, 213

[74] Kalyanasundaram K., Nazeeruddin K., ***Chem. Phys. Lett.***, **1989**, 158, 45

Chapter 7:

Synthesis and Characterisation of a Series of Surface Active Dinuclear Ruthenium(II) and Osmium(II) Complexes

Abstract:

Chapter 7 details the synthesis and preliminary investigations of a series of homonuclear ruthenium(II) and heteronuclear osmium(II)/ruthenium(II) binuclear complexes. The monomeric complexes introduced in Chapter 6 form the subunits of the dinuclear complexes detailed here. The complexes take the form $[Ru(bpy)_2(PnP)_2(bpy)_2RuCl](PF_6)_3$ *and* $[Ru(bpy)_2(PnP)_2(bpy)_2RuCl](PF_6)_3$ *where PnP = 4,4'-bipyridyl (P0P), 1,2-bis(4-pyridyl)ethylene (PEP), 1,2-bis(4-pyridyl)ethane (P2P), and 4,4'-trimethylenedipyridine (P3P). The dinuclear complexes have been designed in such a way as to allow the complexes to bind to a surface.*

Characterisation has been carried out by elemental analysis and ^1H *NMR spectroscopy. The photophysical properties and electrochemical properties are discussed also. This chapter concludes with an attempt to attach one of the mixed metal Os-Ru dinuclear complexes to a Pt surface.*

7.1 Introduction:

Chapter 6 introduced a number of monomeric ruthenium(II) and osmium(II) complexes based on variations of 4,4'-bipyridyl. These monodentate ligands were used to synthesise a series of ruthenium and osmium N6 complexes containing two 2,2'-bipyridyl rings and two monodentate PnP ligands. A series of N5-chloride ruthenium complexes were also synthesised.

This chapter details the synthesis of a series of dinuclear complexes based on these mononuclear complexes, using the PnP ligand as a bridge between two metal centres. Much attention is focussed on the synthesis of these complexes as the synthesis proved more difficult than expected. The characterisation of the complexes is discussed, and in particular, why a different approach had to be taken with these complexes in comparison to the other compounds discussed in this thesis. The photophysical properties of the dinuclear complexes are reported here, however further studies are needed to fully understand the excited state properties of the complexes. The solution phase electrochemistry of these complexes is also reported. Finally it has been shown for one of the complexes, that the complexes are indeed surface active, and a monolayer of a dinuclear complex on a surface has been formed.

7.2 Experimental.

The synthesis of the starting materials for these reaction has already been outlined in the previous chapter (Section 6.2), and will not be discussed further here. The synthesis of *cis*-$[Ru(bpy)_2Cl_2].2H_2O$ has been described in Chapter 3.2.

Synthesis of $[Ru(bpy)_2(P0P)_2(bpy)_2RuCl](PF_6)_3.4H_2O$

$[Ru(bpy)_2(P0P)_2](PF_6)_2$ (100 mg, 9.84 x 10^{-5} mol) and $[Ru(bpy)_2Cl_2].2H_2O$ (51 mg, 9.84 x 10^{-5} mol) were heated at reflux in 20 cm^{-3} of dry MeOH for 6 hours. After this time, the reaction was allowed to cool to room temperature and the solvent removed to dryness *in vacuo*. The product was added as a solid to a saturated aqueous solution of ammonium hexafluorophosphate, and the chloride salt was converted instantly to the PF_6^- salt and was precipitated instantly as a fine brown-red powder. The product was isolated by filtration and washed with a minimum amount of ice-water and diethyl ether and allowed to dry. The complex was recrystallised from a 2:1 mixture of acetone:toluene. No further purification of the complex was necessary and the reaction yielded 125 mg of the desired dinuclear product. (79% yield).

^1H NMR (400 MHz, d_6-acetone) δ = 10.06 (d, 1H), 9.36 (m, 2H), 8.71 (m, 15H), 8.20 (m, 10H), 7.82 (m, 16H), 7.56 (dd, 2H), 7.37 (dd, 1H), 7.30 (dd, 1H).
Total = 48 aromatic protons.

Elemental Analysis for $C_{60}H_{56}N_{12}Ru_2O_4Cl_1P_3F_{18}$: Calculated C 43.05, H 3.11, N 10.04. Found C 43.10, H 3.08, N 9.58 %.

Synthesis of $[Ru(bpy)_2(P2P)_2(bpy)_2RuCl](PF_6)_3.6H_2O$

$[Ru(bpy)_2(P2P)_2](PF_6)_2$ (103 mg, 9.6 x 10^{-5} mol) and $[Ru(bpy)_2Cl_2].2H_2O$ (50 mg, 9.6 x10^{-5} mol) were heated at reflux in 20 cm^{-3} of dry MeOH for 6 hours. After this time, the reaction was allowed to cool to room temperature and the solvent removed to dryness *in vacuo*. The product was added as a solid to a saturated aqueous solution of ammonium hexafluorophosphate, and the chloride salt was converted instantly to the PF_6^- salt and was precipitated instantly as a dark red-brown powder. The product was isolated by filtration and washed with a minimum amount of ice-water and diethyl ether and allowed to dry. The complex was recrystallised from a 2:1 mixture of acetone:toluene.

No further purification of the complex was necessary and the reaction yielded 134 mg of the desired dinuclear product. (84 % yield).

^{1}H NMR (400 MHz, d_6-acetone) δ = 10.08 (d, 1H), 9.24 (m, 2H), 8.59 (m, 17H), 8.14 (m, 16H), 7.80 (dd, 1H), 7.52 (dd, 1H), 7.26 (m, 9H), 2.9 (m, 8H).
Total = 48 aromatic, 8 aliphatic protons.

Elemental Analysis for $C_{66}H_{74}N_{12}Ru_2O_6Cl_1P_3F_{18}$: Calculated C 43.94, H 3.77, N 9.32. Found C 44.25, H 3.51, N 8.99 %.

Synthesis of $[Ru(bpy)_2(P3P)_2(bpy)_2RuCl](PF_6)_3.H_2O$

$[Ru(bpy)_2(P3P)_2](PF_6)_2$ (98 mg, 8.9 x 10^{-5} mol) and $[Ru(bpy)_2Cl_2].2H_2O$ (46 mg, 8.9 x10^{-5} mol) were heated at reflux in 20 cm^{-3} of dry MeOH for 6 hours. After this time, the reaction was allowed to cool to room temperature and the solvent removed to dryness *in vacuo*. The product was added as a solid to a saturated aqueous solution of ammonium hexafluorophosphate, and the chloride salt was converted instantly to the PF_6^- salt and was precipitated instantly as a brown-red powder. The product was isolated by filtration and washed with a minimum amount of ice-water and diethyl ether and allowed to dry. The complex was recrystallised from a 2:1 mixture of acetone:toluene. No further purification of the complex was necessary and the reaction yielded 112 mg of the desired dinuclear product. (78 % yield).

^{1}H NMR (400 MHz, d_6-acetone) δ = 10.06 (d, 1H), 9.24 (m, 2H), 8.55 (m, 17H), 8.03 (m, 16H), 7.79 (dd, 1H), 7.67 (dd, 1H), 7.52 (m, 2H), 7.27 (m, 9H).

Elemental Analysis for $C_{66}H_{62}N_{12}Ru_2OCl_1P_3F_{18}$: Calculated C 46.36, H 3.57, N 9.83. Found C 46.20, H 3.53, N 9.67 %.

Synthesis of $[Ru(bpy)_2(PEP)_2(bpy)_2RuCl](PF_6)_3.4H_2O$

$[Ru(bpy)_2(PEP)_2](PF_6)_2$ (115 mg, 1.08×10^{-4} mol) and $[Ru(bpy)_2Cl_2].2H_2O$ (56 mg, 1.08×10^{-4} mol) were heated at reflux in 20 cm^{-3} of dry MeOH for 6 hours. After this time, the reaction was allowed to cool to room temperature and the solvent removed to dryness *in vacuo*. The product was added as a solid to a saturated aqueous solution of ammonium hexafluorophosphate, and the chloride salt was converted instantly to the PF_6^- salt and was precipitated instantly as a red-brown powder. The product was isolated by filtration and washed with a minimum amount of ice-water and diethyl ether and allowed to dry. The complex was recrystallised from a 2:1 mixture of acetone:toluene. No further purification of the complex was necessary and the reaction yielded 124 mg of the desired dinuclear product. (69 % yield).

^1H NMR (400 MHz, d_6-acetone) δ = 10.05 (d, 1H), 9.37 (m, 2H), 8.66 (m, 14H), 8.19 (m, 9H), 7.95 (m, 5H), 7.79 (d, 1H), 7.60 (m, 14H), 7.38 (dd, 1H), 7.31 (dd, 1H).

Elemental Analysis for $C_{64}H_{60}N_{12}Ru_2O_4Cl_1P_3F_{18}$: Calculated C 44.53, H 3.25, N 9.74. Found C 44.35, H 3.06, N 9.55 %.

Synthesis of $[Os(bpy)_2(P0P)_2(bpy)_2RuCl](PF_6)_3.9H_2O$

$[Os(bpy)_2(P0P)_2](PF_6)_2$ (125 mg, 1.13×10^{-4} mol) and $[Ru(bpy)_2Cl_2].2H_2O$ (59 mg, 1.13×10^{-4} mol) were heated at reflux in 20 cm^{-3} of dry MeOH for 6 hours. After this time, the reaction was allowed to cool to room temperature and the solvent removed to dryness *in vacuo*. The product was added as a solid to a saturated aqueous solution of ammonium hexafluorophosphate, and the chloride salt was converted instantly to the PF_6^- salt and was precipitated instantly as a green-brown powder. The product was isolated by filtration and washed with a minimum amount of ice-water and diethyl ether and allowed to dry. No further purification of the complex was necessary and the reaction yielded 131 mg of the desired dinuclear product. (68% yield).

^{1}H NMR (400 MHz, d_6-acetone) δ = 10.04 (d, 1H), 9.18 (m, 2H), 8.74 (m, 17H), 8.10 (m, 8H), 7.81 (m, 16H), 7.40 (m, 4H). Total = 48 aromatic protons.

Elemental Analysis for $C_{60}H_{66}N_{12}Os_1Ru_1O_9Cl_1P_3F_{18}$: Calculated C 39.09, H 3.09, N 9.12. Found C 38.68, H 2.56, N 8.89 %.

Synthesis of $[Os(bpy)_2(P2P)_2(bpy)_2RuCl](PF_6)_3.9H_2O$

$[Os(bpy)_2(P2P)_2](PF_6)_2$ (108 mg, 9.30 x 10^{-5} mol) and $[Ru(bpy)_2Cl_2].2H_2O$ (48 mg, 9.30 x 10^{-5} mol) were heated at reflux in 20 cm^{-3} of dry MeOH for 6 hours. After this time, the reaction was allowed to cool to room temperature and the solvent removed to dryness *in vacuo*. The product was added as a solid to a saturated aqueous solution of ammonium hexafluorophosphate, and the chloride salt was converted instantly to the PF_6^- salt and was precipitated instantly as a dark green/ brown powder. The product was isolated by filtration and washed with a minimum amount of ice-water and diethyl ether and allowed to dry. No further purification of the complex was necessary and the reaction yielded 118 mg of the desired dinuclear product. (66 % yield).

^{1}H NMR (400 MHz, d_6-acetone) δ = 10.08 (d, 1H), 9.05 (m, 2H), 8.63 (m, 12H), 8.42 (m, 4H), 8.09 (m, 8H), 7.86 (m, 7H), 7.65 (m, 4H), 7.30 (m, 10H). Total = 48 aromatic protons.

Elemental Analysis for $C_{64}H_{78}N_{12}Os_1Ru_1O_9Cl_1P_3F_{18}$: Calculated C 40.47, H 3.43, N 8.85. Found C 40.26, H 2.93, N 8.77 %.

Synthesis of $[Os(bpy)_2(P3P)_2(bpy)_2RuCl](PF_6)_3.9H_2O.2NH_4PF_6$

$[Os(bpy)_2(P3P)_2](PF_6)_2$ (151 mg, 1.27 x 10^{-4} mol) and $[Ru(bpy)_2Cl_2].2H_2O$ (66 mg, 1.27 x 10^{-4} mol) were heated at reflux in 20 cm^{-3} of dry MeOH for 6 hours. After this time, the reaction was allowed to cool to room temperature and the solvent removed to dryness *in vacuo*. The product was added as a solid to a saturated aqueous solution of ammonium hexafluorophosphate, and the chloride salt was converted instantly to the

PF_6^- salt and was precipitated instantly as a dark green/ brown powder. The product was isolated by filtration and washed with a minimum amount of ice-water and diethyl ether and allowed to dry. No further purification of the complex was carried out and the reaction yielded 165 mg of the desired dinuclear product. (73 % yield).

^{1}H NMR (400 MHz, d_6-acetone) δ = 10.10 (d, 1H), 9.05 (m, 2H), 8.87 (m, 2H), 8.55 (m, 15H), 7.96 (m, 17H), 7.70 (m, 2H), 7.29 (m, 9H).
Total = 48 aromatic protons.

Elemental Analysis for $C_{66}H_{86}N_{14}Os_1Ru_1O_9P_5F_{30}$: Calculated C 35.17, H 3.42, N 8.70. Found C 35.35, H 2.79, N 7.77 %.

Synthesis of $[Os(bpy)_2(PEP)_2(bpy)_2RuCl](PF_6)_3.4H_2O$

$[Os(bpy)_2(PEP)_2](PF_6)_2$ (78 mg, 6.74 x 10^{-5} mol) and $[Ru(bpy)_2Cl_2].2H_2O$ (35 mg, 6.74 x 10^{-5} mol) were heated at reflux in 20 cm^{-3} of dry MeOH for 6 hours. After this time, the reaction was allowed to cool to room temperature and the solvent removed to dryness *in vacuo*. The product was added as a solid to a saturated aqueous solution of ammonium hexafluorophosphate, and the chloride salt was converted instantly to the PF_6^- salt and was precipitated instantly as a dark green/ brown powder. The product was isolated by filtration and washed with a minimum amount of ice-water and diethyl ether and allowed to dry. No further purification of the complex was necessary and the reaction yielded 53 mg of the desired dinuclear product. (45 % yield).

^{1}H NMR (400 MHz, d_6-acetone) δ = 10.04 (d, 1H), 9.13 (m, 2H), 8.72 (m, 4H), 8.58 (m, 9H), 8.19 (m, 2H), 8.11 (m, 3H), 8.01 (dd, 2H), 7.90 (m, 8H), 7.78 (d, 2H), 7.72 (dd, 2H), 7.52 (m, 8H), 7.44 (m, 3H), 7.37 (dd, 1H), 7.30 (dd, 1H).
Total = 48 aromatic protons.

Elemental Analysis for $C_{66}H_{72}N_{12}O_4Cl_1Os_1Ru_1P_3F_{18}$: Calculated C 42.16, H 3.07, N 9.22. Found C 42.65, H 2.75, N 8.90 %.

7.3 Discussion of the Synthesis of the Dinuclear Complexes:

The dinuclear complexes have been synthesised using the mononuclear precursors discussed in Chapter 6 as starting materials. Figure 7.1 illustrates the expected mechanism of reaction.

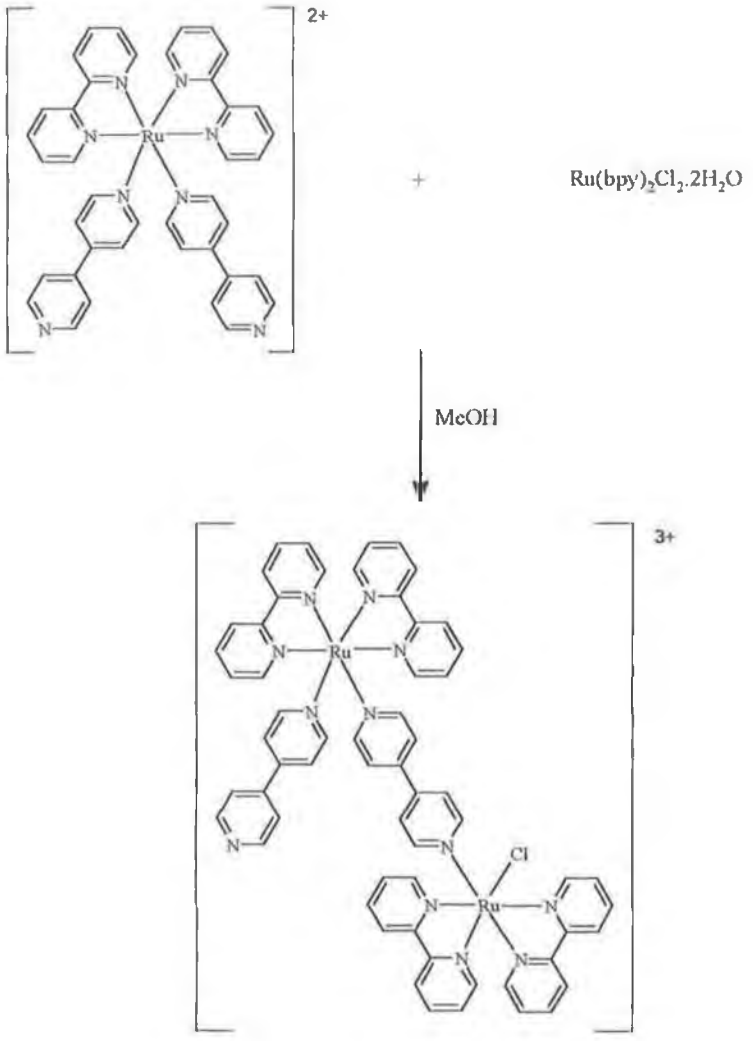

Figure 7.1 Schematic of the expected synthesis of the complex $[Ru(bpy)_2(POP)_2(bpy)_2RuCl]^{3+}$.

The dinuclear complexes have been synthesised with the intention of attaching the free nitrogen of the second pendant arm to a surface, and examining the properties of the complexes while bound to a surface. A representation of this can be seen in Figure 7.2.

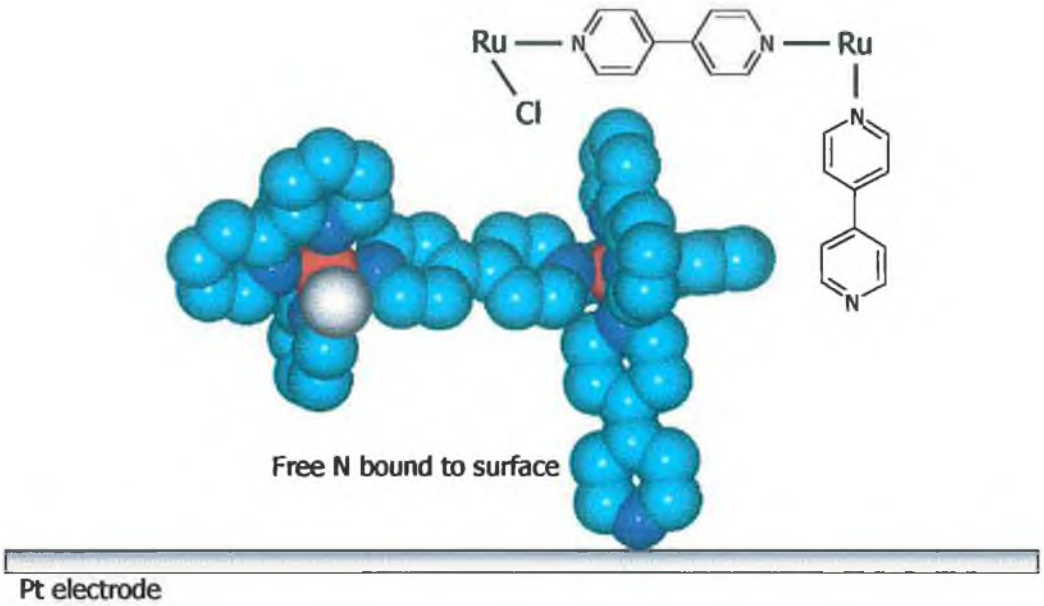

Figure 7.2 Illustration of the complex $[Ru(bpy)_2(POP)_2(bpy)_2RuCl]^{3+}$ bound to the surface via the free nitrogen of the pendant 4,4-bipyridyl

Figure 7.1 is a simplified version of the reality, and the synthesis of the dinuclear complexes proved much more problematic than at first expected. Several problems were discovered and overcome. In order to successfully synthesise the desired pure dinuclear complexes, the purity of the starting materials should be very high. Once the purity of the mononuclear starting materials was determined it was believed the synthesis of the dinuclear complexes would simply involve a 1:1 reaction of the pure monomeric starting material with $[Ru(bpy)_2Cl_2].2H_2O$. As so happens this is the case, but several complications arose. As in the previous chapters the reactions were monitored by HPLC and TLC, and each reaction mixture seemed to give a myriad of products. At no stage did HPLC reveal the disappearance of both the starting materials and the appearance of a single product peak.

After many attempted syntheses and little or no success, a different approach was needed. Instead of assuming the reaction has not worked, and that the HPLC and TLC results were an accurate representation of the actual reaction mixture, it was decided to by-pass these techniques, and to use ^{1}H NMR as the primary characterisation tool, of both the reaction mixture and of the final product. From this it was discovered that the complex was actually being synthesised in reasonable yield, but analysis of the complex by HPLC and by TLC was causing it to either disintegrate on the column or change in such a way as to appear impure under the conditions being used to analyse the purity.

It was realised at this stage that the problems were arising for two separate reasons. The first due to the lability of the chloride ion in aqueous solution, and the second due to the fact that the ligands are monodentate and therefore less securely bound to the metal than bidentate ligands achieve. [1,2,3,4,5,6] These problems have been discussed in more detail in Section 6.3. While the reaction between the $[M(bpy)_2(PnP)_2](PF_6)_2$ monomer and $[Ru(bpy)_2Cl_2].2H_2O$ was carried out in MeOH, the mobile phase being used on the HPLC was 80% MeCN, 20% **H_2O** and 0.08M $LiClO_4$. It was entirely possible therefore that pure $[M(bpy)_2(PnP)_2(bpy)_2RuCl]^{3+}$ dinuclear complex was being injected onto the column from the reaction mixture, but under the conditions being used, this compound was breaking down and exchanging the monodentate ligands causing several products to elute including the aquo dinuclear complex. Based on this assumption, the following complexes may be detected by HPLC analysis of a pure dinuclear complex. (Figure 7.3)

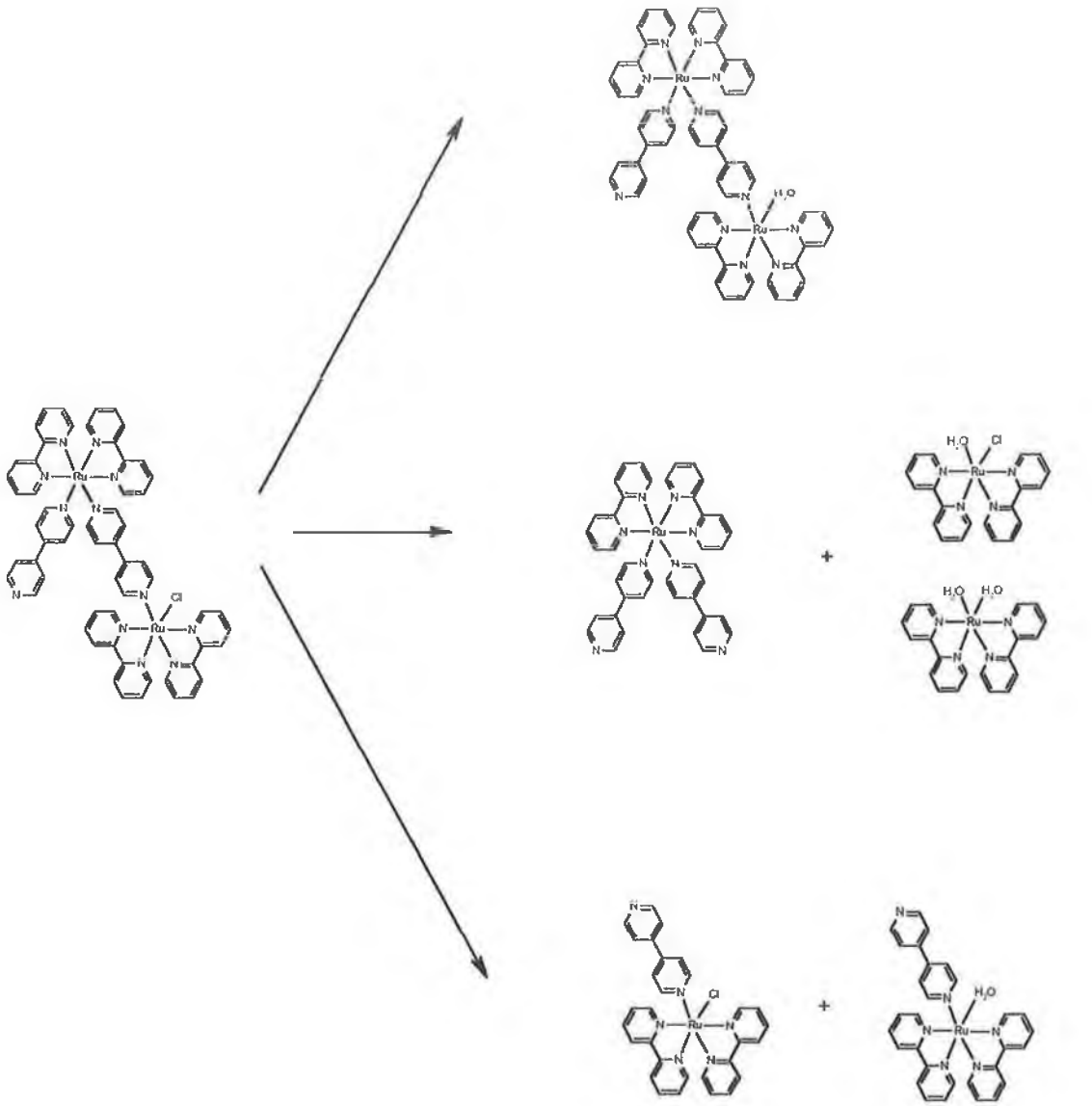

Figure 7.3 Disintegration of the $[Ru(bpy)_2(POP)_2(bpy)_2RuCl]^{3+}$ dinuclear complex could lead to formation of the above compounds by HPLC analysis.

Evidence for this can be seen in Figure 7.4 which is the actual HPLC trace from the complex $[Ru(bpy)_2(POP)_2(bpy)_2RuCl]^{3+}$. The complex before injection is pure by ^1H NMR.

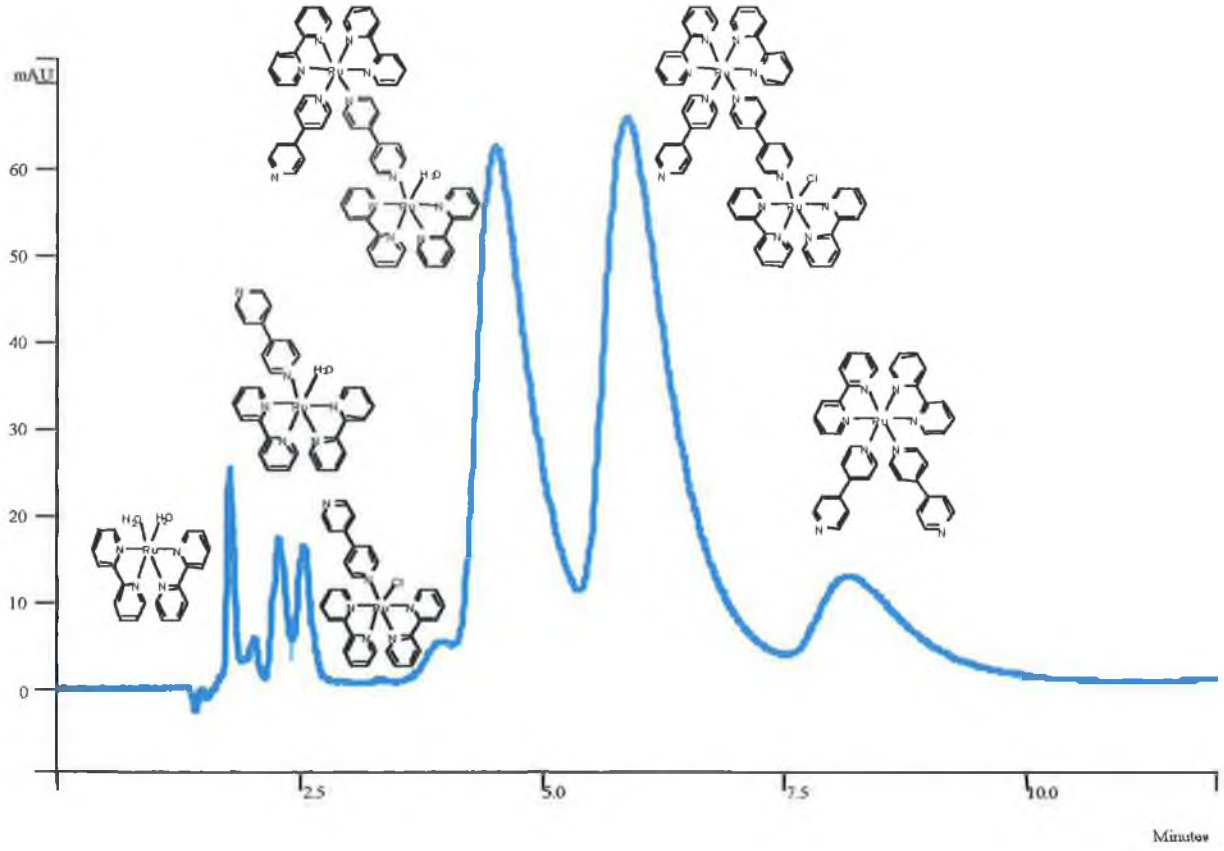

Figure 7.4 Actual HPLC trace of injection of reaction mixture to synthesise $[Ru(bpy)_2(POP)_2(bpy)_2RuCl]^{3+}$

The products have been assigned by comparison of the retention times under the conditions used to previously synthesised products and by known UV/Vis spectra. [2,3,6]

It was decided therefore to use ^1H NMR to analyse the purity of the complexes straight from the reaction rather than HPLC or TLC. Synthesis was carried out in spectroscopy grade MeOH which would contain less water, and hopefully lead to less by-products This approach proved effective, and analysis of the complexes by ^1H NMR in d_6-DMSO,

before conversion from chloride salts to PF_6^- salts, indicated that the compounds had indeed been synthesised in high yield and were reasonably pure. The chloride counter ion was replaced by a PF_6^- counter ion which led to the precipitation of the complex from an aqueous solution. The insolubility of the PF_6^- salts of the complexes in water prevents the chloride from exchanging with water to form the aquo complex.

7.4 ^{1}H NMR of the dinuclear complexes:

In Chapter 6, the spectra of the complexes of the type $[M(bpy)_2(PnP)_2]^{2+}$ were possible to assign. This was because a plane of symmetry existed through the molecule. This symmetry was reflected in the ^{1}H NMR spectra and lead to half the number of expected signals with each signal integrating to two equivalent protons. The ^{1}H spectrum of the complexes of the type $[Ru(bpy)_2(PnP)Cl]^+$ were more complicated. As has already been explained in Chapter 6, the chloride ion removes the symmetry resulting in a more complicated aromatic region with each proton having a discrete signal, many of which overlap. This complexity has made the ^{1}H NMR difficult to assign.

The ^{1}H NMR of the dinuclear complexes is expected to closely resemble the spectrum of the two monomers combined. This is however a simplistic approach as illustrated by Figure 7.5. The ^{1}H NMR spectrum of the dinuclear complex will contain both types of H6 protons, i.e. the H6 protons which interacts with the PnP ligand, and the H6 proton which interacts with the Cl^- ion. However, in the case of the N6 monomer, the H6 protons interacting with the PnP ligand were equivalent. On addition of the N5 chloro moiety to the N6 complex, the two PnP ligands become inequivalent, with one remaining free (for binding to a surface) while the second pendant arm becomes the bridging ligand between the two metal centres.

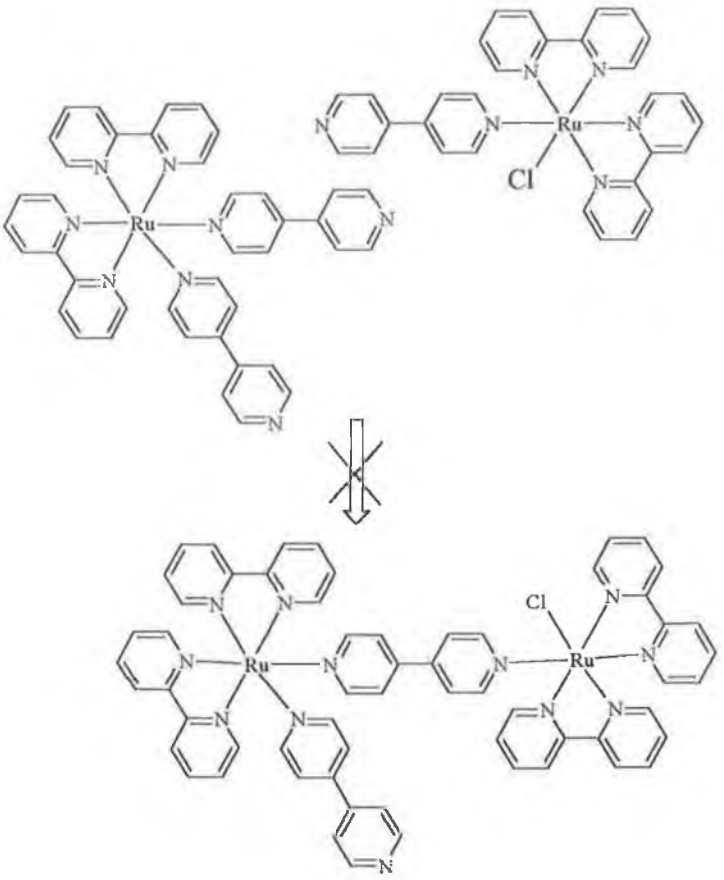

Figure 7.5 Why the addition of the spectra of the two monomers does not give the ^1H NMR spectrum of the dinuclear complex...

This means that the spectrum of the dinuclear complex will differ from the sum of the monomers in two ways. Firstly, the PnP ligands have become inequivalent. The H6 proton over the chloride ion should appear at similar ppm, however the fingerprint H6 protons for the N6 species in the dinuclear complex now split into two separate N6 protons – one hanging over the free PnP ligand, the other over the now bridging PnP ligand.

The diagrams on the next page illustrate these points. The first spectrum consists of the spectra of the two monomers, $[Ru(bpy)_2(POP)_2]^{2+}$ and $[Ru(bpy)_2(POP)Cl]^+$ while the second spectrum is that of the dinuclear complex $[Ru(bpy)_2(POP)_2(bpy)_2RuCl]^{3+}$. All spectra have been performed in d_6-acetone.

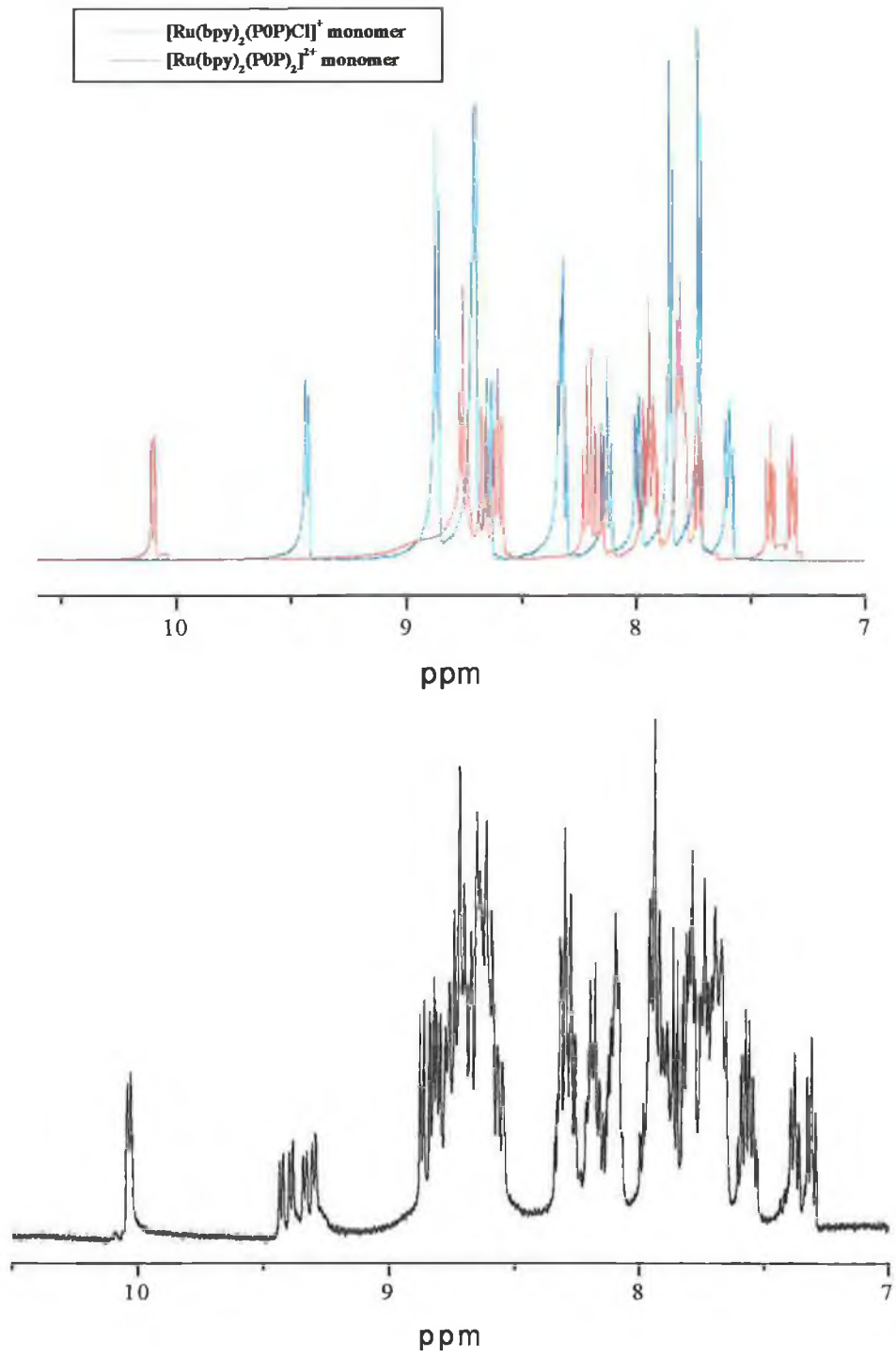

Figure 7.6 Sum of the ^1H NMR spectra of the monomers, $[Ru(bpy)_2(P0P)_2]^{2+}$ and $[Ru(bpy)_2(P0P)Cl]^+$ (above) and $[Ru(bpy)_2(P0P)_2(bpy)_2RuCl](PF_6)_3$ (below) in d_6-acetone.

The reasons for the differences between the spectra illustrated in Figure 7.6 have been given already (Figure 7.5). However, the expected similarities between the combined spectra and the actual spectrum can be seen. The positioning of the "fingerprint" H6 protons are similar for both spectra. As expected the H6 protons over the now inequivalent PnP ligands are split (i.e. one free PnP ligand, one bridging PnP ligand), and the region from 9.25 to 9.45 ppm integrates as two protons. The ^{1}H NMR spectra of the other dinuclear complexes are very similar to that of $[Ru(bpy)_2(POP)_2(bpy)_2RuCl]^{3+}$. Some representative spectra are shown in the Figure 7.7 and 7.8.

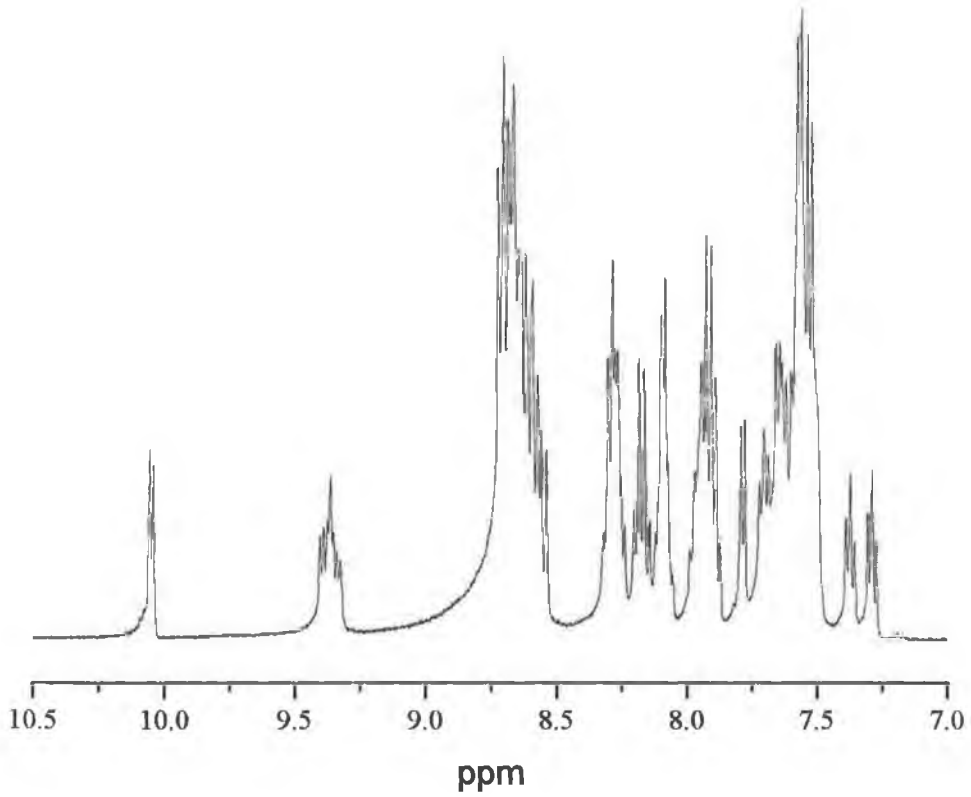

Figure 7.7 ^{1}H NMR of $[Ru(bpy)_2(PEP)_2(bpy)_2RuCl](PF_6)_3$ in d_6-acetone.

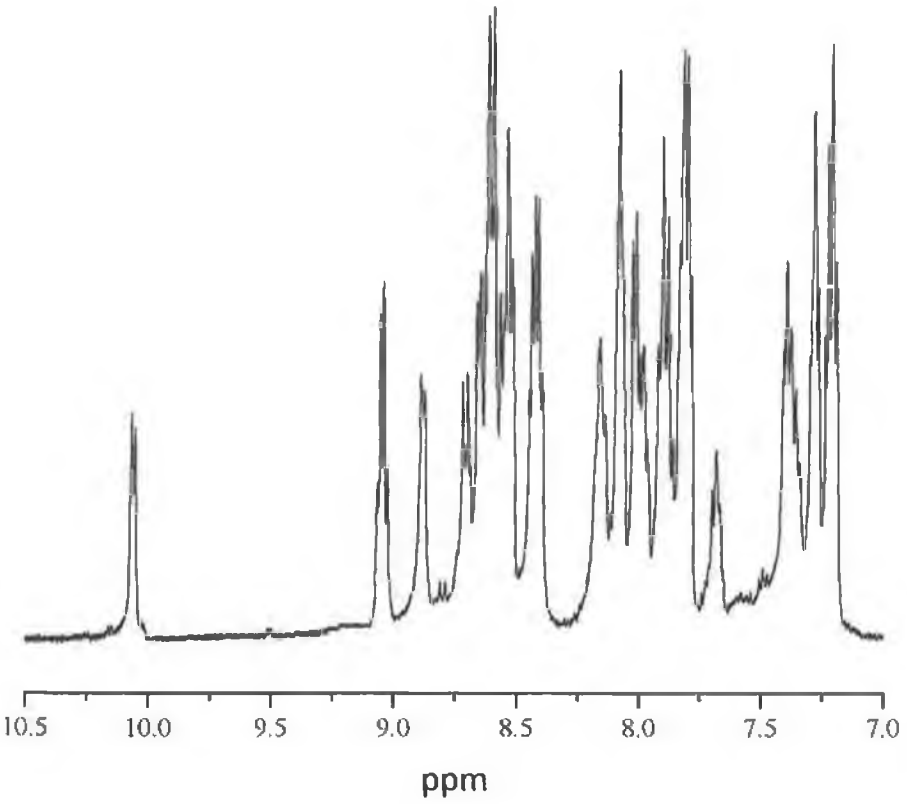

Figure 7.8 ^1H NMR of $[Os(bpy)_2(P2P)_2(bpy)_2RuCl](PF_6)_3$

The table below lists the positioning of both sets of H6 protons. Comparison is possible with the ^1H NMR data found in Tables 6.4, 6.5, 6.6 and 6.8.

Compound	H6 over Cl^-	H6 over PnP ligands
	1 proton	2 protons
$[Ru(bpy)_2(P0P)_2(bpy)_2RuCl]^{3+}$	10.03 (d)	9.35 (m)
$[Ru(bpy)_2(P2P)_2(bpy)_2RuCl]^{3+}$	10.08 (d)	9.24 (m)
$[Ru(bpy)_2(P3P)_2(bpy)_2RuCl]^{3+}$	10.06 (d)	9.24 (m)
$[Ru(bpy)_2(PEP)_2(bpy)_2RuCl]^{3+}$	10.04 (d)	9.36 (m)
$[Os(bpy)_2(P0P)_2(bpy)_2RuCl]^{3+}$	10.04 (d)	9.18 (m)
$[Os(bpy)_2(P2P)_2(bpy)_2RuCl]^{3+}$	10.08 (d)	9.05 (m)
$[Os(bpy)_2(P3P)_2(bpy)_2RuCl]^{3+}$	10.10(d)	9.05 (m)
$[Os(bpy)_2(PEP)_2(bpy)_2RuCl]^{3+}$	10.04 (d)	9.13 (m)

Table 7.1 ^1H NMR data from the Ru-Ru and Os-Ru dinuclear complexes.

Table 7.1 lists the positions of the two fingerprint H6 protons present for the series of dinuclear complexes. The positioning of the H6 over the Cl^- protons are very similar for each of the complexes, with the chemical shift varying from 10.03 – 10.10 ppm. The two protons over the PnP ligands are less similar and vary from 9.05 – 9.36 ppm.

7.5 Absorption and Emission of the $[Ru(bpy)_2(PnP)_2(bpy)_2RuCl]^{3+}$ dinuclear complexes:

The discussion of the absorption and emission of these complexes is divided into several sections. The first and most obvious division is between the Ru-Ru dinuclear complexes and the Os-Ru dinuclear complexes. Within each of these sections other subdivisions, based on the nature of the bridging ligand are possible, i.e. those complexes containing P0P and PEP ligands, vs those containing the P2P and P3P ligands. The absorption spectra of the Ru-Ru dinuclear complexes can be seen in Figure 7.9.

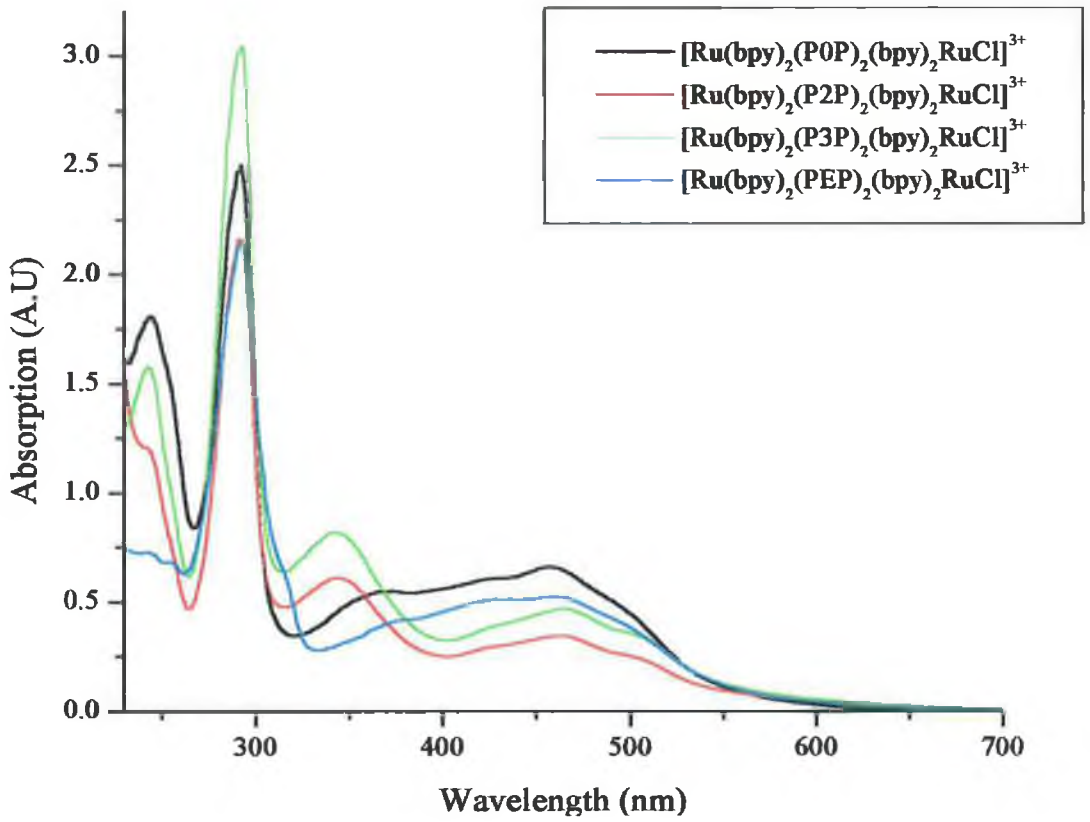

Figure 7.9 UV of the Ru-Ru PnP dinuclear complexes in MeCN.

The data from the absorption and emission spectra of the complexes $[Ru(bpy)_2(PnP)_2(bpy)_2RuCl]^{3+}$ have been collated in Table 7.2. The behaviour observed allows the complexes to be divided into groups based on the properties of the bridging ligand. This will be explained in more detail.

Complex	Absorption (nm)	ε (x10) ($molcm^{-1}$)	Emission, 298K (nm)	Emission, 77K (nm)
$[Ru(bpy)_2(P0P)_2(bpy)_2RuCl]^{3+}$	290	1.08		
	368	.24	612	582
	458	.66	718	666
	490 (sh)	.22		
$[Ru(bpy)_2(PEP)_2(bpy)_2RuCl]^{3+}$	291	1.19		
	372	.23	612	600
	457	.30	719	680
	497 (sh)	.15		
$[Ru(bpy)_2(P2P)_2(bpy)_2RuCl]^{3+}$	291	1.03		
	343	.29	620	593
	462	.35	717	657
	503 (sh)	.25		
$[Ru(bpy)_2(P3P)_2(bpy)_2RuCl]^{3+}$	291	1.16		
	340	.31	620	593
	464	.18	717	658
	507 (sh)	.13		

Table 7.2 Absorption and emission data of the Ru-Ru PnP dinuclear complexes in MeCN. (77K experiments in butyronitrile)

The absorption spectra of the complexes can be assigned easily by comparison to the monomers assuming there is a contribution from both subunits. Before more detailed examination of the data presented in Table 7.2 is carried out, special attention should be paid to the lowest energy absorption bands. As discussed in Section 6.3, the lability of the chloride ion and exchange of the monodentate coordinated PnP ligands are serious problems for the ruthenium centred complexes. [1,4,5,6] The products resulting from either the exchange of the chloride or the PnP ligand are readily identifiable by the resulting UV/Vis spectra. [6] The lowest energy absorption band on the dinuclear complexes consists of a shoulder that appears to have a λ_{max} of between 490 nm and 507 nm.

Previous studies [5] allow this to be confidently assigned as due to the RuN5-Cl, providing strong proof that the complex is intact and in the desired form.

Each of the complexes contain absorption bands at *circa* 290 nm that can be assigned as ligand centred (LC) $\pi \rightarrow \pi^*$ (bpy) based transitions. The extinction coefficients of these transitions should be discussed. For the monomer, ε was generally calculated as being *circa* 5×10^4 $mol^{-1}cm^{-1}$ for the transitions centred at 290 nm. This value has more than doubled in the case of the Ru-Ru PnP dinuclear complexes and is typically 1.1×10^5 $mol^{-1}cm^{-1}$.

The absorption band in the region 320 nm to 400 nm, by comparison to the absorption spectra of the monomeric complexes, may be attributed to the introduction of the PnP ligands into the complex and that this band may be attributed to ligand centred (LC) $\pi \rightarrow \pi^*$ transitions on the PnP ligands. Of most interest however are the $d\pi \rightarrow \pi^*$ metal to ligand charge transfer (MLCT) bands. For the dinuclear complexes, two contributions are expected in the region 400 – 500 nm. The RuN6 monomers have a MLCT centred at *circa* 450 nm while the RuN5Cl complexes the MLCT band is centred at *circa* 490 nm. Both of these bands are observed in the spectra of the dinuclear complexes, often with the contribution of the RuN5Cl moiety appearing as a shoulder of the more intense band centred around 450 nm. As expected, the extinction coefficients of the MLCT bands of the dinuclear complexes are typically 3×10^{-4} $mol^{-1}cm^{-1}$ which corresponds roughly to the sum of the extinction coefficients of the MLCT bands of the mononuclear complexes.

After discussing the general trends in the spectra of the dinuclear complexes, more specific examination of the data is necessary and as mentioned the dinuclear complexes can be split into two separate groups. This division is based on the interaction between the metal centres. Much attention has focussed on the interaction between metal centres in polynuclear systems through bridging ligands in recent years, and the results of the studies using the PnP ligands have been presented in the introduction to Chapter 6. The behaviour of the complexes bridged by the POP and PEP ligands differs from that of the

P2P and P3P ligands. The POP ligand (4,4'-bipyidyl) is an aromatic ring system while the PEP ligand contains two 4'-pyridyl rings bridged by a conjugated ethylene spacer unit. The 4'-pyridyl rings of the P2P and P3P ligands are bridged by saturated -CH_2-CH_2- linkages and (-CH_2-CH_2-CH_2) for P3P.

The PnP bridging ligand is expected to play an important part in the determination of the level of communication between metal centres in a dinuclear complex. Is there evidence of this therefore from the photophysical data? The answer is yes, and a simple experiment has provided graphic evidence of this. Equimolar amounts of the monomeric subunits of the dinuclear complex were combined and absorption spectra of this mixture was examined. Comparison of the spectra of this mixture is made to the dinuclear complex, the results can be seen in Figure 7.10.

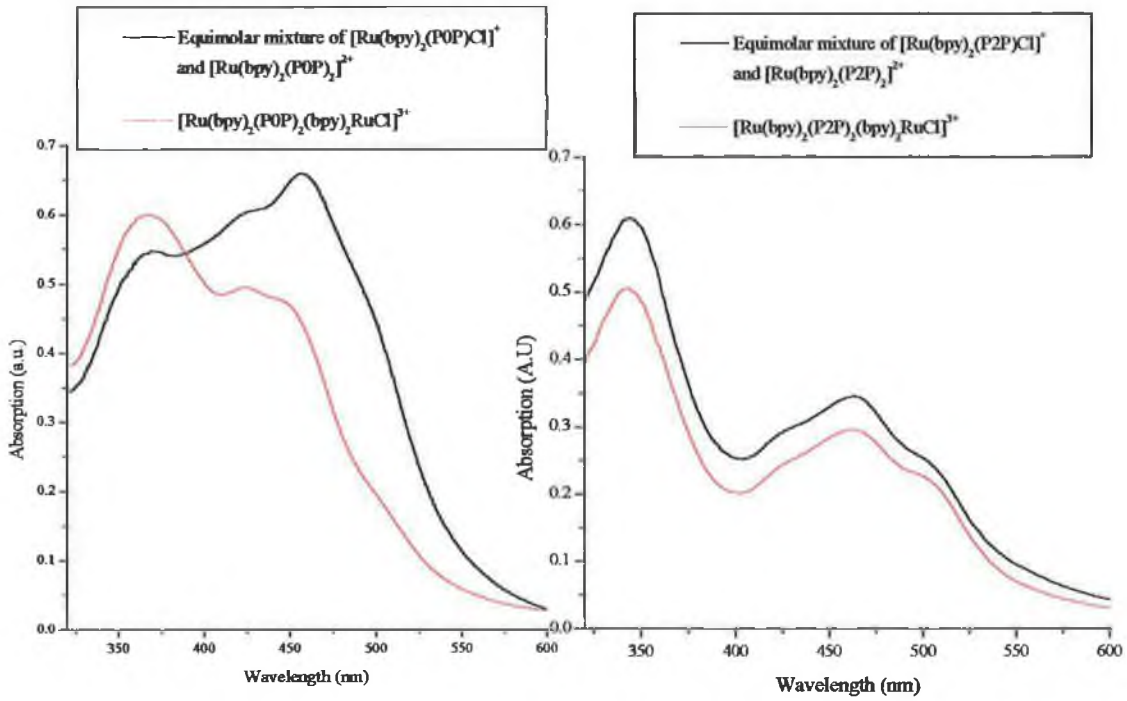

Figure 7.10 Absorption spectra of equimolar solutions of the two monomer components compared to the absorbance of the dinuclear complex. All measurements in MeCN.

This experiment is based on the assumption that if communication between the metal centres is weak, the absorption spectra of the dinuclear complex should closely resemble

that of the sum of the mononuclear components. The absorption spectra on the left have clear differences whereas the spectra on the right are very similar. This clearly illustrates that the bridging ligand POP (and by extension, PEP) facilitates electronic interaction between the two ruthenium metal centres. This communication leads to different (or new) bands in the absorption spectra of the dinuclear complex compared to the sum of the monomers. For the P2P (and P3P) ligand(s), this is not observed. Due to the absence of an extended π system the two ruthenium groups behave as non-interacting chromophores and the absorption spectrum of the dinuclear complex closely resembles that achieved for an equimolar solution of the monomers.

The investigation outlined in Figure 7.10 was performed for a series of similar dinuclear complexes, $[(bpy)_2ClRu(L)RuCl(bpy)_2]^{2+}$ where bpy is 2,2'bipyridine and L = POP, PEP and P2P by Powers and Meyer.[7] The UV/Vis spectra of the series of dinuclear complexes are all similar and the spectra of the mixed valence ions in the UV/Vis spectral region are nearly the sum of the spectra of $[(bpy)_2ClRu^{II}(L)]^{+}$ and $[(bpy)_2ClRu^{III}(L)]^{2+}$.

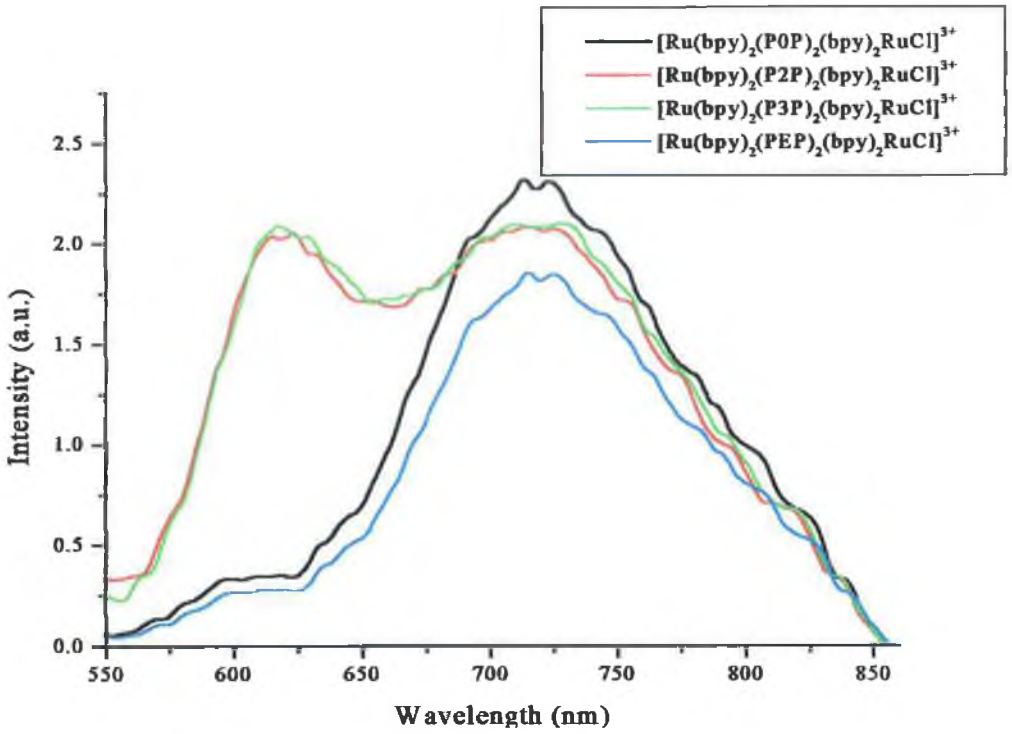

Figure 7.11 Room temperature emission of the Ru-Ru PnP dinuclear complexes in MeCN.

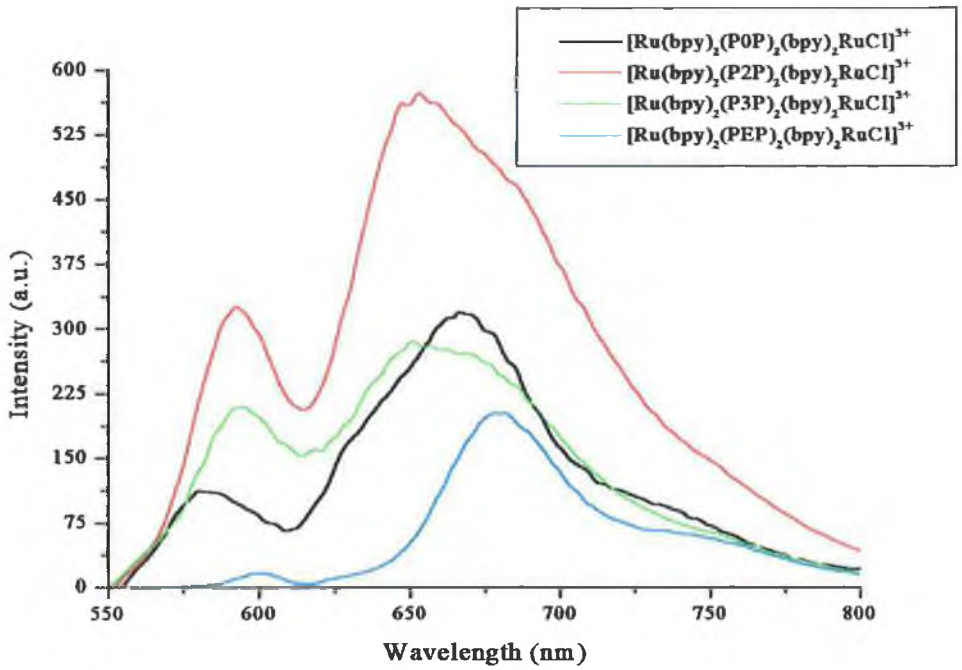

Figure 7.12 Low temperature emission of the Ru-Ru PnP complexes at 77K in MeCN.

The observations made for the absorption spectra, and the conclusions reached after comparison of the equimolar solutions of monomer with the dinuclear complex are verified by analysis of the emission spectra of the complexes.

At room temperature (Figure 7.11) the dinuclear complexes $[Ru(bpy)_2(\mathbf{P2P})_2(bpy)_2RuCl]^{3+}$ and $[Ru(bpy)_2(\mathbf{P3P})_2(bpy)_2RuCl]^{3+}$ exhibit dual emission corresponding to emission from the RuN6 unit at 620 nm, and emission from the RuN5Cl unit at 717 nm. The emissions have been assigned by comparison of these emission spectra to the monomers. (Section 6.5) The complexes of the **P0P** and **PEP** ligands also seem to have a dual emission. The relative intensities of the emissions are completely different than found for the **P2P** and **P3P** ligands. The emission centred on the N5-Cl units (718 nm) appears much stronger than that from the N6 unit (612 nm). This agrees with the assumption that there is increased communication between the metal centres. The emission of the RuN5Cl monomer occurs at lower energy than the RuN6 monomer emission. It is logical therefore that energy transfer should be directed from the RuN6 centre of the dinuclear complex to the N5-Cl moiety and quenching of the emission centred on the RuN6 relative to the emission of the RuN5Cl moiety is observed.

The situation is different at 77K. All complexes exhibit dual emission characteristics. Unlike at room temperature where a very weak emission is attributed to the RuN6 moiety for the P0P and PEP bridged dinuclear complexes, this emission is stronger and the ratio between the relative intensities of the emissions are closer. This can be explained as for other biphenyl-like molecules.[8] At room temperature, in solution, the pyridyl rings of the PnP ligands will be twisted away from co-planarity due to steric effects, but after addition of an electron the rings will become almost planar to maximise delocalisation. Therefore in the ground state the preferred conformation of the POP bridging ligand is expected to be twisted while following optical excitation, the bridging ligand in the excited state is expected to adopt the flattened configuration. At 77K the ligand is unable to adopt the planar configuration and its ability to act as an electron

acceptor is greatly reduced and the photophysics are much the same as for that of the P2P bridged dinuclear complex. However in fluid solution, the bipyridine rings of the PnP ligands are free to become planar and act as an extremely efficient electron trap. This leads to dual emission at 77K which is not observable at room temperature.

This type of dual emission behaviour has been observed before. DeCola et al study photoinduced energy and electron transfer through rigid spacers. [9] The bridging ligand used, 1-4-bis[2-(2,2'-bipyridine-5-yl)ethenyl]bicyclo[2.2.2]octane, contains a bicyclooctane unit linked to two **ethylene-type** units. The homonuclear Ru-Ru and Os-Os complexes as well as the heteronuclear Ru-Os dinuclear complexes have been synthesised. In all these complexes, each Ru-based and Os-based unit displays its own absorption spectrum and electrochemical properties, regardless of the presence of a second metal unit. The homometallic dinuclear complexes exhibit the same luminescence properties as the corresponding mononuclear species. In the heteronuclear Ru-Os complex, 91% of the Ru-based luminescence intensity is quenched by energy transfer to the Os-based unit.

So far, the nature of the emission has not been discussed. The determination of the nature of the emissive state is not as straightforward as for the complexes discussed in Chapters 3, 4 and 5. The PnP ligands are bipyridine based, and should the emission be other than 2,2' bipyridyl based, the differences in the energy will be small. Examination of the reduction potentials (Chapter 7.9) of the complexes reveal a similar pattern to that found for the emissive properties of the dinuclear complexes. The first reduction potentials (i.e. the least negative) for the Ru-Ru P0P and PEP complexes occur at less negative potentials than those observed for the P2P and P3P complexes, and are less negative than those observed for $[Ru(bpy)_3]^{2+}$. This may indicate that the excited state of the P0P and PEP complexes may lie on the bridging ligands, while the excited state of the P2P and P3P complexes lie on the 2,2-bipyridyl units. In order to prove this however further examination of the photophysical and electrochemical properties of the complexes will need to be completed.

7.6 Luminescence Lifetimes Results for the $[Ru(bpy)_2(PnP)_2(bpy)_2RuCl]^{3+}$ dinuclear complexes:

The luminescence lifetime data are presented below. The lifetimes have been obtained using the single photon counting technique (Chapter 2.5). The room temperature measurements have been performed in MeCN while the 77K measurements have been performed in butyronitrile.

Compound	298K, Deaerated, τ (ns)	77K, τ (ns) ex. RuN6	77K, τ (ns) ex. RuN5-Cl	Relative Contribitions (%)
$[Ru(bpy)_2(\mathbf{P0P})_2(bpy)_2RuCl]^{3+}$	3	7,000	7,000	76
	25		2,000	24
$[Ru(bpy)_2(\mathbf{PEP})_2(bpy)_2RuCl]^{3+}$	1	6,000	6,000	60
	50		1,000	40
$[Ru(bpy)_2(\mathbf{P2P})_2(bpy)_2RuCl]^{3+}$	3	6,000	5,700	55
	56		1,200	44
$[Ru(bpy)_2(\mathbf{P3P})_2(bpy)_2RuCl]^{3+}$	6	8,200	5,000	26
	46	1,500	1,200	74

Table 7.3 Luminescent Lifetime Data of the Ru-Ru dimers. Deaerated measurements performed in MeCN. 77K measurements performed in butyronitrile.

As can be seen in Figure 7.11, the complexes exhibit dual emission at room temperature. The room temperature data have been collected in the maximum of emission, that is in this case the maximum of the low energy emission in the dual emitting complexes. The lifetime decays have been best fitted using bi-exponential decay profiles. The lifetime data can be assigned by comparison to that found for the monomeric complexes. The deaerated lifetimes correspond closely with those found for

the $[Ru(bpy)_2(PnP)_2]^{2+}$ complexes (1.1 - 2.9 ns) and the $[Ru(bpy)_2(PnP)Cl]^{+}$ complexes (29 – 37 ns). The two lifetimes observed for the Ru-Ru dinuclear complexes correspond to emission from the RuN6 moiety and from the RuN5-Cl species, with the short lifetime (1 – 6 ns) corresponding to the RuN6 centre and the RuN5-Cl centre is responsible for the longer lived excited state (25 – 56 ns).

At 77K, because of the relatively more intense emission from the RuN6 species it was decided to measure the excited lifetimes in the maxima of both emissions. The results can be seen in Table 7.3. Again the data can be assigned by comparison to the monomeric components of the dinuclear complexes. At 77K, the lifetimes of the $[Ru(bpy)_2(PnP)_2]^{2+}$ complexes range from 3,700 ns – 4,200 ns, while the lifetimes of the $[Ru(bpy)_2(PnP)Cl]^{+}$ complexes range from 580 ns – 700 ns.

The lifetimes recorded for the dinuclear complexes in the high energy emission (i.e. the emission from the RuN6 centre can be fitted as a single decay with a lifetime of between 6,000 and 8,200 ns, with the exception of the $[Ru(bpy)_2(\mathbf{P3P})_2(bpy)_2RuCl]^{3+}$ complex which has a contribution from a species with a shorter lifetime. The long lived excited states are comparable to those observed for the $[Ru(bpy)_2(PnP)_2]^{2+}$ complexes in that they are > 4μs. The data collected in the lower energy emission had a biexponential decay profiles. The longer lived excited state again is assigned to the RuN6 centre, although in this instance the relative contribution is much less than the shorter lived excited states, (1,000 ns – 2,000 ns) which can be attributed to the RuN5Cl centres.

7.7 Absorption and Emission of the $[Os(bpy)_2(PnP)_2(bpy)_2RuCl]^{3+}$ dinuclear complexes:

The absorption and emission spectra of the Os-Ru PnP dinuclear complexes are discussed. As in the case of the Ru-Ru dinuclear complexes, the four dinuclear complexes can be divided into the two separate groups. There are differences however to the Ru-Ru dinuclear complexes discussed in the previous section and these differences

will be highlighted in this section. The absorption spectra of the dinuclear complexes can be seen in Figure 7.13.

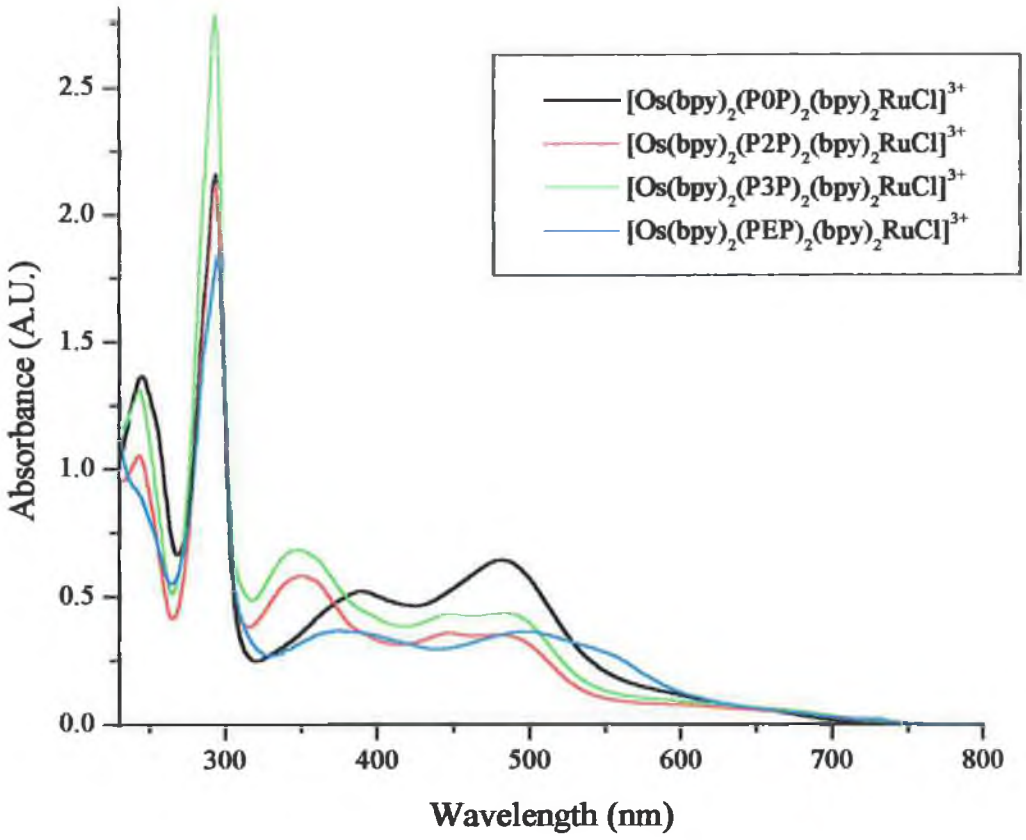

Figure 7.13 Absorption spectra of the $[Os(bpy)_2(PnP)_2(bpy)_2RuCl]^{3+}$ dinuclear complexes in MeCN.

It is important to verify whether the description of the interaction between the metal centres of the Ru-Ru dinuclear complexes can be used to describe the behaviour of the dinuclear complexes being examined in this section. As in the previous section equimolar amounts of the monomeric subunits of the dinuclear complex were combined and compared with the spectrum obtained for the appropriate dinuclear complex. (Figure 7.14). The absorption and emission data are listed in Table 7.4.

Complex	Absorption (nm)	ε (x10) ($mol^{-1}cm^{-1}$)	Emission, 298K (nm)	Emission, 77K (nm)
$[Os(bpy)_2(\mathbf{P0P})_2(bpy)_2RuCl]^{3+}$	292	1.26	740	723 644 (weak)
	389	.31		
	482	.38		
	600 (sh)	.11		
$[Os(bpy)_2(\mathbf{PEP})_2(bpy)_2RuCl]^{3+}$	294	1.21	741	734 652 (weak)
	373	.25		
	497	.25		
	625 (sh)	.06		
$[Os(bpy)_2(\mathbf{P2P})_2(bpy)_2RuCl]^{3+}$	292	1.02	758	654 742
	347	.28		
	445	.18		
	484	.18		
	594 (sh)	.04		
$[Os(bpy)_2(\mathbf{P3P})_2(bpy)_2RuCl]^{3+}$	292	.99	757	648 742
	346	.25		
	446	.17		
	487	.17		
	598 (sh)	.03		

Table 7.4 Absorption and emission data of the Os-Ru PnP dinuclear complexes in MeCN.

Unlike the Ru-Ru dinuclear complexes, the possible products resulting from either the exchange of the chloride or the PnP ligand are not readily identifiable by the resulting UV/Vis spectra [6] in the case of the Os-Ru complexes because of the formally forbidden $d\pi \rightarrow \pi^*$ bpy MLCT transitions, which becomes partially allowed due to the increased spin orbit coupling associated with the larger osmium ion. [10] As discussed in Section 6.3, the lability of the chloride ion and exchange of the monodentate coordinated PnP ligands are serious problems for the ruthenium centred complexes. [1,4,5,6] The bands, with

maxima between 482 nm and 499 nm are most likely due to the Ru-N5Cl moiety. The electrochemistry of the complexes adds to the proof that the complex has retained the chloro moiety.

The sum of the absorption spectra of the monomers is most closely replicated by the dinuclear complex containing the **P2P** ligand. This agrees with the results of the Ru-Ru dinuclear complexes, and allows us to predict that the **P0P** and **PEP** bridging ligands are more able to facilitate interaction between the osmium and ruthenium metal centres in the dinuclear complexes of the type $[Os(bpy)_2(PnP)_2(bpy)_2RuCl]^{3+}$, whereas the non-conjugated bridging ligands, **P2P** and **P3P** cause the metal centres to behave independently. (Figure 7.14)

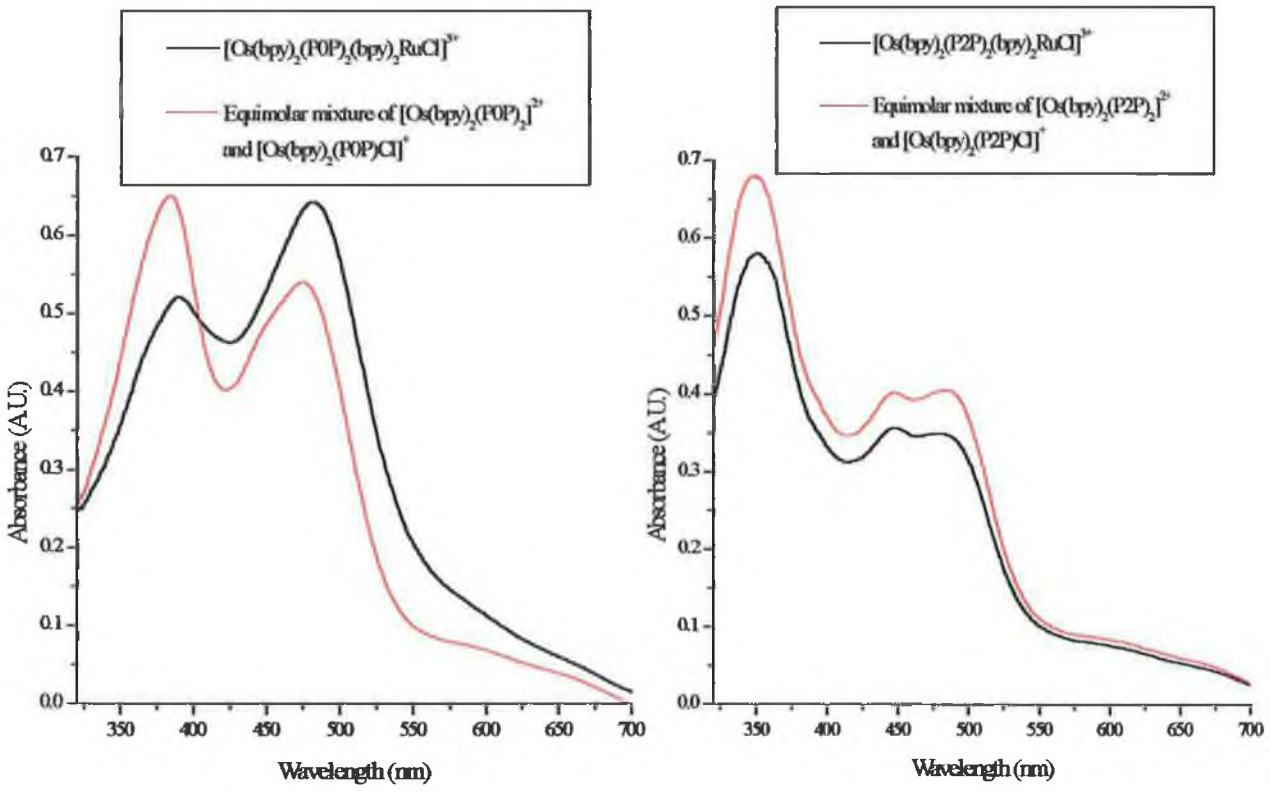

Figure 7.14 Absorption spectra of equimolar solutions of the two monomer components compared to the absorbance of the dinuclear complex. All measurements in MeCN.

The Os-Ru PnP dinuclear complexes exhibit luminescence at room temperature and at 77K. The results are different to those of the Ru-Ru PnP dinuclear complexes. Comparison with the emission spectra of the monomer subunits becomes difficult in this instance, since for example the emission of the $[Os(bpy)_2(P2P)_2]^{2+}$ unit is centred at 749 nm while emission from the $[Ru(bpy)_2(P2P)Cl]^{+}$ unit is centred at 730 nm. If, as in the case of the Ru-Ru PnP dinuclear complexes, emission from both centres is observed, the spectra should overlap considerably, making elucidation impossible. The emission spectra of the complexes are given in Figure 7.15.

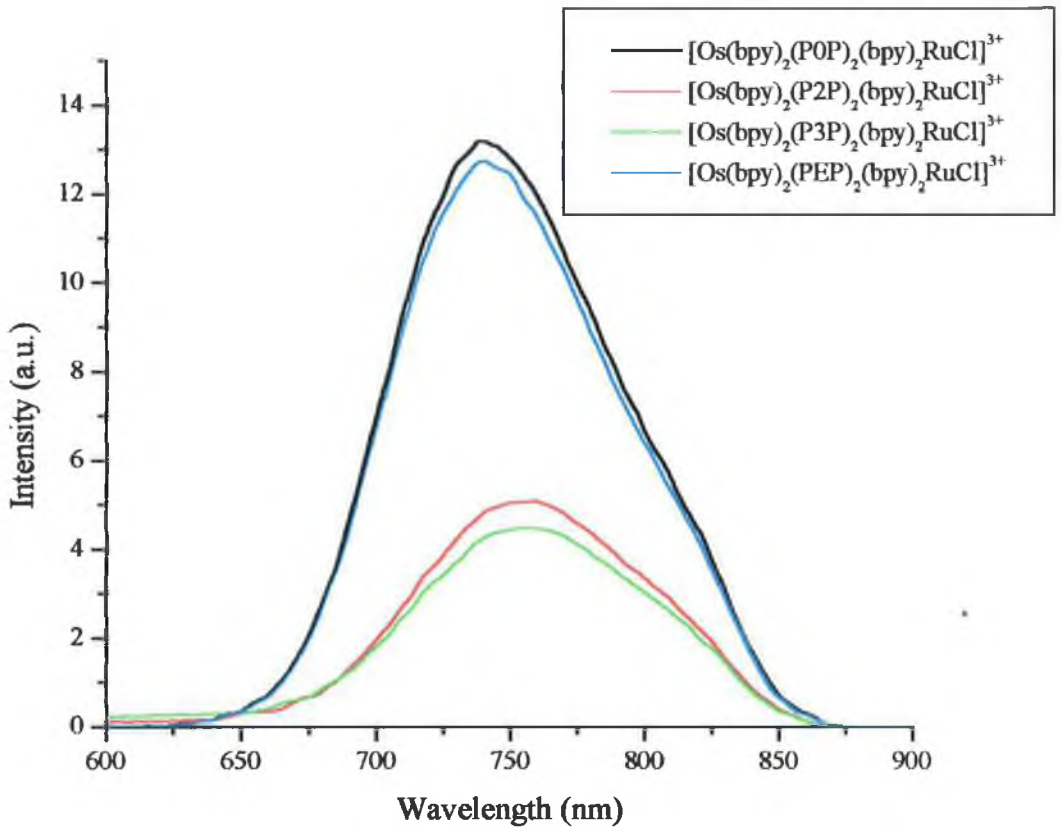

Figure 7.15 Room temperature emission spectra of the Os-Ru PnP dinuclear complexes in MeCN. Spectra have been normalised to allow easier comparison.

At room temperature the emission of both the $[Os(bpy)_2(\mathbf{P2P})_2(bpy)_2RuCl]^{3+}$ and $[Os(bpy)_2(\mathbf{P3P})_2(bpy)_2RuCl]^{3+}$ complexes are centred at 758 nm. Comparison with the monomers allow this to be attributed to emission from the Os centre. It is likely that a

contribution to the emission spectra is made by the RuN5Cl unit but because of the substantial overlap expected it is impossible to quantify.

For the conjugated bridging ligands, where interaction between the metal centres is more likely, the situation is similar. The emission from the $[Os(bpy)_2(\mathbf{P0P})_2(bpy)_2RuCl]^{3+}$ and $[Os(bpy)_2(\mathbf{PEP})_2(bpy)_2RuCl]^{3+}$ complexes are centred at *circa* 740 nm. This compares to an emission centred at 744 nm and 749 nm observed for the $[Os(bpy)_2(P0P)_2]^{2+}$ and $[Os(bpy)_2(PEP)_2]^{2+}$ monomers respectively. Again it is possible a contribution to the emission spectra is made by the RuN5Cl unit but because of the substantial overlap expected this is impossible to quantify.

The situation is changed at 77K. (Figure 7.16) The $[Os(bpy)_2(\mathbf{P0P})_2(bpy)_2RuCl]^{3+}$ and $[Os(bpy)_2(\mathbf{PEP})_2(bpy)_2RuCl]^{3+}$ complexes exhibit a single emission, which is blue shifted in comparison to the room temperature emission (this blue shift has been discussed in previous chapters) and is centred at 723 nm and 734 nm respectively. A very weak emission can also be seen on the high energy side of the intense band which is centred at 644 nm and 652 nm for the $[Os(bpy)_2(\mathbf{P0P})_2(bpy)_2RuCl]^{3+}$ and $[Os(bpy)_2(\mathbf{PEP})_2(bpy)_2RuCl]^{3+}$ complexes, which may be due to the RuN5Cl centre. The emission at 723 nm for the P0P complex compares to the emission centred at 721 nm observed for the $[Os(bpy)_2(\mathbf{P0P})_2]^{2+}$ monomer, while that at 734 nm compares to an emission observed at 725 nm for the $[Os(bpy)_2(\mathbf{PEP})_2]^{2+}$ complex at 77K.

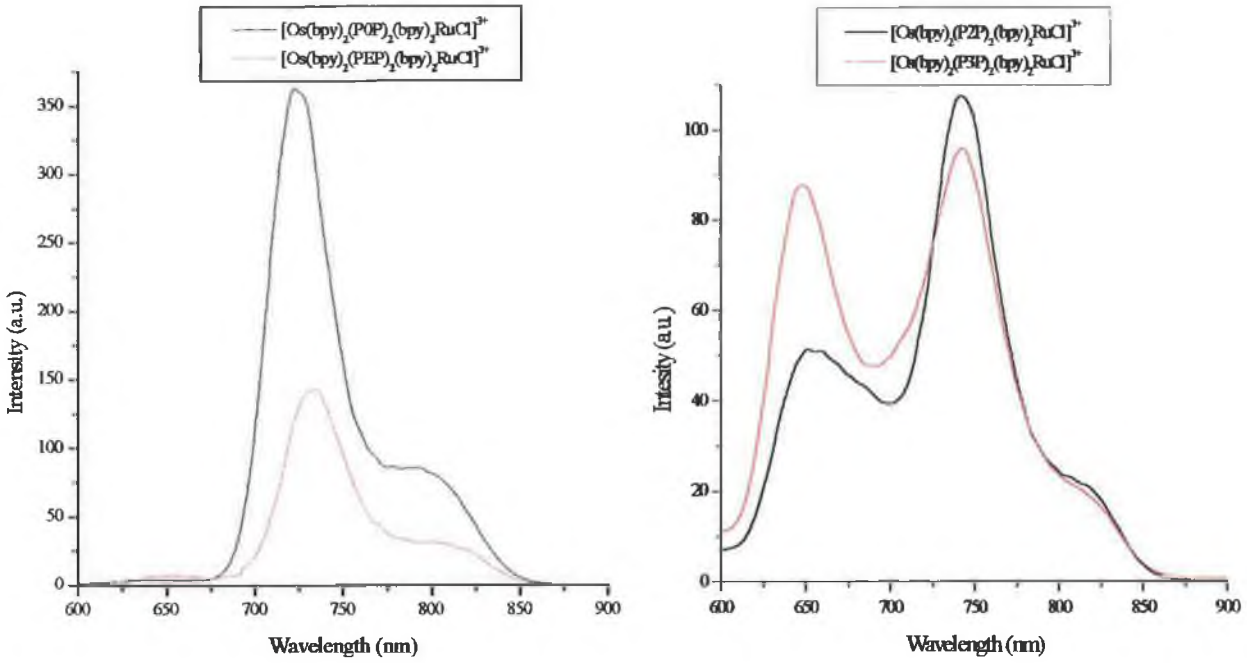

Figure 7.16 Emission spectra of the Os-Ru PnP dinuclear complexes at 77K. All measurements carried out in butyronitrile.

The emission of the complexes containing the non-conjugated P2P and P3P ligands at 77K is different. (Figure 7.16) A dual emissive type behaviour is observed, with intense bands centred at 654 nm and 742 nm for the $[Os(bpy)_2(\mathbf{P2P})_2(bpy)_2RuCl]^{3+}$ complex and bands at 648 nm and 742 nm observed for the $[Os(bpy)_2(\mathbf{PEP})_2(bpy)_2RuCl]^{3+}$ complex. The low energy bands (742 nm) compare to the emission observed from the $[Os(bpy)_2(\mathbf{P2P})_2]^{2+}$ and $[Os(bpy)_2(\mathbf{P3P})_2]^{2+}$ monomers at 77K which are centred at 752 and 749 nm respectively.

The emission at higher energy is at the same energy as the very weak bands found in the spectra of the $[Os(bpy)_2(\mathbf{P0P})_2(bpy)_2RuCl]^{3+}$ and $[Os(bpy)_2(\mathbf{PEP})_2(bpy)_2RuCl]^{3+}$ complexes at 77K.

These bands can be tentatively assigned as emission from the RuN5Cl moiety. The energy of the emission is *circa* 40 nm lower than that observed from the analogous

monomers. The reason this emission is very weak for the POP and PEP bridged dinuclear complexes may be attributed to energy transfer from the RuN5-Cl centre to the OsN6 centre which emits at lower energy. This mirrors the emissive properties observed for the analogous Ru-Ru dinuclear complexes. The non-conjugated nature of the P2P and P3P, and specifically the aliphatic CH_2 spacer unit obviously inhibits this energy transfer phenomenon leading to emission from both centres.

Evidence of similar type dual emission can be quoted from the work of Meyer, Schanze and Neyhart who have also used the PnP ligands to form mixed valence dinuclear complexes of osmium.[8,11] The photophysical properties of these unsymmetrical ligand bridged dinuclear complexes, $[(bpy)_2(CO)Os^{II}(L)Os^{II}(phen)(dppe)(Cl)]^{3+}$ and $[(bpy)_2(CO)Os^{II}(L)Os^{III}(phen)(dppe)(Cl)]^{3+}$ where L = POP, P2P, phen = 1,10-phenanthroline and dppe = 1,2-bis(diphenylphosphino)-cis-ethene have been discussed in the introduction to Chapter 6. Emission from the dinuclear complex $[(bpy)_2(CO)Os(P2P)Os(phen)(dppe)(Cl)]^{3+}$ is superimposable on emission from the monomer $[(phen)Os(dppe(Cl)(P2P)]^{2+}$ except for a weak band appearing on the high energy side of the major band which corresponds in energy to the emission from $[(bpy)_2Os(CO)P2P]^{2+}$. Emission lifetime data at room temperature and 77K gives further evidence in support of a dual emission.

7.8 Luminescent Lifetime of the $[Os(bpy)_2(PnP)_2(bpy)_2RuCl]^{3+}$ dinuclear complexes:

The results of the experiments to determine the luminescent lifetimes of the Os-Ru dinuclear complexes are presented below. As before, the lifetimes were determined using the single photon counting method, and the room temperature measurements were performed in MeCN and the 77K measurements in butyronitrile.

Compound	Deaerated, τ (ns)	77K, τ (ns) ex. RuN5-Cl	77K, τ (ns) ex. OsN6	Relative Contribution (%)
$[Os(bpy)_2(\mathbf{P0P})_2(bpy)_2RuCl]^{3+}$	44	2,000	606	80
			1360	20
$[Os(bpy)_2(\mathbf{PEP})_2(bpy)_2RuCl]^{3+}$	42	2,200	260	9
			2000	91
$[Os(bpy)_2(\mathbf{P2P})_2(bpy)_2RuCl]^{3+}$	40	2,000	470	9
			1720	91
$[Os(bpy)_2(\mathbf{P3P})_2(bpy)_2RuCl]^{3+}$	40	2,100	489	7
			2000	93

Table 7.5 Luminescent Lifetime Data of the Os-Ru dimers. Deaerated measurements performed in MeCN. 77K measurements performed in butyronitrile.

The situation at room temperature is different for the Os-Ru dinuclear complexes than the Ru-Ru dinuclear complexes. At room temperature a single emission is observed and this emission correlates closely with those observed for the $[Os(bpy)_2(PnP)_2]^{2+}$ monomers. The luminescence lifetime data supports this. A single decay seems to exist for all the complexes, and the lifetime of these processes (40 – 44 ns) corresponds to those of the osmium monomers (35 - 46 ns).

At 77K the non conjugated bridged P2P and P3P complexes exhibit dual emission characteristics, while the emission spectra of the P0P and PEP bridged dimers also appear to have a trace of the RuN5-Cl emission also. This is borne out in the lifetime data. Performing the experiment in the maxima of the emission from the RuN5-Cl centre results in a single exponential decay with lifetimes attributable to the RuN5-Cl moiety. As in the case of the Ru-Ru dimers the lifetimes are longer than those of the corresponding monomers. Exciting in the maxima of the OsN6 emission leads to a biexponential decay profile for each of the complexes. The long lived species correlates closely with the species observed upon excitation of the RuN5-Cl centre and is therefore

attributed to that, meaning the second decay process, with lifetimes of between 260 – 600 ns.

7.9 Introduction to the Electrochemistry of the dinuclear complexes:

Electrochemistry plays a vital role in the determination of both the structure and properties of these complexes. As in the discussion of the photophysics, the results obtained for the Ru-Ru PnP complexes will be discussed separately to those of the Os-Ru PnP dinuclear complexes. The electrochemistry of these compounds is very important as they have been designed with the intention of attaching the free nitrogen of the pendant arm to surfaces, and to study the electrochemical properties of the now modified surfaces. This chapter concludes with an investigation of the ability of the $[Os(bpy)_2(\mathbf{P2P})_2(bpy)_2RuCl]^{3+}$ dinuclear complex to form a self assembled monolayer.

The results obtained show that the photophysical properties are determined by the nature of the bridging ligand. Previous studies on similar compounds reveal that the changes in $E_{1/2}(1)$ and $E_{1/2}(2)$ (1^{st} and 2^{nd} metal based oxidations) values, when compared to the monomers are small and this prevents meaningful conclusions about the interaction of the metal centres to be drawn from the electrochemical studies.

For example, the unsymmetrical PnP bridged dinuclear complexes $[(bpy)_2(CO)Os^{II}(L)Os^{II}(phen)(dppe)(Cl)]^{3+}$ and $[(bpy)_2(CO)Os^{II}(L)Os^{III}(phen)(dppe)(Cl)]^{3+}$ where L = POP, P2P, phen = 1,10-phenanthroline and dppe = 1,2-bis(diphenylphosphino)-cis-ethene synthesised by Meyer *et al.*[8] have $E_{1/2}$ values are close to that of the associated monomers, which indicates that at best slight resonance and/or electrostatic interactions exist between the two metal centres. The same group has also investigated mixed valence dinuclear complexes of the type $[(dpte)_2ClRu^{II}(L)Ru^{III/II}Cl(bpy)_2]^{3+/2+}$ and $[(NH_3)_5Ru^{II/III}(L)Ru^{II}Cl(bpy)_2]^{4+/3+}$ where dpte = $PhSCH_2CH_2SPh$ and L = P0P, PEP and P2P in both cases. [12] The

electrochemistry for $[(dpte)_2ClRu(P0P)RuCl(bpy)_2]^{2+}$ does not differ significantly to the electrochemistry of its component monomers. This is characteristic for dinuclear systems where electrostatic and resonance stabilisation effects are small and provides evidence that the electronic coupling between the two sites in the ground state is small.

7.10 Electrochemistry of the $[Ru(bpy)_2(PnP)_2(bpy)_2RuCl]^{3+}$ dinuclear complexes:

Illustrative cyclic voltammograms are presented of a the $[Ru(bpy)_2(PEP)_2(bpy)_2RuCl]^{3+}$ and $[Ru(bpy)_2(P2P)_2(bpy)_2RuCl]^{3+}$ complexes are presented in order to show that the electrochemistry is similar for the systems containing a conjugated and non-conjugated ligand bridge. Tabulated results from the electrochemical experiments are presented in Table 7.6.

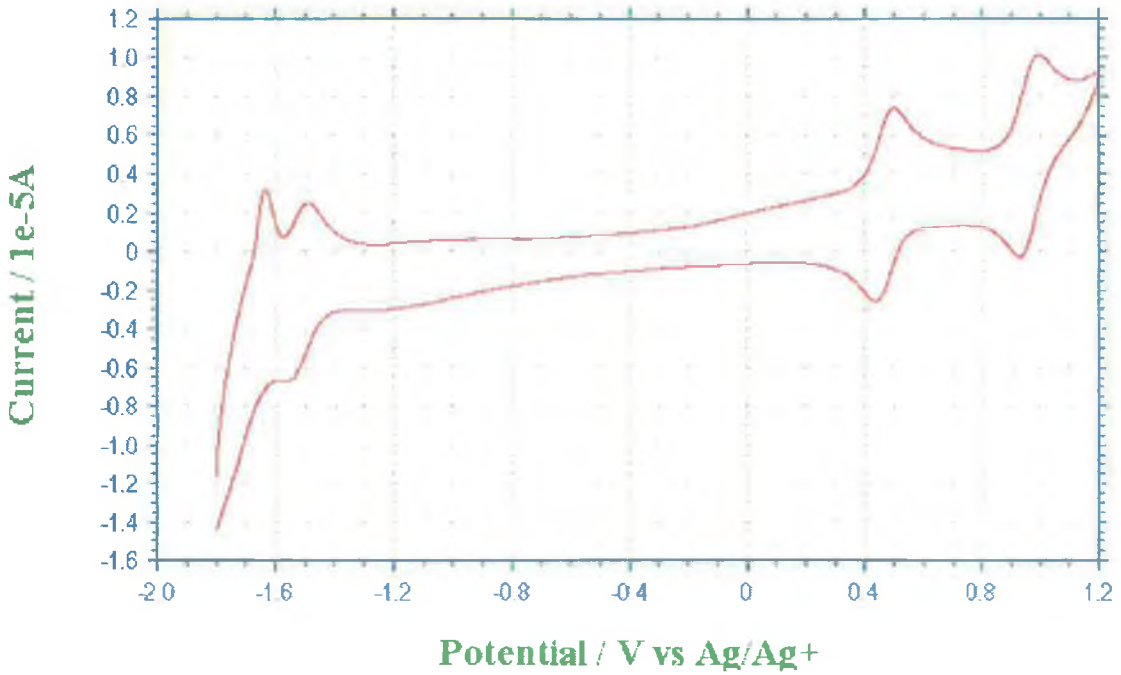

Figure 7.17 Cyclic Voltammogram of $[Ru(bpy)_2(PEP)_2(bpy)_2RuCl]^{3+}$ in MeCN with 0.1M $TBABF_4$.

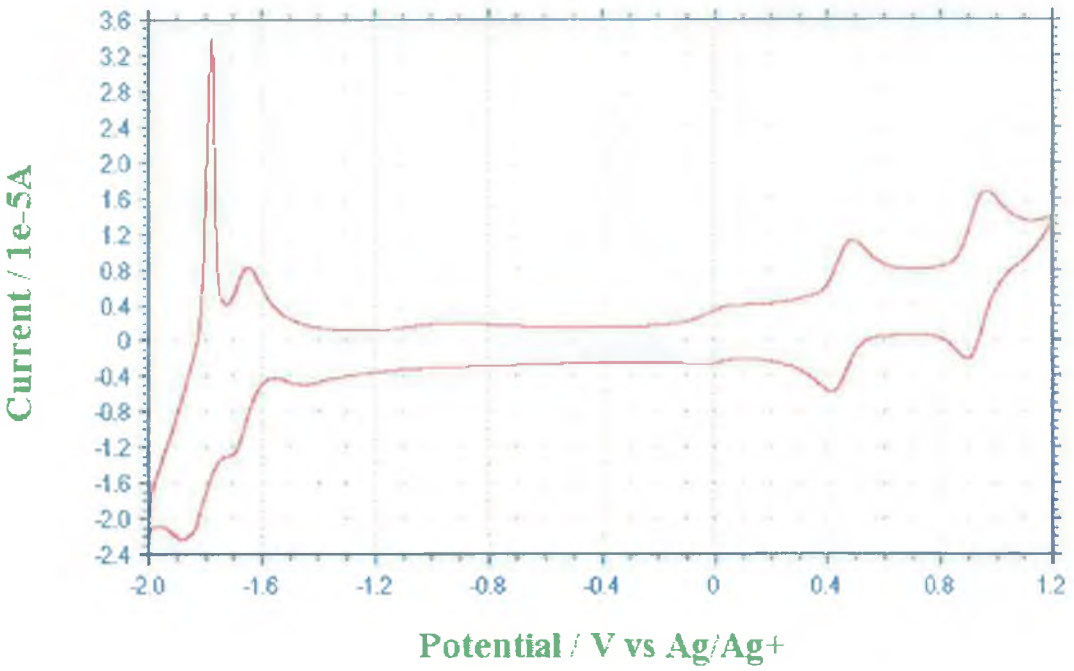

Figure 7.18 Cyclic Voltammogram of $[Ru(bpy)_2(P2P)_2(bpy)_2RuCl]^{3+}$ in MeCN with 0.1M $TBABF_4$.

Compound	Oxidation ($E_{1/2}$)	Reductions, Ligand based.
$[Ru(bpy)_2(P0P)_2(bpy)_2RuCl]^{3+}$	0.40 (63)	-1.61 (55)
	0.92 (65)	
$[Ru(bpy)_2(P2P)_2(bpy)_2RuCl]^{3+}$	0.37 (63)	-1.77 (56)
	0.84 (60)	-1.91 (99)
$[Ru(bpy)_2(P3P)_2(bpy)_2RuCl]^{3+}$	0.36 (65)	-1.76 (67)
	0.83 (68)	-1.88 (99)
$[Ru(bpy)_2(PEP)_2(bpy)_2RuCl]^{3+}$	0.38 (57)	-1.60 (53)
	0.88 (60)	

Table 7.6 Results from the electrochemical analysis of the $[Ru(bpy)_2(PnP)_2(bpy)_2RuCl]^{3+}$ dinuclear complexes in MeCN with 0.1M $TBABF_4$ (V vs Fc/Fc^+)

Many electrochemical investigations on mononuclear and polynuclear ruthenium(II) complexes containing the PnP ligands have been previously reported. (Chapter 6.1). From these studies it is generally accepted the observed oxidation processes are metal-centred while reduction processes are ligand centred. The anodic region of the cyclic voltammograms feature two reversible metal-centred oxidations, while the cathodic region exhibits the reduction waves. For several of the complexes only the first reduction could be determined accurately. Each of the metal based oxidation potentials are reversible. (using the condition of the peak to peak separation of the peaks being between 60 and 100mV).

As expected the electrochemical response can be considered as the sum of the monomer components of the dinuclear complexes. This point is illustrated in Figure 7.19.

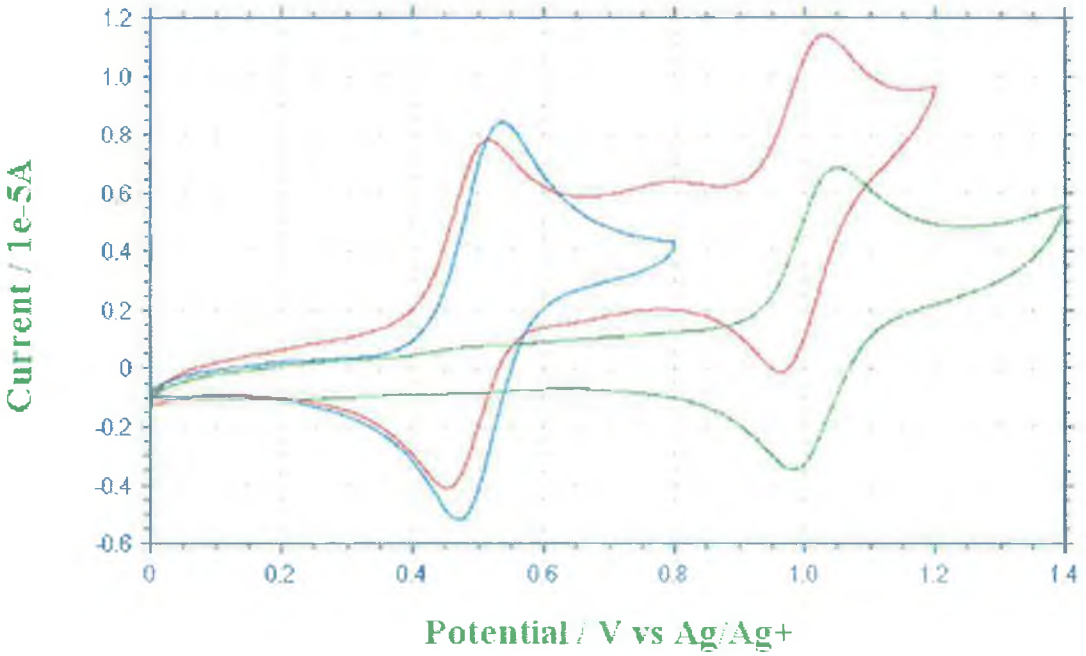

Figure 7.19 Cyclic voltammogram of the monomers $[Ru(bpy)_2(P0P)Cl]^+$ (blue) and $[Ru(bpy)_2(P0P)_2]^{2+}$ (green) overlaid with the dinuclear complex $[Ru(bpy)_2(P0P)(bpy)_2RuCl]^{5+}$ (red trace). All in MeCN with 0.1M $TBABF_4$.

Comparison of the oxidation potentials of the dinuclear complexes with the complexes discussed in Chapter 6, allows the first metal based oxidation to be assigned as based on the RuN5Cl metal centre, while the second oxidation wave is due to the RuN6 metal centre. No significant shift from the results achieved for the monomeric subunits exist which agrees with the results of similar PnP bridged dinuclear complexes which have been discussed earlier in this section.'[12]

The reduction potentials of the complexes are less well defined. For the complexes $[Ru(bpy)_2(POP)_2(bpy)_2RuCl]^{3+}$ and $[Ru(bpy)_2(PEP)_2(bpy)_2RuCl]^{3+}$ only one reduction potential can be determined. The $E_{1/2}$ of this reduction potential is less negative than is expected should this reduction be 2,2' bipyridyl based. It is therefore possible that this reduction is based on the bridging ligand (POP or PEP). This has relevance to the photophysical study of these complexes. This result indicates that the excited state may lie on the bridging POP/PEP ligand rather than on the 2,2'-bypryidyl ligands. In order to confidently assign this further study will be necessary.

For the $[Ru(bpy)_2(P2P)_2(bpy)_2RuCl]^{3+}$ and $[Ru(bpy)_2(P3P)_2(bpy)_2RuCl]^{3+}$ complexes the first two reduction potentials has been determined. The first reduction potential appears at more negative potentials than for the POP and PEP bridged dinuclear complexes. Comparison with the reduction potentials of $[Ru(bpy)_3]^{2+}$ allow assignment of both of these reductions as being 2,2' bipyridyl based.

The spike seen on the return wave of the reduction waves can tentatively be described as a "desorption spike" and is likely to be due to the desorption of complex from the electrode surface at the applied potential. [13,14] This phenomenon has been discussed in more detail in Chapter 5.7 and the same principles apply here. Observation of these desorption spikes provide evidence that the nitrogen of the pendant arm is "free" or unbound. This is the desired state, and should provide the possibility to attach the complex to a surface through this interface.

7.11 Electrochemistry of the $[Os(bpy)_2(PnP)_2(bpy)_2RuCl]^{3+}$ dinuclear complexes:

The electrochemistry of the $[Os(bpy)_2(PnP)_2(bpy)_2RuCl]^{3+}$ dinuclear complexes is complicated by the overlap between the oxidation waves of both metal centres. This was an anticipated problem as the oxidation potentials of the ruthenium N5-Cl and the OsN6 monomers are very similar (Chapter 6.6).

As a result the oxidation waves overlap, and the single oxidation wave in the cyclic voltammogram can be attributed to a two electron process involving simultaneous oxidation of both the RuN5-Cl and OsN6 moiety. As expected the oxidation potentials of the OsN6 moieties are approximately 400mV lower than for those of the analogous ruthenium complexes. This is consistent with the fact that the 5d orbitals of osmium are higher in energy than the 4d orbitals of ruthenium. [15,16,17] Illustrative cyclic voltammograms can be seen below. (Figures 7.20 and 7.21)

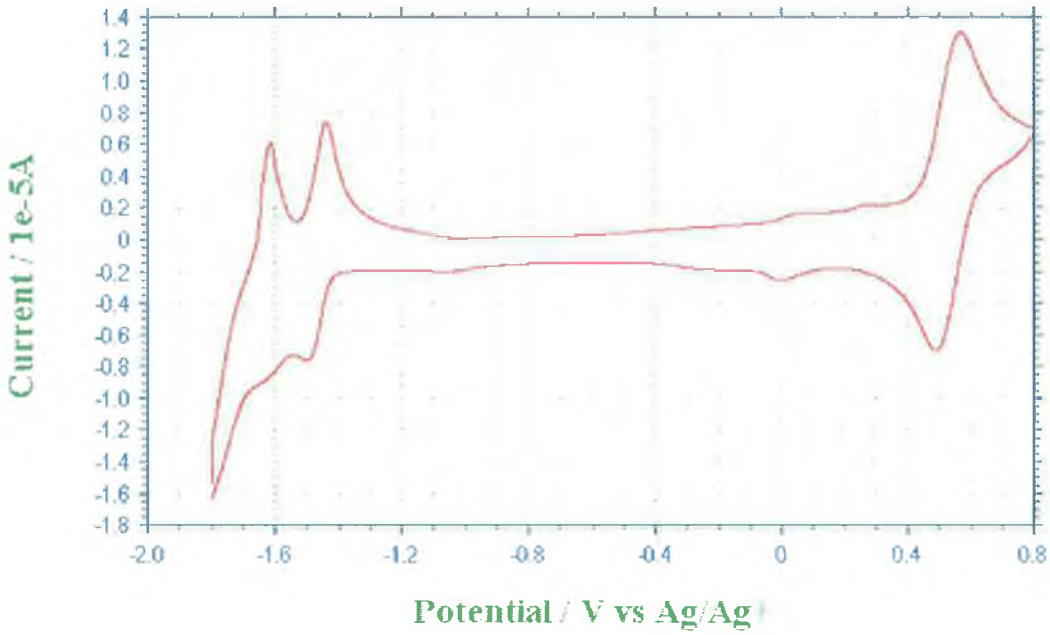

Figure 7.20 Cyclic Voltammogram of $[Os(bpy)_2(P0P)_2(bpy)_2RuCl]^{3+}$ in MeCN with 0.1M $TBABF_4$.

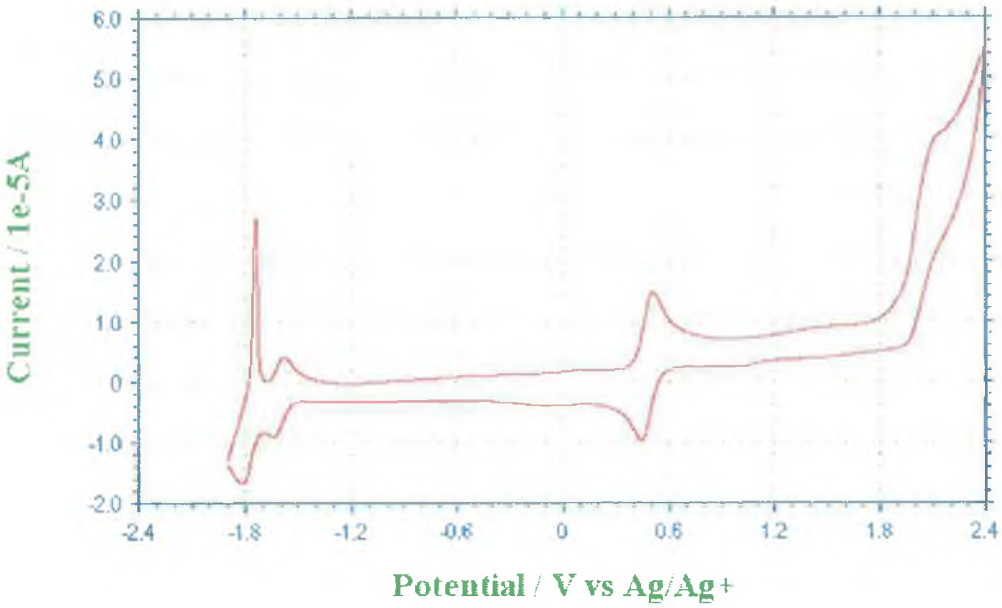

Figure 7.21 Cyclic Voltammogram of $[Os(bpy)_2(P2P)_2(bpy)_2RuCl]^{3+}$ in MeCN with 0.1M $TBABF_4$.

As in the case of the Ru-Ru PnP dinuclear complexes, an example has been given of a dinuclear complex containing a conjugated bridging ligand (Os-Ru POP) and one containing the non-conjugated bridging ligand P2P. Differential Pulse Voltammetry (DPV) has been performed on each of the complexes. It was hoped that the increased sensitivity of this technique compared to cyclic voltammetry may show a splitting of the first oxidation wave, indicating the presence of the two metal centres. The DPV of the complex $[Os(bpy)_2(POP)_2(bpy)_2RuCl]^{3+}$ is presented in Figure 7.22.

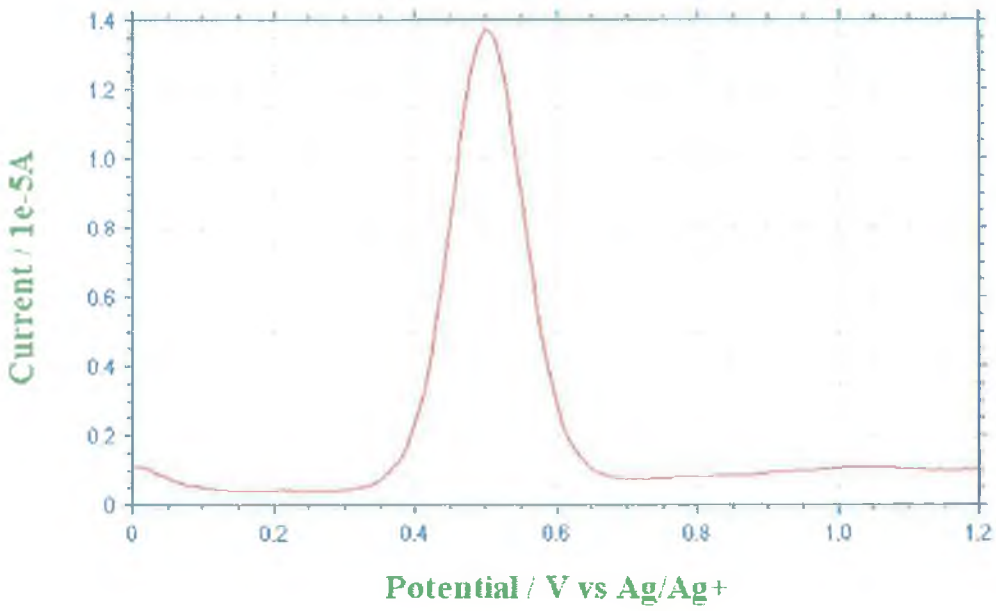

Figure 7.22 DPV of $[Os(bpy)_2(P0P)_2(bpy)_2RuCl]^{3+}$ in MeCN with 0.1M $TBABF_4$.

As can be seen from Figure 7.22 above – no splitting of the first oxidation wave is observed even for the more sensitive technique of differential pulse voltammetry. The data from the electrochemical measurements have been tabulated below in Table 7.7.

Compound	Oxidation, $E_{1/2}$ (ΔE)	Reduction, $E_{1/2}$ (ΔE)
$[Os(bpy)_2(P0P)_2(bpy)_2RuCl]^{3+}$	0.42 (77)	-1.57 (60)
	1.40 (irr)	
$[Os(bpy)_2(P2P)_2(bpy)_2RuCl]^{3+}$	0.37 (66)	-1.71 (59)
	2.01 (irr)	-1.88 (80)
$[Os(bpy)_2(P3P)_2(bpy)_2RuCl]^{3+}$	0.46 (68)	-1.72 (79)
	2.00 (irr)	-1.87 (89)
$[Os(bpy)_2(PEP)_2(bpy)_2RuCl]^{3+}$	0.39 (70)	-1.58 (67)
	1.64 (irr)	

Table 7.7 Results from the electrochemical analysis of the $[Os(bpy)_2(PnP)_2(bpy)_2RuCl]^{3+}$ complexes in MeCN with 0.1M $TBABF_4$ (V vs Fc/Fc^+)

The first oxidation potential has been assigned as a two electron process involving oxidation of both the OsN6 and RuN5-Cl metal centres. For each of the complexes however, a second irreversible oxidation process is observed at higher potentials. Two explanations for this oxidation wave are possible.

The first explanation is that the oxidation wave is due to a second oxidation process at the OsN6 centre corresponding to oxidation of the now $Os^{(III)}$ centre to $Os^{(IV)}$. Evidence of $Os^{(III)}/Os^{(IV)}$ processes have been reported previously, interestingly for the complex $[Os(bpy)_2(POP)Cl]^+$, where the first oxidation, assigned as an $Os^{(II)}/Os^{(III)}$ couple occurs at +0.02 V *vs* Fc/Fc^+ a second oxidation potential is observed. This irreversible wave, which has been assigned as an $Os^{(III)}/Os^{(IV)}$ couple occurs at +1.47 V vs Fc/Fc^+. [18]

This phenomenon has been previously reported by the same group for several other similar complexes. For $[Os(bpy)_2Cl_2]$ the $Os^{(III)}/Os^{(IV)}$ couple is reported as +1.03 V *vs* Fc/Fc^+. For the complex $[Os(bpy)_2(py)Cl]^+$ (where py = pyridine) this rises to +1.45 V *vs* Fc/Fc^+. As expected the potentials are higher again for OsN6 complexes with $[Os(bpy)_2(py)_2]^{2+}$ reported at +2.03 V *vs* Fc/Fc^+ and $[Os(bpy)_2(MeCN)_2]^{2+}$ reported as +2.10 V *vs* Fc/Fc^+. [19] All the potentials were quoted in V *vs* SSCE but have been converted to V *vs* Fc/Fc^+ using a conversion factor of –0.358 V. [20]

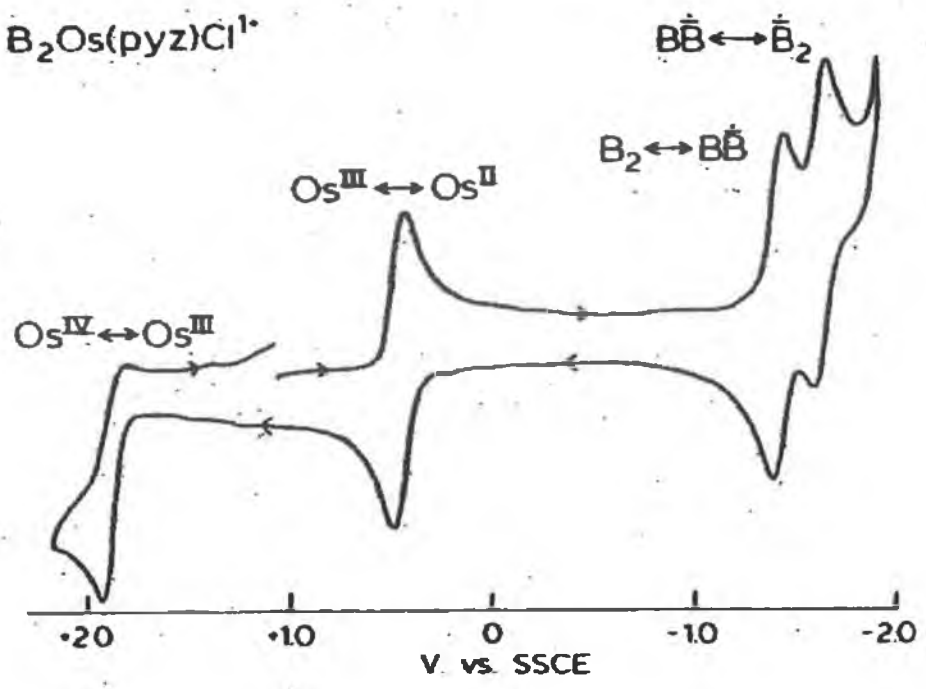

Figure 7.23 Cyclic Voltammogram for cis-[Os(bpy)$_2$(pz)Cl].(PF_6) in 0.1 M TBAH/CH_3CN. Note the irreversible behaviour of the $Os^{(III)}/Os^{(IV)}$ couple. [19]

The oxidation potentials of the second oxidation waves are centred at 1.40 V and 1.64 V for the Os-Ru P0P and PEP bridged dinuclear complexes, and at 2.01 V and 2.00 V for the Os-Ru P2P and P3P bridged dinuclear complexes. The behaviour of this wave is irreversible, which agrees with the observations made by Meyer *et al.* [18,19] who also declare that a significant difference between Ru and Os occurs for the $M^{(III)}/M^{(IV)}$ couple. The $Os^{(III/IV)}$ couple can be observed for several complexes at potentials 1.0-1.5 V more positive than potentials for the $Os^{(II/III)}$ couple. The separation between the $Ru^{(III/IV)}$ and $Ru^{(II/III)}$ couples is considerably larger and the $Ru^{(III/IV)}$ couples are very rarely observed as they often lie at potentials beyond the solvent limit. No oxidations at similar potentials have been observed for the analogous ruthenium dinuclear complexes which seems to add further support to the proposition that the second oxidation waves observed are due to an $Os^{(III/IV)}$ couple on the OsN6 moiety.

A second explanation must also be considered. The oxidation waves observed at higher potentials may simply be due to oxidation of the PnP ligand bridges. An argument

against this has to be the fact that this phenomenon is not observable for the ruthenium complexes.

Comparison of the reduction waves of the $[Os(bpy)_2(PnP)_2(bpy)_2RuCl]^{3+}$ to those observed for the analogous ruthenium complexes show many similarities. As mentioned in the previous sections, irreversible reductions are often observed for complexes containing a halide ligand, and is caused by rapid halide loss and replacement by solvent. [21]

For the complexes $[Os(bpy)_2(P0P)_2(bpy)_2RuCl]^{3+}$ and $[Os(bpy)_2(PEP)_2(bpy)_2RuCl]^{3+}$ only one reduction potential can be determined (at –1.57 and –1.58 V vs Fc/Fc^+). The $E_{1/2}$ of this reduction potential is less negative than is expected should this reduction be 2,2'-bipyridyl based. The possibility must be considered therefore that this reduction is based on the bridging ligand (P0P or PEP). In order to confidently assign this further study will be necessary.

For the $[Os(bpy)_2(P2P)_2(bpy)_2RuCl]^{3+}$ and $[Os(bpy)_2(P3P)_2(bpy)_2RuCl]^{3+}$ complexes the first two reduction potentials has been determined (at circa –1.71 V and –1.87 V vs Fc/Fc^+). The first reduction potential appears at more negative potentials than for the P0P and PEP bridged dinuclear complexes. Comparison with the reduction potentials of $[Ru(bpy)_3]^{2+}$ allow assignment of both of these reductions as being 2,2' bipyridyl based.

"Desorption spikes" are again in evidence on the reduction side of the electrochemical response of the Os-Ru PnP dinuclear complexes. This phenomenon has been discussed for the Ru-Ru PnP dinuclear complexes (Chapter 7.8). The next section deals with the attachment of these complexes to surfaces through the free nitrogen which may be responsible for these spikes.

7.12 Formation of a Self Assembled Monolayer using $[Os(bpy)_2(P2P)_2(bpy)_2RuCl]^{3+}$:

One of the main areas of electrochemical research over the past 20 years has centred on electrodes covered with organised monolayers. This concept has already been introduced and discussed, and relevant examples of work in this field highlighted during the introduction to Chapter 6. The design of this series of homonuclear and heteronuclear dinuclear complexes has purposely provided the opportunity of attaching these complexes to a surface. It was hoped that these compound would provide the opportunity to prepare self assembled monolayers (SAMs). The advantages of SAMs are that they take advantage of a large number of weak and/ or moderate interactions to spontaneously generate organised molecular assemblies. The spontaneous formation and stability of the monolayer depend on favourable if weak, intermolecular forces, as well as on the forces between each of the individual subunits, and the solid substrate for support. In this case, it is anticipated that the free nitrogen on the unbound pendant arm of the dinuclear complex will be free to "bind" to the surface. A full characterisation of the surface active characteristics of the complexes while bound to a surface is beyond the scope of this thesis. What is reported here are the preliminary results from the investigations of the surface active characteristics of one of the dinuclear complexes.

Several differences between the electrochemical experiments previously described in this thesis and the experiments performed here must be highlighted. In order to deposit the compound successfully onto the surface, using techniques which have been previously described, [22,23,24] we have had to move away from organic media, and use aqueous media. This simplifies the performance of the experiment greatly as rigorous drying of solvents and apparatus is no longer necessary. It introduces its own problems however, and one of these problems is specific to the complexes being discussed.

For example, the potential window afforded by the aqueous media is approximately 0.3V to 0.8 V vs Ag/AgCl. This is due to hydrogen evolution at lower potentials and

oxidation of water at higher potentials. This already limits the choice of compound for examination as the oxidation potential of the N6 Ru(II)/Ru(III) couple lies outside of this range. It was necessary to attempt to grow a monolayer from one of the $[Os(bpy)_2(PnP)_2Ru(bpy)_2Cl](PF_6)_3$ complexes. These complexes are far from ideal either. For a start the oxidation potentials of the Os(II)/Os(III) couple and the Ru(II)/Ru(III) couple are so close as to be impossible to separate, and a single wave results. On top of this, a more serious problem exists. As discussed at the start of this Chapter, the main problem in the synthesis of these complexes arose from complications which were caused by exchange of the chloro for an aquo moiety. This problem was overcome by preventing contact with water. This experiment is being performed in aqueous media, and therefore the question of whether the complex is present as the chloro, or as the aquo once again becomes relevant. This problem has been investigated for the mononuclear ruthenium chloro complex $[Ru(bpy)_2(PEP)Cl]^+$. [24] No photosubstitution reactions were observed for the Os-PEP chloro complex.

It is with these considerations that these results are reported. It must be stressed that this is a preliminary examination of only one of the complexes. Much further work is needed to fully characterise these complexes on a surface.

The spontaneously adsorbed monolayers were formed on three Pt electrodes by immersing the freshly polished and electrochemically cleaned (by scanning the potential of the polished Pt electrode between the hygrogen evolution and platinum oxide formation potentials until well defined hydrogen adsorption peaks were visible) platinum disc electrode (radius = 1mm) in a 1:1 MeOH:H_2O solution of the metal complex at millimolar concentrations. The electrodes were allowed to stand in the solution for 72 hours. Before electrochemical measurements were performed, the modified electrodes were rinsed with water, MeOH and acetone to remove any unbound, or loosely bound material. Attempts had also been made to adsorb the complex from pure MeOH, with less success.

The total charge introduced or withdrawn to reduce or oxidise the monolayer can be found from the area under the voltammetric peak, after correcting for the background charging current. This charge together with the real surface area can then be used to calculate the surface coverage, or the number of moles of $[Os(bpy)_2(P2P)_2Ru(bpy)_2Cl]^{3+}$ per cm^2. This figure provides information about the packing density of the monolayer.

The geometric area of the surface was calculated as $0.033cm^2$. The microscopic area was calculated from the Pt oxide re-reduction peak area of the polished electrode in 0.1M $HClO_4$ acid, based on a figure of $420\mu C/cm^2$. [25] The microscopic area was calculated as $0.068cm^2$. This provides a roughness factor of 2.1. The surface coverage was found to be roughly 3.5×10^{-11} mol cm^{-2}. This compares to a value of 2.1×10^{-10} mol cm^{-2} for the $[Os(bpy)_2(P3P)_2]^{2+}$ monomer.

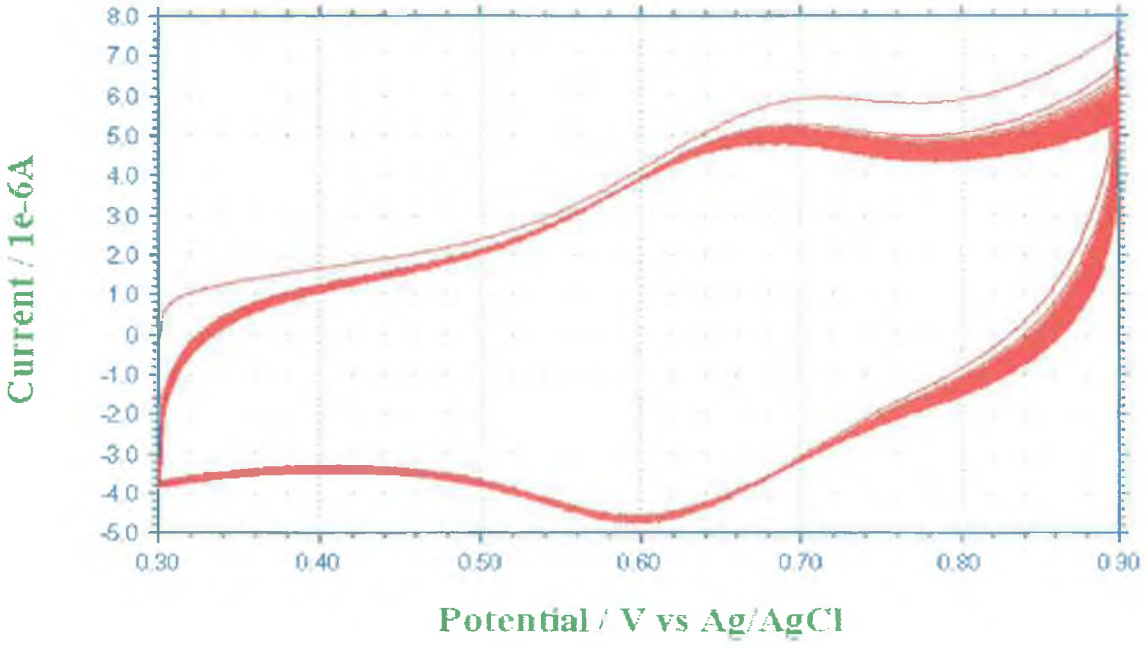

Figure 7.24 Results from 50 scans of surface confined complex $[Os(bpy)_2(P2P)_2Ru(bpy)_2Cl]^{3+}$ in aqueous electrolyte with 0.1M $NaClO_4$.

There are several notable differences between the electrochemical response expected from a surface confined species, and that of a species in solution. Several checks were also performed to prove the electrochemically active species was bound to the surface.

Firstly, as described, the electrode was rinsed with water, MeOH and acetone after deposition of the monolayer. This was to remove any unbound or loosely bound species. Secondly, the electrolyte in which the experiment was performed was checked after the experiment with a clean and polished electrode for evidence of contamination. **No signal was detected by the new electrode**. Both of these checks indicate that the response observed is therefore due to complex bound to the surface of the electrode, and was not due to contamination of the electrolyte.

Since in a SAM, the electroactive centres are all close to the electrode surface, diffusion has no influence on the experiment. Therefore, unlike in experiments with diffusion controlled currents, the peak current, i_p is directly proportional to the scan rate, ν. For diffusion controlled experiments the peak current, i_p is directly proportional to the square root of the scan rate, i.e. $\nu^{1/2}$. A scan rate dependence study, with plots of i_p *vs* ν and $\nu^{1/2}$ should provide further evidence as to the nature of the electroactive species. The results of this experiment can be seen on the next page.

For a surface confined couple the ΔE_p, that is the difference in potential between the anodic and cathodic peak is ideally = 0mV. For a species in solution which must diffuse to the surface, this value is = 59 mV. The value of ΔE_p found during the scan rate study was between 40-55mV, which is lower than the value expected from that of a diffusion controlled species. These values are not ideal however, but it must be remembered that the peaks being analysed are the results of two overlapping redox waves, and therefore a larger peak splitting is entirely possible for this reason.

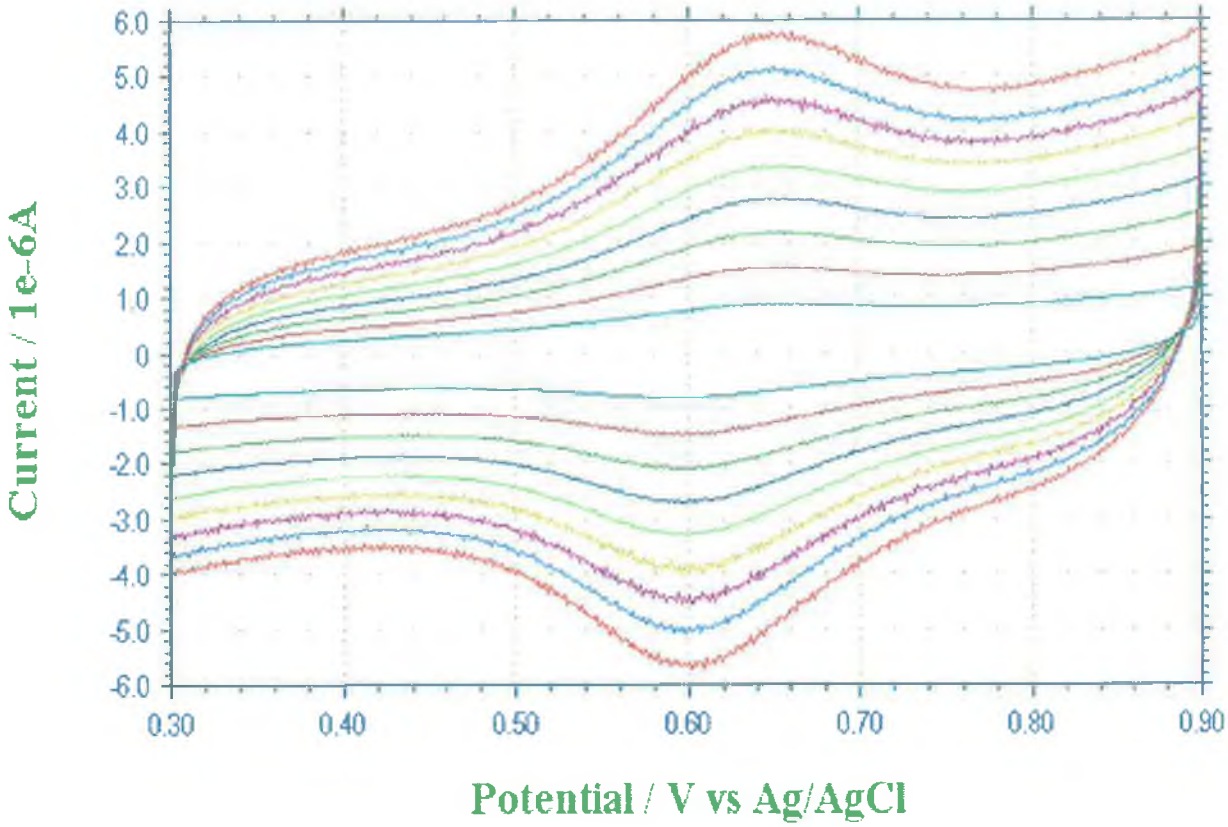

Figure 7.25 Result of scan rate dependence study of a monolayer of $[Os(bpy)_2(P2P)_2Ru(bpy)_2Cl]^{3+}$ in aqueous electrolyte with 0.1M $NaClO_4$ between .1 Vs^{-1} and .9 Vs^{-1}.

From Figure 7.26 and 7.27 it can be seen that the fitting for the plots of scan rate vs i_p for both the cathodic and anodic peak currents fit better than the plots of scan rate vs $(i_p)^{1/2}$. (R^2 values of .9982 and .9954 compared to .9797 and .9727).

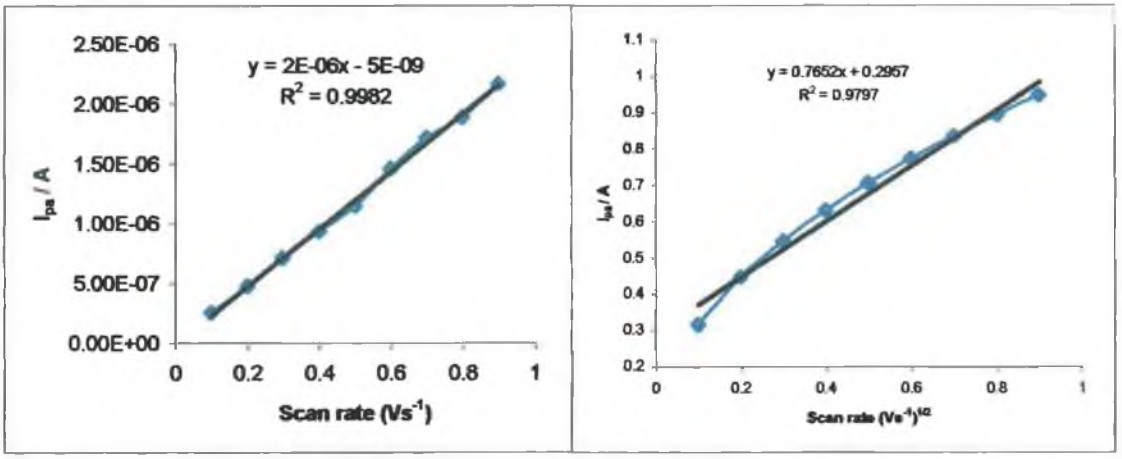

Figure 7.26 Results from the analysis of the scan rate dependence study on the anodic peaks of the surface confined monolayer of $[Os(bpy)_2(P2P)_2(Ru(bpy)_2Cl]^{3+}$ complex in aqueous medium with 0.1M $NaClO_4$.

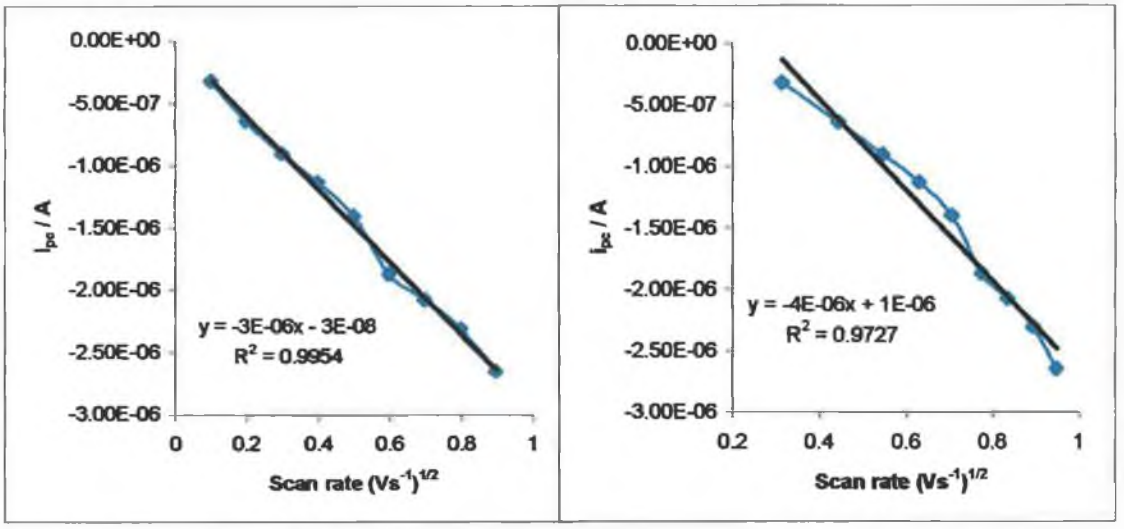

Figure 7.27 Results from the analysis of the scan rate dependence study on the anodic peaks of the surface confined monolayer of $[Os(bpy)_2(P2P)_2(Ru(bpy)_2Cl]^{3+}$ complex in aqueous medium with 0.1M $NaClO_4$.

7.13 Bibliography

[1] Haas O., Kriens M., Vos J. G., ***J. Am. Chem. Soc***., **1981**, 103, 1318.

[2] Moyer B. A., Meyer T. J., ***J. Am. Chem. Soc***., **1978**, 100, 3601.

[3] Moyer B. A., Meyer T. J., ***Inorg. Chem***., **1981**, 20, 436.

[4] Buchanan B. E., McGovern E., Harkin P., Vos J. G., ***Inorg. Chim. Acta***., **1988**, 154, 1.

[5] Forster R. J., Vos J. G., ***Macromolecules***, **1990**, 23, 4372.

[6] Forster R. J., Figgemeier E., Lees A., Hjelm J., Vos J. G., ***Langmuir***, **2000**, 16, 7867.

[7] Powers M. J., Meyer T. J., ***J. Am. Chem. Soc.,*** **1980**, 102, 1289

[8] Schanze K. S., Neyhart G. A., Meyer T. J., ***J. Phys. Chem.,*** **1986**, 90, 2182

[9] DeCola L., Balzani V., Barigelleti F., Flamigni L., Belser P., von Zelewsky A., Frank M., Vögtle F., ***Inorg. Chem.,*** **1993**, 32, 5228.

[10] Haga M., Matsumura-Inoue T., Yamabe S., ***Inorg. Chem.,*** **1987**, 26, 4148.

[11] Schanze K. S., Meyer T. J., ***Inorg. Chem.,*** **1985,** 24, 2122

[12] Curtis J. C., Bernstein J. S., Meyer T. J., ***Inorg. Chem.,*** **1985**, 24, 385

[13] Cleary R. L., Byrom K. J., Bardwell D. A., Jeffrey J. C., Ward M. D., Calogero G., Armoli L., Flamigni L., Barigelleti F., ***Inorg. Chem***., **1997,** 36, 2601.

[14] Tokel-Takvoryan N. E., Hemingway R. E., Bard A. J., ***J. Am. Chem. Soc.***, **1973**, 95, 6582.

[15] Goldsby K. A., Meyer T. J., ***Inorg. Chem.,*** **1984**, 23, 3002.

[16] Kalyanasundaram K., Nazeeruddin K., ***Inorg. Chim. Acta,,*** **1990**, 171, 213

[17] Kalyanasundaram K., Nazeeruddin K***., Chem. Phys. Lett.,*** **1989**, 158, 45

[18] Demadis K. D., Neyhart G. A., Kober E. M., White P. S., Meyer T. J., ***Inorg. Chem.***, **1999**, 38, 5948.

[19] Kober E. M., Caspar J. V., Sullivan B. P., Meyer T. J***., Inorg. Chem.,*** **1988**, 27, 4587.

[20] Kaifer A. E., Gomez-Kaifer M., ***Supramolecular Electrochemistry***, **1999**, Wiley.

[21] Sullivan B. P., Salmon D. J., Meyer T. J., ***Inorg. Chem.***, **1978**, 17, 3334.

[22] Forster R. J., Faulkner L. R., ***Langmuir***, **1995**, 11, 1014.

[23] Forster R. J., Figgemeier E., Loughman P., Lees A., Hjelm J., Vos J. G., ***Langmuir***, **2000**, 16, 7871.

[24] Forster R. J., Figgemeier E., Lees A. C., Hjelm J., Vos J. G., ***Langmuir***, **2000**, 16, 7867

[25] Brown A. P., Anson F. C., ***Anal. Chem.***, **1977**, 49, 1589

Chapter 8: Conclusions and Future Work:

8.1 Conclusions:

Chapter 1 provides an introduction to the area of supramolecular chemistry. The topics discussed in Chapter 1 have been limited to those that are relevant to this thesis as the area of inorganic and supramolecular chemistry is now so large. The development of this area of chemistry is outlined and its relevance to this thesis highlighted. The "parent" complex of many of the complexes discussed in this thesis, $[Ru(bpy)_3]^{2+}$ is introduced, and its importance to the area of inorganic chemistry is highlighted. Chapter 2 provides details of experimental and basic synthetic procedures used in subsequent chapters.

The rest of the thesis can be divided into two separate projects. The first involved the synthesis and characterisation of a series of ruthenium(II) and osmium(II) mixed ligand complexes and is discussed in Chapters 3, 4 and 5. These complexes, containing the LL_x ligands have been successfully synthesised and characterised. Chapter 3 contains the crystal structures of three of the ruthenium(II) complexes, and the complexes containing the LL1, LL2, LL3 and LL8 ligands have had the protons of the LL_x ligands assigned by ^1H NMR. The value of ^1H NMR to the structural determination of these complexes has been illustrated. The presence of rotamers introduces complexity into the determination of the structures of the complexes containing the LL4, LL5 and LL6 ligands, but also produces interesting properties which can be elaborated upon in future studies. The absorption and emission spectra of the ruthenium complexes are as expected, however examination of the LL_x ligands as free ligands have provided interesting results, particularly in the areas of the photochemical behaviour, and the electrochemical behaviour, with the electrochemical investigation revealing that the free ligands are electron rich species. The examination of the free ligands proved crucial in the assignment of photochemical process as well as oxidation waves in the electrochemical behaviour of the complexes. Chapter 3 concludes with a more detailed examination of the rotamers issue. It can be seen from these discussions that each experiment provided more information on this issue. The original concept that the isomers were formed at the

moment of coordination of the LL_x ligand, and the ratio of one isomer to the other was determined at that moment has been disproved by the experiments of Prof. Villani and his group in the University of Rome. It is now believed that in solution, the isomers form an equilibrium, and a solution containing a single isomer will equilibrate to a mixture of the two isomers over time. The half-life of this process at 25°C has also been calculated. We are very grateful for the excellent work that has been achieved on this issue. More work needs to be done however, and this will be discussed in Section 8.2.

Chapter 4 of this thesis has detailed the synthesis and characterisation of a series of osmium(II) bisbipyridyl complexes containing the LL_x ligands. The synthesis, and difficulties of using osmium as opposed to ruthenium has been discussed. Unfortunately no suitable crystals of the osmium complexes were grown, and determination of the structure of any of the complexes by X-Ray Crystal Structure Analysis could not be performed. As in Chapter 3, the purity as well as the structure of the complexes were determined by HPLC and ^{1}H NMR. The differences between the ruthenium and osmium complexes on examination by both of these methods, while small, have been elaborated upon. As expected, the same isomerisation effects are present for the osmium complexes of the LL4, LL5 and LL6 ligands as for the ruthenium complexes. The differences between the ruthenium and osmium complexes were highlighted by the photophysical examination of the complexes. The differences in absorption, emission and lifetime results have been expanded upon and explained. Interestingly, the photochemistry of the osmium complexes provided the most surprising results. In general, it is not expected to observe photochemistry from osmium complexes, however in the case of the osmium complex of the LL1 ligand, the complex decomposes in a similar manner to that of the ruthenium complex. The photochemistry from the osmium complex has been attributed to decomposition of the ligand, rather than a direct effect of irradiating the metal centre. The electrochemistry of the osmium complexes produced the expected results. In general the oxidation potential of the metal based process was 400 mV lower than for the analogous ruthenium complexes. Again the electron rich nature of the LL_x ligands is evident in the additional oxidation potentials observable in the voltammograms.

Chapter 5 details the synthesis of a mononuclear ruthenium(II) complex, and a series of homonuclear Ru-Ru and Os-Os dinuclear complexes and a mixed metal Ru-Os complex, all containing the bridging LL7 ligand. The synthesis of the mononuclear species has been elaborated upon due to the unexpected difficulties involved. The structure of the Ru-Ru dinuclear complex has been determined by X-Ray Crystal Analysis. Assignment of the LL7 protons in the ^{1}H NMR of the complexes has been aided greatly by deuteriation of the 2,2'-bipyridyl ring. The photophysical properties of the mononuclear ruthenium(II) and homonuclear dinuclear complexes are unexceptional, however the mixed metal Ru-Os dinuclear complex exhibits dual emission characteristics at both room temperature and 77K. The luminescence lifetime study of the Ru-Os complex details this dual emission more accurately. The electrochemistry of the complexes is complicated by the presence of several additional oxidation waves which are based on the LL7 ligand. Comparison of the ruthenium and osmium oxidation potentials have allowed the metal based processes to be identified. Bulk electrolysis of the Os-Os dinuclear complex has been performed. This experiment has allowed the assignment of the Os(II)-Os(III) redox couple to be safely assigned as a two electron process. This experiment has proved that both metal centres are oxidised simultaneously, indicating that communication between the metal centres is weak. This fact has also been proven by spectroelectrochemistry. The absence of an observable I.T. band adds further proof to the lack of communication between the metal centres. As in the electrochemical experiments, the oxidation of the LL7 ligand has complicated the experiments, but also provided some interesting results.

The second project is discussed in Chapters 6 and 7. Chapter 6 acts as an introduction to Chapter 7. Chapter 6 begins with an account of work carried out previously using the ligands introduced in this chapter and continues with a description of the synthesis of the ruthenium and osmium complexes which are used as starting materials in the synthesis of the dinuclear complexes discussed in Chapter 7. The problematic synthesis and purification of the complexes is described. As these complexes have been reported previously, full characterisation of the complexes has not been essential. The photophysics of the complexes have been investigated fully as this information has not

been reported previously. The electrochemistry of the complexes has also been examined. The reduction potentials of several of the complexes indicate that the excited state may lie on the PnP ligands and not necessarily on the 2,2'-bipyridyl ligands, but due to time limitations, this has not been investigated further. The electrochemical analysis of these complexes is important as the electrochemistry of the dinuclear complexes of Chapter 7 has proved to be very important, and comparison with the component monomers has proven useful.

Chapter 7 describes the synthesis and characterisation of a series of dinuclear complexes. These complexes have been designed so that they are capable of attachment to suitable surfaces. The chapter describes the unexpected difficulties in the synthesis of what was expected to be a relatively simple series of complexes. As it turns out, the synthesis was straightforward, the complications arose in the method chosen to analyse the products. The photophysical properties of the complexes has provided interesting results. From a simple UV/Vis experiment, it has been shown that the communication between the metal centres can be expected for those complexes bridged by the POP or PEP ligand, while those centres bridged by the P2P or P3P ligand can expect very weak or no communication. This is an expected result and is due to the aliphatic spacer groups between the pyridine rings of the P2P and P3P ligands. The complexes containing the P2P and P3P ligands therefore exhibit dual emission characteristics, while this dual emission is quenched substantially for those complexes containing the POP and PEP bridging ligands. The luminescence lifetime data subscribes to this also. Electrochemistry of these dinuclear complexes has proven very important. The Ru-Ru complexes have well separated potentials, however the oxidation potentials of the Os-Ru complexes overlap, and differentiation between the potentials is impossible. In both cases the electrochemical response can be considered as the sum of the mononuclear components. The reduction potentials of the complexes indicate that the excited state of some of the dinuclear complexes may lie on the bridging PnP ligands, and not necessarily on the 2,2'-bipyridyl ligand. These results need to be examined more, and it is hoped that future work on these complexes will provide the necessary proof. The chapter concludes with the successful formation of a self-assembled monolayer. The

electrochemistry of the complex on the surface has been reported, and scan rate dependence studies point toward the fact that the responses originate from a surface bound species rather than one in solution.

8.2 Future Work:

For the complexes described in Chapters 3, 4 and 5, the photochemistry of the complexes needs to be investigated further in order to be explained better. The photochemical properties have only been investigated for the LL1 and LL3 ligands, and their ruthenium and osmium complexes. Special attention should be paid to the photochemical properties of the osmium complexes as photochemistry from osmium containing complexes is an unusual characteristic. Another issue that could easily be overlooked concerns the free ligands. It has been demonstrated that the LL1 ligand exhibits photochemistry (the LL3 ligand does not). This should be investigated for the other ligands in the series.

As mentioned already, the rotamers issue has not been fully resolved. Each additional experiment seems to add more information, and provides a better understanding of the processes at work. The description of the formation of the isomers appears to be accurate at this stage. It is hoped that collaboration with Prof. Villani in the future will allow the rotamers of not only the LL6 complex to be examined completely, but also the rotamers of the LL4 and LL5 ligands. Also, attention has focussed solely on the ruthenium complexes, however it has also been illustrated in Chapter 4 that the osmium complexes of the LL4, LL5 and LL6 ligands contain the same properties. This should also be investigated.

Much of the future work arising from the projects investigated in this thesis will arise from the dinuclear complexes introduced in Chapter 7. The two sets of dinuclear complexes, RuPnP2-RuCl and OsPnP2-RuCl are not the ideal complexes to be studying. Investigations of the RuPnP2-RuCl complexes are complicated by the aquo-chloro issue, plus the oxidation potentials of the RuN6 species is quite high, and not observable in the

aqueous environment necessary for the study of self-assembled monolayers. The OsPnP2-RuCl are far from ideal also as the aquo-chloro issue is still present, and while the oxidation potentials are lower than for the RuPnP2-RuCl complex, the two oxidation potentials overlay each other, and become indistinguishable from each other. Future work involving this project will therefore concentrate on the synthesis of the Os-Os dinuclear complexes (this has already been attempted with little success) or on the development of a procedure to investigate self assembling monolayers in a way as to avoid the aquo-chloro issue. It should be recognised however, that while the Os-Os dinuclear complexes may be the most interesting complexes for electrochemical study, those already synthesised are the most interesting from a photophysical point of view. The photophysical and electrochemical examinations of these complexes indicate that the excited state of several of the complexes may lie on the PnP bridging ligands. In order to investigate this deuteriation studies may be necessary. It may also prove useful to probe the excited state resonance Raman properties of these complexes. Additionally, the properties of only one of the complexes attached to a surface has been investigated. This should be completed for each of the dinuclear complexes and the results reported.

Appendix A:

X-Ray Crystallography Data

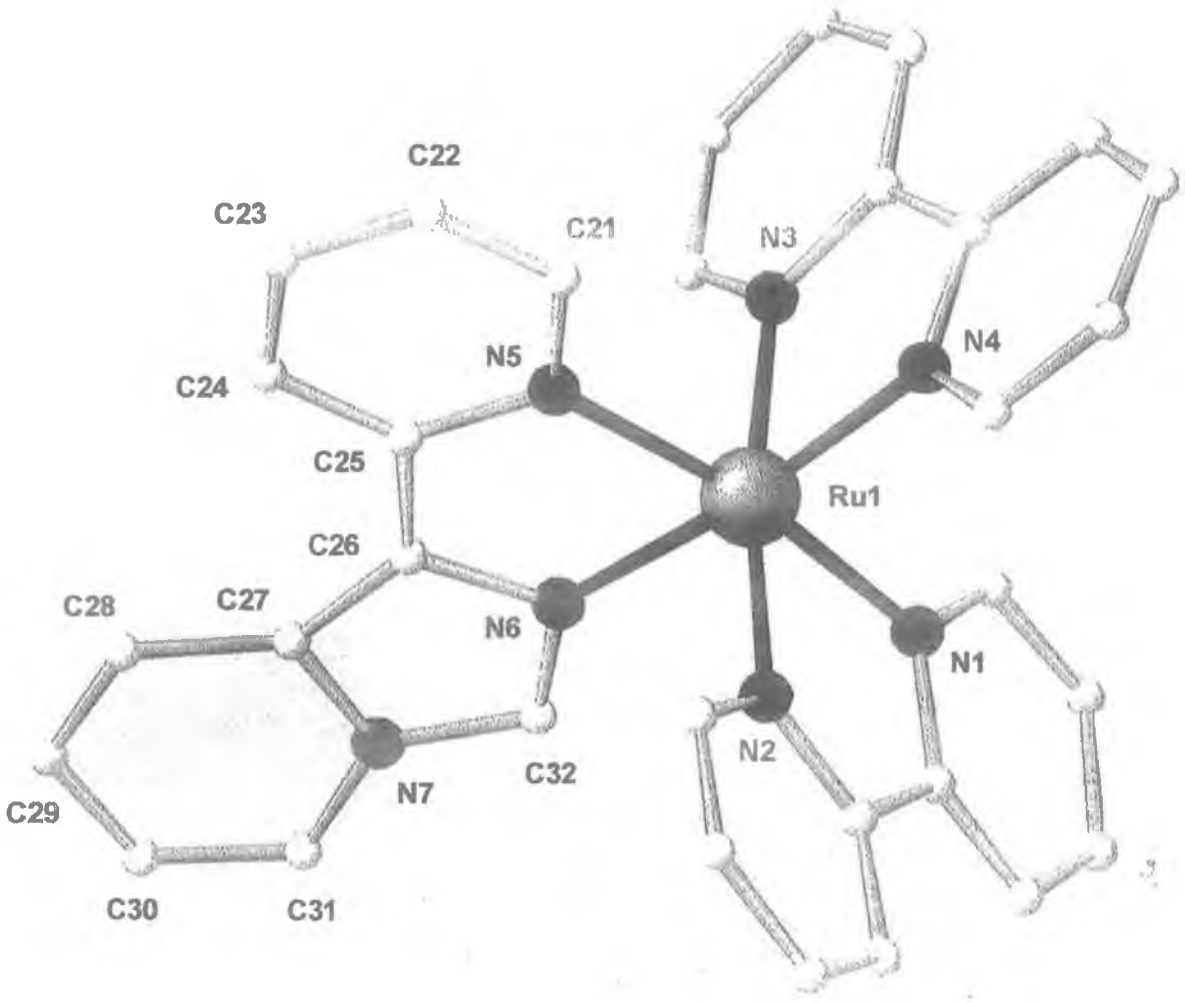

Structure of $[Ru(bpy)_2(LL1)](PF_6)_2$. Detailed X-Ray Crystallography Data from the analysis of this complex follows.

Table 1. Crystal data and structure refinement for ciftab.

Identification code	md1
Empirical formula	C32 H25 F12 N7 P2 Ru
Formula weight	898.60
Temperature	200(2) K
Wavelength	0.71073 A
Crystal system, space group	monoclinic, P2(1)/n (No. 14)
Unit cell dimensions	a = 10.8719(11) A alpha = 90 deg. b = 19.670(2) A beta = 94.846(2) deg. c = 15.7347(16) A gamma = 90 deg.
Volume	3352.9(6) A^3
Z, Calculated density	4, 1.780 Mg/m^3
Absorption coefficient	0.668 mm^-1
F(000)	1792
Crystal size	0.4 x 0.1 x 0.1 mm^3
Theta range for data collection	1.66 to 28.35 deg.
Index ranges	-14<=h<=14, -25<=k<=26, -20<=l<=20
Reflections collected / unique	35986 / 8228 [R(int) = 0.0724]
Completeness to theta = 28.35	97.9%
Refinement method	Full-matrix least-squares on F^2
Data / restraints / parameters	8228 / 0 / 492
Goodness-of-fit on F^2	0.821
Final R indices [I>2sigma(I)]	R1 = 0.0365, wR2 = 0.0660

R indices (all data)	R1 = 0.0896, wR2 = 0.0729
Largest diff. peak and hole	0.589 and -0.517 e.A^-3

Table 2. Atomic coordinates (x 10^4) and equivalent isotropic displacement parameters (A^2 x 10^3) for ciftab. U(eq) is defined as one third of the trace of the orthogonalized Uij tensor.

	x	y	z	U(eq)
Ru(1)	1030(1)	1942(1)	-3289(1)	25(1)
N(1)	-110(2)	2554(1)	-2647(1)	26(1)
N(2)	1086(2)	2835(1)	-3972(1)	26(1)
N(3)	1011(2)	1142(1)	-2446(2)	29(1)
N(4)	2540(2)	2163(1)	-2458(1)	29(1)
N(5)	1973(2)	1334(1)	-4108(1)	25(1)
N(6)	-391(2)	1615(1)	-4145(1)	25(1)
N(7)	-2042(2)	1388(1)	-4998(2)	32(1)
C(1)	-679(3)	2376(2)	-1954(2)	25(1)
C(2)	-1568(3)	2787(2)	-1632(2)	32(1)
C(3)	-1896(3)	3381(2)	-2042(2)	41(1)
C(4)	-1306(3)	3576(2)	-2736(2)	34(1)
C(5)	-404(2)	3164(1)	-3019(2)	25(1)
C(6)	323(3)	3336(2)	-3737(2)	29(1)
C(7)	299(3)	3967(2)	-4130(2)	41(1)

C(8)	1061(3)	4092(2)	-4773(2)	4
6(1)				
C(9)	1839(3)	3591(2)	-5004(2)	3
9(1)				
C(10)	1837(2)	2976(2)	-4591(2)	3
2(1)				
C(11)	182(3)	635(2)	-2471(2)	3
6(1)				
C(12)	218(3)	119(2)	-1872(2)	4
4(1)				
C(13)	1141(3)	122(2)	-1224(2)	5
2(1)				
C(14)	2001(3)	643(2)	-1178(2)	4
5(1)				
C(15)	1920(3)	1153(2)	-1786(2)	3
3(1)				
C(16)	2760(3)	1736(2)	-1785(2)	3
0(1)				
C(17)	3708(3)	1859(2)	-1170(2)	4
3(1)				
C(18)	4485(3)	2405(2)	-1256(2)	4
6(1)				
C(19)	4289(3)	2819(2)	-1948(2)	4
2(1)				
C(20)	3309(3)	2695(2)	-2529(2)	3
5(1)				
C(21)	3196(3)	1203(2)	-4035(2)	3
2(1)				
C(22)	3763(3)	798(2)	-4597(2)	3
4(1)				
C(23)	3064(3)	501(2)	-5258(2)	3
6(1)				
C(24)	1805(3)	617(1)	-5344(2)	3
0(1)				
C(25)	1270(2)	1029(1)	-4768(2)	2
5(1)				
C(26)	-40(2)	1190(1)	-4781(2)	2
4(1)				
C(27)	-1067(3)	1036(1)	-5329(2)	2
7(1)				
C(28)	-1350(3)	652(2)	-6076(2)	3
9(1)				
C(29)	-2520(3)	632(2)	-6449(2)	4
5(1)				
C(30)	-3470(3)	999(2)	-6086(2)	4
4(1)				
C(31)	-3234(3)	1372(2)	-5375(2)	4
2(1)				
C(32)	-1592(3)	1727(1)	-4279(2)	3
0(1)				
P(1)	-4387(1)	3236(1)	-4417(1)	4

0(1)				
	F(11)	-5135(2)	3626(1)	-5182(1) 6
3(1)				
	F(12)	-3500(2)	3875(1)	-4267(1) 7
0(1)				
	F(13)	-5296(2)	3541(1)	-3776(1) 6
8(1)				
	F(14)	-3649(2)	2829(1)	-3665(1) 6
8(1)				
	F(15)	-5286(2)	2592(1)	-4574(1) 6
3(1)				
	F(16)	-3498(2)	2924(1)	-5070(1) 7
2(1)				
	P(2)	-3582(1)	614(1)	-2524(1) 3
7(1)				
	F(21)	-3613(2)	952(1)	-3436(1) 8
5(1)				
	F(22)	-4615(2)	1100(1)	-2258(2) 9
3(1)				
	F(23)	-2555(2)	1139(1)	-2159(1) 5
8(1)				
	F(24)	-3525(2)	251(1)	-1619(1) 8
4(1)				
	F(25)	-2547(2)	101(1)	-2786(1) 7
1(1)				
	F(26)	-4596(2)	77(1)	-2892(1) 5
6(1)				

Table 3. Bond lengths [A] and angles [deg] for ciftab.

Ru(1)-N(1)	2.054(2)
Ru(1)-N(4)	2.057(2)
Ru(1)-N(3)	2.060(2)
Ru(1)-N(2)	2.061(2)
Ru(1)-N(6)	2.064(2)
Ru(1)-N(5)	2.090(2)
N(1)-C(1)	1.346(3)
N(1)-C(5)	1.361(3)
N(2)-C(10)	1.352(3)
N(2)-C(6)	1.359(3)
N(3)-C(11)	1.343(3)
N(3)-C(15)	1.371(3)
N(4)-C(20)	1.349(3)
N(4)-C(16)	1.358(4)
N(5)-C(21)	1.349(3)

N(5)-C(25)	1.374(3)
N(6)-C(32)	1.324(3)
N(6)-C(26)	1.383(3)
N(7)-C(32)	1.367(3)
N(7)-C(31)	1.379(4)
N(7)-C(27)	1.403(3)
C(1)-C(2)	1.387(4)
C(2)-C(3)	1.367(4)
C(3)-C(4)	1.367(4)
C(4)-C(5)	1.375(4)
C(5)-C(6)	1.471(4)
C(6)-C(7)	1.387(4)
C(7)-C(8)	1.382(4)
C(8)-C(9)	1.368(4)
C(9)-C(10)	1.373(4)
C(11)-C(12)	1.384(4)
C(12)-C(13)	1.369(4)
C(13)-C(14)	1.386(4)
C(14)-C(15)	1.384(4)
C(15)-C(16)	1.466(4)
C(16)-C(17)	1.375(4)
C(17)-C(18)	1.380(4)
C(18)-C(19)	1.362(4)
C(19)-C(20)	1.367(4)
C(21)-C(22)	1.375(4)
C(22)-C(23)	1.366(4)
C(23)-C(24)	1.383(4)
C(24)-C(25)	1.381(4)
C(25)-C(26)	1.457(3)
C(26)-C(27)	1.385(4)
C(27)-C(28)	1.409(4)
C(28)-C(29)	1.356(4)
C(29)-C(30)	1.418(4)
C(30)-C(31)	1.345(4)
P(1)-F(13)	1.5887(19)
P(1)-F(12)	1.5897(19)
P(1)-F(14)	1.589(2)
P(1)-F(16)	1.5916(19)
P(1)-F(11)	1.592(2)
P(1)-F(15)	1.6051(19)
P(2)-F(22)	1.560(2)
P(2)-F(21)	1.580(2)
P(2)-F(24)	1.589(2)
P(2)-F(23)	1.5913(18)
P(2)-F(25)	1.5910(19)
P(2)-F(26)	1.5995(18)

N(1)-Ru(1)-N(4)	92.62(9)
N(1)-Ru(1)-N(3)	95.27(9)
N(4)-Ru(1)-N(3)	78.63(10)
N(1)-Ru(1)-N(2)	78.64(9)

N(4)-Ru(1)-N(2)	95.38(9)
N(3)-Ru(1)-N(2)	171.35(9)
N(1)-Ru(1)-N(6)	93.09(8)
N(4)-Ru(1)-N(6)	173.48(9)
N(3)-Ru(1)-N(6)	97.70(9)
N(2)-Ru(1)-N(6)	88.83(8)
N(1)-Ru(1)-N(5)	170.76(9)
N(4)-Ru(1)-N(5)	96.09(8)
N(3)-Ru(1)-N(5)	89.48(8)
N(2)-Ru(1)-N(5)	97.42(9)
N(6)-Ru(1)-N(5)	78.39(9)
C(1)-N(1)-C(5)	118.1(2)
C(1)-N(1)-Ru(1)	125.8(2)
C(5)-N(1)-Ru(1)	115.75(17)
C(10)-N(2)-C(6)	117.8(2)
C(10)-N(2)-Ru(1)	126.6(2)
C(6)-N(2)-Ru(1)	115.45(17)
C(11)-N(3)-C(15)	118.2(3)
C(11)-N(3)-Ru(1)	126.3(2)
C(15)-N(3)-Ru(1)	115.5(2)
C(20)-N(4)-C(16)	118.3(3)
C(20)-N(4)-Ru(1)	125.3(2)
C(16)-N(4)-Ru(1)	116.35(19)
C(21)-N(5)-C(25)	117.6(2)
C(21)-N(5)-Ru(1)	126.01(19)
C(25)-N(5)-Ru(1)	116.37(17)
C(32)-N(6)-C(26)	108.3(2)
C(32)-N(6)-Ru(1)	136.6(2)
C(26)-N(6)-Ru(1)	115.07(17)
C(32)-N(7)-C(31)	128.7(3)
C(32)-N(7)-C(27)	108.6(2)
C(31)-N(7)-C(27)	122.7(3)
N(1)-C(1)-C(2)	121.8(3)
C(3)-C(2)-C(1)	119.2(3)
C(2)-C(3)-C(4)	119.7(3)
C(3)-C(4)-C(5)	119.3(3)
N(1)-C(5)-C(4)	121.9(3)
N(1)-C(5)-C(6)	114.2(2)
C(4)-C(5)-C(6)	123.9(3)
N(2)-C(6)-C(7)	121.1(3)
N(2)-C(6)-C(5)	115.0(2)
C(7)-C(6)-C(5)	123.8(3)
C(8)-C(7)-C(6)	119.7(3)
C(9)-C(8)-C(7)	119.3(3)
C(10)-C(9)-C(8)	118.9(3)
N(2)-C(10)-C(9)	123.1(3)
N(3)-C(11)-C(12)	122.9(3)
C(13)-C(12)-C(11)	118.8(3)
C(12)-C(13)-C(14)	119.4(3)
C(13)-C(14)-C(15)	119.8(3)
N(3)-C(15)-C(14)	120.8(3)

N(3)-C(15)-C(16)	115.0(3)
C(14)-C(15)-C(16)	124.2(3)
N(4)-C(16)-C(17)	120.9(3)
N(4)-C(16)-C(15)	114.5(3)
C(17)-C(16)-C(15)	124.7(3)
C(16)-C(17)-C(18)	119.7(3)
C(19)-C(18)-C(17)	119.3(3)
C(18)-C(19)-C(20)	119.2(3)
N(4)-C(20)-C(19)	122.5(3)
N(5)-C(21)-C(22)	123.2(3)
C(23)-C(22)-C(21)	119.1(3)
C(22)-C(23)-C(24)	119.1(3)
C(25)-C(24)-C(23)	120.1(3)
N(5)-C(25)-C(24)	120.9(2)
N(5)-C(25)-C(26)	113.4(2)
C(24)-C(25)-C(26)	125.7(3)
N(6)-C(26)-C(27)	109.0(2)
N(6)-C(26)-C(25)	116.7(2)
C(27)-C(26)-C(25)	134.2(3)
C(26)-C(27)-N(7)	104.8(2)
C(26)-C(27)-C(28)	138.1(3)
N(7)-C(27)-C(28)	117.1(3)
C(29)-C(28)-C(27)	120.5(3)
C(28)-C(29)-C(30)	119.9(3)
C(31)-C(30)-C(29)	121.2(3)
C(30)-C(31)-N(7)	118.5(3)
N(6)-C(32)-N(7)	109.3(3)
F(13)-P(1)-F(12)	90.49(12)
F(13)-P(1)-F(14)	91.13(12)
F(12)-P(1)-F(14)	91.50(11)
F(13)-P(1)-F(16)	178.93(13)
F(12)-P(1)-F(16)	90.38(12)
F(14)-P(1)-F(16)	89.47(12)
F(13)-P(1)-F(11)	89.54(11)
F(12)-P(1)-F(11)	89.72(11)
F(14)-P(1)-F(11)	178.60(12)
F(16)-P(1)-F(11)	89.84(11)
F(13)-P(1)-F(15)	89.57(11)
F(12)-P(1)-F(15)	179.63(12)
F(14)-P(1)-F(15)	88.87(11)
F(16)-P(1)-F(15)	89.56(11)
F(11)-P(1)-F(15)	89.91(11)
F(22)-P(2)-F(21)	91.38(14)
F(22)-P(2)-F(24)	90.53(14)
F(21)-P(2)-F(24)	178.00(14)
F(22)-P(2)-F(23)	90.24(11)
F(21)-P(2)-F(23)	90.83(11)
F(24)-P(2)-F(23)	89.76(11)
F(22)-P(2)-F(25)	178.48(13)
F(21)-P(2)-F(25)	89.61(13)
F(24)-P(2)-F(25)	88.46(13)

F(23)-P(2)-F(25)	90.90(10)
F(22)-P(2)-F(26)	90.69(11)
F(21)-P(2)-F(26)	89.30(11)
F(24)-P(2)-F(26)	90.09(11)
F(23)-P(2)-F(26)	179.05(11)
F(25)-P(2)-F(26)	88.16(10)

Symmetry transformations used to generate equivalent atoms:

Table 4. Anisotropic displacement parameters (A^2 x 10^3) for ciftab.
The anisotropic displacement factor exponent takes the form:
-2 pi^2 [h^2 a*^2 U11 + ... + 2 h k a* b* U12]

	U11	U22	U33	U23	U13	U12
Ru(1)	23(1)	29(1)	23(1)	-2(1)	2(1)	0(1)
N(1)	27(1)	30(2)	22(1)	-3(1)	3(1)	-2(1)
N(2)	24(1)	32(2)	22(1)	-2(1)	-1(1)	-4(1)
N(3)	26(1)	28(2)	34(2)	-2(1)	9(1)	3(1)
N(4)	29(1)	34(2)	25(1)	-9(1)	0(1)	2(1)
N(5)	23(1)	28(1)	26(1)	-1(1)	4(1)	1(1)
N(6)	25(1)	26(1)	25(1)	0(1)	4(1)	0(1)
N(7)	28(1)	33(2)	35(2)	-1(1)	-4(1)	-2(1)
C(1)	38(2)	36(2)	32(2)	1(2)	9(2)	-1(2)
C(2)	45(2)	49(2)	33(2)	-1(2)	20(2)	3(2)
C(3)	41(2)	40(2)	43(2)	-9(2)	12(2)	9(2)
C(4)	38(2)	32(2)	32(2)	-4(2)	2(2)	4(2)

C(5)	25(2)	27(2)	23(2)	-5(1)	-2(1)
-1(1)					
C(6)	28(2)	32(2)	26(2)	-1(1)	-4(1)
-1(1)					
C(7)	47(2)	37(2)	37(2)	2(2)	3(2)
2(2)					
C(8)	56(2)	39(2)	42(2)	13(2)	0(2)
-8(2)					
C(9)	39(2)	45(2)	33(2)	5(2)	3(2)
-5(2)					
C(10)	26(2)	47(2)	24(2)	-2(2)	0(1)
-3(2)					
C(11)	33(2)	35(2)	42(2)	0(2)	6(2)
5(2)					
C(12)	53(2)	26(2)	53(2)	4(2)	10(2)
2(2)					
C(13)	69(3)	39(2)	49(2)	18(2)	6(2)
11(2)					
C(14)	54(2)	41(2)	40(2)	5(2)	-7(2)
8(2)					
C(15)	33(2)	34(2)	31(2)	-5(2)	2(2)
12(2)					
C(16)	32(2)	31(2)	26(2)	-7(1)	1(1)
8(1)					
C(17)	52(2)	42(2)	33(2)	-2(2)	-9(2)
12(2)					
C(18)	42(2)	52(2)	41(2)	-16(2)	-18(2)
6(2)					
C(19)	35(2)	45(2)	45(2)	-12(2)	-4(2)
-4(2)					
C(20)	34(2)	40(2)	30(2)	-3(2)	-3(2)
-3(2)					
C(21)	23(2)	39(2)	34(2)	2(2)	1(1)
0(1)					
C(22)	21(2)	43(2)	40(2)	4(2)	7(2)
8(2)					
C(23)	40(2)	33(2)	36(2)	-1(2)	15(2)
11(2)					
C(24)	36(2)	29(2)	26(2)	-3(1)	3(1)
0(1)					
C(25)	28(2)	22(2)	25(2)	5(1)	3(1)
0(1)					
C(26)	27(2)	19(2)	26(2)	-1(1)	3(1)
-2(1)					
C(27)	33(2)	21(2)	26(2)	-1(1)	0(1)
-2(1)					
C(28)	42(2)	39(2)	35(2)	1(2)	1(2)
-1(2)					
C(29)	52(2)	44(2)	38(2)	-6(2)	-8(2)
-8(2)					
C(30)	35(2)	48(2)	49(2)	-2(2)	-9(2)

-8(2)					
C(31)	30(2)	44(2)	51(2)	2(2)	0(2)
-2(2)					
C(32)	25(2)	31(2)	35(2)	-3(1)	4(1)
-1(1)					
P(1)	35(1)	38(1)	48(1)	-3(1)	6(1)
-1(1)					
F(11)	56(1)	70(2)	62(1)	14(1)	-4(1)
5(1)					
F(12)	72(1)	56(1)	79(2)	-1(1)	-7(1)
-27(1)					
F(13)	88(2)	50(1)	72(2)	-5(1)	39(1)
9(1)					
F(14)	62(1)	70(2)	70(2)	20(1)	-5(1)
1(1)					
F(15)	50(1)	50(1)	90(2)	-10(1)	6(1)
-14(1)					
F(16)	70(1)	65(2)	86(2)	-2(1)	39(1)
10(1)					
P(2)	37(1)	36(1)	40(1)	-9(1)	6(1)
-4(1)					
F(21)	123(2)	77(2)	53(1)	18(1)	-11(1)
-39(2)					
F(22)	56(1)	75(2)	150(2)	-52(2)	21(2)
11(1)					
F(23)	58(1)	48(1)	66(1)	-18(1)	-2(1)
-18(1)					
F(24)	137(2)	71(2)	44(1)	-1(1)	4(1)
-39(2)					
F(25)	45(1)	74(2)	94(2)	-42(1)	1(1)
7(1)					
F(26)	44(1)	52(1)	72(1)	-14(1)	-3(1)
-15(1)					

Table 5. Hydrogen coordinates (x 10^4) and isotropic displacement parameters (A^2 x 10^3) for ciftab.

	x	y	z	U(eq)
H(1)	-471	1967	-1682	3
6(3)				
H(2)	-1937	2660	-1144	3

6(3)	H(3)	-2517	3651	-1850	3
6(3)	H(4)	-1512	3983	-3013	3
6(3)	H(7)	-228	4305	-3962	3
6(3)	H(8)	1044	4512	-5045	3
6(3)	H(9)	2361	3666	-5433	3
6(3)	H(10)	2378	2640	-4746	3
6(3)	H(11)	-446	630	-2911	4
0(3)	H(12)	-374	-223	-1908	4
0(3)	H(13)	1190	-223	-818	4
0(3)	H(14)	2632	650	-741	4
0(3)	H(17)	3826	1576	-697	4
0(3)	H(18)	5135	2489	-847	4
0(3)	H(19)	4816	3183	-2023	4
0(3)	H(20)	3168	2987	-2991	4
0(3)	H(21)	3679	1397	-3583	2
6(4)	H(22)	4611	726	-4528	2
6(4)	H(23)	3430	224	-5644	2
6(4)	H(24)	1319	418	-5791	2
6(4)	H(28)	-730	411	-6315	3
9(4)	H(29)	-2700	377	-6942	3
9(4)	H(30)	-4271	981	-6345	3
9(4)	H(31)	-3860	1615	-5144	3
9(4)	H(32)	-2057	1995	-3939	4
1(9)					

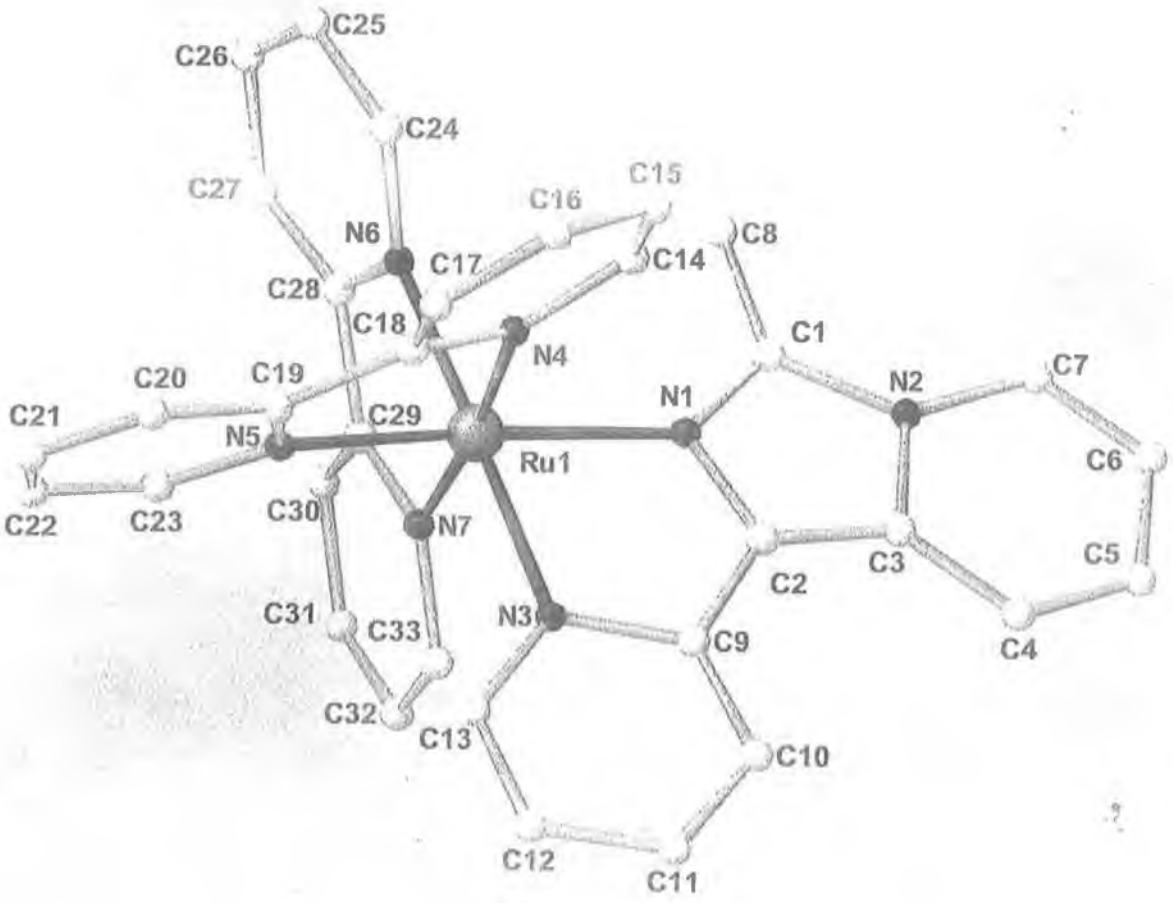

Structure of $[Ru(bpy)_2(LL2)](PF_6)_2$. Detailed X-Ray Crystallography Data from the analysis of this complex follows.

comments: measured with 10 s per frame and delta omega 0.4 d
5598 reflections observed
crystallises with 2 molecule PF6, one full and two half
PF6 anions on special positions (i), one disordered

Table 1. Crystal data and structure refinement for ciftab.

Identification code	md25
Empirical formula	C33 H27 F12 N7 P2 Ru
Formula weight	912.63
Temperature	200(2) K
Wavelength	0.71073 A
Crystal system, space group	monoclinic, P2(1)/n (No. 14)
Unit cell dimensions	a = 13.0742(9) A alpha = 90 deg b = 12.6822(9) A beta = 101.59 deg c = 21.5808(15) A gamma = 90 deg
Volume	3505.3(4) A^3
Z, Calculated density	4, 1.729 Mg/m^3
Absorption coefficient	0.640 mm^-1
F(000)	1824
Crystal size	0.3 x 0.25 x 0.1 mm^3
Theta range for data collection	1.69 to 28.30 deg.
Index ranges	-16<=h<=17, -16<=k<=16, -27<=l<=28
Reflections collected / unique	36830 / 8546 [R(int)] = 0.0665
Completeness to theta = 28.30	93.9%
Refinement method	Full-matrix least-squares on F^2
Data / restraints / parameters	8546 / 0 / 535
Goodness-of-fit on F^2	1.052
Final R indices [I>2sigma(I)]	R1 = 0.0522, wR2 = 0.1296
R indices (all data)	R1 = 0.0910, wR2 = 0.1475
Largest diff. peak and hole	0.797 and -0.711 e.A^-3

Table 2. Atomic coordinates (x 10^4) and equivalent isotr
displacement parameters (A^2 x 10^3) for ciftab.
U(eq) is defined as one third of the trace of the orthogona
Uij tensor.

	x	y	z	U(e
Ru(1)	4216(1)	403(1)	1924(1)	26(
P(1)	3529(1)	3749(1)	1618(1)	47(
P(2)	0	5000	0	59(
P(3)	0	0	0	47(
F(11)	3151(4)	3283(4)	1042(2)	127(
F(12)	4498(3)	2953(3)	1526(2)	90(
F(13)	4240(3)	4588(3)	1190(2)	91(
F(14)	3929(3)	4162(3)	2233(2)	85(
F(15)	2584(4)	4518(4)	1765(3)	122(
F(16)	2840(2)	2906(3)	2070(2)	73(
F(21)	28(4)	6044(15)	226(9)	197(
F(22)	20(.11)	4532(8)	686(3)	118(
F(23)	1149(8)	5427(11)	178(5)	119(
F(21X)	66(3)	6193(14)	100(15)	171(
F(22X)	-591(15)	5024(19)	586(8)	140(
F(23X)	1103(17)	4923 17)	434(14)	186(
F(31)	13(3)	90(1)	66(2)	122(
F(32)	103(3)	641 1)	34(2)	123(
F(33)	5(5)	513 2)	53(2)	126(
N(1)	3692(2)	800(3)	1288(2)	27(
N(2)	2987(3)	2083(3)	641(2)	51(
N(3)	5473 2)	229 2)	1172(2)	28(
N(4)	370(3)	1611 3)	1297(2)	31(
N(5)	1815 3)	1694(3)	2443(2)	31(
N(6)	30(.)	479 3)	2413(2)	30(
N(7)	169(3)	703(3)	2614(2)	34(
C(1)	2853(3)	1445(3)	1153(2)	31(
C(2)	4350(3)	1009(3)	894(2)	29(
C(3)	3942(3)	1808(3)	492(2)	19(
C(4)	4301 1)	2351(1)	20(2)	49(
C(5)	3721(1)	3124(1)	300(2)	57(
C(6)	2721(1)	3397(1)	175(2)	51(
C(7)	2368(1)	2889(3)	290(2)	42(
C(8)	1969(3)	1459(1)	1483(2)	42(
C(9)	5333(3)	454(3)	972(2)	29(
C(10)	6093(1)	573(1)	611(2)	12(
C(11)	7020(1)	23(1)	765(2)	45(
C(12)	7176(1)	636(3)	1287(2)	15(
C(13)	6386 3)	715(1)	1615(2)	38(
C(14)	3005(3)	1534(3)	710(2)	12(
C(15)	2805(1)	2358(1)	324(2)	50(

C(16)	3342(4)	3289(4)	161(2)	51(
C(17)	4033(4)	3385(4)	1024(2)	46(
C(18)	4181(3)	2548(3)	1453(2)	34(
C(19)	4784(3)	2620(3)	2109(2)	37(
C(20)	5192(4)	3544(4)	2396(3)	49(
C(21)	5640(4)	3536(4)	3030(3)	62(
C(22)	5682(4)	2631(4)	3365(2)	53(
C(23)	5280(3)	1703(4)	3062(2)	38(
C(24)	2193(3)	1144(3)	2297(2)	38(
C(25)	1517(3)	1267(4)	2698(2)	42(
C(26)	1690(4)	697(4)	3257(2)	43(
C(27)	2508(4)	10(4)	3379(2)	41(
C(28)	3154(3)	-110(3)	2949(2)	33(
C(29)	4056(3)	848(3)	3036(2)	32(
C(30)	4255(4)	-1599(4)	3589(2)	43(
C(31)	5161(4)	-2215(4)	3567(2)	53(
C(32)	5806(4)	-2057(4)	3152(2)	54(
C(33)	5561(4)	1307(4)	2673(2)	43(

Table 3. Bond lengths [A] and angles [deg] for ciftab.

Ru(1)-N(7)	2.050(3)
Ru(1)-N(6)	2.057(3)
Ru(1) N(5)	2.059(3)
Ru(1) N(1)	2.064(3)
Ru(1) N(4)	2.074(3)
Ru(1) N(3)	2.086(3)
P(1) F(14)	1.544(3)
P(1) F(15)	1.556(4)
P(1) F(13)	1.582(3)
P(1) F(16)	1.599(3)
P(1) F(12)	1.600(4)
P(1) F(11)	1.608(3)
P(2) F(21)#1	1.486(12)
P(2) F(21)	1.486(12)
P(2) F(21X)#1	1.532(19)
P(2) F(21X)	1.533(19)
P(2) F(23X)	1.556(16)
P(2) F(23X)#1	1.556(16)
P(2) F(23)#1	1.570(9)
P(2) F(23)	1.570(9)
P(2) F(22)#1	1.568(6)
P(2) F(22)	1.568(6)
P(2)-F(22X)#1	1.609(18)
P(2) F(22X)	1.609(18)
P(3) F(31)#2	1.561(4)
P(3) F(31)	1.561(4)
P(3) F(32)	1.563(4)
P(3) F(32)#2	1.563(4)
P(3) F(33)#2	1.571(4)

P(3)-F(33)	1.575(4)
F(21)-F(21X)	0.49(6)
F(21)-F(22X)	1.60(3)
F(22)-F(22X)	1.190(15)
F(22)-F(23X)	1.48(3)
F(23)-F(23X)	0.86(3)
F(23)-F(21X)	1.83(3)
F(23)-F(22X)#1	1.759(19)
F(22X)-F(23)#1	1.759(19)
N(1)-C(2)	1.353(5)
N(1)-C(1)	1.352(5)
N(2)-C(3)	1.394(5)
N(2)-C(1)	1.410(6)
N(2)-C(7)	1.425(6)
N(3)-C(13)	1.341(5)
N(3)-C(9)	1.366(5)
N(4)-C(18)	1.352(5)
N(4)-C(14)	1.360(5)
N(5)-C(23)	1.343(5)
N(5)-C(19)	1.372(5)
N(6)-C(24)	1.354(5)
N(6)-C(28)	1.358(5)
N(7)-C(33)	1.351(5)
N(7)-C(29)	1.368(5)
C(1)-C(8)	1.473(6)
C(2)-C(3)	1.371(5)
C(2)-C(9)	1.445(5)
C(3)-C(4)	1.388(5)
C(4)-C(5)	1.343(6)
C(5)-C(6)	1.429(7)
C(6)-C(7)	1.350(6)
C(7)-C(10)	1.390(6)
C(10)-C(11)	1.379(6)
C(11)-C(12)	1.384(6)
C(12)-C(13)	1.371(6)
C(14)-C(15)	1.368(6)
C(15)-C(16)	1.375(7)
C(16)-C(17)	1.366(7)
C(17)-C(18)	1.396(6)
C(18)-C(19)	1.479(6)
C(19)-C(20)	1.382(6)
C(20)-C(21)	1.377(7)
C(21)-C(22)	1.352(8)
C(22)-C(23)	1.397(6)
C(24)-C(25)	1.366(6)
C(25)-C(26)	1.385(6)
C(26)-C(27)	1.364(7)
C(27)-C(28)	1.382(6)
C(28)-C(29)	1.488(6)
C(29)-C(30)	1.382(6)
C(30)-C(31)	1.404(7)
C(31)-C(32)	1.364(7)
C(32)-C(33)	1.394(6)

N(7)-Ru(1) N(6)	79.20(13)
N(7)-Ru(1)-N(5)	96.83(13)
N(6)-Ru(1) N(5)	86.89(13)
N(7)-Ru(1)-N(4)	174.52(13)
N(6) Ru(1) N(4)	97.03(12)
N(5) Ru(1)-N(4)	78.90(13)
N(7) Ru(1) N(1)	89.37(13)
N(6) Ru(1) N(1)	100.92(13)
N(5) Ru(1) N(1)	170.85(12)
N(4)-Ru(1)-N(1)	95.28(13)
N(7)-Ru(1)-N(3)	96.44(13)
N(6)-Ru(1) N(3)	175.62(13)
N(5) Ru(1)-N(3)	91.15(12)
N(4)-Ru(1)-N(3)	87.35(12)
N(1)-Ru(1)-N(3)	78.43(12)
F(11)-P(1)-F(15)	92.0(3)
F(11)-P(1)-F(13)	92.0(2)
F(15)-P(1)-F(13)	92.7(2)
F(11)-P(1)-F(16)	90.17(19)
F(15)-P(1)-F(16)	88.2(2)
F(13)-P(1)-F(16)	177.7(2)
F(11)-P(1)-F(12)	91.8(3)
F(15)-P(1)-F(12)	175.4(3)
F(13)-P(1)-F(12)	89.7(2)
F(16)-P(1)-F(12)	89.32(19)
F(11) P(1)-F(14)	176.4(3)
F(15) P(1) F(14)	90.2(3)
F(13) P(1) F(14)	88.7(2)
F(16) P(1) F(14)	87.13(19)
F(12) P(1) F(14)	92.8(2)
F(21)#1 P(2) F(21)	179.998(2)
F(21)#1-P(2)-F(21X)#1	18(2)
F(21)-P(2)-F(21X)#1	162(2)
F(21)#1 P(2) F(21X)	162(2)
F(21) P(2) F(21X)	18(2)
F(21X)#1 P(2) F(21X)	179.998(3)
F(21)#1-P(2) F(23X)	82.9(7)
F(21) P(2)-F(23X)	97.1(7)
F(21X)#1 P(2)-F(23X)	87.6(12)
F(21X) P(2) F(23X)	92.4(12)
F(21)#1 P(2) F(23X)#1	97.1(7)
F(21) P(2) F(23X)#1	82.9(7)
F(21X)#1 P(2) F(23X)#1	92.4(12)
F(21X) P(2) F(23X)#1	87.6(12)
F(23X) P(2)-F(23X)#1	179.998(4)
F(21)#1-P(2) F(23)#1	84.6(9)
F(21)-P(2) F(23)#1	95.1(9)
F(21X)#1-P(2) F(23)#1	72.3(13)
F(21X) P(2)-F(23)#1	107.7(13)
F(23X) P(2) F(23)#1	148.3(12)
F(23X)#1 P(2) F(23)#1	31.7(12)
F(21)#1 P(2) F(23)	95.4(9)

F(21)-P(2)-F(23)	81.6(9)
F(21X)#1-P(2)-F(23)	107.7(13)
F(21X)-P(2)-F(23)	72.3(13)
F(23X)-P(2)-F(23)	31.7(12)
F(23X)#1-P(2)-F(23)	148.3(12)
F(23')#1-P(2)-F(23)	179.997(1)
F(21')#1-P(2)-F(22')#1	91.8(8)
F(21')-P(2)-F(22')#1	88.2(8)
F(21')#1-P(2)-F(22')#1	104.2(13)
F(21X')-P(2)-F(22)#1	75.8(13)
F(23X)-P(2)-F(22)#1	123.4(12)
F(23X)#1-P(2)-F(22)#1	56.6(12)
F(23')#1-P(2)-F(22)#1	86.0(5)
F(23')-P(2)-F(22')#1	94.0(5)
F(21')#1-P(2)-F(22)	88.2(8)
F(21')-P(2)-F(22)	91.8(8)
F(21X)#1-P(2)-F(22)	75.8(13)
F(21X)-P(2)-F(22)	104.2(13)
F(23X)-P(2)-F(22)	56.6(12)
F(23X)#1-P(2)-F(22)	123.4(12)
F(23')#1-P(2)-F(22)	94.0(5)
F(23')-P(2)-F(22)	86.0(5)
F(22)#1-P(2)-F(22)	180.0
F(21)#1-P(2)-F(22X)#1	62.1(10)
F(21')-P(2)-F(22X)#1	117.9(10)
F(21X)#1-P(2)-F(22X)#1	89.0(17)
F(21X)-P(2)-F(22X)#1	106.0(17)
F(23X')-P(2)-F(22X)#1	84.5(11)
F(23')#1-P(2)-F(22X)#1	95.5(11)
F(21')#1-P(2)-F(22X)	-1-2.998
F(21')-P(2)-F(22X)	[illegible]
F(21X')#1-P(2)-F(22X)	[illegible]
F(21X')-P(2)-F(22X)	138.0(6)
F(23X)-P(2)-F(22X)#1	117.9(10)
F(23X)#1-P(2)-F(22X)	62.1(10)
F(23')-P(2)-F(22X)	169.0(17)
F(23')#1-P(2)-F(22X)	11.97(12)
F(22)-P(2)-F(22X)	95.5(11)
F(23X')-P(2)-F(22X')	86.5(11)
F(23X')#1-P(2)-F(22X)	67.1(8)
F(21')#1-P(2)-F(22X)	112.9(8)
F(21')-P(2)-F(22X)	138.0(6)
F(22')#1-P(2)-F(22X)	41.0(6)
F(22X)#1-P(2)-F(22X)	179.999(2)
F(31)#2-P(3)-F(31)	180.0
F(31)#2-P(3)-F(32)	90.7(3)
F(31)-P(3)-F(32)	89.3(3)
F(31')#2-P(3)-F(31')#2	[illegible]
F(31')-P(3)-F(32)#2	92.7(3)
F(32)-P(3)-F(32)#2	179.996(2)
F(31)#2-P(3)-F(33')#2	[illegible]
F(31')-P(3)-F(33)#2	91.3(3)
F(32)-P(3)-F(33)#2	97.0(3)

F(32)#2 P(3) F(33)#2	88.0(3)
F(31)#2 P(3) F(33)	91.0(3)
F(31) P(3) F(33)	89.0(3)
F(32) P(3) F(33)	88.0(3)
F(32)#2 P(3) F(33)	92.0(3)
F(33)#2 P(3) F(33)	180.0
F(21X) F(21) P(2)	86(4)
F(21X) F(21) F(22X)	116(4)
P(2) F(21) F(22X)	62.8(8)
F(22X) F(22) F(23X)	119.0(15)
F(22X) F(22) P(2)	69.9(10)
F(23X) F(22) P(2)	61.3(8)
F(23X) F(23) P(2)	73.2(17)
F(23X) F(23) F(21X)	107(2)
P(2) F(23) F(21X)	52.9(8)
F(23X) F(23) F(22X)#1	107(2)
P(2) F(23) F(22X)#1	57.5(8)
F(21X) F(23) F(22X)#1	81.2(11)
F(21) F(21X) P(2)	75(3)
F(21) F(21X) F(23)	111(4)
P(2) F(21X) F(23)	54.8(9)
F(22) F(22X) F(21)	102.8(16)
F(22) F(22X) P(2)	66.2(9)
F(21) F(22X) P(2)	55.2(9)
F(22) F(22X) F(23)#1	100.5(10)
F(21) F(22X) F(23)#1	81.5(10)
P(2) F(22X) F(23)#1	55.4(6)
F(23) F(23X) F(22)	136.8(17)
F(23) F(23X) P(2)	74.0(15)
F(22) F(23X) P(2)	69.1(9)
C(2) N(1) C(1)	117.7(3)
C(2) N(1) Ru(1)	113.1(2)
C(1) N(1) Ru(1)	137.2(3)
C(3) N(2) C(1)	107.2(3)
C(3) N(2) C(7)	119.7(4)
C(1) N(2) C(7)	133.1(4)
C(13) N(3) C(9)	117.7(3)
C(13) N(3) Ru(1)	120.1(3)
C(9) N(3) Ru(1)	116.3(3)
C(18) N(4) C(14)	118.5(4)
C(18) N(4) Ru(1)	111.7(3)
C(14) N(4) Ru(1)	126.7(3)
C(23) N(5) C(19)	118.9(4)
C(23) N(5) Ru(1)	126.2(3)
C(19) N(5) Ru(1)	111.9(3)
C(24) N(6) C(28)	117.5(3)
C(24) N(6) Ru(1)	126.5(3)
C(28) N(6) Ru(1)	115.5(3)
C(33) N(7) C(29)	118.2(4)
C(33) N(7) Ru(1)	125.8(3)
C(29) N(7) Ru(1)	115.9(3)
N(1) C(1) N(2)	107.9(3)
N(1) C(1) C(8)	125.8(4)

N(2) C(1) C(8)	127.2(4)
N(1)-C(2) C(3)	109.1(3)
N(1)-C(2)-C(9)	119.6(3)
C(3)-C(2) C(9)	131.2(3)
C(2) C(3) C(4)	133.1(4)
C(2) C(3) N(2)	107.0(3)
C(4) C(3) N(2)	119.9(4)
C(5) C(4) C(3)	119.9(4)
C(4) C(5) C(6)	121.9(5)
C(7) C(6) C(5)	119.3(4)
C(6) C(7) N(2)	119.5(4)
N(3) C(9) C(10)	120.9(4)
N(3) C(9) C(2)	112.1(3)
C(10) C(9) C(2)	126.9(4)
C(11) C(10) C(9)	120.1(4)
C(10) C(11) C(12)	118.8(4)
C(13)-C(12)-C(11)	118.5(4)
N(3) C(13) C(12)	124.0(4)
N(4)-C(14) C(15)	122.1(4)
C(14)-C(15) C(16)	119.5(5)
C(17)-C(16) C(15)	119.1(4)
C(16)-C(17)-C(18)	120.0(5)
N(4) C(18) C(17)	120.6(4)
N(4)-C(18) C(19)	115.0(4)
C(17) C(18)-C(19)	124.3(4)
N(5) C(19) C(20)	120.9(4)
N(5) C(19) C(18)	114.4(4)
C(20) C(19) C(18)	121.4(4)
C(21) C(20) C(19)	119.3(5)
C(22) C(21) C(20)	120.0(5)
C(21) C(22) C(23)	119.7(5)
N(5) C(23) C(22)	121.2(5)
N(6) C(24) C(25)	123.2(4)
C(24) C(25) C(26)	118.7(4)
C(27) C(26) C(25)	119.1(4)
C(26) C(27) C(28)	120.1(4)
N(6) C(28) C(27)	121.3(4)
N(6) C(28) C(29)	114.6(4)
C(27) C(28) C(29)	124.1(4)
N(7) C(29) C(30)	122.4(4)
N(7) C(29) C(28)	111.0(4)
C(30) C(29) C(28)	123.6(4)
C(29) C(30) C(31)	118.6(4)
C(32) C(31) C(30)	118.8(4)
C(31) C(32) C(33)	120.5(5)
N(7) C(33) C(32)	121.4(4)

Symmetry transformations used to generate equivalent atom
#1 -x, y-1, -z #2 -x, y, -z

Table 4. Anisotropic displacement parameters (A^2 x 10^3) for c

The anisotropic displacement factor exponent takes the form:
2 pi^2 | h^2 a*^2 U11 + ... + 2 h k a* b* U12 |

	U11	U22	U33	U23	U13
[illegible]	[illegible]	25(1)	27(1)	1(1)	6(1)
P(1)	38(1)	46(1)	57(1)	9(1)	10(1)
P(2)	52(1)	68(1)	48(1)	18(1)	-14(1)
P(3)	34(1)	59(1)	48(1)	15(1)	9(1)
F(11)	157(4)	175(5)	54(2)	-3(2)	33(2)
F(12)	74(2)	75(2)	104(3)	4(2)	-20(2)
F(13)	88(3)	78(3)	111(3)	-42(2)	29(2)
F(14)	104(3)	75(2)	88(2)	7(2)	45(2)
F(15)	89(3)	114(4)	161(4)	-18(3)	19(3)
F(16)	57(2)	93(3)	67(2)	-12(2)	12(2)
F(21)	197(13)	193(16)	135(10)	119(11)	-128(9)
F(22)	156(11)	138(8)	43(3)	-24(4)	-22(4)
F(23)	65(7)	197(13)	89(6)	27(7)	6(5)
F(21X)	250(3)	32(8)	170(2)	11(11)	-94(18)
F(22X)	126(14)	181(18)	92(11)	57(11)	-28(10)
F(23X)	115(18)	126(17)	250(3)	134(17)	-126(18)
F(31)	106(3)	126(4)	129(4)	71(3)	8(3)
F(32)	86(3)	176(5)	115(3)	55(3)	41(3)
F(33)	170(5)	109(4)	76(3)	-12(2)	30(3)
N(1)	24(2)	25(2)	32(2)	1(1)	3(1)
N(2)	50(3)	47(2)	55(3)	5(2)	4(2)
N(3)	25(2)	26(2)	33(2)	3(1)	5(1)
N(4)	[illegible]	29(2)	32(2)	2(1)	13(2)
N(5)	[illegible]	32(2)	33(2)	6(2)	6(1)
N(6)	39(2)	33(2)	28(2)	2(1)	7(1)
N(7)	31(2)	29(2)	33(2)	-2(1)	3(2)
C(1)	26(2)	34(2)	32(2)	4(2)	3(2)
C(2)	29(2)	27(2)	30(2)	-2(2)	5(2)
C(3)	[illegible]	18(2)	25(2)	4(1)	3(1)
C(4)	36(3)	54(3)	59(3)	22(2)	16(2)
C(5)	55(3)	55(3)	64(3)	30(3)	19(3)
C(6)	47(3)	50(3)	53(3)	19(2)	4(2)
C(7)	36(3)	42(3)	46(3)	8(2)	3(2)
C(8)	34(2)	48(3)	44(3)	2(2)	11(2)
C(9)	25(2)	28(2)	34(2)	-4(2)	6(2)
C(10)	37(2)	47(3)	46(3)	-18(2)	19(2)
C(11)	30(2)	50(3)	61(3)	17(3)	22(2)
C(12)	28(2)	46(3)	62(3)	14(2)	13(2)
C(13)	28(2)	34(2)	51(3)	-12(2)	5(2)
C(14)	42(3)	40(3)	32(2)	0(2)	10(2)
C(15)	64(3)	55(3)	33(2)	5(2)	10(2)
C(16)	82(4)	43(3)	44(3)	16(2)	28(3)
C(17)	62(3)	28(2)	56(3)	3(2)	30(3)
C(18)	38(2)	26(2)	43(2)	1(2)	19(2)
C(19)	29(2)	35(2)	50(3)	-4(2)	13(2)

C(20)	43(3)	32(3)	72(3)	4(2)	8(3)
C(21)	54(3)	45(3)	81(4)	29(3)	-2(3)
C(22)	39(3)	59(4)	55(3)	27(3)	-4(2)
C(23)	32(2)	41(3)	39(2)	11(2)	3(2)
C(24)	41(3)	36(2)	40(2)	9(2)	16(2)
C(25)	33(2)	46(3)	49(3)	2(2)	12(2)
C(26)	40(3)	52(3)	43(3)	4(2)	22(2)
C(27)	42(3)	50(3)	35(2)	3(2)	15(2)
C(28)	39(2)	32(2)	30(2)	3(2)	6(2)
C(29)	34(2)	33(2)	27(2)	3(2)	-1(2)
C(30)	57(3)	36(3)	34(2)	3(2)	8(2)
C(31)	73(4)	38(3)	42(3)	13(2)	0(3)
C(32)	59(3)	45(3)	53(3)	6(2)	1(3)
C(33)	44(3)	41(3)	40(2)	1(2)	1(2)

Table 5. Hydrogen coordinates (x 10^4) and isotropic displacement parameters (A^2 x 10^3) for cifLab.

	x	y	z	U(e
H(4)	4947	2178	-74	57(
H(5)	3979	-3491	-610	57(
H(6)	2324	3920	410	57(
H(7)	1722	3065	379	57(
H(8A)	2215	1655	1917	66(
H(8B)	1453	[illegible]	1082	66(
H(8C)	1615	771	1463	66(
H(10)	5977	1021	264	47(
H(11)	7530	93	524	47(
H(12)	7803	995	1413	47(
H(13)	6488	1205	1957	47(
H(14)	3652	981	639	52(
H(15)	2309	2289	48	52(
H(16)	3236	3845	175	52(
H(17)	4405	4008	1121	52(
H(20)	5164	4165	2164	53(
H(21)	5914	4154	3229	53(
H(22)	5977	2625	3794	53(
H(23)	5314	1080	3293	53(
H(24)	2080	1536	1925	46(
H(25)	951	1724	2598	46(
H(26)	1255	783	3545	46(
H(27)	2631	-380	3752	46(
H(30)	3797	1694	3781	62(
H(31)	5318	2723	3883	62(
H(32)	6414	2153	2748	62(
H(33)	6003	1220	1588	62(

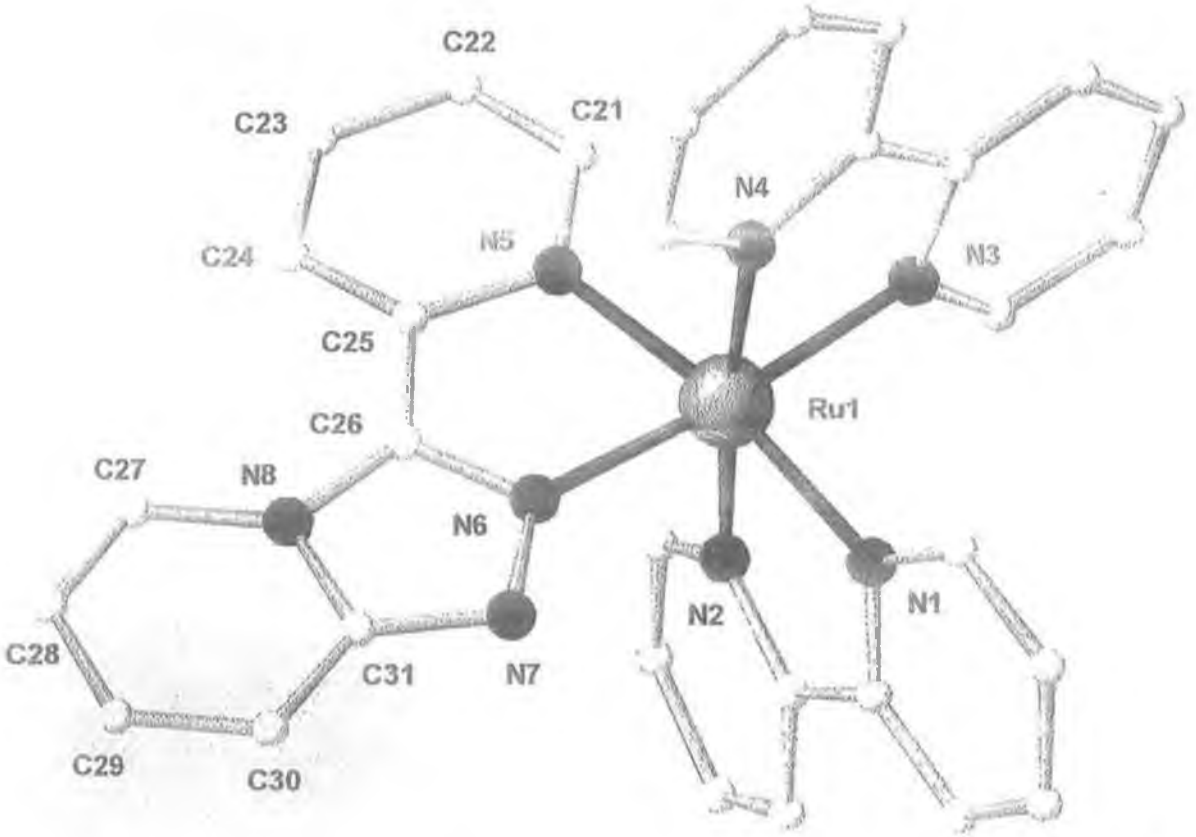

Structure of $[Ru(bpy)_2(LL3)](PF_6)_2$. Detailed X-Ray Crystallography Data from the analysis of this complex follows.

Table 1. Crystal data and structure refinement for ciftab.

Identification code	md2
Empirical formula	C34 H30 F12 N8 O P2 Ru
Formula weight	957.67
Temperature	200(2) K
Wavelength	0.71073 A
Crystal system, space group	monoclinic, P2(1)/c (No. 14)
Unit cell dimensions	a = 17.7163(12) A alpha = 90 deg. b = 13.8631(9) A beta = 112.3450(10) deg. c = 16.3970(11) A gamma = 90 deg.
Volume	3724.8(4) A^3
Z, Calculated density	4, 1.708 Mg/m^3
Absorption coefficient	0.610 mm^-1
F(000)	1920
Crystal size	0.3 x 0.3 x 0.1 mm^3
Theta range for data collection	1.24 to 28.30 deg.
Index ranges	-23<=h<=23, -18<=k<=18, -21<=l<=21
Reflections collected / unique	39757 / 9138 [R(int) = 0.0697]
Completeness to theta = 28.30	94.8%
Refinement method	Full-matrix least-squares on F^2
Data / restraints / parameters	9138 / 0 / 565
Goodness-of-fit on F^2	1.049
Final R indices [I>2sigma(I)]	R1 = 0.0492, wR2 = 0.1041

R indices (all data)	R1 = 0.0941, wR2 = 0.1268
Largest diff. peak and hole	0.846 and -0.697 e.A^-3

Table 2. Atomic coordinates (x 10^4) and equivalent iso
Eropic displacement parameters (A^2 x 10^3) for ciftab.
U(eq) is defined as one third of the trace of the orthogo
nalized Uij tensor.

	x	y	z	U(eq)
Ru(1)	2197(1)	-673(1)	-645(1)	28(1)
N(1)	1064(2)	-1144(2)	-745(2)	30(1)
N(2)	1491(2)	534(2)	-1158(2)	32(1)
N(3)	2008(2)	-1352(2)	-1822(2)	32(1)
N(4)	2823(2)	-1950(2)	-216(2)	31(1)
N(5)	3284(2)	33(2)	-473(2)	32(1)
N(6)	2504(2)	-68(2)	566(2)	29(1)
N(7)	2151(2)	-109(2)	1176(2)	30(1)
C(31)	2628(2)	431(3)	1853(2)	32(1)
C(1)	860(3)	-2058(3)	-627(2)	36(1)
C(2)	95(3)	-2299(3)	-673(3)	45(1)
C(3)	-489(3)	-1584(3)	-830(3)	48(1)
C(4)	-295(2)	-661(3)	-969(3)	41(1)
C(5)	481(2)	-448(3)	-935(2)	32(1)
C(6)	720(2)	494(3)	-1168(2)	31(1)

C(7)	201(3)	1282(3)	-1436(3)	4
1(1)				
C(8)	456(3)	2115(3)	-1720(3)	4
6(1)				
C(9)	1224(3)	2134(3)	-1739(3)	4
5(1)				
C(10)	1723(2)	1341(3)	-1453(2)	3
7(1)				
C(11)	1522(3)	-1036(3)	-2630(3)	3
9(1)				
C(12)	1390(3)	-1560(3)	-3393(3)	4
5(1)				
C(13)	1763(3)	-2439(3)	-3322(3)	5
0(1)				
C(14)	2253(3)	-2782(3)	-2510(3)	4
5(1)				
C(15)	2358(2)	-2236(3)	-1764(2)	3
4(1)				
C(16)	2830(2)	-2566(3)	-860(2)	3
4(1)				
C(17)	3253(3)	-3436(3)	-652(3)	5
0(1)				
C(18)	3665(3)	-3691(3)	211(3)	5
6(1)				
C(19)	3655(3)	-3073(3)	859(3)	5
1(1)				
C(20)	3233(3)	-2216(3)	629(3)	3
9(1)				
C(21)	3639(2)	81(3)	-1073(3)	4
0(1)				
C(22)	4284(3)	68?(3)	-983(3)	5
0(1)				
C(23)	4590(3)	1256(3)	-251(3)	5
1(1)				
C(24)	4264(3)	1209(3)	392(3)	4
4(1)				
C(25)	3617(2)	588(3)	271(2)	3
3(1)				
C(26)	3171(2)	474(2)	848(2)	3
0(1)				
N(8)	3281(2)	811(2)	1678(2)	3
3(1)				
C(27)	3870(3)	1364(3)	2292(3)	4
7(1)				
C(28)	3806(3)	1546(3)	3065(3)	5
6(1)				
C(29)	3149(3)	1179(4)	3263(3)	5
7(1)				
C(30)	2562(3)	625(3)	2666(3)	4
3(1)				
O(100)	-2276(4)	-2946(5)	-1901(4)	14

4(2)				
	C(100)	-2352(4)	-2868(4)	-523(4)	7
7(2)				
	C(101)	-2392(3)	-3362(5)	-1291(4)	7
6(2)				
	C(102)	-2616(4)	-4413(5)	-1399(4)	10
3(3)				
	P(1)	885(1)	5066(1)	-1188(1)	4
3(1)				
	F(11)	635(2)	4232(2)	-671(2)	6
5(1)				
	F(12)	1191(2)	5715(2)	-318(2)	6
4(1)				
	F(13)	-4(2)	5531(2)	-1490(2)	6
5(1)				
	F(14)	1149(2)	5895(2)	-1702(2)	6
8(1)				
	F(15)	585(2)	4417(2)	-2057(2)	6
8(1)				
	F(16)	1778(2)	4596(2)	-899(2)	6
2(1)				
	P(2)	4863(1)	-3763(1)	-1853(1)	5
2(1)				
	F(21)	5225(2)	-4737(2)	-2050(3)	8
9(1)				
	F(24)	4508(2)	-2768(3)	-1667(3)	11
2(2)				
	F(22)	4764(4)	-4285(5)	-1048(4)	8
9(2)				
	F(23)	3955(3)	-4022(4)	-2454(3)	6
0(2)				
	F(25)	4949(4)	-3208(4)	-2661(4)	8
4(2)				
	F(26)	5754(3)	-3405(4)	-1252(5)	9
0(2)				
	F(22X)	4143(17)	-4312(15)	-1810(3)	15
7(17)				
	F(23X)	4475(10)	-4011(13)	-2918(10)	10
0(7)				
	F(25X)	5576(11)	-3325(10)	-2097(14)	8
3(6)				
	F(26X)	5319(19)	-3660(13)	-901(9)	14
4(11)				

Table 3. Bond lengths [A] and angles [deg] for ciftab.

Ru(1)-N(6)	2.030(3)
Ru(1)-N(3)	2.058(3)
Ru(1)-N(1)	2.058(3)
Ru(1)-N(4)	2.065(3)
Ru(1)-N(2)	2.067(3)
Ru(1)-N(5)	2.082(3)
N(1)-C(1)	1.351(5)
N(1)-C(5)	1.360(5)
N(2)-C(10)	1.344(5)
N(2)-C(6)	1.361(5)
N(3)-C(11)	1.348(5)
N(3)-C(15)	1.361(5)
N(4)-C(20)	1.348(5)
N(4)-C(16)	1.363(4)
N(5)-C(21)	1.355(5)
N(5)-C(25)	1.372(5)
N(6)-C(26)	1.327(5)
N(6)-N(7)	1.369(4)
N(7)-C(31)	1.339(5)
C(31)-N(8)	1.396(5)
C(31)-C(30)	1.407(5)
C(1)-C(2)	1.370(6)
C(2)-C(3)	1.385(6)
C(3)-C(4)	1.366(6)
C(4)-C(5)	1.386(5)
C(5)-C(6)	1.468(5)
C(6)-C(7)	1.388(5)
C(7)-C(8)	1.385(6)
C(8)-C(9)	1.373(6)
C(9)-C(10)	1.376(6)
C(11)-C(12)	1.388(5)
C(12)-C(13)	1.371(6)
C(13)-C(14)	1.369(6)
C(14)-C(15)	1.388(5)
C(15)-C(16)	1.471(5)
C(16)-C(17)	1.392(6)
C(17)-C(18)	1.369(6)
C(18)-C(19)	1.369(6)
C(19)-C(20)	1.379(6)
C(21)-C(22)	1.376(6)
C(22)-C(23)	1.370(7)
C(23)-C(24)	1.384(6)
C(24)-C(25)	1.386(6)
C(25)-C(26)	1.451(5)
C(26)-N(8)	1.383(4)
N(8)-C(27)	1.376(5)
C(27)-C(28)	1.340(6)
C(28)-C(29)	1.416(7)
C(29)-C(30)	1.363(6)
O(100)-C(101)	1.238(7)

C(100)-C(101)	1.412(8)
C(101)-C(102)	1.503(9)
P(1)-F(11)	1.594(3)
P(1)-F(14)	1.596(3)
P(1)-F(15)	1.595(3)
P(1)-F(13)	1.596(3)
P(1)-F(12)	1.597(3)
P(1)-F(16)	1.607(3)
P(2)-F(26X)	1.466(15)
P(2)-F(22X)	1.512(15)
P(2)-F(22)	1.572(5)
P(2)-F(23)	1.575(5)
P(2)-F(21)	1.580(3)
P(2)-F(25X)	1.584(13)
P(2)-F(25)	1.588(5)
P(2)-F(26)	1.590(4)
P(2)-F(24)	1.592(4)
P(2)-F(23X)	1.651(14)

N(6)-Ru(1)-N(3)	173.87(12)
N(6)-Ru(1)-N(1)	95.70(11)
N(3)-Ru(1)-N(1)	88.53(11)
N(6)-Ru(1)-N(4)	96.36(12)
N(3)-Ru(1)-N(4)	78.62(12)
N(1)-Ru(1)-N(4)	97.81(12)
N(6)-Ru(1)-N(2)	87.68(11)
N(3)-Ru(1)-N(2)	97.52(12)
N(1)-Ru(1)-N(2)	78.67(12)
N(4)-Ru(1)-N(2)	174.92(12)
N(6)-Ru(1)-N(5)	77.48(12)
N(3)-Ru(1)-N(5)	98.89(12)
N(1)-Ru(1)-N(5)	169.86(12)
N(4)-Ru(1)-N(5)	90.46(12)
N(2)-Ru(1)-N(5)	93.43(12)
C(1)-N(1)-C(5)	118.5(3)
C(1)-N(1)-Ru(1)	126.3(3)
C(5)-N(1)-Ru(1)	115.2(2)
C(10)-N(2)-C(6)	118.1(3)
C(10)-N(2)-Ru(1)	126.9(3)
C(6)-N(2)-Ru(1)	114.9(2)
C(11)-N(3)-C(15)	117.7(3)
C(11)-N(3)-Ru(1)	126.0(3)
C(15)-N(3)-Ru(1)	116.0(2)
C(20)-N(4)-C(16)	117.7(3)
C(20)-N(4)-Ru(1)	126.5(3)
C(16)-N(4)-Ru(1)	115.8(2)
C(21)-N(5)-C(25)	117.3(3)
C(21)-N(5)-Ru(1)	125.8(3)
C(25)-N(5)-Ru(1)	116.5(2)
C(26)-N(6)-N(7)	111.4(3)
C(26)-N(6)-Ru(1)	116.5(2)

N(7)-N(6)-Ru(1)	132.1(2)
C(31)-N(7)-N(6)	105.2(3)
N(7)-C(31)-N(8)	110.7(3)
N(7)-C(31)-C(30)	129.6(4)
N(8)-C(31)-C(30)	119.7(4)
N(1)-C(1)-C(2)	122.3(4)
C(1)-C(2)-C(3)	119.3(4)
C(4)-C(3)-C(2)	119.0(4)
C(3)-C(4)-C(5)	120.0(4)
N(1)-C(5)-C(4)	120.9(4)
N(1)-C(5)-C(6)	115.0(3)
C(4)-C(5)-C(6)	123.9(4)
N(2)-C(6)-C(7)	121.0(4)
N(2)-C(6)-C(5)	114.9(3)
C(7)-C(6)-C(5)	124.1(4)
C(6)-C(7)-C(8)	120.0(4)
C(9)-C(8)-C(7)	118.5(4)
C(10)-C(9)-C(8)	119.4(4)
N(2)-C(10)-C(9)	123.0(4)
N(3)-C(11)-C(12)	122.8(4)
C(13)-C(12)-C(11)	118.6(4)
C(12)-C(13)-C(14)	119.9(4)
C(13)-C(14)-C(15)	119.4(4)
N(3)-C(15)-C(14)	121.6(4)
N(3)-C(15)-C(16)	114.8(3)
C(14)-C(15)-C(16)	123.6(4)
N(4)-C(16)-C(17)	121.0(4)
N(4)-C(16)-C(15)	114.7(3)
C(17)-C(16)-C(15)	124.3(3)
C(18)-C(17)-C(16)	120.2(4)
C(19)-C(18)-C(17)	118.7(4)
C(18)-C(19)-C(20)	119.5(4)
N(4)-C(20)-C(19)	122.7(4)
N(5)-C(21)-C(22)	123.2(4)
C(23)-C(22)-C(21)	118.8(4)
C(22)-C(23)-C(24)	120.0(4)
C(23)-C(24)-C(25)	118.9(4)
N(5)-C(25)-C(24)	121.8(3)
N(5)-C(25)-C(26)	111.2(3)
C(24)-C(25)-C(26)	126.8(4)
N(6)-C(26)-N(8)	107.9(3)
N(6)-C(26)-C(25)	117.9(3)
N(8)-C(26)-C(25)	134.2(3)
C(27)-N(8)-C(26)	133.8(3)
C(27)-N(8)-C(31)	121.2(3)
C(26)-N(8)-C(31)	104.9(3)
C(28)-C(27)-N(8)	118.9(4)
C(27)-C(28)-C(29)	121.5(4)
C(30)-C(29)-C(28)	120.4(4)
C(29)-C(30)-C(31)	118.2(4)
O(100)-C(101)-C(100)	121.9(7)

O(100)-C(101)-C(102)	118.3(7)
C(100)-C(101)-C(102)	119.8(5)
F(11)-P(1)-F(14)	179.16(18)
F(11)-P(1)-F(15)	90.02(16)
F(14)-P(1)-F(15)	90.06(16)
F(11)-P(1)-F(13)	90.95(17)
F(14)-P(1)-F(13)	89.89(16)
F(15)-P(1)-F(13)	89.81(16)
F(11)-P(1)-F(12)	90.08(16)
F(14)-P(1)-F(12)	89.83(16)
F(15)-P(1)-F(12)	179.63(18)
F(13)-P(1)-F(12)	90.54(16)
F(11)-P(1)-F(16)	89.43(16)
F(14)-P(1)-F(16)	89.73(16)
F(15)-P(1)-F(16)	89.49(16)
F(13)-P(1)-F(16)	179.20(16)
F(12)-P(1)-F(16)	90.16(16)
F(26X)-P(2)-F(22X)	97.5(16)
F(26X)-P(2)-F(22)	49.0(8)
F(22X)-P(2)-F(22)	50.3(14)
F(26X)-P(2)-F(23)	135.0(12)
F(22X)-P(2)-F(23)	40.2(15)
F(22)-P(2)-F(23)	90.4(3)
F(26X)-P(2)-F(21)	101.4(10)
F(22X)-P(2)-F(21)	89.7(7)
F(22)-P(2)-F(21)	87.8(3)
F(23)-P(2)-F(21)	94.3(2)
F(26X)-P(2)-F(25X)	93.5(12)
F(22X)-P(2)-F(25X)	167.1(12)
F(22)-P(2)-F(25X)	137.9(8)
F(23)-P(2)-F(25X)	130.7(8)
F(21)-P(2)-F(25X)	81.5(5)
F(26X)-P(2)-F(25)	130.6(9)
F(22X)-P(2)-F(25)	129.5(16)
F(22)-P(2)-F(25)	178.3(3)
F(23)-P(2)-F(25)	89.3(3)
F(21)-P(2)-F(25)	93.9(2)
F(25X)-P(2)-F(25)	42.7(7)
F(26X)-P(2)-F(26)	45.1(10)
F(22X)-P(2)-F(26)	141.6(16)
F(22)-P(2)-F(26)	91.4(4)
F(23)-P(2)-F(26)	174.9(3)
F(21)-P(2)-F(26)	90.5(2)
F(25X)-P(2)-F(26)	48.5(7)
F(25)-P(2)-F(26)	88.8(4)
F(26X)-P(2)-F(24)	79.1(9)
F(22X)-P(2)-F(24)	91.4(7)
F(22)-P(2)-F(24)	93.5(3)
F(23)-P(2)-F(24)	86.2(2)
F(21)-P(2)-F(24)	178.7(2)
F(25X)-P(2)-F(24)	97.3(6)

F(25)-P(2)-F(24)	84.8(3)
F(26)-P(2)-F(24)	89.0(2)
F(26X)-P(2)-F(23X)	170.1(12)
F(22X)-P(2)-F(23X)	85.9(14)
F(22)-P(2)-F(23X)	131.1(8)
F(23)-P(2)-F(23X)	51.4(6)
F(21)-P(2)-F(23X)	69.2(6)
F(25X)-P(2)-F(23X)	82.2(9)
F(25)-P(2)-F(23X)	49.7(7)
F(26)-P(2)-F(23X)	129.5(7)
F(24)-P(2)-F(23X)	110.3(6)

Symmetry transformations used to generate equivalent atoms:

Table 4. Anisotropic displacement parameters (A^2 x 10^3) for ciftab.
The anisotropic displacement factor exponent takes the form:
-2 pi^2 [h^2 a*^2 U11 + ... + 2 h k a* b* U12]

	U11	U22	U33	U23	U13	U12
Ru(1)	30(1)	28(1)	28(1)	0(1)	13(1)	3(1)
N(1)	34(2)	31(2)	25(2)	-3(1)	12(1)	-2(1)
N(2)	35(2)	31(2)	29(2)	-2(1)	12(1)	3(1)
N(3)	33(2)	36(2)	29(2)	-1(1)	14(1)	2(1)
N(4)	33(2)	30(2)	33(2)	2(1)	16(1)	3(1)
N(5)	31(2)	32(2)	35(2)	5(1)	15(1)	6(1)
N(6)	31(2)	25(2)	32(2)	0(1)	14(1)	2(1)
N(7)	33(2)	29(2)	32(2)	0(1)	18(1)	2(1)
C(31)	35(2)	27(2)	37(2)	0(2)	17(2)	5(2)
C(1)	39(2)	33(2)	37(2)	-4(2)	15(2)	

-4(2)					
C(2)	46(3)	43(2)	48(2)	-1(2)	22(2)
-8(2)					
C(3)	35(2)	56(3)	56(3)	-3(2)	21(2)
-9(2)					
C(4)	31(2)	49(2)	43(2)	-2(2)	14(2)
5(2)					
C(5)	31(2)	37(2)	26(2)	-6(2)	10(2)
2(2)					
C(6)	32(2)	34(2)	26(2)	-3(2)	10(2)
6(2)					
C(7)	36(2)	41(2)	42(2)	-7(2)	11(2)
5(2)					
C(8)	52(3)	34(2)	43(2)	0(2)	9(2)
12(2)					
C(9)	52(3)	32(2)	46(2)	3(2)	13(2)
2(2)					
C(10)	36(2)	33(2)	41(2)	3(2)	12(2)
0(2)					
C(11)	40(2)	41(2)	39(2)	1(2)	18(2)
2(2)					
C(12)	49(3)	58(3)	29(2)	1(2)	16(2)
-3(2)					
C(13)	56(3)	62(3)	40(2)	-15(2)	26(2)
-8(2)					
C(14)	47(3)	46(2)	46(2)	-10(2)	22(2)
0(2)					
C(15)	35(2)	35(2)	36(2)	-5(2)	19(2)
1(2)					
C(16)	34(2)	35(2)	39(2)	-5(2)	20(2)
1(2)					
C(17)	56(3)	43(2)	50(3)	-5(2)	20(2)
12(2)					
C(18)	61(3)	39(2)	65(3)	6(2)	22(3)
18(2)					
C(19)	58(3)	44(3)	46(3)	7(2)	14(2)
12(2)					
C(20)	45(3)	38(2)	33(2)	2(2)	14(2)
5(2)					
C(21)	38(2)	49(2)	40(2)	8(2)	23(2)
7(2)					
C(22)	44(3)	61(3)	55(3)	16(2)	31(2)
9(2)					
C(23)	39(3)	50(3)	72(3)	16(2)	29(2)
-1(2)					
C(24)	37(2)	39(2)	57(3)	0(2)	19(2)
-4(2)					
C(25)	32(2)	32(2)	38(2)	2(2)	15(2)
4(2)					
C(26)	32(2)	22(2)	35(2)	-1(1)	15(2)
3(2)					

N(8)	32(2)	27(2)	38(2)	-4(1)	12(1)
1(1)					
C(27)	47(3)	40(2)	51(3)	-10(2)	15(2)
-6(2)					
C(28)	56(3)	51(3)	55(3)	-23(2)	17(2)
-12(2)					
C(29)	70(3)	58(3)	43(3)	-13(2)	24(2)
6(3)					
C(30)	53(3)	42(2)	40(2)	1(2)	24(2)
7(2)					
O(100)	144(5)	201(6)	116(4)	67(4)	82(4)
35(4)					
C(100)	82(4)	73(4)	66(4)	10(3)	16(3)
15(3)					
C(101)	57(4)	99(5)	78(4)	41(4)	32(3)
28(3)					
C(102)	94(5)	125(6)	69(4)	-34(4)	6(4)
49(5)					
P(1)	58(1)	37(1)	36(1)	0(1)	18(1)
4(1)					
F(11)	85(2)	55(2)	64(2)	11(1)	39(2)
0(2)					
F(12)	83(2)	54(2)	45(1)	-11(1)	12(1)
10(2)					
F(13)	58(2)	59(2)	71(2)	-4(1)	16(2)
12(1)					
F(14)	77(2)	62(2)	62(2)	20(1)	22(2)
-7(2)					
F(15)	101(2)	52(2)	43(1)	-9(1)	18(2)
8(2)					
F(16)	64(2)	72(2)	56(2)	11(1)	28(1)
20(2)					
P(2)	47(1)	47(1)	64(1)	-5(1)	22(1)
-9(1)					
F(21)	82(2)	59(2)	146(3)	-22(2)	66(2)
-7(2)					
F(24)	63(2)	65(2)	199(4)	-41(3)	40(3)
-3(2)					
F(22)	89(4)	117(6)	72(3)	31(4)	44(3)
26(4)					
F(23)	46(3)	52(3)	71(3)	-8(2)	9(2)
-15(2)					
F(25)	89(5)	72(3)	107(5)	20(3)	57(4)
-6(3)					
F(26)	40(3)	87(4)	125(6)	-37(4)	12(3)
-8(2)					
F(22X)	160(3)	92(17)	320(5)	-100(3)	200(3)
-69(19)					
F(23X)	85(12)	121(15)	87(10)	-17(9)	23(8)
26(10)					
F(25X)	82(12)	58(8)	118(16)	-1(9)	49(12)

-23(8)					
F(26X)	270(3)	96(12)	50(8)	-9(8)	43(13)
-75(17)					

Table 5. Hydrogen coordinates (x 10^4) and isotropic displacement parameters (A^2 x 10^3) for ciftab.

	x	y	z	U(eq)
H(1)	1253	-2540	-510	4
1(4)				
H(2)	-31	-2937	-600	4
1(4)				
H(3)	-1005	-1729	-842	4
1(4)				
H(4)	-683	-174	-1086	4
1(4)				
H(7)	-320	1250	-1424	4
1(4)				
H(8)	115	2650	-1895	4
1(4)				
H(9)	1406	2678	-1942	4
1(4)				
H(10)	2243	1365	-1464	4
1(4)				
H(11)	1265	-442	-2677	5
0(5)				
H(12)	1055	-1320	-3941	5
0(5)				
H(13)	1684	-2803	-3825	5
0(5)				
H(14)	2512	-3375	-2457	5
0(5)				
H(17)	3256	-3844	-1100	5
0(5)				
H(18)	3946	-4273	354	5
0(5)				
H(19)	3931	-3232	1449	5
0(5)				
H(20)	3231	-1803	1076	5
0(5)				
H(21)	3436	-312	-1569	3

9(6)	H(22)	4508	697	-1412	3
9(6)	H(23)	5017	1678	-186	3
9(6)	H(24)	4475	1588	897	3
9(6)	H(27)	4306	1608	2172	5
8(7)	H(28)	4201	1921	3482	5
8(7)	H(29)	3118	1318	3805	5
8(7)	H(30)	2129	381	2792	5
8(7)	H(10A)	-2200	-2209	-554	14
7(13)	H(10B)	-1954	-3170	-14	14
7(13)	H(10C)	-2877	-2889	-477	14
7(13)	H(10D)	-2620	-4638	-1954	14
7(13)	H(10E)	-3148	-4498	-1382	14
7(13)	H(10F)	-2223	-4775	-929	14
7(13)					

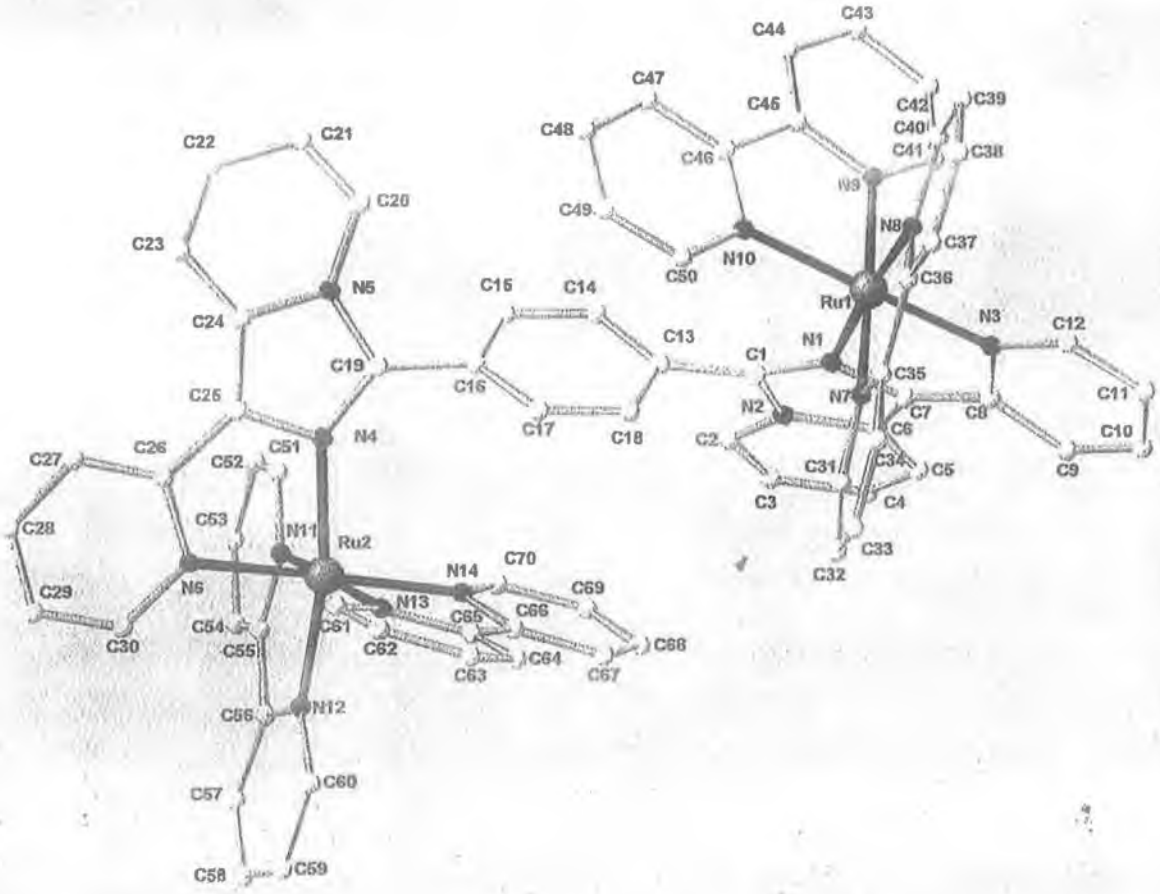

Structure of $[Ru(bpy)_2(LL7)(bpy)_2Ru](PF_6)_4$. Detailed X-Ray Crystallography Data from the analysis of this complex follows.

comments: measured with 20 s per frame and delta omega = 0.4 c
8985 reflections observed
crystallises with 1.7 molecules of acetone per unit
(H-atoms of the solvent molecules are omitted, so the final
formular has to be corrected as the H-atoms for 1.7 acetone mc
are missing, the influence on density is neglectible)
3 of the 4 PF6 anions are disordered, the F-atoms with lower
occupancies are refined isotropically
The P-F distances are refined using the same distance restrair
for all.

Table 1. Crystal data and structure refinement for ciftab.

Identification code	md26
Empirical formula	C75.10 H52 F24 N14 O1.70 P4
Formula weight	1959.73
Temperature	200(2) K
Wavelength	0.71073 A
Crystal system, space group	monoclinic, P2(1)/c (No. 14)
Unit cell dimensions	a = 15.0193(15) A alpha = b = 24.332(3) A beta = 9(c = 21.810(2) A gamma = 9(
Volume	7911.9(14) A^3
Z, Calculated density	4, 1.645 Mg/m^3
Absorption coefficient	0.575 mm^-1
F(000)	3913
Crystal size	0.3 x 0.3 x 0.1 mm^3
Theta range for data collection	1.26 to 28.31 deg.
Index ranges	-20<=h<=19, -30<=k<=32, -26< :(
Reflections collected / unique	85840 / 19449 [R(int) = 0.12
Completeness to theta = 28.31	96.5%
Refinement method	Full-matrix least-squares or
Data / restraints / parameters	19449 / 84 / 1156

Goodness-of-fit on F^2	0.941
Final R indices [I>2sigma(I)]	R1 = 0.0560, wR2 = 0.1360
R indices (all data)	R1 = 0.1576, wR2 = 0.1723
Largest diff. peak and hole	0.783 and -0.988 e.A^-3

Table 2. Atomic coordinates (x 10^4) and equivalent isotr displacement parameters (A^2 x 10^3) for ciftab.
U(eq) is defined as one third of the trace of the orthogona Uij tensor.

	x	y	z	U(e
Ru(1)	4631(1)	4195(1)	6858(1)	27(
Ru(2)	-409(1)	2179(1)	5879(1)	29(
P(1)	-1429(1)	1280(1)	3348(1)	62(
F(11)	-1365(3)	787(2)	2866(2)	81(
F(12)	-543(4)	1533(2)	3132(2)	113(
F(13)	-810(3)	935(2)	3846(2)	98(
F(14)	-1478(3)	1762(2)	3823(2)	92(
F(15)	-2285(3)	1002(2)	3562(3)	115(
F(16)	-2016(4)	1621(2)	2843(2)	124(
P(2)	-1495(1)	4327(1)	4196(1)	54(
F(21)	-452(3)	4358(2)	4159(2)	110(
F(24)	-2537(3)	4317(2)	4255(2)	78(
F(22)	-1637(4)	4933(3)	3928(5)	98(
F(23)	-1337(5)	4623(5)	4855(4)	119(
F(25)	-1336(5)	3775(4)	4537(8)	146(
F(26)	-1669(7)	4077(6)	3536(4)	158(
F(22X)	-1659(12)	4407(7)	3493(6)	66(
F(23X)	-1374(13)	4912(6)	4399(11)	91(
F(25X)	-1312(13)	4123(10)	4859(6)	80(
F(26X)	-1573(15)	3689(6)	4021(11)	93(
P(3)	5699(1)	894(1)	5933(1)	40(
F(32)	6104(3)	348(2)	6240(2)	98(
F(35)	5274(3)	1437(2)	5646(2)	93(
F(31)	6337(5)	1261(2)	6413(3)	74(
F(33)	6403(5)	937(4)	5461(4)	109(
F(34)	5072(5)	552(2)	5442(3)	86(
F(36)	4986(5)	880(3)	6408(3)	121(
F(31X)	6724(11)	1072(14)	5980(2)	125(
F(33X)	5950(2)	678(12)	5291(9)	91(
F(34X)	4799(14)	547(12)	5788(15)	96(
F(36X)	5780(3)	1139(15)	6601(9)	130(
P(4)	3791(1)	2813(1)	4289(1)	57(
F(41)	4339(3)	2299(2)	4567(2)	80(
F(44)	3260(3)	3337(2)	4012(2)	94(

F(42)	4648(5)	3193(3)	4428(6)	134(
F(43)	3367(5)	2883(3)	4918(2)	88(
F(45)	2973(4)	2441(2)	4037(3)	61(
F(46)	4101(6)	2732(4)	3618(4)	102(
F(42X)	4345(11)	3166(7)	4819(7)	75(
F(43X)	2895(16)	2553(14)	4490(19)	212(
F(45X)	3500(3)	2355(11)	3805(14)	199(
F(46X)	4618(11)	2877(7)	3913(8)	71(
N(1)	3393(3)	4322(2)	7171(2)	27(
N(2)	2185(3)	4363(2)	7651(2)	34(
N(3)	4611(3)	5044(2)	6935(2)	31(
N(4)	764(3)	1766(2)	6217(2)	28(
N(5)	2019(3)	1391(2)	6651(2)	31(
N(6)	-726(3)	1379(2)	5598(2)	37(
N(7)	4231(3)	4318(2)	5938(2)	31(
N(8)	5835(3)	4132(2)	6501(2)	32(
N(9)	5087(3)	4033(2)	7774(2)	29(
N(10)	4642(3)	3351(2)	6851(2)	28(
N(11)	-1035(3)	2048(2)	6651(2)	32(
N(12)	-1678(3)	2451(2)	5583(2)	35(
N(13)	168(3)	2412(2)	5114(2)	33(
N(14)	-71(3)	2986(2)	6094(2)	28(
C(1)	2731(4)	4021(2)	7353(2)	28(
C(2)	1421(4)	4239(3)	7920(3)	39(
C(3)	1001(4)	4636(3)	8185(3)	54(
C(4)	1331(4)	5184(3)	8201(3)	54(
C(5)	2065(4)	5319(3)	7939(3)	47(
C(6)	2520(4)	4897(2)	7647(3)	34(
C(7)	3265(4)	4863(2)	7344(2)	29(
C(8)	3882(4)	5267(2)	7144(2)	31(
C(9)	3725(4)	5835(2)	7130(3)	43(
C(10)	4343(5)	6165(3)	6889(3)	54(
C(11)	5113(5)	5942(3)	6698(3)	51(
C(12)	5219(4)	5386(2)	6722(3)	42(
C(13)	2493(3)	3454(2)	7175(3)	30(
C(14)	2357(4)	3047(2)	7599(3)	38(
C(15)	2048(4)	2533(2)	7401(3)	37(
C(16)	1883(3)	2412(2)	6778(3)	29(
C(17)	2064(3)	2810(2)	6349(3)	32(
C(18)	2354(3)	3323(2)	6548(3)	32(
C(19)	1536(4)	1871(2)	6554(3)	32(
C(20)	2868(4)	1311(3)	6952(3)	50(
C(21)	3221(5)	803(3)	6966(3)	60(
C(22)	2719(5)	357(3)	6687(3)	61(
C(23)	1890(4)	432(2)	6404(3)	45(
C(24)	1508(4)	964(2)	6369(3)	33(
C(25)	731(4)	1208(2)	6097(2)	31(
C(26)	-74(4)	987(2)	5753(3)	32(
C(27)	-219(4)	436(2)	5600(3)	40(
C(28)	-1036(4)	276(3)	5299(3)	48(
C(29)	-1677(4)	660(3)	5144(3)	54(
C(30)	-1504(4)	1200(3)	5298(3)	44(
C(31)	3395(4)	4465(2)	5693(3)	34(

C(32)	3158(4)	4544(2)	5081(3)	43(
C(33)	3818(5)	4471(3)	4685(3)	53(
C(34)	4681(5)	4343(3)	4925(3)	49(
C(35)	4881(4)	4271(2)	5556(3)	37(
C(36)	5786(4)	4153(2)	5871(3)	33(
C(37)	6553(4)	4085(3)	5572(3)	49(
C(38)	7355(5)	3993(3)	5911(3)	55(
C(39)	7417(4)	3966(3)	6541(3)	53(
C(40)	6657(4)	4035(2)	6825(3)	42(
C(41)	5224(4)	4397(2)	8232(3)	37(
C(42)	5458(4)	4259(3)	8836(3)	44(
C(43)	5558(5)	3720(3)	8986(3)	59(
C(44)	5388(5)	3331(3)	8526(3)	52(
C(45)	5154(4)	3492(2)	7930(3)	36(
C(46)	4944(4)	3107(2)	7400(3)	32(
C(47)	5041(4)	2546(2)	7439(3)	51(
C(48)	4833(4)	2220(2)	6920(3)	45(
C(49)	4537(4)	2462(2)	6366(3)	38(
C(50)	4445(4)	3026(2)	6350(3)	36(
C(51)	-644(4)	1868(2)	7205(3)	40(
C(52)	-1081(5)	1832(3)	7714(3)	49(
C(53)	-1973(5)	1980(3)	7665(3)	58(
C(54)	-2390(4)	2159(3)	7107(3)	51(
C(55)	-1910(4)	2194(2)	6604(3)	37(
C(56)	-2286(4)	2386(2)	5990(3)	38(
C(57)	-3190(4)	2487(3)	5815(3)	54(
C(58)	-3485(4)	2666(3)	5232(4)	62(
C(59)	-2862(5)	2753(3)	4825(3)	62(
C(60)	-1954(4)	2641(3)	5006(3)	48(
C(61)	353(4)	2080(3)	4655(3)	45(
C(62)	746(5)	2266(3)	4146(3)	53(
C(63)	951(5)	2818(3)	4117(3)	56(
C(64)	766(4)	3172(3)	4588(3)	49(
C(65)	390(4)	2958(2)	5090(3)	35(
C(66)	207(4)	3281(2)	5624(3)	33(
C(67)	349(4)	3843(2)	5675(3)	45(
C(68)	194(4)	4112(2)	6210(3)	48(
C(69)	-84(4)	3813(2)	6682(3)	41(
C(70)	-220(4)	3249(2)	6604(3)	34(
O(100)	1220(3)	3703(2)	2898(2)	59(
C(100)	1211(5)	4172(3)	3062(3)	51(
C(101)	1850(8)	4389(4)	3559(6)	155(
C(102)	520(5)	4573(3)	2774(4)	77(
O(200)	1728(4)	1011(2)	4685(3)	62(
C(200)	2502(6)	1091(3)	4761(4)	37(
C(201)	2885(6)	1470(3)	5252(4)	40(
C(202)	3145(6)	839(4)	4371(5)	65(

Table 3. Bond lengths [A] and angles [deg] for ciftab.

Ru(1)-N(7)	2.046(4)
Ru(1)-N(10)	2.053(4)
Ru(1)-N(8)	2.060(4)
Ru(1)-N(9)	2.069(4)
Ru(1)-N(3)	2.073(4)
Ru(1)-N(1)	2.081(4)
Ru(2)-N(12)	2.046(4)
Ru(2)-N(11)	2.048(4)
Ru(2)-N(13)	2.052(4)
Ru(2)-N(14)	2.065(4)
Ru(2)-N(6)	2.079(5)
Ru(2)-N(4)	2.084(4)
P(1)-F(16)	1.562(5)
P(1)-F(14)	1.573(4)
P(1)-F(15)	1.574(5)
P(1)-F(13)	1.583(5)
P(1)-F(12)	1.587(5)
P(1)-F(11)	1.606(4)
P(2)-F(23X)	1.495(12)
P(2)-F(25X)	1.523(12)
P(2)-F(22X)	1.535(12)
P(2)-F(25)	1.540(6)
P(2)-F(26)	1.555(6)
P(2)-F(21)	1.581(5)
P(2)-F(24)	1.587(4)
P(2)-F(22)	1.592(6)
P(2)-F(23)	1.600(6)
P(2)-F(26X)	1.598(12)
F(22)-F(23X)	1.06(2)
F(22)-F(22X)	1.591(17)
F(23)-F(25X)	1.217(18)
F(23)-F(23X)	1.21(2)
F(25)-F(25X)	1.098(18)
F(25)-F(26X)	1.157(19)
F(26)-F(22X)	0.811(18)
F(26)-F(26X)	1.41(2)
P(3)-F(36X)	1.565(15)
P(3)-F(35)	1.563(4)
P(3)-F(33)	1.567(5)
P(3)-F(34)	1.576(5)
P(3)-F(32)	1.578(4)
P(3)-F(36)	1.577(5)
P(3)-F(33X)	1.584(14)
P(3)-F(31)	1.602(4)
P(3)-F(31X)	1.590(15)
P(3)-F(34X)	1.593(14)
F(31)-F(36X)	1.02(4)
F(31)-F(31X)	1.26(4)
F(33)-F(33X)	0.97(3)
F(33)-F(31X)	1.22(4)
F(34)-F(34X)	0.90(3)
F(34)-F(33X)	1.43(3)
F(36)-F(36X)	1.37(4)

F(36)-F(34X)	1.57(3)
P(4)-F(45X)	1.560(14)
P(4)-F(42X)	1.591(12)
P(4)-F(42)	1.583(6)
P(4)-F(46X)	1.576(12)
P(4)-F(41)	1.577(4)
P(4)-F(46)	1.600(7)
P(4)-F(44)	1.585(4)
P(4)-F(45)	1.571(5)
P(4)-F(43)	1.590(6)
P(4)-F(43X)	1.596(15)
F(42)-F(42X)	1.015(16)
F(42)-F(46X)	1.355(17)
F(43)-F(42X)	1.658(18)
F(43)-F(43X)	1.36(4)
F(45)-F(45X)	1.01(4)
F(45)-F(43X)	1.04(4)
F(46)-F(46X)	1.011(17)
F(46)-F(45X)	1.38(4)
N(1)-C(1)	1.334(6)
N(1)-C(7)	1.389(6)
N(2)-C(1)	1.384(6)
N(2)-C(2)	1.385(7)
N(2)-C(6)	1.394(7)
N(3)-C(8)	1.348(7)
N(3)-C(12)	1.358(7)
N(4)-C(19)	1.321(6)
N(4)-C(25)	1.381(6)
N(5)-C(20)	1.376(7)
N(5)-C(19)	1.377(6)
N(5)-C(24)	1.390(7)
N(6)-C(30)	1.341(7)
N(6)-C(26)	1.378(7)
N(7)-C(31)	1.352(7)
N(7)-C(35)	1.362(7)
N(8)-C(40)	1.367(7)
N(8)-C(36)	1.368(7)
N(9)-C(41)	1.333(7)
N(9)-C(45)	1.360(6)
N(10)-C(50)	1.353(7)
N(10)-C(46)	1.365(6)
N(11)-C(51)	1.350(7)
N(11)-C(55)	1.354(7)
N(12)-C(56)	1.357(7)
N(12)-C(60)	1.359(7)
N(13)-C(61)	1.339(7)
N(13)-C(65)	1.373(7)
N(14)-C(70)	1.327(7)
N(14)-C(66)	1.358(7)
C(1)-C(13)	1.465(7)
C(2)-C(3)	1.325(8)
C(3)-C(4)	1.422(9)
C(4)-C(5)	1.343(9)

C(5)-C(6)	1.424(8)
C(6)-C(7)	1.368(7)
C(7)-C(8)	1.454(7)
C(8)-C(9)	1.403(7)
C(9)-C(10)	1.379(9)
C(10)-C(11)	1.387(9)
C(11)-C(12)	1.362(8)
C(13)-C(14)	1.386(7)
C(13)-C(18)	1.396(7)
C(14)-C(15)	1.384(7)
C(15)-C(16)	1.383(7)
C(16)-C(17)	1.395(7)
C(16)-C(19)	1.479(7)
C(17)-C(18)	1.373(7)
C(20)-C(21)	1.344(8)
C(21)-C(22)	1.416(9)
C(22)-C(23)	1.335(9)
C(23)-C(24)	1.414(7)
C(24)-C(25)	1.378(7)
C(25)-C(26)	1.449(7)
C(26)-C(27)	1.393(7)
C(27)-C(28)	1.376(8)
C(28)-C(29)	1.356(9)
C(29)-C(30)	1.372(8)
C(31)-C(32)	1.353(7)
C(32)-C(33)	1.402(9)
C(33)-C(34)	1.373(9)
C(34)-C(35)	1.386(8)
C(35)-C(36)	1.474(8)
C(36)-C(37)	1.401(8)
C(37)-C(38)	1.354(9)
C(38)-C(39)	1.368(9)
C(39)-C(40)	1.372(8)
C(41)-C(42)	1.363(8)
C(42)-C(43)	1.357(8)
C(43)-C(44)	1.381(8)
C(44)-C(45)	1.364(8)
C(45)-C(46)	1.490(8)
C(46)-C(47)	1.375(7)
C(47)-C(48)	1.386(8)
C(48)-C(49)	1.368(8)
C(49)-C(50)	1.379(7)
C(51)-C(52)	1.361(8)
C(52)-C(53)	1.379(9)
C(53)-C(54)	1.372(9)
C(54)-C(55)	1.385(8)
C(55)-C(56)	1.466(8)
C(56)-C(57)	1.386(8)
C(57)-C(58)	1.368(9)
C(58)-C(59)	1.380(10)
C(59)-C(60)	1.400(9)
C(61)-C(62)	1.396(8)
C(62)-C(63)	1.382(9)

C(63)-C(64)	1.394(9)
C(64)-C(65)	1.392(8)
C(65)-C(66)	1.459(8)
C(66)-C(67)	1.387(7)
C(67)-C(68)	1.381(8)
C(68)-C(69)	1.367(8)
C(69)-C(70)	1.395(7)
O(100)-C(100)	1.196(7)
C(100)-C(101)	1.456(10)
C(100)-C(102)	1.506(9)
O(200)-C(200)	1.171(9)
C(200)-C(201)	1.477(11)
C(200)-C(202)	1.493(13)

N(7)-Ru(1)-N(10)	98.01(17)
N(7)-Ru(1)-N(8)	78.87(18)
N(10)-Ru(1)-N(8)	85.10(16)
N(7)-Ru(1)-N(9)	176.45(17)
N(10)-Ru(1)-N(9)	79.30(17)
N(8)-Ru(1)-N(9)	98.52(17)
N(7)-Ru(1)-N(3)	85.89(16)
N(10)-Ru(1)-N(3)	175.77(17)
N(8)-Ru(1)-N(3)	97.30(18)
N(9)-Ru(1)-N(3)	96.87(17)
N(7)-Ru(1)-N(1)	97.55(17)
N(10)-Ru(1)-N(1)	99.16(16)
N(8)-Ru(1)-N(1)	174.82(17)
N(9)-Ru(1)-N(1)	85.22(16)
N(3)-Ru(1)-N(1)	78.62(17)
N(12)-Ru(2)-N(11)	78.88(19)
N(12)-Ru(2)-N(13)	97.10(18)
N(11)-Ru(2)-N(13)	172.85(18)
N(12)-Ru(2)-N(14)	87.64(17)
N(11)-Ru(2)-N(14)	95.02(17)
N(13)-Ru(2)-N(14)	78.82(18)
N(12)-Ru(2)-N(6)	92.15(18)
N(11)-Ru(2)-N(6)	89.10(18)
N(13)-Ru(2)-N(6)	97.01(18)
N(14)-Ru(2)-N(6)	175.76(18)
N(12)-Ru(2)-N(4)	169.19(17)
N(11)-Ru(2)-N(4)	94.95(17)
N(13)-Ru(2)-N(4)	89.91(17)
N(14)-Ru(2)-N(4)	101.83(16)
N(6)-Ru(2)-N(4)	78.79(17)
F(16)-P(1)-F(14)	90.1(3)
F(16)-P(1)-F(15)	91.5(4)
F(14)-P(1)-F(15)	91.1(3)
F(16)-P(1)-F(13)	178.2(4)
F(14)-P(1)-F(13)	90.8(3)
F(15)-P(1)-F(13)	90.0(3)
F(16)-P(1)-F(12)	90.4(3)
F(14)-P(1)-F(12)	90.8(3)
F(15)-P(1)-F(12)	177.3(3)

F(13)-P(1)-F(12)	88.0(3)
F(16)-P(1)-F(11)	90.5(3)
F(14)-P(1)-F(11)	179.2(3)
F(15)-P(1)-F(11)	89.4(3)
F(13)-P(1)-F(11)	88.7(3)
F(12)-P(1)-F(11)	88.7(3)
F(23X)-P(2)-F(25X)	91.5(11)
F(23X)-P(2)-F(22X)	100.0(11)
F(25X)-P(2)-F(22X)	168.2(11)
F(23X)-P(2)-F(25)	132.9(11)
F(25X)-P(2)-F(25)	42.0(7)
F(22X)-P(2)-F(25)	126.2(9)
F(23X)-P(2)-F(26)	130.4(11)
F(25X)-P(2)-F(26)	137.9(10)
F(22X)-P(2)-F(26)	30.4(7)
F(25)-P(2)-F(26)	96.0(7)
F(23X)-P(2)-F(21)	83.3(8)
F(25X)-P(2)-F(21)	89.9(8)
F(22X)-P(2)-F(21)	89.1(7)
F(25)-P(2)-F(21)	88.2(4)
F(26)-P(2)-F(21)	91.7(5)
F(23X)-P(2)-F(24)	94.4(8)
F(25X)-P(2)-F(24)	89.0(8)
F(22X)-P(2)-F(24)	92.5(7)
F(25)-P(2)-F(24)	92.5(4)
F(26)-P(2)-F(24)	90.7(5)
F(21)-P(2)-F(24)	177.4(3)
F(23X)-P(2)-F(22)	39.9(8)
F(25X)-P(2)-F(22)	130.6(9)
F(22X)-P(2)-F(22)	61.1(7)
F(25)-P(2)-F(22)	172.6(7)
F(26)-P(2)-F(22)	91.3(6)
F(21)-P(2)-F(22)	91.5(3)
F(24)-P(2)-F(22)	87.4(3)
F(23X)-P(2)-F(23)	46.0(8)
F(25X)-P(2)-F(23)	45.8(7)
F(22X)-P(2)-F(23)	145.9(8)
F(25)-P(2)-F(23)	87.7(7)
F(26)-P(2)-F(23)	176.2(7)
F(21)-P(2)-F(23)	89.1(4)
F(24)-P(2)-F(23)	88.5(3)
F(22)-P(2)-F(23)	84.9(5)
F(23X)-P(2)-F(26X)	175.8(12)
F(25X)-P(2)-F(26X)	84.8(11)
F(22X)-P(2)-F(26X)	83.6(10)
F(25)-P(2)-F(26X)	43.2(7)
F(26)-P(2)-F(26X)	53.2(8)
F(21)-P(2)-F(26X)	94.5(8)
F(24)-P(2)-F(26X)	87.7(8)
F(22)-P(2)-F(26X)	144.1(9)
F(23)-P(2)-F(26X)	130.5(9)
F(23X)-F(22)-F(22X)	121.2(10)
F(23X)-F(22)-P(2)	65.1(8)

F(22X)-F(22)-P(2)	57.7(5)
F(25X)-F(23)-F(23X)	125.7(11)
F(25X)-F(23)-P(2)	63.8(7)
F(23X)-F(23)-P(2)	62.4(7)
F(25X)-F(25)-F(26X)	138.0(13)
F(25X)-F(25)-P(2)	68.2(8)
F(26X)-F(25)-P(2)	71.1(8)
F(22X)-F(26)-F(26X)	138.5(14)
F(22X)-F(26)-P(2)	73.5(10)
F(26X)-F(26)-P(2)	65.0(7)
F(26)-F(22X)-P(2)	76.1(11)
F(26)-F(22X)-F(22)	136.8(15)
P(2)-F(22X)-F(22)	61.2(6)
F(22)-F(23X)-F(23)	143.2(15)
F(22)-F(23X)-P(2)	75.0(9)
F(23)-F(23X)-P(2)	71.6(8)
F(25)-F(25X)-F(23)	140.1(13)
F(25)-F(25X)-P(2)	69.8(8)
F(23)-F(25X)-P(2)	70.5(8)
F(25)-F(26X)-F(26)	126.9(11)
F(25)-F(26X)-P(2)	65.7(7)
F(26)-F(26X)-P(2)	61.9(6)
F(36X)-P(3)-F(35)	91.9(13)
F(36X)-P(3)-F(33)	127.1(17)
F(35)-P(3)-F(33)	87.5(4)
F(36X)-P(3)-F(34)	143.8(17)
F(35)-P(3)-F(34)	89.6(3)
F(33)-P(3)-F(34)	89.1(4)
F(36X)-P(3)-F(32)	86.7(13)
F(35)-P(3)-F(32)	178.0(3)
F(33)-P(3)-F(32)	94.5(4)
F(34)-P(3)-F(32)	90.7(3)
F(36X)-P(3)-F(36)	51.7(16)
F(35)-P(3)-F(36)	90.3(4)
F(33)-P(3)-F(36)	177.5(4)
F(34)-P(3)-F(36)	92.2(4)
F(32)-P(3)-F(36)	87.7(4)
F(36X)-P(3)-F(33X)	162(2)
F(35)-P(3)-F(33X)	93.2(11)
F(33)-P(3)-F(33X)	35.8(11)
F(34)-P(3)-F(33X)	53.8(12)
F(32)-P(3)-F(33X)	88.5(11)
F(36)-P(3)-F(33X)	145.7(13)
F(36X)-P(3)-F(31)	37.5(15)
F(35)-P(3)-F(31)	88.5(3)
F(33)-P(3)-F(31)	89.7(4)
F(34)-P(3)-F(31)	177.8(3)
F(32)-P(3)-F(31)	91.2(3)
F(36)-P(3)-F(31)	89.0(4)
F(33X)-P(3)-F(31)	125.1(13)
F(36X)-P(3)-F(31X)	83(2)
F(35)-P(3)-F(31X)	98.1(12)
F(33)-P(3)-F(31X)	45.5(15)

F(34)-P(3)-F(31X)	132.9(16)
F(32)-P(3)-F(31X)	83.1(12)
F(36)-P(3)-F(31X)	133.8(16)
F(33X)-P(3)-F(31X)	79.3(18)
F(31)-P(3)-F(31X)	46.3(15)
F(36X)-P(3)-F(34X)	111(2)
F(35)-P(3)-F(34X)	94.2(12)
F(33)-P(3)-F(34X)	121.9(12)
F(34)-P(3)-F(34X)	33.1(10)
F(32)-P(3)-F(34X)	84.9(12)
F(36)-P(3)-F(34X)	59.4(11)
F(33X)-P(3)-F(34X)	86.3(15)
F(31)-P(3)-F(34X)	148.3(12)
F(31X)-P(3)-F(34X)	161.5(18)
F(36X)-F(31)-F(31X)	132.4(17)
F(36X)-F(31)-P(3)	69.3(11)
F(31X)-F(31)-P(3)	66.3(10)
F(33X)-F(33)-F(31X)	135.2(19)
F(33X)-F(33)-P(3)	73.1(11)
F(31X)-F(33)-P(3)	68.3(10)
F(34X)-F(34)-F(33X)	136.1(16)
F(34X)-F(34)-P(3)	74.5(11)
F(33X)-F(34)-P(3)	63.4(8)
F(36X)-F(36)-P(3)	63.7(9)
F(36X)-F(36)-F(34X)	124.1(12)
P(3)-F(36)-F(34X)	60.8(7)
F(31)-F(31X)-F(33)	129.1(16)
F(31)-F(31X)-P(3)	67.4(10)
F(33)-F(31X)-P(3)	66.2(10)
F(33)-F(33X)-F(34)	132.5(15)
F(33)-F(33X)-P(3)	71.1(10)
F(34)-F(33X)-P(3)	62.8(8)
F(34)-F(34X)-F(36)	131.4(15)
F(34)-F(34X)-P(3)	72.4(11)
F(36)-F(34X)-P(3)	59.8(8)
F(31)-F(36X)-F(36)	137.4(15)
F(31)-F(36X)-P(3)	73.2(12)
F(36)-F(36X)-P(3)	64.6(10)
F(45X)-P(4)-F(42X)	162.8(14)
F(45X)-P(4)-F(42)	134.5(16)
F(42X)-P(4)-F(42)	37.3(6)
F(45X)-P(4)-F(46X)	83.9(16)
F(42X)-P(4)-F(46X)	87.0(9)
F(42)-P(4)-F(46X)	50.8(7)
F(45X)-P(4)-F(41)	77.6(12)
F(42X)-P(4)-F(41)	86.9(7)
F(42)-P(4)-F(41)	90.8(3)
F(46X)-P(4)-F(41)	82.6(6)
F(45X)-P(4)-F(46)	51.9(14)
F(42X)-P(4)-F(46)	123.1(7)
F(42)-P(4)-F(46)	85.8(6)
F(46X)-P(4)-F(46)	37.1(6)
F(41)-P(4)-F(46)	93.4(3)

F(45X)-P(4)-F(44)	103.3(13)
F(42X)-P(4)-F(44)	92.2(7)
F(42)-P(4)-F(44)	87.9(3)
F(46X)-P(4)-F(44)	96.5(7)
F(41)-P(4)-F(44)	178.7(3)
F(46)-P(4)-F(44)	86.5(3)
F(45X)-P(4)-F(45)	37.7(14)
F(42X)-P(4)-F(45)	151.9(7)
F(42)-P(4)-F(45)	170.6(6)
F(46X)-P(4)-F(45)	120.6(8)
F(41)-P(4)-F(45)	91.6(3)
F(46)-P(4)-F(45)	84.9(5)
F(44)-P(4)-F(45)	89.6(3)
F(45X)-P(4)-F(43)	123.5(16)
F(42X)-P(4)-F(43)	62.9(7)
F(42)-P(4)-F(43)	99.9(6)
F(46X)-P(4)-F(43)	149.4(8)
F(41)-P(4)-F(43)	89.9(3)
F(46)-P(4)-F(43)	173.3(5)
F(44)-P(4)-F(43)	90.4(3)
F(45)-P(4)-F(43)	89.1(4)
F(45X)-P(4)-F(43X)	74.1(17)
F(42X)-P(4)-F(43X)	113.5(17)
F(42)-P(4)-F(43X)	150.6(16)
F(46X)-P(4)-F(43X)	157.8(16)
F(41)-P(4)-F(43X)	89.9(13)
F(46)-P(4)-F(43X)	123.4(16)
F(44)-P(4)-F(43X)	91.2(13)
F(45)-P(4)-F(43X)	38.5(14)
F(43)-P(4)-F(43X)	50.7(15)
F(42X)-F(42)-F(46X)	133.2(12)
F(42X)-F(42)-P(4)	71.7(8)
F(46X)-F(42)-P(4)	64.3(6)
F(42X)-F(43)-F(43X)	123.4(11)
F(42X)-F(43)-P(4)	58.6(5)
F(43X)-F(43)-P(4)	64.9(9)
F(45X)-F(45)-F(43X)	135(2)
F(45X)-F(45)-P(4)	70.6(11)
F(43X)-F(45)-P(4)	72.1(11)
F(46X)-F(46)-F(45X)	121.5(16)
F(46X)-F(46)-P(4)	70.2(8)
F(45X)-F(46)-P(4)	62.6(9)
F(42)-F(42X)-F(43)	129.0(11)
F(42)-F(42X)-P(4)	70.9(8)
F(43)-F(42X)-P(4)	58.5(5)
F(45)-F(43X)-F(43)	133.8(14)
F(45)-F(43X)-P(4)	69.5(10)
F(43)-F(43X)-P(4)	64.4(9)
F(45)-F(45X)-P(4)	71.7(11)
F(45)-F(45X)-F(46)	126(2)
P(4)-F(45X)-F(46)	65.5(10)
F(46)-F(46X)-F(42)	132.2(13)
F(46)-F(46X)-P(4)	72.7(9)

F(42)-F(46X)-P(4)	64.9(6)
C(1)-N(1)-C(7)	107.9(4)
C(1)-N(1)-Ru(1)	138.0(4)
C(7)-N(1)-Ru(1)	112.9(3)
C(1)-N(2)-C(2)	129.5(5)
C(1)-N(2)-C(6)	108.9(5)
C(2)-N(2)-C(6)	121.6(5)
C(8)-N(3)-C(12)	118.5(5)
C(8)-N(3)-Ru(1)	116.6(3)
C(12)-N(3)-Ru(1)	124.4(4)
C(19)-N(4)-C(25)	107.7(4)
C(19)-N(4)-Ru(2)	138.7(4)
C(25)-N(4)-Ru(2)	113.5(3)
C(20)-N(5)-C(19)	129.3(5)
C(20)-N(5)-C(24)	122.4(5)
C(19)-N(5)-C(24)	108.3(4)
C(30)-N(6)-C(26)	116.4(5)
C(30)-N(6)-Ru(2)	127.1(4)
C(26)-N(6)-Ru(2)	116.4(3)
C(31)-N(7)-C(35)	118.7(5)
C(31)-N(7)-Ru(1)	125.1(4)
C(35)-N(7)-Ru(1)	116.1(4)
C(40)-N(8)-C(36)	117.5(5)
C(40)-N(8)-Ru(1)	126.6(4)
C(36)-N(8)-Ru(1)	115.7(4)
C(41)-N(9)-C(45)	117.1(5)
C(41)-N(9)-Ru(1)	126.8(4)
C(45)-N(9)-Ru(1)	115.6(4)
C(50)-N(10)-C(46)	118.0(5)
C(50)-N(10)-Ru(1)	126.3(4)
C(46)-N(10)-Ru(1)	115.5(3)
C(51)-N(11)-C(55)	117.7(5)
C(51)-N(11)-Ru(2)	126.3(4)
C(55)-N(11)-Ru(2)	115.8(4)
C(56)-N(12)-C(60)	119.4(5)
C(56)-N(12)-Ru(2)	115.6(4)
C(60)-N(12)-Ru(2)	124.8(4)
C(61)-N(13)-C(65)	118.8(5)
C(61)-N(13)-Ru(2)	126.0(4)
C(65)-N(13)-Ru(2)	115.2(4)
C(70)-N(14)-C(66)	118.4(5)
C(70)-N(14)-Ru(2)	126.0(4)
C(66)-N(14)-Ru(2)	114.9(4)
N(1)-C(1)-N(2)	108.3(4)
N(1)-C(1)-C(13)	127.3(5)
N(2)-C(1)-C(13)	123.4(5)
C(3)-C(2)-N(2)	119.3(6)
C(2)-C(3)-C(4)	120.8(6)
C(5)-C(4)-C(3)	121.3(6)
C(4)-C(5)-C(6)	118.6(6)
C(7)-C(6)-N(2)	105.2(5)
C(7)-C(6)-C(5)	136.3(6)
N(2)-C(6)-C(5)	118.4(5)

C(6)-C(7)-N(1)	109.7(5)
C(6)-C(7)-C(8)	133.9(5)
N(1)-C(7)-C(8)	116.3(5)
N(3)-C(8)-C(9)	122.0(5)
N(3)-C(8)-C(7)	113.9(5)
C(9)-C(8)-C(7)	124.1(6)
C(10)-C(9)-C(8)	117.6(6)
C(9)-C(10)-C(11)	120.7(6)
C(12)-C(11)-C(10)	118.4(6)
N(3)-C(12)-C(11)	122.7(6)
C(14)-C(13)-C(18)	118.2(5)
C(14)-C(13)-C(1)	123.2(5)
C(18)-C(13)-C(1)	118.5(5)
C(13)-C(14)-C(15)	120.6(5)
C(16)-C(15)-C(14)	120.8(5)
C(15)-C(16)-C(17)	119.0(5)
C(15)-C(16)-C(19)	121.9(5)
C(17)-C(16)-C(19)	119.2(5)
C(18)-C(17)-C(16)	120.0(5)
C(17)-C(18)-C(13)	121.4(5)
N(4)-C(19)-N(5)	109.4(5)
N(4)-C(19)-C(16)	127.3(5)
N(5)-C(19)-C(16)	123.2(5)
C(21)-C(20)-N(5)	118.7(6)
C(20)-C(21)-C(22)	120.5(6)
C(23)-C(22)-C(21)	120.9(6)
C(22)-C(23)-C(24)	119.9(6)
C(25)-C(24)-N(5)	105.1(5)
C(25)-C(24)-C(23)	137.3(6)
N(5)-C(24)-C(23)	117.6(5)
C(24)-C(25)-N(4)	109.5(5)
C(24)-C(25)-C(26)	132.4(5)
N(4)-C(25)-C(26)	118.1(5)
N(6)-C(26)-C(27)	121.5(5)
N(6)-C(26)-C(25)	113.2(5)
C(27)-C(26)-C(25)	125.3(5)
C(28)-C(27)-C(26)	119.5(6)
C(29)-C(28)-C(27)	119.2(6)
C(28)-C(29)-C(30)	119.5(6)
N(6)-C(30)-C(29)	124.0(6)
N(7)-C(31)-C(32)	123.3(6)
C(31)-C(32)-C(33)	117.9(6)
C(34)-C(33)-C(32)	120.0(6)
C(33)-C(34)-C(35)	119.2(6)
N(7)-C(35)-C(34)	120.8(6)
N(7)-C(35)-C(36)	114.9(5)
C(34)-C(35)-C(36)	124.3(6)
N(8)-C(36)-C(37)	121.0(5)
N(8)-C(36)-C(35)	114.2(5)
C(37)-C(36)-C(35)	124.7(5)
C(38)-C(37)-C(36)	119.5(6)
C(37)-C(38)-C(39)	120.3(6)
C(38)-C(39)-C(40)	119.2(6)

N(8)-C(40)-C(39)	122.5(6)
N(9)-C(41)-C(42)	124.0(6)
C(43)-C(42)-C(41)	118.7(6)
C(42)-C(43)-C(44)	118.8(6)
C(45)-C(44)-C(43)	120.0(6)
N(9)-C(45)-C(44)	121.3(5)
N(9)-C(45)-C(46)	114.3(5)
C(44)-C(45)-C(46)	124.4(5)
N(10)-C(46)-C(47)	120.5(5)
N(10)-C(46)-C(45)	115.0(5)
C(47)-C(46)-C(45)	124.5(5)
C(46)-C(47)-C(48)	120.4(6)
C(49)-C(48)-C(47)	119.5(6)
C(48)-C(49)-C(50)	118.0(6)
N(10)-C(50)-C(49)	123.5(5)
N(11)-C(51)-C(52)	123.5(6)
C(51)-C(52)-C(53)	118.7(6)
C(54)-C(53)-C(52)	119.2(6)
C(53)-C(54)-C(55)	119.7(6)
N(11)-C(55)-C(54)	121.3(6)
N(11)-C(55)-C(56)	114.5(5)
C(54)-C(55)-C(56)	124.2(6)
N(12)-C(56)-C(57)	120.9(6)
N(12)-C(56)-C(55)	114.8(5)
C(57)-C(56)-C(55)	124.3(6)
C(58)-C(57)-C(56)	120.6(7)
C(57)-C(58)-C(59)	118.6(6)
C(58)-C(59)-C(60)	120.1(6)
N(12)-C(60)-C(59)	120.4(6)
N(13)-C(61)-C(62)	123.0(6)
C(63)-C(62)-C(61)	118.0(6)
C(62)-C(63)-C(64)	120.1(6)
C(65)-C(64)-C(63)	119.0(6)
N(13)-C(65)-C(64)	121.0(5)
N(13)-C(65)-C(66)	114.9(5)
C(64)-C(65)-C(66)	124.0(5)
N(14)-C(66)-C(67)	121.3(5)
N(14)-C(66)-C(65)	115.0(5)
C(67)-C(66)-C(65)	123.6(5)
C(68)-C(67)-C(66)	119.6(6)
C(69)-C(68)-C(67)	118.9(6)
C(68)-C(69)-C(70)	119.0(6)
N(14)-C(70)-C(69)	122.7(5)
O(100)-C(100)-C(101)	122.6(7)
O(100)-C(100)-C(102)	121.6(7)
C(101)-C(100)-C(102)	115.8(7)
O(200)-C(200)-C(201)	120.0(8)
O(200)-C(200)-C(202)	123.4(8)
C(201)-C(200)-C(202)	116.6(8)

Symmetry transformations used to generate equivalent aton

Table 4. Anisotropic displacement parameters (A^2 x 10^3) for c
The anisotropic displacement factor exponent takes the form:
-2 pi^2 [h^2 a*^2 U11 + ... + 2 h k a* b* U12]

	U11	U22	U33	U23	U13
Ru(1)	32(1)	24(1)	24(1)	1(1)	6(1)
Ru(2)	25(1)	29(1)	33(1)	1(1)	5(1)
P(1)	68(1)	62(1)	54(1)	-4(1)	3(1)
F(11)	115(4)	59(3)	68(3)	-12(2)	13(3)
F(12)	138(5)	116(4)	95(4)	-39(3)	55(3)
F(13)	101(4)	132(4)	57(3)	8(3)	3(3)
F(14)	95(4)	96(4)	83(3)	-40(3)	9(3)
F(15)	74(3)	105(4)	173(6)	-16(4)	46(4)
F(16)	192(6)	68(3)	94(4)	-9(3)	-59(4)
P(2)	50(1)	67(1)	45(1)	10(1)	6(1)
F(21)	53(3)	172(5)	111(4)	47(4)	27(3)
F(24)	54(3)	87(3)	94(3)	11(3)	17(2)
F(22)	61(4)	80(5)	155(8)	64(5)	26(5)
F(23)	94(6)	204(10)	55(5)	-48(6)	-9(4)
F(25)	88(6)	83(6)	253(13)	92(8)	-33(7)
F(26)	154(9)	202(12)	103(7)	-112(8)	-42(6)
P(3)	44(1)	40(1)	36(1)	-1(1)	4(1)
F(32)	129(4)	50(3)	100(4)	13(2)	-44(3)
F(35)	107(4)	52(3)	111(4)	3(3)	-26(3)
F(31)	91(4)	51(3)	70(4)	1(3)	-28(3)
F(33)	77(5)	175(8)	86(5)	-4(5)	52(4)
F(34)	113(5)	57(4)	73(5)	-12(3)	-45(4)
F(36)	130(6)	143(6)	108(5)	-21(5)	93(5)
P(4)	48(1)	48(1)	72(1)	10(1)	-2(1)
F(41)	65(3)	60(3)	114(4)	35(3)	1(3)
F(44)	89(3)	69(3)	118(4)	26(3)	-12(3)
F(42)	79(5)	93(6)	212(11)	86(7)	-55(6)
F(43)	141(6)	98(5)	26(3)	-10(3)	11(4)
F(45)	54(4)	67(4)	59(4)	-15(3)	-7(3)
F(46)	80(5)	121(7)	113(7)	10(5)	49(5)
N(1)	30(2)	26(2)	26(3)	0(2)	-1(2)
N(2)	33(3)	40(3)	31(3)	-1(2)	6(2)
N(3)	39(3)	26(2)	29(3)	-2(2)	6(2)
N(4)	26(2)	23(2)	35(3)	-1(2)	7(2)
N(5)	27(2)	31(3)	34(3)	4(2)	5(2)
N(6)	29(3)	43(3)	41(3)	-3(2)	6(2)
N(7)	39(3)	25(3)	30(3)	-4(2)	3(2)
N(8)	35(3)	31(3)	30(3)	2(2)	7(2)
N(9)	28(2)	32(3)	29(3)	1(2)	7(2)
N(10)	29(2)	28(2)	28(3)	-3(2)	9(2)
N(11)	30(3)	34(3)	34(3)	-1(2)	7(2)
N(12)	31(3)	34(3)	40(3)	3(2)	2(2)

N(13)	31(3)	38(3)	30(3)	1(2)	6(2)
N(14)	25(2)	27(2)	31(3)	2(2)	3(2)
C(1)	34(3)	31(3)	21(3)	0(2)	4(2)
C(2)	33(3)	53(4)	32(3)	-6(3)	9(3)
C(3)	46(4)	73(5)	48(4)	-3(4)	18(3)
C(4)	45(4)	67(5)	52(4)	-18(4)	14(3)
C(5)	51(4)	43(4)	46(4)	-13(3)	2(3)
C(6)	36(3)	34(3)	32(3)	-2(3)	5(3)
C(7)	36(3)	25(3)	25(3)	-4(2)	1(2)
C(8)	47(4)	22(3)	24(3)	-4(2)	1(3)
C(9)	57(4)	31(3)	40(4)	-7(3)	-2(3)
C(10)	81(5)	22(3)	54(5)	1(3)	-8(4)
C(11)	69(5)	37(4)	45(4)	3(3)	2(4)
C(12)	55(4)	34(3)	36(4)	-3(3)	10(3)
C(13)	27(3)	26(3)	37(3)	4(2)	7(2)
C(14)	45(4)	44(4)	25(3)	4(3)	4(3)
C(15)	44(4)	39(3)	27(3)	14(3)	0(3)
C(16)	21(3)	35(3)	32(3)	-1(3)	4(2)
C(17)	33(3)	37(3)	25(3)	0(3)	1(2)
C(18)	35(3)	27(3)	35(3)	7(3)	6(3)
C(19)	33(3)	27(3)	37(3)	6(3)	7(3)
C(20)	39(4)	54(4)	56(4)	5(3)	-5(3)
C(21)	52(4)	56(5)	68(5)	12(4)	-11(4)
C(22)	69(5)	39(4)	74(5)	1(4)	5(4)
C(23)	46(4)	31(3)	56(4)	6(3)	1(3)
C(24)	34(3)	30(3)	38(4)	5(3)	12(3)
C(25)	32(3)	26(3)	35(3)	2(2)	12(3)
C(26)	33(3)	29(3)	37(3)	-2(3)	18(3)
C(27)	46(4)	33(3)	45(4)	-7(3)	20(3)
C(28)	45(4)	46(4)	56(4)	-20(3)	22(3)
C(29)	38(4)	63(5)	62(5)	-26(4)	13(3)
C(30)	31(3)	54(4)	47(4)	-10(3)	10(3)
C(31)	35(3)	37(3)	30(3)	3(3)	0(3)
C(32)	45(4)	52(4)	30(4)	5(3)	1(3)
C(33)	58(5)	70(5)	27(4)	6(3)	-6(3)
C(34)	59(4)	61(4)	27(4)	1(3)	7(3)
C(35)	44(4)	37(4)	31(3)	1(3)	11(3)
C(36)	37(3)	34(3)	29(3)	4(3)	9(3)
C(37)	51(4)	58(4)	42(4)	-1(3)	23(3)
C(38)	43(4)	69(5)	58(5)	5(4)	23(4)
C(39)	28(3)	71(5)	61(5)	5(4)	9(3)
C(40)	40(4)	50(4)	36(4)	2(3)	0(3)
C(41)	46(4)	36(3)	29(3)	-5(3)	3(3)
C(42)	60(4)	46(4)	27(3)	-2(3)	3(3)
C(43)	88(6)	60(5)	25(4)	2(3)	-3(3)
C(44)	72(5)	44(4)	37(4)	4(3)	1(3)
C(45)	44(4)	29(3)	34(3)	5(3)	2(3)
C(46)	39(3)	30(3)	29(3)	7(2)	6(3)
C(47)	71(5)	31(4)	52(4)	8(3)	5(4)
C(48)	52(4)	23(3)	61(5)	-6(3)	8(3)
C(49)	33(3)	36(3)	45(4)	-7(3)	10(3)
C(50)	38(3)	35(3)	37(4)	-3(3)	6(3)
C(51)	36(3)	41(4)	44(4)	9(3)	7(3)

C(52)	55(4)	54(4)	39(4)	8(3)	13(3)
C(53)	72(5)	60(5)	49(5)	7(4)	31(4)
C(54)	34(4)	53(4)	69(5)	-1(4)	21(3)
C(55)	35(3)	30(3)	48(4)	4(3)	12(3)
C(56)	31(3)	30(3)	53(4)	1(3)	7(3)
C(57)	31(4)	62(5)	70(5)	9(4)	5(3)
C(58)	25(4)	69(5)	86(6)	2(4)	-11(4)
C(59)	47(4)	74(5)	58(5)	16(4)	-20(4)
C(60)	42(4)	54(4)	45(4)	2(3)	-6(3)
C(61)	47(4)	50(4)	39(4)	-2(3)	10(3)
C(62)	62(4)	60(5)	40(4)	-5(3)	20(3)
C(63)	63(5)	66(5)	46(4)	9(4)	26(4)
C(64)	59(4)	47(4)	43(4)	8(3)	11(3)
C(65)	33(3)	37(3)	35(3)	9(3)	3(3)
C(66)	34(3)	33(3)	32(3)	1(3)	4(3)
C(67)	55(4)	34(4)	48(4)	8(3)	10(3)
C(68)	57(4)	25(3)	62(5)	-4(3)	9(4)
C(69)	42(4)	37(4)	44(4)	-4(3)	5(3)
C(70)	30(3)	33(3)	37(4)	-1(3)	2(3)
O(100)	65(3)	48(3)	64(3)	-7(2)	5(3)
C(100)	57(4)	46(4)	48(4)	-3(3)	4(3)
C(101)	173(11)	78(7)	179(12)	-33(7)	-120(10)
C(102)	80(6)	70(5)	81(6)	12(4)	10(5)
O(200)	33(4)	35(4)	115(6)	-21(4)	-7(4)
C(200)	36(5)	19(4)	54(6)	-3(4)	-1(4)
C(201)	47(5)	48(5)	27(5)	-7(4)	7(4)
C(202)	46(6)	86(8)	58(7)	-33(6)	-16(5)

Table 5. Hydrogen coordinates (x 10^4) and isotropic displacement parameters (A^2 x 10^3) for ciftab.

	x	y	z	U(e
H(2)	1205	3880	7915	56
H(3)	483	4556	8363	56
H(4)	1032	5455	8397	56
H(5)	2271	5679	7947	56
H(9)	3222	5984	7278	60
H(10)	4243	6542	6855	60
H(11)	5547	6166	6557	60
H(12)	5729	5234	6586	60
H(14)	2475	3119	8019	23
H(15)	1951	2266	7690	23
H(17)	1988	2729	5930	23
H(18)	2460	3588	6258	23
H(20)	3192	1603	7143	62
H(21)	3799	744	7161	62
H(22)	2971	7	6702	62

H(23)	1563	134	6229	62(
H(27)	233	179	5700	42(
H(28)	-1146	-92	5202	42(
H(29)	-2229	559	4935	42(
H(30)	-1954	1457	5189	42(
H(31)	2961	4515	5958	62(
H(32)	2575	4644	4927	62(
H(33)	3672	4510	4261	62(
H(34)	5125	4305	4666	62(
H(37)	6512	4104	5143	62(
H(38)	7866	3947	5715	62(
H(39)	7967	3902	6775	62(
H(40)	6703	4014	7253	62(
H(41)	5156	4768	8134	51(
H(42)	5548	4530	9138	51(
H(43)	5737	3614	9392	51(
H(44)	5434	2959	8623	51(
H(47)	5246	2383	7816	51(
H(48)	4895	1840	6947	51(
H(49)	4402	2252	6010	51(
H(50)	4237	3191	5976	51(
H(51)	-44	1763	7240	56(
H(52)	-784	1710	8089	56(
H(53)	-2287	1959	8006	56(
H(54)	-2993	2257	7065	56(
H(57)	-3598	2433	6098	56(
H(58)	-4092	2728	5111	56(
H(59)	-3046	2886	4430	56(
H(60)	-1538	2698	4730	56(
H(61)	212	1709	4678	47(
H(62)	867	2025	3835	47(
H(63)	1212	2954	3782	47(
H(64)	892	3545	4568	47(
H(67)	549	4038	5351	47(
H(68)	277	4489	6247	47(
H(69)	-180	3983	7050	47(
H(70)	-424	3050	6923	47(

Appendix B:

Publications and Presentations:

- "Ruthenium and Osmium Polypyridyl Complexes as Precursors to Surface Active Dinuclear Complexes", Oral Presentation, EU TMR, "Heterosupramolecular Chemistry", Uppsala, Sweden, 1999.

- "The synthesis and characterisation of a new type of $[Ru(bpy)_2(LL_x)]^{2+}$ complex", Poster Presentation, SOLAR '01, Cairo, Egypt.

- "An examination of the synthesis and characterisation of a series of Ruthenium(II) complexes", Oral Presentation, Research Seminar Series, Dublin City University, April 2002.

- "Routes to regioselective deuteriation of heteroaromatic compounds", Publication, ***Inorg. Chem.***, In Press.

Inorg. Chem. XXXX, XX,

Inorganic Chemistry

: Article

Routes to Regioselective Deuteration of Heteroaromatic Compounds

Wesley R. Browne,[†] Christine M. O'Connor,[‡] J. Scott Killeen,[†] Adrian L. Guckian,[†] Micheal Burke,[§] Paraic James,[∥] Maurice Burke,[§] and Johannes G. Vos*,[†]

National Centre for Sensor Research, School of Chemical Sciences, Dublin City University, Dublin 9, Ireland, Department of Chemistry, Dublin Institute of Technology, Dublin 2, Ireland, School of Chemical Sciences, Dublin City University, Dublin 9, Ireland, and National Institute for Cellular Biotechnology, Dublin City University, Dublin 9, Ireland

Received March 22, 2002

A systematic approach to the deuteration of polypyridyl type ligands is reported. A range of isotopologues of heteroaromatic compounds containing pyrazyl, pyridyl, 1,2,4-triazole, thienyl, methyl, and phenyl moieties, have been prepared in a cost-effective manner, using a range of methods based on subcritical aqueous media. Selectively and fully deuteriated ligands are characterized by mass spectrometry and ^{1}H, ^{2}D, and ^{13}C NMR spectroscopy. The application of deuteriation to supramolecular chemistry is discussed.

Introduction

The application of transition metal complexes incorporating polypyridyl type ligands in inorganic photochemistry and supramolecular chemistry, in particular, has increased rapidly since the mid 1970s.[1] In particular, ruthenium(II) and osmium(II) based polypyridyl complexes have been utilized as building blocks for large multinuclear structures, mostly because of their synthetic versatility and suitable photophysical and electrochemical properties.[2] However, with the ever-increasing complexity of supramolecular systems, the ability to characterize these molecules fully by standard NMR techniques has become difficult.[3] An additional challenge often encountered is the identification of the nature of the emitting state, which, for heteroleptic compounds, may be located on different parts of the molecular assembly. Deuteriation of ligands has been proposed as a tool to help overcome these problems, at least in part.[4]

To date, however, the widespread use of deuteriation as a general spectroscopic aid has been limited, primarily because of the lack of generally applicable, high yield, and low cost H/D exchange procedures for polypyridyl type ligands. In this contribution, a general and systematic approach to the deuteriation of polypyridyl type heteroaromatic compounds is reported. This approach is based on the use of subcritical D_2O. The methods reported in this contribution are a significant improvement on traditional routes reported for the deuteriation of 2,2′-bipyridyl, which require several synthetic steps or the use of the environmentally unfriendly material asbestos.[5,6] Both methods yield only fully deuteriated compounds, in low to moderate yields. With the systematic approach reported in this contribution, more than 30 partially and fully deuteriated compounds (Figure 1) are obtained in high yields (~90%). The procedures used are relatively low cost and straightforward and can be carried out on at least gram scale. The approach reported is of a general nature and can be applied to a wide range of compounds, and as a result, the widespread use of partial deuteriation to elucidate the properties of supramolecular structures is now possible.

* To whom correspondence should be addressed. E-mail: johannes.vos@dcu.ie. Fax: 00353 1 7005503. Phone: 00353 1 7005307.

† National Centre for Sensor Research.

‡ Dublin Institute of Technology.

§ School of Chemical Sciences, Dublin City University.

∥ National Institute for Cellular Biotechnology.

(1) (a) Juris, A.; Balzani, V.; Barigelletti, F.; Campagna, S.; Belser, P.; von Zelewsky, A. *Coord. Chem. Rev.* **1988**, *84*, 85. (b) Balzani, V.; Campagna, S.; Denti, G.; Juris, A.; Ventura, M. *Coord. Chem. Rev.* **1994**, *132*, 1. (c) Balzani, V.; Scandola, F. *Supramolecular Photochemistry*; Ellis Horwood: Chichester, U.K., 1991. (d) *Supramolecular Photochemistry*; Balzani, V., Ed.; Reidel: Dordrecht, The Netherlands, 1997. (e) Kalyanasundaram, K. *Coord. Chem. Rev.* **1962**, *46*, 159.

(2) (a) Balzani, V.; Juris, A.; Venturi, M.; Campagna, S.; Serroni, S. *Acc. Chem. Res.* **1998**, *31*, 26. (b) Slate, C. A.; Striplin, D. R.; Moss, J. A.; Chen, P.; Erickson, B. W.; Meyer, T. J. *J. Am. Chem. Soc.* **1998**, *120*, 4885. (c) Hu, Y.-Z.; Tsukiji, S.; Shinkai, S.; Oishi, S.; Hamachi, I. *J. Am. Chem. Soc.* **2000**, *122*, 241. (d) Balzani, V.; Juris, A.; Venturi, M.; Campagna, S.; Serroni, S. *Chem. Rev.* **1996**, *96*, 759.

(3) (a) Thummel, R. P.; Williamson, D.; Hery, C. *Inorg. Chem.* **1993**, *32*, 1587. (b) Chirayil, S.; Thummel, R. P. *Inorg. Chem.* **1989**, *28*, 812. (c) O'Brien, J. R.; McMurry, T. B. H.; O'Callaghan, C. N. *J. Chem. Res., Synop.* **1998**, 448 and references therein.

(4) For a recent review see: Browne, W. R.; Vos, J. G. *Coord. Chem. Rev.* **2001**, *219*, 761 and references therein.

(5) Cook, M. J.; Lewis, A. P.; McAuliffe, G. S. G.; Skarda, V.; Thomson, A. J.; Glasper, J. L.; Robbins, D. J. *J. Chem. Soc., Perkin Trans. 2* **1984**, 1293.

(6) Fischer, G.; Puza, M. *Synthesis* **1973**, *4*, 218.

10.1021/ic020226y CCC: $22.00
Published on Web 00/00/0000

Table 1. Conditions, Yields, and Extent of Isotope Exchange Reactions

	compound	overall % H−D exchange (site)[a]	method[b]	% yield[c]	reaction time (days)
1b	[D_8]-2,2′-bipyridine	>98	A	80	2 × 3 days
		>98	C	90	6
2b	[D_8]-4,4′-bipyridine	>98 (C2/C6); <15 (C3/C5)	B	95	3
2c	[D_8]-4,4′-bipyridine	>98	A	80	4
		>98	C	90	6
3b	[D_{12}]-4,4′-dimethyl-2,2′-bipyridine	>98 (50% exchange at C3)	A	70	4
		>98	C	95	6
4b	[D_8]-1,10-phenanthroline	>98	A	70	4
		>98	C	95	6
5b	[D_6]-4,7-diphenyl-1,10-phenanthroline	>98 phenanthroline protons (<5% for phenyl rings, C5/C6 show incomplete exchange)	C	95	6
5c	[D_{10}]-4,7-diphenyl-1,10-phenanthroline	~95% for phenyl rings	D (from **5d**)	95	6
5d	[D_{14}]-4,7-diphenyl-1,10-phenanthroline	>98 (<5 at C5/C6)	A	60	6
5e	[D_{16}]-4,7-diphenyl-1,10-phenanthroline	>98	A then C	80	2 × 3 days
6b	[D_{12}]-2,2′-biquinoline	>98	A	80	3
6c	[D_4]-2,2′-biquinoline	>98 C2/C3/C4 (<10 at remaining positions)	C	60	4
7b	[D_{10}]-2,3-di-(pyrid-2yl)-pyrazine	> 98	C	90	6
8b	[D_2]-2-(thien-2′-yl)-pyridine	>98 (py-H6/th-H5′)	B	85	6
8c	[D_7]-2-(thien-2′-yl)-pyridine	>98	C	95	6

[a] In the case of partially deuteriated compounds, exchange at individual positions is given in parentheses. [b] **A** 0.1 g of 10% Pd/C in 20 mL of D_2O at 200 °C; **B** in 20 mL of D_2O at 200 °C; **C** in 20 mL of 1 M NaOD/D_2O at 200 °C; **D** in 20 mL of 1 M NaOH/H_2O at 200 °C. [c] Based on recovered yield.

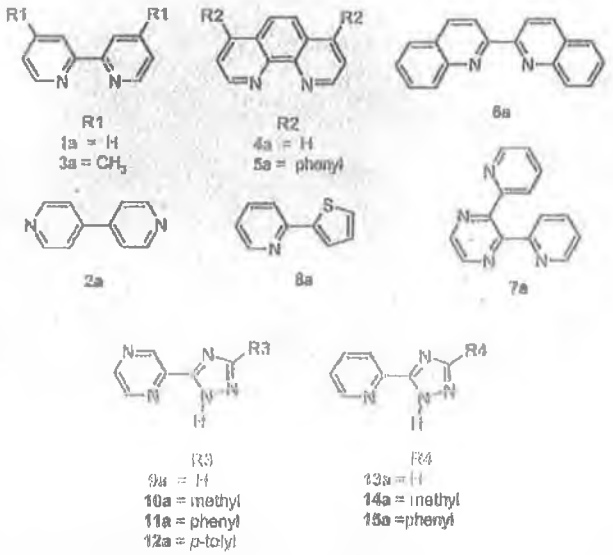

Figure 1. Structures of compounds examined.

Preliminary results on the deuteriation of 2,2′-bipyridyl using a Pd/C catalyst and D_2O as deuterium source were reported in an earlier communication.[7] Subsequently, this approach was applied to the full deuteriation of 1,10-phenanthroline,[7,8] pyridyl- and pyrazyl-1,2,4-triazole,[9] imidazole,[10] and 2-(thien-2′-yl)-pyridine.[11]

Results

As outlined in the Experimental Section, several H/D exchange procedures, methods A, B, and C, have been developed. In method A, Pd/C is used as a catalyst in the presence of D_2O, and in method B, only D_2O is used, while method C is based on the use of basic D_2O (pD = 10/11). In addition, "reverse" D/H exchange has been used to achieve further regioselectivity. The approaches taken are basic H_2O, method D, neutral H_2O, method E, and neutral H_2O in the presence of Pd/C, method F. In all methods, the reaction is carried out in a sealed steel container with a Teflon liner at 200 °C. The products obtained, together with yields, the degree of deuteriation, and experimental conditions are given in Tables 1 and 2. Spectroscopic characterization of the products has been carried out using mass spectrometry and ^1H, ^2D, and ^{13}C NMR spectroscopy. Data are given as Supporting Information. The degree of deuteriation was determined using both ^1H NMR spectroscopy and mass spectrometry. In Tables 1 and 2 (and for convenience throughout this paper), the exchange of the N−H proton of 1,2,4-triazole rings is not considered because exchange at this position is fast and occurs under ambient conditions in protic solvents.

Discussion

General. The application of high temperature and supercritical aqueous media in organic reactions has attracted significant interest in recent years.[12] Much less attention has been focused on medium temperature (150−250 °C) aqueous media despite it being the more accessible temperature range. H/D exchange of pyridine under acidic, neutral, and basic conditions was investigated in some detail in the medium (150−250 °C) and low (<150 °C) temperature range.[13−15] The usefulness of transition metal catalysts was examined,

(7) Keyes, T. E.; Weldon, F.; Müller, E.; Pechy, P.; Grätzel, M. J. G. Vos, J. *J. Chem. Soc., Dalton Trans.* **1995**, 2705.
(8) Coates, C. G.; Callaghan, P. L.; McGarvey, J. J.; Kelly, J. M.; Kruger, P. E.; Higgins, M. E. *J. Raman Spectrosc.* **2000**, *31*, 283.
(9) Fanni, S.; Keyes, T.; O'Connor, C. M.; Hughes, H.; Wang, R. Y.; Vos, J. G. *Coord. Chem. Rev.* **2000**, *208*, 77.
(10) Hanfarer, C.; Holbrey, J. D.; McMath, S. E. J. *Chem. Commun.* **2001**, 367.
(11) Yersin, H.; Humbs, W. *Inorg. Chem* **1999**, *38*, 5820.
(12) (a) Katritzky, A. R.; Nichols, D. A.; Siskin, M.; Murugan, R.; Balasubramanian, M. *Chem Rev.* **2001**, *101*, 837. (b) Junk, T.; Catallo, W. J. *Chem. Soc Rev.* **1997**, *26*, 401.
(13) (a) Zoltewicz, J. A.; Smith, C. L. *J. Am Chem. Soc.* **1967**, *89*, 3358. (b) Yao, J.; Evilia, R. F. *J. Am. Chem. Soc.* **1994**, *116*, 11229. (c) Riesen, H.; Wallace, L.; Krausz, E. *J. Phys. Chem.* **1996**, *100*, 17138.

Table 2. Conditions, Yields, and Extent of Hydrogen/Deuterium Exchange Reactions

	compound	overall % H−D exchange (site)[a]	method[b]	% yield[c]	reaction time (days)
9b	[D_4]-Hpztr	>98%	B	95	3
10b	[D_6]-Hmepztr	>98%	B	95	3
11b	[D_3]-Hphpztr	>98% (pz)	B	95	3
11c	[D_5]-Hphpztr	>98% (ph)	E (*#*)	95	3
11d	[D_8]-Hphpztr	>98%	A	80	2 × 3 days
12b	[D_3]-Htolpztr	>98% (pz)	B	95	3
12c	[D_3]-Htolpztr	>98% (Me)	E (prepared from 12e)	95	2
12d	[D_4]-Htolpztr	>80% (tolyl, see Scheme 2)	F (*#*)	95	6
12e	[D_6]-Htolpztr	>98% (pz and Me)	A	95	6
12f	[D_7]-Htolpztr	>98% (tolyl)	E (*#*)	95	3(§)
12g	[D_{10}]-Htolpztr	>98%	C	95	2 × 10 days
13b	[D_5]-Hpytr	>98%	C	80	3
14b	[D_7]-Hmepytr	>98%	C	80	3
15b	[D_1]-Hphpytr	>95% (py H6)	B	95	30
15c	[D_4]-Hphpytr	>95% (py), <15% (ph)	C	90	3
15d	[D_5]-Hphpytr	>95% (ph), <15% (py)	E (*#*)	90	3
15e	[D_9]-Hphpytr	>98%	A	80	6
	[$Ru(bpy)_2$(**11a**)](PF_6)	>98% pz C3/5, <20% at pz C6	B	70	3
	[$Ru(bpy)_3$](PF_6)	no exchange obsd	B	90	3
		no exchange obsd	B	90	3

[a] In the case of partially deuteriated compounds, exchange at individual positions is given in parentheses. [b] **E** in 20 mL of H_2O at 200 °C; **F** 0.1 g of 10% Pd/C in 20 mL of H_2O at 200 °C; *#* indicates preparation from perdeuteriated reagents (see Experimental Section). For other reaction conditions, see Table 1. [c] On the basis of recovered yield, § indicates that when species reacted for 30 days, no further exchange was observed. For **12b−g**, see Scheme 2 for further information.

with Pt and Pd receiving the most attention.[15] However, to the authors' knowledge, no detailed study on the general application of such methods has been reported. The motivation behind the interest in the deuteriation of polypyridyl ligands is their potential applicability in the study of supramolecular systems. One approach taken has been the direct deuteriation of the metal complexes.[16−18] For example, deuteriation of $[Ru(bpy)_3]^{2+}$ in 0.1 M $NaOCD_3/(CD_3)_2SO/CD_3OD$ at 35 °C was found to occur rapidly at the 3,3′-positions and more slowly at the 5,5′-positions. In the present study, $[Ru(bpy)_3]^{2+}$ is found to be inert to H/D exchange in both neutral and basic D_2O (Table 2). When using method B, $[Ru(bpy)_2(11a)]^{2+}$ shows a very slow exchange at the H6 position of the pyrazyl ring (adjacent to the coordinating nitrogen), whereas the H3 and H5 positions of the pyrazine ring undergo complete exchange. Overall deuteriation of metal complexes is slow and has severe limitations, especially in the case of heteroleptic complexes; for this reason, a general strategy for the H/D exchange of ligands is needed.

With the strategy reported in this contribution, deuteriation has been achieved on the gram scale, with high yields (typically >80% after purification) and to high degrees of isotopic purity (typically >98%). No impurities were observed for any of the reactions listed in Tables 1 and 2. The yields reported are recovered yields, and the less than quantitative values obtained for method A reflect the difficulty of removing the substrates from the Pd/C catalyst. It is also important to realize that there is a theoretical limit to the extent of deuteriation. This limit is dependent on the molar ratio between the substrate and the solvent D_2O. For example, 3 g of 2,2′-bipyridine contains 0.1538 mol equiv of protons, and 20 mL of D_2O contains 2.214 mol equiv of deuterons; for this reaction mixture, the maximum theoretical deuteriation is 93.5%. When 1 g of bpy is employed, the maximum theoretical limit is raised to 98%. When large amounts are deuteriated (>1 g) by any of the procedures, the sample is subjected to two cycles rather than one, and after the second cycle, the equilibrium limit rises to greater than 99.5%. This is indicated in the tables. We thank one of the reviewers for highlighting this issue. By careful manipulation of the conditions employed and by the combination of different methods, regioselective deuteriation is achieved. The behavior of the compounds studied is discussed in more detail in the next sections.

Deuteriation of Heterocyclic Groups. Compounds **1a**−**8a** (Figure 1) are among the most commonly employed bidentate ligands in the preparation of inorganic polypyridyl complexes.[1] Table 1 shows that Pd/C is not needed to achieve full deuteriation. Neutral and basic D_2O solutions also yield high deuteriation ratios and high yields. The absence of a catalyst has the advantage that the workup of the reaction mixture is easier, and hence, yields improve (See Table 1).

The effect of the reaction conditions used (e.g., time, pH/pD and catalyst) is found to be dependent on the type of proton to be exchanged. For example, as shown in Figure 2,

(14) (a) Wong, J. L.; Heck, J. H., Jr. *J. Org. Chem.* **1974**, *39*, 2398. (b) Buncel, E.; Clement, O.; Onyido, I. *J. Am. Chem. Soc.* **1994**, *116*, 2679. (c) Clement, O.; Rouzak, A. W.; Buncel, E. *J. Am. Chem. Soc.* **1996**, *118*, 612. (d) Hardacre, C.; Holbrey, J. D.; McMath, S. E. J. *Chem. Commun.* **2001**, 367. (e) Anto, S.; Getvoldsen, G. S.; Harding, J. R.; Jones, J. R.; Lu, S.-Y.; Russell, J. C. *J. Chem. Soc., Perkin Trans. 2* **2000**, 2208.

(15) (a) Buncel, E.; Clement, O. *J. Chem. Soc., Perkins Trans. 2* **1995**, 1333. (b) Olofson, R. A.; Landesberg, J. M. *J. Am. Chem. Soc.* **1966**, *88*, 4263. (c) Olofson, R. A.; Landesberg, J. M.; Houk, K. N.; Michealman, J. S. *J. Am Chem. Soc.* **1966**, *88*, 4265. (d) Coburn, R. A.; Landesberg, J. M.; Kemp, D. S.; Olofson, R. A. *Tetrahedron* **1970**, *26*, 685.

(16) Constable, E. C.; Seddon, K. R. *J. Chem. Soc., Chem. Commun.* **1982**, 34.

(17) McClanahan, S. F.; Kincaid, J. R. *J. Am Chem. Soc.* **1986**, *108*, 3840.

(18) Strommen, D. P.; Mallick, P. K.; Danzer, G. D.; Lumpkin, R. S.; Kincaid, J. R. *J. Phys. Chem.* **1990**, *94*, 1357.

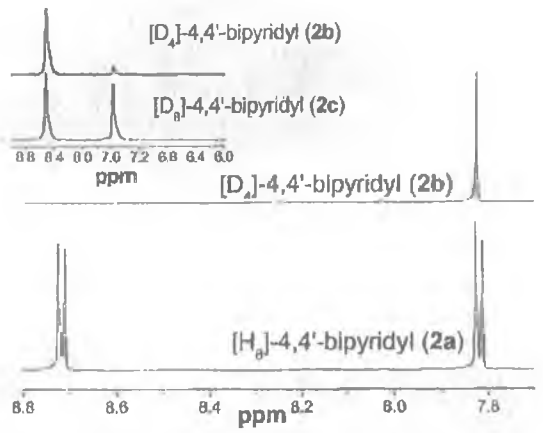

Figure 2. ^{1}H NMR spectra of [H_8]-4,4′-bipyridine (**2a**) (lower spectrum) and [D_4]-4,4′-bipyridine (**2b**) (upper spectrum) in [D_6]-acetone. Inset: ^{2}D NMR spectra of [D_8]-4,4′-bipyridine (**2c**) (lower spectrum) and [D_4]-4,4′-bipyridine (**2b**) (upper spectrum) in [D_6]-acetone).

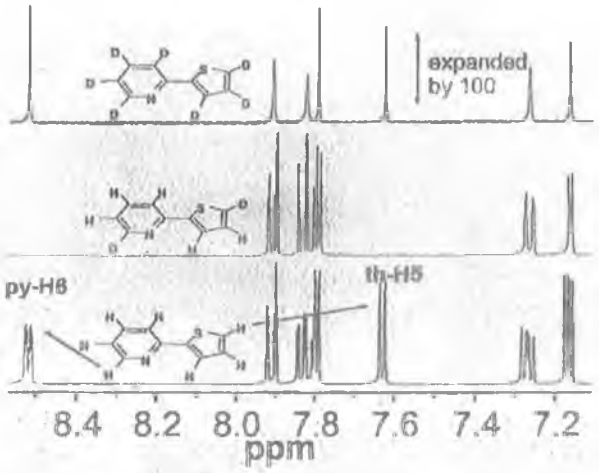

Figure 3. ^{1}H NMR spectra of [H_7]-2-(thien-2′-yl)-pyridine (**8a**) (lower spectrum), [D_2]-2-(thien-2′-yl)-pyridine (**8b**) (middle spectrum), and [D_7]-2-(thien-2′-yl)-pyridine (**8c**) (upper spectrum) in [D_6]-DMSO (all spectra were obtained at equal concentrations).

by using method B, little exchange is observed for the H3/H5 position of 4,4′-bipyridine (**2a**). Another example is illustrated in Figure 3 for compounds **8a**−**c**. This figure shows that after use of method B only the pyridine H6 and the thienyl H5 are exchanged, while full exchange is obtained with method C. In general, with method B, only exchange at the positions adjacent to heteroatoms (e.g., N and S) takes place even with extended reaction times (see Tables 1 and 2). Pyrazyl groups (compounds **9a**−**12a**) readily undergo complete exchange. This is not unexpected because every position can be considered as analogous to the H2/H6 position of pyridine.

Under basic conditions, much less variation is observed in exchange rates at different positions, with thienyl, pyridyl, and pyrazyl groups showing complete H/D exchange. However, with this method, a significant level of control over the deuteriation of the aryl and pyridyl moieties in **5a** and **6a** can be achieved. It should be noted that with method C the regioselectively observed for **5a** is different than that observed with method B. This is discussed later in more detail.

Deuteriation of Aromatic and Aliphatic Groups. H/D exchange of methyl groups depends on the nature of the moiety to which they are attached. When bound directly to pyridyl (**3a**) or 1,2,4-triazole (**10a**, **14a**) groups, complete exchange occurs under all conditions examined (Tables 1 and 2). In contrast, methyl groups attached to phenyl rings (**12a**) show no exchange using method B but deuteriate completely in basic media and with method A. Phenyl (**5a**, **11a**, and **15a**) and tolyl groups (**12a**) are the least reactive moieties. No exchange of aromatic protons was observed using method B, but phenyl groups do exchange in the presence of Pd/C catalyst (method A). Using method C, complete exchange of both phenyl and methyl protons is observed, albeit at a much slower rate than for heteroaromatic groups.

Regioselective Deuteriation. The differences in the reactivities of the various moieties allow for the development of strategies for the regioselective isotope exchange. Two examples of how different methods can be combined to achieve particular selectively deuteriated compounds are shown in Schemes 1 and 2. Scheme 1 (and Table 1) illustrates the routes taken in the preparation of four isotopologues of 4,7-diphenyl-1,10-phenanthroline (ph_2phen), namely [D_6]-ph_2phen, [D_{10}]-ph_2phen, [D_{14}]-ph_2phen, and [D_{16}]-ph_2phen. H/D exchange of the phenyl groups is achieved in the presence of the Pd/C catalyst in neutral D_2O but occurs only very slowly in basic D_2O. Consequently, using method A, the D_{14}- isotopologue (**5d**) is obtained in good yield with excellent regioselectivity. Interestingly, it is the phenanthroline H5 and H6 positions, which do not exchange under these conditions. However, deuteriation of the complete phenanthroline moiety takes place using method C. The fact that these reactions are high yield and can be carried out on a gram scale opens the possibility to use the products obtained as materials for further reaction. Therefore, a reverse D/H exchange as shown in Scheme 1 becomes a viable option. With this approach, compounds such as **5c** can be prepared from **5d**. In this process, the moiety that is most easily exchanged, namely the phenanthroline grouping, is regenerated in the perprotio form.

In Scheme 2, the different reactivities of pyrazine, aromatic, and methyl groupings are illustrated. On the basis of the behavior observed in Scheme 1, it is surprising that the tolyl aromatic protons do not exchange in any significant manner using method A, and this suggests that the methyl group deactivates the tolyl ring toward H/D exchange. Exchange of these protons is more efficient in the presence of base, albeit at a slower rate than for methyl or pyrazinyl protons. In contrast to the results obtained for **3a** and **10a**, the protons of the methyl group in **12a** can be exchanged using method A, but not by the use of method B. Again, the reverse D/H exchange can be used to yield isotopologues, such as **12c**, **12d**, and **12f**, which contain deuterium atoms in positions, which undergo H/D exchange with most difficulty.

Routes to Regioselective Deuteriation

Scheme 1. Routes Examined in the Deuteriation of **5a**

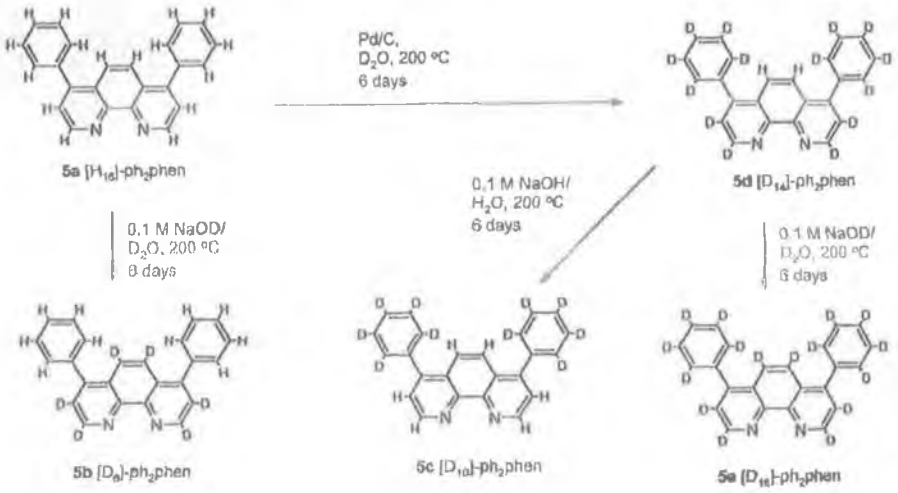

Scheme 2. Routes Examined for the Deuteriation of **12a**

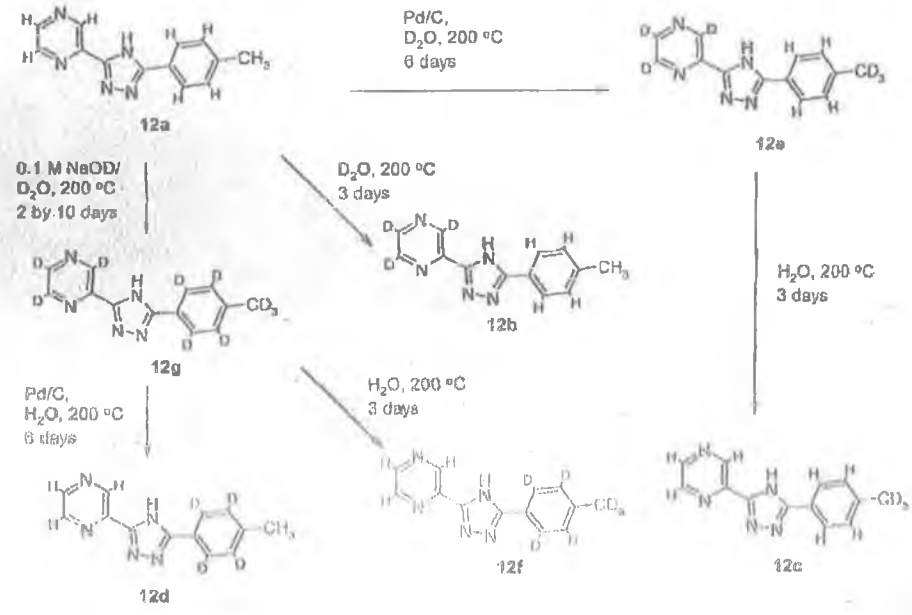

Application of Deuteriation in Supramolecular Systems. The effect of deuteriation on ^1H and ^{13}C NMR spectroscopy is already well-known.[3,4] Deuteriation results not only in a loss in intensity but also in the splitting of ^{13}C signals into multiplets. An example of this is shown in Figure 4, which shows the ^{13}C spectra for **4a** and **4b**. In the spectrum of **4b**, only the signals that can be attributed to the quaternized carbon atoms remain as singlets; the others appear as triplets. Selective deuteriation is therefore useful in the assignment of ^{13}C resonances.[3c] In addition, ^2D NMR spectroscopy can be used to monitor specific sites in complexes, which have complicated ^1H NMR spectra (see Figure 2 and Supporting Information). Furthermore, for large molecules such as ruthenium(II) and osmium(II) polypyridyl complexes, deuteriation has been shown to be very useful in simplifying ^1H NMR spectra,[3] and an example of this can be seen in Figure 5 (and Supporting Information), where ^1H NMR resonances are eliminated by selective deuteriation. The spectra shown illustrate how well-defined NMR based information can be obtained for compounds, which contain a large number of hydrogen atoms. It is also important to point out that no evidence for H/D exchange was observed, under the reaction conditions employed to prepare ruthenium complexes from deuteriated ligands.[9] This is in agreement with the observed temperature dependence of the deuteriation methods discussed, which indicates that no measurable exchange occurs below 140 °C.[19]

The application of deuteriation is not limited to structural characterization. Isotope exchange has found application as a probe for studying excited-state processes in transition metal complexes in time-resolved resonance Raman spectroscopy.[18] In addition, deuteriation has received considerable attention, in the study of the excited-state properties of rare earth ions and ruthenium(II) polypyridyl complexes.[4] Selec-

(19) O'Dwyer, C. MSc Thesis., Dublin City University, Dublin, Ireland, 1997.

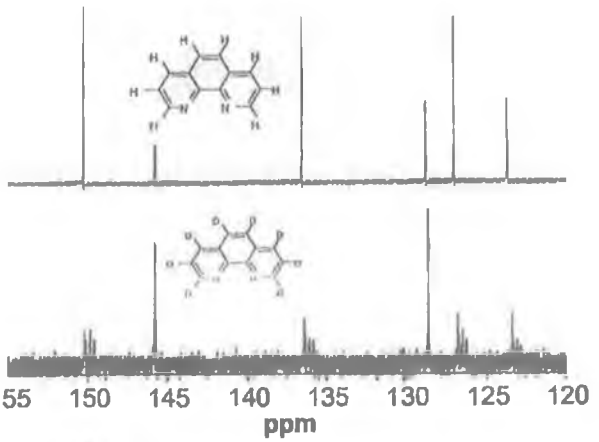

Figure 4. ^{13}C (proton decoupled) NMR spectra of [H_8]-1,10-phenanthroline (**4a**) (upper spectrum) and [D_8]-1,10-phenanthroline (**4b**) (lower spectrum) in [D_6]-DMSO.

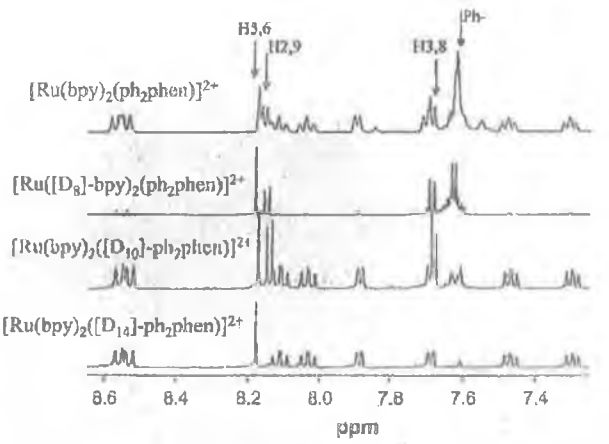

Figure 5. ^1H NMR spectra (400 MHz) of [Ru([D_x]-bpy)([D_y]-ph$_2$phen)]-$(PF_6)_2$ in [D_3]-acetonitrile. (x = 0 or 8, y = 10, 14, 16). Resonances due to ph$_2$phen ligand are indicated.

tive deuteriation of mixed ligand complexes was shown to yield important information about the location of the emitting state in mixed ligand complexes by its effect on emission lifetime.[7,8] For example, this approach can now be applied in the study of 2,3-bis(pyrid-2′-yl)-pyrazine (**7a**) based multinuclear ruthenium and osmium based bis(bipyridyl) complexes.[20] Deuteriation of either **7a** or **1a** would allow for the detailed study of the possible isomers present, and selective deuteriation could also be used to study the excited state behavior of such compounds.

Limitations. During the course of this study, 1,2,4-triazines and compounds containing functional groups (e.g., carboxylic acids, esters, and carbonitriles) were found to decompose under the conditions employed. However, the deuteriation of relatively large amounts of material (up to 3 g in this study), coupled with high yields, allows for the preparation of a much larger range of deuteriated compounds through the deuteriation of precursors in synthetically useful amounts. Therefore, the preparation of perdeuteriated compounds containing thermally unstable functional groups such as carboxylic acids, carbonitriles, amides, and so forth may be achieved indirectly via perdeuteriated methyl precursors (e.g., [D_6]-4,4′-dicarboxy-2,2′-bipyridine can be prepared from **3b**).

(20) Campagna, S.; Giannetto, A.; Serroni, S.; Denti, G.; Trusso, S.; Mallamace, F.; Micali, N. *J. Am. Chem. Soc.* **1995**, *117*, 1754.

Conclusions

In this contribution, a general approach to the deuteriation of heteroaromatic compounds is described. The potential for regioselective deuteriation is identified. The procedures employed allow for the reduction and often the complete elimination of the requirement for catalysts or derivatization (e.g., via *N*-oxide intermediates[5]) and much improved yields. The applicability of deuteriation in inorganic photophysics and supramolecular chemistry is already well-known.[4] However, its use has been severely limited by the cost and difficulty in preparing well-defined deuteriated materials. In this regard, the methods described here allow for the widespread application of deuteriation in such studies and provide an additional tool for the study of the spectroscopic and photophysical properties of supramolecular compounds.

Experimental Section

Materials. All reagents for synthesis were used as received without further purification. D_2O (99.9%) and 10% w/w Pd/C (Sigma-Aldrich) were used as received. NaOD/D_2O solution (1 M) was prepared in situ by addition of 460 mg of sodium metal to 20 mL of D_2O. 2,2′-Bipyridine (**1a**), 4,4′-bipyridine (**2a**), 4,4′-dimethyl-2,2′-bipyridine (**3a**), 1,10-phenanthroline (**4a**), 4,7-diphenyl-1,10-phenanthroline (ph$_2$phen) (**5a**), 2,2′-biquinoline (**6a**) (Sigma-Aldrich), and 2-(thien-2′-yl)-pyridine (2-thpy) (**8a**) (Lancaster) were obtained from commercial sources and used as received without further purification. The syntheses of 2,3-bis(pyrid-2′-yl)-pyrazine (**7a**),[21] 3-(pyrazin-2′-yl)-1,2,4-triazole (Hpztr) (**9a**), 3-methyl-5-(pyrazin-2′-yl)-1,2,4-triazole (Hmepztr) (**10a**), 3-(pyridin-2′-yl)-1,2,4-triazole (Hpytr) (**13a**), 3-methyl-5-(pyridin-2′-yl)-1,2,4-triazole (Hmepytr) (**14a**),[22] and 3-phenyl-5-(pyridin-2′-yl)-1,2,4-triazole (Hphpytr) (**15a**)[7] have been carried out using previously reported procedures. [Ru(bpy)$_3$](PF$_6$)$_2$,[23] [Ru(d_x-bpy)$_2$(d_y-ph$_2$phen)](PF$_6$)$_2$,[24] and [Ru(bpy)$_2$(**11a**)](PF$_6$)$_2$[25] (where bpy = **1a**, ph$_2$phen = **5a**, x = 0 or 8 and y = 0, 10, and 14) were prepared by literature procedures. The compounds 3-phenyl-5-(pyrazin-2′-yl)-1,2,4-triazole (Hphpztr) (**11a**) and 3-tolyl-5-(pyrazin-2′-yl)-1,2,4-triazole (Htolpztr) (**12a**) were carried out by previously reported procedures.[22]

Hydrogen−Deuterium Exchange Reactions. H−D exchange reactions were carried out using a Teflon cup contained in a general purpose dissolution Bomb P/N 4744 from Scientific Medical Products. Typical examples of each reaction type A−F are given in following paragraphs. Spectroscopic data for each partially and fully deuteriated compound are summarized as Supporting Information. In the case of method A, the solvent employed to remove deuteriated compound from the catalyst varied depending on the solubility of the compound. The extent of isotope exchange was determined from the isotopic pattern of the mass spectra of the compounds and by comparison of the ^1H NMR spectra of the

(21) Goodwin, H. A.; Lions, F. *J. Am. Chem. Soc.* **1959**, *81*, 6415.
(22) Hage, R. Ph.D. Thesis, Leiden University, The Netherlands, 1991.
(23) Casper, J. V.; Meyer, T. J. *J. Am. Chem. Soc.* **1983**, *105*, 5583.
(24) Baggot, J.; Gregory, G.; Piling, M.; Anderson, S.; Seddon, K. R.; Turp, J. *J. Chem. Soc., Faraday Trans. 2* **1983**, *79*, 195.
(25) Browne, W. R.; Guckian, A.; Vos, J. G. To be published.

deuteriated compound with its perprotio analogue at known concentrations using the residual solvent peak as an internal standard.

Method A. [D_8]-2,2′-Bipyridine (1b). 2,2′-Bipyridine (**1a**) (3 g) was reacted with 50 mg of 10% Pd/C in 20 mL of D_2O at 200 °C under pressure for 3 days. On cooling, the reaction mixture was filtered, and the catalyst was washed with 2 × 50 mL of diethyl ether to remove any 2,2′-bipyridine from the catalyst surface. The diethyl ether washings and the aqueous filtrate were evaporated to dryness to yield [D_8]-2,2′-bipyridine. It should be noted that with this method yields are sometimes lower than quantitative because of difficulty in removing the product from the catalyst.

Method B. [D_3]-Hphpztr (11b). A 1 g portion of 3-phenyl-5-(pyrazin-2-yl)-1,2,4-triazole (**11a**) was reacted at 200 °C in 20 mL of D_2O for 3 days. After cooling, the compound precipitated and was filtered and air-dried.

Method C. [D_4]-Hphpytr (15c). A 1.5 g portion of 3-phenyl-5-(pyridin-2-yl)-1,2,4-triazole (**15a**) was reacted at 200 °C in 20 mL of 1 M NaOD/D_2O for 3 days. On cooling, the reaction mixture was neutralized with concentrated HCl, and the white precipitate was filtered and air-dried.

Method D. [D_5]-Hphpytr (15d). A 0.5 g portion of [D_9]-3-phenyl-5-(pyridin-2-yl)-1,2,4-triazole (**15e**) was reacted at 200 °C in 20 mL of 1 M NaOH/H_2O for 3 days. On cooling, the reaction mixture was neutralized with concentrated HCl, and the white precipitate was filtered and air-dried.

Method E. [D_5]-Hphpztr (11c). A 0.5 g portion of [D_8]-3-phenyl-5-(pyrazin-2-yl)-1,2,4-triazole (**11d**) was reacted at 200 °C in 20 mL of H_2O for 3 days. On cooling the reaction mixture, the white precipitate was filtered and air-dried.

Method F. As for method A except H_2O was used in place of D_2O.

^{1}H, ^{13}C, and ^{2}D NMR Spectroscopic and Mass Spectral Data. Assignments of ^{1}H and ^{2}D NMR resonances were made by comparison with assignments made for ^{1}H NMR spectra of their perprotio analogues and are available as Supporting Information. Assignments of ^{13}C spectra were made on the basis of comparison with assignments made for their perprotio analogues using HMQC and HMBC NMR experiments and on the basis of the loss of intensity and splitting upon deuteriation. ^{1}H, ^{2}D, ^{13}C and ^{1}H COSY, HMQC, and HMBC spectra were recorded on a Bruker Avance 400 (400 MHz) NMR spectrometer equipped with a QNP probe (a broad band probe was employed for ^{2}D NMR spectroscopy). All measurements were carried out in [D_6]-acetone or [D_6]-dimethyl sulfoxide. ^{2}D NMR spectra were acquired in [H_6]-acetone or [H_6]-dimethyl sulfoxide. Peak positions are relative to residual solvent peaks. Mass spectra were obtained using a Bruker-Esquire-LC_00050 electrospray ionization mass spectrometer at positive polarity with cap-exit voltage of 167 V. Spectra were recorded in the scan range of 50−2200 *m/z* with an acquisition time of between 300 and 900 μs and a potential between 30 and 70 V. Each spectrum was recorded by summation of 20 scans. The limited solubility of some compounds precluded the measurement of their ^{2}D and ^{13}C NMR spectra.

Acknowledgment. The authors thank Enterprise Ireland for financial support.

Supporting Information Available: ^{1}H NMR spectra and characterization information. This material is available free of charge via the Internet at http://pubs.acs.org.

IC020226Y